VOLUME 112 NUMBER 1

THE ASTROPHYSICAL JOURNAL

AN INTERNATIONAL REVIEW OF SPECTROSCOPY AND ASTRONOMICAL PHYSICS

JULY 1950

THE AMOUNT OF POLARIZATION BY INTERSTELLAR GRAINS *H. C. van de Hulst* 1
PULSATION PROPERTIES OF GIANT-STAR MODELS *I. Epstein* 6
RADIATIVE EQUILIBRIUM IN AN ATMOSPHERE IN WHICH PURE SCATTERING AND PURE ABSORPTION BOTH PLAY A ROLE *A. D. Cole* 22
RADIAL VELOCITIES, SPECTRAL TYPES, AND LUMINOSITY CLASSES OF 920 STARS *J. H. Moore and C. P. Parkhurst* 48
ADDITIONAL STARS WHOSE SPECTRA HAVE A BRIGHT H_α LINE *Paul W. Merrill and Cora G. Burwell* 72
STELLAR SPECTRA IN MILKY WAY REGIONS. II. A REGION IN CYGNUS *S. W. McCuskey and C. E. Seyfert* 90
OH EMISSION BANDS IN THE SPECTRUM OF THE NIGHT SKY. II *A. B. Meinel* 120
ON THE IDENTIFICATION OF THE 3670 A BAND OF THE C_3 MOLECULE *John G. Phillips* 131
FINE STRUCTURE OF N_2O BANDS IN THE INFRARED SOLAR SPECTRUM *Manuel F. Migeotte* 136
PHOTOELECTRIC STUDIES. IV. COLOR-LUMINOSITY ARRAY FOR STARS IN THE REGION OF THE SUN *Olin J. Eggen* 141
SPECTROGRAPHIC OBSERVATIONS OF W URSAE MAJORIS *Otto Struve and Henry C. Horak* 178
SPECTROGRAPHIC OBSERVATIONS OF THE ECLIPSING BINARIES TW CASSIOPEIAE, TY PUPPIS, AND VV URSAE MAJORIS *Otto Struve* 184
THE RADIAL VELOCITY OF GAMMA CASSIOPEIAE *Burke Smith and O. Struve* 192
ON THE CHANGE OF PERIOD OF ECLIPSING VARIABLE STARS *Frank Bradshaw Wood* 196
NOTES
A Note on Energy Generation *I. Epstein* 207
On the Transition Probabilities of C_2 Swan Bands *N. R. Tawde and J. M. Patel* 310
Apparent Magnitudes and Color Indices for Seventy-four White Dwarfs and Degenerate Stars *W. J. Luyten* 212
The Spectrum of YY Geminorum (Castor C) *O. Struve, G. Herbig, and H. Horak* 216
The Spectrum of GP Orionis *William P. Bidelman* 219
Twenty-seven New Variable Stars in the Globular Cluster M 13 *L. Rosino* 221
Zeeman Shifts for Stellar Dipoles and Quadrupoles with Inclined Axes *Martin Schwarzschild* 222
REVIEWS 224

THE UNIVERSITY OF CHICAGO PRESS
CHICAGO, ILLINOIS, U.S.A.

July 1960 Vol. LXXXI, No. 1

THE ASTROPHYSICAL JOURNAL

AN INTERNATIONAL REVIEW OF SPECTROSCOPY AND ASTRONOMICAL PHYSICS

Edited by

W. W. MORGAN
Managing Editor

[illegible]
Associate Editor

PAUL W. MERRILL
Mount Wilson Observatory of the Carnegie Institution of Washington

[illegible]
Associate Editor

N. U. MAYALL
Lick Observatory
University of California

With the Collaboration of the American Astronomical Society

Collaborating Editors
1959-60

CECILIA H. PAYNE-GAPOSCHKIN
Harvard College Observatory

W. SAARE
Mount Wilson Observatory

[illegible]
Yerkes Observatory

H. H. BARBIER
Princeton University

LEO GOLDBERG
Observatory of the University of Michigan

[illegible]
Kitt Peak National Observatory

ANDREW McELLAR
Dominion Astrophysical Observatory, Victoria

O. STRUVE
National Science Foundation, Observatory

[illegible]
Associate Editor

The Astrophysical Journal is published bimonthly by the University of Chicago at the University of Chicago Press, 5750 Ellis Avenue, Chicago 37, Illinois, during July, September, November, January, March, and May. Two volumes are published per year, each beginning with the January issue and ending with the July issue. The subscription price is $6.00 per volume net in advance for the regular issues of the Journal, including postage. The price per single copy is $3.00. Orders for numbers of less than a volume will be charged at the single-copy rate. Postage is prepaid by the publishers on all orders from the United States and its possessions. No extra charge is made for postage to countries in the Pan American Postal Union. Postage is charged extra on orders as follows: for Canada, 40 cents per volume, 20 cents per part (total $6.40 per volume); for all other countries in the Postal Union, 80 cents per volume, 40 cents per part (total $6.80 per volume). Subscriptions may be entered at any time (prices, $6.00 per year; $3.00 per volume, $1.50 per part). All single copies are sent postpaid. Remittances should be made payable to The University of Chicago Press, in United States currency or its equivalent by postal or express money order or bank draft.

The following is an authorized agent:

For the British Empire except North America and Australasia: The Cambridge University Press, Bentley House, 200 Euston Road, London, N.W. 1, England. Prices of yearly subscriptions and of single copies may be had on application.

Claims for missing numbers should be made within the month following the regular month of publication. The publishers expect to supply missing numbers free only when they are lost in the mail. Claims must be received when the reserve stock will permit.

Business correspondence should be addressed to The University of Chicago Press, Chicago 37, Illinois. Communications for the editors and manuscripts should be addressed to W. W. Morgan, Editor of The Astrophysical Journal, Yerkes Observatory, Williams Bay, Wisconsin.

Line drawings and photographs suitable for reproduction should be made by the author, and all manuscript must be in publishable form, even lengths, etc., should be indicated in the copy. It will not be possible to alter or add to the contents in proof.

One copy of the corrected author's proof should be returned as soon as possible to the editor, Yerkes Observatory, Williams Bay, Wisconsin. Authors should take notice that the manuscript will not be sent to them with the proof.

The cable address is "Observatory, Williamsbay, Wisconsin."

The articles in this Journal are indexed in the *International Index to Periodicals*, New York, N.Y.

Applications for permission to quote from the Journal should be addressed to the University of Chicago Press, and will be freely granted.

Microfilms of complete Journal volumes are available to regular subscribers only, and may be obtained at the end of the year. Orders and remittance should be addressed to University Microfilms, 313 North First Street, Ann Arbor, Michigan.

Notice to subscribers: If you change your address, please notify us and your local postmaster immediately. The Post-Office does not forward second-class mail.

Entered as second-class matter July 25, 1930, at the Post-Office at Chicago, Ill., under the Act of March 3, 1879.

Acceptance for mailing at special rate of postage provided for in Section 1103, Act of October 3, 1917, authorized February 28, 1925.

[over]

THE ASTROPHYSICAL JOURNAL

AN INTERNATIONAL REVIEW OF SPECTROSCOPY AND ASTRONOMICAL PHYSICS

VOLUME 112 JULY 1950 NUMBER 1

THE AMOUNT OF POLARIZATION BY INTERSTELLAR GRAINS

H. C. VAN DE HULST

Leiden Observatory

Received April 21, 1950

ABSTRACT

The extinction of light by long dielectric cylinders is computed for different directions of polarization. Cylinders with diameters of the order of the wave length give the correct dependence of interstellar polarization on wave length, whereas cylinders or ellipsoids small compared to the wave length do not. The computed amount of polarization is barely sufficient to explain the observations, even if the grains are strongly elongated and fully aligned.

The important discovery by Hiltner[1] and its confirmation by Hall,[2] that the light of many distant stars is polarized, has been followed by several explanations. These suggestions contain many speculative points, but, unless some quite different possibility is overlooked, we may assert these facts: (1) The phenomenon is interstellar rather than stellar, for it appears in stars of diverse types and only at large distances. (2) The phenomenon has the character of a differential extinction, light vibrating in one direction (electric vector roughly parallel to galactic plane) being less strongly attenuated in interstellar space than light vibrating in the perpendicular direction. Hall has found for one star that the transmitted light is indeed linearly, not elliptically, polarized. (3) This extinction is caused by the same solid grains that are believed to cause the ordinary interstellar extinction; for no other constituent of interstellar matter is known to be able to give even the minimum extinction needed for one polarized component if the other component is assumed to suffer no extinction at all. Hiltner[3] has shown that this holds true also for free electrons.

Admitting that interstellar grains are responsible, we may estimate the ratio of the extinction values of the two polarized components. Let these values, expressed in magnitudes, be A_1 and A_2, where $A_1 > A_2$. The magnitude difference, $A_1 - A_2$, is the polarization measured by Hiltner. The photographic extinction for unpolarized light follows from

$$\tfrac{1}{2}(A_1 + A_2) = 9E_1 ,$$

where E_1 is the color excess on Stebbins' scale. Several stars have a well-observed value of $(A_1 - A_2)/E_1$ as high as 0.50. This gives

$$\frac{A_1 - A_2}{A_1 + A_2} = 0.03 ; \qquad \text{so} \qquad \frac{A_1}{A_2} = 1.06$$

[1] *Ap. J.*, **109**, 471, 1949.

[2] J. S. Hall and A. H. Mikesell, *A.J.*, **54**, 187, 1949.

[3] *Phys. Rev.*, **78**, 170, 1950.

for blue light. Hiltner's observations[3] show that $A_1 - A_2$ is nearly independent of λ, but, since $A_1 + A_2$ decreases by a factor of 2 if the wave length increases from λ 4400 to λ 8000, the ratio A_1/A_2 increases with increasing λ, reaching the value 1.12 for strongly polarized stars in the infrared.

All previous explanations suggest that the grains are elongated and aligned by magnetic forces.[4] Apart from the physical difficulties in this suggestion, one simple question has to be answered: Do such particles give a sufficiently different extinction for different directions of polarization of the incident light? I started some calculations on this question soon after the discovery of interstellar polarization was announced; the preliminary results are reported below.

Scattering problems are simple applications of Maxwell's theory, in principle, but few of them have solutions that admit of a simple numerical evaluation. Such solutions are obtained, for instance, if the scattering particles are (*a*) homogeneous ellipsoids that are small compared to the wave length of the incident light and (*b*) long, circular cylinders with arbitrary radii, with light incident in a direction perpendicular to the cylinder axis. The formal solution for ellipsoids of arbitrary size has also been obtained,[5] but its evaluation would require very lengthy computations; *a* and *b* are special cases of this more general problem.

Problem *a* is the only one that I have seen referred to in the papers on interstellar polarization; it leads to simple formulae, first derived by Gans.[6] The authors[4] who suggest that these formulae are applicable make the implicit assumption that the grains causing interstellar polarization are small compared with the wave length. These grains would thus form a class separate from the grains causing ordinary extinction, which must have sizes of the order of the wave length in order to explain the observed reddening law. Such a superposition of two classes of interstellar grains would seem artificial, but not impossible. For instance, if the polarizing grains have the extinction values $A_1' > A_2'$ and the ordinary grains have the values $A_1'' = A_2''$, the observed ratio is

$$\frac{A_1' + A_1''}{A_2' + A_2''} = 1.06 .$$

We may estimate that the wave-length dependence of interstellar reddening is not affected if $A_1' + A_2' \leqslant \frac{1}{10}(A_1'' + A_2'')$. Combining these equations, we find that A_1'/A_2' has to be about 2, or larger. Such a large ratio requires prolate spheroids with the axial ratios 2/1 or 6/1, for refractive indices 2 or 1.4, respectively. This makes this explanation very improbable. An even stronger argument against it is found from the dependence of polarization on wave length. The difference, $A_1 - A_2 = A_1' - A_2'$, which is a constant according to observation, would have to be proportional to λ^{-4} (nonabsorbing grains), or λ^{-1} (absorbing grains), according to the theory for small particles. It thus seems fairly certain that a solution based on the formulae of Gans must be rejected.

Problem *b* leads to more complex formulae,[7] analogous in many details to Mie's formulae for scattering by spheres. For instance, if the electric vector of the incident light is parallel to the cylinder axis, which gives the strongest effects of scattering and extinction, the principal quantities to be computed are the complex coefficients

$$b_n(x, m) = \frac{mJ_n'(y)\,J_n(x) - J_n(y)\,J_n'(x)}{mJ_n'(y)\,H_n(x) - J_n(y)\,H_n'(x)} . \qquad (1)$$

[3] L. Spitzer and J. W. Tukey, *Science*, **109**, 461, 1949; L. Davis and J. L. Greenstein, *Phys. Rev.*, **75**, 1605, 1949.

[4] F. Möglich, *Ann. d. Phys.*, **83**, 609, 1927.

[5] *Ann. d. Phys.*, **37**, 881, 1912.

[6] Cl. Schaeffer and F. Grossman, *Ann. d. Phys.*, **31**, 455, 1910.

Here n is an integer, m is the refractive index, $y = mx$, and x is the ratio $2\pi r/\lambda$, where r is the radius of the cylinder and λ is the wave length. Further, $J_n(x)$ are Bessel functions, $H_n(x)$ are Hankel functions of the second kind, and primes denote derivatives. The efficiency factor for extinction, defined as the ratio between the extinction cross-section and the geometrical cross-section, is found from

$$Q_1(x, m) = \frac{2}{x}\sum_{n=-\infty}^{\infty} \Re\, b_n , \tag{2}$$

where $b_n = b_{-n}$ and the symbol $\Re$ means that the real part is taken. If the magnetic vector of the incident light is parallel to the cylinder axis, the solution is found from

$$Q_2(x, m) = \frac{2}{x}\sum_{n=-\infty}^{\infty} \Re\, a_n , \tag{3}$$

where the coefficients $a_n(x,m)$ are obtained by removing the factors m in equation (1) from the first terms of the numerator and denominator and placing them with the second terms.

The results of computations for refractive indices 1.25 and 1.50 are shown in Figure 1. The actual procedure was to write b_n and a_n in the form

$$b_n = \tfrac{1}{2}\,(1 - e^{-i\beta_n}), \qquad a_n = \tfrac{1}{2}\,(1 - e^{-i\alpha_n}),$$

and to compute the real angles β_n and α_n. The *Tables of Amplitudes and Phase Angles*,[8] a copy of which was very kindly made available to me by Dr. A. N. Lowan, were of great help in this computation. Very effective use was also made of graphs of the angles β_n and α_n, as suggested earlier for spheres.[9] The "nodes," where $\beta_n = \alpha_n$, have some very curious properties that afford checks in so many ways that errors are detected easily from these graphs and a full check is obtained at the stage of the computation where it is most needed. Additional values were found by interpolation from these graphs. The largest number of terms needed in the series for Q_1 and Q_2 was from $n = 0$ to $n = 10$ for $m = 1.25$, $x = 8.0$.

The bottom curve of Figure 1 refers to refractive indices close to 1. A derivation similar to the one made for spheres[10] leads to the formula

$$Q(x, m) = \pi \mathfrak{S}_1(\rho)$$

for both directions of polarization alike. Here $\mathfrak{S}_1$ is Struve's function tabulated by Jahnke and Emde[11] and $\rho = 2x(m - 1)$. The curves of Figure 1 have been drawn to a common scale of ρ, which equals x for $m = 1.50$ and $\frac{1}{2}x$ for $m = 1.25$. The values corresponding to the first terms of the series expansion for small ρ, or x, are indicated by dotted curves. The formulae are:

$$\text{For } m = 1.50: \quad Q_1 = 1.93x^3, \quad Q_2 = 0.364x^3, \quad \frac{Q_1}{Q_2} = 5.30;$$

$$\text{For } m = 1.25: \quad Q_1 = 0.39x^3, \quad Q_2 = 0.128x^3, \quad \frac{Q_1}{Q_2} = 3.03;$$

[8] A. N. Lowan, P. M. Morse, H. Feshbach, and M. Lax, *Scattering and Radiation from Circular Cylinders and Spheres: Tables of Amplitudes and Phase Angles* (U.S. Navy Department, 1946).

[9] H. C. van de Hulst, *Rech. Astr. Obs. Utrecht*, Vol. 11, Part I, chap. viii, 1946.

[10] *Ibid.*, chap. vii.

[11] Jahnke and Emde, *Tables of Functions* ("Dover Publications" [New York, 1945]), esp. Fig. 117.

and for any real value of m:

$$Q_1 = \frac{x^2(m^2-1)^2}{8}x^3, \qquad Q_2 = \frac{x^2(m^2-1)^2}{4(m^2+1)^2}x^3, \qquad \frac{Q_1}{Q_2} = \frac{(m^2+1)^2}{2}.$$

The further discussion follows closely the pattern set by previous discussions of interstellar reddening.[12] The argument, ρ, is proportional to λ^{-1}; the ordinates, Q_1 and Q_2, are

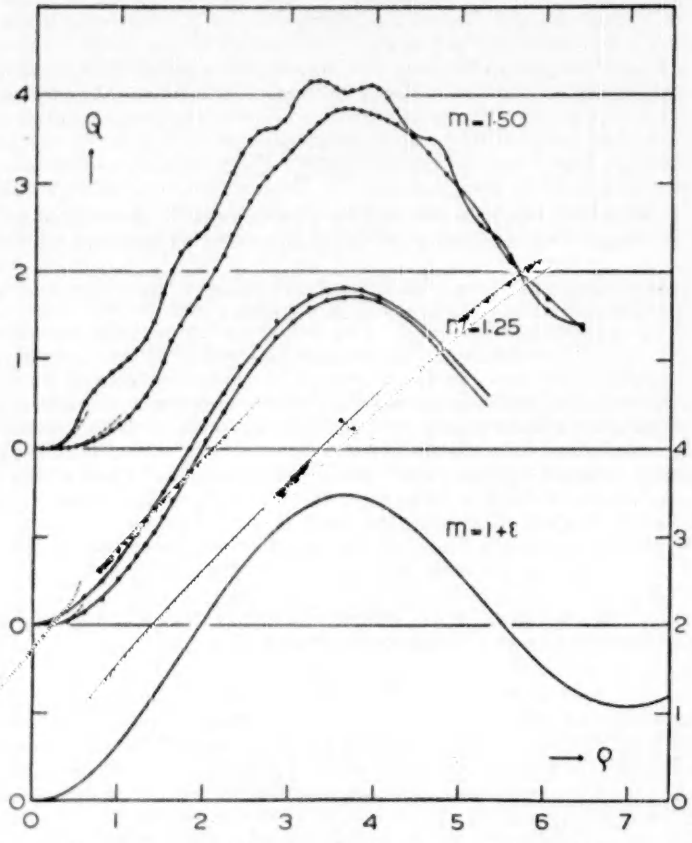

FIG. 1.—Extinction by long, circular cylinders for different values of the refractive index m, as a function of their size with respect to the wave length (perpendicular incidence). Q is the efficiency factor; the upper curve of each set refers to linear polarization with the electric vector parallel to the cylinder axis (Q_1), the lower curve to electric vector perpendicular to the cylinder axis (Q_2). The scale of abscissae: $\rho = 2x(m-1)$, where $x = 2\pi r/\lambda$, is common to all curves.

proportional to the extinction values, A_1 and A_2, at a given wave length. The observed reddening law is well represented by cylinders of a single size if λ^{-1} is about equal to ρ, the wave length being expressed in microns. So blue light, $\lambda = 0.41\mu$, corresponds to $\rho = 2.44$; yellow light, $\lambda = 0.55\ \mu$, to $\rho = 1.82$; and the near infrared, $\lambda = 0.80\ \mu$, to

[12] H. C. van de Hulst, *op. cit.*, Part II, chap. iii, 1949.

$\rho = 1.25$. All these values lie outside the region where the theory for thin rods holds, so that the ratio $A_1/A_2 = Q_1/Q_2$ is notably smaller than the values 5.3 and 3.0 mentioned above. In fact, we read from the curves that $Q_1/Q_2 = 1.22$ for $m = 1.50$ and $Q_1/Q_2 = 1.07$ for $m = 1.25$ in the region corresponding to blue light. Since the strongest observed value is $A_1/A_2 = 1.06$ for blue light, we may infer that ice needles ($m = 1.25$) can just explain the observed amount of polarization if they are very long and perfectly aligned. No margin at all is left for the effects of imperfect alignment and of reduced length, both of which tend to reduce the expected polarization. For $m = 1.50$, which is already an improbably high value, the margin is still small. Rough estimates, that cannot be explained in the present context, show that the amount of polarization, $Q_1 - Q_2$, is reduced by a factor of 2 if long cylinders are replaced by prolate spheroids with the axial ratio 2 to 1. It is reduced by a factor of 4 if the spheroids have the axial ratio 1.3 to 1. So glass spheroids ($m = 1.50$) with the axial ratio 1.5 to 1, all perfectly aligned, would also be capable of explaining the observed ratio $A_1/A_2 = 1.06$ for blue light.

The dependence of $Q_1 - Q_2$ on ρ is very interesting. Apart from the irregular bumps, that will be smoothed out if particles of various sizes are mixed, we see that $Q_1 - Q_2$ is almost independent of ρ in the entire range of interest. So, while Q_1 and Q_2 increase rapidly with increasing ρ, their difference is virtually constant, so that the ratio Q_1/Q_2 decreases. If Q_1 and Q_2 are replaced by A_1 and A_2, and ρ by λ^{-1}, this is exactly what Hiltner's recent observations show. The sign is such that the long axes of the grains have to be perpendicular to the galactic plane. It would seem premature to make any more detailed computations at this stage.

The conclusion is that interstellar grains of the ordinary size, as indicated by reddening measurements, may give a barely sufficient amount of polarization, which, however, has the correct dependence on wave length. We hope that partly absorbing grains will leave a better margin by giving a stronger polarization effect. Computations on such particles are in preparation.

PULSATION PROPERTIES OF GIANT-STAR MODELS

I. EPSTEIN
Princeton University Observatory
Received April 15, 1950

ABSTRACT

The pulsation equation is solved numerically for the fundamental and first-overtone modes for three giant-star models having very high central concentrations. The period–mean-density relationships derived from these integrations are practically identical with one another and are very similar to those derived in earlier investigations.

It is found that the properties of the fundamental mode are determined largely by the physical conditions prevailing in the layers of the star around $r = (0.7)R$. The properties of the first overtone are determined primarily by the conditions obtaining at $(0.8)R$ and, to a lesser degree, by those around $(0.5)R$. The pulsation periods were found to be little influenced by the conditions in the central regions of the star.

Agreement between theory and observations with regard to the period-density relationship may be attained by (1) reducing the cepheid masses, deduced from the empirical mass-luminosity relation, by a factor of about 4 or by (2) reducing the effective temperatures, estimated for the cepheids from their colors, by about 13 per cent, or by (3) lengthening the theoretical periods by supposing that the hydrogen convection layer may have a depth of about one-fifth the stellar radius.

I. INTRODUCTION

In recent investigations on the internal constitution of giant stars the attempt has been made to construct models which give radii large enough to apply to the largest of the red giant stars, while at the same time yielding a central temperature high enough for the carbon cycle to operate as the energy-producing mechanism. The results of these investigations indicate that giant stars may be represented by models having an extremely high central concentration.

The pulsation integrations on pure polytropes show a decrease in pulsation period with increasing central concentration.[1] From this one might suspect that the recent giant models might give very short periods, which would still further increase the discrepancy between theory and observation. To ascertain whether or not this suspicion is justified, one can perform the pulsation integrations and compare the results with the observed periods of cepheids.

The present investigation consists in an analysis of the pulsation properties of three of the above-mentioned models. Two are of the noise-zone type. One of these is case 4 of the six noise-zone models investigated by R. S. Richardson and M. Schwarzschild,[2] the other (case 7) has been computed in the present investigation and is described in Section II. Despite the fact that the main physical assumption underlying this type of model has been shown to be untenable,[3] these models nevertheless represent examples of density distributions of high central concentration. The third model considered here is case 15 of the models with chemical inhomogeneities published by Li Hen and M. Schwarzschild.[4] The results of the pulsation integrations are given in Section III.

In addition to the pulsation integrations of the three particular models, investigation was undertaken to discover which specific characteristics of the stellar interior determine the pulsation properties in general. This investigation is described in Section IV. Pos-

[1] For a description of the early developments in the theory of pulsating stars see S. Rosseland, *The Pulsation Theory of Variable Stars* (Oxford: Clarendon Press, 1949), esp. chaps. i and iii.

[2] *Ap. J.*, **108**, 373, 1948.

[3] See, e.g., T. Gold, *M.N.*, **109**, 115, 1949.

[4] *M.N.*, **109**, 631, 1949.

sible explanations of the remaining discrepancies between theory and observations are discussed in Section V.

II. THE STATIONARY MODEL, CASE 7

In order to extend the noise-zone-type model over a larger range of the characteristic quantity C, defined by

$$C = \frac{3\kappa_0}{4ac}\left(\frac{k}{\mu HG}\right)^{7.5}\left(\frac{1}{4\pi}\right)^{2.75}\frac{LR^{1.25}}{M^{5.75}}, \tag{1}$$

an additional noise-zone model, case 7, was constructed. For this model was chosen a log C of -5.2, an isothermal zone characterized by $\xi_1 = 2.7$, and a convective core of polytropic index $\frac{3}{2}$. Case 7 was constructed by the same methods as those used in the construction of the earlier six noise-zone cases.[5]

The radiative-envelope solution was integrated for case 7 ($\log C = -5.2$) and is given in Table 1. The extension of the isothermal-zone integration for $\xi_1 = 2.7$, necessary for case 7, is given in Table 2. The nondimensional characteristics of the complete model are listed in Table 3. Tables 1, 2, and 3 are identical in form to the corresponding tables in the paper by Richardson and Schwarzschild.[6]

Table 4 gives a summary of the physical quantities of the three models considered in this investigation, the models having been fitted to a star of fixed mass, composition, and central temperature. The mass is taken to be 1.35×10^{34} gm in each of the three cases. This mass corresponds to the mass of η Aquilae as given by the empirical mass-luminosity relation. The central temperature taken is 30,000,000°, so that the carbon cycle may be regarded as the energy-producing mechanism. The composition taken is $X = 0.50$ (hydrogen), $Y = 0.40$ (helium), and $Z = 0.10$ (all other elements) for cases 4 and 7. In case 15 the envelope composition is taken as $X = 0.90$, $Y = 0.00$, $Z = 0.10$, while in the intermediate zone and convective core the composition taken is $X = 0.00$, $Y = 0.90$, and $Z = 0.10$.

III. THE PULSATION INTEGRATIONS FOR CASES 4, 7, AND 15

To determine the pulsation periods of the models here considered, well-behaved solutions must be sought for the equation

$$\frac{d^2y}{d\tau^2} + \frac{dy}{d\tau}\left(\frac{4}{\tau} - \frac{GM_r\rho}{r^2P}\right) + y\left[\frac{4-3\gamma}{\gamma}\frac{GM_r\rho}{r^3P} + \frac{\rho}{\gamma P}\left(\frac{2\pi}{\tau}\right)^2\right] = 0, \tag{2}$$

which occurs as a result of the usual assumptions concerning the nature of the pulsations.[7] This equation may be rewritten in terms of nondimensional variables defined by

$$P = p\frac{GM^2}{4\pi R^4}; \qquad T = t\mu_e\frac{HGM}{kR}; \qquad M_r = qM; \qquad r = xR, \tag{3}$$

where μ_e denotes the molecular weight in the envelope. With these variables, the pulsation equation takes the following form:

$$\frac{d^2y}{dx^2} + \frac{dy}{dx}\left(\frac{4}{x} - \frac{lq}{tx^2}\right) + y\left(\frac{4-3\gamma}{\gamma}\frac{lq}{tx^3} + \frac{l\omega^2}{t}\right) = 0. \tag{4}$$

[5] For the properties of the six noise-zone models previously investigated and for the definitions of the symbols used in this section see Richardson and Schwarzschild, *op. cit.*

[6] *Ibid.*

[7] A. S. Eddington, *The Internal Constitution of the Stars* (Cambridge: At the University Press, 1930), chap. viii.

TABLE I

INTEGRATION FOR RADIATIVE ENVELOPE, CASE 7

$\text{Log}(\frac{1}{x}-1)$	-Log q	$\frac{-d\,\text{Log}\,q}{d\,\text{Log}(\frac{1}{x}-1)}$	Log t	$\frac{d\,\text{Log}\,t}{d\,\text{Log}(\frac{1}{x}-1)}$	Log p	$\frac{d\,\text{Log}\,p}{d\,\text{Log}(\frac{1}{x}-1)}$	U	V
			LOG C = -5.2					
-1.00	0.00000	0.0000	-1.67342	1.0000	-5.30234	4.7143	0.0002	51.857
-0.95	.00000	.0000	-1.62342	1.0000	-5.06663	4.7143	.0003	46.730
-.90	.00000	.0000	-1.57342	1.0000	-4.83092	4.7142	.0004	42.161
-.85	.00001	.0001	-1.52342	1.0000	-4.59520	4.7142	.0006	38.088
-.80	.00001	.0001	-1.47342	1.0000	-4.35949	4.7142	.0008	34.459
-.75	.00002	.0002	-1.42342	1.0000	-4.12379	4.7141	.0012	31.223
-.70	.00003	.0003	-1.37342	1.0000	-3.88808	4.7140	.0018	28.340
-.65	.00005	.0005	-1.32342	0.9999	-3.65239	4.7138	.0026	25.770
-.60	.00008	.0007	-1.27343	.9999	-3.41670	4.7135	.0037	23.478
-.55	.00013	.0012	-1.22343	.9998	-3.18104	4.7131	.0052	21.436
-.50	.00020	.0018	-1.17344	.9998	-2.94540	4.7124	.0074	19.614
-.45	.00031	.0027	-1.12346	.9996	-2.70980	4.7114	.0104	17.990
-.40	.00048	.0041	-1.07348	.9994	-2.47427	4.7098	.0146	16.540
-.35	.00073	.0062	-1.02352	.9991	-2.23883	4.7074	.0202	15.246
-.30	.00112	.0092	-0.97358	.9986	-2.00354	4.7039	.0277	14.090
-.25	.00168	.0135	-.92366	.9979	-1.76847	4.6988	.0376	13.055
-.20	.00250	.0196	-.87379	.9968	-1.53370	4.6913	.0507	12.127
-.15	.00368	.0281	-.82399	.9953	-1.29939	4.6807	.0677	11.292
-.10	.00536	.0397	-.77427	.9932	-1.06571	4.6657	.0896	10.539
-.05	.00771	.0553	-.72468	.9902	-0.83292	4.6448	.1173	9.8564
.00	.01097	.0760	-.67527	.9861	-.60135	4.6164	.1520	9.2327
+.05	.01542	.1031	-.62610	.9804	-.37144	4.5781	.1949	8.6583
+.10	.02141	.1378	-.57726	.9729	-.14375	4.5274	.2473	8.1237
+.15	.02935	.1817	-.52885	.9631	+.08105	4.4616	.3103	7.6202
+.20	.03975	.2361	-.48100	.9504	+.30211	4.3777	.3851	7.1398
+.25	.05316	.3023	-.43386	.9344	+.51847	4.2727	.4722	6.6754
+.30	.07019	.3811	-.38762	.9146	+.72899	4.1441	.5721	6.2211
+.35	.09149	.4731	-.34247	.8906	+.93245	3.9901	.6844	5.7724
+.40	.11771	.5778	-.29864	.8622	+1.12756	3.8100	.8078	5.3268
+.45	.14946	.6939	-.25633	.8295	+1.31303	3.6047	.9401	4.8837
+.50	.18725	.8191	-.21575	.7927	+1.48766	3.3768	1.0781	4.4446
+.55	.23146	.9498	-.17711	.7525	+1.65041	3.1308	1.2175	4.0131
+.60	.28225	1.0815	-.14055	.7096	+1.80053	2.8728	1.3532	3.5944
+.65	.33954	1.2089	-.10618	.6652	+1.93760	2.6100	1.4795	3.1943
+.70	.40297	1.3260	-.07404	.6203	+2.06158	2.3500	1.5906	2.8189
+.75	.47187	1.4271	-.04413	.5762	+2.17278	2.1002	1.6809	2.4737
+.80	.54532	1.5066	-.01639	.5338	+2.27187	1.8667	1.7454	2.1625
+.85	.62210	1.5598	+.00929	.4940	+2.35980	1.6543	1.7801	1.8880
+.90	.70080	1.5829	+.03306	.4573	+2.43770	1.4660	1.7822	1.6506
+0.95	.77984	1.5735	+.05508	.4241	+2.50683	1.3034	1.7500	1.4496
+1.00	.85759	1.5309	+.07553	.3946	+2.56847	1.1665	1.6840	1.2831
+1.05	0.93241	1.4568	+.09460	.3688	+2.62389	1.0544	1.5866	1.1483
+1.10	1.00280	1.3547	+.11247	.3465	+2.67429	0.9655	1.4623	1.0421
+1.15	1.06751	1.2308	+.12930	.3276	+2.72079	.8978	1.3179	0.9614
+1.20	1.12564	1.0926	+.14528	.3118	+2.76439	.8493	1.1616	.9029
+1.25	1.17668	0.9487	+.16053	.2989	+2.80601	.8181	1.0020	.8641
+1.30	1.22055	.8069	+.17522	.2888	+2.84645	.8021	0.8474	.8423
+1.35	1.25752	.6739	+.18945	.2811	+2.88645	.7999	.7040	.8356
+1.40	1.28816	.5541	+.20336	.2758	+2.92665	.8100	.5762	.8422
+1.45	1.31319	.4500	+.21706	.2726	+2.96764	.8313	.4660	.8608
+1.50	1.33343	.3619	+.23066	.2715	+3.00995	.8628	.3734	.8901
+1.55	1.34964	.2892	+.24425	.2725	+3.05408	.9039	.2975	.9293
+1.60	1.36257	.2302	+.25784	.2754	+3.10048	0.9539	.2359	0.9778
+1.65	1.37285	.1829	+.27182	.2802	+3.14960	1.0123	.1870	1.0350
+1.70	1.38102	.1454	+.28599	.2870	+3.20185	1.0789	.1483	1.1004
+1.75	1.38753	.1159	+.30055	.2956	+3.25762	1.1533	.1179	1.1738
+1.80	1.39272	.0927	+.31559	.3063	+3.31730	1.2351	.0942	1.2547
+1.85	1.39688	.0746	+.33121	.3188	+3.38125	1.3241	.0756	1.3428
+1.90	1.40024	.0604	+.34750	.3333	+3.44982	1.4199	.0611	1.4378
+1.95	1.40297	.0492	+.36457	.3496	+3.52335	1.5222	.0498	1.5393
+2.00	1.40520	.0405	+.38250	.3678	+3.60214	1.6304	.0409	1.6467
+2.05	1.40705	.0336	+.40138	.3878	+3.68648	1.7441	.0339	1.7596
+2.10	1.40859	.0282	+.42130	.4093	+3.77663	1.8625	.0284	1.8773
+2.15	1.40989	.0239	+.44234	.4323	+3.87281	1.9851	.0241	1.9991
+2.20	1.41099	.0205	+.46455	.4565	+3.97519	2.1108	.0206	2.1241
+2.25	1.41195	0.0177	+0.48801	0.4817	+4.08393	2.2390	0.0178	2.2516

All symbols used are identical with those of Richardson and Schwarzschild.

The dependent variable y is the relative amplitude (displacement divided by mean distance from center). The variable l denotes the ratio of the molecular weight at the point x to μ_c. Correspondingly, l equals 1 throughout the two noise-zone models, as well as in the envelope of case 15, while l equals 2.547 in the core and intermediate zone of case 15. The eigen-parameter, ω^2, is defined by

$$\omega^2 = \frac{4\pi^2 R^3}{\tau^2 \gamma G M}, \tag{5}$$

TABLE 2*

INTEGRATIONS FOR ISOTHERMAL ZONE, $\xi_1 = 2.7$

x	ψ	$-d\psi/dx$	U	V
0.070	7.9643	32.29	0.031	2.260
.065	8.1259	32.37	.033	2.104
.060	8.2880	32.46	.036	1.948
.055	8.4506	32.56	.039	1.791
.050	8.6137	32.70	.044	1.635
.045	8.7776	32.86	.051	1.479
.040	8.9424	33.08	.062	1.323
.035	9.1085	33.38	.077	1.168
.030	9.2764	33.84	.102	1.015
.025	9.4474	34.60	.146	0.865
.020	9.6235	36.03	.230	0.721
.015	9.8106	39.36	.413	0.590
0.010	10.0279	51.44	0.858	0.514

* Continuation of Table 2, by Richardson and Schwarzschild, *Ap. J.*, **108**, 381, 1948.

TABLE 3

MATHEMATICAL QUANTITIES CHARACTERIZING CASE 7
($\log C = -5.2$)

ξ_1	2.7	z_2	1.964
θ_1	0.24966	$100\, x_2$	1.075
x_1	0.33138	$-\log q_2$	1.4036
ψ_1	0.0	$\log l_2$	0.3694
$(-d\psi/dx)_1$	26.142	$\log p_2$	3.5445
U_2	0.0471	$100\, x_1$	0.1553
V_2	1.568	$\log p_1$	7.3154
x_2	0.04787	$-\log q_1$	1.5016
ψ_2	8.683	$\log l_c$	0.9721
$(-d\psi/dx)_2$	32.76	$\log p_c$	8.8220

where τ is the period in seconds. In the pulsation equation all variables except y refer to their equilibrium values. The value of γ used in all the present integrations was $\frac{5}{3}$. The effect upon the period of using an improved value of γ, as well as the effects of including other refinements in the models, are discussed in Section IV.

The general method of solution was to choose a trial value of ω^2 and, with it, to carry through two integrations, one originating at the stellar center, the other at the surface. The proximity of the trial value of ω^2 to its eigen-value was estimated by comparing the logarithmic first derivatives of the two integrations at an interior fitting point near $x = \frac{1}{2}$. Improved trial values of ω^2 were then assumed, and the integrations and fittings were repeated. That value of ω^2 which led to equality between inside-out and outside-in

TABLE 4

PHYSICAL CHARACTERISTICS OF MODELS WITH HIGH CENTRAL CONCENTRATIONS, APPLIED TO STARS WITH MASS OF 1.35×10^{34} GRAMS AND CENTRAL TEMPERATURE OF 30 MILLION DEGREES.

	Case 4	Case 7	Case 15 interior	Case 15 envelope
X	0.50	0.50	0.00	0.90
Y	0.40	0.40	0.90	0.00
Z	0.10	0.10	0.10	0.10
μ	0.74	0.74	1.38	0.54
R/RO	40.053	36.370	44.906	
r_1/RO	0.169	0.056	0.254	
r_2/RO	0.701	0.391	0.689	
M_{r_1} / MO	0.554	0.214	0.205	
M_{r_2} / MO	1.428	0.268	1.363	
log $\bar{\rho}$	−3.826	−3.700	−3.975	
log ρ_c	2.457	3.673	1.344	
log ρ_1	2.001	2.769	1.206	
log ρ_2	−0.129	−1.002	0.230	−0.176
$T_1 \times 10^{-6}$	14.88	7.49	24.28	
$T_2 \times 10^{-6}$	14.88	7.49	10.40	
log L/LO	4.32	3.17	3.15	
log κ_2	−1.07	−0.68	−0.39	−0.48
log κ_1	+0.53	+2.15	−0.94	

In Tables 3 and 4, the subscript c denotes the center of the star. The subscript 1 denotes the inner interface between the convective core and the intermediate zone. The subscript 2 denotes the outer interface between the intermediate zone and the radiative envelope. All symbols have the definitions as used in Richardson and Schwarzschild, op. cit.

logarithmic derivatives is the eigen-value corresponding to the mode of pulsation considered. Since the corresponding solution, $y(x)$, is arbitrary to the extent of a multiplicative constant factor, the eigen-amplitudes were normalized to unity at the surface.

The actual integrations were performed with the aid of the auxiliary variables v (for the outside-in integrations) and w (for the inside-out integrations), defined by

$$v = y x^2 p^{1/2}; \qquad w = \left(\frac{y}{y_c}\right) \xi^2 \left(\frac{p}{p_c}\right)^{1/2}. \tag{6}$$

The two differential equations to be solved numerically are

$$\frac{d^2 v}{dx^2} + I(x)\, v = 0; \qquad \frac{d^2 w}{d\xi^2} + I(\xi)\, K^2 w = 0, \tag{7}$$

where $I(x)$ and K are defined by the following two equations:

$$I(x) = -\frac{3}{5}\frac{lq}{tx^3} + \frac{l\omega^2}{t} - \frac{1}{2}\frac{d}{dx}\left(\frac{4}{x} - \frac{lq}{tx^2}\right) - \frac{1}{4}\left(\frac{4}{x} - \frac{lq}{tx^2}\right)^2, \tag{8}$$

$$K = \frac{x}{\xi} = t_c p_c^{-1/2} (2.5)^{1/2} l^{-1}. \tag{9}$$

The letter ξ denotes the independent Emden variable; and $I(x)$ may be pre-computed as a function of x (or of ξ) for each model under consideration.

Since singularities occur in the coefficients of the pulsation equation both at the center and at the surface, it was necessary to develop y at the beginning of both the outside-in and the inside-out integrations. The development for y used at the surface was in the form of a power series in $(1 - x)/x$, where the coefficients of this series depend on the value ω^2 chosen for the particular integration to be performed. Values of v were computed from the development for y at the points $x = 0.994$ and $x = 0.993$, separately for each ω^2 and for each model. With these starting values for v, the outside-in numerical integrations were begun. Five or more significant figures were carried in the integrations, each of which consisted of approximately fifty steps. The step-values used were adjusted to the magnitude of $I(x)$ and ranged from $\Delta x = 0.001$ near the surface to $\Delta x = 0.020$ at the end of these outside-in integrations, near $x = \frac{1}{2}$.

The development for y at the center is given by

$$\frac{y}{y_c} = 1 + (0.0500000)\,\xi^2 + (0.0041667)\,\xi^4 + (0.0003549)\,\xi^6 + (0.0000296)\,\xi^8 + \ldots \tag{10}$$

and is valid with no sensible dependence on ω^2 for the lower modes of oscillation, for all stars having convective cores of polytropic index $\frac{3}{2}$. The inside-out integrations were begun at $\xi = 0.5$, values of w at that point and at $\xi = 0.4$ being available from the development at the center. Seven significant figures were carried in the integrations. The step-value used in the numerical integration was $\Delta\xi = 0.1$ in the convective core and no greater than $\Delta\xi = 0.2$ in the intermediate zone. In all cases the inside-out integrations were continued into the radiative zone, the independent variable being changed from ξ to x at the interface, until a point convenient for fitting the inside-out integrations to the corresponding outside-in integrations was reached. The step-value in the radiative zone ranged from $\Delta x = 0.001$ at the beginning to $\Delta x = 0.020$ at the termination of the inside-out integrations. Each complete integration of this type involved between 55 and 165 steps.

The inside-out integrations were carried across the two interfaces under the condition

of continuity of y and its first derivative. As a consequence of this condition, w and its first derivative were also continuous, except at the outer interface of case 15, where dw/dx has a discontinuity due to the discontinuity in the composition at that point in the star.

In each of the cases considered, the fundamental and first overtone eigen-solutions were computed by means of integrations performed with a series of trial values of ω^2. The eigen-parameters ω_0^2 and ω_1^2 (the zero subscript denoting the fundamental mode and the unit subscript the first overtone), were fixed when equality between $(1/w)\ (dw/dx)$ and $(1/v)\ (dv/dx)$ was obtained at some convenient fitting point near $x = \frac{1}{2}$.

Finally, the eigen-solutions $y(x)$ were computed from w and v by the use of equations (6). The value of y_c occurring in the second of these equations is fixed by the ratio v/w found at the fitting point.

The complete tabulation of $y(x)$, the relative amplitude, for the fundamental and first overtone modes for cases 4, 7, and 15, along with their first derivatives, may be found in Tables 5, 6, and 7, respectively. These tables show that the relative pulsation amplitudes at the center of these highly concentrated models reach exceedingly small values relative to their surface values.

Tables 5, 6, and 7 also list the nondimensional pressures (p), masses (q), and temperatures (t) as functions of x. The equilibrium values of the corresponding physical quantities may be obtained for any specific star from p, q, and t by applying equations (3).

Table 8 gives the results for ω^2 for cases 4, 7, and 15, along with a tabulation of Q, defined by

$$Q^2 = (\text{Period in days})^2 \frac{\bar{\rho}}{\bar{\rho}_\odot} = \frac{0.008049}{\omega^2}. \tag{11}$$

Also listed are the corresponding values of Q arrived at by earlier integrations on other models.[8] One feature apparent in this table is the similarity in all the Q values, even though the density distribution and log C values in the different cases tabulated show considerable variation. The central densities of the models listed vary radically (by as much as a factor of 10^5 between case 7 and the Russell-mixture model); yet the period–mean-density relationships for these cases differ by, at most, 10 per cent.

IV. THE VARIATIONAL FORMULATION OF THE PULSATION PROBLEM

The formulation of the pulsation problem by the variational method was used to investigate further the implications of the similarity of the Q values listed in Table 8. The expression for the period in this method is given by

$$\left(\frac{2\pi}{\tau}\right)^2 = \frac{\gamma \int_0^R (dy/dr)^2 P r^4 dr + (3\gamma - 4) \int_0^R y^2 GM_r \rho r dr}{\int_0^R y^2 r^4 \rho dr}, \tag{12}$$

where all the symbols have their conventional meaning and where y and dy/dr are the relative amplitude and its first derivative for the individual mode considered.[9] Equation (12) may be rewritten in terms of the nondimensional variables defined by equations (3),

[8] Russell-mixture model: G. Keller, *On the Physical and Chemical Composition of the Sun* (Ph.D. Diss.; Columbia University, 1948); oxygen model: *ibid.*; standard model: M. Schwarzschild, *Ap. J.*, **94**, 245, 1941.

[9] P. Ledoux and C. L. Pekeris, *Ap. J.*, **94**, 124, 1941.

TABLE 5

PULSATION TABLE, CASE 4

x	p	q	t	y_0	$\frac{dy_0}{dx}$	$f_0 \times 10^4$	y_1	$\frac{dy_1}{dx}$	$f_1 \times 10^4$
0.000	5.948 +7	0.000	1.033 +1	1.633 -6	0.000	0.000	-9.559 -7	0.000	0.0000
.001	5.419 +7	1.857 -3	9.950 0	1.652 -6	3.78 -5		-9.668 -7	-2.21 -5	
.002	4.089 +7	1.345 -2	8.889 0	1.713 -6	8.73 -5		-1.003 -6	-5.11 -5	
.003	2.533 +7	3.855 -2	7.339 0	1.831 -6	1.63 -4		-1.072 -6	-9.51 -5	
.004	1.257 +7	7.303 -2	5.549 0	2.054 -6	3.11 -4		-1.202 -6	-1.82 -4	
.005	5.636 +6	1.051 -1	5.122 0	2.490 -6	5.46 -4		-1.458 -6	-3.20 -4	
.006	2.575 +6	1.265 -1	5.122 0	3.147 -6	7.71 -4		-1.842 -6	-4.51 -4	
.007	1.347 +6	1.415 -1	5.122 0	4.036 -6	9.93 -4		-2.363 -6	-5.81 -4	
.008	8.056 +5	1.529 -1	5.122 0	5.122 -6	1.16 -3		-2.998 -6	-6.82 -4	
.009	5.248 +5	1.620 -1	5.122 0	6.346 -6	1.28 -3		-3.715 -6	-7.49 -4	
.010	3.663 +5	1.697 -1	5.122 0	7.669 -6	1.34 -3		-4.489 -6	-7.83 -4	
.020	5.579 +4	2.217 -1	4.753 0	2.116 -5	1.26 -3		-1.239 -5	-7.39 -4	
.030	2.155 +4	2.709 -1	3.782 0	3.238 -5	1.068 -3		-1.895 -5	-6.249 -4	
.040	1.063 +4	3.235 -1	3.185 0	4.291 -5	1.053 -3		-2.512 -5	-6.157 -4	
.050	5.915 +3	3.771 -1	2.763 0	5.364 -5	1.100 -3	0.001	-3.139 -5	-6.429 -4	0.0004
.060	3.531 +3	4.300 -1	2.440 0	6.505 -5	1.187 -3		-3.805 -5	-6.936 -4	
.070	2.210 +3	4.810 -1	2.182 0	7.750 -5	1.308 -3		-4.532 -5	-7.632 -4	
.080	1.432 +3	5.290 -1	1.970 0	9.131 -5	1.459 -3		-5.337 -5	-8.502 -4	
.090	9.528 +2	5.739 -1	1.791 0	1.068 -4	1.640 -3		-6.238 -5	-9.543 -4	
.100	6.482 +2	6.152 -1	1.639 0	1.242 -4	1.851 -3	0.004	-7.252 -5	-1.075 -3	0.0015
.150	1.197 +2	7.721 -1	1.119 0	2.528 -4	3.460 -3	0.012	-1.468 -4	-1.986 -3	0.0040
.200	2.892 +1	8.655 -1	8.181 -1	4.912 -4	6.345 -3	0.027	-2.824 -4	-3.573 -3	0.0088
.250	8.313 0	9.204 -1	6.242 -1	9.204 -4	1.125 -2	0.057	-5.207 -4	-6.155 -3	0.0173
.300	2.693 0	9.528 -1	4.898 -1	1.668 -3	1.932 -2	0.108	-9.215 -4	-1.014 -2	0.0304
.350	9.475 -1	9.722 -1	3.917 -1	2.933 -3	3.228 -2	0.191	-1.566 -3	-1.597 -2	0.0484
.400	3.523 -1	9.837 -1	3.172 -1	5.019 -3	5.274 -2	0.317	-2.556 -3	-2.399 -2	0.0691
.450	1.355 -1	9.907 -1	2.588 -1	8.394 -3	8.457 -2	0.496	-4.003 -3	-3.415 -2	0.0872
.500	5.290 -2	9.948 -1	2.119 -1	1.376 -2	1.335 -1	0.730	-5.993 -3	-4.528 -2	0.0945
.550	2.060 -2	9.972 -1	1.735 -1	2.217 -2	2.080 -1	1.008	-8.499 -3	-5.383 -2	0.0829
.600	7.859 -3	9.986 -1	1.414 -1	3.519 -2	3.205 -1	1.294	-1.121 -2	-5.123 -2	0.0519
.650	2.874 -3	9.993 -1	1.142 -1	5.515 -2	4.894 -1	1.527	-1.317 -2	-1.922 -2	0.0189
.700	9.802 -4	9.997 -1	9.090 -2	8.548 -2	7.408 -1	1.623	-1.210 -2	+7.872 -2	0.0212
.750	2.998 -4	9.999 -1	7.071 -2	1.312 -1	1.114 0	1.505	-3.133 -3	+3.129 -1	0.0931
.800	7.726 -5	1.000 0	5.303 -2	1.998 -1	1.663 0	1.154	+2.346 -2	+8.136 -1	0.2133
.850	1.496 -5	1.000 0	3.743 -2	3.018 -1	2.471 0	0.662	+8.633 -2	+1.819 0	0.2735
.900	1.689 -6	1.000 0	2.357 -2	4.528 -1	3.644 0	0.226	+2.202 -1	+3.749 0	0.1745
0.950	4.987 -8	1.000 0	1.116 -2	6.748 -1	5.345 0	0.023	+4.879 -1	+7.330 0	0.0279
1.000	0.000	1.000 0	0.000	1.000 0	7.849 0	0.000	+1.000 0	+1.384 +1	0.0000

The smaller numbers to the right are the powers of 10 by which the corresponding entries must be multiplied. The two interfaces for this Case are at X = 0.00423 and , at X = 0.0175 .

TABLE 6

PULSATION TABLE, CASE 7

x	p	q	t	y_0	$\frac{dy_0}{dx}$	$f_0 \times 10^4$	y_1	$\frac{dy_1}{dx}$	$f_1 \times 10^4$
0.000	6.637 +4	0.000	9.378 0	1.555 -4	0.000	0.000	-1.051 -4	0.000	0.000
.001	1.806 +4	1.517 -2	5.569 0	1.867 -4	8.40 -4		-1.262 -4	-5.68 -4	
.002	2.574 +4	3.599 -2	2.341 0	7.983 -4	2.22 -2		-5.396 -4	-1.50 -2	
.003	1.709 +5	3.771 -2	2.341 0	5.442 -3	7.41 -2		-3.679 -3	-5.01 -2	
.004	4.642 +4	3.820 -2	2.341 0	1.514 -4	1.14 -1		-1.023 -4	-7.71 -2	
.005	2.060 +4	3.845 -2	2.341 0	2.744 -4	1.28 -1		-1.855 -4	-8.64 -2	
.006	1.191 +4	3.863 -2	2.341 0	4.017 -4	1.25 -1		-2.715 -4	-8.44 -2	
.007	8.035 +3	3.882 -2	2.341 0	5.219 -4	1.15 -1		-3.528 -4	-7.79 -2	
.008	5.970 +3	3.898 -2	2.341 0	6.311 -4	1.03 -1		-4.266 -4	-6.95 -2	
.009	4.745 +3	3.912 -2	2.341 0	7.272 -4	8.99 -2		-4.915 -4	-6.09 -2	
.010	3.937 +3	3.931 -2	2.341 0	8.126 -4	7.80 -2		-5.493 -4	-5.29 -2	
.020	1.554 +3	4.174 -2	1.920 0	1.294 -3	3.21 -2		-8.746 -4	-2.17 -2	
.030	1.043 +3	4.606 -2	1.711 0	1.511 -3	1.588 -2		-1.021 -3	-1.071 -2	
.040	8.141 +2	5.293 -2	1.577 0	1.643 -3	1.084 -2		-1.110 -3	-7.294 -3	
.050	6.751 +2	6.269 -2	1.476 0	1.738 -3	8.321 -3	0.029	-1.174 -3	-5.578 -3	0.013
.060	5.756 +2	7.593 -2	1.392 0	1.813 -3	6.963 -3		-1.224 -3	-4.645 -3	
.070	4.971 +2	9.253 -2	1.319 0	1.879 -3	6.257 -3		-1.268 -3	-4.150 -3	
.080	4.316 +2	1.128 -1	1.255 0	1.940 -3	5.917 -3		-1.308 -3	-3.899 -3	
.090	3.750 +2	1.365 -1	1.195 0	1.998 -3	5.795 -3		-1.346 -3	-3.793 -3	
.100	3.253 +2	1.636 -1	1.140 0	2.056 -3	4.708 -3	0.126	-1.384 -3	-3.030 -3	0.057
.150	1.512 +2	3.338 -1	9.078 -1	2.382 -3	7.538 -3	0.327	-1.592 -3	-4.720 -3	0.144
.200	6.403 +1	5.189 -1	7.263 -1	2.845 -3	1.126 -2	0.574	-1.876 -3	-6.755 -3	0.240
.250	2.566 +1	6.774 -1	5.831 -1	3.549 -3	1.741 -2	0.867	-2.287 -3	-9.884 -3	0.332
.300	1.008 +1	7.938 -1	4.716 -1	4.644 -3	2.711 -2	1.259	-2.886 -3	-1.432 -2	0.422
.350	3.968 0	8.728 -1	3.836 -1	6.348 -3	4.214 -2	1.821	-3.745 -3	-2.026 -2	0.510
.400	1.574 0	9.237 -1	3.135 -1	8.988 -3	6.507 -2	2.605	-4.935 -3	-2.752 -2	0.576
.450	6.280 -1	9.557 -1	2.572 -1	1.305 -2	9.979 -2	3.637	-6.510 -3	-3.535 -2	0.589
.500	2.504 -1	9.751 -1	2.112 -1	1.926 -2	1.524 -1	4.921	-8.454 -3	-4.184 -2	0.522
.550	9.865 -2	9.865 -1	1.733 -1	2.871 -2	2.307 -1	6.332	-1.059 -2	-4.177 -2	0.365
.600	3.788 -2	9.931 -1	1.413 -1	4.297 -2	3.474 -1	7.694	-1.237 -2	-2.497 -2	0.177
.650	1.389 -2	9.967 -1	1.141 -1	6.437 -2	5.206 -1	8.681	-1.249 -2	+2.912 -2	0.095
.700	4.745 -3	9.986 -1	9.089 -2	9.630 -2	7.688 -1	8.764	-8.278 -3	+1.566 -1	0.294
.750	1.452 -3	9.994 -1	7.072 -2	1.437 -1	1.164 0	8.131	+5.552 -3	+4.327 -1	0.863
.800	3.712 -4	9.998 -1	5.303 -2	2.145 -1	1.678 0	5.827	+3.905 -2	+9.629 -1	1.461
.850	7.253 -5	1.000 0	3.743 -2	3.162 -1	2.458 0	3.276	+1.097 -1	+1.971 0	1.590
.900	8.192 -6	1.000 0	2.357 -2	4.664 -1	3.613 0	1.110	+2.500 -1	+3.829 0	0.905
0.950	2.418 -7	1.000 0	1.116 -2	6.854 -1	5.246 0	0.112	+5.160 -1	+7.120 0	0.133
1.000	0.000	1.000 0	0.000	1.000 0	7.584 0	0.000	+1.000 0	+1.286 +1	0.000

The smaller numbers to the right are the powers of 10 by which the corresponding entries must be multiplied. The two interfaces for this Case are at X = 0.00155 and at X = 0.01075.

TABLE 7

PULSATION TABLE, CASE 15

x	p	q	f	y_0	$\frac{dy_0}{dx}$	$f_0 \times 10^4$	y_1	$\frac{dy_1}{dx}$	$f_1 \times 10^4$
0.000	3.898 +6	0.000	1.587 +1	5.821 -6	0.000	0.000	-3.405 -6	0.000	0.0000
.001	3.833 +6	2.076 -4	1.576 +1	5.832 -6	2.36 -5		-3.412 -6	-1.38 -5	
.002	3.645 +6	1.630 -3	1.545 +1	5.868 -6	4.87 -5		-3.433 -6	-2.84 -5	
.003	3.350 +6	5.340 -3	1.494 +1	5.930 -6	7.64 -5		-3.469 -6	-4.46 -5	
.004	2.976 +6	1.214 -2	1.424 +1	6.022 -6	1.06 -4		-3.522 -6	-6.22 -5	
.005	2.553 +6	2.247 -2	1.340 +1	6.145 -6	1.41 -4		-3.594 -6	-8.22 -5	
.006	2.114 +6	3.639 -2	1.244 +1	6.305 -6	1.82 -4		-3.688 -6	-1.06 -4	
.007	1.689 +6	5.345 -2	1.150 +1	6.512 -6	2.34 -4		-3.809 -6	-1.37 -4	
.008	1.306 +6	7.276 -2	1.062 +1	6.777 -6	2.98 -4		-3.964 -6	-1.74 -4	
.009	9.804 +5	9.323 -2	9.780 0	7.113 -6	3.77 -4		-4.160 -6	-2.20 -4	
.010	7.181 +5	1.138 -1	8.994 0	7.535 -6	4.56 -4		-4.408 -6	-2.66 -4	
.020	5.579 +4	2.217 -1	4.753 0	1.940 -5	1.27 -3		-1.135 -5	-7.41 -4	
.030	2.155 +4	2.709 -1	3.782 0	3.140 -5	1.133 -3		-1.837 -5	-6.625 -4	
.040	1.063 +4	3.235 -1	3.185 0	4.225 -5	1.074 -3		-2.471 -5	-6.276 -4	
.050	5.915 +3	3.771 -1	2.763 0	5.314 -5	1.112 -3	0.001	-3.107 -5	-6.495 -4	0.0004
.060	3.531 +3	4.300 -1	2.440 0	6.465 -5	1.195 -3		-3.779 -5	-6.975 -4	
.070	2.210 +3	4.810 -1	2.182 0	7.716 -5	1.313 -3		-4.509 -5	-7.655 -4	
.080	1.432 +3	5.290 -1	1.970 0	9.101 -5	1.462 -3		-5.316 -5	-8.516 -4	
.090	9.528 +2	5.739 -1	1.791 0	1.065 -4	1.643 -3		-6.218 -5	-9.551 -4	
.100	6.482 +2	6.152 -1	1.639 0	1.240 -4	1.858 -3	0.004	-7.232 -5	-1.078 -3	0.0015
.150	1.197 +2	7.721 -1	1.119 0	2.526 -4	3.460 -3	0.012	-1.466 -4	-1.985 -3	0.0040
.200	2.892 +1	8.655 -1	8.181 -1	4.910 -4	6.344 -3	0.027	-2.821 -4	-3.570 -3	0.0088
.250	8.313 0	9.204 -1	6.242 -1	9.201 -4	1.124 -2	0.057	-5.202 -4	-6.148 -3	0.0172
.300	2.693 0	9.528 -1	4.898 -1	1.668 -3	1.932 -2	0.108	-9.206 -4	-1.013 -2	0.0304
.350	9.475 -1	9.722 -1	3.917 -1	2.932 -3	3.228 -2	0.191	-1.565 -3	-1.596 -2	0.0483
.400	3.523 -1	9.837 -1	3.172 -1	5.019 -3	5.274 -2	0.317	-2.555 -3	-2.398 -2	0.0690
.450	1.355 -1	9.907 -1	2.588 -1	8.393 -3	8.457 -2	0.496	-4.002 -3	-3.414 -2	0.0872
.500	5.290 -2	9.948 -1	2.119 -1	1.376 -2	1.335 -1	0.730	-5.990 -3	-4.527 -2	0.0945
.550	2.060 -2	9.972 -1	1.735 -1	2.217 -2	2.080 -1	1.008	-8.496 -3	-5.382 -2	0.0828
.600	7.859 -3	9.986 -1	1.414 -1	3.519 -2	3.205 -1	1.294	-1.121 -2	-5.124 -2	0.0518
.650	2.874 -3	9.993 -1	1.142 -1	5.515 -2	4.894 -1	1.527	-1.317 -2	-1.926 -2	0.0189
.700	9.802 -4	9.997 -1	9.090 -2	8.548 -2	7.408 -1	1.622	-1.210 -2	+7.871 -2	0.0212
.750	2.998 -4	9.999 -1	7.071 -2	1.312 -1	1.114 0	1.506	-3.133 -3	+3.129 -1	0.0931
.800	7.726 -5	1.000 0	5.303 -2	1.998 -1	1.663 0	1.154	+2.346 -2	+8.136 -1	0.2133
.850	1.496 -5	1.000 0	3.743 -2	3.018 -1	2.471 0	0.662	+8.633 -2	+1.819 0	0.2736
.900	1.689 -6	1.000 0	2.357 -2	4.528 -1	3.644 0	0.226	+2.202 -1	+3.749 0	0.1745
0.950	4.987 -8	1.000 0	1.116 -2	6.748 -1	5.345 0	0.023	+4.879 -1	+7.330 0	0.0279
1.000	0.000	1.000 0	0.000	1.000 0	7.849 0	0.000	+1.000 0	+1.384 +1	0.0000

The smaller numbers to the right are the powers of 10 by which the corresponding entries must be multiplied. The two interfaces for this Case are at X = 0.00559 and at X = 0.0183.

and ω^2, the eigen-parameter, as defined by equation (5). The resulting expression is

$$\omega^2 = \frac{\int_0^1 f(x)\,dx}{\int_0^1 g(x)\,dx}, \tag{13}$$

where the functions $f(x)$ and $g(x)$ are defined by the equations

$$f(x) = x^4\left(\frac{dy}{dx}\right)^2 p + \frac{3}{5} l y^2 \frac{q x p}{t}, \tag{14}$$

$$g(x) = l x^4 \frac{y^2 p}{t}. \tag{15}$$

TABLE 8

EIGEN-PARAMETERS AND PERIOD–MEAN-DENSITY RELATIONSHIPS FOR SEVERAL STELLAR MODELS

Model	ω_0^2	ω_1^2	Q_0	Q_0'
Case 4	8.449	14.439	0.0309	0.039₆
Case 7	8.184	13.461	.0314	.0425
Case 15	8.449	14.439	.0309	.0410
Russell mixture*			.0320	
Oxygen model†			.0292	
Standard model‡			0.0381	
Observed§				0.09

* G. Keller, *On the Physical and Chemical Composition of the Sun* (Ph.D. Diss.; Columbia University, 1948).

† *Ibid.*

‡ M. Schwarzschild, *Ap. J.*, **94**, 245, 1941.

§ A. S. Eddington, *The Internal Constitution of the Stars* (Cambridge: At the University Press, 1930), p. 182; and M. Schwarzschild, B. Schwarzschild, and W. S. Adams, *Ap. J.*, **108**, 107, 1948.

The function $g(x)$ has the role of a normalization factor for ω^2. The function $f(x)$ plays the role of a weight function for the period. The period may be thought of as constituted of contributions by the various portions of the star, some portions contributing more, some less. The function $f(x)$ indicates the relative contributions of the various stellar layers in fixing the period of a particular mode of oscillation.

For the use of the function $f(x)$ in the above sense, the stationary (minimal) character of the right-hand side of equation (12) is essential for the following reason: If the model (that is, P, M_r, and ρ) is changed in a limited range of r, the eigen-solution y and its first derivative, dy/dr, will, in general, be changed throughout the complete range of r. These changes of the eigen-solution will, however, not produce first-order changes in the period because of the stationary character of equation (12). Thus changes in the model at a limited range of r are reflected by changes in equation (12) in the same limited interval only.

The functions $f(x)$ were computed[10] for the pulsation modes and models considered here, with the aid of the eigen-solutions y and dy/dx listed in Tables 5, 6, and 7. The results are listed in these same tables. Figures 1 and 2 show the weight functions, f_0 and f_1,

[10] The functions $g(x)$ were also computed, and ω^2 was rederived by eq. (13). In all cases the agreement with the original results for ω^2 was very satisfactory.

for the fundamental and first-overtone modes. Thus it appears that, in all cases considered, the value of the fundamental period is most strongly influenced by the physical conditions in the stellar layers located around $x = 0.75$. One notices also that, in all cases considered, the maximum for the weight function for the first overtone occurs at a region somewhat nearer the stellar surface than does the maximum for the fundamental mode. Thus, as a result of superficial phenomena, one might expect a more profound effect on the overtone pulsation periods than on the fundamental period. In addition, the figures show a secondary broad maximum occurring farther toward the center for the first overtone.

The shapes of Figures 1 and 2 emphasize the fact that conditions near the center of the star can have little influence on the pulsation periods, since in that region the weight func-

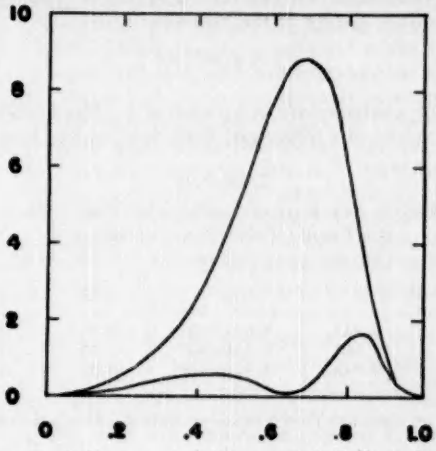

FIG. 1.—Weight function, case 7. *Upper curve*, f_0; *lower curve*, f_1. *Ordinate*, $f \times 10^4$; *abscissa*, $x = r/R$

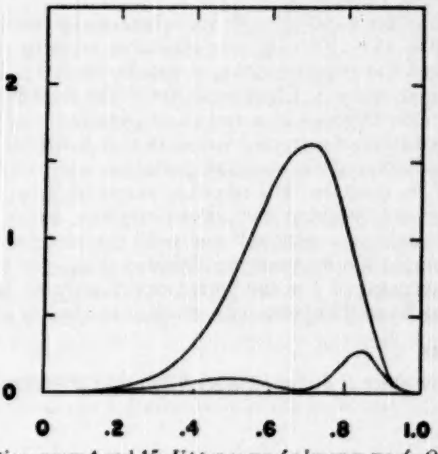

FIG. 2.—Weight function, cases 4 and 15. *Upper curve*, f_0; *lower curve*, f_1. *Ordinate*, $f \times 10^4$; *abscissa*, $x = r/R$.

tions are indeed small. This is in agreement with the result of the previous section that models with widely differing core conditions still have similar periods.

An attempt could now be made to estimate the effects on the fundamental period of neglected physical processes operative in regions where the weight function is large.

Since hydrogen and helium are already more than 99 per cent ionized at a depth where the weight function has a value less than one-tenth its maximum, this physical process can have little effect on the fundamental period, except if ionization should produce a convection zone reaching far into the interior.

Next the opacity law in the region of highest weight was investigated. Mrs. M. H. Harrison's tables were used (the model having 70 per cent oxygen and 30 per cent Russell mixture),[11] in conjunction with the dimensional models listed in Table 4, to obtain the variation of the guillotine factor with density. Electron scattering was included, and a fit was sought for the total opacity of the following form:

$$\kappa'_T = \kappa'_0 \rho^s T^{-3.5} . \tag{16}$$

Values of s and κ'_0 giving a satisfactory fit for each of the three cases considered are given in Table 9. Since the values of s differ only little from unity, Kramers' law is found to

TABLE 9*

OPACITY AND RADIATION-PRESSURE CORRECTIONS FOR HIGHLY CONCENTRATED MODELS

Model	s	κ'_0	$(1-\beta)$	n'	Γ_1
Case 4	0.943	5.023×10^{24}	0.45	3.9	1.4
Case 7	.961	3.334×10^{24}	.17	3.4	1.5
Case 15	0.948	3.971×10^{24}	0.18	3.4	1.5

* The values listed are those which apply in regions where the weight function for the fundamental mode is a maximum.

apply reasonably well in this region. The ratios of radiation pressure to total pressure, $(1 - \beta)$, are also listed in Table 9.

Since the values found for s and $(1 - \beta)$ are substantially different from those originally used [$s = 0.75$ and $(1 - \beta) = 0$], new estimates must be made of the effective polytropic indices n' and the effective ratios of specific heats Γ_1. These quantities were computed by formulae given by S. Chandrasekhar.[12] The resulting values of n' and Γ_1 are listed in Table 9. The revisions of n and Γ_1 (originally $n = 3.71$ and $\Gamma_1 = \gamma = \frac{5}{3}$) necessitated the computation of corrected values of Q (labeled "Q'"). The values of Q' were derived by interpolation of the available pulsation integrations[13] corresponding to the ranges of n' and Γ_1 in question. The resulting values of Q_1 are indicated in Table 8.

The observed value of Q is about 0.09, if one employs, for cepheids, masses determined from the mass-luminosity relation[14] and radii computed with the effective temperature scale. The comparison between the observed Q and the theoretical Q' shows a discrepancy of about a factor of 2 in the period, which may be due to other neglected physical conditions which are of importance in a region of the star where the weight func-

[11] *Ap. J.*, **108**, 310, 1948.

[12] *An Introduction to the Study of Stellar Structure* (Chicago: University of Chicago Press, 1939), pp. 324 and 59.

[13] Keller, *op. cit.*

[14] Eddington, *op. cit.*, p. 182; and M. Schwarzschild, B. Schwarzschild, and W. S. Adams, *Ap. J.*, **108**, 207, 1948.

tion for the fundamental mode is large. One such neglected physical condition may be the presence of a convection layer extending from the surface into the star to a sufficient depth to lower the local polytropic index in the regions of high weight. Another explanation of the discrepancy between observation and theory may be sought in a revision of cepheid masses. Still another possibility is that the effective temperature scale (and consequently the radii) as applied to cepheids is in error. These three possibilities are discussed in the next section.

V. DISCUSSION OF THE REMAINING DISCREPANCY

Employing a corrected value of Q, one may now compute a mean density as a function of the period. For the mean value of Q' (Table 8), $\bar{Q}' = 0.041$, the period–mean-density relationship takes the form $\bar{\rho} = 0.00237/\Pi^2$, where Π is the period in days. Thus, a means is available for determining the mass of a cepheid of known period in terms of its radius. Comparison with observations was here restricted to the cepheid η Aquilae. The mean radius of η Aquilae, derived from its effective temperature, is 2.55×10^{12} cm, while its period is 7.176+ days.[15] These data, when incorporated into the period–mean-density relationship above, yield a value for the mass of 3.2×10^{33} gm = 1.6 solar masses, figures which seem unexpectedly small. To pursue further the consequences of attaining accord between theory and observations by means of adjusting the masses of the cepheids, a value of C (eq. [1]) in the theoretical mass-luminosity relationship was computed with the values of the radius and mass stated above and with the observed luminosity of η Aquilae. The resulting value of log C was -0.74, a value which indicates that such a model, even if it should perhaps be found reasonable in its physical properties, would be completely beyond the range of models considered here (log $C = -4.0$ and -5.2).

A second method of attacking the above discrepancy is to use a theoretical mass-luminosity law for a fixed model (case 15, e.g.) in conjunction with the period–mean-density relationship. With an observed luminosity, unique values of the mass and mean radius (and consequently of the effective temperature) may be derived. Using case 15 to represent a model cepheid, with composition as given in Table 4, the derived radius was $R = 4.07 \times 10^{12}$ cm, while the mass, 1.3×10^{34} gm = 6.6 solar masses. The radius at minimum light, r, was computed by applying the known difference, $r - R$, to the mean radius R. With r and the observed luminosity at minimum light, an effective temperature of $T_e = 4100°$ K was derived for η Aquilae at minimum. This method, when revised by the use of corrected values of the opacity constant κ_0', yielded values of $R = 3.76 \times 10^{12}$ cm; $M = 1.0 \times 10^{33}$ gm = 5.1 solar masses; and an effective temperature at minimum light of $T_e = 4170°$ K. Compared with an observed T_e at a minimum of 4800° K, this calculation shows that accord between theory and observation[16] can be brought about by lowering the effective temperature by about 13 per cent, a procedure difficult to justify in view of recent color measurements. The mass obtained by this method seems of the right order.

A third possibility is that a convection layer extends into the interior to such an extent as to provide a substantial reduction in the effective polytropic index. To relate polytropic indices to pulsation periods, reference was made to available pulsation integrations.[17] In Figure 3, the logarithms of the periods were plotted against effective polytropic index. The polytropic index which would increase the value of the fundamental period by a factor of 2 over that arrived at in the previous analyses, in which $n_{eff} = 3.5$, was

[15] Schwarzschild, Schwarzschild, and Adams, *op. cit.*

[16] All observational quantities for η Aquilae listed in this section are from Schwarzschild, Schwarzschild, and Adams, *op. cit.*

[17] Homogeneous model: T. Sterne, *M.N.*, **97**, 582, 1937; polytrope 1.5: T. G. Cowling, *M.N.*, **94**, 779, 1934 (fundamental only); standard model: M. Schwarzschild, *Ap. J.*, **94**, 245, 1941; Russell-mixture model: Keller, *op. cit.*; oxygen model: *ibid.*

estimated from Figure 3.[18] This value proved to be in the neighborhood of $n = 1.8$, in conformity with Eddington's view.[19] The work of L. Biermann[20] would tend to confirm the possibility that the convection zone may extend through the layers in which the weight function for the fundamental mode is appreciable. Hence the possibility that n_{eff} in the region of highest weight equals 1.8 (above the limiting value of 1.5) is not ex-

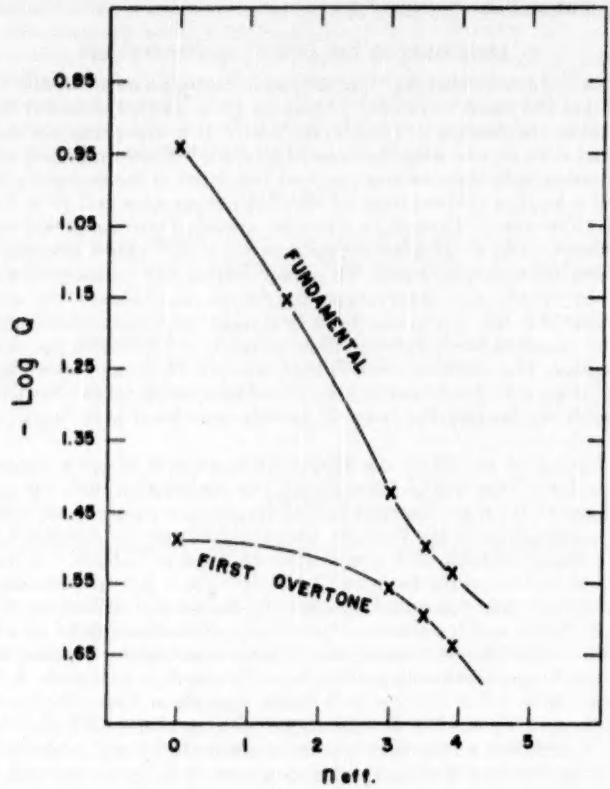

FIG. 3.—Pulsation periods for modes of differing effective polytropic indices. *Ordinate, log Q* = log (period in days) + ½ log ($\bar{\rho}/\bar{\rho}_\odot$); *abscissa*, effective polytropic index.

cluded. One must, however, consider the consequences of a convection zone on other modes of pulsation, particularly on the first overtone.

The observational data[21] suggests that $\log \tau_1/\tau_0 = -0.16$ for the variables in Messier 3. Figure 3 shows that this value for $\log \tau_1/\tau_0$ can be attained only if the effective polytropic index for the first overtone were to be reduced to a greater extent than that for

[18] The effective polytropic index, n_{eff}, is 3.5 for all three cases in the present investigation, as well as in Keller's pulsation integration for the Russell-mixture model, since the same absorption law holds in all four cases.

[19] Rosseland, *op. cit.*

[20] *A.N.*, **264**, 361, 1938.

[21] M. Schwarzschild, *Pub. A.A.S.*, **10**, 117, 1941.

the fundamental mode. If the convection were to extend down to $x = 0.8$, then, according to Figures 1 and 2, the pulsation properties of the overtone mode would have been more seriously altered in the direction of lower polytropic index than those of the fundamental mode.

Making the assumption that, with the above depth of convection, the period of the fundamental mode may be approximated by that of a polytrope $n = 2.5$ and the period of the overtone by a polytrope of $n = 1.5$, a value of $\log \tau_1/\tau_0 = -0.18$ is obtained, in good agreement with the value of -0.16 for the variables observed in Messier 3. The increase in the value for the fundamental period indicated by these assumptions amounted to a factor of about 1.6. Thus the possibility of invoking a convection layer to raise the fundamental period is not in conflict with the observed ratios of overtone to fundamental periods.

VI. GENERAL CONCLUSIONS

The period-density relationship for the highly concentrated models, constructed to represent giant stars, was found not to differ to any significant extent from the period-density law for models representing main-sequence stars. The fundamental pulsation period proved to be virtually independent of physical conditions in the inner half of the star.

Agreement between observed and theoretical values for the period-density relationship of η Aquilae, taken as a typical cepheid, may be accomplished by (1) reducing the mass, as determined by the empirical mass-luminosity relation, by a factor of 4.3 or by (2) reducing the effective temperature, as determined from color measurements, by 13 per cent or by (3) altering the theoretically derived period-density relationship. The mechanism operating to produce condition 3 may possibly be a convection layer reaching into the star to a depth corresponding to one-fifth the stellar radius.

The author takes pleasure in thanking Professor Martin Schwarzschild for his generous guidance throughout all phases of this investigation.

RADIATIVE EQUILIBRIUM IN AN ATMOSPHERE IN WHICH PURE SCATTERING AND PURE ABSORPTION BOTH PLAY A ROLE

A. D. CODE
Yerkes Observatory
Received March 21, 1950

ABSTRACT

In this paper a solution of the equation of transfer for an atmosphere in which both scattering by free electrons and pure absorption play a role is given. The laws of darkening, the temperature distribution, and the degree of polarization for atmospheres with different values of $\lambda = \bar{\kappa}/\sigma + \bar{\kappa}$ are given for a gray atmosphere. The extension to cases of small departures from grayness is also considered. A perturbation theory for $\lambda \to 1$ is given, and it is found that accurate results for an atmosphere with an arbitrary λ may be obtained by linear interpolation between two different values of λ differing by 0.2.

Finally, the laws of darkening and the degree of polarization in monochromatic light are considered. The degree of polarization decreases from short to long wave lengths. For a star whose effective temperature is of the order of 20,000° K, the polarization has reduced to about half the value of the integrated light at the ordinary photographic region for a star in which $\lambda = 0.5$. The law of darkening at this wave length is intermediate between that expected in a gray body and that in a pure scattering atmosphere.

I. INTRODUCTION

In discussions of the problem of radiative transport in stellar atmospheres, appeal is generally made either to the concept of local thermodynamic equilibrium or to that of monochromatic equilibrium. If the main source of opacity is due to pure absorption, the atmosphere is said to be in "local thermodynamic equilibrium," and the source function is specified by Kirchhoff's law. On the other hand, if a pure scattering process assumes the dominant role, then the atmosphere is considered to be in monochromatic equilibrium, and the corresponding source function is given by the law of scattering. These two concepts represent useful limiting cases and are susceptible of exact solution. It is generally accepted that in early-type stars the opacity is due to the scattering by free electrons and absorption by hydrogen and helium. It is of importance, then, to consider the problem of transfer of radiation in an atmosphere in which pure scattering and pure absorption both play a role.

In this paper we shall formulate the problem of transfer for the case in which the scattering by free electrons is governed by Thomson's laws. In this law the scattering coefficient may be regarded as independent of frequency over the entire frequency range of interest. It is an essential feature of such a problem, involving scattering, that polarization of the radiation be allowed for, since the scattering function is different for different states of polarization.

The concept of temperature does not enter into the problem of an atmosphere in monochromatic equilibrium. The treatment here provides appropriate representation of the temperature distribution in an atmosphere combining pure absorption and pure scattering and permits a generalization of the temperature distribution to the limiting case of pure scattering.

The degree of polarization and the laws of darkening in the two states of polarization, both in integrated light and for monochromatic radiation, for varying ratios of absorption to scattering represent the significant features to be studied.

We shall confine our discussion to the transfer of radiation in a semi-infinite, plane-parallel atmosphere. The neglect of the curvature of the stellar atmosphere may not always be justifiable in the case of early supergiants, but even there it will be a safe approximation with regard to the continuous spectrum and will provide a definite lower limit for the degree of polarization.

II. EQUATION OF TRANSFER FOR TWO COMPONENTS OF POLARIZATION IN AN ATMOSPHERE IN WHICH BOTH SCATTERING BY FREE ELECTRONS AND PURE ABSORPTION GOVERN TRANSFER OF RADIATION

We shall restrict our discussion to the transfer problem in a semi-infinite, plane-parallel atmosphere with a constant net flux of radiation and in which the scattering takes place in accordance with Thomson's laws of scattering by free electrons. In formulating the equation of transfer appropriate to the case under consideration, it is clear that we must allow for contributions to the source function by scattering and by thermal emission. S. Chandrasekhar[1] has formulated the laws of scattering in a manner suitable for this discussion. In specifying the nature of the re-emission of the absorbing matter, we shall make use of the concept of local thermodynamic equilibrium. If a sufficient number of radiative processes is involved, we can expect a Maxwellian distribution at each depth, characterized by a particular temperature, and we can expect Kirchhoff's law to give the emission from these sources. This emission will be unpolarized and may be considered as contributing equally to both states of polarization. Under these conditions the equation of transfer is expressible in the following forms:

$$\cos\vartheta\,\frac{dI_{l,\nu}}{\rho dx} = -(\sigma+\kappa_\nu)\,I_{l,\nu} + \sigma\,[\mathfrak{J}_{l,l,\nu}(x,\vartheta) + \mathfrak{J}_{r,l,\nu}(x,\vartheta)] + \tfrac{1}{2}\kappa_\nu B_\nu \tag{1}$$

and

$$\cos\vartheta\,\frac{dI_{r,\nu}}{\rho dx} = -(\sigma+\kappa_\nu)\,I_{r,\nu} + \sigma\,[\mathfrak{J}_{l,r,\nu}(x,\vartheta) + \mathfrak{J}_{r,r,\nu}(x,\vartheta)] + \tfrac{1}{2}\kappa_\nu B_\nu, \tag{2}$$

where, as usual,

$$\sigma = \frac{8\pi}{3}\,\frac{e^6}{m^2c^4}\,N_e \tag{3}$$

is the Thomson mass scattering coefficient and is independent of frequency, similarly κ_ν is the mass absorption coefficient; also $I_{l,\nu}$ and $I_{r,\nu}$ denote the specific intensities at frequency ν in a particular direction and polarized with the electric vector vibrating in the principal meridian and at right angles to it, respectively. $\mathfrak{J}_{l,l,\nu}$ and $\mathfrak{J}_{r,l,\nu}$ are the contributions to the source function for the radiation in a particular direction and polarized with the electric vector in the meridian plane, arising from the scattering from all other directions of radiation polarized with the electric vectors parallel, respectively, perpendicular to the appropriate meridian planes. Similarly, $\mathfrak{J}_{l,r,\nu}$ and $\mathfrak{J}_{r,r,\nu}$ are the corresponding contributions to the source function for radiation in a particular direction and polarized with the electric vector at right angles to the meridian plane, arising from scattering from all other directions of radiation polarized with the electric vectors parallel, respectively, perpendicular to the appropriate meridian planes. B_ν is the Planck function for the temperature prevailing at depth x.

Chandrasekhar has evaluated the quantities $[\mathfrak{J}_{l,l} + \mathfrak{J}_{r,l}]$ and $[\mathfrak{J}_{l,r} + \mathfrak{J}_{r,r}]$ for the case of Thomson scattering,[2] and, in terms of the quantities J and K, defined in the usual manner, they are

$$\mathfrak{J}_{l,l,\nu} + \mathfrak{J}_{r,l,\nu} = \tfrac{3}{4}\,[2(J_{l,\nu} - K_{l,\nu}) + \mu^2(3K_{l,\nu} - 2J_{l,\nu} + K_{r,\nu})] \tag{4}$$

and

$$\mathfrak{J}_{l,r,\nu} + \mathfrak{J}_{r,r,\nu} = \tfrac{3}{4}\,[J_{r,\nu} + K_{l,\nu}], \tag{5}$$

where $\mu = \cos\vartheta$.

We shall let

$$\kappa_\nu = \bar{\kappa} + \delta_\nu\bar{\kappa}, \tag{6}$$

[1] *Ap. J.*, **103**, 351, 1942. In the future this paper will be referred to as "Paper X."

[2] Cf. Paper X, eqs. (39) and (40).

where δ_ν is a measure of the departure from grayness of the absorbing matter and $\bar{\kappa}$ is some suitably chosen mean absorption coefficient which we shall leave undefined for the present. We shall further let

$$\lambda = \frac{\bar{\kappa}}{\sigma + \bar{\kappa}}, \tag{7}$$

and in terms of σ and the mean absorption coefficient $\bar{\kappa}$ we introduce an optical depth defined by the equation

$$d\tau = -(\sigma + \bar{\kappa})\,\rho dx\,. \tag{8}$$

By virtue of equations (4), (5), (6), (7), and (8), the equations of transfer (1) and (2) take on the forms

$$\mu \frac{dI_{\tau,\nu}}{d\tau} = I_{\tau,\nu} - \tfrac{3}{4}(1-\lambda)\{2(J_{\tau,\nu} - K_{\tau,\nu}) + \mu^2(3K_{\tau,\nu} - 2J_{\tau,\nu} + J_{\tau,\nu})\} - \tfrac{1}{2}\lambda B_\nu + \lambda\delta_\nu(I_{\tau,\nu} - \tfrac{1}{2}B_\nu) \tag{9}$$

and

$$\mu \frac{dI_{\tau,\nu}}{d\tau} = I_{\tau,\nu} - \tfrac{3}{4}(1-\lambda)\{J_{\tau,\nu} + K_{\tau,\nu}\} - \tfrac{1}{2}\lambda B_\nu + \lambda\delta_\nu(I_{\tau,\nu} - \tfrac{1}{2}B_\nu)\,. \tag{10}$$

These are the fundamental equations with which we shall be concerned in this paper.

III. GENERAL SOLUTION OF EQUATIONS OF TRANSFER IN $(n, 1)$ APPROXIMATION FOR INTEGRATED INTENSITIES

If the atmosphere is gray, δ_ν vanishes, and the equations of transfer integrated over all frequencies become

$$\mu \frac{dI_\tau}{d\tau} = I_\tau - \tfrac{3}{4}(1-\lambda)\{2(J_\tau - K_\tau) + \mu^2(3K_\tau - 2J_\tau + J_\tau)\} - \tfrac{1}{2}\lambda\int_0^\infty B_\nu d\nu \tag{11}$$

and

$$\mu \frac{dI_\tau}{d\tau} = I_\tau - \tfrac{3}{4}(1-\lambda)\{J_\tau + K_\tau\} - \tfrac{1}{2}\lambda\int_0^\infty B_\nu d\nu\,. \tag{12}$$

The condition of constant net flux requires that

$$\frac{dF_\tau}{d\tau} + \frac{dF_\tau}{d\tau} = \frac{dF}{d\tau} = 0\,. \tag{13}$$

If we integrate equations (11) and (12) over μ, we obtain

$$\frac{1}{2}\frac{dF_\tau}{d\tau} = \tfrac{3}{2}K_\tau - \tfrac{1}{2}J_\tau + \lambda\{2J_\tau + \tfrac{1}{2}J_\tau - \tfrac{3}{2}K_\tau\} - \lambda B \tag{14}$$

and

$$\frac{1}{2}\frac{dF_\tau}{d\tau} = -\tfrac{3}{2}K_\tau + \tfrac{1}{2}J_\tau + \lambda\{\tfrac{3}{2}J_\tau + \tfrac{3}{2}K_\tau\} - \lambda B\,; \tag{15}$$

therefore, adding equations (14) and (15) and applying the condition of constant net flux (13), we have

$$B = J_\tau + J_\tau = J\,. \tag{16}$$

Substituting equation (16) in equations (11) and (12), multiplying these equations by μ, and integrating over all μ's, we find

$$\frac{dK_l}{d\tau} = \tfrac{1}{4}F_l; \qquad \frac{dK_r}{d\tau} = \tfrac{1}{4}F_r; \tag{17}$$

we therefore have the "K integral,"

$$K_l + K_r = \tfrac{1}{4}F(\tau + Q), \tag{18}$$

where Q is a constant.

In solving equations (11) and (12), we shall follow the method developed by S. Chandrasekhar[3] and replace the various integrals which occur on the right-hand sides of the equations by sums according to Gauss's formula for numerical quadrature. Thus in the nth approximation, equations (11) and (12) are replaced by the following system of $4n$ linear equations, in which B has been set equal to $J_l + J_r$:

$$\mu_i \frac{dI_{l,i}}{d\tau} = I_{l,i} - \tfrac{3}{8}(1-\lambda)[2\Sigma a_j I_{l,j}(1-\mu_j^2) + \mu_i^2\{\Sigma a_j I_{l,j}(3\mu_j^2-2) + \Sigma a_j I_{r,j}\}] - \tfrac{1}{4}\lambda[\Sigma a_j I_{l,j} + \Sigma a_j I_{r,j}] \qquad (i = \pm 1, \ldots, \pm n) \tag{19}$$

and

$$\mu_i \frac{dI_{r,i}}{d\tau} = I_{r,i} - \tfrac{3}{8}(1-\lambda)[\Sigma a_j I_{r,j} + \Sigma a_j I_{l,j}\mu_j^2] - \tfrac{1}{4}\lambda[\Sigma a_j I_{l,j} + \Sigma a_j I_{r,j}] \qquad (i = \pm 1, \ldots, \pm n), \tag{20}$$

where the μ_i's ($i = \pm 1, \ldots, \pm n$) are the zeros of the Legendre polynomial of order $2n$ and the a_i's are the appropriate Gaussian weights.

We shall first seek a solution of equations (19) and (20) of the form

$$I_{l,i} = g_i e^{-k\tau} \quad \text{and} \quad I_{r,i} = h_i e^{-k\tau} \qquad (i = \pm 1, \ldots, \pm n), \tag{21}$$

where the g_i's, h_i's, and k are constants. Substituting these equations in (19) and (20), we obtain

$$g_i(1+\mu_i k) = \tfrac{3}{8}(1-\lambda)[2\Sigma a_j g_j(1-\mu_j^2) + \mu_i^2\{\Sigma a_j g_j(3\mu_j^2-2) + \Sigma a_j h_j\}] + \tfrac{1}{4}\lambda[\Sigma a_j g_j + \Sigma a_j h_j] \tag{22}$$

and

$$h_i(1+\mu_i k) = \tfrac{3}{8}(1-\lambda)[\Sigma a_j g_j \mu_j^2 + \Sigma a_j h_j] + \tfrac{1}{4}\lambda[\Sigma a_j g_j + \Sigma a_j h_j]. \tag{23}$$

It follows from equations (22) and (23) that g_i and h_i must be expressible in the forms

$$g_i = \frac{\alpha\mu_i^2 + \beta}{1+\mu_i k} \quad \text{and} \quad h_i = \frac{\gamma}{1+\mu_i k} \qquad (i = \pm 1, \ldots, \pm n), \tag{24}$$

where α, β, and γ are certain constants, independent of i. Inserting equation (24) back in equations (22) and (23), we obtain

$$\alpha\mu_i^2 + \beta = \tfrac{3}{8}(1-\lambda)[2\{\alpha(D_2 - D_4) + \beta(D_0 - D_2)\} + \mu_i^2\{\alpha(3D_4 - 2D_2) + \beta(3D_2 - 2D_0) + \gamma D_0\} + \tfrac{1}{4}\lambda[\alpha D_2 + \beta D_0 + \gamma D_0] \tag{25}$$

and

$$\gamma = \tfrac{3}{8}(1-\lambda)[\alpha D_4 + \beta D_2 + \gamma D_0] + \tfrac{1}{4}\lambda[\alpha D_2 + \beta D_0 + \gamma D_0], \tag{26}$$

[3] *Ap. J.*, **100**, 76, 1944.

where the D's are defined according to the formula

$$D_m = \Sigma \frac{a_j \mu_j^m}{1 + \mu_j k}. \tag{27}$$

Since equations (25) and (26) must be valid for all i, it follows that

$$\tfrac{8}{3}\alpha = [\alpha(3D_4 - 2D_2) + \beta(3D_2 - 2D_0) + \gamma D_0](1 - \lambda), \tag{28}$$

$$\tfrac{8}{3}\beta = 2[\alpha(D_2 - D_4) + \beta(D_0 - D_2)](1 - \lambda) + \tfrac{2}{3}\lambda[\alpha D_2 + \beta D_0 + \gamma D_0], \tag{29}$$

and

$$\tfrac{8}{3}\gamma = [\alpha D_4 + \beta D_2 + \gamma D_0](1 - \lambda) + \tfrac{2}{3}\lambda[\alpha D_2 + \beta D_0 + \gamma D_0]. \tag{30}$$

Adding equations (28) and (29), we see that

$$\gamma = \alpha + \beta. \tag{31}$$

Substituting for γ in the above equations and adding equations (29) and (30), we obtain

$$\frac{\alpha}{\beta} = \frac{2(D_0 - 2)}{(\frac{8}{3} - D_2 - D_0)}. \tag{32}$$

To simplify equation (32) still further, we shall make use of the following recursion formulae:[4]

$$D_{2m} = \frac{1}{k^2}\left(D_{2m-2} - \frac{2}{2m-1}\right) \quad \text{and} \quad D_{2m-1} = -kD_{2m}, \tag{33}$$

which the D's satisfy. By virtue of these recursion formulae, it is readily established that equation (32) becomes

$$\frac{\alpha}{\beta} = -\frac{2D_2}{D_2 + D_4} = -A(k) \quad \text{(say)}. \tag{34}$$

From equations (21), (24), and (35) it follows that

$$I_{l,\,i} = \text{Constant}\ \frac{1 - \mu_i^2 A(k)}{1 + \mu_i k}\, e^{-kr} \qquad (i = \pm 1, \ldots, \pm n) \tag{35}$$

and

$$I_{r,\,i} = \text{Constant}\ \frac{1 - A(k)}{1 + \mu_i k}\, e^{-kr} \qquad (i = \pm 1, \ldots, \pm n). \tag{36}$$

We must next establish the characteristic equation determining k. Solving equation (28) for α/β, we obtain

$$\frac{\alpha}{\beta} = \frac{3D_2 - D_0}{[2D_2 - 3D_4 - D_0 + \frac{8}{3}(1 - \lambda)]}. \tag{37}$$

Combining equations (34) and (37) and reducing them by means of the recursion formulae (33), we find that

$$(1 - \lambda)\left(1 - \frac{1}{k^2}\right)^2 (D_0 - 2)^2 = \tfrac{16}{9}\lambda D_0 - 4\lambda + \tfrac{4}{9}. \tag{38}$$

[4] Cf. *Ap. J.*, **101**, 328, 1945 (eqs. [54] and [56]).

Equation (38) is the characteristic equation of order $4n$ in k; there are, however, only $4n - 2$ pairs of nonvanishing roots. The characteristic roots determined by equation (38) are related to the roots of the pure scattering problem considered by Chandrasekhar[5] in a simple manner, which will be discussed later. It is convenient for this reason to consider two sets of characteristic roots; the κ_β's, of which there are $n - 1$ pairs, and the n pairs of roots k_α, which are the analogues of the corresponding roots of the pure scattering problem, $\lambda = 0$.

Since zero is a root of equation (38), a linear solution of the form

$$I_{l,\,i} = I_{r,\,i} = b\,(\tau + \mu_i + Q) \qquad (i = \pm 1, \ldots, \pm n)\,, \tag{39}$$

where b and Q are arbitrary constants, must also satisfy the equation of transfer, as may be readily verified.

Combining the solutions (35), (36), and (39), we observe that the general solution of the system of equations (19) and (20) can be written in the following form:

$$I_{l,\,i} = b\Big\{\tau + \mu_i + Q + \sum_{\beta=-(n-1)}^{n-1} L_\beta \frac{1-\mu_i^2 A_\beta}{1+\mu_i\kappa_\beta}\, e^{-\kappa_\beta\tau} + \sum_{\alpha=-n}^{n} M_\alpha \frac{1-\mu_i^2 A_\alpha}{1+\mu_i k_\alpha}\, e^{-k_\alpha\tau}\Big\} \qquad (i = \pm 1, \ldots, \pm n) \tag{40}$$

and

$$I_{r,\,i} = b\Big\{\tau + \mu_i + Q + \sum_{\beta=-(n-1)}^{n-1} L_\beta \frac{1-A_\beta}{1+\mu_i\kappa_\beta}\, e^{-\kappa_\beta\tau} + \sum_{\alpha=-n}^{n} M_\alpha \frac{1-A_\alpha}{1+\mu_i k_\alpha}\, e^{-k_\alpha\tau}\Big\} \qquad (i = \pm 1, \ldots, \pm n)\,, \tag{41}$$

where $L_{\pm\beta}$ ($\beta = 1, \ldots, n-1$), $M_{\pm\alpha}$ ($\alpha = 1, \ldots, n$), b, and Q are the $4n$ constants of integration.

IV. SOLUTIONS SATISFYING THE NECESSARY BOUNDARY CONDITIONS

The boundary conditions appropriate to the problem in hand are that none of the I_i's tend to infinity exponentially as $\tau \to \infty$ and that there is no radiation incident on the surface $\tau = 0$. The first of these conditions implies that, in the general solutions (40) and (41), we omit all terms in exp $(+k_\alpha\tau)$ and exp $(+\kappa_\beta\tau)$; hence

$$I_{l,\,i} = b\Big\{\tau + \mu_i + Q + \sum_{\beta=1}^{n-1} L_\beta \frac{1-\mu_i^2 A_\beta}{1+\mu_i\kappa_\beta}\, e^{-\kappa_\beta\tau} + \sum_{\alpha=1}^{n} M_\alpha \frac{1-\mu_i^2 A_\alpha}{1+\mu_i k_\alpha}\, e^{-k_\alpha\tau}\Big\} \qquad (i = \pm 1, \ldots, \pm n) \tag{42}$$

and

$$I_{r,\,i} = b\Big\{\tau + \mu_i + Q + \sum_{\beta=1}^{n-1} \frac{L_\beta(1-A_\beta)}{1+\mu_i\kappa_\beta}\, e^{-\kappa_\beta\tau} + \sum_{\alpha=1}^{n} \frac{M_\alpha(1-A_\alpha)}{1+\mu_i k_\alpha}\, e^{-k_\alpha\tau}\Big\} \qquad (i = \pm 1, \ldots, \pm n)\,. \tag{43}$$

[5] Paper X.

Next the nonexistence of any radiation incident on $\tau = 0$ requires that

$$I_{l,\,i} = I_{r,\,i} = 0 \qquad \text{at} \qquad \tau = 0 \qquad \text{and for} \qquad i = -1, \ldots, -n\,; \tag{44}$$

or, from equations (42) and (43),

$$\sum_{\beta=1}^{n-1} \frac{L_\beta (1 - \mu_i^2 A_\beta)}{1 - \mu_i \kappa_\beta} + \sum_{\alpha=1}^{n} \frac{M_\alpha (1 - \mu_i^2 A_\alpha)}{1 - \mu_i k_\alpha} - \mu_i + Q = 0 \qquad (i = 1, \ldots, n) \tag{45}$$

and

$$\sum_{\beta=1}^{n-1} \frac{L_\beta (1 - A_\beta)}{1 - \mu_i \kappa_\beta} + \sum_{\alpha=1}^{n} \frac{M_\alpha (1 - A_\alpha)}{1 - \mu_i k_\alpha} - \mu_i + Q = 0 \qquad (i = 1, \ldots, n)\,. \tag{46}$$

These are the $2n$ equations which determine the $2n$ constants L_β ($\beta = 1, \ldots, n-1$), M_α ($\alpha = 1, \ldots, n$), and Q. The constant b is left arbitrary and is related to the constant net flux of radiation in the atmosphere.

Now, defining the net flux in terms of F_l and F_r, where

$$F_q = 2 \int_{-1}^{+1} I_q \mu \, d\mu \simeq 2 \Sigma a_i I_{q,\,i} \mu_i \qquad (q = l,\ r)\,, \tag{47}$$

we have, according to equations (43) and (44),

$$F_l = 2b \left\{ \frac{2}{3} + \sum_{\beta=1}^{n-1} L_\beta \left[D_1(\kappa_\beta) - A_\beta D_3(\kappa_\beta) \right] e^{-\kappa_\beta \tau} + \sum_{\alpha=1}^{n} M_\alpha \left[D_1(k_\alpha) - A_\alpha D_3(k_\alpha) \right] e^{-k_\alpha \tau} \right\} \tag{48}$$

and

$$F_r = 2b \left\{ \frac{2}{3} + \sum_{\beta=1}^{n-1} L_\beta \left[D_1(\kappa_\beta) - A_\beta D_1(\kappa_\beta) \right] e^{-\kappa_\beta \tau} + \sum_{\alpha=1}^{n} M_\alpha \left[D_1(k_\alpha) - A_\alpha D_1(k_\alpha) \right] e^{-k_\alpha \tau} \right\}; \tag{49}$$

then

$$F_l + F_r = 2b \left\{ \frac{4}{3} + \sum_{\beta=1}^{n-1} L_\beta \left[2 D_1(\kappa_\beta) - A_\beta \left\{ D_1(\kappa_\beta) + D_3(\kappa_\beta) \right\} \right] e^{-\kappa_\beta \tau} + \sum_{\alpha=1}^{n} M_\alpha \left[2 D_1(k_\alpha) - A_\alpha \left\{ D_1(k_\alpha) + D_3(k_\alpha) \right\} \right] e^{-k_\alpha \tau} \right\}. \tag{50}$$

We may conclude, however, from equations (33) and (34) that

$$2 D_1 - A (D_1 + D_3) = \frac{2 D_1 (D_2 + D_4) - 2 D_2 (D_1 + D_3)}{D_2 + D_4} = 0\,. \tag{51}$$

Hence,

$$F_l + F_r = \tfrac{8}{3} b = F = \text{Constant}\,. \tag{52}$$

We can therefore rewrite equations (42) and (43) as follows:

$$I_{l,\,i} = \tfrac{3}{8}F\left\{\tau + \mu_i + Q + \sum_{\beta=1}^{n-1} \frac{L_\beta(1-\mu_i^2 A_\beta)}{1+\mu_i \kappa_\beta}\, e^{-\kappa_\beta \tau} + \sum_{\alpha=1}^{n} \frac{M_\alpha(1-\mu_i^2 A_\alpha)}{1+\mu_i k_\alpha}\, e^{-k_\alpha \tau}\right\} \tag{53}$$

$$(i = \pm 1, \ldots, \pm n)$$

and

$$I_{r,\,i} = \tfrac{3}{8}F\left\{\tau + \mu_i + Q + \sum_{\beta=1}^{n-1} \frac{L_\beta(1-A_\beta)}{1+\mu_i \kappa_\beta}\, e^{-\kappa_\beta \tau} + \sum_{\alpha=1}^{n} \frac{M_\alpha(1-A_\alpha)}{1+\mu_i k_\alpha}\, e^{-k_\alpha \tau}\right\} \tag{54}$$

$$(i = \pm 1, \ldots, \pm n).$$

In terms of the foregoing solutions for $I_{l,\,i}$ and $I_{r,\,i}$, we may establish the following formulae:

$$J_l = \tfrac{1}{2}\Sigma a_j I_{l,\,j} = \tfrac{3}{8}F\left\{\tau + Q + \frac{1}{2}\sum_{\beta=1}^{n-1} L_\beta(D_0 - D_2 A_\beta)\, e^{-\kappa_\beta \tau} + \frac{1}{2}\sum_{\alpha=1}^{n} M_\alpha(D_0 - D_2 A_\alpha)\, e^{-k_\alpha \tau}\right\}, \tag{55}$$

$$J_r = \tfrac{1}{2}\Sigma a_j I_{r,\,j} = \tfrac{3}{8}F\left\{\tau + Q + \frac{1}{2}\sum_{\beta=1}^{n-1} L_\beta D_0(1 - A_\beta)\, e^{-\kappa_\beta \tau} + \frac{1}{2}\sum_{\alpha=1}^{n} M_\alpha D_0(1 - A_\alpha)\, e^{-k_\alpha \tau}\right\}, \tag{56}$$

$$K_l = \tfrac{1}{2}\Sigma a_j I_{l,\,j}\mu_j^2 = \tfrac{3}{8}F\left\{\tfrac{1}{3}(\tau + Q) + \frac{1}{2}\sum_{\beta=1}^{n-1} L_\beta(D_2 - D_4 A_\beta)\, e^{-\kappa_\beta \tau} + \frac{1}{2}\sum_{\alpha=1}^{n} M_\alpha(D_2 - D_4 A_\alpha)\, e^{-k_\alpha \tau}\right\}, \tag{57}$$

and

$$K_r = \tfrac{1}{2}\Sigma a_j I_{r,\,j}\mu_j^2 = \tfrac{3}{8}F\left\{\tfrac{1}{3}(\tau + Q) + \frac{1}{2}\sum_{\beta=1}^{n-1} L_\beta D_2(1 - A_\beta)\, e^{-\kappa_\beta \tau} + \frac{1}{2}\sum_{\alpha=1}^{n} M_\alpha D_2(1 - A_\alpha)\, e^{-k_\alpha \tau}\right\}. \tag{58}$$

Now the Planck re-emission in the gray atmosphere is given by

$$B = J_l + J_r; \tag{59}$$

it now follows from equations (55) and (56) that

$$B = \tfrac{3}{4}F\left\{\tau + Q + \sum_{\beta=1}^{n-1} L_\beta\left[\tfrac{1}{2}D_0 - \tfrac{1}{4}(D_0 + D_2)\, A_\beta\right] e^{-\kappa_\beta \tau} + \sum_{\alpha=1}^{n} M_\alpha\left[\tfrac{1}{2}D_0 - \tfrac{1}{4}(D_0 + D_2)\, A_\alpha\right] e^{-k_\alpha \tau}\right\}. \tag{60}$$

On the other hand, from equation (32), we have

$$1 - \tfrac{3}{5} A = \tfrac{1}{2} D_0 - \tfrac{1}{4} (D_0 + D_2) A \; ; \tag{61}$$

hence

$$B = \tfrac{3}{4} F\{\tau + q[\tau]\} = \tfrac{3}{4} \sigma T_e^4 \{\tau + q[\tau]\} \; , \tag{62}$$

where

$$q[\tau] = Q + \sum_{\beta=1}^{n-1} L_\beta (1 - \tfrac{3}{5} A_\beta) \; e^{-\kappa_\beta \tau} + \sum_{\alpha=1}^{n} M_\alpha (1 - \tfrac{3}{5} A_\alpha) \; e^{-k_\alpha \tau} . \tag{63}$$

The temperature distribution in the atmosphere is therefore given by

$$T^4 = \tfrac{3}{4} T_e^4 \{\tau + q[\tau]\} . \tag{64}$$

Now the source functions for the two states of polarization are

$$\mathfrak{J}_l = \tfrac{3}{4} (1 - \lambda) \{2 (J_l - K_l) + \mu^2 (3 K_l - 2 J_l + J_r)\} + \tfrac{3}{2} \lambda (J_l + J_r) \tag{65}$$

and

$$\mathfrak{J}_r = \tfrac{3}{4} (1 - \lambda) \{J_r + K_l\} + \tfrac{1}{2} \lambda (J_l + J_r) ; \tag{66}$$

or, substituting for J_l, J_r, and K_l from equations (55), (56), and (57) and making use of equation (25), we obtain

$$\mathfrak{J}_l = \tfrac{3}{8} F \left\{ \tau + Q + \sum_{\beta=1}^{n-1} L_\beta (1 - \mu^2 A_\beta) \; e^{-\kappa_\beta \tau} + \sum_{\alpha=1}^{n} M_\alpha (1 - \mu^2 A_\alpha) \; e^{-k_\alpha \tau} \right\} , \tag{67}$$

and, from equation (26), equation (66) reduces to

$$\mathfrak{J}_r = \tfrac{3}{8} F \left\{ \tau + Q + \sum_{\beta=1}^{n-1} L_\beta (1 - A_\beta) \; e^{-\kappa_\beta \tau} + \sum_{\alpha=1}^{n} M_\alpha (1 - A_\alpha) \; e^{-k_\alpha \tau} \right\} . \tag{68}$$

With the explicit forms for the source functions now found, we can readily obtain formulae for the emergent intensity distribution from the general equation

$$I(0, \mu) = \int_0^\infty \mathfrak{J}(\tau, \mu) \; e^{-\tau/\mu} \frac{d\tau}{\mu} . \tag{69}$$

We have

$$I_l(0, \mu) = \tfrac{3}{8} F \left\{ \mu + Q + \sum_{\beta=1}^{n-1} L_\beta \frac{1 - \mu^2 A_\beta}{1 + \kappa_\beta \mu} + \sum_{\alpha=1}^{n} M_\alpha \frac{1 - \mu^2 A_\alpha}{1 + k_\alpha \mu} \right\} \tag{70}$$

and

$$I_r(0, \mu) = \tfrac{3}{8} F \left\{ \mu + Q + \sum_{\beta=1}^{n-1} L_\beta \frac{1 - A_\beta}{1 + \kappa_\beta \mu} + \sum_{\alpha=1}^{n} M_\alpha \frac{1 - A_\alpha}{1 + k_\alpha \mu} \right\} . \tag{71}$$

These expressions for $I_l(0, \mu)$ and $I_r(0, \mu)$ are in agreement with the solutions (53) and (54) for $\tau = 0$ at the points of the Gaussian division. This completes the solution of the problem in the $(n, 1)$ approximation.

V. NUMERICAL SOLUTION IN THE (2, 1) AND (3, 1) APPROXIMATIONS

i) SECOND APPROXIMATION

The dependence of the roots of the characteristic equation (38) on λ is best studied by rewriting equation (38) in the form

$$f = \left(1 - \frac{1}{k^2}\right)^2 (D_0 - 2)^2 = g = \frac{16}{9} \frac{\lambda}{1 - \lambda} D_0 - \frac{4\lambda}{1 - \lambda} + \frac{4}{9(1 - \lambda)} \tag{72}$$

and considering the behavior of f and g separately. The quantity g depends linearly on D_0, the slope depending on λ. In the second approximation, f spirals twice to infinity with increasing k^2. These functions are plotted in Figure 1. The intersections of these two functions for a given λ are the desired roots. The three roots of the pure scattering prob-

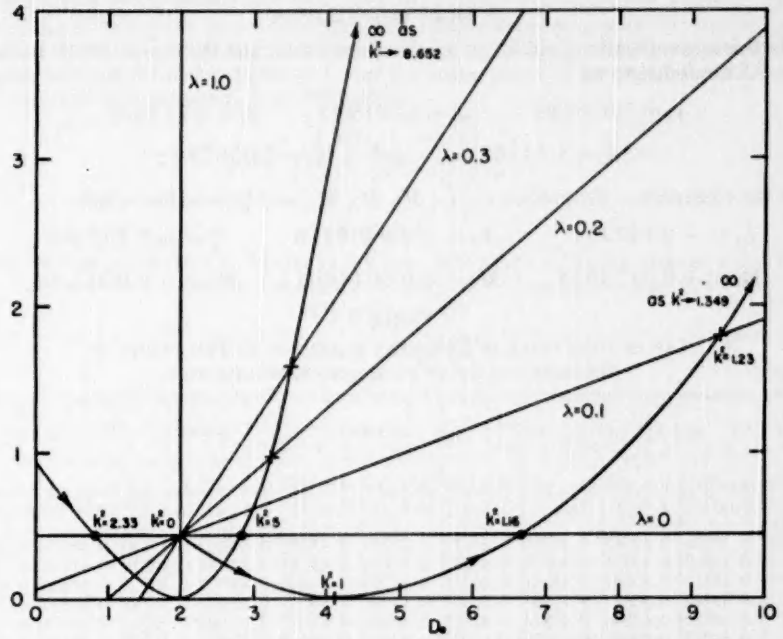

FIG. 1.—The ordinate gives the values of the f and g functions. The straight lines are the function g whose slope is determined by the value of λ. The intersections of the curve f with g correspond to the characteristic roots for a particular λ.

TABLE 1

CHARACTERISTIC ROOTS AND CONSTANTS OF INTEGRATION IN SECOND APPROXIMATION

λ	k_1^2	k_1^2	k_2^2	L_1	M_1	M_2	Q
0.0	2.33333	5.00000	1.16666	−0.19265	0.021830	0.029516	0.69638
0.1	2.64279	5.16668	1.22942	− .20056	.026086	.013964	.69596
0.2	2.92828	5.38307	1.26644	− .19828	.027410	.0069761	.69561
0.5	3.51820	6.35782	1.31843	− .16470	.014470	.000999	.69484
0.8	3.79150	7.67956	1.34006	− .13157	.002022	.0000823	.69441
0.9	3.84560	8.15974	1.34467	− .12336	0.000461	0.0000169	.69416
1.0	3.88889	.....	.....	−0.11668	.....	.....	0.69403

lem considered by Chandrasekhar[6] are the intersections of f with the horizontal line $g = 0.444$. The single root $k^2 = 3.889$ of the pure absorption problem is the intersection of f with the vertical line at $D_0 = 2$. This form of the characteristic equation is a convenient representation for computational purposes as well. In Table 1 the characteristic roots $\lambda = 0$, 0.1, 0.2, 0.5, 0.8, 0.9, and 1.0 are given along with the values for the con-

[6] Cf. Paper X, eq. (114).

stants L_1, M_1, M_2, and Q determined from the boundary conditions (45) and (46). The quantity $A(k)$ was computed from equation (34) for each characteristic root. The values of $I_l(0, \mu)$ and $I_r(0, \mu)$ were obtained for each of these cases from equations (70) and (71), and the law of darkening in the emergent radiation is tabulated in Table 2.

ii) THIRD APPROXIMATION

In this approximation f spirals to infinity three times, and the characteristic roots for $\lambda = 0.5$ are found to be

$$\kappa_1 = 3.088167\,, \qquad \kappa_2 = 1.208943\,; \qquad k_1 = 3.725616\,, \qquad k_2 = 1.444011\,, \quad \text{and} \quad k_3 = 1.070789\,; \tag{73}$$

and the constants of integration L_1, L_2, M_1, M_2, M_3, and Q have the values

$$L_1 = -0.141231\,, \qquad L_2 = -0.0400918\,, \qquad Q = +0.702509\,; \tag{74}$$
$$M_1 = +0.0124928\,, \qquad M_2 = +0.0014601\,, \qquad M_3 = -0.0002295\,.$$

TABLE 2

LAW OF DARKENING IN EMERGENT RADIATION IN TWO STATES OF POLARIZATION GIVEN BY SECOND APPROXIMATION

μ	$\lambda=0.1$		$\lambda=0.2$		$\lambda=0.5$		$\lambda=0.8$		$\lambda=0.9$	
	$\lvert I_l(0,\mu)\rvert/\lvert I_l(0,1)\rvert$	$\lvert I_r(0,\mu)\rvert/\lvert I_r(0,1)\rvert$	$\lvert I_l(0,\mu)\rvert/\lvert I_l(0,1)\rvert$	$\lvert I_r(0,\mu)\rvert/\lvert I_r(0,1)\rvert$	$\lvert I_l(0,\mu)\rvert/\lvert I_l(0,1)\rvert$	$\lvert I_r(0,\mu)\rvert/\lvert I_r(0,1)\rvert$	$\lvert I_l(0,\mu)\rvert/\lvert I_l(0,1)\rvert$	$\lvert I_r(0,\mu)\rvert/\lvert I_r(0,1)\rvert$	$\lvert I_l(0,\mu)\rvert/\lvert I_l(0,1)\rvert$	$\lvert I_r(0,\mu)/\rvert\lvert I_r(0,1)\rvert$
0.0	0.30416	0.36593	0.31077	0.36279	0.32739	0.35716	0.34087	0.35190	0.34503	0.35041
0.1	0.37939	0.43424	0.38598	0.43232	0.40184	0.42740	0.41400	0.42339	0.41761	0.42211
0.2	0.45217	0.50067	0.45781	0.49901	0.47299	0.49488	0.48373	0.49163	0.48686	0.49062
0.3	0.52246	0.56538	0.52898	0.56398	0.54201	0.56055	0.55132	0.55793	0.55399	0.55713
0.4	0.59319	0.62898	0.59824	0.62781	0.60956	0.62502	0.61746	0.62292	0.61971	0.62229
0.5	0.66223	0.69181	0.66654	0.69087	0.67606	0.68865	0.67782	0.68699	0.68443	0.68650
0.6	0.73062	0.75409	0.73413	0.75336	0.74179	0.75166	0.74696	0.75039	0.74842	0.75003
0.7	0.79850	0.81597	0.80117	0.81544	0.80694	0.81420	0.81078	0.81329	0.81186	0.81304
0.8	0.86597	0.87754	0.86777	0.87719	0.87163	0.87640	0.87416	0.87580	0.87488	0.87566
0.9	0.93312	0.93887	0.93379	0.93857	0.93596	0.93831	0.93720	0.93801	0.93758	0.93795
1.0	1.00000	1.00000	1.00000	1.00000	1.00000	1.00000	1.00000	1.00000	1.00000	1.00000

The corresponding laws of darkening for the emergent radiation in the two states of polarization take the numerical forms

$$I_l(0,\mu) = \tfrac{3}{8}F\Big\{\mu + 0.702509 - 0.141231\,\frac{1-0.494543\mu^2}{1+3.088167\mu} - 0.0400918\,\frac{1-0.4558133\mu^2}{1+1.208943\mu} + 0.0124928\,\frac{1-2.561096\mu^2}{1+3.725616\mu} + 0.0014601\,\frac{1-1.447584\mu^2}{1+1.444011\mu} - 0.0002295\,\frac{1-1.0717898\mu^2}{1+1.070789\mu}\Big\} \tag{75}$$

and

$$I_r(0,\mu) = \tfrac{3}{8}F\Big\{\mu + 0.702509 - \frac{0.0713861}{1+3.088167\mu} - \frac{0.0218174}{1+1.208943\mu} - \frac{0.0195024}{1+3.725616\mu} - \frac{0.0006535}{1+1.444011\mu} - \frac{0.00001648}{1+1.070789\mu}\Big\}. \tag{76}$$

Values of $I_l(0, \mu)$ and $I_r(0, \mu)$ obtained from the foregoing formulae for the case $\lambda = 0.5$ are given in Table 3. These results are compared with the values in the third approximation obtained by Chandrasekhar for the two limiting cases; pure scattering, $\lambda = 0$, and pure absorption, $\lambda = 1$.[7]

Comparison of the second and third approximations for $\lambda = 0.5$ and a similar comparison of the values for the second, third, and infinite approximations[8] for the limiting cases $\lambda = 0$ and $\lambda = 1$ indicate that the solution obtained in the third approximation is certainly accurate to within 1 per cent over the entire range of the variables.

The degree of polarization, $\delta(\mu)$, defined by

$$\delta(\mu) = \frac{I_r(0, \mu) - I_l(0, \mu)}{I_r(0, \mu) + I_l(0, \mu)}, \tag{77}$$

TABLE 3

LAWS OF DARKENING IN TWO STATES OF POLARIZATION GIVEN BY THIRD APPROXIMATION FOR $\lambda = 0.5$, 1.0, AND 0.0; DEGREE OF POLARIZATION OF EMERGENT RADIATION FOR $\lambda = 0.5$ AND 0.0

μ	$\lambda = 0.5$					$\lambda = 0.0$			$\lambda = 1.0$
	$[I_l(0, \mu)]/F$	$[I_r(0, \mu)]/F$	$[I_l(0, \mu)]/[I_l(0, 1)]$	$[I_r(0, \mu)]/[I_r(0, 1)]$	$\delta(\mu)$	$[I_l(0, \mu)]/[I_l(0, 1)]$	$[I_r(0, \mu)]/[I_r(0, 1)]$	$\delta(\mu)$	$\frac{1}{2}[I(0, \mu)]/[I(0, 1)]$
0.0	0.2006	0.2209	0.3202	0.3526	0.0482	0.2914	0.3659	0.1134	0.3460
0.1	.2510	.2677	0.4006	0.4272	.0321	0.3728	0.4382	.0806	0.4175
0.2	.2972	.3109	0.4743	0.4963	.0226	0.4486	0.5053	.0594	0.4926
0.3	.3411	.3524	0.5444	0.5625	.0164	0.5213	0.5699	.0445	0.5597
0.4	.3836	.3929	0.6122	0.6270	.0119	0.5921	0.6330	.0334	0.6249
0.5	.4250	.4326	0.6783	0.6905	.0089	0.6616	0.6953	.0248	0.6889
0.6	.4658	.4719	0.7434	0.7532	.0072	0.7303	0.7569	.0179	0.7520
0.7	.5064	.5109	0.8082	0.8154	.0044	0.7983	0.8181	.0122	0.8149
0.8	.5466	.5496	0.8724	0.8772	.0027	0.8659	0.8789	.0075	0.8767
0.9	.5867	.5882	0.9364	0.9387	0.0012	0.9331	0.9396	0.0034	0.9385
1.0	0.6265	0.6265	1.0000	1.0000	0	1.0000	1.0000	0	1.0000

is listed in Table 3. Comparison of the degree of polarization for $\lambda = 0$ with that for $\lambda = 0.5$ indicates that the reduction in polarization due to absorbing matter varies nearly linearly with λ. In Figure 2 the degree of polarization in the integrated light at the limb is plotted as a function of λ for the second and third approximations. It must be remembered, however, that only in the case of pure scattering, $\lambda = 0$, is the degree of polarization independent of frequency and, further, that all observations of early-type stars in which electron scattering is believed to play a dominant role are made far to the red of the energy maximum. We shall return to the question of frequency dependence in Section VIII.

The temperature distribution given by equation (64) is of value in providing a first approximation in the construction of model atmospheres for early-type stars. The temperature distribution in an atmosphere in which there is a small amount of gray absorbing matter in a predominantly electron-scattering atmosphere would be given by the limiting form of equation (63) for $\lambda = 0$. The equivalent of the Hopf-Bronstein relation for a pure scattering atmosphere may be found from the exact solution given by S.

[7] Cf. *Ap. J.*, **100**, 76, 1944, and Paper X, p. 365.

[8] For $\lambda = 0$ see *Ap. J.*, **105**, 439, 1947; for $\lambda = 1$ see *ibid.*, p. 445, eq. (30).

Chandrasekhar[9] as

$$J(0) = \frac{1}{2\sqrt{2}} F(c + \tfrac{1}{2}q), \tag{78}$$

where c and q are certain constants. This gives

$$J(0) = 0.43059\, F; \tag{79}$$

and the corresponding value of $q[0]$ in equation (64) defining the boundary temperature is $q[0] = 0.57412$, as compared to $q[0] = 0.57735$ for the gray-body case, $\lambda = 1$. As would be expected, $q[0]$ in the second approximation for $\lambda = 0.5$ is $q[0] = 0.57642$.

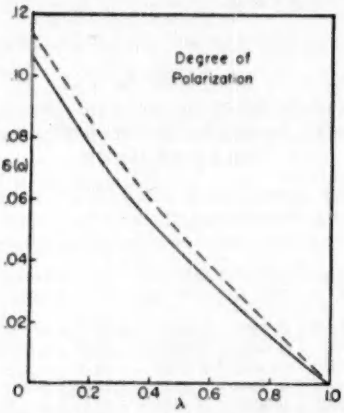

FIG. 2.—Degree of polarization at the limb. The solid line is the second approximation, and the dotted line the third approximation.

VI. FORMAL DISCUSSION OF THE $(n, 2)$ APPROXIMATION

The extension of the solution for the gray atmosphere given in Sections IV and V to the case in which the departures from grayness are slight is formally possible but one which may not be practicable. However, one important conclusion may be drawn from the existence of the K integral.

Returning to equations (9) and (10), we shall write them in their integrated form. We have

$$\mu \frac{dI_l}{d\tau} = I_l - \tfrac{3}{4}(1-\lambda)\{2(J_l - K_l) + \mu^2(3K_l - 2J_l + J_r)\} - \tfrac{1}{2}\lambda B + \lambda \int_0^\infty \delta_\nu (I_{l,\nu} - \tfrac{1}{2}B_\nu)\, d\nu \tag{80}$$

and

$$\mu \frac{dI_r}{d\tau} = I_r - \tfrac{3}{4}(1-\lambda)\{J_r + K_l\} - \tfrac{1}{2}\lambda B + \lambda \int_0^\infty \delta_\nu (I_{r,\nu} - \tfrac{1}{2}B_\nu)\, d\nu. \tag{81}$$

Integrating equations (80) and (81) over μ and using the condition of constant net flux, we obtain

$$B = J_l + J_r + \int_0^\infty \delta_\nu (J_{l,\nu} + J_{r,\nu} - B_\nu)\, d\nu. \tag{82}$$

[9] *Ap. J.*, **105**, 437, 1947.

If we now replace B in equations (80) and (81) by equation (82), we are able to express the equation of transfer completely in terms of I_l and I_r and their integrals in the following form:

$$\mu \frac{dI_l}{d\tau} = I_l - \tfrac{3}{4}(1-\lambda)\{2(J_l - K_l) + \mu^2(3K_l - 2J_l + J_r)\} - \tfrac{1}{2}\lambda(J_l + J_r) + \lambda\int_0^\infty \delta_\nu (I_{l,\nu} - \tfrac{1}{2}J_{l,\nu} - \tfrac{1}{2}J_{r,\nu})\, d\nu \tag{83}$$

and

$$\mu \frac{dI_r}{d\tau} = I_r - \tfrac{3}{4}(1-\lambda)\{J_r + K_l\} - \tfrac{1}{2}\lambda(J_l + J_r) + \lambda\int_0^\infty \delta_\nu (I_{r,\nu} - \tfrac{1}{2}J_{l,\nu} - \tfrac{1}{2}J_{r\nu})\, d\nu . \tag{84}$$

Multiplying equations (83) and (84) by μ and integrating, we have

$$\frac{dK_l}{d\tau} = \tfrac{1}{4}F_l + \tfrac{1}{4}\lambda\int_0^\infty \delta_\nu F_{l,\nu}\, d\nu \tag{85}$$

and

$$\frac{dK_r}{d\tau} = \tfrac{1}{4}F_r + \tfrac{1}{4}\lambda\int_0^\infty \delta_\nu F_{r,\nu}\, d\nu . \tag{86}$$

If we are to satisfy the K integral, then $\bar{\kappa}$ must be chosen so that

$$\int_0^\infty \delta_\nu F_\nu d\nu = 0 . \tag{87}$$

This implies that $\bar{\kappa}$ is to be defined as

$$\bar{\kappa} = \frac{1}{F}\int_0^\infty \kappa_\nu F_\nu^{(1)}\, d\nu , \tag{88}$$

where the superscript (1) refers to the values in the first approximation. This is the familiar mean-absorption coefficient first introduced by Chandrasekhar[10] for a pure absorbing atmosphere. An important conclusion may be drawn from equation (87) if δ_ν is independent of the optical depth τ. In that case equation (88) is equivalent to

$$\int_{-1}^{+1}\int_0^\infty \delta_\nu \mu \frac{dI_\nu^{(1)}}{d\tau}\, d\mu\, d\nu = 0 . \tag{89}$$

Returning to the equations of transfer (9) and (10), we can readily verify that

$$\int_{-1}^{+1}\int_0^\infty \delta_\nu \mu \frac{dI_\nu^{(1)}}{d\tau}\, d\mu\, d\nu = 2\int_0^\infty \delta_\nu (J_\nu^{(1)} - B_\nu^{(1)})\, d\nu . \tag{90}$$

From equations (90), (89), and (82) it now follows that

$$B = J_l + J_r . \tag{91}$$

This means that the temperature distribution is still defined by the mean intensities in the second approximation if δ_ν is independent of depth.

Since the term $\lambda\delta_\nu(I_{q,\nu} - \tfrac{1}{2}B_\nu)$ in equations (9) and (10) is of the second order itself in the small quantities λ and δ_ν, it should be expected, by virtue of equation (91), that

[10] *Ap. J.*, **101**, 334, eq. (42), 1945.

the temperature distribution determined in the $(n, 1)$ approximation will provide a satisfactory representation for the true temperature distribution of a star with a given value of λ.

Equations (83) and (84) may be solved by the method of variation of parameters. The numerical evaluation, however, is not possible without a knowledge of the monochromatic intensities. These could be obtained from the formal solution of the equation of transfer by iteration if approximate values are known; however, this would be a long, tedious task. We shall return to the discussion of the monochromatic intensities in the final section of this paper.

VII. PERTURBATION THEORY FOR $\lambda \to 1$

i) FORMULATION OF PROBLEM

In view of the near-linearity of the behavior of the solutions with λ and difficulties in computing values for each particular λ, it is worth while to consider perturbation methods for expressing the solutions in terms of λ. We shall first consider the case of λ near unity. The appropriate equations of transfer can obviously be written as follows:

$$\mu \frac{dI_i}{d\tau} = I_i - \tfrac{1}{2}\lambda (J_i + J_r) - (1-\lambda)\, \mathfrak{J}_i \tag{92}$$

and

$$\mu \frac{dI_r}{d\tau} = I_r - \tfrac{1}{2}\lambda (J_i + J_r) - (1-\lambda)\, \mathfrak{J}_r . \tag{93}$$

We shall let

$$I = I_i + I_r , \qquad J = J_i + J_r , \qquad \text{and} \qquad X = I_i - I_r ; \tag{94}$$

it then follows that

$$\mu \frac{dI}{d\tau} = I - J - (1-\lambda)(\mathfrak{J}_i + \mathfrak{J}_r - J) \tag{95}$$

and

$$\mu \frac{dX}{d\tau} = X - (1-\lambda)(\mathfrak{J}_i - \mathfrak{J}_r) . \tag{96}$$

When $(1-\lambda) \to 0$ the solution of the gray-atmosphere problem without scattering provides a first approximation. Thus

$$\mu \frac{dI^{(1)}}{d\tau} = I^{(1)} - J^{(1)} \tag{97}$$

and

$$X^{(1)} = 0 . \tag{98}$$

The solution of equation (97) in the nth approximation is

$$I_i^{(1)} = \tfrac{1}{4}F\left\{\tau + \mu_i + Q^{(1)} + \sum_{a=1}^{n-1} L_a^{(1)} \frac{e^{-k_a\tau}}{1+\mu_i k_a}\right\} \qquad (i = \pm 1, \ldots, \pm n) , \tag{99}$$

where the $L_a^{(1)}$'s and $Q^{(1)}$ are the constants given for solution of the gray-body problem;[11] also

$$J^{(1)} = \tfrac{1}{4}F\left\{\tau + Q^{(1)} + \sum_{a=1}^{n-1} L_a^{(1)}\, e^{-k_a\tau}\right\} , \tag{100}$$

$$K^{(1)} = \tfrac{1}{4}F\{\tau + Q^{(1)}\} \tag{101}$$

[11] *Ap. J.*, **100**, 80, 1944.

and

$$I_l^{(1)} = I_r^{(1)} = \tfrac{1}{2} I^{(1)}\,; \qquad J_l^{(1)} = J_r^{(1)} = \tfrac{1}{2} J^{(1)}\,; \qquad \text{and} \qquad K_l^{(1)} = K_r^{(1)} = \tfrac{1}{2} K^{(1)}\,. \tag{102}$$

Now, returning to equation (95), we shall evaluate the third term on the right-hand side in terms of the solutions (100) and (101). This provides us with a second approximation.

Now from equations (4) and (5) we see that

$$(\mathfrak{I}_l + \mathfrak{I}_r - J) = \tfrac{3}{4}\{2J_l + J_r - K_l + \mu^2(3K_l - 2J_l + J_r)\} - J\,; \tag{103}$$

but in our first approximation, by virtue of equations (102), we have

$$[\mathfrak{I}_l^{(1)} + \mathfrak{I}_r^{(1)} - J^{(1)}] = \tfrac{3}{8}\{(\tfrac{1}{3} - \mu^2)[J^{(1)} - 3K^{(1)}]\}. \tag{104}$$

Substituting equations (100) and (101) in (104), we obtain

$$[\mathfrak{I}_l^{(1)} + \mathfrak{I}_r^{(1)} - J^{(1)}] = \tfrac{9}{32} F(\tfrac{1}{3} - \mu^2) \sum_{a=1}^{n-1} L_a^{(1)} e^{-k_a \tau}. \tag{105}$$

Inserting this expression in equation (95) and replacing it by a system of linear equations in the usual manner, we obtain the following set of nonhomogeneous equations:

$$\mu_i \frac{dI_i^{(2)}}{d\tau} = I_i^{(2)} - \tfrac{1}{2}\Sigma a_j I_j^{(2)} - (1-\lambda)\tfrac{9}{32} F(\tfrac{1}{3} - \mu^2) \sum_{a=1}^{n-1} L_a^{(1)} e^{-k_a \tau} \tag{106}$$

$$(i = \pm 1, \ldots, \pm n).$$

The most convenient method of solving this system of equations is the method of variation of parameters. Thus, writing the general solution in the form

$$I_i^{(2)} = \tfrac{3}{4} F\left\{\tau + \mu_i + Q^{(2)}(\tau) + \sum_{a=1}^{n-1} \frac{L_a^{(2)}(\tau)\, e^{-k_a \tau}}{1 + \mu_i k_a} + \sum_{a=1}^{n-1} \frac{L_{-a}^{(2)}(\tau)\, e^{+k_a \tau}}{1 - \mu_i k_a}\right\} \tag{107}$$

$$(i = \pm 1, \ldots, \pm n),$$

we readily obtain the variational equation

$$\mu_i \left\{\frac{dQ^{(2)}}{d\tau} + \sum_{a=1}^{n-1} \frac{e^{-k_a \tau}}{1 + \mu_i k_a} \frac{dL_a^{(2)}}{d\tau} + \sum_{a=1}^{n-1} \frac{e^{+k_a \tau}}{1 - \mu_i k_a} \frac{dL_{-a}^{(2)}}{d\tau}\right\} \tag{108}$$

$$= -\tfrac{3}{8}(1-\lambda)(\tfrac{1}{3} - \mu^2) \sum_{a=1}^{n-1} L_a^{(1)} e^{-k_a \tau} \qquad (i = \pm 1, \ldots, \pm n).$$

On multiplying equation (108) by a_i and summing over all i's, the equation is satisfied identically. This corresponds to the assumption of constant net flux. Next, multiplying by $a_i \mu_i$ and summing, we obtain

$$\frac{dQ^{(2)}}{d\tau} = 0\,, \qquad Q^{(2)} = Q^{(1)} + \Delta Q(\lambda)\,. \tag{109}$$

This is equivalent to the K integral.

The variational equations now become

$$\mu_i \left\{\sum_{a=1}^{n-1} \frac{e^{-k_a \tau}}{1 + \mu_i k_a} \frac{dL_a^{(2)}}{d\tau} + \sum_{a=1}^{n-1} \frac{e^{+k_a \tau}}{1 - \mu_i k_a} \frac{dL_{-a}^{(2)}}{d\tau}\right\} \tag{110}$$

$$= -\tfrac{3}{8}(1-\lambda)(\tfrac{1}{3} - \mu^2) \sum_{a=1}^{n-1} L_a^{(1)} e^{-k_a \tau} \qquad (i = \pm 1, \ldots, \pm n),$$

which represents $(2n-2)$ linearly independent equations for the determination of the $(2n-2)$ constants $L_a^{(2)}$ and $L_{-a}^{(2)}$. Now, multiplying equations (110) by $a_i\mu_i^{m-1}$ $(m=1, \ldots, 2n)$ and summing over all, we obtain

$$\sum_{a=1}^{n-1} D_{m,a}\, e^{-k_a\tau}\frac{dL_a^{(2)}}{d\tau} + (-1)^m \sum_{a=1}^{n-1} D_{m,a}\, e^{+k_a\tau}\frac{dL_{-a}^{(2)}}{d\tau} = \frac{3}{8}\left(\frac{2}{m+2}-\frac{2}{3m}\right)\epsilon_{m,\,\text{odd}}\,(1-\lambda)\sum_{a=1}^{n-1} L_a^{(1)}\, e^{-k_a\tau} \qquad (m=1, \ldots, 2n), \tag{111}$$

where all the quantities have their usual meanings.[12] We shall now pass directly to the solution of the equations in the second approximation, (2, 2).

ii) SOLUTION IN THE (2, 2) APPROXIMATION

In the (2, 2) approximation, equations (111) yield the following pair of equations:

$$D_{3,1}\, e^{-k_1\tau}\frac{dL_1^{(2)}}{d\tau} - D_{3,1}\, e^{+k_1\tau}\frac{dL_{-1}^{(2)}}{d\tau} = \tfrac{1}{15}\,(1-\lambda)\,L_1^{(1)}\, e^{-k_1\tau} \tag{112}$$

and

$$e^{-k_1\tau}\frac{dL_1^{(2)}}{d\tau} + e^{+k_1\tau}\frac{dL_{-1}^{(2)}}{d\tau} = 0\,. \tag{113}$$

Solving these equations for $L_1^{(2)}$ and $L_{-1}^{(2)}$, we find

$$L_1^{(2)} = (1-\lambda)\frac{L_1^{(1)}\tau}{30\,D_{3,1}} + L_1^{(1)} + \Delta L_1 \tag{114}$$

and

$$L_{-1}^{(2)} = (1-\lambda)\frac{L_1^{(1)}}{30\,D_{3,1}k_1}\, e^{-2k_1\tau} + \Delta L_{-1}\,, \tag{115}$$

where a superscript (1) refers to the values of these constants in the limit $\lambda = 1$. Substituting equations (109), (114), and (115) in equation (107), we obtain

$$I_i^{(2)} = \tfrac{3}{4}F\Big\{\tau+\mu_i+Q^{(1)}+\frac{L_1^{(1)}\, e^{-k_1\tau}}{1+\mu_i k_1}+\Delta Q+\frac{\Delta L_1\, e^{-k_1\tau}}{1+\mu_i k_1}+\frac{\Delta L_{-1}\, e^{+k_1\tau}}{1-\mu_i k_1}+(1-\lambda) \times\left[\frac{L_1^{(1)}\tau}{30\,D_{3,1}}\,\frac{e^{-k_1\tau}}{1+\mu_i k_1}+\frac{L_1^{(1)}}{60\,D_{3,1}k_1}\,\frac{e^{-k_1\tau}}{1-\mu_i k_1}\right]\Big\} \qquad (i=\pm 1, \pm 2)\,. \tag{116}$$

Now the boundary conditions require that no I_i's increase exponentially as $\tau\to\infty$. Applying this condition, we obtain

$$I_i^{(2)} = \tfrac{3}{4}F\Big\{\tau+\mu_i+Q^{(1)}+\frac{L_1^{(1)}\, e^{-k_1\tau}}{1+\mu_i k_1}+\Delta Q+\frac{\Delta L_1\, e^{-k_1\tau}}{1+\mu_i k_1} + (1-\lambda)\left[\frac{L_1^{(1)}\tau}{30\,D_{3,1}}\,\frac{e^{-k_1\tau}}{1+\mu_i k_1}+\frac{L_1^{(1)}}{60\,D_{3,1}k_1}\,\frac{e^{-k_1\tau}}{1-\mu_i k_1}\right]\Big\} \qquad (i=\pm 1, \pm 2)\,. \tag{117}$$

The second boundary condition, that at $\tau = 0$ there is no incident radiation, gives

$$-\mu_i+Q^{(1)}+\frac{L_1^{(1)}}{1-\mu_i k_1}+\Delta Q+\frac{\Delta L_1}{1-\mu_i k_1}+(1-\lambda)\frac{L_1^{(1)}}{60\,D_{3,1}k_1}\,\frac{1}{1+\mu_i k_1}=0 \qquad (i=+1,+2) \tag{118}$$

[12] Cf. *Ap. J.*, **101**, 335, 1945.

but $Q^{(1)}$ and $L_1^{(1)}$ are determined by the equation

$$-\mu_i + Q^{(1)} + \frac{L_1^{(1)}}{1-\mu_i k_1} = 0 \qquad (i = +1, +2); \tag{119}$$

hence

$$\Delta Q + \frac{\Delta L_1}{1-\mu_i k_1} = -(1-\lambda)\frac{L_1^{(1)}}{60 D_{3,1} k_1}\frac{1}{1+\mu_i k_1} \qquad (i = +1, +2). \tag{120}$$

These two equations may be solved for ΔQ and ΔL_1, and we obtain

$$\Delta Q = (1-\lambda)\, c_1; \qquad \Delta L_1 = (1-\lambda)\, c_2, \tag{121}$$

where

$$c_1 = \frac{-L_1^{(1)}}{60 D_{3,1} k_1}\frac{1}{(1+\mu_1 k_1)(1+\mu_2 k_1)} = +0.001294 \tag{122}$$

and

$$c_2 = \frac{-L_1^{(1)}}{60 D_{3,1} k_1}\frac{(1-\mu_1 k_1)(1-\mu_2 k_1)}{(1+\mu_1 k_1)(1+\mu_2 k_1)} = -0.0001489. \tag{123}$$

Equation (117) now becomes

$$I_i^{(2)} = \tfrac{3}{4}F\Big\{\tau + \mu_i + Q^{(1)} + \frac{L_1^{(1)} e^{-k_1\tau}}{1+\mu_i k_1} + (1-\lambda)\Big[c_1 + \frac{c_2 e^{-k_1\tau}}{1+\mu_i k_1} + \frac{2 c_3 k_1 \tau e^{-k_1\tau}}{1+\mu_i k_1} + \frac{c_3 e^{-k_1\tau}}{1-\mu_i k_1}\Big]\Big\} \qquad (i = \pm 1, \pm 2), \tag{124}$$

where

$$c_3 = \frac{L_1^{(1)}}{60 D_{3,1} k_1} = -0.0029169. \tag{125}$$

It follows from equation (124) that

$$J^{(2)} = \tfrac{3}{4}F\{\tau + Q^{(1)} + L_1^{(1)} e^{-k_1\tau} + (1-\lambda) \times [c_1 + c_2 e^{-k_1\tau} + 2 c_3 k_1 \tau e^{-k_1\tau} + c_3 e^{-k_1\tau}]\}. \tag{126}$$

The source function of equation (95) in the present approximation is

$$\mathfrak{J}^{(2)} = J^{(2)} + \tfrac{3}{8}(1-\lambda)(\tfrac{1}{3} - \mu^2)[J^{(1)} - 3K^{(1)}], \tag{127}$$

or

$$\mathfrak{J}^{(2)} = \tfrac{3}{4}F\{\tau + Q^{(1)} + L_1^{(1)} e^{-k_1\tau} + (1-\lambda)[c_1 + c_2 e^{-k_1\tau} + 2 c_3 k_1 \tau e^{-k_1\tau} + c_3 e^{-k_1\tau} + \tfrac{3}{8}(\tfrac{1}{3} - \mu^2) L_1^{(1)} e^{-k_1\tau}]\}; \tag{128}$$

and, evaluating the emergent intensity according to

$$I(0, \mu) = \int_0^\infty \mathfrak{J} e^{-\tau/\mu}\frac{d\tau}{\mu}, \tag{129}$$

we obtain

$$I^{(2)}(0, \mu, \lambda) = \tfrac{3}{4}F\Big\{\mu + Q^{(1)} + \frac{L_1^{(1)}}{1+\mu k_1} + (1-\lambda)\Big[c_1 + \frac{c_2}{1+\mu k_1} + \frac{c_3}{1+\mu k_1} + \frac{3}{8}\frac{(\tfrac{1}{3} - \mu^2) L_1^{(1)}}{1+\mu k_1} + \frac{2 c_3 \mu}{(1+\mu k_1)^2}\Big]\Big\}. \tag{130}$$

This may be written as

$$I(0, \mu, \lambda) = I(0, \mu, 1) + (1 - \lambda) F \Delta_I(\mu), \tag{131}$$

where

$$\Delta_I(\mu) = c_1 + \left[c_2 + c_3 + \tfrac{3}{8} (\tfrac{1}{3} - \mu^2) L_1^{(1)} + \frac{2 c_2 \mu}{1 + \mu k_1} \right] \frac{1}{1 + \mu k_1}; \tag{132}$$

We now return to equation (96). This may be integrated directly. Evaluating the terms proportional to $(1 - \lambda)$ in this equation in terms of the solution for the case $\lambda = 1$, we have

$$\mu \frac{d X^{(2)}}{d \tau} = X^{(2)} - (1 - \lambda) \tfrac{9}{32} F \left\{ \tfrac{1}{2} (1 - \mu^2) \sum_{a=1}^{n-1} L_a^{(1)} e^{-k_a \tau} \right\}. \tag{133}$$

Hence

$$\int_\tau^\infty d [X e^{-\tau/\mu}] = - \frac{(1 - \lambda)}{\mu} \tfrac{9}{32} F \int_\tau^\infty \left\{ \tfrac{1}{2} (1 - \mu^2) \sum_{a=1}^{n-1} L_a^{(1)} e^{-k_a t} \right\} e^{-t/\mu} dt, \tag{134}$$

or

$$X = (1 - \lambda) \tfrac{9}{32} F (1 - \mu^2) \sum_{a=1}^{n-1} \frac{L_a^{(1)}}{1 + \mu k_a} e^{-k_a \tau}. \tag{135}$$

In the (2, 2) approximation we have, therefore, the following form for the intensity difference in the emergent radiation:

$$X(0, \mu, \lambda) = (1 - \lambda) F \Delta_X(\mu), \tag{136}$$

where

$$\Delta_X(\mu) = \tfrac{9}{32} (1 - \mu^2) \frac{L_1^{(1)}}{1 + \mu k_1} = - 0.032815 \frac{1 - \mu^2}{1 + \mu k_1}. \tag{137}$$

The values of $\Delta_I(\mu)$ and $\Delta_X(\mu)$ are tabulated in Table 4.

The degree of polarization is

$$\delta(\mu) = \frac{X(0, \mu, \lambda)}{I(0, \mu, \lambda)}, \tag{138}$$

while the intensities in the two states of polarization are

$$I_l(0, \mu, \lambda) = \tfrac{1}{2} [I(0, \mu, \lambda) + X(0, \mu, \lambda)] \tag{139}$$

and

$$I_r(0, \mu, \lambda) = \tfrac{1}{2} [I(0, \mu, \lambda) - X(0, \mu, \lambda)]. \tag{140}$$

In Table 5 the results of the law of darkening have been tabulated for the case $\lambda = 0.9$. A comparison of these results with those found earlier, in Table 2, by the general method indicates that, for values of $(1 - \lambda)$ less than 0.1, the agreement is better than 0.4 per cent over the entire range of the variables. It is better than 0.8 per cent for the range from $\lambda = 0.8$ to $\lambda = 1.0$.

It is of interest to point out that the perturbation method provides a means for discussing the problem when λ is a function of the optical depth. For each of the constants of integration involving λ there is an integral equation defining the appropriate mean value of λ to be used. For example, the mean value of λ for the differences of intensities X is defined according to the equation

$$\overline{(1 - \lambda)} \int_0^\infty e^{-(k_1 + 1/\mu)\tau} d\tau = \int_0^\infty (1 - \lambda) e^{-(k_1 + 1/\mu)\tau} d\tau; \tag{141}$$

this follows from equation (143).

A similar perturbation theory may be developed for small departures around any value of λ. This has been done for $\lambda \to 0$. The development is somewhat lengthy because of the more complicated nature of the solution for $\lambda = 0$ and will not be given here. The results are perhaps significant only in that they would provide a method for calculating the mean value of λ when λ varies with optical depth and, further, that they indicate that linear interpolation for intermediate values of λ from Table 2 provides an accuracy of 1 per cent within the second approximation.

TABLE 4

CORRECTION TERMS $\Delta(\mu)_I$ AND $\Delta(\mu)_X$ PROPORTIONAL TO $(1-\lambda)$ FOR $\lambda \to 1$ IN SECOND APPROXIMATION AND LAW OF DARKENING FOR $\lambda = 1$

μ	$\Delta(\mu)_I$	$\Delta(\mu)_X$	$[I(0,\mu,1)]/F$	μ	$\Delta(\mu)_I$	$\Delta(\mu)_X$	$[I(0,\mu,1)]/F$
0.0	−0.01636	−0.03282	0.43301	0.6	−0.00032	−0.00962	0.93044
0.1	− .01349	− .02714	.52243	0.7	+ .00216	− .00703	1.00876
0.2	− .01071	− .02259	.60776	0.8	+ .00460	− .00458	1.08657
0.3	− .00802	− .01876	.69054	0.9	+ .00701	− .00225	1.16398
0.4	− .00539	− .01541	.77160	1.0	+0.00941	0.00000	1.24108
0.5	−0.00283	−0.01239	0.85146				

TABLE 5

COMPARISON OF PERTURBATION THEORY, $\lambda \to 1$, FOR $\lambda = 0.9$ WITH LAW OF DARKENING FROM GENERAL THEORY IN SECOND APPROXIMATION

μ	PERTURBATION THEORY FOR $\lambda=0.9$ (2, 2) APPROXIMATION							GENERAL THEORY $\lambda=0.9$	
	$[X(\mu,\lambda)]/F$	$[I(\mu,\lambda)]/F$	$[I_I(0,\mu,\lambda)]/F$	$[I_r(0,\mu,\lambda)]/F$	$\delta(\mu)$	$[I_I(0,\mu)]/[I_I(0,1)]$	$[I_r(0,\mu)]/[I_r(0,1)]$	$[I_I(0,\mu)]/[I_I(0,1)]$	$[I_r(0,\mu)]/[I_r(0,1)]$
0.0	−0.00328	0.43138	0.21405	0.21733	0.0076	0.34468	0.34996	0.34502	0.35041
0.1	− .00271	0.52108	.25918	.26190	.0052	0.41774	0.42173	0.41761	0.42211
0.2	− .00226	0.60669	.30222	.30448	.0037	0.48666	0.49029	0.48686	0.49062
0.3	− .00188	0.68974	.34393	.34581	.0027	0.55383	0.55685	0.55399	0.55713
0.4	− .00154	0.77106	.38476	.38630	.0020	0.61951	0.62206	0.61971	0.62229
0.5	− .00124	0.85118	.42497	.42621	.0015	0.68432	0.68632	0.68443	0.68650
0.6	− .00096	0.93041	.46472	.46568	.0010	0.74834	0.74988	0.74842	0.75003
0.7	− .00070	1.00897	.50414	.50489	.0007	0.81180	0.81301	0.81186	0.81304
0.8	− .00046	1.08703	.54329	.54374	.0004	0.87485	0.87558	0.87488	0.87566
0.9	− .00022	1.16468	.58223	.58245	.0002	0.93756	0.93792	0.93758	0.93795
1.0	−0.00000	1.24202	0.62101	0.62101	0.0000	1.00000	1.00000	1.00000	1.00000

VIII. MONOCHROMATIC DISTRIBUTION OF THE EMERGENT RADIATION

i) *n*TH APPROXIMATION

It is clear that at a frequency ν, the equations of transfer (1) and (2) may be written in the form

$$\mu \frac{dI_{I,\nu}}{d\tau} = I_{I,\nu} - \tfrac{3}{4}(1-\lambda_\nu)\{2(J_{I,\nu} - K_{I,\nu}) + \mu^2(3K_{I,\nu} - 2J_{I,\nu} + J_{r,\nu})\} - \tfrac{1}{2}\lambda_\nu B_\nu(\tau) \tag{142}$$

and

$$\mu \frac{dI_{r,\nu}}{d\tau} = I_{r,\nu} - \tfrac{3}{4}(1-\lambda_\nu)\{J_{r,\nu} + K_{I,\nu}\} - \tfrac{1}{2}\lambda_\nu B_\nu(\tau), \tag{143}$$

where

$$\lambda_\nu = \frac{\kappa_\nu}{\sigma + \kappa_\nu}. \tag{144}$$

We shall assume that λ_ν is independent of the optical depth, τ, and that the Planck intensity, $B_\nu(\tau)$, is expressible as a linear function of τ, thus:

$$B_\nu(\tau) = B^{(0)} + B^{(1)}\tau . \tag{145}$$

Expressions for $B^{(0)}$ and $B^{(1)}$ may be obtained by expanding B_ν as a Taylor series from $\tau = 0$, using the temperature distribution given by equation (64). Substituting for $B_\nu(\tau)$ in equations (142) and (143) and following the usual procedure of replacing the integrals by sums, we obtain the following system of $4n$ nonhomogeneous linear equations:

$$\mu_i \frac{dI_{i,i}}{d\tau} = I_{i,i} - \tfrac{3}{8}(1-\lambda)\{2\Sigma a_j I_{i,j}(1-\mu_j^2) + \mu_i^2[\Sigma a_j I_{i,j}(3\mu_j^2 - 2) + \Sigma a_j I_{r,j}]\} - \tfrac{1}{2}\lambda[B^{(0)} + B^{(1)}\tau] \qquad (i = \pm 1, \ldots, \pm n) \tag{146}$$

and

$$\mu_i \frac{dI_{r,i}}{d\tau} = I_{r,i} - \tfrac{3}{8}(1-\lambda)[\Sigma a_j I_{r,j} + \Sigma a_j I_{i,j}\mu_j^2] - \tfrac{1}{2}\lambda[B^{(0)} + B^{(1)}\tau] \qquad (i = \pm 1, \ldots, \pm n), \tag{147}$$

where, for convenience, we have suppressed the suffix ν.

Consider, first, the homogeneous parts of equations (146) and (147). We shall seek a solution of the form

$$I_{i,i} = g_i e^{-k\tau} \quad \text{and} \quad I_{r,i} = h_i e^{-k\tau} . \tag{148}$$

Substituting these in the corresponding homogeneous equations, we find that the constants g_i and h_i must be expressible in the forms

$$g_i = \frac{\alpha\mu_i^2 + \beta}{1 + \mu_i k} \quad \text{and} \quad h_i = \frac{\alpha + \beta}{1 + \mu_i k}, \tag{149}$$

where α and β are constants. On substituting equations (149) back in the original equations and equating coefficients of the different powers of μ_i, we obtain

$$\tfrac{8}{3}\alpha = [\alpha(3D_4 - 2D_2 + D_0) + \beta(3D_2 - D_0)](1-\lambda) \tag{150}$$

and

$$\tfrac{4}{3}\beta = [\alpha(D_2 - D_4) + \beta(D_0 - D_2)](1-\lambda) . \tag{151}$$

The determinant of these equations must vanish, therefore, as follows:

$$\begin{vmatrix} [3D_4 - 2D_2 + D_0](1-\lambda) - \frac{8}{3} & [3D_2 - D_0](1-\lambda) \\ [D_2 - D_4](1-\lambda) & [D_0 - D_2](1-\lambda) - \frac{4}{3} \end{vmatrix} = 0 . \tag{152}$$

This is the characteristic equation. We shall return to the discussion of the evaluation of the characteristic roots from the characteristic equation later.

From equation (151) we now obtain

$$-\frac{\alpha}{\beta} = A(k) = \frac{D_2 - D_0 + \frac{4}{3}(1-\lambda)}{D_4 - D_2} . \tag{153}$$

In terms of $A(k)$ the general solution of the homogeneous part of equations (146) and (147) may be written in terms of the integrals

$$I_{l,\,i} = \text{Constant}\left[\frac{1-\mu_i^2 A\,(k_a)}{1 \pm k_a\mu_i}\right] e^{\mp k_a\tau}$$
$$I_{r,\,i} = \text{Constant}\left[\frac{1-A\,(k_a)}{1 \pm k_a\mu_i}\right] e^{\mp k_a\tau} \qquad \begin{cases} (i = \pm 1, \ldots, \pm n) \\ (a = 1, \ldots, 2n)\,. \end{cases} \tag{154}$$

Now a particular integral of the equations of transfer (146) and (147) is

$$I_{l,\,i} = I_{r,\,i} = \tfrac{1}{2}\left[\mu B^{(1)} + \tau B^{(1)} + B^{(0)}\right]. \tag{155}$$

When we combine solutions (154) and (155), the general solution of the equations of transfer becomes

$$I_{l,\,i} = \tfrac{1}{2}B^{(1)}\left\{\sum_{a=-2n}^{2n} M_a \frac{1-\mu_i^2 A_a}{1+k_a\mu_i}\, e^{-k_a\tau} + \mu_i + \tau + \frac{B^{(0)}}{B^{(1)}}\right\} \qquad (i = \pm 1, \ldots, \pm n) \tag{156}$$

and

$$I_{r,\,i} = \tfrac{1}{2}B^{(1)}\left\{\sum_{a=-2n}^{2n} M_a \frac{1-A_a}{1+k_a\mu_i}\, e^{-k_a\tau} + \mu_i + \tau + \frac{B^{(0)}}{B^{(1)}}\right\} \qquad (i = \pm 1, \ldots, \pm n)\,. \tag{157}$$

The boundary condition that none of the I_i's tend to infinity exponentially as $\tau \to \infty$ implies that we omit the terms in exp $(+k_a\tau)$. The condition that there be no incident radiation on $\tau = 0$ requires that

$$\sum_{a=1}^{2n} M_a \frac{1-\mu_i^2 A_a}{1-k_a\mu_i} = \mu_i - \frac{B^{(0)}}{B^{(1)}} \qquad (i = 1, \ldots, n) \tag{158}$$

and

$$\sum_{a=1}^{2n} M_a \frac{1-A_a}{1-k_a\mu_i} = \mu_i - \frac{B^{(0)}}{B^{(1)}} \qquad (i = 1, \ldots, n)\,. \tag{159}$$

Equations (158) and (159) determine the $2n$, M_a's, while $B^{(0)}$ and $B^{(1)}$ are related to the emergent flux. It is more convenient for the practical determination of these constants to rewrite equations (158) and (159) in the form

$$\sum_{a=1}^{2n} \frac{M_a}{1-\mu_i k_a} = \mu_i - \frac{B^{(0)}}{B^{(1)}} \qquad (i = 1, \ldots, n) \tag{160}$$

and

$$\sum_{a=1}^{2n} \frac{M_a A_a}{1-\mu_i k_a} = 0 \qquad (i = 1, \ldots, n)\,. \tag{161}$$

Now, as with the earlier problem in the integrated flux, it is not difficult to pass over from the intensities at the points of the Gaussian division to the explicit form for the intensity distribution of the emergent radiation, by evaluating the source function. The resulting expressions for the emergent intensity are

$$I_l(0, \mu) = \tfrac{1}{2}B^{(1)}\left\{\sum_{a=1}^{2n} M_a \frac{1-\mu^2 A_a}{1+k_a\mu} + \mu + \frac{B^{(0)}}{B^{(1)}}\right\} \tag{162}$$

and

$$I_r(0, \mu) = \tfrac{1}{2}B^{(1)}\left\{\sum_{a=1}^{2n} M_a \frac{1-A_a}{1+k_a\mu} + \mu + \frac{B^{(0)}}{B^{(1)}}\right\}. \tag{163}$$

ii) NUMERICAL SOLUTION IN THE SECOND APPROXIMATION

In the numerical solution the first task is that of evaluating the characteristic roots. After some minor reductions, equation (152) becomes

$$[(D_0 - D_2)^2 + 4D_4 - \tfrac{4}{3}D_2](1-\lambda)^2 - 4[D_0 - D_4 - \tfrac{4}{3}D_2](1-\lambda) + \tfrac{32}{9} = 0\,. \quad (164)$$

In the second approximation

$$D_0 = \frac{2a_1}{1-\mu_1^2 x} + \frac{2a_2}{1-\mu_2^2 x}; \qquad D_2 = \frac{2a_1\mu_1^2}{1-\mu_1^2 x} + \frac{2a_2\mu_2^2}{1-\mu_2^2 x}; \qquad D_4 = \frac{2a_1\mu_1^4}{1-\mu_1^2 x} + \frac{2a_2\mu_2^4}{1-\mu_2^2 x}, \quad (165)$$

where μ_1 and μ_2 are the points of the Gaussian division, a_1 and a_2 the corresponding weights, and x the square of the characteristic root. Combining equations (164) and (165) and using the numerical values of a_1, a_2, μ_1, and μ_2, we find

$$\begin{aligned}[2.48889 - 2.94603x + 0.82866x^2](1-\lambda)^2 - [6.04444 - 8.68571x \\ + 3.52217x^2 - 0.30041x^3](1-\lambda) + [3.55556 - 6.09523x \\ + 3.22176x^2 - 0.52245x^3 + 0.026122x^4] = 0\,.\end{aligned} \quad (166)$$

This quartic equation in X may be solved by standard methods for a given value of λ.

We shall consider here the case $\lambda = 0.5$ as a representative intermediate case. The solution of equation (166) for $\lambda = 0.5$ gives the four roots

$$k_1^2 = 0.94368\,; \qquad k_2^2 = 1.32273\,;$$

$$k_3^2 = 5.31137\,; \qquad k_4^2 = 6.67235\,.$$

Now, for $\lambda = 0.5$, equation (153) for $A(k)$ becomes

$$A(k) = \frac{D_2 - D_0 + \frac{8}{3}}{D_4 - D_2}, \quad (167)$$

or, by virtue of the recursion formulae (33),

$$A(k) = k^2 \frac{(1-k^2)D_2 + \frac{2}{3}}{(1-k^2)D_2 - \frac{2}{3}}. \quad (168)$$

From equations (160) and (161) we obtain the constants of integration,

$$\begin{aligned} M_1 &= +0.067090 - 0.083963\,\frac{B^{(0)}}{B^{(1)}}, \\ M_2 &= +0.004847 - 0.006701\,\frac{B^{(0)}}{B^{(1)}}, \\ M_3 &= +0.055287 - 0.225262\,\frac{B^{(0)}}{B^{(1)}}, \end{aligned} \quad (169)$$

and

$$M_4 = -0.002870 + 0{,}021559\,\frac{B^{(0)}}{B^{(1)}},$$

while from equation (168) we have

$$A(k_1) = -1.30177\,; \qquad A(k_2) = 1.13572\,;$$
$$A(k_3) = 0.86669 \qquad A(k_4) = 4.24401\,. \tag{170}$$

Using the foregoing expressions, we find equations (162) and (163) to be

$$I_l(0,\mu) = \tfrac{1}{2}\,[P_l B^{(1)} + S_l B^{(0)}] \tag{171}$$

and

$$I_r(0,\mu) = \tfrac{1}{2}\,[P_r B^{(1)} + S_r B^{(0)}]\,, \tag{172}$$

where

$$P_l = \mu + 0.067089\,\frac{1+1.30177\mu^2}{1+0.97143\mu} + 0.004847\,\frac{1-1.13572\mu^2}{1+1.15010\mu} + 0.055287\,\frac{1-0.86669\mu^2}{1+2.30464\mu} - 0.002869\,\frac{1-4.24401\mu^2}{1+2.58309\mu}\,; \tag{173}$$

$$S_l = 1 - 0.083963\,\frac{1+1.30177\mu^2}{1+0.97143\mu} - 0.0067013\,\frac{1-1.13572\mu^2}{1+1.15010\mu} - 0.225262\,\frac{1-0.86669\mu^2}{1+2.30464\mu} + 0.021559\,\frac{1-4.24401\mu^2}{1+2.58309\mu}\,; \tag{174}$$

$$P_r = \mu + \frac{0.154423}{1+0.97143\mu} - \frac{0.0006578}{1+1.15010\mu} + \frac{0.0073704}{1+2.30464\mu} + \frac{0.0093097}{1+2.58309\mu}\,; \tag{175}$$

and

$$S_r = 1 - \frac{0.193263}{1+0.97143\mu} + \frac{0.0009095}{1+1.15010\mu} - \frac{0.0300297}{1+2.30464\mu} - \frac{0.0699366}{1+2.58309\mu}\,. \tag{176}$$

The P and S functions are tabulated in Table 6. Now the law of darkening is clearly dependent only on the ratio $B^{(0)}/B^{(1)}$, while the total intensity is dependent on the absolute values of $B^{(0)}$ and $B^{(1)}$. The ratio $B^{(0)}/B^{(1)}$ is a function of frequency for a star of a given temperature; the constant $B^{(1)}$ is related to the monochromatic flux. There is some arbitrariness in the value of $B^{(0)}/B^{(1)}$.[13] The question is essentially one of determining the "best" linear representation of the Planck intensity at a particular wave length as a function of depth. Presumably, the "best" representation would be obtained by putting the appropriate straight line through a point representing the average depth of the photosphere ($\tau \sim 0.7$) rather than expanding from $\tau = 0$. This degree of arbitrariness, however, will not affect the conclusions which we shall derive; it is of importance only when discussing a particular star.

The accuracy of this linear approximation may be estimated by considering the integrated form of equations (171) and (172). In the integrated intensity

$$B^{(0)} + B^{(1)}\bar{\tau} \simeq \tfrac{3}{4}F\{\bar{\tau} + q\,[\bar{\tau}]\}\,, \tag{177}$$

from equation (62).[14] From this we find that

$$B^{(1)} = 0.83F \qquad \text{and} \qquad \frac{B^{(0)}}{B^{(1)}} \simeq 0.5\,. \tag{178}$$

[13] D. L. Harris, *Ap. J.*, **109**, 56, 1949.

[14] Here $\bar{\tau}$ refers to the optical depth in the continuum rather than to the optical depth at a given wave length.

A comparison of the law of darkening and the integrated intensities derived from equations (171) and (172) for the foregoing values of $B^{(0)}$ and $B^{(1)}$ are in reasonable agreement with those results obtained from the general theory in Section V.

For a star of a given temperature, $B^{(0)}/B^{(1)}$ is a function of wave length alone. Despite the element of arbitrariness associated with values of $B^{(0)}/B^{(1)}$, it is frequently sufficient to regard the linear expansion of the Planck function as being a straight line through the values of $B_\nu(\tau)$ at $\tau = 0$ and $\tau = 1$; that is,

$$1 + \frac{B^{(1)}}{B^{(0)}} = \frac{(e^{c_2/\lambda T_0} - 1)}{(e^{c_2/\lambda T_1} - 1)}, \tag{179}$$

TABLE 6

$\lambda = 0.5$

μ	P_l	S_l	P_r	S_r	μ	P_l	S_l	P_r	S_r
0.0	0.12435	0.70563	0.17045	0.70768	0.6	0.68050	0.85025	0.70391	0.83841
0.1	.20859	.75146	.25355	.74468	0.7	0.77987	.85862	0.79769	.84907
0.2	.29782	.78379	.33995	.77225	0.8	0.88016	.86510	0.89218	.85836
0.3	.39241	.80761	.42869	.79387	0.9	0.98119	.87006	0.98727	.86653
0.4	.48542	.82563	.51917	.81142	1.0	1.08285	0.87379	1.08285	0.87379
0.5	0.58298	0.83949	0.61101	0.82602					

TABLE 7

REPRESENTATIVE VALUES OF $B^{(0)}$–$B^{(1)}$

$T_e \times 10^{-3}$ K	$B^{(0)}/B^{(1)}$		$T_e = 30{,}000°$ K		$T_e \times 10^{-3}$ K	$B^{(0)}/B^{(1)}$		$T_e = 30{,}000°$ K	
	λ_{Ph} 4250 A	λ_{vis} 5290 A	λ	$B^{(0)}/B^{(1)}$		λ_{Ph} 4250 A	λ_{vis} 5290 A	λ	$B^{(0)}/B^{(1)}$
10	0.576	0.779	4000 A	1.66	30	1.70	1.93	2000 A	0.90
20	1.29	1.45	3000	1.34	40	2.02	2.21	1000	0.36

where T_0 is the boundary temperature and T_1 is the temperature prevailing at the depth $\tau = 1$ according to equation (65). In Table 7 the values of $B^{(0)}/B^{(1)}$ for the effective wave lengths of the visual and photographic region, respectively, are given for several effective temperatures. In addition, the values of $B^{(0)}/B^{(1)}$ for a star of 30,000° K are given for several wave lengths.

The law of darkening in an atmosphere in which $\lambda = 0.5$ is tabulated for three values of $B^{(0)}/B^{(1)}$ for both states of polarization is shown in Table 8. For an effective temperature of 20,000° K the values 0.5, 1.0, and 1.5 of $B^{(0)}/B^{(1)}$ correspond, respectively, to 2000 A, 3400 A, and 5700 A, while at a temperature of 30,000° K these correspond to 1200 A, 2200 A, and 3500 A, respectively. The degree of darkening is intermediate between that found for a pure scattering atmosphere and that found at these wave lengths for a gray atmosphere.

The degree of polarization of the emergent radiation is given by

$$\delta(\mu) = \frac{I_r - I_l}{I_r + I_l} = \frac{(P_r - P_l)B^{(1)} + (S_r - S_l)B^{(0)}}{(P_r + P_l)B^{(1)} + (S_r + S_l)B^{(0)}}. \tag{180}$$

In Table 9 the degree of polarization at the limb is given for values of $B^{(0)}/B^{(1)}$. It is seen that the degree of polarization decreases toward longer wave lengths. It is of interest to compare these values of $\delta(0)$ with the corresponding value of the degree of polarization in the integrated light. For $\lambda = 0.5$, $\delta(0) = 0.048$ for the integrated light; this corresponds to the value at $B^{(0)}/B^{(1)} = 0.5$. For an effective temperature of 20,000° K, this occurs far in the ultraviolet. The degree of polarization in the photographic region is only 2 per cent; this is probably on the border line of observational detectability.

TABLE 8

LAW OF DARKENING IN SECOND APPROXIMATION FOR $\lambda = 0.5$ AND $B^{(0)}/B^{(1)} = 0.5$, 1.0, 1.5, FOR BOTH STATES OF POLARIZATION

μ	$B^{(0)}/B^{(1)} = 0.5$		$B^{(0)}/B^{(1)} = 1.0$		$B^{(0)}/B^{(1)} = 1.5$	
	$[I_l(0,\mu)]/[I_l(0,1)]$	$[I_r(0,\mu)]/[I_r(0,1)]$	$[I_l(0,\mu)]/[I_l(0,1)]$	$[I_r(0,\mu)]/[I_r(0,1)]$	$[I_r(0,\mu)]/[I_l(0,1)]$	$[I_r(0,\mu)]/[I_l(0,1)]$
0.0	0.31398	0.34498	0.42419	0.44880	0.49416	0.47293
0.2	0.45384	0.47776	0.55279	0.56842	0.61562	0.62599
0.4	0.59104	0.60857	0.67005	0.68004	0.72022	0.72541
0.6	0.72751	0.73902	0.78234	0.78825	0.81715	0.81951
0.8	0.86377	0.86946	0.89197	0.89466	0.90987	0.91067
1.0	1.00000	1.00000	1.00000	1.00000	1.00000	1.00000

TABLE 9

$\lambda = 0.5$—DEGREE OF POLARIZATION AT LIMB AS FUNCTION OF $B^{(0)}/B^{(1)}$

$B^{(0)}/B^{(1)}$	$\delta(0)$	$B^{(0)}/B^{(1)}$	$\delta(0)$	$B^{(0)}/B^{(1)}$	$\delta(0)$	$B^{(0)}/B^{(1)}$	$\delta(0)$
0	0.156	0.6	0.041	1.2	0.025	1.8	0.018
0.2	.075	0.8	.033	1.4	.021	2.0	.016
0.4	0.056	1.0	0.028	1.6	0.019	∞	0.015

Detailed calculations along these lines for a particular stellar model will determine the darkening coefficient appropriate for computation of the light-curves of early-type eclipsing binaries; or, conversely, accurate determinations of the coefficient of darkening in eclipsing binaries will permit a determination of the mean value of λ and hence of the nature of the opacity in the atmosphere. It is intended that this aspect of the problem will be discussed more thoroughly in a future paper.

In conclusion, I wish to express my appreciation to Dr. S. Chandrasekhar for suggesting the course that this discussion should take and for his advice and encouragement.

RADIAL VELOCITIES, SPECTRAL TYPES, AND LUMINOSITY CLASSES OF 820 STARS*

J. H. MOORE† AND G. F. PADDOCK
Lick Observatory, University of California
Received January 20, 1950

ABSTRACT

Radial velocities and spectral and luminosity classes are given for 820 stars of types F–M in the HD photographic magnitude range of 8.5–8.6. The velocities were determined with a one-prism dispersion of 75 A/mm and were reduced to the Lick system by means of observations of 260 brighter stars having velocities based on three-prism Mills spectrograms. Two plates were obtained for two-thirds of the stars, and three plates for most of the remaining stars. The average probable error is ±3.6 km/sec for one plate of unit weight. Comparison of velocities in common with Victoria and Mount Wilson determinations indicates that the systematic errors are satisfactorily small, of the order of 1 km/sec or less.

The spectral-class estimates agree well with the HD, Yerkes, and Mount Wilson classifications, except among the early F stars, where the Lick estimates average somewhat later. The luminosity-class assignments are on the Yerkes system, and those for the bright-star velocity standards show no appreciable deviation from the classes given by Morgan, Keenan, and Kellman in their *Atlas of Stellar Spectra*. Because of the basis for selection, statistically significant data on the luminosity function are obtained only for the class IV stars (subgiants). The frequency maximum for these stars appears to be at F4–F5, and practically no stars are found later than K1 or K2, as previously noted by several other investigators.

Solar-motion solutions for giants (III), subgiants (IV), and main-sequence dwarfs (V) give results that show hardly any real differences depending on luminosity: solar motions of 24, 23, and 19 km/sec for class III, IV, and V stars, respectively, toward essentially the same apex at $\alpha_\odot = 280°$ and $\delta_\odot = +44\frac{1}{2}°$. No significant K-terms were found, and the mean residual velocities show the usual tendency to increase with advancing spectral class.

Two solutions including a galactic-rotation term were made for the giants. The first, for 348 class III stars (including a few II–III and III–IV) and with assumed values of $K = 0$ and $L_\odot = 325°$, gave $\bar{r}A = 4.2 \pm 1.9$ km/sec. The second, for 147 class III stars in the galactic zone limited by $b = \pm 20°$ and based on the residual velocities, gave $\bar{r}A = 6.7 \pm 1.5$ km/sec and $L_\odot = 309° \pm 7°$. These results show that the giants included in this material participate in the differential galactic rotation characteristic of the region around the sun.

I. INTRODUCTION

The Lick Observatory general program of radial velocities included all stars to visual magnitude 5.51. In the course of this program many velocities of fainter stars were obtained, but without systematic selection. After the completion of the program of bright stars, it was decided to extend the Lick system of radial velocities to a representative group of fainter stars. In order to avoid too much duplication of work at other observatories on stars fainter than about magnitude 5.5, it was decided to select a group of stars within the rather narrow range of photographic magnitude from 8.5 to 8.6, inclusive, as given in the *Henry Draper Catalogue*.

With the general aim of providing data for studies of the apparent and peculiar motions of a representative sample of faint stars of spectral classes F–M, the observational program was made up more specifically as follows:

* *Contributions from the Lick Observatory*, Ser. II, No. 28.

† [Dr. Moore was engaged in preparing this material for publication at the time of his death on March 15, 1949. Dr. Paddock had retired from the Lick Observatory. While all the basic data, such as those in Table 1, had been obtained and several of the least-squares solutions were finished or well along toward completion, hardly any text had been written. The responsibility for finishing the calculations, writing the brief discussion, and preparing the final copy for publication was assumed by the undersigned, who wishes to make grateful acknowledgment to Messrs. H. F. Weaver and O. J. Eggen for their expert advice.—N. U. MAYALL.]

1. The selection of the stars was on the basis of random distribution of the line of sight to the star, that is to say, stars were selected so as to give a fairly uniform distribution over the sky from declination $-21°$ to $+90°$. Over this part of the sky, however, there are many more HD stars of $m_{pg} = 8.5$–8.6 than can be observed in a reasonable time. Accordingly, for spectral classes F, G, and K, only those stars in the even zones of declination were chosen. No such limitation was needed for the K5 and M stars, because of their relatively small number.

2. A dispersion of 75 A/mm was chosen because experience with a one-prism 12-inch camera spectrograph showed that this instrument, in combination with the 36-inch refractor, would yield velocities having probable errors of ± 3 to ± 4 km/sec for a single observation—a precision that appeared sufficient for the purpose.

3. A brightness of $m_{pg} \sim 8.5$ was decided upon because, with good seeing, it resulted in reasonably constant exposure times, 1–1½ hours, for the fastest available emulsion, Eastman 40, regardless of spectral class.

In the early part of the work, three plates were taken of each star to find out how accordant the measures would be. It was soon found that the velocities from two or three plates generally were in good agreement, and thereafter only two satisfactory plates were taken for each star. The frequency distribution of the number of observations per star is given in the accompanying tabulation. The majority of the plates were taken by Moore

No. of obs. per star	1	2	3	4	5	6
No. of stars	14	562	208	26	8	2
Percentage	1.7	68.5	25.4	3.2	1.0	0.2

and Paddock, a few by some of the assistants. Observations for the program were begun in July, 1928, and were completed in December, 1937.

II. THE RADIAL VELOCITIES

MEASUREMENT AND REDUCTION

In order to refer the one-prism velocities for these fainter stars to the Lick three-prism Mills spectrograph system, 260 brighter stars having velocities determined with the Mills spectrograph were observed with the one-prism spectrograph. This set of plates for the brighter stars and that for the fainter stars, totaling over two thousand spectrograms, were measured on a Hartmann spectrocomparator. Paddock measured all plates, and Miss Mary L. Miller about two-thirds of the total.

For the Hartmann standards, five plates of bright stars of spectral classes F, G, K, K5, and M were selected, as noted below. Each one-prism plate was measured against the Hartmann standard of nearest corresponding spectral class. Such a measurement yielded for every plate a velocity difference, ΔV, which may be written as

$$\Delta V = (V_1 - \odot) - V_s , \tag{1}$$

where V_1 is the star's velocity reduced to the sun, $\odot$ is the sun reduction, and V_s is the velocity of the Hartmann standard. Once V_s is known, the velocity of any star may be found.

In order to obtain V_s and, at the same time, to refer the one-prism velocities to the three-prism system, the measures of the 260 brighter stars were used. For each of these stars a three-prism velocity, V_3, was available from *Lick. Obs. Pub.*, Volume **16**, 1928. Therefore, to refer the one-prism system to the three-prism system, V_1 was replaced by V_3 in equation (1), and each bright star gave an equation for V_s as follows:

$$V_s = (V_3 - \odot) - \Delta V . \tag{2}$$

Average values, $\bar{V}_s$, were computed for each Hartmann standard for each measurer, as indicated in the accompanying tabulation.

VELOCITIES FOR HARTMANN STANDARD SPECTROGRAMS

Spectral Class	Star	One-Prism Plate No.	$\bar{V}_s$ (Km/Sec)	
			GFP	MLM
F	α Per	16396 T	+22.10	+22.11
G	Sky	16404 M	− 3.35	+ 1.55
K	β Gem	16402 P	+13.43	+14.43
K5	α Tau	16397 N	+73.03	+76.64
M	δ Oph	16559 Q	−20.21	−21.31

Because some of the plates were measured by only one person, those plates measured in common were compared, and the average systematic differences were evaluated according to spectral class, in order to reduce the smaller set of measures to the larger, as follows:

Spectral class	F	G	K	K5	M
GFP–MLM (km/sec)	+2.23	−0.84	+0.06	+2.77	−1.32

These differences have been applied as corrections to Miss Miller's measures to make the latter consistent with Paddock's. The average of Paddock's measures and those of Miss Miller, including the above corrections, are the velocities listed in column 9 of Table 1.

ACCURACY

The internal consistency of these radial-velocity determinations may be indicated as follows: From 1796 plates of 820 stars, the average probable error of one observation of unit weight was found to be ± 3.6 km/sec.

The external consistency, or systematic errors, of these radial velocities may be indicated by a comparison of the results for stars observed in common at the Lick, Mount Wilson, and Victoria observatories. The data for comparison are in column 11 of Table 1, which notes the determinations from other observatories,[1] the stars of variable ("var") or probably variable ("var?") velocity, and the number of observations in parentheses. In the following comparisons, the variable (var) and probably variable (var?) velocities have been omitted. Because of the rather small number of stars included, comparisons also are given for averages omitting differences greater than 10 km/sec.

Mount Wilson: 51 stars, MW−LO = −0.87 km/sec
47 stars, MW−LO = +0.60 km/sec (HD 37453, 123598, 125455, 217580 omitted)

Victoria: 27 stars, DAO−LO = −2.18 km/sec
24 stars, DAO−LO = −0.75 km/sec (HD 81069, 175545, 183681 omitted)

The smallness of these average differences suggests that the radial velocities in Table 1 are not affected by any serious systematic errors.

[1] Through the kindness of Dr. R. E. Wilson, of the Mount Wilson Observatory, a number of his unpublished measures were made available for comparison. These velocities, indicated in column 11 by "MW*," were obtained from plates of comparable dispersion. Since many depend on only one plate, a number of above-average differences may be expected.

TABLE 1

RADIAL VELOCITIES, SPECTRAL CLASSES, AND LUMINOSITIES OF 820 STARS

HD	α (1900)	δ (1900)	VIS. MAG.	SPEC. CL.		LUM. CLASS	NO. OBS.	V (KM/SEC)	p.e. (KM/SEC)	REMARKS
				HD	LO					
(1)	(2)	(3)	(4)	(5)	(6)	(7)	(8)	(9)	(10)	(11)
153..	0h01m3	+42° 11′	8.0	G0	G1	V	2	− 32	± 1.0	
233..	02.0	−16 24	8.2	F5	F5	V	2	− 10	0.2	
334..	02.9	− 8 06	8.2	F5	F5	V	2	− 22	0.5	
377..	03.3	+ 6 04	8.0	F8	G2	V	3	− 4	0.3	
489..	04.3	+18 33	7.8	G5	G3	V	2	− 24	1.9	
502..	04.4	+18 59	7.8	G5	G8	IV	3	+ 2	2.0	
615..	05.4	+14 41	8.2	F5	F6	V	3	− 4	3.0	
737..	06.6	+26 58	8.1	F5	F5	V	3	− 9	3.0	
949..	08.8	+43 57	8.2	F5	F4	V	1	+ 15	.....	
966..	08.9	− 4 27	7.5	K0	G6	III	2	− 23	2.5	
975..	09.0	+34 51	8.1	F5	F5	V	2	+ 1	1.5	
982..	09.1	+43 17	8.0	F8	F8	V	1	+ 17	.....	
1228..	11.5	+ 1 18	7.3	Ma	M5	III	2	− 4	1.0	MW −7.9±1.6 (4)
1364..	12.7	+19 41	7.3	Mb	M4	II–III	2	+ 9	1.7	
1552..	14.7	+42 19	8.2	F2	F2	III	2	+ 15	0.6	
1736..	16.5	−16 45	8.2	F5	F5	IV	2	− 5	0.1	
2344..	22.2	+ 2 15	7.7	G5	G4	III	3	0	2.9	
2506..	23.7	+58 55	7.8	G5	G4	III	2	− 55	1.0	
2624..	24.7	− 0 53	7.7	G5	G6	III	3	+ 14	7.4	Var?
2730..	25.7	+42 49	8.1	F8	F7	V	2	− 11	1.6	
2779..	26.2	+20 16	7.4	K5	K4	III	3	+ 4	1.1	
2841..	26.7	+19 05	7.3	K5	K5	III	3	+ 4	0.8	
3070..	28.8	+ 2 46	7.8	G5	G4	III	2	− 10	2.8	
3141..	29.6	+42 09	7.7	G5	K0	IV	2	+ 1	2.8	
3265..	30.7	+37 42	7.4	K5	M0	III	2	− 16	2.6	
3370..	31.5	+26 29	8.2	F2	F3	IV	3	− 1	0.4	
3397..	31.8	+30 57	8.2	F0	F0	III	2	+ 11	0.1	
3726..	35.0	+26 08	8.0	F8	F6	V	3	− 10	3.6	
3790..	35.5	+30 34	8.2	F5	F4	V	2	+ 14	3.7	
3989..	37.4	+45 21	7.4	K5	K5	III	2	− 24	1.7	MW −18.7±0.9 (4)
4270..	40.0	+14 37	8.2	F0	F3	IV	4	− 14	5.3	Var?
4277..	40.1	+54 26	8.0	F8	F8	V	2	− 17	4.1	
4549..	42.4	+26 34	7.8	G5	G4	III	2	− 26	1.4	
4565..	42.5	− 2 52	7.3	K5	M1	III	2	+ 20	1.4	
4647..	43.4	+56 32	7.2	Ma	M2	III	2	− 36	0.2	
5072..	47.5	+38 29	8.0	G0	F7	IV	3	− 11	2.0	
5308..	49.8	+22 53	8.2	F5	F5	V	2	− 2	2.1	
5362..	50.4	− 0 31	7.6	K0	K4	III	4	− 29	2.9	
5453..	51.2	− 8 07	8.2	F5	F6	IV	2	+ 6	0.7	
5494..	51.6	+34 20	8.2	F5	F7	V	2	− 33	1.9	
5650..	53.1	+26 15	7.5	K2	K5	III	3	− 19	3.1	
5892..	55.3	+ 6 49	8.2	F5	F5	V	3	− 3	1.0	
6064..	56.8	+ 2 00	8.0	F8	F6	V	3	+ 1	3.7	
6262..	58.5	+38 09	7.3	Ma	M3	III	2	− 30	1.0	
6424..	1 00.0	+10 48	8.1	F5	F5	V	3	+ 9	2.6	
6529..	01.1	− 0 47	8.2	F2	F4	IV	2	− 1	4.0	
6645..	02.1	+46 19	7.5	K2	K0	II–III	2	− 26	1.9	
6664..	02.3	+38 44	8.0	F8	G1	V	2	+ 6	2.9	
6876..	04.2	+34 05	8.1	F5	F5	IV	2	+ 8	1.3	
7189..	07.1	+46 39	7.7	G5	G6	III	2	− 21	1.3	
8262..	16.8	+18 10	8.0	F8	G3	V	3	+ 4	1.4	MW 0±2 (3)
8447..	18.5	−18 28	7.2	Ma	M3	III	3	0	2.2	
8507..	19.0	+46 39	7.8	G5	G5	II	2	− 28	4.2	
8583..	19.7	+46 36	7.7	G5	G4	III	2	− 10	0.9	
8586..	19.7	+22 25	8.1	F8	F5	V	3	− 6	1.1	
8626..	20.0	+15 44	7.4	K5	K5	III	3	− 4	3.1	
8865..	22.3	− 0 28	8.3	F2	F3	V	3	+ 23	1.7	

TABLE 1—*Continued*

HD	α (1900)	δ (1900)	Vis. Mag.	Spec. Cl.		Lum. Class	No. Obs.	V (Km/Sec)	p.e. (Km/Sec)	Remarks
				HD	LO					
(1)	(2)	(3)	(4)	(5)	(6)	(7)	(8)	(9)	(10)	(11)
8884	1h22m5	+42° 16′	7.7	G5	G7	III	2	− 17	± 2.9	
9500	28.2	+35 06	7.3	Ma	M4	III	2	+ 1	3.0	MW* +5 (1)
9956	32.2	+22 04	8.1	F5	F6	V	2	+ 47	6.1	Var?
10100	33.6	−16 23	7.5	K0	K1	III	2	+ 28	2.8	
10108	33.8	+54 20	8.2	F0	F4	IV	2	− 15	2.8	
10572	37.9	−20 40	7.3	K0	K4	III	2	+ 25	4.6	
11012	43.1	+46 45	8.2	F0	F2	IV	2	+ 7	0.8	
11170	44.7	+ 6 44	7.9	G0	G1	IV	2	− 14	0.5	
11274	45.6	−12 50	8.1	F5	F5	V	2	+ 17	4.8	
11719	49.9	+42 34	7.5	K2	K4	III	3	+ 2	1.8	
11961	52.3	+30 39	7.2	Mb	M6	III	2	− 46	0.7	MW* −47 (1)
12102	53.7	+ 6 11	8.3	F2	F3	IV	4	+ 2	2.0	
12246	55.1	+34 49	8.1	F5	F3	V	2	+ 24	3.1	
12460	57.0	−12 18	8.1	F5	F6	V	2	+ 8	2.0	
12568	58.1	+62 28	8.0	F8	G1	II	2	+ 12	0.1	
12637	58.7	+38 58	8.1	F5	F3	III	2	+ 10	2.4	
12783	2 00.2	− 0 10	8.0	G0	G5	V	3	+ 22	0.9	
13364	05.5	+22 45	8.2	F2	F5	IV	2	− 13	2.1	
13565	07.3	+30 06	7.8	G5	G4	III	2	+ 14	1.7	
13830	09.7	+62 43	8.0	F8	F6	IV	2	− 22	2.1	
13834	09.7	+46 13	8.2	F5	F4	V	2	− 9	2.0	
14376	14.2	−19 59	7.1	K5	M0	III	2	− 7	1.4	
14385	14.3	+ 2 22	7.8	G5	G5	III	2	+ 11	2.7	
14625	16.6	− 0 36	7.6	K0	G8	III	2	+ 5	1.5	
14738	17.5	+26 15	8.1	F8	F6	II	2	− 11	0.9	
14797	18.0	+46 55	7.6	K0	M0	III	4	+ 26	1.8	
15084	20.7	+18 27	8.0	G0	F7	V	3	+ 20	0.9	
15128	21.1	+30 50	8.1	F5	F6	V	2	+ 18	0.1	
15164	21.4	+10 08	8.3	F0	F2	IV	3	+ 34	0.6	
16090	30.0	+30 44	7.9	G0	G1	IV	2	+ 2	1.9	
16314	32.0	+ 2 00	8.2	F0	F5	III	4	− 16	2.1	
16497	33.7	+14 05	8.2	F5	F5	IV	3	+ 3	1.2	
16638	34.9	+26 12	8.1	F5	F7	V	2	+ 1	4.7	
16708	35.6	+ 2 28	7.8	G5	G5	IV	3	+ 65	1.8	
17055	39.2	+22 58	8.1	F8	F6	III	3	+ 13	4.1	
17238	40.9	+42 59	7.6	K0	G9	III	2	− 27	1.1	
18142	49.7	+30 38	7.2	Ma	M3	II–III	2	− 25	2.8	MW* −21 (1)
19178	3 00.0	−12 33	8.2	F5	F5	V	2	+ 3	0.7	
19258	00.8	+11 17	7.3	K5	M1	III	3	− 74	1.7	
19286	01.1	+74 41	8.2	F5	F2	V	2	+ 52	2.2	
19301	01.2	+38 42	8.2	F0	F3	V	2	− 2	0.9	
19511	03.1	+ 6 21	7.8	G5	G4	III	2	+ 20	0.2	
19522	03.2	−12 25	8.0	G0	G3	IV	3	+ 50	2.5	
19534	03.5	+73 51	7.2	Ma	M2	III	1	+ 12	.....	MW* +16 (1)
19790	05.9	+ 6 47	8.3	F0	F3	III	3	− 3	2.0	
19808	06.1	+34 36	8.1	F8	F5	IV	2	+ 38	7.7	Var?
19855	06.5	+81 47	7.3	Ma	M2	III	2	− 7	3.1	
19882	06.7	+38 36	8.3	F0	F3	IV	2	− 13	1.1	
20358	11.4	−12 22	7.5	K2	K4	III	2	− 24	2.5	
20692	14.8	+38 22	8.1	F5	F5	V	2	− 4	4.7	
20909	17.2	−12 41	8.2	F5	F4	V	2	+ 8	2.1	
20988	18.1	+ 2 30	8.3	F0	F4	V	3	+ 7	2.6	
21183	20.0	+34 59	8.1	F8	F9	V	3	0	1.2	
21910	26.9	+74 26	7.6	K0	G9	IV	2	−104	1.3	
21971	27.4	+62 59	7.6	K0	K4	III	2	− 22	1.0	
22007	27.7	− 0 50	8.0	G0	G5	IV	5	+ 18	1.9	
22156	29.1	+46 14	7.7	G5	G6	III	2	− 26	0.8	
22373	31.0	+34 50	8.1	F8	F9	V	1	− 9	.....	

* Unpublished Mount Wilson measures (see n. 1).

TABLE 1—*Continued*

HD	α (1900)	δ (1900)	Vis. Mag.	Spec. Cl.		Lum. Class	No. Obs.	V (Km/Sec)	p.e. (Km/Sec)	Remarks
				HD	LO					
(1)	(2)	(3)	(4)	(5)	(6)	(7)	(8)	(9)	(10)	(11)
22872	3h35m3	+50° 51′	7.9	G0	F9	V	2	+ 56	± 4.9	
23107	37.4	+38 04	7.4	K5	K5	III	2	+ 12	3.2	MW +15.7±1.0 (3)
23141	37.7	+26 04	7.5	K0	K0	III	2	− 28	0.8	
23317	39.1	− 8 11	7.8	G5	G6	III	2	− 16	1.4	
23393	39.7	−12 22	8.2	F0	F0	III	2	− 1	0.5	
23450	40.2	+66 51	7.7	G5	G8	III	2	+ 6	1.6	
23502	40.6	+10 15	7.7	G5	G8	III	2	+ 3	1.7	
23806	42.9	+ 2 28	8.3	F	F2:	V:	2	+ 32	2.2	Weak plates
23825	43.0	+10 31	7.9	G0	G3	IV	2	− 13	2.1	
23962	44.1	+33 45	7.4	K5	K5	III	2	+ 16	10.2	Var?
24107	45.3	− 4 12	7.5	K0	K1	II	2	+ 39	0.8	
24301	46.9	+26 22	8.0	G0	G0	IV	2	+ 22	1.7	
24622	49.8	− 0 17	8.3	F0	F3	IV	3	+ 24	1.8	
24694	50.4	−20 47	8.8	F0	F0	.....	3	+ 45	13.7	V. br. lines; Var?
25189	55.0	−20 37	7.7	K0	K2	II	2	+ 14	0.1	
25322	56.3	+22 09	8.2	F5	F5	V	2	− 13	2.8	
25391	57.0	+14 47	8.0	G0	G0	V:	2	− 39	3.0	Plates underexposed
25518	58.1	+38 38	8.1	F5	F5	IV	2	− 29	1.9	
25661	59.2	−20 26	7.4	K2	K2	II	2	+ 24	0.6	
25749	59.9	+14 02	7.6	K0	G9	III–II	2	− 41	2.2	
25921	4 01.2	−10 34	7.3	Mb	M4	III	3	+ 49	1.6	
26004	01.9	−19 47	7.6	K5	K0	II	2	− 12	0.4	
26297	04.5	−16 10	7.7	G5	G1	V	2	+ 15	3.0	
26395	05.4	+42 39	8.2	F5	F4	V	2	+ 31	20.7	Var?
26596	07.3	+54 44	8.0	F8	F9	IV:	2	+ 2	3.1	Weak plates
26717	08.5	+62 20	8.0	G0	F7	V	2	− 15	1.1	
27129	11.9	+22 06	8.2	F5	F5	IV	2	+ 15	0.5	
27135	12.0	+70 36	8.2	F0	F4	III	2	+ 17	0.5	
27372	14.1	+14 03	7.8	G5	G7	III	2	− 17	3.0	
27498	15.3	− 2 52	7.3	Mb	M4	III	2	+ 86	2.0	
27598	16.2	−17 04	7.3	Ma	M5	II	4	+ 99	0.9	
27816	18.4	+58 01	8.1	F8	F7	IV	2	+ 11	1.9	
28159	21.4	− 0 44	7.5	K2	M1	II	4	− 6	0.3	
28387	23.5	−18 04	7.5	K5	K5	II	2	+ 26	0.3	
28395	23.6	+ 2 09	8.2	F5	F3	V	3	− 37	4.5	
28486	24.4	+14 06	8.0	G0	F7	V	2	− 49	3.5	
28487	24.4	+ 4 56	7.2	Mb	M3	II	2	− 6	1.0	
29146	30.3	+78 58	8.1	F5	F4	V	2	− 7	4.4	
29936	37.9	− 0 47	7.8	G5	F9	V	2	+ 3	6.7	Var?
30247	40.8	+14 21	8.2	F0	F2	V	2	+ 22	3.8	
30436	42.6	− 0 16	8.2	F2	F4	III	2	− 12	2.3	
31324	49.7	+58 28	7.8	G5	G7	III	3	+ 35	1.7	
31355	50.0	+ 2 49	8.2	F2	F3	IV	2	+ 18	4.1	
31706	53.0	+30 55	8.0	F8	F5	IV	1	+ 19	.....	
31923	54.5	−12 55	8.3	F2	F4	IV	3	+ 46	1.4	
32024	55.2	− 0 20	8.2	F2	F4	III	3	+ 41	2.4	
33053	5 02.5	+14 25	7.7	G5	G3	III	2	− 18	0.8	
33072	02.6	−20 14	8.6	F2	F4	IV	2	+ 29	0.1	
33239	03.7	−20 15	7.3	K0	G9	II	2	− 11	1.2	
34616	13.7	−16 18	7.6	K0	G9	III	2	+ 24	1.8	
34624	13.8	+42 16	7.8	G5	G6	III–IV	2	+ 9	0.8	
34786	14.9	+58 51	7.8	K5	G8	III	3	− 17	3.9	
34860	15.4	− 4 54	8.1	F5	F6	V	2	+ 18	1.5	
35062	16.9	+18 55	7.6	K0	G8	III	2	+ 39	0.4	
35146	17.6	+18 31	7.5	K2	K5	III	3	+ 9	2.1	DAO +10 (1)
35441	19.6	−20 49	7.8	K2	K2	III	2	+ 15	2.0	
36042	23.8	+34 08	7.8	G5	G7	III	2	+ 7	4.5	
36067	24.0	+50 57	7.6	K0	K1	II	2	− 15	0.3	

TABLE 1—*Continued*

HD	α (1900)	δ (1900)	Vis. Mag.	Spec. Cl.		Lum. Class	No. Obs.	V (Km/Sec)	p.e. (Km/Sec)	Remarks
				HD	LO					
(1)	(2)	(3)	(4)	(5)	(6)	(7)	(8)	(9)	(10)	(11)
36724	5h28m7	+26° 54′	8.0	F8	F6	IV	3	− 19	± 4.0	
37453	33.6	+30 02	8.2	F5	F4	III	2	+ 56	1.6	MW +22 (1)†
37847	36.3	−20 20	7.0	K0	G4	III	2	+ 36	3.0	
38092	38.1	+38 27	7.5	K0	G9	III	2	+ 30	1.0	
38164	38.7	+ 6 29	7.7	G5	G5	III	2	+ 36	1.0	
38411	40.5	+10 45	8.3	F0	F3	III	3	+ 28	0.6	MW +19 (1)
38455	40.8	−12 29	7.6	K0	G7	IV	2	− 33	1.6	
38699	42.5	−16 41	7.6	K0	K4	III	2	+ 30	0.1	
39008	44.6	− 0 23	7.4	K2	K3	III	2	− 12	1.5	
39116	45.3	+30 43	8.2	F5	F4	V	2	+ 4	0.5	
39645	48.8	+22 30	7.6	K0	G7	III	3	+ 19	1.0	
39688	49.0	−16 17	7.9	G0	F7	V	2	+ 3	0.8	
39699	49.1	+17 23	7.4	K5	K5	III	3	+ 32	0.2	DAO +28 (1)
39967	50.9	+42 50	8.0	F8	F6	IV	2	− 60	7.2	Var?
40170	52.1	−20 02	8.4	G0	F6	V	2	− 6	1.0	
40259	52.1	+ 2 04	8.3	F0	F0	V	2	− 30	5.4	
40300	52.8	+ 6 31	8.1	F8	F3	IV	2	− 12	0.3	
40512	54.2	+ 2 28	8.1	F5	F5	IV	2	+ 45	0.1	
40567	54.6	+66 58	8.2	F5	F5	IV	2	− 9	5.8	
40931	56.9	+13 02	7.4	K5	M0	III	2	+ 17	1.8	DAO +13 (1)
40960	57.1	+18 00	7.8	G5	K1	III	3	+ 42	2.7	
41028	57.5	+14 21	8.2	F5	F4	IV	3	− 3	3.1	
41159	58.2	+74 32	8.1	F8	F5	III	2	− 19	0.9	
41255	58.8	−16 02	8.0	G0	F7	V	2	− 3	0.6	
41456	6 00.2	+26 32	7.6	K0	G5	III	2	− 19	2.8	
41563	00.8	+26 40	7.5	K0	G6	III	2	− 5	1.5	DAO −9 (1)
41608	01.1	− 5 52	7.2	Ma	M1	III	3	+ 7	4.7	
41658	01.4	+18 49	8.3	F0	F3	III	2	+ 22	1.3	
42061	03.6	+70 42	7.8	G5	G7	III	2	+ 13	0.2	
42106	03.8	+30 34	7.8	G5	G7	III	2	+ 24	3.7	
42176	04.2	+30 59	8.1	F8	F7	V	2	− 43	3.7	
42820	07.8	+42 10	8.0	F8	F8	V	2	+ 22	5.0	
42911	08.3	− 4 58	7.5	K0	G7	III	2	+ 43	2.3	DAO +40 (1)
43236	10.0	−19 30	7.9	Ma	M3	III	3	+ 72	0.8	
43502	11.4	−20 10	7.5	K0	K0	III	2	+ 49	2.4	
43748	12.9	+78 02	7.8	G5	G5	III–IV	3	+ 8	3.1	
43795	13.1	+42 50	7.8	G5	G6	III	2	− 50	0.7	
43856	13.4	+ 6 46	8.1	F5	F6	V	3	− 58	1.4	
44019	14.3	− 0 53	7.6	K0	K2	IV–	2	+ 39	0.4	
44073	14.7	+18 05	7.6	K0	G7	III	2	+ 16	1.1	
44252	15.7	+22 57	8.1	F5	F3	IV	3	+ 35	0.8	MW +37.3 ±2.5 (4)
44415	16.6	+14 44	8.3	F0	F4	Ib	3	+ 27	1.8	
44420	16.6	− 0 29	7.7	G5	G4	V	3	+ 5	1.4	
44630	17.7	+58 47	8.0	F8	F5	IV	2	− 38	0.1	
44894	19.2	−20 53	8.3	K0	G6	II–III	2	+ 19	2.8	
45379	21.9	− 0 59	8.2	F0	F3	III	3	+ 25	1.5	
45528	22.9	+62 50	7.6	K0	G9	III	2	− 47	1.9	
46122	26.4	+ 6 51	7.7	G5	G3	IV	2	− 8	3.2	
46217	27.0	+54 08	8.0	F8	F7	V	2	+ 17	2.4	
46377	27.9	+ 1 20	7.4	K5	K4	III	2	+ 15	1.3	DAO +14 (1)
46423	28.2	+14 22	8.2	F5	F6	V	2	+ 14	0.6	
47194	32.3	+34 23	8.2	F0	A8	.....	3	*+ 8	1.6	
47668	34.7	−18 06	7.4	K5	M2	III	2	+ 5	3.3	
47821	35.4	− 6 15	7.2	Ma	M3	III	2	− 14	1.1	
47930	35.9	+57 01	7.2	Ma	M2	III	2	+ 22	3.2	
48688	39.5	+10 52	7.9	G0	G0	III	2	+ 32	1.6	
48796	41.1	+ 9 18	7.4	K5	K5	III	2	+ 21	2.1	
49068	41.5	−20 45	7.5	K2	K0	Ib	2	+ 22	0.1	

† Bright hydrogen lines, cF5e, Merrill, *Pub. A.S.P.*, **54**, 155, 1942.

TABLE 1—*Continued*

HD	α (1900)	δ (1900)	Vis. Mag.	Spec. Cl.		Lum. Class	No. Obs.	V (Km/Sec)	p.e. (Km/Sec)	Remarks
				HD	LO					
(1)	(2)	(3)	(4)	(5)	(6)	(7)	(8)	(9)	(10)	(11)
49317	6h42m7	−20° 34′	8.4	F8	G6	III	2	+ 24	± 0.7	
49367	43.0	+ 6 19	7.7	G5	K1	II	2	+ 2	0.2	
49435	43.3	− 1 43	7.4	K5	K5	III	2	+ 70	1.8	DAO +74 (1)
49633	44.3	+46 38	7.6	K0	G8	II	2	+ 6	0.9	
50060	46.4	+10 55	7.8	G5	F9	V	2	+ 71	1.4	
50067	46.4	− 9 58	7.4	K5	K4	III	2	+ 7	0.2	
50372	47.8	+ 2 52	7.7	G5	G6	II	2	+ 15	0.2	
50434	48.2	+14 53	7.8	G5	G5	III	2	− 5	1.9	
50735	49.3	− 8 39	8.3	F0	F0	V	2	+ 55	7.7	V. br. lines
50746	49.4	+ 2 44	8.1	F8	F7	V	3	+ 41	4.0	
51002	50.5	+14 38	8.2	F5	F4	IV	2	+ 26	0.1	
51710	53.4	+42 13	7.8	G5	G7	IV	2	+ 12	0.3	
51833	53.8	+30 26	7.8	K0	G8	III	2	+ 55	2.0	
52340	55.8	+ 2 16	8.3	F2	F4	V	2	− 5	4.8	
53561	7 00.4	+14 08	7.4	K5	K5	III	3	+ 42	2.7	
53590	00.5	− 0 38	7.6	K0	G8	IV	2	+ 15	2.0	
53598	00.5	−20 41	7.2	K2	M0	II	2	+ 54	1.5	
54489	03.9	+ 2 25	7.5	K0	G9	III	2	+ 20	4.2	
54519	04.0	−20 42	6.9	K2	K5	II	2	+ 15	0.5	
54684	04.7	+70 41	7.8	G5	G2	IV	2	− 38	2.3	
54983	06.0	+50 44	8.2	F0	A9	.....	2	+ 28	2.3	
55054	06.3	+10 41	7.9	G0	F7	V	2	− 45	2.8	
55055	06.3	+ 6 55	8.2	F0	F0	V	2	+ 1	4.6	
55438	07.8	− 8 32	8.3	F0	F0	IV	2	+ 34	9.1	Var?
55760	09.1	−20 57	8.4	F0	A9	.....	2	− 26	19.0	Var?
55847	09.6	+22 09	7.4	K5	K5	III	3	+ 62	3.2	
56274	11.3	−12 52	7.7	G5	G0	V	3	+ 63	0.5	MW +57.0±1.5 (3)
56418	11.8	+26 31	7.6	K0	G7	III	3	− 4	4.3	Var (−16 to +5)
56819	13.5	+70 09	8.2	F0	A9:	.....	4	+ 10	19.0	Var (+76 to −60)
56965	14.1	+10 35	7.4	K2	M0	III	2	+ 29	1.5	DAO +23 (1)
57046	14.5	+46 25	8.0	F8	F8	V	2	− 27	0.8	
57267	15.4	+26 21	7.9	G0	G5	III	3	+ 15	5.0	Var?‡
57362	15.8	+30 01	8.1	F5	F4	V	4	− 16	1.5	
57840	17.9	− 8 51	8.3	F0	A9	III	2	+ 47	0.1	
57890	18.1	−20 19	7.4	Mb	M6	III	2	+ 36	0.7	
58121	19.1	+ 6 21	7.7	G5	G7	III	2	+ 14	0.7	
58477	20.7	+18 44	8.3	F0	F2	IV	2	+ 39	6.9	Var?
59058	23.2	+38 40	7.7	G5	G5	V	2	+ 14	2.9	
59076 and 77	23.2	−20 57	7.7	G0+A2	G5+A	III	2	+ 20	19.2	Var (−9 to +49)
59980	27.3	− 0 17	8.1	F5	F6	III	2	+ 28	1.7	
60265	28.5	−20 35	8.6	F0	.....	.....	2	+ 52	7.5	Var?
60381	29.1	+54 36	8.1	F5	F4	IV	2	− 6	0.4	
60618	30.3	+30 00	8.2	F2	F5	IV	2	0	0.8	
60983	32.0	+54 41	8.0	F8	F5	III	2	+ 8	0.9	
61367	33.8	− 0 02	7.3	Ma	M2	III	2	+ 17	0.7	
61787	35.9	+18 17	8.1	F5	G4	IV	2	− 1	1.3	
62094	37.2	+78 28	8.0	F8	F6	V	2	− 4	2.9	
62549	39.4	− 4 49	7.9	G0	G1	V	2	+ 85	1.5	
63210	42.6	+18 36	7.7	G5	G8	III	2	+ 13	2.5	
63348	43.4	+55 00	7.4	K5	M0	III	2	− 5	2.2	
63653	44.9	− 8 04	8.0	F8	F5	IV	2	+ 35	0.7	
64207	47.7	+26 49	8.0	F8	F9	V	3	+ 25	1.6	
64291	48.1	+10 57	7.7	G5	G6	III	2	+ 67	5.5	
64372	48.5	+30 37	7.8	G5	G7	III	2	+ 82	0.9	
64493	49.1	+18 21	7.4	K2	K4	III	3	− 12	2.0	
64512	49.2	+18 13	7.5	K0	G6	III	3	+ 5	2.5	

‡ 57267. On first two plates, spectrum G5 + A, av. vel. = +24; and on third plate, G5, vel. = 0.

TABLE 1—*Continued*

HD	α (1900)	δ (1900)	Vis. Mag.	Spec. Cl.		Lum. Class	No. Obs.	V (Km/Sec)	p.e. (Km/Sec)	Remarks
				HD	LO					
(1)	(2)	(3)	(4)	(5)	(6)	(7)	(8)	(9)	(10)	(11)
65174	7h52m4	+ 2° 55′	8.1	F8	F5	V	2	+ 28	± 2.7	
65477	53.8	+ 6 36	8.3	F0	F0	IV	2	+ 1	2.8	
66633	59.4	+74 39	8.2	F0	.....	.....	2	+ 6	0.3	MW* +2±3 (3)
66686	59.6	+10 47	7.7	G5	G5	III	2	+ 17	0.2	
66823	8 00.2	+65 57	7.3	K5	K5	III	2	− 10	1.6	
67141	01.5	−20 39	8.2	G5	G1	IV	2	+ 58	0.1	
67517	03.3	+54 32	8.0	F8	F8	V	3	− 23	3.4	
68706	08.5	+ 2 19	8.0	F8	F7	V	2	− 29	2.3	
68793	08.9	− 4 21	8.2	F5	F4	V	2	− 6	2.1	
69229	10.9	−13 19	7.2	Ma	M2	III	2	− 4	2.9	
69285	11.2	+67 51	7.2	Ma	M3	III	2	+ 10	0.9	
69287	11.2	+38 11	8.2	F2	F2	III	3	+ 24	6.7	Var (+9 to +42)
69438	11.9	−16 01	7.6	K0	G9	III	2	+ 26	1.7	
71053	20.2	+18 10	7.9	G0	F9	V	2	+ 28	1.1	
71228	21.1	+ 2 48	7.6	K0	K1	III	2	+ 2	1.1	
71495	22.7	+34 04	8.1	F5	F4	V	4	+ 9	2.8	
71659	23.5	+50 37	8.0	F8	F8	V	2	− 50	6.4	Var?
72052	25.7	+30 03	8.2	F2	F3	V	3	− 26	3.8	MW −22.8±1.9 (3)
72132	26.1	+42 28	7.7	G5	G5	III	2	− 28	0.5	
72528	28.3	− 4 59	8.0	F8	F7	V	3	+ 16	2.7	
72854	30.0	−20 51	7.9	F2	F0	IV	3	+ 21	1.4	
73039	31.0	−20 00	8.4	F2	F3	V	2	+ 20	4.5	
73668	34.4	+ 6 08	7.8	G5	G1	V	2	− 20	2.1	MW −17.1±0.6 (3)§
74225	37.7	+78 33	7.3	Mb	M5	III	2	− 43	1.1	
74360	38.5	+46 33	8.2	F5	F4	V	2	− 24	1.8	
74492	39.2	−16 39	8.0	F8	F7	V	3	− 13	2.7	
75107	42.9	+66 49	7.8	G5	G8	III	2	− 57	0.1	
75646	46.1	+26 05	7.5	K0	G9	III	2	− 8	0.2	
75775	46.8	−20 09	8.0	F8	F7	IV	2	+ 19	4.0	
75786	46.9	− 8 45	8.2	F5	F3	V	3	+ 30	3.6	
75994	48.3	+18 37	7.8	G5	G5	IV	2	− 34	3.6	
76122	49.1	−16 50	8.2	F0	F3	IV	2	+ 26	0.7	
76318	50.3	+26 45	8.2	F2	F2	V	3	+ 27	1.5	
76646	52.4	− 0 16	8.2	F0	F3	V	2	+ 34	0.9	
77015	54.6	−16 06	7.6	K0	K1	III	3	+ 56	4.6	
77024	54.7	+22 52	8.1	F8	F7	V	2	− 14	1.4	
77098	55.2	−20 25	8.4	F8	F6	V	2	− 19	3.2	
77173	55.8	+26 47	8.3	F0	F0	IV	2	+ 21	13.1	V. br. lines
77189	55.9	+39 03	7.3	K5	K5	III	3	+ 8	4.8	
77378	57.0	+18 10	8.2	F0	F3	V	3	+ 25	7.6	Var?
77391	57.1	+22 40	7.8	G5	G6	IV	2	+ 43	1.3	
77572	58.3	+10 17	8.2	F2	F4	V	2	+ 14	1.7	
77772	59.5	+38 50	8.1	F5	F6	V	2	− 12	2.2	
77930	9 00.3	+38 28	8.1	F5	F6	V	2	+ 47	7.4	Var?
78195	01.8	+10 03	7.5	K0	G9	III	2	+ 3	3.2	
78670	04.4	−16 22	8.1	F8	F9	V	2	+ 71	2.7	
80388	14.4	+78 51	8.0	G	G1	V	4	− 12	4.0	Var (+1 to −33)‖
80547	15.4	+26 26	8.1	F5	F4	IV	3	+ 16	1.6	
80731	16.3	+62 12	8.3	F0	F0	V	2	+ 4	1.7	
80743	16.4	+42 38	8.1	F8	F5	V	3	− 23	2.8	
81028	18.1	+ 8 09	7.2	Ma	M4	III	2	+ 58	0.1	MW* +57.8±1.7 (2)
81069	18.4	+ 2 50	7.5	K0	K0	III	3	− 16	1.6	DAO −28 (1)
81109	18.6	−20 36	7.1	Ma	M3	III	2	+ 17	0.2	MW* +11 (1)
81265	19.5	+30 56	7.8	G5	G7	IV	2	0	3.1	MW* −1.0±0.8 (3)
81373	20.1	+ 6 41	7.5	K0	G9	III	3	− 2	1.7	
81548	21.2	+ 2 57	8.1	F5	F7	V	4	+ 21	1.7	
81704	22.2	+46 02	8.1	F8	F9	IV	2	+ 8	0.5	MW* +8.6±0.3 (2)
82333	26.2	+ 2 43	7.7	G5	G5	III	3	+ 13	3.9	

§ 73668. Brighter component of Σ 1255.

‖ 80388. Brighter component of β 5017, d = 29″.

TABLE 1—*Continued*

HD	α (1900)	δ (1900)	Vis. Mag.	Spec. Cl.		Lum. Class	No. Obs.	V (Km/Sec)	p.e. (Km/Sec)	Remarks
				HD	LO					
(1)	(2)	(3)	(4)	(5)	(6)	(7)	(8)	(9)	(10)	(11)
82394	9h26m6	+22° 18′	7.5	K0	G7	II	3	− 4	± 3.9	
82957	30.1	− 4 27	7.4	K2	G8	III	2	0	4.3	
83140	31.3	+78 00	8.3	F2	F3	IV	2	− 7	1.5	
83395	33.0	+30 36	8.0	G0	G6	III	2	+ 13	1.1	
83423	33.2	+42 44	8.0	F8	F8	V	2	− 6	1.3	
83839	36.0	+51 44	7.3	Ma	M2	III	2	− 11	1.2	
84165	38.1	+66 05	7.2	Ma	M1	III	3	− 32	1.6	MW* −26 (1)
84606	41.3	+18 36	7.9	G0	G0	IV	2	+ 19	2.0	
84660	41.7	+42 54	8.1	F5	F1	III	2	+ 9	3.8	
85162	44.9	+31 52	7.3	Ma	M2	III	2	− 34	0.6	MW* −33.4±0.2 (2)
85198	45.2	+18 12	7.9	G0	F6	V	2	+ 24	3.7	
85431	46.6	−16 05	8.2	F5	F6	V	3	+ 20	0.9	
85958	50.3	+30 15	8.1	F8	F5	V	3	− 14	2.7	
86391	53.1	−20 42	7.8	G5	G7	III	2	0	0.5	
86476	53.7	+ 5 16	7.3	Ma	M2	III	2	− 32	0.3	
86871	56.3	+50 21	7.5	K0	G5	III	2	− 11	2.1	
87161	58.1	− 8 24	8.0	G0	G2	IV	2	+ 1	1.0	
87209	58.4	+42 52	8.4	F8	F6	V	2	+ 24	0.4	
87386	59.6	+82 53	7.6	K0	K0	III	3	− 35	2.7	
87481	10 00.2	+61 24	7.4	K5	K5	III	3	+ 33	1.3	
87621	01.0	+38 31	8.2	F2	F3	V	2	− 26	2.7	
87646	01.2	+18 23	7.9	G0	G1	IV	3	+ 21	2.4	
88108	04.5	−12 52	7.3	Ma	M2	III	3	− 13	1.5	MW* −10.6±1.7 (2)
88513	07.4	+42 23	8.2	F2	F3	IV	3	+ 8	2.1	
88785	09.4	+42 22	8.2	F2	F3	III	2	+ 23	2.1	
88865	09.9	+70 30	8.3	F2	F6	IV	3	+ 6	4.2	Var?
89276	12.9	+30 20	8.2	F0	F0	V	2	− 13	13.6	Var?
89312	13.1	−20 31	7.4	K5	K5	II–III	4	− 4	3.4	Var (+9 to −16)
89885	17.2	−20 04	7.2	K0	K1	III	3	+ 19	1.8	
89945	17.7	− 8 54	7.2	Ma	M3	III	3	0	1.5	
90068	18.6	+34 41	7.3	Ma	M6	III	3	+ 1	0.5	MW* 0 (1)
90164	19.4	+30 52	7.8	G5	F8	V	1	− 28	.....	
92547	36.0	−12 37	8.1	F8	F8	V	2	− 9	1.5	
92855	38.2	+46 44	8.1	F8	F9	V	2	− 2	9.6	Var? MW* +13 var (9)
93238	40.9	+66 08	7.2	Ma	M4	III	2	− 18	1.4	
93391	41.9	+27 26	7.3	K5	K5	III	3	+ 9	1.3	
93542	42.8	+14 45	8.2	F2	F5	V	3	− 2	2.6	
93552	42.9	+22 38	8.3	F2	F2	V	2	+ 9	2.2	
94270	47.7	−16 29	7.9	G0	G0	V	2	+ 21	3.2	
94336	48.2	+26 44	7.3	Ma	M3	III	2	0	2.9	MW* −5.8±0.6 (3)
94467	49.2	+66 16	8.1	F8	F9	V	2	− 61	5.5	
94500	49.4	− 0 59	8.3	F2	F4	IV	2	+ 16	0.9	
94574	50.0	+70 34	8.1	F5	F4	V	2	− 11	1.5	
94794	51.5	+14 07	8.1	F8	F8	V	3	+ 11	1.5	
94937	52.5	+78 13	8.1	F8	F7	V	2	− 7	2.7	
94978	52.8	+66 50	8.3	F2	F0	IV	6	− 4	2.7	Var (+13 to −17)
95532	56.5	−16 24	7.9	G0	F7	IV	2	− 25	5.4	
95660	57.4	+30 58	8.2	F2	F3	V	2	+ 5	0.5	V. br. lines
95680	57.5	−20 52	7.4	K0	G6	III	2	+ 8	4.0	
96161	11 00.3	+38 56	7.5	K2	G5	III	1	+ 13	.....	
96294	01.0	+54 14	8.2	F0	F2	III	2	0	0.5	
96497	02.1	+22 35	7.9	G0	G1	V	2	+ 3	0.1	
96696	03.2	−20 59	7.7	K0	G7	III	2	+ 5	5.0	
97406	07.5	+46 45	8.2	F2	F1	V	2	− 2	2.5	
97486	08.0	+62 48	7.8	G5	G5	III	2	− 30	0.7	
97658	09.2	+26 16	7.6	K0	G7	V	2	+ 2	3.3	
97876	10.4	−11 02	7.3	Ma	M4	III	3	− 27	2.8	

TABLE 1—*Continued*

HD	α (1900)	δ (1900)	Vis. Mag.	Spec. Cl.		Lum. Class	No. Obs.	V (Km/Sec)	p.e. (Km/Sec)	Remarks
				HD	LO					
(1)	(2)	(3)	(4)	(5)	(6)	(7)	(8)	(9)	(10)	(11)
97904	11^{h}10^m.6	+74° 53′	7.6	K0	G7	III	2	− 23	± 0.7	
98019	11.3	−20 09	7.8	K0	G7	III	3	+ 33	0.9	
98487	14.7	+62 54	8.2	F2	F1	V	2	− 4	2.3	
98500	14.8	+30 40	7.4	K5	M0	III	4	+ 31	0.6	
98932	18.0	−16 04	8.1	F5	F5	III	2	+ 8	2.4	
99058	18.9	−20 43	8.1	G0	F6	V	3	+ 16	2.0	
99331	20.7	−13 59	7.4	K5	K5	III	2	+ 25	1.9	
99873	24.3	− 0 18	7.4	K2	K4	III	1	− 15	.....	
100551	29.2	−12 19	8.1	F8	F5	V	2	− 6	1.3	
100738	30.5	+66 54	8.1	F5	F5	IV	2	− 30	0.4	
101025	32.5	+22 15	8.2	F5	F2	IV	3	− 6	1.2	
101178	33.5	+39 45	7.4	K5	M1	III	2	− 36	1.5	
101642	36.7	+26 29	8.0	F8	F8	V	2	− 23	1.0	
101828	38.1	+82 53	7.8	G5	G5	II	2	− 16	1.0	
101969	39.0	− 4 15	8.1	F5	F4	V	2	+ 19	1.7	
102159	40.4	+36 26	7.2	Mb	M6	III	2	+ 58	0.7	MW* +63 (1)
102165	40.4	−20 55	7.6	F5	F7	IV	2	+ 19	1.9	
102570	43.3	+46 41	8.2	F0	F3	V	2	+ 5	0.0	
102651	44.0	− 8 34	7.5	K0	G6	III	2	+ 14	0.9	
102652	44.0	−12 04	8.3	F2	F2	IV	2	+ 16	5.7	Var?
102686	44.3	+30 03	7.6	K0	G6p	III#	3	0	1.4	
102885	45.6	−12 18	7.3	K5	K5	III	4	− 25	1.9	
103628	50.9	+22 34	8.0	F8	F7	IV	2	+ 23	3.3	
104415	56.3	−20 58	8.3	F8	F6	V	3	+ 61	3.4	
104986	12 00.2	+74 00	7.6	K0	G9	III	3	− 54	3.3	
105187	01.6	− 8 51	8.1	F5	F7	V	2	− 6	2.7	
105548	04.1	+17 45	7.4	K5	M1	III	3	+ 36	1.7	
105679	04.9	+42 51	8.0	F8	F7	V	2	+ 4	3.8	
105730	05.1	−19 13	7.7	K5	K5	III	3	− 6	1.5	
106127	07.6	− 1 55	7.4	K5	K5	III	3	+ 8	4.4	
106348	09.0	+42 43	8.1	F5	F4	V	2	− 15	3.4	
106691	11.1	+26 19	8.1	F5	F5	IV	2	+ 8	6.2	Trumpler +0.7±1.5 (4)
107582	16.8	+62 19	8.0	G0	G1	V	2	− 82	0.5	
108203	20.7	− 4 18	8.1	F8	F6	V	2	− 15	1.1	
108468	22.6	+18 24	7.5	K0	G5	III	4	− 24	0.7	
108649	23.8	+66 02	8.1	F2	F3	V	2	− 6	4.0	
108832	25.2	+82 33	8.2	F5	F3	IV	3	− 8	0.8	
109031	26.6	+22 08	8.2	F2	F0	IV	2	+ 3	2.0	
109035	26.6	−20 25	7.3	K2	K0	III	2	+ 4	0.5	
109497	30.0	+30 45	8.2	F5	F6	IV	1	− 6	.....	
109695	31.5	−20 45	7.9	K2	G9	III	5	+ 9	2.2	
110194	35.3	+34 42	7.5	K2	K3	III	2	− 44	0.7	
110375	36.6	+38 56	8.1	F5	F2	IV	2	− 23	5.2	
110950	40.6	+30 19	8.0	G0	G2	V	3	+ 8	4.6	
111384	43.8	− 8 40	7.6	K0	K2	III	3	+ 16	1.0	
111420	44.1	+71 29	7.3	K5	K3	II–III	2	− 39	0.4	
111603	45.4	+42 46	8.2	F5	F6	IV	3	+ 11	6.2	Var (−3 to +28)
111957	47.9	+50 49	8.2	F5	F4	V	2	+ 4	1.5	
112311	50.7	+58 41	8.2	F0	F0	IV	2	− 12	2.7	
112574	52.6	−12 36	8.1	F8	F7	V	3	− 10	5.4	Var?
113036	55.8	+42 28	8.2	F0	F0	V	2	− 1	0.4	
113284	57.6	+30 53	8.2	F0	F1	IV	2	+ 7	4.4	
113406	58.4	+24 21	7.2	Ma	M1	III	4	+ 1	2.4	MW* +3.5±3.1 (3)
113449	58.7	− 4 37	7.5	K0	G5	V	2	0	6.9	Var?
113516	59.2	−22 25	7.8	G5	F7	V	2	− 10	6.7	Var?
113577	59.6	+46 59	8.2	F5	F4	IV	2	+ 6	1.9	
113621	59.9	+50 36	8.0	G0	F9	V	2	− 5	1.3	

102686. λ 4077 gives III; λ 4215 gives IV.

TABLE 1—*Continued*

HD	α (1900)	δ (1900)	Vis. Mag.	Spec. Cl.		Lum. Class	No. Obs.	V (Km/Sec)	p.e. (Km/Sec)	Remarks
				HD	LO					
(1)	(2)	(3)	(4)	(5)	(6)	(7)	(8)	(9)	(10)	(11)
113637	13h00m0	+54° 29′	7.5	K2	K3	III	2	− 32	± 0.5	
113892	01.7	+41 27	7.4	K5	M1	III	4	− 33	3.2	
114217	04.1	+42 41	8.2	F2	F4	IV	1	− 20	.....	
114494	05.8	+ 2 16	8.1	F8	F6	III	3	− 5	6.7	Var (−16 to +14)**
114662	06.8	−20 20	8.0	K2	K0	II	3	+ 4	1.7	
114913	08.6	+58 59	8.0	G0	F7	V	2	− 12	3.1	
115322	11.4	+ 7 02	7.2	Mb	M6	III	3	− 24	1.0	MW* −22 (1)
115427	12.0	−12 00	8.1	F5	F4	IV	3	− 14	7.6	Var (−1 to −36)
115832	14.6	+ 6 00	8.1	F5	F5	III	3	− 11	1.2	
116961	22.0	−12 47	7.7	G5	G5	III	3	+ 2	1.4	
117125	23.2	+ 2 45	7.6	K0	G8	III	3	− 1	1.6	
117403	25.0	+46 54	8.0	F8	F4	III	2	0	0.4	
118186	30.1	−16 25	8.1	F8	F8	V	2	− 16	3.3	
118643	33.1	+34 15	7.5	K2	K3	II	2	− 4	1.9	
118942	35.1	−16 50	8.1	F5	F3	IV	3	+ 4	1.9	
118957	35.2	− 4 45	8.1	F5	F5	IV	2	− 10	4.5	
119272	37.2	+78 24	8.2	F5	F4	V	3	− 17	2.0	
120335	43.7	+18 44	8.1	F5	F3	IV	2	+ 5	7.5	Var?
120893	47.2	+38 13	8.2	F5	F6	V	2	− 8	3.1	
120980	47.7	+66 29	8.2	F0	F1	III	2	− 10	2.5	
121766	52.4	− 4 59	8.1	F5	F4	IV	2	− 9	2.1	
121785	52.5	−20 09	8.6	F0	A	.....	6	+ 50	12.0	Var? v. br. lines
121829	52.8	+18 44	7.7	G5	G6	III–IV	3	− 5	2.1	
122132	54.8	+47 06	7.2	Ma	M2	III	3	− 60	1.7	MW* −57.9±2.0 (3)
122149	54.9	+54 04	7.9	G0	G2	IV	2	− 2	2.3	
122694	58.3	+22 33	8.2	F2	F6	V	2	− 45	2.2	
122751	58.6	−20 50	8.2	F8	F2	V	3	− 29	2.9	
122967	59.9	+62 46	8.2	F0	F3	V	2	− 7	1.0	
123011	14 00.1	+70 49	7.6	K0	G8	III	2	− 38	2.1	
123280	01.6	+42 51	8.0	F8	F6	V	2	+ 7	11.7	Var (+25 to −10)
123413	02.4	−20 43	8.1	K0	G5	III	3	+ 28	4.2	
123598	03.5	−18 46	7.2	Ma	M3	III	2	+ 65	3.5	MW* +50 (1)
123673	04.0	+18 06	7.8	G5	G6	III	3	− 8	1.1	
123760	04.5	+10 44	7.9	G0	G5	V	2	+ 2	1.1	MW* −3.5±2.7 (5)
124304	07.7	−13 23	7.2	Mb	M5	II	3	− 46	1.5	MW* −43 (1)
124330	07.9	+54 53	7.8	G5	G4	IV	3	− 30	1.4	
124370	08.1	+62 59	8.2	F5	F2	IV	2	+ 4	1.3	
124575	09.3	−20 36	7.7	K0	K5	II–III	2	− 21	5.1	
125272	13.3	+58 32	8.0	G0	F9	V	2	− 22	0.4	
125455	14.4	− 4 42	7.6	K0	K0	V	2	− 1	3.6	MW −13.0±1.6 (3)
126101	18.4	−12 28	8.1	F8	F5	V	2	+ 2	1.3	
126140	18.6	+38 57	8.3	F0	F0	IV	3	− 4	2.5	
126381	20.0	+ 6 04	7.6	K0	G4	III	2	+ 7	2.1	
126516	20.9	− 0 15	8.2	F2	F3	V	3	− 37	4.2	
126898	23.2	−16 31	8.3	F0	F4	V	3	+ 11	12.4	Var?
127007	23.9	− 4 29	8.1	F5	F2	III	3	+ 9	1.4	
127227	25.1	+16 40	7.4	K5	K5	III	3	− 41	1.0	
127824	28.4	+50 02	8.2	F0	F4	IV	2	+ 24	1.6	
127825	28.4	+ 6 44	8.1	F5	F7	V	2	+ 1	1.6	
128164	30.3	+70 41	8.2	F2	F2	IV	2	− 8	0.5	
128200	30.5	− 4 50	7.5	K0	K0	III	2	+ 2	1.9	
128684	33.2	− 3 11	7.4	Ma	M2	III	3	− 11	2.7	MW* −2.0±1.6 (3)
129209	36.2	+30 57	7.9	G0	G2	IV	2	− 7	4.8	
129391	37.2	+18 55	7.6	K0	G7	III	3	− 15	1.0	
130155	41.5	+14 56	7.3	Ma	M1	III	3	+ 6	3.9	
130342	42.5	+18 45	8.0	G0	F4	V	2	+ 4	8.3	Var?
130768	44.9	+10 37	7.5	K0	G9	III	2	+ 16	3.5	
130893	45.6	+58 29	8.2	F5	F3	IV	2	− 16	2.4	

** 114494, λ 4077 strong.

TABLE 1—*Continued*

HD	α (1900)	δ (1900)	Vis. Mag.	Spec. Cl.		Lum. Class	No. Obs.	V (Km/Sec)	p.e. (Km/Sec)	Remarks
				HD	LO					
(1)	(2)	(3)	(4)	(5)	(6)	(7)	(8)	(9)	(10)	(11)
130991	14h46m0	−20° 12′	7.5	K0	G7	III	3	− 2	± 3.5	MW −7.1±1.1 (3)
131271	47.5	− 8 17	8.1	F8	F6	V	2	+ 12	5.0	
131958	51.5	−16 07	8.3	F2	F1	V	2	+ 34	6.4	Var?
133460	59.5	+26 25	7.9	G0	F7	V	3	− 9	5.5	Var (−22 to +6)
133644	15 00.5	− 0 55	8.1	F8	F7	V	3	+ 6	1.0	
134063	02.8	+22 57	7.7	G5	G4	III	2	−108	1.1	
134228	03.6	+10 30	7.9	G0	F8	V	2	+ 7	0.3	
134630	05.8	−12 41	7.5	K0	G7	III	2	− 37	0.7	
135633	11.1	+22 55	8.1	F8	G0	V	3	− 29	4.3	Var (−19 to −41)††
136010	13.2	− 8 02	7.6	K0	K1	II–III	2	+ 1	0.7	
136711	17.1	+18 48	7.6	K0	K3	II–III	3	− 76	0.1	
136866	17.9	−16 13	7.6	K0	K4	II–III	3	+ 35	2.9	
136927	18.2	+ 6 24	8.1	F5	F6	IV	3	− 48	0.6	
137719	22.5	+44 39	7.4	K5	K5	III	2	− 14	2.2	
137945	23.9	+22 49	8.3	F2	F3	V	2	− 48	2.0	
139784	35.0	−16 25	8.3	F2	F1	IV	3	+ 22	2.8	
140489	38.8	+ 2 44	7.6	K0	G8	III	2	− 12	2.5	
140514	38.9	+22 01	7.9	G0	G2	IV	2	+ 14	1.9	
140700	40.0	+16 50	7.4	K5	K5	II–III	2	− 26	2.4	
141247	43.0	− 4 29	7.9	G0	F9	V	3	− 68	4.0	
142176	48.0	+30 11	7.4	K5	K5	III	2	− 53	2.2	
143840	57.6	− 4 32	8.2	F5	F1	V	3	− 29	1.7	
144492	16 01.1	− 4 30	8.0	F8	F4	V	3	− 14	5.4	Var?
144639	01.8	−12 52	8.2	F2	F3	III	3	+ 10	3.7	
144955	03.4	+58 26	8.2	F2	F1	IV	3	− 4	0.3	
145059	03.8	−16 55	8.0	G0	G1	V	2	+ 45	0.5	
145153	04.3	−12 37	7.6	K0	G8	III	3	− 15	1.7	
145404	05.7	+26 16	7.7	G5	G0	V	2	− 8	3.2	
145710	07.3	+62 45	8.2	F2	F0	V	2	− 20	3.6	
145748	07.5	−14 51	7.4	K5	M0	III	3	− 34	2.3	
146264	10.3	+18 28	7.5	K0	G8	III	3	− 21	1.7	
146815	13.1	+ 6 19	7.6	K0	G7	II	2	+ 31	0.4	
146929	13.7	+34 31	8.3	F2	F2	IV	2	− 27	0.3	
147144	15.0	+42 52	8.3	F2	F4	IV	2	− 18	5.5	
147644	18.0	− 0 29	7.9	G0	F9	V	2	+ 10	2.1	
148180	21.2	− 8 30	8.2	F0	F0	IV	2	− 8	3.1	
148365	22.4	+50 41	7.8	G5	G6	III	2	− 43	2.1	
150415	35.8	−16 45	8.2	F5	F5	V	2	+ 10	3.6	
150466	36.1	− 4 02	8.2	F0	F5	V	3	− 10	5.3	Var (+4 to −22)
150553	36.7	+22 57	8.3	F0	F0	V	2	− 11	7.7	Var?
150826	38.4	+58 19	8.2	F5	F6	IV	2	− 24	3.4	
151061	39.9	− 2 54	7.2	Mb	M6	III	3	− 6	1.9	MW* −10.6±1.1 (3)
151120	40.3	+42 48	8.2	F0	F2	IV	2	− 13	0.8	
151445	42.3	+42 37	8.0	F8	F5	IV	2	+ 2	4.7	
151451	42.3	−20 46	8.7	F8	F5	III	4	+ 46	1.2	
152112	46.3	+10 03	7.3	Ma	M3	III	4	− 45	1.9	
152484	48.5	− 4 09	7.7	G5	G9	III	2	+ 45	6.3	Var?
152794	50.4	+30 36	8.2	F2	F0	IV	2	− 15	0.8	
153033	52.0	+ 6 39	7.5	K0	K5	III	3	− 42	0.5	
153240	53.1	− 4 11	8.0	F8	F6	V	2	− 22	1.4	
153540	55.1	+11 05	7.3	K5	K4	III	3	− 18	1.0	
153698	55.9	+27 29	7.3	Mb	M4	III	3	− 20	3.7	MW* −24.2±0.8 (3)
153741	56.1	−20 26	7.6	K0	G6	II	2	− 27	0.3	
153777	56.3	+38 00	8.1	F5	F2	IV	2	− 12	7.7	Var?
154578	17 01.2	+46 14	8.0	F8	F7	V	2	+ 28	0.3	
154617	01.5	+26 36	8.1	F5	F5	IV	2	− 24	0.2	
155105	04.5	− 8 24	8.0	G0	G3	V	2	− 33	0.1	
155467	06.7	− 0 52	8.1	F5	F7	V	2	− 11	1.3	

†† Brighter component of ADS 9555 (7.5–11.0 mag.); separation 10″.8.

TABLE 1—*Continued*

HD	α (1900)	δ (1900)	Vis. Mag.	Spec. Cl.		Lum. Class	No. Obs.	V (Km/Sec)	p.e. (Km/Sec)	Remarks
				HD	LO					
(1)	(2)	(3)	(4)	(5)	(6)	(7)	(8)	(9)	(10)	(11)
155581	17h07m4	+14° 38′	7.4	K5	K5	III	3	+ 13	± 1.0	
155967	09.7	+14 42	8.1	F5	F6	V	3	− 15	1.7	MW −16.7±1.9 (3)
156282	11.6	+42 21	7.9	G0	F8	V	1	− 1	.....	
156392	12.2	−12 12	8.2	F5	F3	V	4	− 32	1.5	
156536	13.0	+26 49	8.1	F5	F3	IV	2	− 38	1.1	
156649	13.7	+63 28	7.4	K5	K5	III	3	+ 16	2.4	
157031	15.8	−20 08	8.5	G0	G0	V	2	− 10	3.5	
157072	16.0	−20 28	7.1	K2	K4	IV	3	+ 1	1.5	
157463	18.3	+42 19	7.6	K0	G5	III	2	+ 8	0.3	
157606	19.1	+13 30	7.4	K5	K4	III	2	− 8	2.8	
157683	19.6	+22 00	8.2	F5	F1	V	2	− 25	0.8	
157925	21.1	+22 31	8.3	F2	F0	III	2	− 25	4.3	
158211	22.9	+18 00	7.5	K0	G9	III	2	− 1	3.2	
158671	25.5	+46 09	8.2	F2	F2	V	2	− 22	3.9	
159119	27.8	+14 28	7.4	K5	K5	III	2	− 20	0.4	
159410	29.5	+46 24	7.5	K2	K3	III	2	− 52	3.6	
159714	31.1	+24 25	7.4	K5	K4	III	4	− 20	4.9	Var (−8 to −36)
159754	31.3	+74 34	8.2	F2	F2	V	2	− 5	0.7	
159972	32.4	+ 6 30	8.1	F8	F6	V	2	0	0.7	
161227	39.2	−16 44	8.2	F0	F0	II	2	+ 4	1.7	
162262	45.1	+ 2 16	8.1	F5	F5	V	5	− 1	0.9	Var (+32 to −44)
162949	48.6	+34 13	7.9	G0	F3	V	3	− 11	2.3	
163418	51.0	+42 41	7.6	K0	G6	III	2	− 1	1.1	MW −0.7±0.6 (3)
163572	51.7	−20 37	8.8	F0	F2	II	2	+ 24	2.9	
164809	57.8	+22 28	7.5	K2	K0	II–III	2	− 51	1.7	
165042	59.0	+19 33	7.2	Ma	M5	II–III	2	− 23	3.6	MW* −20.0±0.2 (2)
165073	59.1	+30 21	8.1	F8	F7	V	2	− 35	1.1	
165374	18 00.6	+16 55	7.2	Ma	M2	III	2	− 17	11.3	Var (0 to −34) MW* −11 var (+50 to −41) (4)
166091	04.0	+63 47	7.4	K5	K5	II–III	2	− 69	3.5	
166408	05.4	+50 52	8.3	F0	A8	.....	2	− 40	1.3	
166601	06.3	+30 49	8.0	F8	F5	V	2	− 67	0.1	
166780	07.1	+57 57	7.4	K5	K5	III	2	− 43	2.8	
166781	07.1	+26 38	7.7	G5	G3	II	2	− 39	1.9	
167225	09.1	−20 54	8.9	K0	G7	III	3	− 13	2.5	
167391	09.9	+26 44	8.1	F5	F5	IV	2	− 15	10.0	Var (−1 to −29)
168245	13.7	− 4 09	7.6	K0	G7	II	3	+ 41	11.0	Var (+25 to +73)
168451	14.6	−20 15	8.1	F5	F6	IV	4	− 30	0.5	
168621	15.6	+34 05	8.1	F8	F4	V	2	− 20	1.0	
170002	22.2	+46 12	8.1	F5	F5	IV	2	− 11	1.6	
170053	22.4	+ 6 56	7.6	K0	K2	II	3	− 30	0.5	
170456	24.4	−16 16	8.3	F0	F1	V	3	− 7	9.1	Var (−22 to +19)
170698	25.7	+18 32	7.6	K0	G6	III	2	0	0.8	
171662	31.0	−16 01	7.4	K5	K5	III	3	− 18	0.8	
171706	31.2	− 4 38	8.0	G0	F9	V	2	+ 20	4.2	
172237	34.0	−20 46	8.8	F5	F6	IV	2	− 20	2.7	
172381	34.8	+30 22	7.3	Ma	M2	III	2	− 61	2.7	
172508	35.5	− 4 36	7.5	K0	K0	II–III	4	− 11	1.8	DAO −14 (1)
172669	36.4	+66 49	7.6	K0	G3	V	2	− 6	0.6	MW −5.8±1.5 (3)
173051	38.3	+58 08	8.3	F0	F2	IV	2	− 20	0.3	
173189	39.0	+54 49	8.1	F5	F5	V	2	+ 11	1.8	
173297	39.4	−20 45	8.1	F5	G0	*Ib*	2	+ 19	13.3	Var (−1 to +39) V 350 Sgr
173435	40.2	+26 08	7.7	G5	G7	III	2	− 12	1.8	
173511	40.6	+61 27	7.4	K5	K5	III	2	− 8	0.8	
173526	40.7	+22 27	7.5	K0	G4	II	2	+ 10	0.2	DAO +14 (1)
173651	41.3	+ 2 52	8.1	F5	F7	V	2	− 1	3.4	

TABLE 1—*Continued*

HD	α (1900)	δ (1900)	Vis. Mag.	Spec. Cl.		Lum. Class	No. Obs.	V (Km/Sec)	p.e. (Km/Sec)	Remarks
				HD	LO					
(1)	(2)	(3)	(4)	(5)	(6)	(7)	(8)	(9)	(10)	(11)
173741	18h41m8	+38° 13′	7.6	K0	K5	III	3	− 6	± 2.8	
173854	42.4	−19 19	7.0	K5	K5	III	3	+ 7	3.0	
173883	42.6	− 0 21	7.9	G0	F9	V	2	− 82	1.4	
174349	45.0	+10 25	7.5	K2	K4	II–III	2	− 21	2.2	
174719	46.8	+ 2 55	7.7	G5	G6	V	3	− 18	2.9	
175036	48.4	+26 24	7.9	G0	F8	V	2	− 51	0.5	
175545	50.7	− 0 52	7.5	K0	K2	III	2	− 14	1.7	DAO −30 (1)
175905	52.5	− 0 39	7.5	K0	K1	III	2	+ 24	2.3	DAO +18 (1)
176391	55.0	+42 32	8.2	F2	F5	III	2	− 18	0.4	
176886	57.2	−20 52	8.5	F5	F5	IV	2	0	0.5	
177433	59.6	+14 57	7.6	K0	K0	II–III	2	− 31	2.4	
178011	19 01.9	+ 5 05	8.3	F0	F3	IV	1	+ 1	.....	
178165	02.4	+ 5 04	7.6	K0	K3	III–IV	2	− 2	2.5	
178612	04.2	+48 46	7.3	K5	K4	III	2	− 9	0.5	
179070	06.0	+38 33	8.0	G0	F6	IV	2	− 28	2.2	
179177	06.4	−16 36	8.1	F5	F5	III	2	− 33	1.8	
179757	08.7	+18 58	8.3	F0	F0	V	3	+ 21	12.4	Var (−1 to +57) broad lines
179785	08.8	+14 46	7.4	K2	K4	III	2	− 26	3.6	MW −32.1±1.1 (3) DAO −29 (1)
179869	09.1	+41 04	7.3	Ma	M3	III	2	− 11	0.8	
179985	09.6	+34 19	8.0	G0	F7	III	2	− 25	0.1	
180015	09.7	−16 17	7.5	K0	G8	III	2	+ 41	1.1	
180714	12.5	+18 39	8.3	F0	F0	IV	2	− 18	3.8	
180867	13.1	+46 53	8.1	F8	F6	V	2	− 14	0.1	
180940	13.4	+18 40	7.6	K0	G2	III–IV	2	+ 4	2.1	
181312	14.9	−10 44	7.3	Ma	M5	III	3	− 68	3.4	
181358	15.1	+54 07	8.1	F8	F6	IV	2	− 54	3.0	
181475	15.5	− 4 41	7.4	K5	K5	II	3	+ 3	1.6	DAO +1 (1)
181604	16.0	+10 28	7.9	G0	F7	IV	2	− 20	4.7	
181681	16.3	+40 05	7.4	K5	K4	III	2	− 21	0.1	
182549	20.1	+46 06	7.8	G5	G6	II	2	− 25	1.9	
183127	22.9	− 0 37	8.1	F5	F6	IV	2	− 10	0.9	
183681	25.6	+22 30	7.5	K2	M0	III	5	− 8	2.0	DAO −21 (1)
183791	26.1	+ 6 10	7.8	G5	G2	II	2	+ 15	2.6	
184025	27.3	+ 6 27	8.1	F5	F2	IV	3	− 23	4.9	Var (−11 to −36)
184590	30.1	+25 08	7.2	Ma	M1	II–III	2	+ 15	0.7	MW* +24.0±1.0 (2)
184881	31.4	+18 21	7.8	G5	G5	III–IV	2	+ 3	0.1	
184909	31.5	+14 18	7.5	K2	K3	III	3	− 20	1.9	
185115	32.5	+46 22	8.2	F0	F1	IV	3	− 15	1.2	
186176	37.8	+46 09	7.8	G5	G6	III	2	− 1	0.6	
185497	39.6	− 8 53	8.3	F0	F0	V	5	− 3	4.8	Var (+20 to −22)
186752	41.2	−20 08	8.5	G0	F8	V	3	− 15	1.4	
186962	42.3	+18 34	7.6	K0	K0	II–III	3	− 18	2.8	
186981	42.4	+18 38	8.1	F8	F4	III	3	− 21	2.1	
187317	44.3	+58 08	7.9	G0	F6	III	2	− 21	0.3	
187401	44.7	+14 58	7.7	G5	G5	II	3	− 16	1.3	
187663	46.0	−12 52	7.5	K0	G9	III	2	− 11	1.3	
188169	48.8	+50 24	8.0	F8	F4	V	2	− 10	0.1	
188398	49.9	+50 46	8.2	F5	F4	III	1	+ 34	.....	
189063	53.1	+60 33	7.3	K5	M0	III	2	− 22	0.1	MW −23.0±1.6 (4)
189084	53.2	+60 21	7.4	K5	M0	III	3	− 6	2.6	
189148	53.5	+34 45	8.2	F5	F6	V	3	− 9	0.9	
189578	55.6	+14 37	8.1	F8	F5	V	2	+ 12	7.9	Var (−22 to +46)
190149	58.5	+43 50	7.3	Ma	G9	III	2	− 61	1.4	
190315	59.3	+75 27	7.3	K5	K4	III	2	− 27	1.0	
190464	20 00.0	+54 23	8.3	F0	F2	III	2	+ 6	2.8	
191373	04.5	+54 22	8.1	F5	F3	V	2	− 9	1.1	

TABLE 1—*Continued*

HD	α (1900)	δ (1900)	Vis. Mag.	Spec. Cl.		Lum. Class	No. Obs.	V (Km/Sec)	p.e. (Km/Sec)	Remarks
				HD	LO					
(1)	(2)	(3)	(4)	(5)	(6)	(7)	(8)	(9)	(10)	(11)
191737	20h06m4	+58° 30′	7.8	G5	G3	III	2	− 5	± 0.2	
191878	07.0	+18 12	8.1	F8	F7	IV	2	− 23	1.0	
192020	07.7	+38 06	7.8	G5	G8	V	2	− 6	1.8	
192260	08.9	+34 53	7.6	K0	K0	IV	2	− 26	1.2	
192343	09.3	+ 6 18	8.0	G	G4	V	5	− 2	2.0‡‡	
192344	09.3	+ 6 18	7.8	G5	G4	IV	5	− 1	1.3‡‡	
192635	10.8	+74 08	8.1	F5	F4	IV	3	− 35	1.4	
192804	11.7	+30 56	7.7	G5	F8	V	2	− 25	0.1	
192867	12.1	+43 50	7.4	K5	M1	III	2	− 5	6.8	Var? DAO −18 (1)
192869	12.1	+42 03	7.9	G0	F6	IV	2	− 28	1.5	
193054	13.1	+52 12	7.3	K5	K5	III	2	− 57	0.5	DAO −54 (1)
193533	15.6	+72 16	7.3	Ma	M3	III	2	− 25	0.8	
193799	17.1	+ 6 51	7.6	K0	G9	III	2	− 2	0.5	
194299	19.8	+63 07	7.3	K5	M0	III	2	+ 21	1.4	
194595	21.4	+26 23	8.2	F5	F2	IV	2	− 18	4.2	
194737	22.2	+54 41	7.5	K2	K0	II–III	2	− 47	2.5	
194917	23.1	−12 07	7.4	K5	M0	III	4	+ 17	1.4	
195075	24.0	−12 55	7.5	K0	G7	III	2	+ 28	0.3	
195100	24.2	+42 44	7.5	K0	G6	III	2	+ 2	1.7	
195534	26.8	− 0 29	7.6	K0	G8	III	2	− 49	0.7	
195668	27.6	+18 17	7.2	Mb	M4	II–III	3	− 3	0.5	
195767	28.1	− 6 33	7.3	Ma	M3	III	2	− 21	1.9	
195807	28.4	+54 15	8.2	F0	F2	III	2	+ 7	3.3	
195850	28.7	+82 02	8.1	F5	F5	IV	2	+ 4	20.9	Var (−27 to +36)
195993	29.4	+17 51	7.3	K5	K5	III	2	− 3	4.7	
196090	30.0	+46 49	7.8	G5	G7	III	2	− 42	1.6	
196245	31.0	+ 6 44	8.1	F5	F4	IV	2	− 6	5.8	
196282	31.2	+49 25	7.3	K5	K4	III	2	− 26	1.0	DAO −26 (1)
196346	31.7	+ 2 08	7.6	K0	G9	III	3	− 49	1.8	
196643	33.6	+37 45	7.4	K5	K5	III	2	− 11	0.1	DAO −20 (1)
196674	33.8	+26 43	8.0	F8	F7	IV	2	− 56	1.5	
196972	35.6	+30 28	7.5	K2	K0	II	2	+ 15	1.3	DAO +14 (1)
197206	37.2	+30 54	7.4	K2	K1	IV	2	− 26	1.0	
197315	37.8	+ 2 38	8.3	F2	F4	V	2	− 21	0.1	
197577	39.5	− 8 21	8.0	K0	G2	III	2	+ 6	5.6	
197976	42.1	+18 25	8.3	F0	F0	III	1	− 24	.....	
198025	42.5	+ 1 29	7.3	K5	K4	III	2	+ 19	4.5	
198075	42.8	−12 49	8.0	G0	G3	V	2	− 16	1.3	
198188	43.5	−20 59	8.0	G5	G0	V	2	− 90	3.6	MW* −82.6±2.6 (3)
198330	44.5	+30 25	7.4	K5	K4	III	2	− 4	5.8	DAO +4 (1)
198861	48.2	+10 36	8.1	F8	F7	IV	3	− 34	1.2	
199120	50.0	+58 16	7.6	K0	G7	II–III	2	− 6	3.7	
199378 / 199379	51.7	−14 27	7.5	K0 +A2	G0	IVp‖‖	2	− 15	1.8	
199523	52.6	−12 21	7.5	K0	G7	III	2	+ 13	2.0	
199761	54.1	+46 48	8.1	F8	F4	III	2	− 16	4.3	
200043	55.9	+32 06	7.2	Mb	M3	III	3	− 16	0.7	
200451	58.4	+26 06	7.4	K5	M0	III	2	− 25	3.7	
200531	58.9	+34 38	8.2	F2	F3	V	2	+ 11	1.6	
200580	59.2	+ 2 36	8.1	F8	F8	V	3	− 4	4.2	Var? MW −9.3±1.5 (3)
200925	21 01.4	+50 24	8.2	F5	F5	III	2	+ 15	2.4	
201525	05.1	+22 32	8.0	F8	F7	IV	2	− 31	1.6	
202712	12.6	+22 05	8.2	F2	F4	IV	2	+ 3	7.1	Var?
202783	13.1	−12 41	8.0	F8	F7	V	3	− 18	1.2	
203135	15.3	+53 45	7.4	K5	K3	II–III	2	− 45	2.1	DAO −37 (1)
203140	15.3	+12 33	7.3	K5	M0	III	3	− 16	0.6	
203378	16.7	+55 01	7.2	Mb	M6	III	2	− 27	9.0	Var (−1 to −41)

‡‡ 192343. Precedes 192344 0ˢ.0 and is south 0″.6.

‖‖ 199378. Spectrum suspected to be composite (G5 III + A).

TABLE 1—*Continued*

HD	α (1900)	δ (1900)	Vis. Mag.	Spec. Cl. HD	Spec. Cl. LO	Lum. Class	No. Obs.	V (Km/Sec)	p.e. (Km/Sec)	Remarks
(1)	(2)	(3)	(4)	(5)	(6)	(7)	(8)	(9)	(10)	(11)
203600	21h18m2	+62°06′	8.0	F8	F5	IV	2	− 17	± 0.9	
203712	18.9	+40 30	7.3	Mb	M7	III	2	− 53	1.4	MW* −50 (1)
203844	19.6	− 8 37	8.0	G0	G1	V	2	− 18	0.6	
205025	27.4	+34 06	8.2	F2	F3	IV	3	− 17	0.8	
205837	32.9	+14 46	7.5	K0	G4	III	2	− 29	3.7	
205966	33.8	+50 37	7.4	K5	M0	III	2	− 24	1.7	DAO −23 (1)
205998	34.0	+40 38	7.4	K5	K5	III	2	− 39	1.7	DAO −35 (1)
206146	35.0	−19 21	7.4	K5	M0	III	3	− 2	1.7	
206311	36.2	+63 56	7.4	K5	K5	III	5	− 7	1.0	DAO −14 (1)
206367	36.5	+21 46	7.4	K5	M2	III	2	− 17	3.2	
206469	37.2	− 8 55	8.2	F5	F4	V	2	+ 18	2.5	
206485	37.3	+18 30	7.6	K0	G7	III	2	− 10	2.5	
206507	37.4	+70 00	8.0	F8	F5	V	2	+ 8	1.1	
207076	41.4	− 2 40	7.2	Mb	M8	III	3	− 37	1.2	
207583	44.9	−16 40	7.8	G5	G5	V	2	+ 24	0.6	
207858	47.0	+26 16	8.0	F8	F6	V	2	− 20	2.7	
208609	52.3	+17 13	7.3	K5	K4	III	2	− 28	2.6	
208745	53.3	+58 09	8.3	F0	F0	V	2	− 8	9.0	Var?
208785	53.6	+50 01	7.6	K0	K3	II–III	2	− 17	2.4	
209394	58.0	+36 29	7.2	Mb	M2	III	2	− 60	3.2	
209712	22 00.3	− 8 11	8.1	F8	F6	V	2	− 17	2.5	
209977	02.1	+11 17	7.3	Ma	M1	III	2	− 68	2.9	MW* −64 (3)
210266	04.1	+ 6 59	8.0	F8	F7	V	3	− 3	1.2	
210342	04.7	+22 03	8.1	F5	F4	III	3	− 28	1.9	
210483	05.6	+18 18	7.8	G0	G1	V	2	− 72	1.2	
210514	05.8	+31 48	7.3	Mb	M4	III	3	− 25	1.4	
210698	07.1	+39 13	7.4	K5	K5	III	2	− 15	0.1	
210891	08.4	+10 22	8.2	F0	F0	IV	3	− 3	12.9	Var (+24 to −39)
210922	08.6	+54 36	7.4	K2	K1	III	2	− 12	0.3	DAO −15 (1)
210957	08.8	+18 25	8.2	F0	A9	IV	2	+ 5	5.7	
211244	10.7	+18 07	8.1	F5	F3	IV	2	+ 47	23.6	Var (+12 to +82)
211362	11.4	−16 53	8.1	F8	F6	IV	2	− 12	1.4	
211472	12.2	+54 10	7.8	G5	K1	V	2	− 7	1.0	
211489	12.3	+54 20	8.2	F0	F1	V	2	− 12	3.0	
211645	13.4	+38 31	7.5	K2	G9	III	2	− 25	2.8	
212882	22.4	+62 49	7.2	Mb	M4	III	2	+ 8	2.6	
213199	24.6	−16 58	8.1	F8	G0	V	2	+ 4	1.5	
213758	28.7	+58 31	8.0	F8	F3	V	2	+ 8	1.2	
213863	29.3	−20 22	8.7	F0	F1	V	2	− 38	5.2	
213890	29.5	+14 31	8.0	F8	F4	IV	2	+ 12	5.5	
214245	31.8	+12 39	7.3	K5	K5	III	3	− 30	3.1	
214422	32.9	+26 54	8.1	F8	F6	V	3	+ 2	1.7	
215166	38.2	−16 40	8.1	F8	F7	V	2	− 18	3.2	
215290	39.0	+32 19	7.3	K5	M0	III	2	− 23	1.0	
215399	39.8	+46 06	8.2	F0	F1	V	2	+ 13	6.3	
215763	42.4	+ 2 22	8.0	G0	F9	V	3	− 22	1.3	
215772	42.5	+46 39	8.2	F5	F5	V	3	− 2	5.8	Var (−15 to +14)
215953	43.8	+49 03	7.2	Ma	M3	III	2	− 52	2.5	MW* −50 (1)
216085	44.8	−16 50	8.3	F2	F3	IV	4	+ 14	1.2	
217276	54.5	−16 56	8.0	G0	G0	V	2	+ 52	1.8	
217577	56.6	+18 44	8.0	G0	G2	V	2	− 2	0.5	
217580	56.6	− 4 23	7.6	K0	K4	V	2	− 39	1.6	MW −50.7±0.5 (3)
217694	57.4	+50 18	7.4	K5	K4	III	2	− 81	2.5	DAO −83 (1)
217786	58.0	− 0 58	7.7	G5	F9	V	2	+ 7	2.0	
218081	23 00.1	− 8 18	7.6	K0	G8	III	3	− 25	1.1	MW* −23 var? (4)
218159	00.6	−16 00	8.1	F5	F3	V	2	+ 8	0.3	
218170	00.7	+28 29	7.4	K5	M2	III	3	− 54	3.5	Var?
218234	01.3	+18 27	7.6	K0	G8	III	2	+ 14	1.9	

TABLE 1—*Continued*

HD	α (1900)	δ (1900)	Vis. Mag.	Spec. Cl.		Lum. Class	No. Obs.	V (Km/Sec)	p.e. (Km/Sec)	Remarks
				HD	LO					
(1)	(2)	(3)	(4)	(5)	(6)	(7)	(8)	(9)	(10)	(11)
218852	23h06m2	+30° 37′	7.6	K0	G8	III	2	+ 5	± 2.1	
219066	07.9	− 0 30	7.7	G5	G6	III	2	0	4.3	
210497	11.1	+34 09	8.0	G0	F6	IV	2	+ 56	3.1	
219828	13.8	+18 06	8.0	G0	G0	IV	3	− 23	2.7	
220008	15.3	+ 6 19	7.8	G5	G4	V	3	− 15	1.0	
220140	16.3	+78 27	7.7	G5	G9	V	2	− 19	0.9	MW* −15.1±1.3 (3)
221247	25.3	+30 49	8.2	F2	F2	V	2	− 3	2.6	
221477	27.4	+34 47	8.1	F8	F8	V	2	+ 13	2.8	
221584	28.2	+62 44	8.0	G0	F7	V	2	− 27	1.5	
221777	29.9	− 8 14	7.4	K5	K4	III	2	+ 9	0.4	
221913	31.0	+50 43	7.2	Ma	M1	III	2	− 19	1.3	
222928	39.9	− 1 13	7.3	K5	K5	III	2	+ 8	0.4	
223110	41.7	+54 36	8.1	F5	F5	V	3	− 13	4.1	Var?
223835	47.9	+40 47	7.2	Ma	M2	III	3	− 12	3.2	MW* −11 (1)
223847	48.0	+58 52	7.8	G5	G7	III	2	− 15	1.4	
223963	48.9	− 9 51	7.4	K5	M1	III	2	− 34	2.1	
224060	49.7	+18 12	7.6	K0	K3	III	2	− 11	3.4	
224839	56.0	− 0 37	8.0	G0	F8	V	2	0	0.8	
224882	56.4	+30 11	8.0	G0	G2	IV	2	− 6	1.6	
225191	59.2	+42 02	8.2	F5	F7	IV	3	+ 21	1.3	

III. THE SPECTRAL AND LUMINOSITY CLASSES

All the estimates of spectral and luminosity class were made by Miss Emilia Pisani according to the Yerkes two-dimensional system[2] that includes the spectral class and Roman numerals indicative of luminosity. A total of 32 stars was selected from the *Atlas*, and, with their spectra as standards, spectral- and luminosity-class estimates were made of (*a*) all but nine of the 820 stars in Table 1 and (*b*) the 260 brighter stars used to bring the system of one-prism velocities into agreement with the three-prism Mills system. This latter group served to give some notion of the consistency of the spectral- and luminosity-class estimates, because for most of these brighter stars Mount Wilson, Victoria, and HD spectral class were available, while, for 41 of them, spectral and luminosity classes were contained in the *Atlas*.

The detailed results of the comparison of spectral classes are not given here because it was found that most of the estimates were in good agreement. The only differences of statistical significance are in the early F's, where the Lick estimates are appreciably later than the HD and Mount Wilson classes but agree well with those in the *Atlas*.

Since a comparison of the luminosity classes is relatively more important, the individual estimates for the 41 stars mentioned above are included in Table 2. An inspection of this table shows that the luminosity classes estimated for these brighter stars are in satisfactory agreement with the *Atlas* assignments. In most cases the estimates differ by less than one luminosity class, and there is only one instance (ξ Peg) in which the difference exceeds one luminosity class.

Because of the basis for selection of these stars—only those within a narrow range of apparent magnitude (HD m_{pg} 8.5–8.6)—the frequencies in Table 3 have only limited usefulness. Thus there are so few stars of the higher luminosity classes I and II and such

[2] Morgan, Keenan, and Kellman, *An Atlas of Stellar Spectra* (Chicago: University of Chicago Press, 1943).

TABLE 2

Comparison of Luminosity Classes

Star	MKK *Atlas*	Lick Obs.	Star	MKK *Atlas*	Lick Obs.
χ Peg	M2 III	M1 III	β Boo	G8 III	G7 II
α Cas	K0 II–III	G7 II–III	δ Boo	G8 III	G5 IV
η Cas A	G0 V	G0 V	α Ser	K2 III–IV	K2 III
τ Cet	G8 V	G6 V	λ Ser	G2 V	G0 V
ι Per	G0 V	G2 V	γ Ser	F6 IV	F7 V
δ Eri	K0 IV	K1 IV	ε CrB	K3 III	K3 III
π^2 Ori	F6 V	F6 V	ε Oph	G8 III	G9 III
χ^1 Ori	G0 V	F8 V	η Dra	G8 III	G7 III
κ Gem	G8 III	G9 III	κ Oph	K2 III	G9 III
β Cnc	K5 III	K4 III	λ Her	K3 III	K4 III
σ^2 UMa	F6 IV	F5 V	β Oph	K2 III–IV	K3 III
α Hya	K3 III	K4 II–III	ξ Her	G5 III	G6 III
ε Leo	G0 I–II	G0 *Ib*	η Ser	K0 III–IV	K0 IV
36 UMa	F8 V	F6 V	κ Lyr	K2 III	K2 II
ρ Hya	K2 III	K3 III–IV	109 Her	K2 III	K2 IV
46 LMi	K0 III–IV	K0 III	α Sct	K3 III	K3 III
ψ UMa	K2 III	K1 II	ε Aql	K2 III	K2 II
ε Crv	K2 III	K2 II–III	δ Dra	G8 III	G7 III
ε Vir	G8 III	G6 III	γ Aql	K3 I–II	K4 II
70 Vir	G5 IV–V	G6 IV–V	52 Cyg	K0 III	K1 III
τ Boo	F6 IV	F6 IV	1 Lac	K3 III	K3 II
α Boo	K2 pec	K0 III	ξ Peg	F6 III–IV	F7 V
ρ Boo	K3 III	K3 III			

TABLE 3

Frequencies of Spectral and Luminosity Classes

Luminosity Class	Spectral Class																															Totals
	F										G										K						M						
	0	1	2	3	4	5	6	7	8	9	0	1	2	3	4	5	6	7	8	9	0	1	2	3	4	5	0	1	2	3	4	5	6	7	8	
Ib					1						1										1															3
II	1		1				1					1	1	1	1	3	3	3	1	1	3	3	3	2		3	1	1		1		2				37
II–III																	1	1		1	7	1		4	2	3		1		1	2	1				25
III	5	2	6	7	9	9	4	1			1		2	2	11	17	21	24	19	18	6	7	3	6	24	41	18	13	19	15	9	3	7	1	1	331
III–IV													1			2	2							1												6
IV	12	4	15	20	19	22	17	12		2	4	4	6	3	3	3	1	3	2	1	2	1	1		1											158
V	11	9	9	22	26	27	32	34	21	17	9	11	3	5	3	5	1	1	1	1	1	1			1											251
Unclass.*																																				9
9	29	15	31	49	55	58	54	47	21	19	15	16	13	11	18	30	29	32	23	22	20	13	7	13	28	47	19	15	19	17	11	6	7	1	1	820
Subtotals	179					199					73					136					128						81					15				

* HD 24694 (F0), 47194 (A8), 54983 (A9), 55760 (A9), 56819 (A9:), 60265, 66633, 121785 (A), 166408 (A8).

a marked absence of main-sequence dwarfs of class V from about G5 through M that the tabulated data contribute little to a knowledge of the luminosity function for high and low luminosities. On the other hand, for giants, class III, and for the subgiants, class IV, the frequency distributions may be indicative of the true character of the luminosity function for these classes. For example, Morgan, Keenan, and Kellman,[2] Keenan,[3] and McCuskey[4] give evidence that subgiants later than K1 or K2 may not occur. The frequencies of the spectral and luminosity classes are given in Table 3 for all the stars listed in Table 1.

Quite recently Eggen,[5] has shown by precise photoelectric photometry that, among the nearer stars, those of class IV have very nearly the same photographic absolute magnitude, $M = +3.6$, with a very small dispersion, in the range F2–K1. The class IV stars in this material are therefore all at nearly the same distance, approximately 100 parsecs. Consequently, the frequency distribution for class IV in Table 3 may be typical for the volume of space concerned—a relatively thick shell of radius 100 parsecs. Within this shell there appears to be a maximum frequency of subgiants at F4–F5, with a fairly definite drop to zero frequency at K5. At the present time, however, no similar statement appears appropriate for class III stars because correspondingly precise information regarding their absolute magnitudes has not yet been published.

IV. SOLAR MOTION

Solar-motion solutions were made for three groupings according to luminosity class: (1) giants, classes II and III (including II–III and III–IV); (2) subgiants, class IV; and (3) main-sequence dwarfs, class V. Before the solutions were made, however, it was decided to reject certain stars, namely, a few of high velocity (>80 km/sec) and a number of variable or probably variable velocity. The latter are listed in Table 4.

The numbers of stars of constant velocity available for the solar-motion solutions for the several luminosity classes are indicated in Table 5. In the case of stars of luminosity class V, only those stars in the spectral range from F5 to G4, inclusive, were used in the solution.[6] The results from the solar-motion solutions are collected in Table 6.

The results from the solar-motion solutions indicate that there probably are no significant differences between the several luminosity groups, since the differences are of the order of the sums of the probable errors. Certainly, the co-ordinates of the apex agree well within their probable errors, and for this reason rounded mean values, $\bar{\alpha}_0 = 280^\circ$ and $\bar{\delta}_0 = +44\frac{1}{2}^\circ$, were used to compute the mean residual radial velocities from the appropriate values of the solar motions, V_0, for giants, subgiants, and dwarfs. Table 7 gives the mean residual velocities computed in this manner; quantities in parentheses are the numbers of stars in the means. Stars with residual velocities greater than 60 km/sec are individually listed in Table 8.

Comparison of the solar-motion results in Table 6 with those for other groups of stars, such as those included in the extensive computations of Nordström,[7] does not reveal outstanding differences. For the group of fainter stars included in Table 1 the galactic

[3] *Ap. J.*, **91**, 518, 1940.

[4] *Ap. J.*, **109**, 426, 1949.

[5] A.A.S. meeting, Ottawa, June 18–21, 1949.

[6] [Dr. Moore left no manuscript notes giving a reason for omitting the fairly large group of 62 F0–F4 stars and the small group of 12 G5–K4 stars from the solar-motion solution. Among the early F stars, however, it probably was difficult to separate those of luminosity class IV from class V. Thus within the spectral-class range from F0 to F4, inclusive, the class V assignments may include a number of class IV stars. Most of the class IV assignments in the same spectral range, on the other hand, probably are correct, since such assignments presumably would not have been made unless the luminosity criteria were fairly evident.—N. U. Mayall.]

[7] *Lund Obs. Medd.*, Ser. II, No. 79, 1936.

TABLE 4

STARS OF VARIABLE OR PROBABLY VARIABLE VELOCITY

Lum. Class	Var		Var?		Lum. Class	Var		Var?	
	HD	Sp. Cl.	HD	Sp. Cl.		HD	Sp. Cl.	HD	Sp. Cl.
Ib	173297 (V350 Sgr)	G0	.....	.....	V	80388	G1	9956	F6
						123280	F6	26395	F4
						133460	F7	29936	F9
II	168245	G7	.....	.....		135633	G0	71659	F8
						150466	F5	77378	F3
II–III	89312	K5	.....	.....		162262	F5	77930	F6
						170456	F1	89276	F0
III	56418	.....	2624	G6		179757	F0	92855	F9
	59076/77	G7+A	23962	K5		186497	F0	112574	F7
	69287	F2	57267	G5		189578	F5	113449	F5
	114494	F6	152484	G9		215772	F5	113516	F7
	159714	K4	192867	M1				126898	F4
	165374	M2	218170	M2				130342	F4
	203378	M6	.....	.....				131958	F1
								144492	F4
IV	94978	F0	4270	F3				150553	F0
	111603	F6	19808	F5				200580	F8
	115427	F4	39967	F6				208745	F0
	167391	F5	55438	F0				223110	F5
	184025	F2	58477	F2					
	195850	F5	88865	F6	Unclass.	56819	A9	24694	F0
	210891	F0	102652	F2				60265	.....
	211244	F3	120335	F3				121785	A
			153777	F2					
			202712	F4					

TABLE 5

NUMBERS OF STARS OMITTED AND USED IN SOLAR-MOTION SOLUTIONS

Lum. Class	No. of Stars	Omitted		Constant Vel.	Used in Sol.
		Var Vel.	Var? Vel.		
II	37	1	0	36	
II–III	25	1	0	24	
III	331	7	6	318	
III–IV	6	0	0	6	
	.....	.....	.....	.....	
	399	9	6	384	
		V>80		−3*	381
IV	158	8	10	140	
		V>80		−1†	139
V	251	11	19	221	
		F0–F4		−62	
		G5–K4		−12	
		V>80		− 1‡	146

* HD 19258, 27598, 134063. † HD 21910. ‡ HD 198188.

TABLE 6

SOLAR-MOTION SOLUTIONS, WITH PROBABLE ERRORS

Lum. Class	No. of Stars	V_0 (Km/Sec)	K (Km/Sec)	Equatorial		Galactic	
				α_0	δ_0	l	b
II, II–III III, III–IV	381	24.2±1.8	+1.5±1.1	282°.2±5°.2	+46°.7±2°.3	43°.7±4°.0	+18°.6±4°.0
IV	139	23.0±2.3	+3.0±1.5	275.7±6.4	+43.6±3.0	38.9±4.7	+22.5±3.4
V*	146	18.7±3.1	−2.0±1.7	285.0±9.5	+43.0±5.0	40.9±7.7	+15.3±4.2

* Only spectral classes F5–G4 (inclusive).

TABLE 7

MEAN RESIDUAL VELOCITIES (KM/SEC)
(Co-ordinates of Apex: α_0=280°, δ_0= +44 1/2°)

Lum. Class	V_0 (Km/Sec)	F		G		K	M		All Sp. Cl.
		0–4	5–9	0–4	5–9	0–5	0–4	5–8	
II, II–III III, III–IV	24	19.3 (30)	15.4 (14)	18.7 (20)	17.3 (112)	17.8 (112)	20.4 (79)	25.9 (14)	18.6 (381)
III	24	19.0 (28)	15.1 (13)	15.9 (14)	17.6 (96)	17.8 (81)	20.1 (72)	25.8 (12)	18.6 (316)
IV	23	11.2 (59)	15.0 (47)	17.4 (20)	23.5 (8)	13.0 (5)	.....	.....	14.1 (139)
V	19	16.3 (62)	17.2 (115)	24.1 (30)	12.1 (8)	15.0 (3)	.....	.....	17.7 (218)

TABLE 8

STARS WITH RESIDUAL RADIAL VELOCITIES >60 KM/SEC*

Star HD	Class		Obs. Vel.	Sun Corr.	Res. Vel.	Star HD	Class		Obs. Vel.	Sun Corr.	Res. Vel.
	Sp.	Lum.					Sp.	Lum.			
19258	M1	III	− 74	− 7	−81	102159	M6	III	+ 58	+ 6	+64
19286	F2	V	+ 52	+10	+62	107582	G1	V	− 82	+11	−71
21910	G9	IV	−104	+13	−91	123598	M3	III	+ 65	0	+65
27498	M4	III	+ 86	−15	+71	134063	G4	III	−108	+16	−92
27598	M5	II	+ 99	−18	+81	136711	K3	II–III	− 76	+15	−61
43856	F6	V	− 58	−12	−70	173883	F9	V	− 82	+13	−69
50060	F9	V	+ 71	−10	+61	198188	G0	V	− 90	+ 6	−84
62549	G1	V	+ 85	−14	+71	217694	K4	III	− 81	+18	−63
64372	G7	III	+ 82	− 6	+76	219497	F6	IV	+ 56	+14	+70

* Var and var? velocities omitted.

longitude of the apex is somewhat greater, by 15°–20°; but the latitude of the apex is about the same as for the stars represented, for example, in Nordström's Table 29. The apparently systematically lower latitude for Nordström's group of 500 dwarf G–M stars fainter than sixth magnitude, included in his Table 19, is not obtained from the luminosity class V stars in this material. Also, the solar motion for the luminosity class III stars appears to be a little larger, by 4–5 km/sec, than for the giants included in Nordström's investigation.

As regards the mean residual motions, Table 7 shows the usual tendency for them to increase with advancing spectral type, for the several luminosity classes. While there is an apparent exception in the case of the early F III stars, it probably cannot be regarded as significant, for the late F III stars do not show the same effect.

V. GALACTIC ROTATION

To investigate the possibility that differential galactic rotation may be represented in the radial velocities of some of these stars, several solutions that included a rotational term were made for the giants. This group was selected, of course, because its greater average distance would be expected to lead to a larger rotational term.

Since the direction to the center of the galaxy is now known to be toward $L_0 = 325°$, with an uncertainty of only a few degrees, this value was assumed in the first solution, which included 348 stars, mainly of luminosity class III (318 III, 24 II–III, 6 III–IV). Also, since the K-term for these stars was found to be $+1.5 \pm 1.1$ km/sec (Table 6), it was assumed to be zero, and the following results were obtained:

$$V_0 = 24.7 \pm 3.3 \text{ km/sec};$$

$$a_0 = 281^{\circ}.9 \pm 1^{\circ}.5, \quad \text{or} \quad l = 38^{\circ}.4 \pm 1^{\circ}.4;$$

$$\delta_0 = +41.3 \pm 0.9, \quad \text{or} \quad b = +16.7 \pm 1.0;$$

$$\bar{r}A = 4.2 \pm 1.9 \text{ km/sec}.$$

The solar motion is essentially the same as before, and there appears to be a significant rotational term, although the latter is only a little more than twice as large as its probable error. Since the stars included in the solution are distributed fairly uniformly over the sky, it is possible that those in higher galactic latitudes, for example, those with $|b| > 20°$, might tend to reduce the value of $\bar{r}A$ and to increase its probable error. To check this possibility, a second solution was made for $\bar{r}A$ and L_0, the longitude of the galactic center, from the residual radial velocities (computed as indicated in Table 7) for 147 giants having $|b| < 20°$, with the following results:

$$\bar{r}A = 6.7 \pm 1.5 \text{ km/sec};$$

$$L_0 = 309^{\circ}.2 \pm 7^{\circ}.0.$$

In this case the rotational term is four and a half times as large as its probable error, and it may therefore be concluded that the normal giants included in this material participate in the differential galactic rotation characteristic of the region around the sun. This conclusion supports Nordström's extensive computations for stars brighter and fainter than $m = 6.0$[8] and his analysis[9] of the radial velocities of a group of nearly 400 faint K stars observed by Redman, who had previously found little evidence for galactic rotation in his material.[10]

[8] *Ibid.*, Table 34.

[9] *Arkiv för Mat., Astr. och Fysik*, **23A**, No. 14, 1933; *Lund Obs. Medd.*, Ser. I, No. 131.

[10] *M.N.*, **92**, 107, 1931.

That a value for $\bar{r}A$ of the order of 5 km/sec is approximately correct for the luminosity class III stars in this material may be shown from the data in Table 9, which gives the mean distances for the stars concerned.

TABLE 9

MEAN DISTANCES OF 348 LUMINOSITY-CLASS III STARS*

Sp. Cl.	No. of Stars	Mean Sp. Cl.	Mean m_{vis}	Mean M_{vis}†	Mean Distance (Pcs)	Wt.
F	41	F4	8.2	+1.4	230	4
G	119	G6	7.7	+0.4	288	12
K	101	K4	7.4	−0.1	316	10
M	87	M2	7.3	−0.3	331	9

* Including 24 II–III and 6 III–IV stars.
† *An Atlas of Stellar Spectra*, Fig. 2, p. 34.

The weighted average of the mean distances in Table 9 is $\bar{r} = 300$ parsecs, which, with a generally accepted value of $A = 0.017$ km/sec/parsec, gives $\bar{r}A = 5.1$ km/sec for these stars. Thus the observed and expected galactic-rotational terms agree as well as may be expected.

ADDITIONAL STARS WHOSE SPECTRA HAVE A BRIGHT *Hα* LINE

PAUL W. MERRILL AND CORA G. BURWELL
Mount Wilson and Palomar Observatories
Received March 24, 1950

ABSTRACT

This paper lists 519 objects not previously published which have a bright *Hα* line on objective-prism photographs taken with the 10-inch telescope on Mount Wilson. Most of these objects are probably stars of spectral type B or A.

The objective-prism photographs taken during the last thirty years with the 10-inch telescope on Mount Wilson have shown a bright *Hα* line in some two thousand objects. About half these, of types B and A, are listed in the three sections of the *Mount Wilson Catalogue and Bibliography of Stars of Classes B and A Whose Spectra Have Bright Hydrogen Lines*.[1] Table 1 lists 519 additional objects, for only about 80 of which are spectral types known (type W, 2; O, 5; B, 33; A, 10; F, 15; G and K, 11; N or S, 3; peculiar, 10). Most of the remaining objects are probably of types O, B, and A, although a few are undoubtedly of other types; a very few faint planetary nebulae may possibly be included.

The chief groups of bright-line objects omitted are: (1) objects previously announced by ourselves or others to have bright lines; (2) planetary nebulae, known or suspected, under investigation by R. Minkowski; and (3) objects in which the reality of the bright *Hα* line appears uncertain.

In Table 1, stars for which catalogue numbers (HD, BD, or CD) or variable star names are not available are designated by their numbers on our objective-prism photographs. For example, "MHα 321-5" means star No. 5 on Plate 321 of the MHα series.

The galactic longitudes and latitudes, l and b, are for the pole, R.A. = 12^h40^m, Dec. = $+28°$ (1900).

For most stars in the HD, BD, or CD catalogues we have adopted the catalogue magnitude. For other stars the magnitudes are estimates from the objective-prism photographs; for the fainter stars these are quite uncertain because the continuous spectrum may be weak or even invisible. For some of the stars listed as 9.5 in the BD or 10 in the CD we have substituted our own estimates. For variable stars the maximum magnitude is given.

The last column of Table 1 gives the estimated intensity of the bright *Hα* line on the following scale: w = weak; m = medium; s = strong; s! = very strong.

Our best thanks are due to the volunteer observers, Mr. W. C. Miller and Dr. A. G. Mowbray, for taking most of the objective-prism photographs on which these bright-line stars were detected. We are appreciative also of the continued co-operation of our colleague, Rudolph Minkowski.

[1] Merrill and Burwell, *Mt. W. Contr.*, No. 471; *Ap. J.*, **78**, 87, 1933; *Mt. W. Contr.*, No. 682; *Ap. J.*, **98**, 153, 1943; *Mt. W. and P. Obs. Reprint*, No. 8; *Ap. J.*, **110**, 387, 1949.

TABLE I

ADDITIONAL STARS WHOSE SPECTRA HAVE A BRIGHT Hα LINE ON OBJECTIVE-PRISM PHOTOGRAPHS TAKEN AT MOUNT WILSON

No.	Star	R.A. 1900	Dec. 1900	l	b	Mag.	Int. Bright Hα
1	BD +62°11	0h 5m.5	+62° 37'	86°	+1°	9.2	m
2	MHα 321-5	0 7.6	+65 45	87	+4	10	m
3	MHα 284-4	0 29.7	+68 9	89	+6	10.5	m
4	MHα 295-122	0 38.7	+63 21	90	+1	10	m
5	MHα 295-108	0 39.0	+63 14	90	+1	11	m
6	D 130-19	0 40.5	+61 5	90	-1	10	s
7	MHα 325-81	0 40.9	+64 47	90	+3	10.4	v
8	BM Cas	0 48.7	+63 33	91	+2	9.1	m
9	MHα 295-99	0 51.8	+61 21	91	-1	10.5	v
10	MHα 224-71	0 58.0	+63 11	92	+1	10.5	m
11	HD 6744	1 3.1	+64 30	92	+3	8.9	m
12	MHα 325-72	1 6.5	+64 27	93	+3	12	m
13	MHα 295-95	1 8.7	+60 28	94	-1	10.5	m
14	MHα 295-44	1 9.7	+58 37	94	-3	10	m
15	(BD +57°251)	1 13.2	+57 44	94	-4	10	m
16	MHα 223-41	1 16.0	+61 0	94	-1	10.2	s
17	(BD +57°273)	1 16.9	+57 33	95	-4	12	m
18	BD +62°245	1 17.7	+62 18	94	+1	10	v
19	MHα 295-49	1 17.7	+58 19	95	-3	11	m
20	BD +59°246	1 18.0	+59 46	95	-2	9.3	m
21	MHα 224-7	1 19.6	+60 30	95	-1	12	m
22	MHα 295-84	1 22.2	+60 32	95	-1	11	m
23	MHα 354-101	1 24.4	+62 6	95	+1	11	v
24	MHα 224-12	1 24.5	+61 50	95	0	12	m
25	MHα 295-53	1 26.9	+58 59	96	-2	11	m
26	MHα 224-13	1 27.2	+61 23	96	0	11	s
27	MHα 224-64	1 27.9	+63 46	95	+2	11.5	v
28	MHα 354-111	1 28.5	+60 52	96	-1	11.5	v
29	MHα 326-10	1 28.8	+60 50	96	-1	11	s
30	(BD +60°274)	1 29.0	+60 46	96	-1	10	m
31	MHα 325-67	1 30.2	+66 31	95	+5	11	m
32	MHα 295-83	1 31.0	+61 34	96	0	11	m
33	MHα 224-63	1 31.1	+63 21	96	+2	12	m
34	MHα 224-15	1 31.4	+62 11	96	+1	11	m
35	MHα 224-61	1 32.8	+62 34	96	+1	12	s
36	BD +62°287	1 33.4	+62 36	96	+1	8.3	v
37	BD +62°292	1 35.0	+63 6	96	+2	9.4	v
38	MHα 354-121	1 37.3	+62 18	97	+1	10.5	v
39	MHα 224-57	1 37.8	+65 7	96	+4	10.5	m
40	MHα 224-55	1 37.9	+63 54	96	+3	12	s
41	BD +62°300	1 38.1	+62 22	97	+1	9.4	m
42	(BD +60°341)	1 39.5	+60 38	97	-1	10.0	m
43	BD +60°343	1 39.6	+60 46	97	-1	9.1	v
44	MHα 5-12	1 39.8	+59 3	98	-2	11	m
45	BD +59°330	1 43.2	+59 41	98	-1	10	m
46	MHα 295-60	1 47.1	+59 22	98	-2	12	m
47	MHα 295-69	1 47.5	+59 37	98	-1	12	s
48	BD +61°353	1 48.9	+61 45	98	+1	9.3	v
49	BD +60°393	1 50.9	+61 5	98	0	11	m
50	MHα 354-50	1 54.4	+59 52	99	-1	10.5	v
51	MHα 326-28	1 55.3	+59 9	99	-1	11	m
52	BD +61°371	1 56.9	+61 55	99	+1	10.5	m
53	MHα 224-50	1 58.7	+62 53	99	0	10	v
54	(BD +57°485)	2 0.3	+57 26	101	-3	9.4	m
55	MHα 354-40	2 10.2	+58 33	102	-1	10	v
56	MHα 224-46	2 10.3	+64 7	100	+4	10	m
57	(BD +56°511)	2 11.8	+56 37	102	-3	8.8	v
58	HD 14947	2 19.5	+58 25	103	-1	8.0	v
59	MHα 125-9	2 21.9	+61 3	102	+1	10	m
60	MHα 379-17	2 22.6	+55 50	104	-3	10.5	v

TABLE I (Cont'd)

No.	Star	R. A. 1900	Dec. 1900	l	b	Mag.	Int. Bright Ha
61	MWa 5-86	$2^h\ 22.^m9$	+56° 52'	104°	-2°	11	s
62	MD 15570	2 25.2	+60 56	102	+1	8.0	m
63	MWa 379-57	2 25.9	+57 6	104	-2	10.5	m
64	MWa 5-75	2 26.4	+57 7	104	-2	11	s
65	MWa 5-76	2 29.7	+57 31	104	-1	10	s
66	MWa 5-83	2 32.9	+56 41	105	-2	10.5	s
67	MWa 125-6	2 33.8	+61 53	103	+3	11	s
68	MWa 125-56	2 40.8	+58 36	105	0	9.5	m
69	MD 17306	2 41.6	+53 44	107	-4	7.8	m
70	(BD +52°651)	2 56.2	+52 20	110	-4	10.5	m
71	MWa 248-52	2 59.2	+63 47	105	+6	10	m
72	MWa 302-25	3 2.1	+51 59	111	-4	10	m
73	MWa 125-64	3 19.9	+64 0	106	+7	10	s
74	BD +54°686	3 22.8	+54 34	112	0	10	m
75	BD +50°796	3 32.6	+51 5	115	-2	9.4	m
76	MWa 248-54	3 34.5	+64 17	108	+8	10	m
77	MWa 313-33	3 47.8	+44 38	121	-6	10	m
78	MWa 58-24	3 51.0	+55 54	115	+3	10.5	s:
79	MWa 58-26	3 54.5	+53 47	116	+2	10	s
80	MD 26909	4 10.1	+44 41	124	-3	10.2	s
81	MWa 313-38	4 10.8	+46 26	123	-2°	11	s
82	BD +47°1000	4 24.1	+47 44	124	+1	9.5	m
83	MWa 334-3	4 26.7	+17 18	147	-19	11	s
84	MWa 313-40	4 35.6	+46 27	126	+2	11.5	s
85	MWa 58-7	4 44.6	+53 30	122	+7	11	m
86	MWa 58-3	4 47.4	+49 15	125	+5	9.5	m
87	MWa 350-33	4 48.4	+41 28	131	0	10	m
88	BD +44°1051	4 48.6	+44 6	129	+2	9.3	m
89	MD 277413	4 54.4	+39 38	134	0	10.5	m
90	BD +37°1016	4 55.2	+37 14	136	-2	10	m
91	BD +32°869	4 55.6	+32 26	139	-4	10	v
92	(MD 282671)	4 56.5	+33 21	139	-4	10.5	m
93	MWa 1-65	4 58.4	+41 2	133	+1	10	s
94	BD +44°1103	5 1.3	+44 34	131	+4	9.4	v
95	BD +46°965	5 1.4	+46 33	129	+5	9.0	v
96	BD +44°1108	5 2.0	+44 18	131	+4	9.1	v
97	MWa 1-56	5 11.9	+43 41	132	+5	9.5	m
98	MWa 129-32	5 18.8	+36 28	139	+2	10	m
99	MWa 330-33	5 22.7	+34 25	141	+1	10	v
100	BD +37°1207	5 23.0	+37 27	139	+3	9.1	v
101	BD +24°879	5 30.2	+24 43	150	-3	10	m
102	(MD 245405)	5 30.9	+17 0	157	-7	10.6	v
103	RR Tau	5 33.3	+26 19	149	-1	10.2	m
104	(BD +37°1285)	5 35.0	+37 24	140	+5	9.5	m
105	BD +37°1292	5 36.0	+37 57	140	+6	8.7	v
106	BD +52°996	5 39.6	+52 10	127	+13	9.1	m
107	MWa 126-51	5 46.4	+25 44	151	+1	10.5	s
108	MWa 310-50	5 46.6	+40 17	139	+9	10	m
109	MWa 267-104	5 47.3	+28 46	149	+3	10.5	m
110	BD +28°936	5 48.2	+29 1	149	+3	9.5	s
111	MWa 267-71	5 48.9	+29 36	148	+4	10	m
112	MWa 126-56	5 50.8	+23 35	154	+1	10	m
113	MWa 239-46	5 53.3	+23 43	154	+1	11	m
114	(MD 250160)	5 54.3	+19 56	157	0	11.0	m
115	BD +24°1063	5 55.3	+24 29	153	+2	11	m
116	BD -10°1351	5 57.5	-10 2	184	-14	10	s
117	BD -14°1319	5 59.1	-14 53	189	-16	9.4	m
118	MD 251726	6 1.0	+19 2	159	+1	10.0	s
119	MWa 385-52	6 4.7	- 9 37	185	-12	11	s:
120	MWa 271-41	6 8.7	+18 30	160	+ 2	10	m
121	MWa 239-16	6 9.6	+18 6	161	+ 2	10.5	s
122	MD 43246	6 10.1	+28 54	151	+ 7	7.3	m
123	MD 254878	6 12.9	+14 40	164	+ 1	11.5	m
124	(MD 255137)	6 13.8	+21 13	158	+ 4	10.8	s
125	MWa 271-35	6 19.5	+19 50	160	+ 5	10	s

TABLE I (Cont'd)

No.	Star	R. A. 1900	Dec. 1900	l	b	Mag.	Int. Bright Hα
126	BD -21°1449	6h 21m0	-21° 17'	197°	-14°	9.8	m
127	BD -10°1563	6 27.0	-10 27	188	- 8	9.8	m
128	HD 288805	6 27.1	+ 1 14	177	- 2	9.3	v
129	MHa 260-35	6 27.2	+ 4 31	175	- 1	10.5	m
130	MHa 260-36	6 29.0	+ 5 21	174	0	10	m
131	HD 260378	6 30.6	+13 11	167	+ 4	11.0	m
132	HD 288847	6 31.3	+ 1 45	177	- 1	9.3	m
133	HD 260698	6 31.6	+12 45	168	+ 4	10.5	m
134	HD 263072	6 39.2	+ 5 4	175	+ 2	10.8	m
135	MHa 9-14	6 45.4	+ 5 6	176	+ 3	10	s
136	MHa 268-35	6 46.3	- 3 13	184	0	10	m
137	MHa 185-17	6 48.1	-12 2	192	- 4	9	m
138	BD -15°1548	6 48.1	-15 29	195	- 5	9.3	m
139	BD -12°1700	6 51.3	-12 52	193	- 4	9.9	s
140	MHa 268-28	6 57.0	- 5 28	187	+ 1	9.5	v
141	MHa 268-26	6 58.1	- 4 42	186	+ 2	10	m
142	BD -2°1911	6 59.5	- 2 10	184	+ 3	9.8	v
143	MHa 268-23	6 59.6	- 3 55	186	+ 2	10	m
144	MHa 9-28	7 1.0	+ 7 16	176	+ 8	10	s
145	BD -14°1751	7 6.3	-14 12	196	- 1	9.5	s
146	MHa 62-65	7 11.1	-19 43	201	- 3	9.5	m
147	(CD -30°4279)	7 14.8	-30 39	211	- 7	10	s
148	MHa 261-74	7 15.0	- 9 26	193	+ 3	9.5	m
149	CD -26°4310	7 20.2	-26 19	208	- 4	9.2	s
150	MHa 61-12	7 20.4	- 3 24	188	+ 7	10	s!
151	BD -19°1871	7 20.6	-19 55	202	- 1	9.5	m
152	MHa 62-45	7 21.5	-14 14	197	+ 2	11	m
153	MHa 390-56	7 23.3	-27 9	209	- 4	10	s
154	MHa 62-44	7 26.5	-14 12	198	+ 3	11	s
155	(BD -15°1889)	7 28.1	-15 7	199	+ 3	10	m
156	CD -32°4140	7 29.2	-32 20	214	- 5	9.8	s
157	(CD -30°4705)	7 29.8	-30 4	212	- 4	10	s!
158	CD -22°4761	7 31.5	-22 40	206	0	9.9	s
159	MHa 390-43	7 34.7	-31 46	214	- 4	10	s
160	(CD -24°5721)	7 34.9	-24 31	208	0	9.8	s!
161	BD -18°1948	7 35.0	-18 35	203	+ 3	10	m
162	CD -28°4667	7 35.5	-28 56	212	- 2	9.3	s
163	(CD -25°4885)	7 36.4	-25 35	209	- 1	10.5	s
164	MHa 390-41	7 36.7	-31 26	214	- 3	10	s!
165	CD -30°4978	7 39.2	-30 37	214	- 2	9.3	m
166	MHa 390-64	7 39.3	-28 14	212	- 1	10.3	s
167	CD -28°4778	7 39.9	-28 44	212	- 1	9.8	s!
168	(CD -23°6121)	7 41.0	-23 54	208	+ 1	9.7	s!
169	(CD -31°5007)	7 41.1	-31 54	215	- 3	10	s
170	(CD -27°4497)	7 41.3	-28 3	212	- 1	9.8	s!
171	MHa 390-7	7 41.5	-32 33	215	- 3	11	m
172	(CD -25°5038)	7 42.2	-25 23	209	+ 1	10	s
173	(CD -26°4955)	7 42.5	-26 27	210	0	9.7	s!
174	(CD -31°5070)	7 43.6	-31 36	215	- 2	10	s
175	(CD -31°5076)	7 43.7	-31 31	215	- 2	9.7	s
176	(CD -23°6234)	7 43.9	-23 46	208	+ 2	10	m
177	(CD -29°4961)	7 44.1	-29 35	213	- 1	10	s
178	CD -26°5045	7 45.4	-26 45	211	0	9.5	s
179	(CD -31°5110)	7 45.6	-31 34	215	- 2	10	s
180	(CD -28°4944)	7 46.1	-28 16	212	0	9.9	s!
181	(CD -27°4612)	7 46.4	-27 10	211	+ 1	10	s!
182	(CD -28°4976)	7 47.4	-28 14	213	0	9.7	s!
183	MHa 390-80	7 50.8	-27 30	212	+ 1	10	s
184	CD -32°4567	7 51.4	-32 11	216	- 1	10	s
185	(CD -27°4743)	7 51.7	-27 53	213	+ 1	9.7	s!
186	(CD -29°5159)	7 51.7	-29 18	214	0	9.7	s
187	(CD -33°4318)	7 52.3	-33 11	217	- 2	9.5	m
188	CD -23°6539	7 52.4	-23 37	209	+ 4	10	s
189	(CD -28°5151)	7 53.3	-28 22	213	+ 1	9.7	m
190	(CD -28°5154)	7 53.3	-28 26	213	+ 1	9.8	m

TABLE I (Cont'd)

No.	Star	R. A. 1900	Dec. 1900	l	b	Mag.	Int. Bright Hα
191	CD -32°4657	7h 55m0	-32° 17'	217°	- 1°	9.0	s
192	(CD -28°5247)	7 55.6	-28 44	214	+ 1	10	s
193	(CD -28°5249)	7 55.7	-28 28	214	+ 2	9.8	s
194	CD -30°5382	7 55.8	-30 26	215	+ 1	9.9	m
195	MHα 382-6	7 59.4	-32 17	217	0	10.5	m
196	CD -30°5559	8 0.5	-30 41	216	+ 1	9.5	s
197	(CD -27°5181)	8 9.9	-28 1	215	+ 4	9.8	s
198	MHα 382-39	8 12.6	-26 37	214	+ 6	11	m
199	CD -37°4605	8 18.3	-37 11	224	0	9.2	m
200	MHα 392-16	8 24.8	-39 4	226	0	12	s
201	MHα 382-43	8 27.5	-27 25	217	+ 8	11	s
202	CD -37°4883	8 28.8	-37 39	225	+ 2	9.6	m
203	(CD -27°5934)	8 43.8	-27 20	219	+11	10	m
204	MHα 392-12	8 49.8	-39 41	229	+ 4	11.5	s!
205	MHα 365-14	16 5.8	-18 23	323	+22	11	s
206	MHα 365-12	16 19.9	-24 6	321	+16	11	s
207	(CD -24°12689)	16 21.6	-24 8	321	+16	10.5	m
208	MHα 300-58	16 42.3	-35 35	315	+ 5	11.5	s
209	MHα 362-3	16 43.6	-14 13	333	+17	11	s
210	MHα 276-52	16 45.1	-25 49	323	+10	11.5	s!
211	HD 152408	16 48.0	-41 0	312	0	6.0	s
212	MHα 71-6	16 48.3	-30 14	320	+ 7	10	s!
213	MHα 71-5	16 48.5	-30 28	320	+ 7	11	s!
214	HD 322447	16 49.4	-40 32	312	0	9.3	s
215	(HD 322422)	16 50.4	-40 13	313	0	9.6	m
216	(CD -27°11363)	16 54.4	-27 29	323	+ 8	9.7	s
217	MHα 71-15	17 0.8	-33 57	319	+ 3	13	s!
218	MHα 276-48	17 1.0	-27 5	325	+ 7	11	s
219	(HD 326971)	17 3.4	-41 45	313	- 2	11	s
220	MHα 276-46	17 3.8	-27 8	325	+ 6	12	s
221	MHα 276-12	17 5.7	-32 28	321	+ 3	17	s!
222	MHα 192-53	17 7.4	-38 52	316	- 1	10.5	s
223	CD -38°11746	17 12.1	-38 43	316	- 2	10	m
224	HD 156409	17 12.3	-39 42	316	- 3	9.3	m
225	MHα 192-100	17 14.1	-37 54	317	- 2	11	s
226	MHα 276-33	17 15.1	-30 15	324	+ 2	10	m
227	CD -32°12653	17 15.2	-32 59	321	+ 1	9.7	m
228	MHα 192-37	17 15.2	-38 3	317	- 2	10	m
229	HD 323097	17 16.6	-37 54	317	- 2	9.7	s
230	CD -40°11454	17 19.8	-40 9	316	- 4	9.9	m
231	CD -33°12119	17 23.8	-33 40	322	- 1	9.7	v
232	HD 323771	17 27.1	-39 19	317	- 5	10.5	m
233	CD -22°12093	17 27.3	-22 47	331	+ 4	10	m
234	HD 317861	17 27.5	-32 36	323	- 1	9.5	m
235	F 6-6	17 33.1	-18 14	336	+ 5	11	s
236	HD 320483	17 36.6	-35 13	322	- 4	10.5	m
237	UU Ser	17 36.9	-15 22	339	+ 6	14.6	s
238	HD 316179	17 37.1	-27 13	329	0	8.9	v
239	MHα 79-52	17 37.4	-22 43	333	+ 2	12	s!
240	MHα 375-1	17 37.8	- 8 55	345	+ 9	11	s
241	MHα 363-30	17 38.4	-38 14	320	- 6	12	m
242	(CD -25°12254)	17 38.7	-25 12	331	+ 1	10	m
243	MHα 304-68	17 40.3	-28 3	329	- 1	11	m
244	MHα 304-74	17 42.9	-29 44	327	- 3	10.5	s
245	MHα 359-110	17 45.0	-22 17	334	+ 1	11	s
246	HD 316375	17 45.4	-27 57	329	- 2	9.2	s
247	CD -24°13552	17 45.6	-25 1	332	- 1	10	m
248	HD 316520	17 45.7	-28 45	329	- 2	10	s
249	(HD 316587)	17 45.8	-29 54	328	- 3	10.5	m
250	CD -22°12292	17 45.9	-22 59	334	0	10	m
251	(CD -28°13765)	17 46.9	-28 56	329	- 3	9.7	m
252	HD 316608	17 47.8	-30 12	327	- 4	9.8	m
253	CD -29°14172	17 48.3	-29 43	328	- 3	9.6	m
254	MHα 304-92	17 50.1	-27 37	330	- 3	10.5	s
255	MHα 363-45	17 50.5	-35 14	323	- 7	12	s

TABLE I (Cont'd)

No.	Star	R. A. 1900	Dec. 1900	l	b	Mag.	Int. Bright Hα
256	MHa 304-10	17h 50.7m	-34° 9'	324°	- 6°	12	s
257	HD 163514	17 51.4	-18 11	338	+ 2	9.2	w
258	MHa 304-168	17 51.7	-24 11	333	- 1	10.5	s
259	(CD -25°12493)	17 52.0	-25 13	332	- 2	10	m
260	HD 318710	17 52.6	-31 18	327	- 5	10.5	m
261	MHa 304-167	17 53.3	-25 3	333	- 2	10.5	m
262	MHa 304-14	17 53.5	-33 52	325	- 7	12	s
263	HD 312462	17 54.7	-17 39	339	+ 1	10	m
264	HD 316870	17 55.0	-29 40	329	- 5	9.7	m
265	(HD 316989)	17 55.1	-29 19	329	- 5	9.8	s
266	(HD 324802)	17 55.7	-37 31	322	- 9	10.5	s
267	MHa 359-71	17 55.9	-23 41	334	- 2	9.5	w
268	MHa 359-70	17 56.3	-23 34	334	- 2	10	s
269	MHa 304-52	17 56.8	-32 42	326	- 7	12	s
270	F 6-7	17 59.6	-20 21	337	- 1	11	s:
271	HD 313820	17 59.7	-22 18	336	- 2	10	m
272	MHa 82-21	18 0.8	-29 14	330	- 6	11.5	s
273	BD -8°4559	18 1.0	- 8 11	348	+ 5	9.6	m
274	(HD 315177)	18 1.0	-25 17	333	- 4	9.9	m
275	(HD 317086)	18 1.2	-28 52	330	- 6	10	m
276	MHa 363-7	18 2.1	-41 14	319	-12	11.5	m
277	MHa 79-19	18 2.2	-19 26	338	- 1	10	m
278	MHa 79-25	18 2.4	-22 18	336	- 3	11	s
279	HD 165895	18 3.1	-24 43	334	- 4	10.9	m
280	MHa 304-17	18 3.3	-33 20	326	- 8	12	s
281	MHa 208-83	18 4.4	-27 59	331	- 6	12	s
282	MHa 304-113	18 4.7	-28 35	331	- 6	12	s
283	MHa 304-120	18 5.2	-28 24	331	- 6	11	s
284	MHa 304-121	18 5.7	-29 36	330	- 7	11	s
285	F 1-37	18 6.1	-14 52	343	0	10	s
286	CD -25°12867	18 6.1	-25 11	334	- 5	10	m
287	HD 166612,3	18 6.3	-28 16	331	- 6	7.4	m
288	MHa 304-119	18 6.5	-28 21	331	- 6	12	s
289	F 1-11	18 6.7	-11 39	346	+ 2	10.5	s
290	MHa 77-52	18 6.7	-32 21	328	- 8	12	s:
291	HD 312984	18 7.3	-20 34	338	- 3	9.8	s
292	HD 319139	18 7.6	-32 50	327	- 9	9.7	s:
293	MHa 304-122	18 8.2	-29 51	330	- 7	11.5	s
294	MHa 304-123	18 9.6	-27 56	332	- 7	11	s
295	MHa 304-41	18 9.6	-30 54	329	- 8	12	m
296	D 143-2	18 10.0	- 0 21	356	+ 6	10.5	s:
297	MHa 352-34	18 10.3	+20 58	16	+16	10	s
298	MHa 312-68	18 11.0	-17 1	342	- 2	10.5	m
299	MHa 208-92	18 11.0	-28 12	332	- 7	10	s:
300	MHa 304-149	18 12.8	-24 8	336	- 5	11	s
301	MHa 304-145	18 14.0	-24 18	336	- 6	12	s
302	MHa 304-33	18 15.0	-31 35	329	- 9	12	s:
303	MHa 366-101	18 18.8	-25 45	335	- 8	11	m
304	(CD -28°14567)	18 19.2	-28 39	332	- 9	11.5	s
305	BD +16°3492	18 20.4	+16 1	12	+12	8.7	w
306	F 1-17	18 21.5	-12 26	347	- 2	11	s
307	MHa 204-53	18 24.1	-13 22	346	- 3	11	m
308	F 4-37	18 25.7	-19 20	341	- 6	11	m
309	F 5-12	18 27.9	-13 58	346	- 4	10.5	s
310	MHa 375-17	18 28.1	- 5 3	354	0	10	m
311	MHa 345-39	18 29.7	- 3 35	356	+ 1	11	m
312	F 5-56	18 30.4	-11 14	349	- 3	11	s
313	MHa 208-51	18 32.0	-22 47	339	- 9	11.5	s
314	BD -13°5061	18 33.8	-13 57	347	- 5	9.2	s
315	D 143-20	18 35.6	- 5 33	355	- 2	10.5	s:
316	MHa 208-58	18 36.6	-21 23	341	- 9	12	s
317	MHa 345-51	18 37.5	- 3 35	357	- 1	11	m
318	MHa 345-30	18 37.6	- 5 14	355	- 2	10.5	m
319	MHa 345-31	18 38.0	- 5 11	355	- 2	11	s
320	MHa 345-32	18 39.2	- 3 54	356	- 2	11	s

TABLE I (Cont'd)

No.	Star	R. A. 1900	Dec. 1900	l	b	Mag.	Int. Bright Nb
321	BD -11°4747	18h 41m.5	-11° 47'	350°	- 6°	9.3	m
322	MWn 345-52	18 41.7	- 2 12	358	- 1	10.5	m
323	MWn 369-39	18 43.2	- 6 48	354	- 4	12	s
324	MWn 352-9	18 43.8	+10 29	10	+ 4	10	m
325	CD -26°13521	18 43.8	-26 31	337	-13	9.5	s:
326	MWn 204-32	18 45.1	-13 38	348	- 7	12	s
327	MWn 208-67	18 47.2	-24 30	339	-13	11.5	s
328	SV Sct	18 48.0	-14 19	348	- 8	12.0	s
329	FN Sgr	18 48.0	-19 7	344	-11	9	s
330	(CD -32°14673	18 49.1	-32 23	331	-16	9.8	s
331	BD -5°4819	18 51.9	- 5 39	356	- 5	10.3	m
332	BD -5°4823	18 52.9	- 5 38	357	- 6	9.4	m
333	CD -23°14922	18 53.6	-23 50	340	-14	9.1	m
334	MWn 305-5	18 55.8	+17 7	17	+ 5	11.5	m
335	MWn 214-24	18 56.4	+ 2 28	4	- 2	10	m
336	(BD +0°4080)	18 56.4	+ 0 29	2	- 3	9.5	s
337	MWn 277-6	18 58.0	-17 8	347	-12	10.5	s
338	MWn 305-6	18 59.3	+16 18	17	+ 3	11.5	s
339	MWn 214-22	19 1.3	+ 3 8	5	- 3	10	s
340	HD 230767	19 4.3	+10 57	13	0	10.6	s
341	MWn 339-4	19 4.7	- 2 57	0	- 7	11	s
342	MWn 277-26	19 4.8	-12 46	351	-11	10	m
343	BD +2°3806	19 5.4	+ 2 45	5	- 4	9.5	m
344	HD 349853	19 9.0	+19 47	21	+ 3	9.5	m
345	MWn 305-11	19 9.6	+17 21	19	+ 2	11	m
346	MWn 305-10	19 9.8	+17 11	19	+ 2	10.5	s
347	MWn 214-17	19 10.1	+ 4 43	8	- 4	9.8	m
348	(BD -9°5069)	19 11.0	- 9 14	355	-11	10	s:
349	MWn 215-6	19 12.2	+14 23	16	0	9.5	s
350	MWn 319-34	19 12.8	-11 16	354	-12	14	s
351	MWn 308-19	19 13.1	+14 5	16	0	11	m
352	MWn 308-44	19 14.5	+15 59	18	0	11	m
353	MWn 308-18	19 15.8	+10 51	14	- 3	11.5	m
354	HD 344191	19 16.2	+24 4	25	+ 4	9.4	m
355	MWn 308-17	19 17.8	+11 47	15	- 3	9.8	v
356	MWn 215-33	19 19.0	+24 16	26	+ 3	10	m
357	MWn 92-20	19 24.7	+26 58	29	+ 3	11	s
358	BD +53°2262	19 30.6	+53 40	53	+15	9.4	m
359	MWn 215-36	19 31.0	+23 6	26	0	10	m
360	MWn 80-5	19 41.4	+18 22	23	- 4	11	s:
361	HD 350485	19 44.4	+19 54	25	- 4	9.3	v
362	HD 226100	19 46.9	+34 14	38	+ 3	10.4	v
363	HD 338970	19 46.9	+26 53	31	- 1	9.4	m
364	HD 345105	19 46.9	+22 51	28	- 3	10	v
365	HD 350799	19 47.8	+18 6	24	- 6	11	v
366	(HD 333003)	19 48.5	+28 44	33	0	10.5	m
367	HD 345122	19 48.6	+21 59	27	- 4	9.4	s
368	MWn 92-28	19 48.7	+28 31	33	0	10	m
369	BS Cyg	19 49.2	+53 26	54	+13	11.0	s
370	MWn 328-117	19 51.1	+39 32	42	+ 5	11	m
371	MWn 316-52	19 51.9	+26 31	32	- 2	11	m
372	HD 351123	19 53.1	+17 6	24	- 7	9.0	m
373	MWn 328-116	19 53.6	+39 33	43	+ 5	12	s
374	MWn 316-29	19 55.3	+31 11	36	0	11	m
375	MWn 92-31	19 55.4	+31 37	36	0	10.5	m
376	MWn 328-10	19 57.5	+36 3	40	+ 2	10.5	m
377	MWn 328-9	19 58.6	+36 25	41	+ 2	11	m
378	HD 351808	19 59.4	+31 1	36	- 1	10.5	v
379	MWn 328-112	20 0.8	+37 2	41	+ 2	10	m
380	MWn 104-29	20 2.4	+33 4	38	0	11.5	s
381	MWn 316-47	20 2.8	+32 57	38	0	11.5	s
382	(HD 228023)	20 6.0	+34 50	40	0	11.2	m
383	MWn 328-20	20 6.0	+34 32	40	0	10.7	m
384	HD 351582	20 6.3	+19 27	28	- 9	9.0	v
385	MWn 328-23	20 7.0	+36 14	41	+ 1	10.5	s

TABLE I (Cont'd)

No.	Star	R. A. 1900	Dec. 1900	l	b	Mag.	Int. Bright Ha
386	MHa 148-48	20h 7m.2	+38° 1'	43°	+ 2	10	m
387	(HD 228207)	20 7.8	+35 34	41	0	10.8	s
388	MHa 328-105	20 8.6	+39 18	44	+ 2	10.5	m
389	MHa 328-107	20 8.8	+40 27	45	+ 3	12	s
390	MHa 328-102	20 9.6	+37 11	43	+ 1	11	m
391	MHa 148-64	20 10.1	+38 50	44	+ 2	10.5	m
392	(HD 228510)	20 10.9	+35 34	41	0	11.4	m
393	MHa 148-69	20 11.2	+39 3	44	+ 2	10.5	s
394	(HD 228576)	20 11.6	+36 37	42	0	11.7	s
395	MHa 328-91	20 13.7	+36 51	43	0	10.5	m
396	MHa 328-87	20 13.8	+37 48	44	+ 1	10	s
397	MHa 328-84	20 13.9	+38 38	44	+ 1	10.5	m
398	MHa 328-88	20 14.4	+37 35	43	0	10	m
399	MHa 148-103	20 14.6	+41 48	47	+ 3	10.5	m
400	D 146-37	20 14.8	+38 1	44	+ 1	11	m
401	MHa 328-89	20 15.0	+37 41	44	0	10	m
402	BD +40°4112	20 15.4	+40 38	46	+ 2	9.5	v
403	MHa 328-80	20 16.2	+38 20	44	+ 1	11	s
404	MHa 328-81	20 16.3	+39 27	45	+ 1	10	m
405	MHa 328-79	20 16.7	+38 19	44	0	11	m
406	MHa 328-71	20 17.7	+37 47	44	0	11	m
407	MHa 328-74	20 17.8	+37 7	43	- 1	10.5	m
408	MHa 328-68	20 17.9	+39 56	46	+ 1	11	s
409	MHa 328-76	20 18.2	+36 41	43	- 1	10.5	m
410	MHa 328-69	20 18.4	+38 8	44	0	11	m
411	FHa 3-44	20 18.6	+37 42	44	0	10.5	s
412	HD 194208	20 19.3	+35 21	42	- 2	8.2	v
413	MHa 148-76	20 20.4	+39 30	46	+ 1	10.5	s
414	MHa 148-77	20 20.4	+38 20	45	0	12	s
415	MHa 148-88	20 21.1	+40 54	47	+ 1	12	s!
416	MHa 76-40	20 21.3	+37 56	45	- 1	10.5	s
417	FHa 3-6	20 23.2	+37 53	45	- 1	10.5	s
418	MHa 148-99	20 24.4	+43 25	49	+ 2	10	m
419	MHa 76-34	20 25.2	+42 26	49	+ 2	10	s
420	MHa 328-130	20 26.1	+40 50	47	+ 1	11	v
421	MHa 328-131	20 28.1	+41 28	48	+ 1	11.5	m
422	MHa 328-53	20 28.5	+40 28	47	0	10.5	m
423	BD +47°3133	20 29.0	+47 37	53	+ 4	9.3	v
424	MHa 289-51	20 29.1	+40 54	48	0	9.5	m
425	MHa 328-51	20 29.4	+37 44	45	- 2	10	v
426	MHa 328-133	20 29.6	+40 54	48	0	9.5	m
427	MHa 328-134	20 30.0	+40 57	48	0	12	s
428	MHa 148-90	20 30.1	+41 2	48	0	10.5	s
429	MHa 328-40	20 30.2	+35 18	44	- 4	11	m
430	MHa 148-91	20 31.1	+41 8	48	0	11.5	m
431	MHa 328-50	20 33.1	+40 0	48	- 1	10.5	m
432	MHa 328-41	20 33.1	+34 57	44	- 4	10	m
433	MHa 328-142	20 35.2	+41 46	49	0	12	s
434	MHa 328-141	20 35.4	+41 41	49	0	11	v
435	BD +48°3184	20 36.8	+48 27	55	+ 4	8.8	v
436	MHa 328-42	20 37.9	+35 21	45	- 5	11	m
437	BD +54°2399	20 38.2	+54 59	60	+ 8	10	m
438	HD 197406	20 38.4	+52 14	58	+ 6	10.3	s
439	BD +53°2476	20 40.2	+54 7	59	+ 7	10.5	m
440	BD +50°3188	20 42.1	+50 12	56	+ 4	9.2	v
441	MHa 235-37	20 43.2	+43 23	51	0	11.5	s
442	MHa 235-36	20 44.1	+43 24	51	0	10.3	m
443	MHa 148-94	20 44.6	+43 24	52	- 1	10.8	s
444	MHa 148-95	20 44.8	+43 16	51	- 1	10	m
445	MHa 221-39	20 46.0	+50 33	57	+ 4	10.5	v
446	MHa 255-56	20 47.6	+48 37	56	+ 2	9.5	v
447	(BD +46°3080)	20 48.4	+46 34	54	+ 1	9.3	v
448	MHa 235-59	20 49.4	+45 11	53	0	10.5	m
449	MHa 255-55	20 52.1	+49 11	57	+ 2	10.5	m
450	BD +36°4330	20 52.8	+36 58	48	- 6	8.5	v

TABLE I (Cont'd)

No.	Star	R. A. 1900	Dec. 1900	l	b	Mag.	Int. Bright Nb
451	BD +44°3657	20h 55m.1	+44° 41'	54	- 1	10.5	m
452	(BD +44°3666)	20 56.6	+44 37	54	- 1	9.5	m
453	MHa 289-90	20 58.6	+45 22	55	- 1	11.5	s
454	MHa 235-19	20 59.3	+40 31	51	- 4	10	m
455	MHa 235-54	21 1.2	+45 50	55	- 1	10	m
456	MHa 255-53	21 4.3	+50 41	59	+ 2	10.5	m
457	MHa 81-12	21 4.8	+44 53	55	- 2	10	s
458	BD +47°3302	21 5.0	+47 16	57	- 1	10	v
459	MHa 255-52	21 5.7	+48 41	58	0	10.5	m
460	MHa 255-26	21 10.2	+48 21	58	0	10	m
461	MHa 255-51	21 11.2	+49 5	59	0	10.5	m
462	MHa 170-24	21 14.6	+55 31	64	+ 4	9.3	m
463	MHa 255-48	21 20.1	+49 55	60	0	10.5	m
464	MHa 297-51	21 20.5	+58 7	66	+ 6	10	m
465	MD 204185	21 21.8	+60 51	68	+ 8	8.1	v
466	MHa 221-64	21 24.2	+52 33	63	+ 1	10	m
467	BD +48°3416	21 29.3	+48 35	61	- 2	9.4	m
468	BD +41°4191	21 29.7	+41 25	56	- 8	9.4	m
469	MHa 297-36	21 33.0	+54 53	65	+ 2	10	s
470	MHa 297-55	21 33.2	+56 54	67	+ 4	11	s
471	BD +63°1757	21 35.2	+63 26	71	+ 8	9.4	m
472	BD +57°2358	21 36.1	+57 21	67	+ 4	9.3	s
473	MHa 297-34	21 37.7	+56 8	66	+ 3	9.5	m
474	MHa 297-35	21 37.8	+56 36	67	+ 3	9.5	m
475	BD +65°1637	21 40.6	+65 39	73	+10	9.4	m
476	MHa 258-37	21 46.8	+54 20	66	0	9.5	m
477	BD +46°3471	21 48.7	+46 46	62	- 6	9.5	m
478	BD +58°2341	21 48.8	+58 26	69	+ 3	9.5	m
479	BD +48°3561	21 54.1	+48 36	64	- 5	8.9	v
480	MHa 174-63	21 54.9	+52 56	67	- 1	9.5	s
481	MHa 73-11	21 57.0	+53 9	67	- 1	10.5	s
482	BD +46°3577	22 2.1	+46 16	64	- 8	9.4	m
483	BD +49°3735	22 2.2	+49 25	65	- 5	9.0	v
484	MHa 258-33	22 3.6	+54 57	69	- 1	10.5	m
485	MHa 258-95	22 4.0	+48 32	65	- 6	9.5	s
486	BD +65°1744	22 13.9	+65 27	76	+ 8	9.2	m
487	MHa 258-26	22 17.4	+54 46	70	- 2	11	m
488	BD +45°3899	22 17.4	+45 33	66	-10	9.5	s
489	MHa 258-70	22 18.8	+52 48	70	- 4	10.5	s
490	BD +61°2292	22 19.7	+62 13	74	+ 4	9.4	m
491	AC +55°64276	22 24.7	+55 30	72	- 2	10.8	m
492	MHa 217-26	22 24.8	+62 14	75	+ 4	9.5	m
493	BD +60°2405	22 27.6	+61 6	75	+ 3	9.4	m
494	AC +57°60526	22 27.6	+57 57	73	0	11.1	m
495	MHa 258-78	22 32.8	+53 46	72	- 4	10.5	m
496	AC +57° 61154	22 35.8	+57 10	74	- 1	11.5	s
497	MHa 217-83	22 39.4	+54 42	73	- 3	10.3	m
498	BD +64°1709	22 41.7	+65 2	78	+ 6	9.2	v
499	MHa 47-30	22 52.1	+58 7	76	- 1	11.5	s
500	MHa 217-49	22 52.8	+56 56	76	- 2	11	m
501	MHa 73-59	22 53.6	+58 15	76	- 1	10.5	m
502	MHa 217-55	22 57.0	+59 24	77	0	10.5	m
503	BD +58°2536	22 59.5	+59 9	77	0	9.5	v
504	BD +66°1576	23 0.2	+67 14	81	+ 7	9.1	m
505	MHa 217-18	23 1.0	+61 42	79	+ 2	10	m
506	MHa 217-58	23 2.8	+57 21	77	- 2	10.5	m
507	BD +73°1031	23 17.0	+73 42	84	+13	9.5	s
508	BD +60°2527	23 17.9	+60 29	80	0	10	m
509	PHa 7-6	23 27.3	+60 52	81	0	10.5	m
510	BD +60°2584	23 31.1	+60 38	82	0	10	m
511	MHa 217-68	23 33.3	+55 29	81	- 5	10	s
512	BD +60°2600	23 35.6	+60 47	82	0	9.0	m
513	MHa 217-9	23 38.7	+61 23	83	0	11	m
514	MHa 256-51	23 50.0	+61 32	84	0	11	m
515	MHa 256-53	23 51.7	+62 57	85	+ 1	9.7	m
516	MHa 223-53	23 51.8	+63 27	85	+ 2	9.5	m
517	BD +65°1970	23 52.5	+65 53	85	+ 4	9.3	m
518	MHa 284-27	23 52.6	+72 19	86	+11	10.5	m
519	BD +65°2090	23 55.2	+63 31	85	+ 2	9.6	m

NOTES TO TABLE 1

No.

2. MHα 321-5. Slightly south of the midpoint of the line joining BD+65°14 and +65°21.
3. MHα 284-4. 5′ n.p. BD+67°57. The following and visually fainter of two stars separated by nearly 2′. It may be variable.
4. MHα 295-122. 16′ s.f. BD+63°82. A star of about the same magnitude is 5′ n.p.
5. MHα 295-108. 9′ n.f. BD+62°138. A slightly brighter star precedes by 2′.5.
6. D 130-19. 8′ north of and slightly preceding BD+60°100.
7. MHα 325-81. 8′ n.f. BD+64°79. A star of about the same magnitude precedes by 4′.
8. BM Cas. An eclipsing variable of period 198 days, spectrum *Fe*. Under investigation by Dr. D. M. Popper.
9. MHα 295-99. 5′ s.p. BD+61°187.
10. MHα 224-71. 5′ n.f. BD+62°191.
11. HD 6744. On an objective-prism photograph, taken on July 26, 1946, the image of this star, although near the edge of the plate, appears to show a bright *Hα* line of low intensity. On another plate, taken on September 1, 1946, *Hα* appears as a strong dark line. Further observations should be made.
12. MHα 325-72. 2′.5 s.f. BD+64°129.
13. MHα 295-95. 5′ n.f. BD+60°193.
14. MHα 295-44. 9′ s.f. BD+58°203. 2′.5 north of another faint star of the same R.A.
16. MHα 223-41. 5′ n.f. BD+60°214.
17. (BD+57°273). A brighter star which may be BD+57°273 is about 2′ s.p.
19. MHα 295-49. 6′ n.p. BD+58°232.
20. BD+59°246. On slit spectrograms taken in September and November, 1947, the spectrum appears to be that of a highly reddened A-type star, but bright *Hα* is not seen, although it appeared on an objective-prism photograph taken on September 27, 1946.
21. MHα 224-7. 10′ following and slightly north of BD+60°230. Southern and following of two stars separated by 3′.
22. MHα 295-84. 8′ n.p. BD+60°246. Southern and faintest of three stars.
23. MHα 354-101. 6′.5 s.f. BD+61°277. 2′.5 n.p. one or possibly two stars of about the same magnitude.
24. MHα 224-12. 2′.5 s.p. BD+61°282.
25. MHα 295-53. 10′ following and slightly north of BD+58°257. A slightly fainter star is 4′ n.f.
26. MHα 224-13. 6′.5 n.f. BD+61°288. A somewhat brighter star is 3′ north.
27. MHα 224-64. 10′ n.p. BD+63°206. A star of the same magnitude is 7′ following.
28. MHα 354-111. 6′.5 s.p. BD+60°273.
29. MHα 326-10. 2′.5 north of and slightly preceding the triple star BD+60°274, 275, 276.
30. (BD+60°274). May be BD+60°275 or +60°276.
31. MHα 325-67. 5′ n.p. BD+66°142.
32. MHα 295-83. 9′ following and slightly north of BD+61°297.
33. MHα 224-63. 10′ n.p. BD+62°284. Following of two stars.
34. MHα 224-15. 6′ s.f. BD+62°281.
35. MHα 224-61. 1′.5 north of and slightly preceding BD+62°286.
38. MHα 354-121. 6′.5 s.p. BD+62°300.
39. MHα 224-57. 8′ n.f. BD+64°228. A slightly fainter star is 2′ s.p.
40. MHα 224-55. 5′ n.f. BD+63°230.
42. (BD+60°341). Southern star of a cluster in NGC 663.
44. MHα 5-12. 4′ s.p. BD+58°298. Northern and preceding of two faint stars.
45. BD+59°330. Northern, preceding, and brighter of two stars separated by 1′.5.
46. MHα 295-60. 5′ preceding and slightly north of BD+59°351.
47. MHα 295-69. 2′.5 s.p. BD+59°352.
50. MHα 354-50. Lies halfway between BD+59°378 and +59°385.
51. MHα 326-28. 4′ s.p. BD+58°356.
53. MHα 224-50. 12′ north of and slightly following BD+62°345. Southern and following of three faint stars.
54. (BD+57°485). Southern and brightest of three stars. Bright *Hα*, detected on a plate taken in November, 1938, could not be seen on three plates taken in September, October, and November, 1946.
55. MHα 354-40. 6′ south of BD+58°430.
56. MHα 224-46. 9′ n.p. BD+63°317.
58. HD 14947. *Hα* is bright on a one-prism spectrogram taken on August 31, 1947. This spectrum of type Of is under investigaton by O. C. Wilson.
59. MHα 125-9. 4′ following and slightly south of BD+60°482, 483.
60. MHα 379-17. 1′.5 south of BD+55°633.
61. MHα 5-86. 4′ north of BD+56°635, 636.
62. HD 15570. Classified O5f on slit spectrograms.
63. MHα 379-57. 2′.5 n.f. BD+56°652.

NOTES TO TABLE 1—*Continued*

No.

64. MHa 5-75. 1′.5 n.f. BD+56°656. One of two extremely faint stars.
65. MHa 5-76. 4′ n.f. BD+57°597. Northern, following, and fainter of two stars.
66. MHa 5-83. 13′ s.p. BD+56°683. The following of two stars.
67. MHa 125-6. 6′ s.p. BD+61°462.
68. MHa 125-56. 12′ north and slightly preceding BD+58°521. A fainter star is 5′ s.f.
69. HD 17306. The *Hα* line was bright on October 13, 1944, October 26, 1945, and August 20, 1948. The type is cK0e*α*. This star deserves further study.
70. (BD+52°651). Southern and following of two stars separated by 3′.
71. MHa 248-52. 10′ n.f. BD+63°390.
72. MHa 302-25. Precedes BD+51°686 by 10′. Brightest star between BD+51°681 and +51°686.
73. MHa 125-64. 5′ s.p. BD+63°417. A brighter star is 2′.5 s.p.
76. MHa 248-54. 4′ s.p. BD+64°405.
77. MHa 313-33. 2′.5 n.f. BD+44°809.
78. MHa 58-24. 18′ s.p. BD+56°867. A slightly fainter star lies at the midpoint of the line joining them. Southern, following, and faintest of three stars.
79. MHa 58-26. 8′ s.p. BD+53°724. A much fainter star is 1′.5 s.f. *Hα* is a strong, bright line on a low-dispersion slit spectrogram taken by W. C. Miller in September, 1949. On a low-dispersion slit spectrogram of the photographic region taken in November, 1941, the type appears to be Fp. This star deserves further investigation.
81. MHa 313-38. Follows BD+46°859 by 8′.
83. MHa 334-3. Northern of two stars of equal magnitude separated by 5′.
84. MHa 313-40. 5′ n.p. two somewhat brighter stars.
85. MHa 58-7. Halfway between BD+53°821 and +53°824.
86. MHa 58-3. 3′ south of BD+49°1267.
87. MHa 350-33. Halfway between BD+41°1002 and +41°1005. A slightly brighter star is 2′.5 s.p.
89. HD 277413. 10′ south of BD+39°1138.
92. (HD 282671). 10′ s.p. BD+33°945.
93. MHa 1-65. 5′ s.f. BD+41°1052. Southern, preceding, and fainter of two stars.
97. MHa 1-56. 6′.5 n.f. BD+43°1241.
98. MHa 129-32. Follows BD+36°1128 by 2′.5.
99. MHa 330-33. 13′ north of and slightly preceding BD+34°1065. A star of similar magnitude is 3′.5 following and slightly south.
102. (HD 245405). Possibly HD 245406. 6′ preceding and slightly north of BD+16°822.
104. (BD+37°1285). Northern of three stars.
107. MHa 126-51. 2′ n.p. BD+25°1012.
108. MHa 310-50. Southern, following, and fainter of two stars separated by 2′.5.
109. MHa 267-104. Between BD+28°931 and +28°932. Northern and preceding of two stars of the same magnitude separated by 2′.
111. MHa 267-71. 4′ preceding and slightly south of BD+29°1040.
112. MHa 126-56. 4′ s.p. BD+23°1118. Halfway between BD+23°1116 and +23°1118.
113. MHa 239-46. 1′.5 s.p. BD+23°1138.
114. (HD 250160). 4′ south and slightly following BD+19°1165. Southern, preceding, and slightly brighter of two stars separated by 1′.5.
118. HD 251726. Spectrum is given as F5 in HD but appears to be of class B on a poor slit spectrogram of low dispersion taken on February 8, 1946.
119. MHa 385-52. Follows BD−9°1343 by 6′.5.
120. MHa 271-41. 5′ south and slightly following BD+18°1137.
121. MHa 239-16. Near HD 253963. Northern and following of two stars separated by 2′.5.
122. HD 43246. *Hα* is a well-marked bright line on a slit spectrogram taken on January 24, 1948. Several slit spectrograms of the photographic region in the years 1922–1948 appear to show slight changes, especially in the *Hβ* and *Hγ* lines. Class gF2e.
123. HD 254878. Precedes BD+14°1242 by 8′.
124. (HD 255137). 2′.5 s.f. a slightly fainter star.
125. MHa 271-35. Follows BD+19°1341 by 5′. A somewhat brighter star is 1′.5 s.f.
128. HD 288805. BD+1°1384.
129. MHa 260-35. 6′.5 s.f. BD+4°1301. Southern, preceding, and fainter of two stars.
130. MHa 260-36. 4′ north of BD+5°1305.
131. HD 260378. 6′.5 s.f. BD+13°1327. A fainter star is 2′.5 following.
132. HD 288847. BD+1°1417.
133. HD 260698. 3′.5 n.f. BD+12°1217. Northern and preceding of two stars.
134. HD 263072. 11′ following and slightly north of BD+5°1383.
135. MHa 9-14. 4′ north and slightly following BD+5°1439.
136. MHa 268-35. 6′ preceding and slightly south of BD−3°1624. A star of the same magnitude is 3′.5 s.f.
137. MHa 185-17. 2′ s.p. BD−11°1673.

NOTES TO TABLE 1—*Continued*

No.

140. MHα 268-28. 8′ north and slightly preceding BD−5°1926.
141. MHα 268-26. 4′.5 south and slightly preceding BD−4°1790.
143. MHα 268-23. Precedes BD−3°1717 by 2′.
144. MHα 9-28. 4′ north and slightly preceding BD+7°1597. Preceding of two stars.
146. MHα 62-65. 4′ s.f. BD−19°1777.
147. (CD−30°4279). 2′.5 s.f. CD−30°4276. Two faint stars lie north of the line joining them.
148. MHα 261-74. 9′ north of and slightly following BD−9°1986.
150. MHα 61-12. 4′ n.f. BD−3°1887. BD−3°1889 is 4′ north.
152. MHα 62-45. 4′ n.f. BD−14°1891.
153. MHα 390-56. 3′ n.p. CD−27°4097. A brighter star is 2′ north and slightly preceding.
154. MHα 62-44. 1′.5 s.f. BD−14°1940. A brighter star is 1′.5 s.f.
155. (BD−15°1889). Following of two stars separated by 1′.5.
156. CD−32°4140. 6′.5 n.p. CD−32°4145. Two stars of similar magnitude having the same R.A. but 2′ apart in declination are s.p.
158. CD−22°4761. 5′.5 s.f. BD−22°1945 (CD−22°4756).
159. MHα 390-43. 8′ south and slightly following CD−31°4847. Central and probably faintest of three stars.
160. (CD−24°5721). 13′ preceding and slightly south of CD−24°5746. Two faint stars are 2′.5 and 5′ south, respectively.
163. (CD−25°4885). 4′ s.f. CD−25°4881. The central one of three stars forming a straight line with CD−25°4881.
164. MHα 390-41. May be CD−31°4897. Northern and preceding of two stars separated by 0′.7.
166. MHα 390-64. Following of three stars 2′ apart, which form an equilateral triangle.
167. CD−28°4778. 1′.5 following CD−28°4774.
168. (CD−23°6121). 13′ n.p. CD−23°6155. A star of approximately the same magnitude is 5′.5 s.f.
169. (CD−31°5007). 3′ north and slightly following CD−31°5006.
170. (CD−27°4497). 6′ preceding and slightly north of CD−28°4822.
171. MHα 390-7. 10′ north of CD−32°4366. A brighter star, probably CD−32°4367, is 5′ s.f.
172. (CD−25°5038). 5′ n.f. CD−25°5031.
173. (CD−26°4955). 4′ n.f. CD−26°4942.
174. (CD−31°5070). 5′.5 n.f. CD−31°5064. A fainter star is 2′.5 south and slightly following.
175. (CD−31°5076). Brightest star within a radius of 5′.
176. (CD−23°6234). May be CD−23°6235. 10′ n.f. CD−23°6228. Brightest star within a radius of 5′.
177. (CD−29°4961). 2′ n.p. CD−29°4963.
179. (CD−31°5110). 3′ s.f. a star of the same magnitude.
180. (CD−28°4944). 1′.5 south and slightly preceding CD−28°4948.
181. (CD−27°4612). 5′ s.p. CD−27°4615. Preceding of three stars having almost the same declination.
182. (CD−28°4976). 15′ south and slightly following CD−27°4630. 12′ s.p. CD−27°4646.
183. MHα 390-80. 2′ n.f. CD−27°4710.
184. CD−32°4567. 2′ s.f. a star of the same magnitude.
185. (CD−27°4743). 5′.5 n.p. CD−27°4751. A fainter star is 2′ s.p.
186. (CD−29°5159). 2′ s.p. CD−29°5169.
187. (CD−33°4318). Northern of two stars separated by 2′.5.
188. CD−23°6539. 2′.5 n.f. CD−23°6532.
189. (CD−28°5151). 3′ s.p. CD−28°5157.
190. (CD−28°5154). 6′.5 south and slightly preceding CD−28°5157. A fainter star is 2′.5 n.f.
192. (CD−28°5247). 4′ north and slightly preceding a star of the same magnitude. A similar pair of stars follows by about 3′.
193. (CD−28°5249). 1′ n.p. a somewhat fainter star.
194. CD−30°5382. 5′.5 n.p. CD−30°5387. A slightly brighter star is 2′ n.p.
195. MHα 382-6. 1′.5 n.p. a brighter star, probably CD−32°4772.
197. (CD−27°5181). 6′.5 s.p. CD−27°5193.
198. MHα 382-39. 1′.5 north of and slightly following CD−26°5792.
200. MHα 392-16. 5′.5 n.p. CD−39°4376. A brighter star is 2′.5 s.f.
201. MHα 382-43. 1′ n.f. CD−27°5582.
202. CD−37°4833. 3′ n.f. CD−37°4828.
203. (CD−27°5934). 4′ north and slightly preceding CD−27°5937.
204. MHα 392-12. 4′.5 s.p. CD−39°4921. A somewhat brighter star is 3′ s.f.
205. MHα 365-14. 13′ n.p. BD−18°4242. A fainter star is 4′ preceding and slightly south.
206. MHα 365-12. 10′ n.f. CD−24°12684.
207. (CD−24°12689). 21′ n.p. CD−24°12691.
208. MHα 300-58. 27′ following and slightly north of CD−35°11100. A brighter star is 4′.5 n.p.
209. MHα 362-3. 13′ n.p. BD−14°4489.

NOTES TO TABLE 1—*Continued*

No.

210. MHa 276-52. 7′ following and slightly south of CD−25°11723. A slightly brighter star is 1′.5 n.p. R. Minkowski has found the spectrum to have bright lines of *He* I and [*Fe* VII] in addition to those of *H*.
212. MHa 71-6. 2′.5 n.f. CD−30°13590. A brighter star is 1′.5 north.
213. MHa 71-5. 4′ s.f. CD−30°13594. A slightly brighter star is 4′ following and slightly south.
214. HD 322447. CD−40°10963.
215. (HD 322422). (CD−40°11001). 4′.5 s.f. CD−40°10989.
216. (CD−27°11363). 8′ following CD−27°11351. Type Fe.
217. MHa 71-15. Southern, following, and faintest of three stars in a line approximately 8′ long. Peculiar, probably a combination spectrum.
218. MHa 276-48. 8′ south and somewhat following CD−26°11900. Equidistant from CD−26°11900 and −27°11457.
219. (HD 326971). 8′ s.p. CD−40°11324.
220. MHa 276-46. Near CD−27°11001. A slightly brighter star is 2′.5 n.p.
221. MHa 276-12. 9′ preceding CD−32°12467. A brighter star is 1′ following. R. Minkowski has found the spectrum to have bright lines of [*Fe* VII] in addition to those of *H*.
222. MHa 192-53. 5′ n.p. CD−38°11671.
223. CD−38°11746. Preceding of two stars separated by 1′.
225. MHa 192-100. 2′.5 n.f. CD−37°11487.
226. MHa 276-33. 9′ s.f. CD−30°14064. A brighter star is 4′ s.f.
227. CD−32°12653. 9′ s.p. CD−32°12663. Brightest star in the field.
228. MHa 192-37. 8′ n.p. CD−38°11801. Central one of three stars.
229. HD 323097. CD−37°11520. 2′ s.f. CD−37°11514.
230. CD−40°11454. 2′ south of CD−40°11455.
231. CD−33°12119. 4′ s.f. CD−33°12117. Type may be later than B.
232. HD 323771. (CD−39°11602). 4′ s.f. CD−39°11597.
233. CD−22°12093. 9′ n.p. BD−22°4367 (CD−22°12097). A fainter star is 2′.5 n.f.
234. HD 317861. CD−32°12908.
235. F 6-6. 8′ south of and slightly following BD−18°4595.
236. HD 320483. 2′.5 n.f. CD−35°11839. Northern and preceding of two faint stars.
237. UU Ser. 2′.5 north and slightly following BD−15°4654.
238. HD 316179. CD−27°11855.
239. MHa 79-52. 5′ n.p. BD−22°4399. A brighter star is 1′.5 n.p. R. Minkowski reports that this very peculiar spectrum shows lines of highly ionized iron atoms. He will publish a description later.
240. MHa 375-1. 5′ n.p. BD−8°4489.
241. MHa 363-30. 1′.5 north of the midpoint of the line joining CD−38°12156 and −38°12175. A brighter star is 2′ n.p.
242. (CD−25°12254). 2′.5 preceding a star of the same magnitude.
243. MHa 304-68. 6′ north and slightly preceding CD−28°13571.
244. MHa 304-74. Near CD−29°14029. 1′.5 north and slightly preceding a somewhat fainter star.
245. MHa 359-110. 12′ n.p. BD−22°4437. A tenth-magnitude star is 3′ preceding. R. Minkowski has found the spectrum to be very peculiar, with prominent bright lines of *He* I and [*Fe* VII].
246. HD 316375. CD−27°12020.
247. CD−24°13552. 4′ preceding and slightly south of a star of the same magnitude, probably CD−24°13553.
248. HD 316520. CD−28°13727. 3′ north and slightly following CD−28°13724. Another tenth-magnitude star is 3′ north.
249. (HD 316587). (CD−29°14098). 5′ preceding and slightly south of a much fainter star.
250. CD−22°12292. 10′ s.p. CD−22°12299. Northern and following of two stars.
251. (CD−28°13765). 1′.5 s.p. a slightly fainter star.
252. HD 316608. (CD−30°14896). 1′.5 n.f. CD−30°14891.
253. (HD 316568). CD−29°14172. 7′.5 n.p. CD−29°14183. A faint red star lies between.
254. MHa 304-92. 2′.5 preceding and slightly north of CD−27°12131.
255. MHa 363-45. Between two brighter stars separated by 3′. The northern, preceding, and brighter is probably CD−35°12088.
256. MHa 304-10. 5′ n.f. CD−34°12297. Central one of three extremely faint stars.
258. MHa 304-168. 2′.5 south of a brighter star, probably CD−24°13678.
259. (CD−25°12499). 5′ n.p. a star of magnitude 9.5. The following (and of intermediate declination) of three stars of similar magnitude.
260. HD 318710. CD−31°14905. 8′ north and slightly preceding CD−31°14907.
261. MHa 304-167. Near HD 314916. 7′ n.p. CD−25°12544. A brighter star is 3′ north and slightly preceding.
262. MHa 304-14. 2′ n.f. CD−33°12697. An eleventh-magnitude star, probably CD−33°12702, is 1′ s.p. Magnitude variable; possibly a nova.

NOTES TO TABLE 1—*Continued*

No.
263. HD 312462. 7′ preceding BD−17°4985. Bright *Hα* may have been less intense on May 16, 1947, than on August 31, 1946.
264. HD 316870. CD−29°14345. 5′ south and slightly preceding CD−29°14349.
265. (HD 316989). (CD−29°14350). 1′ following and slightly north of a fainter star.
266. (HD 324802). (CD−37°12105). 4′ n.f. a brighter star.
267. MHα 359-71. Near CD−23°13793. Preceding and fainter of two stars separated by less than 1′.
268. MHα 359-70. 1′.2 south of CD−23°13802.
269. MHα 304-52. 1′.5 s.f. CD−32°13660.
270. F 6-7. 13′ preceding and slightly north of BD−20°4986. A brighter star is 6′.5 n.f. Probably the southern star of several. R. Minkowski has found very strong bright *H* lines superposed on a continuous spectrum with dark *TiO* bands.
271. HD 313820. CD−22°12543.
272. MHα 82-21. 1′.5 preceding CD−29°14508. A slightly brighter star is 1′.5 n.p.
274. (HD 315177). (CD−25°12733 or −25°12736). May be HD 315178.
275. (HD 317086). (CD−28°14164). Follows a fainter star by 1′.
276. MHα 363-7. 8′ s.p. CD−41°12468. An eleventh-magnitude star is 3′ north.
277. MHα 79-19. 2′.5 s.f. BD−19°4854.
278. MHα 79-25. 4′ following BD−22°4576. Forms an equilateral triangle with two brighter stars following.
279. HD 165895. 4′ s.p. CD−24°13971. 5′.5 n.p. CD−24°13975.
280. MHα 304-17. 1′.5 n.p. a brighter star, probably CD−33°12894. Southern and faintest of three stars.
281. MHα 208-83. 1′ following and slightly south of a brighter star, probably CD−27°12510.
282. MHα 304-113. 3′.5 preceding a brighter star, probably CD−28°14255.
283. MHα 304-120. 3′ south and slightly following a brighter star, probably CD−28°14256.
284. MHα 304-121. 1′ s.f. CD−29°14632.
285. F 1-37. 3′ preceding and slightly south of BD−14°4924.
286. HD 315277. CD−25°12867.
287. HD 166612, 3. *Hα* is a bright line of moderate intensity on a low-dispersion slit spectrogram taken in August, 1948. Spectrum Fe.
288. MHα 304-119. 4′ s.p. CD−28°14290. 2′.5 s.p. CD−28°14291.
289. F 1-11. 9′ n.p. BD−11°4558. 7′ south of and slightly preceding a brighter star.
290. MHα 77-52. 1′.5 south of CD−32°13890.
291. HD 312984. Halfway between BD−20°5033 and −20°5039.
292. HD 319139. CD−32°13906. Classified K5e at Harvard. The star deserves further investigation.
293. MHα 304-122. 1′.5 south of an M-type star, CD−29°14700.
294. MHα 304-123. 5′.5 following CD−27°12619. 3′ s.f. a brighter star.
295. MHα 304-41. 2′ n.p. HD 167362.
296. D 143-2. 16′ s.p. BD−0°3449. A brighter star is 9′ s.p.
297. MHα 352-34. 8′ s.p. BD+21°3358.
298. MHα 312-68. 4′.5 north and slightly preceding BD−17°5108. A slightly brighter object is 2′.5 n.p.
299. MHα 208-92. Probably Nova Sagittarii, 1945. 1′.5 s.p. a brighter star, probably CD−28°14410.
300. MHα 304-149. 9′ north and slightly preceding CD−24°14166. 9′ s.p. CD−24°14179. A brighter star is 1′.5 preceding.
301. MHα 304-145. 2′.5 n.f. a brighter star, probably CD−24°14186.
302. MHα 304-33. 6′.5 n.p. CD−31°15441. A faint star is 2′ north. Minkowski reports that this star is variable.
303. MHα 366-101. 3′ n.f. a slightly brighter star, probably CD−25°13093. 5′ north and slightly preceding a brighter star, probably CD−25°13094.
304. (CD−28°14567). 2′.5 n.p. a red star.
306. F 1-17. Halfway between BD−12°5047 and −12°5055. A tenth-magnitude star is 1′.5 n.f.
307. MHα 204-53. 8′ n.p. BD−13°5006. The southern of several faint stars.
308. F 4-37. 1′.5 south of the midpoint of the line joining BD−19°5038 and −19°5043.
309. F 5-12. 6′.5 following and slightly north of BD−14°5102. A brighter star is 3′ following.
310. MHα 375-17. 12′ north of and slightly following BD−5°4686. 5′ n.p. BD−5°4689.
311. MHα 345-39. 2′ following a star of about the same magnitude.
312. F 5-56. Brightest star within a radius of 5′.
313. MHα 208-51. 3′ following and slightly south of BD−22°4807.
315. D 143-20. 8′ s.f. BD−5°4721. Preceding and northern of two stars separated by 2′.
316. MHα 208-58. 7′ south of BD−21°5108.
317. MHα 345-51. 2′.5 s.p. a star of similar magnitude.
318. MHα 345-30. 2′ n.p. a star of the same magnitude.
319. MHα 345-31. 4′ south of and slightly following BD−5°4735. A brighter star is 3′ south.
320. MHα 345-32. 6′ south and slightly preceding BD−3°4366. A very interesting Wolf-Rayet star. The emission line λ 4650 of *C* III has a wide, strong absorption line on its shortward side.

NOTES TO TABLE 1—*Continued*

No.
321. BD−11°4747. R. Minkowski has found the [*N* II] lines near *Hα* to be strong.
322. MHα 345-52. 6′ south and slightly following BD−2°4737. A slightly fainter star is 4′ n.f.
323. MHα 369-39. 1′ south and slightly following a faint red star. R. Minkowski has found the spectrum to have bright lines of *He* I in addition to those of *H*.
324. MHα 352-9. 5′ s.f. BD+10°3663. A much fainter star is 2′.5 preceding.
325. CD−26°13521. *Hβ* is a very strong, bright line on low-dispersion slit spectrograms taken in August, 1948; *Hγ* and *Hδ* also are bright. The type is Fe. The star deserves further observation.
326. MHα 204-32. 5′ n.f. BD−13°5119. On a straight line joining BD−13°5119 and −13°5123.
327. MHα 208-67. 1′.5 s.p. a brighter star, probably CD−24°14797.
328. SV Sct. 8′ n.f. BD−14°5215. The following of three stars. The spectrum is probably Se.
329. FN Sgr. 4′.5 north and slightly preceding BD−19°5213. A low-dispersion slit spectrogram taken by R. Minkowski shows bright lines of *H*, *He* I, and possibly other elements. The type may be earlier than B.
330. (CD−32°14673). 6′.5 south and slightly preceding CD−32°14678. Southern, following, and faintest of three stars in a straight line.
331. BD−5°4819. Bright *Hα* was independently discovered by C. K. Seyfert of the Warner and Swasey Observatory.
332. BD−5°4823. *Hα* is bright on slit spectrograms taken on August 15 and October 23, 1948, and July 15, 1949. The type is not well shown.
334. MHα 305-5. 6′.5 south and slightly following BD+17°3812. A brighter star is 2′.5 n.f. Northern, preceding, and faintest of three stars.
335. MHα 214-24. 2′.5 n.p. BD+2°3756. A brighter star is 2′.5 n.p.
336. (BD+0°4080). Northern and following of two stars separated by 1′.5. *Hα* is bright on three slit spectrograms taken in July, 1947. Bright *Hβ* and other peculiarities in the blue are shown by a weak slit spectrogram taken on July 23, 1948. The type is estimated to be gK(3)pe. This star deserves further observation.
337. MHα 277-6. Halfway between BD−17°5439 and −17°5445.
338. MHα 305-6. 4′ preceding and slightly south of BD+16°3715. Two slightly brighter stars are 4′ south. R. Minkowski has found the spectrum to have bright lines of [*Fe* VII] in addition to those of *H*.
339. MHα 214-22. 3′ n.f. BD+3°3893.
341. MHα 339-4. 4′ s.p. BD−2°4875.
342. MHα 277-26. 9′ s.p. BD−12°5298. A brighter star is 3′ n.p. Southern of two or more faint stars.
344. HD 349853. BD+19°3948.
345. MHα 305-11. 2′.5 n.p. BD+17°3895.
346. MHα 305-10. 4′ n.p. BD+17°3897.
347. MHα 214-17. 2′ n.f. BD+4°4036.
348. (BD−9°5069). 3′ north of a brighter star.
349. MHα 215-6. 5′ n.f. BD+14°3852.
350. MHα 319-34. 4′ n.f. BD−11°4942. R. Minkowski has found the spectrum to be of type W.
351. MHα 308-19. 1′.5 s.f. BD+14°3858.
352. MHα 308-44. 3′ following BD+15°3764.
353. MHα 308-18. 8′ n.p. BD+10°3867. Brightest star on line joining BD+10°3763 and +10°3867.
354. HD 344191. BD+23°3632.
355. MHα 308-17. 8′ s.p. BD+11°3817.
356. MHα 215-33. 4′.5 s.p. BD+24°3729. Probably type N or S.
357. MHα 92-20. 2′.5 following and slightly south of a tenth-magnitude star, probably HD 338351.
359. MHα 215-36. 2′.5 preceding BD+23°3703.
360. MHα 80-5. 5′ north of BD+18°4227. R. Minkowski has found this star to have a combination spectrum.
361. HD 350485. BD+19°4163.
362. HD 226100. 1′.5 s.p. BD+34°3751.
363. HD 338970. BD+26°3687. The *Hα* line appears bright on objective-prism photographs taken in September, 1940, August, 1946, and August, 1947; it is a well-marked bright line, possibly slightly widened, on a low-dispersion slit spectrogram taken in August, 1947. From a low-dispersion slit spectrogram of the photographic region taken in October, 1947, the spectrum was classified dF5e.
364. HD 345105. 2′.5 n.f. BD+22°3834.
365. HD 350799. BD+17°4126.
366. (HD 333003). 3′ preceding BD+28°3513.
367. HD 345122. BD+21°3959.
368. MHα 92-28. Northern of two stars of similar magnitude separated by 2′.5.
369. BS Cyg. Halfway between BD+53°2311 and +53°2312. The spectrum appears to be banded.
370. MHα 328-17. Southern, following, and brighter of two stars separated by less than 1′. Northern and following of three stars making a line 5′ in length.
371. MHα 316-52. 2′.5 n.f. BD+26°3729.

NOTES TO TABLE 1—*Continued*

No.

372. HD 351123. BD+16°4079.
373. MHα 328-116. 5′ south of BD+39°3965. A slightly brighter star is 1′ following.
374. MHα 376-29. 1′.5 s.f. BD+31°3872.
375. MHα 92-31. 6′.5 n.p. BD+31°3878.
376. MHα 328-10. 4′ s.p. BD+35°3917.
377. MHα 328-9. 3′.5 s.f. BD+36°3825. A faint star is 2′ following.
378. HD 331808. 6′.5 s.p. BD+30°3867.
379. MHα 328-112. 1′.5 n.f. BD+36°3853.
380. MHα 104-29. 2′ n.p. BD+32°3706.
381. MHα 376-47. 5′ preceding and slightly north of BD+32°3709. A star of similar magnitude is 5′ south.
382. (HD 228023). 5′ n.p. BD+34°3896. Preceding of four stars of similar magnitude.
383. MHα 328-20. 9′ s.p. BD+34°3890. Southern and preceding of three stars forming a straight line.
384. HD 351582. BD+19°4308.
385. MHα 328-23. 6′ following BD+36°3918.
386. MHα 148-48. 6′ n.p. BD+37°3810. Brightest star in the field.
387. (HD 228207). 1′.5 s.f. BD+35°4011 (HD 228200).
388. MHα 328-105. 3′.5 following BD+39°4074. Southern and following of two stars separated by 1′.5. Possibly peculiar bands.
389. MHα 328-107. 1′.5 north and slightly preceding a star of magnitude 10.5.
390. MHα 328-102. 10′ s.f. BD+37°3826. Preceding and fainter of two stars separated by less than 1′.
391. MHα 148-64. 2′.5 preceding BD+38°3963. A brighter star is approximately 1′ preceding.
392. (HD 228510). Follows a brighter star by less than 1′.
393. MHα 148-69. 8′ s.p. BD+39°4100. A slightly fainter star is 2′.5 following.
394. (HD 228576). 3′.5 north of and slightly following BD+36°3963. A red star is 1′ following and slightly north.
395. MHα 328-91. 6′.5 n.p. BD+36°3992.
396. MHα 328-87. 2′ preceding and slightly south of a star of the same magnitude.
397. MHα 328-84. 2′ north and somewhat preceding BD+38°3990.
398. MHα 328-88. 4′ s.f. BD+37°3870. Two slightly brigher stars lie between.
399. MHα 148-103. 4′ north of BD+41°3866.
400. D 146-37. 4′ n.p. BD+37°3879. A star of equal magnitude is 3′ n.p.
401. MHα 328-89. 9′ north and slightly preceding BD+37°3878. Brightest star within a radius of 5′.
402. BD+40°4112. Type probably later than B.
403. MHα 328-80. 4′ north of and slightly following BD+38°4016.
404. MHα 328-81. 4′ n.p. BD+39°4139.
405. MHα 328-79. 4′ south of BD+38°4025. In declination it is halfway between two much brighter stars preceding.
406. MHα 328-71. 2′ n.p. BD+37°3902.
407. MHα 328-74. 3′.5 n.p. BD+36°4031. A brighter star is 2′ south.
408. MHα 328-68. 5′ n.p. BD+39°4154. Probably northern and brightest of several faint stars.
409. MHα 328-76. 9′ north of BD+36°4033.
410. MHα 328-69. 4′ n.f. BD+37°3906. A brighter star is 4′ south.
411. FHα 3-44. 1′.5 n.f. BD+37°3907. A brighter star is 3′.5 south.
413. MHα 148-76. 5′ preceding BD+39°4179. A fainter star is less than 1′ s.p.
414. MHα 148-77. Less than 1′ s.p. a tenth-magnitude star.
415. MHα 148-88. Southern, preceding, and faintest of three stars forming a straight line 5′.5 in length.
416. MHα 76-40. 8′ north and slightly following BD+37°3926. A slightly fainter star follows by less than 1′.5.
417. FHα 3-6. 5′ north and slightly following BD+37°3936. A brighter star is 2′ n.p.
418. MHα 148-99. 8′ n.f. BD+43°3613. Brightest star within a radius of 8′.
419. MHα 76-34. 4′ north of and slightly preceding a ninth-magnitude star.
420. MHα 328-130. 4′ following and slightly north of BD+40°4195. Preceding of three stars of about the same declination.
421. MHα 328-131. 1′.5 preceding and slightly south of BD+41°3791.
422. MHα 328-53. 9′ south of BD+40°4218. Southern and brightest of three stars.
424. MHα 289-51. 5′ s.f. BD+40°4220.
425. MHα 328-51. Northern of three stars forming an equilateral triangle, 4′ on each side.
426. MHα 328-133. 4′ south and slightly preceding BD+40°4227. Northern, following, and brighter of two stars separated by 1′.5.
427. MHα 328-134. 4′ following BD+40°4227. A brighter star is 1′.5 n.f.
428. MHα 148-90. 6′.5 n.f. BD+40°4227. A star of magnitude 9.5 is 4′ south.
429. MHα 328-40. 2′ following a slightly brighter star.
430. MHα 148-91. 6′.5 s.f. BD+41°3808. 6′.5 n.f. BD+40°4234.

NOTES TO TABLE 1—*Continued*

No.

431. MHa 328-50. 2′.5 n.p. a tenth-magnitude star.
432. MHa 328-41. 9′ s.p. BD+34°4095. 10′ n.p. BD+34°4098. Brightest star in the field.
433. MHa 328-142. 4′ n.f. BD+41°3837. A ninth-magnitude star is 3′ n.f.
434. MHa 328-141. 2′.5 n.f. BD+41°3840.
436. MHa 328-42. 2′.5 following and slightly south of BD+35°4217. BD+35°4221 is 2′.5 south and somewhat preceding.
438. HD 197406. Spectrum Of. The HD classification of Ma was later changed by Miss Cannon to Oc. The spectrum is under investigation by O. C. Wilson.
441. MHa 235-37. 2′.5 south of BD+43°3714.
442. MHa 235-36. 4′ n.f. BD+43°3720. Northern, preceding, and brighter of two stars.
443. MHa 148-94. 8′ n.f. BD+43°3720. BD+43°3725 is 9′ north.
444. MHa 148-95. 6′ s.f. BD+43°3722.
445. MHa 221-39. Southern, preceding, and brighter of two stars separated by 4′. A brighter star is 4′.5 n.p.
446. MHa 255-56. 4′ n.p. BD+48°3223. Preceding of two stars.
447. (BD+46°3080). N.f. of two stars separated by less than 1′.
448. MHa 235-59. 7′ north and slightly preceding BD+44°3615. A fainter star precedes by less than 1′.
449. MHa 255-55. Northern, following, and probably fainter of two stars separated by 2′. Approximately at the midpoint of the line joining BD+48°3242 and +49°3420.
451. BD+44°3657. 4′ s.f. BD+44°3656.
452. (BD+44°3666). 4′ north and slightly following BD+44°3661.
453. MHa 289-90. 5′ s.f. BD+45°3368. A brighter star is 4′ north. R. Minkowski has found this star to have a combination spectrum.
454. MHa 235-19. 5′ n.p. BD+40°4396. Northern, following, and brighter of two stars.
455. MHa 235-54. 2′.5 n.p. BD+45°3392.
456. MHa 255-53. 13′ north of and somewhat following BD+50°3257. Central and probably brightest of three stars.
457. MHa 81-12. 8′ n.p. BD+44°3714.
459. MHa 255-52. Approximately equidistant from BD+48°3298 and +48°3299. Northern and following of two stars separated by 2′.5.
460. MHa 255-26. 8′ north of and slightly preceding BD+48°3316.
461. MHa 255-51. 2′.5 s.p. BD+48°3320.
462. MHa 170-24. 12′ north of and slightly following BD+55°2549.
463. MHa 255-48. 3′.5 following BD+49°3512.
464. MHa 297-51. Southern and following of two stars separated by 3′.
466. MHa 221-54. Southern of two stars separated by 1′.5.
468. BD+41°4191. 12′ n.p. BD+41°4196.
469. MHa 297-36. 12′ s.f. BD+54°2577. Two brighter stars are 8′ s.p. and 8′ s.f., respectively.
470. MHa 297-55. 4′ north and slightly following BD+56°2601.
473. MHa 297-34. 4′ preceding and slightly south of a brighter star.
474. MHa 297-35. 4′ south of BD+56°2624. A red star is 2′.5 preceding.
475. BD+65°1637. Preceding and northern of two stars separated by 1′.
476. MHa 258-37. 5′ n.p. BD+54°2631.
477. BD+46°3471. Preceding and brighter of two stars separated by 2′.
480. MHa 174-63. Probably late type. 4′ s.f. a star of similar magnitude. A fainter star is 4′ south.
481. MHa 73-11. 2′ n.f. a star of similar magnitude.
484. MHa 258-33. Northern and following of two stars separated by 1′.5.
485. MHa 258-95. 12′ south and somewhat preceding BD+48°3621. 5′.5 n.f. a star of similar magnitude. A fainter star lies between.
487. MHa 258-26. 2′ n.p. BD+54°2746.
489. MHa 258-70. 4′ following a much brighter star. Southern and following of three stars.
491. AC+55°64276. 1′ preceding and slightly south of BD+55°2754. Bright *Hα* was detected independently by Morgan and Bidelman.
492. MHa 217-26. 6′.5 following and slightly north of BD+61°2298.
494. AC+57°60526. Southern and following of two stars separated by 2′.5. Independently discovered by Morgan and Bidelman.
495. MHa 258-78. 4′ n.p. BD+53°2933. A slightly fainter star is 2′ preceding.
496. AC+57°61154. 1′.5 south of a slightly brighter star. Bright *Hα* was independently discovered by Morgan and Bidelman.
497. MHa 217-83. 6′ south and slightly preceding BD+54°2843.
499. MHa 47-30. 4′ n.f. BD+57°2643. A. H. Joy has found the spectrum to be of the T Tauri type. See *Ap. J.*, **110**, 435, 1949.
500. MHa 217-49. 3′ n.f. a slightly brighter star.

NOTES TO TABLE 1—*Continued*

No.

501. MHα 73-59. 4′ s.f. BD+58°2517. Probably late type. *Hα* not distinctly bright on an objective-prism plate taken on September 21, 1944.
502. MHα 217-55. 8′ preceding and slightly south of BD+59°2628. A star of similar magnitude is 4′ n.f.
505. MHα 217-18. 6′ south and slightly preceding BD+61°2388.
506. MHα 217-58. 6′ north and slightly following BD+57°2692. 6′.5 s.p. BD+57°2696.
507. BD+73°1031. Probably K type.
509. FHα 7-6. 5′ s.f. BD+60°2567. A fainter star is 4′ north.
511. MHα 217-68. 5′ north and slightly following BD+55°2992. Probably N type.
513. MHα 217-9. 1′.5 preceding and slightly south of BD+61°2508. Spectrum Of. The spectrum is under investigation by O. C. Wilson.
514. MHα 256-51. 1′.5 north and slightly following BD+61°2564.
515. MHα 256-53. 1′ north and slightly preceding BD+62°2329.
516. MHα 223-53. 5′ n.f. BD+63°2078.
518. MHα 284-27. 2′ n.f. BD+72°1127. *Hα* appears distinctly bright on objective-prism photographs taken on July 26 and August 31, 1946, but is not seen on a similar plate taken on September 24, 1946. Does it change?

STELLAR SPECTRA IN MILKY WAY REGIONS
II. A REGION IN CYGNUS

S. W. McCuskey and C. K. Seyfert
Case Institute of Technology and Vanderbilt University
Received March 9, 1950

ABSTRACT

Observations of spectra, photographic magnitudes, and red color indices are given for a region in Cygnus R.A. 19^h36^m; Dec. $+30°$. The area of the sky covered is 13.4 square degrees. Tables 1 and 2 list the data. Identification charts are shown in Figure 1, *A–L*.

An analysis of spectral type distributions for a study of the galactic structure in Aquila and in Cygnus was published[1] by the authors in 1947. The present note supplies a catalogue of the observational data on spectral types, colors, and photographic magnitudes for the region LF2 in Cygnus. Similar data for region LF1 in Aquila have been published recently in the *Astrophysical Journal*.[2]

Region LF2 lies in the Milky Way at R.A. 19^h36^m; Dec. $+30°$; $l = 33°$, $b = +3°$ (1945). The field is circular and covers 13.4 square degrees. All the observations of spectra have been made with the 4° objective prism attached to the 24–36-inch Schmidt-type telescope of the Warner and Swasey Observatory.

Sectional charts covering the area are presented in Figure 1, *A–L*. The numbering is explained below. A key to the sectioning of the field is included in the upper left-hand corner of Figure 1, *A*. The printing on each section reads correctly when the chart is held with north up.

Table 1 gives the observational data for 2170 stars in this area. The numbering scheme given in the first column is similar to the system of the BD catalogue, the stars being listed approximately in order of right ascension in each degree zone of declination. Zone boundaries are for 1950 and are not to be considered very precise. The network has been established by reference to the computed positions for only four stars.

An asterisk following a star's serial number in Table 1 indicates that it is a BD star. An "R" indicates a reference to the remarks given in Table 2. Attached to the latter table are the BD numbers for a few stars in each zone to provide quick orientation with the BD catalogue and chart.

Table 1 lists about 600 more stars than were used in our analysis of LF2 mentioned above. Most of these are faint stars whose spectra became classifiable only on the better plates which were taken after the original work of 1945 and 1946. A reanalysis of these data will be made when the results for all the LF regions are summarized.

The second and third columns of Table 1 give, respectively, the apparent photographic magnitudes for all stars and the red color indices for stars of spectral type earlier than F0. The colors have been determined from the given m_{pg} and from red magnitudes based upon the North Polar Sequence as given by Nassau and Berger.[3] Eastman 103*a*-E plates combined with a No. 22 Wratten filter were used for the red-magnitude work. The effective wave length of this combination is about λ 6200. Eastman 103*a*-O and II*a*-O plates were used for the blue photometry. The tabulated m_{pg}'s have an average probable error of ±0.09 mag.; the colors, an average p.e. of ±0.12 mag. All the photometry was done with a graduated scale of stellar images on plates taken with the Schmidt telescope.

[1] *Ap. J.*, **106**, 1, 1947.

[2] S. W. McCuskey, *Ap. J.*, **109**, 426, 1949.

[3] *Ap. J.*, **103**, 25, 1946.

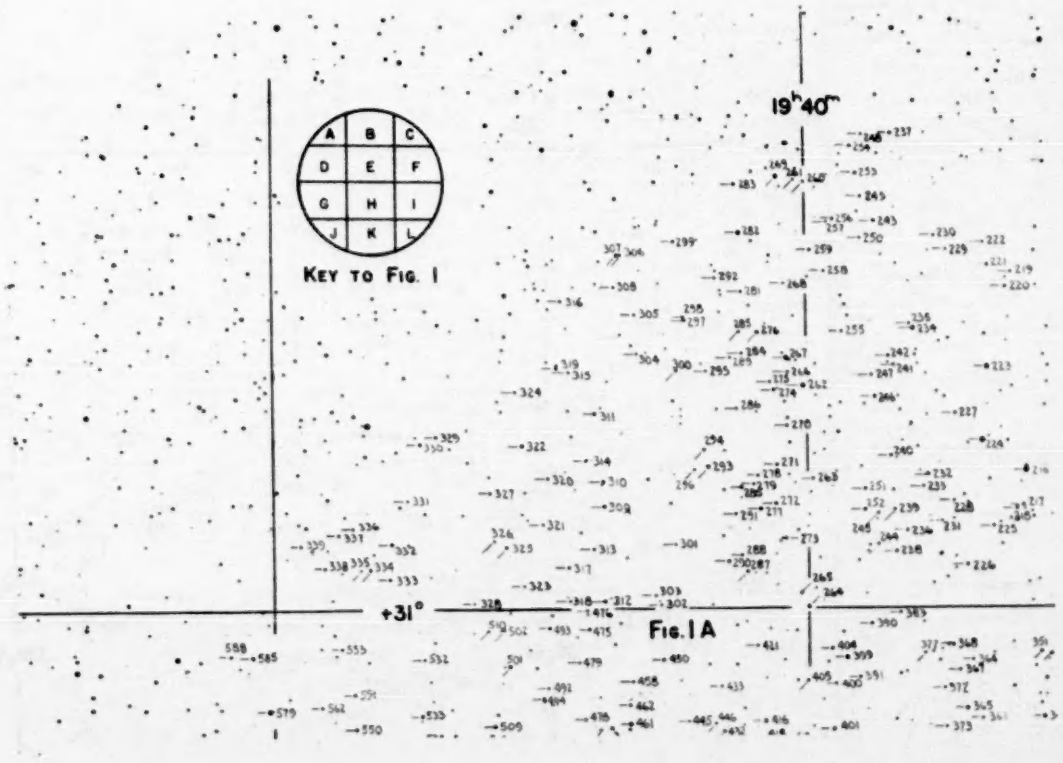

FIG. 1A

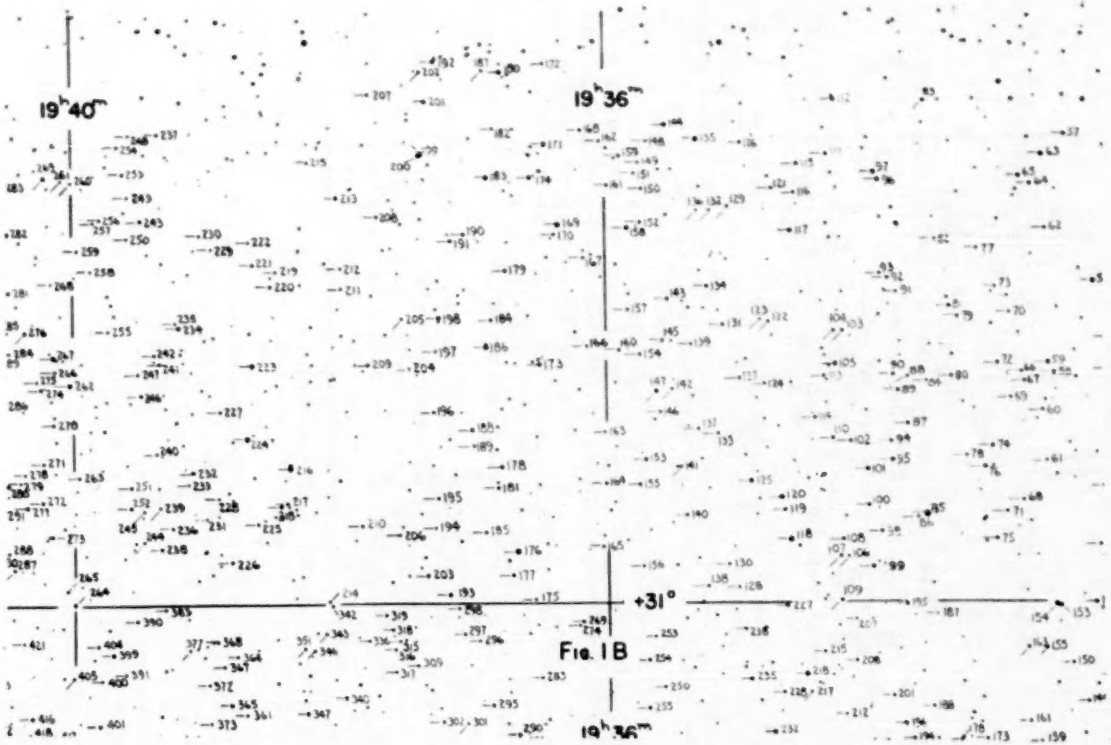

Fig. 1B

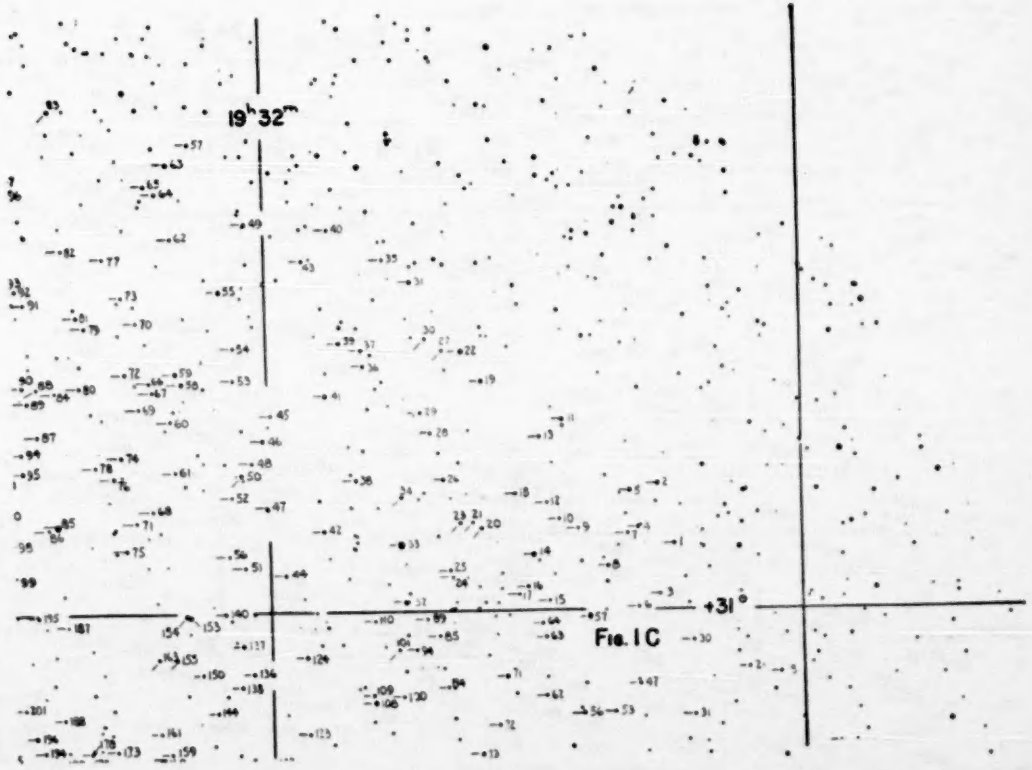

Fig. 1C

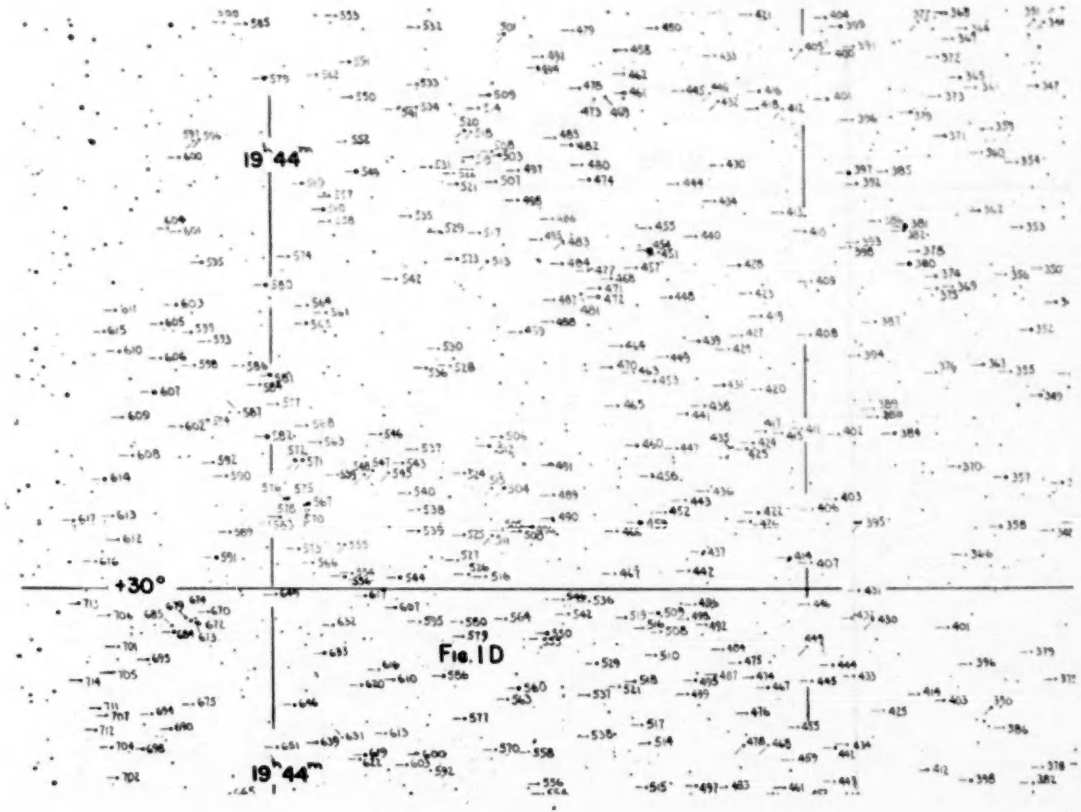

Fig. 1 D

19h36m
+30°
Fig. I E

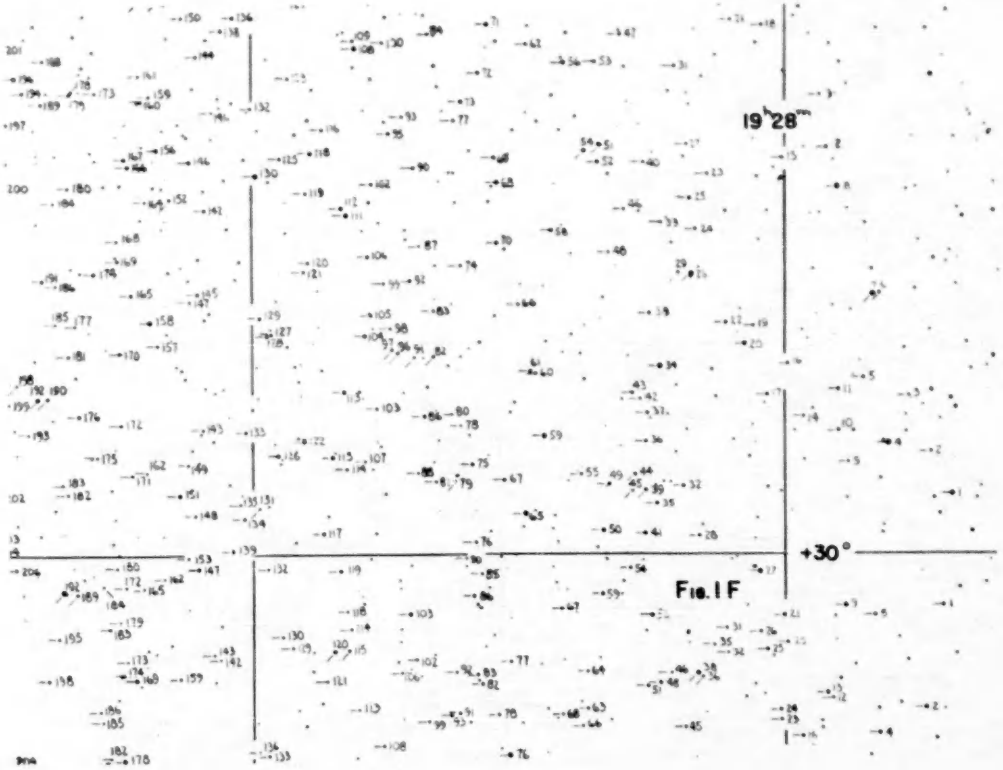

FIG. 1 F

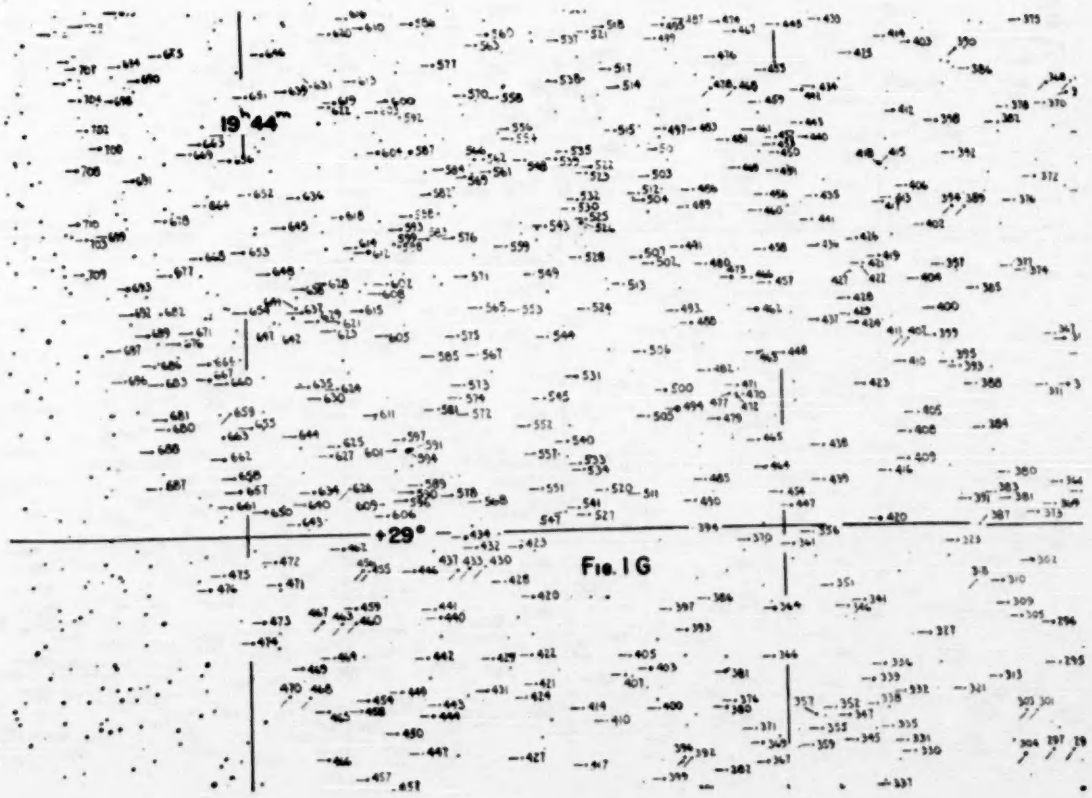

Fig. I G

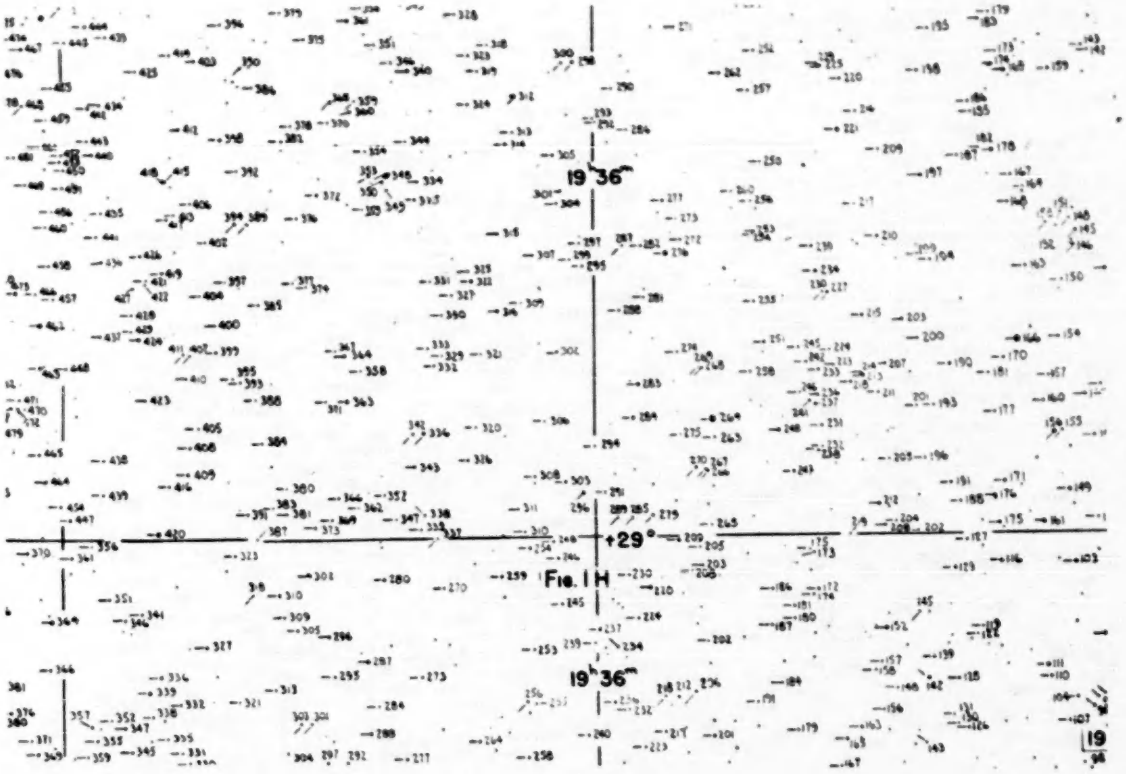

Fig. 1 H

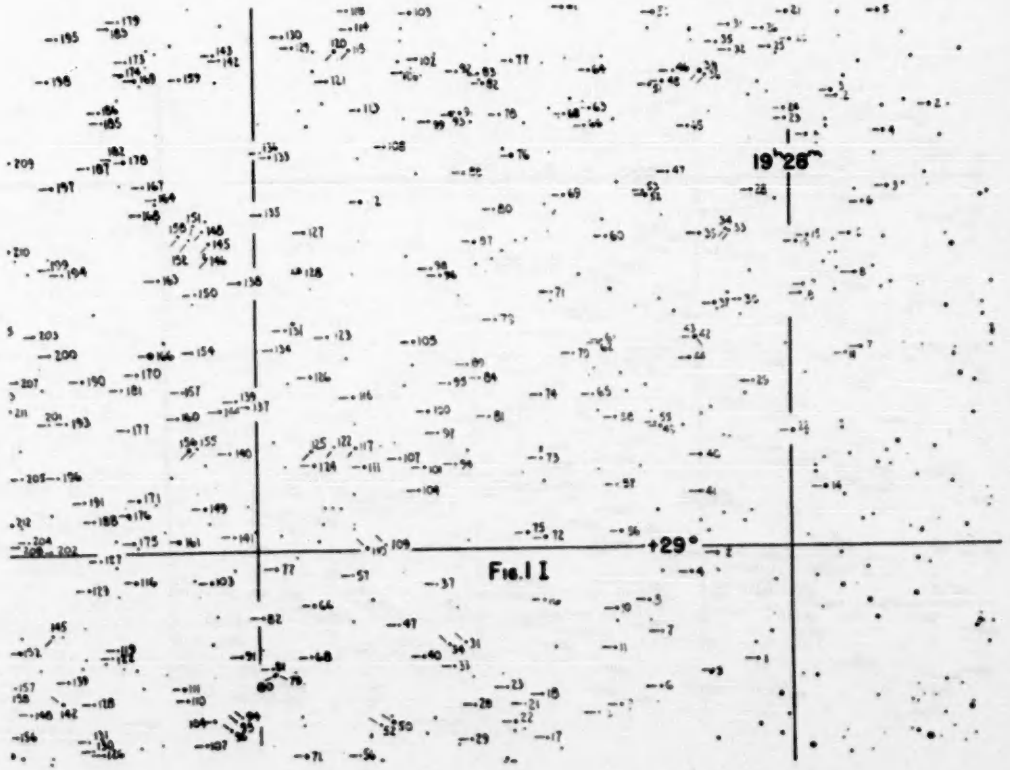

FIG. I I

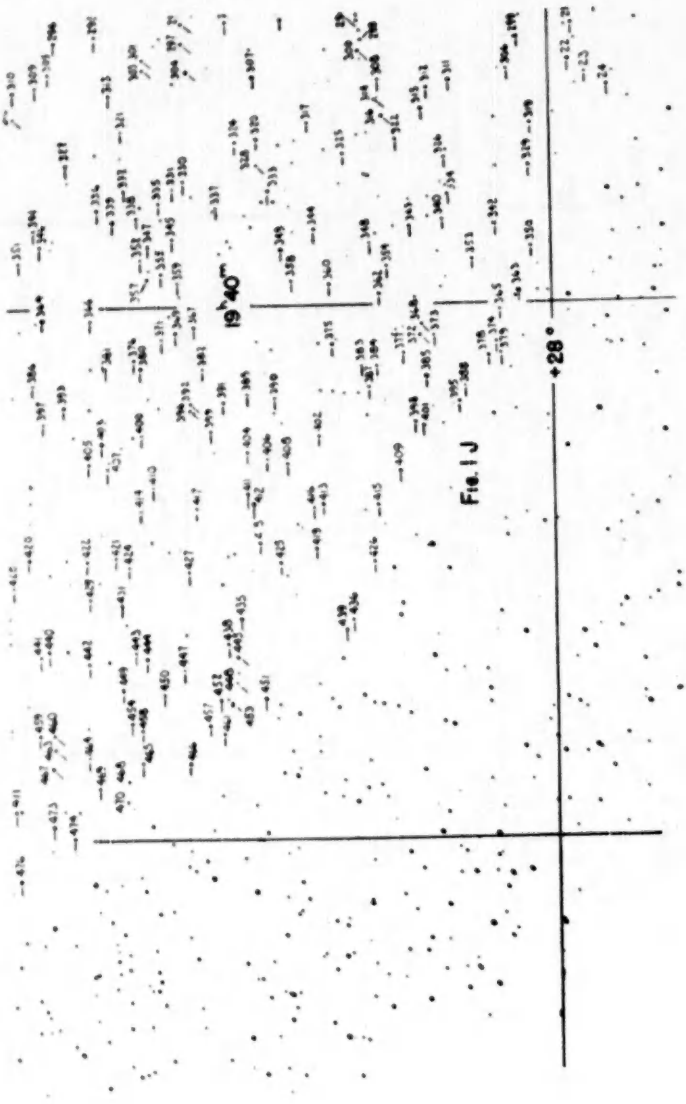

Fig. 1 J

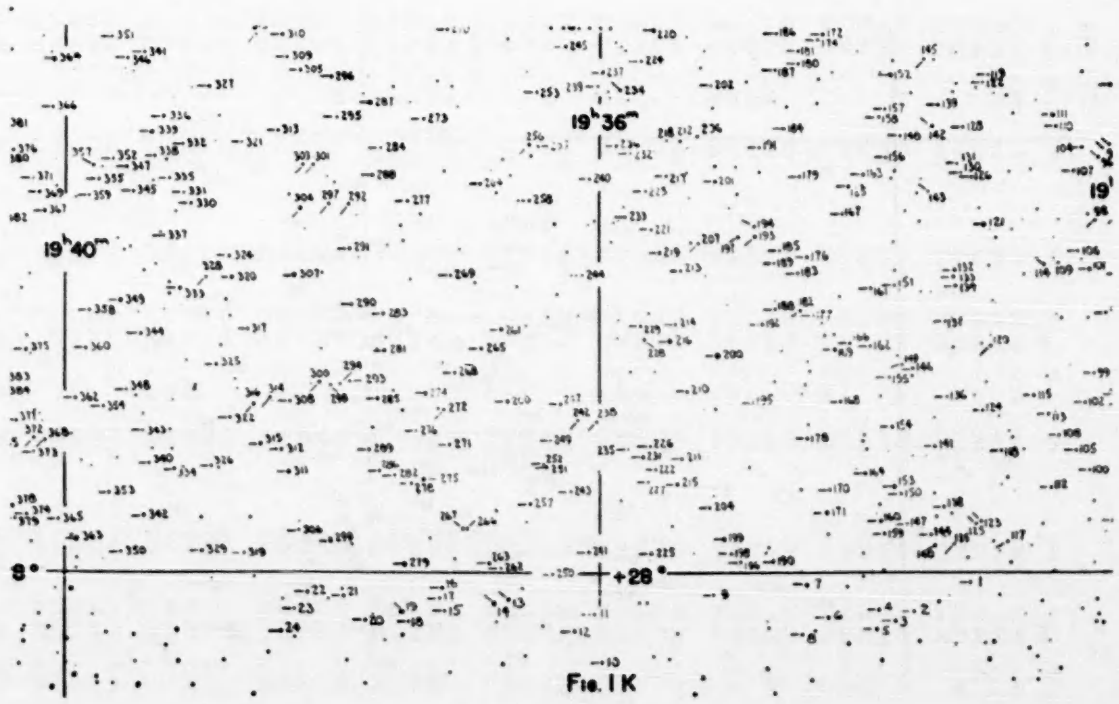

Fig. 1K

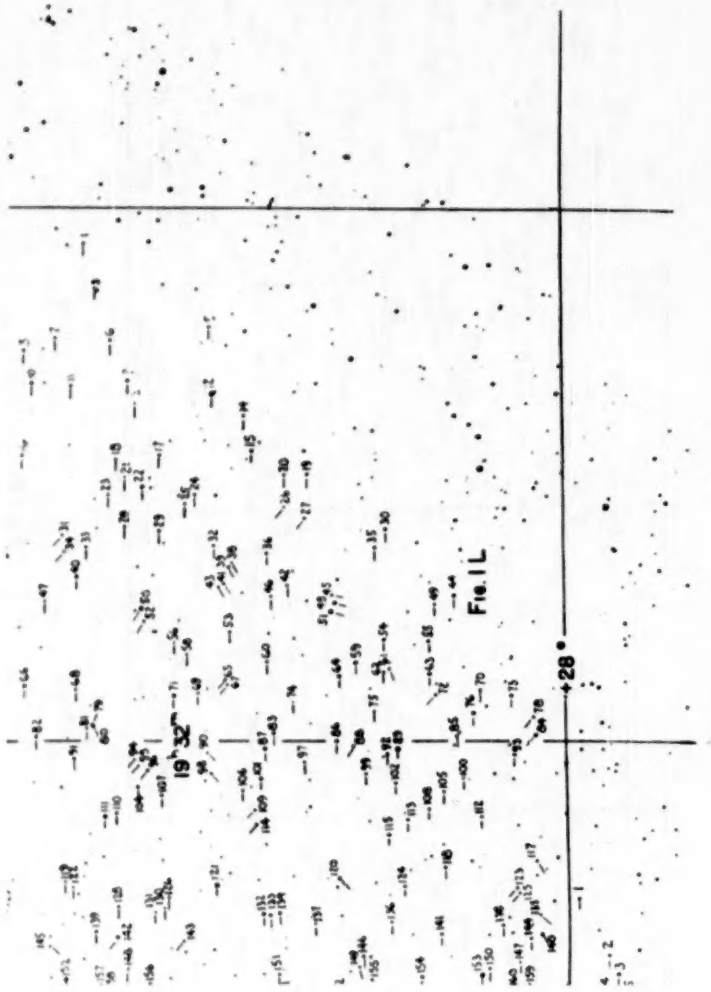
Fig. 1 L
+28°
1932

Table 1

Observational Data for Region LF2

Zone +27°

No.	m_{pg}	R.I.	Sp.
1	11.90	+.57	A0
2	12.00	+.39	A0
3*	10.46	...	G0V
4	11.43	...	G0
5	10.68	...	F0V
6	11.04	+.67	A2
7*	9.89	...	F5V
8	11.92	...	A0
9	12.55	...	B9
10	12.11	...	G5III
11	12.35	...	K0
12	11.70	+.21	B9
13*	9.95	-.39	A0
14*	9.62	+.07	B9
15	12.03	+.38	A0
16	10.84	...	G2V
17	12.39	...	F2:
18	12.30	...	G0
19*	10.70	+.39	A3
20	11.37	+.14	B9
21	11.70	...	G8III
22	11.04	+.38	B9
23	12.57	...	K3
24	11.48	...	K2V

Zone +28°

No.	m_{pg}	R.I.	Sp.
1	11.88	+.15	A0
2	10.98	+.08	A0
3	11.81	+.37	A5
4	11.04	-.04	B9
5	11.98	...	F0
6	11.93	+.69	A3
7	12.48	...	G8III
8*	11.86	...	K0III
9	11.47	+.23	A0
10	10.73	...	G5IV
11	12.17	...	A0
12*	7.46	...	F0V
13	12.69	...	G0
14	11.81	...	F8
15*	10.53	...	F0V
16	12.33	...	A2
17	11.98	...	F2
18	12.29	...	G0
19	11.52	...	F0
20	12.15	...	A0
21	12.83	...	M0
22	10.60	-.04	A3
23	12.52	...	G8
24	12.06	...	A3
25	12.29	...	G0
26	12.79	+.21	A0
27	12.16	...	G5IV
28	12.04	+.29	A2
29	11.20	...	K0III
30*	11.32	...	G5V
31	12.04	...	M0III
32	12.33	...	F0
33	12.46	...	G0
34	12.12	...	A3
35	11.98	+.58	A5
36	13.50:	...	N
37	12.45	...	A5
38	12.75	...	F8
39	11.37	+.49	A5
40	9.93	+.01	A2
41	12.37	...	F0
42	12.06	...	G0
43	12.36	...	G2
44	10.70	-.28	B5
45	12.36	...	G2
46R	12.14	...	F0
47	12.37	...	G2V
48	9.89	+.09	F0III
49	12.51	...	G5III
50*	8.77	-.33	B8
51*	8.72	-.42	B8
52	12.16	...	K0III
53	11.96	...	G0
54	11.57	...	F5
55	11.80	...	F2
56	12.81	...	K2
57	12.75	...	A3
58	12.47	...	K0III
59*	10.10	+.07	B9
60	12.25	...	A0
61	12.06	...	G2
62*	11.90	...	K0III
63	10.41	-.12	B9
64*	10.26	-.13	B8
65	11.63	+.19	A0
66*	9.30	...	G0V
67	12.37	...	G0
68	11.53	-.16	B8
69R	12.26	...	M2III
70	12.10	...	G0
71*	9.30	-.23	B9
72	12.20	...	G2
73	10.97	...	F2III
74	13.03	...	K0
75	12.54	...	A2
76*	10.21	+.40	A0
77*	9.97	...	F0V
78	12.06	...	G0
79	11.07	-.01	A3
80*	11.47	...	F0
81	11.87	...	F0
82*	10.80	...	F2V
83	10.80	+.58	A3
84	10.34	-.23	B8
85	11.85	...	K0III
86*	9.92	...	G0V
87*	9.32	-.06	A3
88	12.03	...	K0
89*	7.72	-.27	B5
90	12.67	...	A0
91	11.10	+.17	A2
92	10.61	...	G2V
93	11.30	...	F2
94	12.00	...	G8III
95	12.35	...	A2
96	10.50	-.25	A0
97	12.46	...	A2
98	11.85	...	F0
99	12.03	+.21	A3
100	12.26	...	G0
101*	9.53	...	G5III
102	11.80	-.10	A0
103*	9.15	-.24	B9
104	11.17	+.24	A0
105	12.22	+.36	A0
106	11.70	+.25	A2
107	11.41	...	K5III
108	11.94	+.12	B9
109	12.35	+.49	A2
110	10.83	+.03	A2
111*	9.27	...	K0V
112	12.00	+.35	A3
113	11.81	+.14	A2
114	11.18	...	G8III
115*	11.15	...	G5V
116*	9.03	+.14	F5V
117	12.28	...	K5
118	11.89	...	F5
119	12.30	...	K0
120	12.52	+.26	A5
121*R	8.50	+.20	B9
122	12.52	...	A0
123	11.90	+.04	B8
124	12.15	...	G0
125	12.46	...	A0

Table 1

Observational Data for Region LF2 (Cont'd)

Zone +28° (Cont'd)

No.	m_{pg}	R.I.	Sp.	No.	m_{pg}	R.I.	Sp.	No.	m_{pg}	R.I.	Sp.
126	11.61	...	F2	176	11.41	...	F8	226	12.41	+.11	B9
127	11.84	...	G8V	177	12.77	...	M2	227	12.37	...	G0
128	11.86	...	F8	178	11.67	...	K0V	228	11.56	+.11	B9
129	10.54	-.25	A0	179	11.88	+.02	B8	229	11.93	...	F0
130	12.75	...	G8	180	11.71	...	G0	230	11.98	-.06	A2
131	12.63	+.05	A2	181	11.69	...	G0	231*	11.30	...	M0III
132*	10.33	...	A2	182R	11.66	...	F5	232	12.51	+.13	A5
133	10.69	...	F0	183	11.95	...	F8	233	12.39	...	F8
134	10.59	...	A3	184	12.21	...	G8	234	11.58	...	F8
135	12.32	...	A2	185	12.62	...	A0	235	13.00	...	G0
136	12.34	...	G0	186	11.75	...	F8	236	11.59	+.03	B9
137	12.56	...	A0	187	11.98	...	F8	237	11.84	-.07	A0
138	11.70	...	F0	188	11.90	+.21	A2	238	12.37	...	K3
139	11.20	...	F0	189	12.65	...	K5	239	12.23	...	A0
140	11.03	-.01	B8	190	12.00	...	M2III	240*	11.88	...	K2III
141	11.82	...	G0	191	12.41	...	K0III	241	11.84	+.28	A0
142	10.54	...	F0III	192	11.28	...	F5	242	11.92	+.16	B8
143	12.46	-.05	A0	193*	10.21	...	G2	243	12.63	...	G0
144	12.06	...	G0	194	11.12	...	A0	244	12.71	...	A0
145	12.15	...	G0	195	12.66	...	M2	245	11.57	-.04	A0
146	11.55	-.18	B5	196	11.95	...	K2V	246	11.70	+.17	A5
147	12.81	...	A0	197	11.04	+.06	B8	247	12.01	...	G0
148	12.41	...	G0	198	12.45	+.27	A0	248R	11.75	+.22	A0-F2
149	12.36	...	F0	199*	9.03	...	K0III	249	12.86	...	A2
150	12.17	...	F2	200*	7.05	...	G2V	250	12.46	+.20	B9
151	12.19	...	B8	201*	10.32	...	K2V	251	11.83	+.16	B5
152*	9.92	-.07	A3	202	12.48	...	A0	252	12.46	...	B8:
153*	9.56	-.22	A0	203	11.92	...	G0	253	11.93	...	F5
154*	11.58	...	G5V	204	12.04	...	K0III	254	11.07	+.09	B9
155	12.48	...	A3	205	12.32	...	F8	255	12.57	...	A0
156	12.20	...	G8III	206*	11.60	...	K0V	256	11.41	+.05	B8
157	12.36	...	G0	207	11.87	...	K2III	257	11.77	...	F0
158	11.94	...	G0	208	12.42	...	G8	258	11.85	...	K0III
159	11.53	+.30	A0	209*	9.30	-.31	B9	259*	10.37	+.29	A2
160	10.75	-.02	A2	210	11.96	+.18	A0	260*	11.04	...	G8III
161	11.64	...	K0III	211	12.05	...	G5III	261*R	9.97	+.26	A3
162	12.11	...	Go	212	11.92	+.15	A0	262	12.64	...	G0
163*	10.84	+.11	A0	213	12.42	+.43	A0	263	11.17	-.11	B8
164	10.84	-.02	A0	214*	12.08	+.04	A0	264	11.37	+.35	A2
165	11.26	-.10	A0	215	10.54	-.08	A0	265R	11.08	...	M8V
166	11.99	+.13	B9	216	8.68	-.27	B8	266	12.10	+.49	A5
167	11.54	...	G5V	217	12.00	...	K0V	267	12.02	...	F0
168	12.21	+.22	A0	218	12.69	...	A0	268	11.85	...	F2
169*	10.21	-.18	B8	219	11.04	+.56	A5	269	12.30	...	K0III
170	12.34	...	A0	220*	8.99	-.54	B5	270	11.97	...	G8III
171*	9.33	...	F5V	221	12.18	-.21	A0	271	12.08	...	K0III
172	10.60	...	F2V	222	12.35	...	K2	272	12.10	+.07	B9
173	11.88	+.17	A2	223	12.55	+.17	A0	273	11.82	...	G8V
174	12.06	...	A0	224	12.07	...	G5V	274*	9.66	-.07	B3
175	12.64	...	K0III	225	10.08	...	F5V	275*	9.67	...	F5III

Table 1

Observational Data for Region LF2 (Cont'd)

Zone +28° (Cont'd)

No.	m_{pg}	R.I.	Sp.	No.	m_{pg}	R.I.	Sp.	No.	m_{pg}	R.I.	Sp.
276	12.77	...	K2	326	12.26	...	F0	376*	11.39	...	G2V
277	11.75	...	F2	327	11.08	+.09	B8	377	12.39	...	G0
278	11.80	...	F5	328	12.69	...	G5	378*	11.97	...	M5III
279*	8.77	...	F5V	329*	11.18	...	K0III	379	12.61	...	A0
280*	11.12	...	K5III	330	12.05	+.01	B9	380*	9.83	-.14	B9
281*R	10.89	+.41	A0	331	12.77	...	A0	381*	10.09	+.06	A2
282	12.10	...	F0	332	12.42	...	G0	382	12.61	...	A0
283	12.21	...	G5V	333	11.41	-.11	B9	383	12.71	...	G0
284R	12.61	...	A3	334	11.90	-.05	A0	384	11.97	-.02	B9
285	10.90	+.04	B8	335	12.49	...	M0	385*	8.76	...	F5III
286	12.04	+.35	A0	336	11.10	+.20	A2	386	12.54	...	A3
287*	9.03	...	K0III	337	12.59	...	G8	387	11.84	...	G5V
288	11.40	...	F0	338	12.54	...	A0	388	13.07	...	K2
289*	11.20	...	G8V	339*	9.41	...	K0III	389	12.54	...	A0
290	11.37	...	G0	340	12.48	...	G0	390	12.42	...	G0
291	11.57	...	G5III	341	11.73	...	F2	391	11.44	+.33	A2
292	12.39	...	F0	342	11.24	...	G0	392	12.17	...	G2
293	12.36	...	G0	343	11.90	-.09	B8	393*	11.07	+.14	B8
294	12.60	+.22	A2	344	11.70	...	G5V	394*	11.25	...	G0
295	12.36	...	G0	345	12.28	-.10	A2	395*	11.64	...	K0III
296	11.32	+.39	B9	346	11.82	+.29	A3	396	11.73	...	G2V
297	12.21	+.13	A0	347	11.63	...	F8	397	12.61	...	A5
298	12.35	...	M2II	348	12.69	...	A2	398*	11.69	...	K5V
299	11.91	+.02	A0	349*	9.36	-.40	B8	399	11.90	...	A5
300*	11.25	...	K0IV	350	12.29	...	B9	400	12.54	...	G8
301	12.36	....	G8	351	12.35	...	F5	401	11.82	...	F8
302	11.05	+.15	B8	352	12.86	...	A0	402	11.98	+.16	B8
303	12.37	...	G0	353	12.16	+.26	A2	403*	9.18	...	G0V
304*	9.97	...	K0III	354	12.38	-.11	A0	404	11.84	+.19	A0
305	11.72	...	G8III	355	11.90	...	K0V	405	12.41	+.38	Ao
306	12.61	...	A0	356	12.69	...	G8	406	12.69	...	G5
307*	9.21	-.23	A0	357	11.90	...	G5V	407	12.23	...	G0
308	12.39	...	A5:	358	12.36	...	G0	408	12.00	+.35	A0
309	12.28	+.38	A2	359	12.75	...	G0:	409	11.69	+.38	A0
310	10.61	-.01	A0	360	11.64	-.09	B8	410	12.83	...	B9
311*	9.62	+.05	B8	361	11.45	...	F0	411	11.27	+.37	A3
312R	11.86	+.25	A5	362*	11.68	...	K2III	412*	9.06	-.02	B5
313	12.06	...	A0:	363*	8.71	-.44	B8	413	11.41	...	F0
314	12.35	+.27	B8	364*	8.69	-.46	B3	414	12.57	...	A0
315	11.05	...	G0	365R	12.42	...	F8	415	11.80	...	K3III
316	11.54	...	G0	366	11.92	...	G5	416	12.65	...	K0
317	12.40	...	F0	367	11.32	+.47	A0	417	12.41	...	A2
318	12.67	...	K0	368	11.90	...	G8III	418	11.28	...	F8
319	12.15	+.16	A0	369*	11.32	...	M2III	419	11.74	...	F5
320	11.10	...	F0	370	11.94	...	A5	420R	10.95	+.20	A2
321	12.88	...	K5	371	12.62	...	A2	421	12.54	...	G0
322	12.10	...	F2	372	11.89	...	B9	422	11.88	...	A3
323	11.96	...	K2III	373	12.57	...	A3	423*	10.42	...	G8III
324	11.86	+.06	B8	374	12.25	...	G2V	424	12.45	...	G5
325	11.88	+.19	A0	375*	10.51	+.25	B9	425	11.62	...	G8V

Table 1

Observational Data for Region LF2 (Cont'd)

Zone +28° (Cont'd)				Zone +29°							
No.	m_{pg}	R.I.	Sp.	No.	m_{pg}	R.I.	Sp.	No.	m_{pg}	R.I.	Sp.
426	12.35	...	F8	1	11.82	...	K0III	51	11.16	...	F0
427	12.65	...	K0	2	10.85	-.03	A2	52*	9.62	...	K5III
428	12.67	...	F8	3*	10.62	...	G5V	53	11.23	...	G5III
429	12.06	...	G0	4	11.30	...	A3	54	11.77	...	K0III
430	12.39	...	A5	5R	11.37	+.32	A0	55	12.37	...	G8
431*	11.64	...	G8III	6	11.94	...	K2	56*	10.57	...	F8III
432	11.79	-.07	B9	7	11.32	+.50	A2	57	12.73	...	A0
433*	10.60	+.30	B9	8	11.89	...	F2	58R	11.93	...	F0
434*	9.06	-.26	B5	9*	9.30	-.03	A3	59	10.80	...	G5V
435	11.05	...	F5	10	11.43	+.06	A2	60*	11.97	...	K2
436	12.52	...	G0	11	12.00	...	K0III	61	12.42	...	K0
437	12.14	...	A3	12	12.13	...	A2	62	11.82	...	F0
438	12.15	...	B5:	13*	10.58	+.32	A2	63	11.85	...	F8
439	11.80	...	K0V	14*	9.29	...	F0III	64	12.03	...	G2
440	11.07	-.08	B8	15	11.58	...	F0	65	12.73	...	G0
441	12.09	....	F0	16	11.46	+.35	A0	66	12.16	+.17	A3
442	11.36	...	F0	17	12.05	...	F8	67*	10.85	-.05	A2
443	12.54	...	A0	18	11.90	...	G0	68	12.13	...	F5
444*	10.35	+.09	A0	19*	11.58	...	K2III	69	11.45	+.21	A0
445*R	11.07	+.31	B8	20	11.58	+.34	A5	70	12.52	...	F8
446	11.57	...	G0	21	10.64	...	F0V	71	12.57	...	A2
447	12.91	...	K0III	22*	9.31	-.17	A0	72*	9.41	...	G8III
448	12.67	...	A3	23	12.03	...	G0	73*	12.20	...	G0
449	12.16	...	K3III	24	11.48	...	G0	74	11.82	+.21	A5
450	12.36	...	G2	25	11.51	-.14	A0	75	10.80	+.36	A5
451*	10.20	+.19	Ao	26	11.81	...	G5V	76*	8.79	-.36	A0
452	11.47	+.37	B8	27*	9.00	...	F2V	77	11.75	...	F0
453	12.54	...	G0	28*	11.66	...	K0V	78	11.93	...	G5V
454	11.32	+.34	A2	29	12.39	...	A2	79R	11.90	+.09	B9
455	12.59	...	B9	30	12.64	...	G8	80	12.20	...	G8III
456	11.32	...	F8	31	11.96	...	A5	81	12.31	...	G5III
457	11.62	+.55	A0	32	12.59	...	A2	82	11.48	...	G8V
458	11.85	...	F8	33	12.18	...	G8III	83*	11.45	...	G5V
459*	11.34	...	G0	34	12.12	...	F0	84	12.51	...	G0
460	11.84	...	A2:	35	12.10	+.11	A0	85	12.52	...	G0
461	11.90	...	G5V	36	12.27	+.14	A2	86*	11.43	...	G8III
462*	9.97	-.14	B8	37	10.44	-.26	B9	87*	9.95	...	G8Ib
463	11.89	+.44	A0	38*	9.00	+.12	B9	88	11.61	...	F2
464	12.50	...	G0	39	11.63	+.35	A5	89	11.93	...	G0
465	12.04	...	G5III	40	11.16	...	B8	90	12.65	...	F0
466	11.41	+.26	A0	41	12.58	...	A0	91	11.05	-.07	A0
467	10.59	-.01	B5	42	12.21	...	A0	92	12.10	...	G8III
468	12.30	...	K0III	43*	10.33	...	F5V	93*	10.54	...	M0III
469	11.75	+.27	A5	44	11.24	...	K0III	94	11.81	...	F8
470	12.10	...	K3III	45	11.98	-.11	B9	95	11.97	...	K5
471	11.32	+.47	B8	46	12.37	...	G8III	96	11.32	...	F2
472	11.50	...	F0	47	12.45	...	A3	97	12.65	...	K0V
473*	10.10	...	G0	48	11.04	+.02	B9	98*	11.74	...	K3III
474	11.31	...	G8V	49	11.46	+.18	A2	99	11.83	...	F8
475	12.62	...	A0	50*	9.97	-.06	B9	100*	10.95	...	G8III
476	10.67	+.42	B9								

Table 1

Observational Data for Region LF2 (Cont'd)

Zone +29° (Cont'd)

No.	m_{pg}	R.I.	Sp.	No.	m_{pg}	R.I.	Sp.	No.	m_{pg}	R.I.	Sp.
101	11.17	-.11	A0	151	11.97	...	F5	201	12.48	...	G0
102	12.29	-.17	A0	152	12.30	...	K0III	202	12.28	...	G0
103*	9.72	-.21	A2	153	11.90	...	G5V	203	11.04	...	G0
104	12.05	...	G0	154*	11.70	...	K0III	204	12.41	...	G2
105*R	10.94	+.13	A2-F0	155	11.97	...	G2	205	12.41	...	F0
106	12.29	...	A2	156*	8.71	-.36	A0	206	10.54	-.36	B9
107	12.23	...	G5	157	11.96	...	A3	207	11.90	...	F8
108	11.93	...	G8V	158	12.05	...	G0	208	12.34	...	G0
109	12.28	...	F2	159	11.07	+.05	A2	209	11.78	+.03	A2
110*	9.76	...	F0V	160	11.05	+.41	A3	210	11.04	-.24	B8
111*	10.22	-.40	B8	161*	8.56	...	K3III	211	12.01	+.11	A0
112*	9.62	...	G8III	162	12.54	...	F8:	212	10.63	-.19	A0
113	11.97	-.03	A3	163	11.05	...	F5	213*	9.59	...	G0V
114	12.06	...	G0	164	11.64	...	B8	214	11.40	...	F0
115	11.54	+.22	A2	165	12.27	...	G5	215*	10.82	+.17	B9
116	10.91	-.02	A2	166*R	(5.84)	...	A3-F5	216	11.95	...	G0
117	10.25	...	F0III	167	11.71	+.04	B9	217	12.60	...	A2
118	12.21	...	G5	168	11.21	...	G8IV	218R	10.94	+.06	A3
119*	10.54	...	G5V	169*	9.29	-.56	B9	219	12.50	...	K0III
120	9.70	...	B5	170	10.32	+.12	A0	220	11.65	+.16	A0
121	12.23	...	F0	171*	9.66	-.29	A2	221*	8.74	-.47	B5
122	12.15	...	F5	172	12.19	...	F0	222	12.02	+.20	A3
123	11.41	-.19	B8	173	12.18	...	K0V	223	12.02	...	G5III
124*	9.30	-.34	A0	174	11.07	...	F2	224	12.37	...	K0III
125	10.97	+.02	A2	175	10.87	+.21	A0	225	10.19	+.06	A2
126*	10.43	...	K5IV	176*	9.90	-.23	B9	226	11.64	-.01	A2
127*	11.15	...	F0	177	11.82	...	G2V	227*	10.62	...	G5III
128	11.25	...	G5III	178*	8.57	...	F2V	228*	10.07	-.36	A0
129	11.68	-.03	A3	179	12.10	...	F5	229	11.62	...	G0
130	11.64	-.14	B8	180	11.68	...	F5	230R	12.06	...	Bep
131*	11.17	...	B5	181	11.85	...	G0	231	11.33	...	B9
132	12.23	...	F0	182	12.26	+.22	A5	232	12.37	...	K2III
133	11.60	+.11	A3	183	11.85	-.01	A2	233	11.03	+.13	A0
134	11.88	+.50	A5	184	12.29	...	G0	234*	9.34	-.39	A2
135	11.64	-.18	A0	185	11.98	...	F2	235	11.95	+.09	A2
136	12.64	...	M2	186	11.32	-.20	B9	236	11.36	...	G0
137	11.63	...	F5	187	11.85	...	F0	237*	9.97	-.11	A5
138*	9.67	-.55	B8	188	11.88	...	F0	238	11.07	+.05	A0
139	11.97	...	G8V	189	11.12	...	G8V	239	11.54	-.28	B8
140	11.83	...	G2	190*	9.73	-.22	A5	240*	9.80	...	G2V
141	12.15	...	G0	191	11.60	...	F5	241	11.51	+.23	A0
142	12.19	...	F5	192*	8.29	+.07	A0	242	11.57	...	K2V
143	11.78	+.07	A3	193	11.88	...	G0	243	11.99	...	K0III
144*	11.04	...	M2III	194	11.82	-.09	B9	244	12.21	...	F5
145	10.50	-.25	A0	195	11.64	...	F5	245	11.80	...	F2
146	10.70	.00	B8	196R	11.66	...	F8	246	12.52	...	A0
147*	9.97	-.46	A0	197*	9.62	...	K0III	247R	10.99	-.07	A0
148	12.13	...	G0	198	11.08	...	F8	248*	9.95	...	G8IV
149*	9.80	-.33	B8	199	12.62	...	A2	249	12.00	-.18	A0
150	12.05	...	K0V	200	11.57	...	F5	250	12.01	-.03	A0

Table 1

Observational Data for Region LF2 (Cont'd)

Zone +29° (Cont'd)

No.	m_{pg}	R. I.	Sp.	No.	m_{pg}	R. I.	Sp.	No.	m_{pg}	R. I.	Sp.
251*	10.54	...	F2V	301	12.03	-.35	A2	351	12.12.	...	F8
252	11.59	...	F8	302	12.86	...	K2	352	12.77	...	K0
253	12.04	...	G8	303	11.04	...	G8III	353	10.24	-.58	B8
254	12.58	...	K0	304	11.56	...	F0	354	12.25	...	A0
255	11.70	...	G0	305	11.08	...	G2V	355	12.48	...	G8
256	12.29	...	K0III	306	12.54	...	G0	356	12.45	...	G0
257	11.57	...	G0	307	12.10	...	K0III	357	11.93	-.02	A0
258	11.86	...	G0	308	11.90	...	G0	358	12.33	...	A0
259*	10.06	...	A3	309	12.64	...	A0	359	12.35	+.22	A0
260	12.36	...	G5III	310	12.42	...	G0:	360	11.25	...	K0III
261*	9.31	-.60	B9	311	12.12	-.01	A3	361*	9.19	-.34	B9
262	10.61	-.46	A0	312*	9.27	...	F5III	362	12.60	...	A0
263	11.98	...	G0	313R	11.40	...	F8	363*	8.83	-.32	B8
264*	(6.14)	-.45	B5	314	10.47	...	F8V	364*	9.63	-.28	B9
265	12.57	...	A2	315	11.64	+.11	B9	365	12.64	...	K0
266	10.87	+.09	A2	316*	9.64	-.29	A0	366	11.62	+.13	A3
267	12.10	...	F0	317	12.23	...	G0	367	12.15	...	G0
268*	11.52	...	G5V	318	12.57	...	K0III	368	10.24	...	F0III
269	12.65	...	K0	319	12.15	-.23	A2	369	12.21	...	G0:
270	10.83	+.21	A5	320	12.03	...	G5V	370	12.21	...	G8
271	12.03	...	K0III	321	12.42	...	B8	371	12.13	...	G0
272	11.49	...	G8V	322*	9.34	-.23	A2	372*	10.54	...	G0III
273	12.47	...	A0	323	11.68	-.10	B8	373	11.41	+.18	A5
274	11.98	+.03	A0	324	11.32	+.21	A2	374	12.37	...	K0III
275	12.65	...	K0	325	11.64	+.07	A3	375	12.05	...	G0
276*	7.58	+.12	A2	326	11.63	...	G5V	376	11.66	...	F8
277	11.42	...	K0III	327R	12.06	...	G0	377	12.38	...	G2
278	11.75	-.07	A0	328	12.29	...	G0	378	12.10	-.36	A0
279	10.56	-.27	B9	329	12.46	...	A2	379	12.45	...	G0
280	11.55	...	G0	330	11.88	...	G0	380	12.64	...	A5
281	11.94	...	G0	331	12.10	+.20	A3	381	12.33	...	A2
282	11.65	...	G5V	332	11.32	...	F5	382	11.82	+.05	A3
283*	9.14	...	G8III	333	11.54	...	G0	383	12.60	...	A0
284*	9.17	-.47	B8	334	11.70	...	K0III	384	12.05	...	F5
285	11.32	...	F0	335	11.82	-.01	B9	385	11.85	...	K0V
286	12.05	+.06	B8	336*	9.31	...	G8III	386	12.34	...	K3
287	12.19	...	G0	337	12.63	...	K0	387	12.39	...	G0
288	11.75	...	G8III	338	11.50	...	F2	388	12.29	...	F0
289	11.82	...	G8V	339R	12.15	...	A2-F0	389	11.08	...	A2
290	11.92	-.07	A0	340*	9.69	...	M2III	390	11.96	...	G0
291	11.61	...	F0	341	11.51	...	F2	391*	11.85	...	G8IV
292	12.31	...	B8	342	11.17	+.05	A3	392	11.88	-.12	B8
293	12.17	...	G0	343	11.16	+.15	A0	393R	11.25	...	A3-F2
294	12.18	...	G0	344	12.18	+.23	A3	394	10.28	-.32	A0
295	11.14	+.11	A2	345	12.23	...	G5	395	12.16	+.34	B9
296*	11.12	...	G5III	346	11.57	+.04	A0	396	12.09	-.33	B8
297	11.87	...	G0:	347	12.69	...	A3	397	12.50	-.11	A3
298*	9.47	-.38	A2	348*	7.64	+.12	B8	398	9.71	-.67	B8
299	11.87	...	K0V	349	10.24	...	B9	399*	10.32	...	G0V
300	11.12	+.18	A0	350	10.99	-.06	B9	400	11.77	...	K0III

Table 1

Observational Data for Region LF2 (Cont'd)

Zone +29° (Cont'd)

No.	m_{pg}	R. I.	Sp.	No.	m_{pg}	R. I.	Sp.	No.	m_{pg}	R. I.	Sp.
401	11.82	-.03	A0	451*	11.45	...	G8	501	12.50	...	K0
402	12.18	...	G8III	452	11.81	...	B9	502	12.06	...	F5
403	11.38	...	M5III	453	11.98	...	F0:	503	11.98	...	G0
404	12.30	+.01	A0	454	11.97	...	F8	504*	10.51	...	K0III
405	12.02	+.15	A5	455	12.07	...	A5	505	12.32	+.07	A0
406	12.19	...	G0	456	12.61	...	A0	506	12.21	-.01	A0
407	12.64	...	F0	457R	11.98	...	A3-F2	507*	11.25	...	F8
408	11.47	...	G5III	458	11.97	-.02	A2	508	12.23	...	G0
409*	10.01	...	F5V	459	12.67	...	G0	509*	9.16	-.37	A0
410	12.08	...	F5	460	12.18	+.05	A2	510	11.91	...	A3
411	11.85	...	F8	461	12.35	...	G2	511	12.52	...	K0III
412	11.12	-.32	B8	462*	8.31	...	F8V	512	12.28	...	A2
413	12.30	+.12	A3	463*	9.88	-.35	A0	513	12.54	...	A0
414	11.95	...	K0V	464	11.21	-.19	A0	514	11.60	...	F0
415	11.17	...	A0	465	11.64	...	F5	515	11.49	.00	B9
416	11.97	+.20	A0	466	12.18	...	G0	516	13.18	...	K0
417	11.50	+.10	A3	467	10.54	-.27	B8	517	12.03	...	A0
418*	9.72	-.32	B8	468	12.08	...	Go	518	11.37	-.03	B8
419	10.62	+.18	A5	469	12.46	...	F8	519	11.37	...	G0
420*	8.37	-.17	B2	470	12.61	...	G2	520	12.41	+.38	A2
421	12.21	...	A5	471	11.81	...	G0	521	11.77	...	G5V
422	12.23	...	F0:	472	11.89	...	G0	522	11.25	+.17	A2
423	12.02	...	F0	473*	9.50	-.47	B8	523	12.12	...	G0
424*R	9.56	-.13	A3-F2	474	11.75	...	K0V	524	12.42	...	G0
425	12.61	...	K0III	475	11.96	...	G0	525	12.01	...	K2
426	12.75	...	G0	476	12.27	...	G0	526*	9.16	...	B5
427	12.27	...	A3	477	12.15	...	F0	527	12.33	...	K0
428	11.92	...	G0	478	11.43	...	F0	528	12.29	...	K0
429	12.18	...	G0	479	9.97	-.25	B9	529*	10.27	-.21	B9
430	12.30	...	G0	480	12.45	...	F5	530	11.85	+.20	B9
431	11.75	...	G8III	481	12.83	...	G8	531*	9.83	...	F0V
432	11.75	...	F0	482	12.07	+.27	A2	532	11.85	...	F0
433	12.67	...	G0	483	11.91	...	A0	533*	11.59	...	K2III
434	11.60	...	K0III	484	12.56	...	K0	534	12.35	-.34	A0
435	12.08	...	G0	485	12.69	...	A3	535	12.13	...	F8
436	11.77	...	K0III	486	12.28	+.59	A2	536	12.29	...	A2
437	11.36	...	A5	487	12.16	+.16	A2	537	12.31	...	G0
438	11.72	...	G8V	488*	10.86	-.16	B8	538	12.38	...	F2
439	12.23	...	A2	489	11.97	+.11	A0	539	11.66	...	F2
440R	11.75	...	A3	490	12.13	...	G0	540	11.70	...	F0
441	12.65	...	G5V	491	11.82	...	F8	541	12.08	...	A2
442*	10.57	...	G8III	492	12.06	...	F0	542	11.88	...	G8III
443	12.29	...	K0	493	12.21	...	A5	543	11.63	...	K5III
444	11.20	...	F0	494*	7.12	...	F2III	544	12.27	...	F0
445	12.10	...	G0	495	10.58	-.40	B5	545	11.75	...	F0
446	12.45	...	K2	496	12.18	...	F5	546	12.30	-.23	A0
447	11.96	...	A2	497	11.88	+.27	A0	547	12.45	...	A2
448	11.61	...	A3	498	12.58	...	F5	548	12.23	...	G0
449	12.52	...	A0	499	12.24	...	G5III	549	12.82	...	G8
450	12.21	...	A0	500*	9.47	...	G0V	550*	8.83	-.32	B8

Table 1

Observational Data for Region LF2 (Cont'd)

Zone +29° (Cont'd)

No.	m_{pg}	R. I.	Sp.	No.	m_{pg}	R. I.	Sp.	No.	m_{pg}	R. I.	Sp.
551*	11.88	...	K0IV	601	11.57	...	K0III	651	12.31	...	F0
552	11.93	...	F5	602	12.10	+.24	A2	652	12.57	...	A2
553	12.77	...	M0	603	11.98	...	A0	653	10.42	-.32	B8
554	12.42	...	G0	604*	8.80	-.15	A0	654	12.27	...	A2
555	12.64	...	G8	605	12.27	...	F8	655R	11.50	-.11	A2
556	12.10	...	A2	606	11.82	...	G0	656*	9.34	...	K0III
557	12.36	...	F5	607	11.57	+.21	A2	657*	9.36	-.23	B9
558	12.54	...	A2	608	12.62	...	A0	658	11.73	...	B8
559	12.17	+.22	A2	609	12.69	...	K2	659	12.73	...	A0
560*	9.16	-.19	A0	610	11.46	+.27	A0	660	11.90	+.25	B8
561	11.88	...	G2	611	11.50	...	K3V	661	11.63	...	F8
562	12.20	...	F2	612*	8.29	+.42	A0	662	11.77	...	A0
563	12.08	...	F2	613	12.33	...	G0	663*	11.12	...	G8III
564	11.63	+.36	A5	614	11.88	...	F2	664	12.73	...	A3
565	12.41	...	G0	615	10.60	+.12	A0	665	11.92	...	K0III
566	12.06	...	A3	616	12.29	...	G0	666*	10.07	...	B9
567	12.79	...	A0	617*	11.17	+.01	B9	667*	9.06	...	B8
568	12.42	...	G2	618*	9.88	-.24	B9	668	12.45	...	G8V
569	12.35	...	G8III	619*R	9.57	-.16	A3	669	12.57	...	G5III
570	12.21	...	A5	620R	11.80	+.27	A0	670	12.45	...	A2:
571	11.12	-.03	B9	621	12.13	...	F8	671	12.41	...	B5
572	12.31	...	G5V	622	12.05	...	F8	672	12.45	...	G8III
573	12.43	...	G8V	623	12.61	...	K0	673*	9.76	...	B8
574	12.52	...	K0	624	11.86	...	G5V	674	10.74	...	F8
575	12.03	+.47	A0	625	12.31	...	F8	675	12.61	...	G2
576	12.47	...	G0	626	12.32	...	G2	676	12.15	...	A2
577	11.08	...	F8V	627	11.61	...	F0	677	12.20	...	G0
578	12.03	-.05	A0	628	11.32	+.30	A0	678	11.53	...	G2V
579	11.79	...	G8III	629	11.45	-.03	B8	679	11.67	+.56	A5
580	12.10	+.02	A2	630	12.47	...	A3	680	12.03	...	G8
581	12.15	...	A2	631	12.64	...	F0	681	12.00	...	K0III
582*	11.78	...	K5III	632	11.54	+.14	A3	682	11.90	...	K0III
583	11.85	...	K0III	633*R	10.17	...	K5V	683	12.33	...	A0
584	12.52	...	B9	634	10.74	-.10	B9	684	10.57	-.12	A0
585	12.69	...	B9	635	11.73	...	F2	685	11.81	...	G0
586*	9.33	-.24	B8	636	11.72	+.16	A2	686	11.79	...	G0
587*	8.29	-.19	B8	637	11.72	...	G0	687	12.45	...	A2
588	11.71	...	K0III	638	12.27	...	A0	688	11.61	...	G0
589	12.69	...	A0	639	12.12	...	B9	689*	9.70	...	K0III
590	12.03	...	K5	640	12.01	+.32	A2	690	11.45	+.17	A0
591	11.08	+.23	A0	641	11.61	...	G2	691*	9.80	...	G8III
592	12.42	...	K0	642	11.68	...	F8	692	12.10	...	F8
593	11.07	+.02	B8	643	12.10	...	G8III	693*	8.19	...	B8
594*R	(7.5 var)	...	F2III	644	12.61	...	A0	694	12.26	-.08	A0
595	12.19	...	G0	645	11.49	+.45	B9	695	12.12	...	B8
596	11.90	...	B8	646	11.45	...	G8IV	696	12.50	...	G2
597	11.60	...	F8	647	12.19	...	F5	697	12.64	...	B9
598	11.91	...	F8:	648	12.10	+.15	A0	698	11.83	+.31	A0
599	11.62	+.43	A3	649	11.83	...	G8III	699	12.71	...	B9
600	12.52	...	B8	650*	9.31	-.35	B9	700*	9.79	-.07	A2

Table 1

Observational Data for Region LF2 (Cont'd)

Zone +29° (Cont'd)

No.	m_{pg}	R. I.	Sp.
701	12.37	...	A2
702	11.57	...	F5
703	11.85	-.23	B5
704	11.61	+.50	A3
705	12.77	...	A0
706	12.50	+.20	B9
707	12.41	...	A0
708*	10.00	...	B8
709	12.27	+.10	A0
710	11.62	+.34	A3
711R	12.23	...	G0
712	12.05	...	G8III
713	11.73	+.29	A2
714	12.52	...	A0

Zone +30°

No.	m_{pg}	R. I.	Sp.
1	12.06	...	G5V
2	12.03	...	F2
3	12.03	...	G5V
4*	8.21	-.08	B8
5*	11.29	...	F0
6	11.82	...	F2
7*	8.40	...	K0III
8*	8.50	+.16	A2
9	12.37	...	K0III
10	11.98	...	G0
11*	11.02	...	K2III
12	11.04	...	F5
13	12.51	...	A5
14	11.96	...	G8III
15	11.92	...	K0III:
16	11.57	...	G2V
17*	11.86	...	K2V
18*	11.80	...	G8IV
19	11.97	-.11	B9
20*	10.08	...	G0V
21	12.06	...	M5III
22*	11.41	...	G8V
23	11.98	...	F0
24R	12.03	...	F0
25*	10.55	...	F2V
26*R	9.48	...	M2III
27	12.32	+.24	A0
28R	11.61	...	A3-F2
29	12.08	...	G8III
30	11.94	...	G8V
31	11.87	...	K0III
32	10.63	-.09	A0
33	11.85	...	G0
34*	8.60	+.20	A0
35	11.32	...	F5
36	11.58	...	G8:
37	11.29	+.01	B8
38	11.63	...	F0
39	10.76	-.14	B9
40	12.30	+.31	A5
41	10.46	+.08	A3
42	12.10	+.01	A5
43	11.54	...	F0
44	11.32	-.21	B8
45	12.00	+.17	A3
46	12.28	...	K0III
47	12.19	...	K0III
48	12.03	+.08	A5
49*	10.91	+.01	A3
50*	9.73	-.55	B9
51	9.97	...	F5V
52	11.81	+.48	A5
53	11.88	...	G8V
54	10.84	+.31	B9
55	11.85	...	F2
56*	10.54	...	G8III
57*	9.88	-.01	A0
58	11.01	+.08	A2
59*	8.72	-.37	A0
60	11.49	...	G5V
61*	11.21	...	G8IV
62	12.24	-.29	A0
63	11.77	...	K0V
64	12.02	...	K0
65*	8.60	...	K2III
66	11.78	...	F0
67	10.79	+.31	A2
68*	9.49	-.28	B9
69*	11.04	...	K2III
70	11.04	+.02	A2
71*	10.48	...	F2V
72	11.80	...	K0III
73*	10.56	...	K2IV
74	11.93	...	F5
75	10.54	-.44	B5
76	11.61	...	G0
77	11.98	...	G0
78	12.15	...	K5
79	12.35	-.33	A0
80	12.16	-.26	A5
81	12.05	...	G2
82	12.05	...	G0
83	12.19	...	K0
84	12.33	...	A0
85	12.12	+.13	A0
86*	11.17	...	K0III
87	12.64	...	G2
88*	12.46	...	K3III
89	12.12	...	G5III
90	11.64	...	F2
91	12.27	...	G8III
92	11.36	...	F2
93	12.08	...	G5V
94	11.90	...	G8III
95	11.72	...	G0
96	11.46	+.13	A2
97	12.04	...	B9
98	11.93	...	A2
99	12.60	...	G5
100	12.23	...	A0
101	12.12	...	G0
102	11.85	...	F2
103	11.85	...	G8V
104	10.91	...	F2V
105	11.90	...	K0III
106	11.23	+.12	A2
107	12.36	...	F5
108*	9.03	...	K0III
109	12.06	...	A5
110	12.40	+.01	B9
111*	8.96	...	F5V
112	10.54	...	F8V
113*	9.62	...	B8
114	11.67	...	F8
115*	9.90	...	G0V
116	11.72	...	F5
117	11.57	...	K0III
118*	10.07	.00	A0
119	12.17	...	K0V
120	11.99	...	G0
121	12.13	...	G0
122*	8.88	-.39	A0
123	12.07	...	G0
124*	9.97	...	G0V
125	11.97	+.26	A5
126	10.70	+.05	A2
127	11.84	...	F2
128*	11.62	...	K0III
129	11.46	+.05	A3
130*	8.92	-.41	A0
131	12.20	...	G0
132	12.41	...	K0III
133	12.05	+.22	A0
134	11.37	+.09	A3
135*	12.27	...	M0

Table 1

Observational Data for Region LF2 (Cont'd)

Zone +30° (Cont'd)

No.	m_{pg}	R. I.	Sp.	No.	m_{pg}	R. I.	Sp.	No.	m_{pg}	R.I.	Sp.
136	11.08	. . .	F2	186	11.88	-.11	A2	236*	7.56	-.18	B5
137	10.05	. . .	F0V	187	12.45	. . .	K0	237	12.27	. . .	G0
138	10.97	. . .	F2	188	11.93	+.20	A2	238	12.17	. . .	G8III
139	12.05	. . .	B8	189	11.69	-.17	A0	239	11.32	. . .	G8III
140	10.54	. . .	G0V	190	11.08	+.02	A2	240	10.90	. . .	F5III
141	12.78	.00	A0	191	10.95	-.12	A0	241	10.31	-.59	A0
142	11.66	+.07	A3	192*	8.92	. . .	G5III	242	11.79	+.14	A2
143	12.07	+.24	A5	193	12.21	. . .	G0	243	11.66	. . .	G0
144	11.92	. . .	F0	194	11.56	. . .	F0	244	11.62	-.03	A2
145*	11.45	. . .	G8IV	195*	11.08	. . .	M0III	245	11.24	+.05	A2
146*	10.82	. . .	K0IV	196*	9.66	. . .	G8IV	246	11.81	+.03	A2-F2
147	12.12	. . .	F8	197	11.89	. . .	G5V	247	11.66	. . .	G0
148	11.64	-.01	A0	198	12.21	. . .	K3	248*	7.99	+.06	B9
149	12.19	. . .	G0	199	12.37	+.03	A2	249	11.29	-.03	A2
150	11.69	. . .	F2	200	11.79	-.15	A3	250R	11.72	. . .	F8
151*	9.73	. . .	F0III	201	11.93	-.01	A3	251*	10.54	-.23	A2
152	11.98	. . .	F2	202	12.36	. . .	A3	252	11.53	+.21	A3
153*	9.82	-.29	B9	203	12.00	. . .	G0	253	12.01	. . .	K0III
154*	9.15	-.58	A0	204	11.53	. . .	G5V	254*	10.67	+.07	A3
155	11.05	+.03	A5	205*	9.04	-.39	A0	255*	10.80	. . .	A0
156*	10.85	. . .	G8III	206	11.63	. . .	B8	256*	10.21	-.30	A2
157	12.39	. . .	G0	207	11.85	. . .	F8	257	12.10	. . .	B5
158*R	9.09	. . .	O	208	11.82	. . .	F5	258*	11.59	. . .	M2III
159	12.10	. . .	K0III	209*	12.55	. . .	K2	259*R	10.05	. . .	K0V:
160	11.85	. . .	K0III	210	11.68	. . .	G5V		10.05		
								260	11.73	+.08	A0
161	12.10	. . .	K2V	211*	10.42	-.35	A0	261	12.14	+.06	A0
162	12.43	. . .	F2	212	12.36	. . .	K0III	262	10.70	+.22	A3
163	11.29	. . .	G0	213*	10.55	. . .	K0IV	263	11.64	. . .	F0
164	12.52	. . .	K5	214	11.87	. . .	G5IV	264*	9.09	-.52	B9
165	11.32	. . .	K0III	215	11.98	. . .	M2	265*	11.02	. . .	K0III
166*	10.61	. . .	K0III	216*	11.32	. . .	K2III	266	11.05	+.28	A3-F2
167*	10.70	. . .	K0III	217	11.90	+.12	A2	267*	11.12	. . .	M0III
168	12.06	. . .	G0	218*	8.60	-.42	B9	268*	10.60	. . .	K0III
169	11.82	-.04	A2	219*	10.07	-.27	A0	269*	10.46	. . .	K0III
170	12.19	. . .	G0	220	12.45	. . .	G8III	270	11.41	+.27	A3
171	11.82	. . .	F8	221	11.05	+.17	A0	271	11.78	-.17	B9
172	12.08	. . .	G0	222	11.88	. . .	G8	272*	11.78	. . .	K0
173	11.97	. . .	G8IV	223	12.17	. . .	K0III	273*	10.75	. . .	G2V
174*	9.95	. . .	G2V	224	12.06	. . .	G0	274	12.07	. . .	A0
175	11.88	-.11	B9	225	12.15	. . .	G5	275*	10.42	-.47	A0
176*	9.74	-.48	B8	226	12.31	. . .	K0	276	10.42	. . .	G0V
177	12.31	. . .	G5V	227	10.54	. . .	F0III	277*	8.95	-.43	B9
178	12.00	+.01	A2	228	11.47	-.31	B8	278	11.51	. . .	K0
179	11.90	. . .	G8:	229	11.54	. . .	F5	279	11.37	. . .	G0
180	11.80	. . .	F5	230	12.42	. . .	G0	280	11.64	. . .	K3III
181	11.07	-.16	B8	231	11.07	. . .	K0IV	281*	9.66	-.33	A2
182	11.60	. . .	G5V	232*	9.25	-.59	A0	282	11.68	-.28	B8
183	12.05	. . .	F5	233	11.61	. . .	F0	283	12.04	. . .	F2
184	12.27	. . .	F5	234	11.61	. . .	K2III	284*	10.52	. . .	G8III
185	12.22	. . .	K0	235*	10.39	-.06	B9	285	10.97	-.08	B9

Table 1

Observational Data for Region LF2 (Cont'd)

Zone +30° (Cont'd)

No.	m_{pg}	R. I.	Sp.	No.	m_{pg}	R. I.	Sp.	No.	m_{pg}	R. I.	Sp.
286	12.47	-.14	A0	336	11.97	...	F0	386	12.47	+.39	A5
287	11.37	...	G2V	337	11.88	+.65	A3	387	11.78	-.02	B9
288	11.10	...	G2V	338	11.73	...	G5V	388	11.90	...	F2
289	11.63	...	F0	339*	10.61	...	K0III	389	12.47	...	M2
290*	10.07	...	K2III	340*	10.36	...	K0III	390	11.57	...	G5III
291	12.10	-.11	A0	341	12.06	...	K0V	391	11.61	-.26	B8
292	11.91	...	F2	342	11.63	...	K2III	392	11.07	+.09	A2
293	12.32	-.06	A0	343*	11.60	...	K5III	393	12.17	...	G0
294	11.85	...	G5III	344	11.12	...	F2	394	11.96	...	F8
295	11.36	...	G2V	345	10.56	...	F8V	395*	11.12	...	K2III
296	11.90	-.05	A2	346	11.55	...	G0	396	12.31	...	F0
297	11.46	-.23	A0	347*	9.72	...	K0III	397*R	8.29	...	M0III
298	11.88	...	F5	348	11.96	...	A3	398	12.15	...	F8
299	11.57	...	A5	349*	10.19	...	A2	399*	8.96	...	G0V
300	11.36	...	K0	350	12.36	...	A0	400	12.08	...	K0V
301	12.42	...	G8III	351	11.78	...	F5	401	10.16	...	F8IV
302	11.48	...	F8	352*	9.66	-.09	A2	402	12.07	...	G8V
303	11.33	-.11	A2	353	11.85	...	F8	403	11.60	-.17	A0
304	12.52	...	A3	354	11.90	...	F2	404	10.81	...	F8V
305*	11.07	...	G5III	355	11.75	...	G5V	405	11.61	+.21	A0
306*R	(5.79)	...	K0III	356	12.10	...	G8III	406	12.21	...	A3
307	9.88	+.07	A2	357*	9.23	-.45	A0	407	12.27	...	G0
308	11.60	...	G5:	358*	10.26	+.17	A5	408	12.10	...	F2
309	11.96	...	F8	359	12.26	.00	A3	409	12.03	...	A3
310*	7.18	-.12	B5	360	12.44	+.01	A0	410	11.37	+.01	A0
311	11.12	+.14	A5	361	11.66	...	K0V	411	12.42	...	F0
312	12.12	...	G5V	362	11.25	...	F5	412	11.73	...	F8
313	12.61	...	G0	363	11.14	+.24	A2	413	12.31	...	F8
314	11.93	+.07	A5	364	12.05	-.21	B9	414*	8.76	-.45	B8
315	12.06	...	G0	365*	9.57	...	K2III	415	12.13	...	G0
316	11.64	...	G0	366	12.35	-.11	A0	416*	9.86	+.29	F8III
317	12.45	...	A2	367	11.70	+.18	A5	417	11.64	...	K0IV
318	11.57	+.13	A2	368	11.12	-.52	A0	418	11.47	...	K0III
319	11.61	-.07	A2	369	12.12	+.09	A0	419	11.96	...	F2
320	11.32	...	G8V	370	11.85	...	F0	420	12.50	...	G5III
321	11.54	...	G5V	371	11.92	...	G0	421	12.41	+.15	A3
322	11.12	...	G5V	372	11.95	-.08	A0	422*	9.90	...	G8IV
323	11.51	...	A0	373	11.98	...	F0	423	12.29	...	A5
324*	10.45	...	K2III	374*	10.21	...	B8	424	11.60	...	G8V
325	9.92	...	A0	375	11.03	...	A0	425*R	11.21	...	A3-F2
326	9.71	...	A0	376	12.12	+.22	A2	426	11.37	...	G8IV
327*	9.80	-.63	B8	377	12.10	+.20	A0	427	12.52	...	G2
328	10.42	-.44	B9	378	11.72	...	G8III	428*	9.84	...	K0III
329	10.54	-.32	B8	379*	11.07	...	K2V	429	12.52	...	A3
330*	9.36	-.42	B9	380*	8.29	-.17	B9	430	12.46	-.28	B9
331	10.99	-.45	B9	381*R	7.70	...	A3-F5	431	10.55	-.19	A0
332	11.33	...	G0	382	11.74	...	A0	432	11.90	+.13	A2
333	12.19	...	F8	383	11.66	...	G8III	433	12.40	+.02	A2
334*	8.83	-.50	B9	384*	10.61	-.18	A2	434	12.42	...	K0III
335	12.35	...	G8III	385	12.12	...	G0	435	12.47	...	M0

Table 1

Observational Data for Region LF2 (Cont'd)

Zone +30° (Cont'd)

No.	m_{pg}	R. I.	Sp.	No.	m_{pg}	R. I.	Sp.	No.	m_{pg}	R. I.	Sp.
436	12.50	-.03	A3	486	12.28	+.29	A0	536	11.50	...	G2V
437	11.45	-.11	B9	487	12.39	+.40	B9	537	12.67	...	A0
438	11.93	...	G2V	488	12.45	...	G8	538	11.81	...	K0III
439	10.02	-.28	A2	489	12.05	...	K0	539	11.71	...	K0III
440	11.62	+.26	A3	490	11.74	...	A2	540	12.38	...	A5
441	11.37	...	F0	491	11.73	+.39	A5	541	12.45	...	A2
442	11.85	...	G5III	492	12.10	...	G2	542	12.28	...	F0
443	11.85	...	K2III	493	11.91	+.59	A0	543	11.92	+.10	B8
444	12.35	+.36	A0	494*	10.96	...	F5V	544*	9.51	-.33	B5
445	12.67	...	G2V	495	12.10	+.07	A2	545	11.84	...	F0
446	12.18	...	F8	496*	9.13	-.53	B8	546	11.96	+.10	A2
447	12.08	...	G0	497	11.85	+.18	A0	547	12.10	+.32	A2
448	10.93	-.11	B8	498	11.71	...	A3	548	11.96	...	F2
449	12.30	+.04	A0	499	11.90	-.05	B9	549*	8.36	+.01	A2
450	11.66	+.01	A0	500	11.29	...	F8	550*	11.62	...	K0III
451	12.28	...	A5	501*	10.36	...	F8III	551	11.46	+.14	A0
452	12.00	...	F0	502	12.19	...	F0	552	12.35	...	K0
453	11.25	...	F8	503*	9.37	-.47	B9	553	12.15	...	G0
454*R	(6.04)	...	A0	504	11.73	...	G8III	554	12.06	...	A3
455	12.05	+.01	A3	505	12.08	...	K0	555	12.41	...	A2
456	12.05	...	G0	506	11.08	+.03	B9	556*R	10.09	+.20	A2-F2
457	11.85	+.14	B9	507	11.09	-.19	B5	557	12.10	...	A3
458	12.06	...	F5	508	11.98	...	F8	558	12.41	...	A0:
459*	7.37	+.18	A0	509*R	10.15	+.07	A3	559	12.50	...	F5
460*	9.79	-.01	A2	510	12.48	...	K0III	560*R	9.67	-.13	A0
461*	9.24	...	K3III	511	12.10	...	G8	561	11.92	...	G0
462	11.60	+.32	B9	512	10.57	-.21	A0	562	11.93	...	K0III
463	12.03	+.42	A3	513	11.46	-.02	B9	563	12.36	...	K0
464	11.57	...	F2	514	11.74	-.09	B8	564	12.06	...	A0
465	11.85	...	G5V	515	12.41	...	A2:	565	11.37	+.33	A0
466	11.40	...	F0	516*	12.01	...	G8V	566	12.06	...	F8
467	12.23	...	G8V	517	11.88	+.10	A0	567*	9.06	...	M5III
468	11.82	+.03	B9	518	12.20	...	A2	568	12.33	...	A2:
469	11.56	+.03	A2	519	11.90	+.21	A5	569	12.31	...	F5
470	11.63	...	G8III	520*	10.44	.00	A3	570	11.85	+.12	B9
471	10.28	-.02	A3	521*	10.70	-.14	A0	571*	9.97	-.19	B8
472*	9.06	+.02	A2	522	12.39	...	A2	572	11.65	...	G0
473	12.42	...	A0	523*	10.52	...	K0III	573	11.85	+.05	A0
474	9.97	...	F8V	524	11.82	...	F2	574	11.82	...	G8IV
475	11.59	...	G0	525	11.82	+.38	A2	575*	9.72	-.33	B5
476	12.08	+.09	A0	526*	11.85	...	K0III	576	12.08	...	G0
477	11.62	...	G2	527	12.38	...	K0III	577	12.32	...	F5
478	11.29	...	K0IV	528	12.41	...	B8	578	11.84	+.36	A5
479	12.23	...	F8	529	12.79	...	M5	579*	8.52	+.17	B9
480	11.90	...	F0	530	12.60	...	G0	580*	8.89	-.43	B9
481	11.37	-.03	B8	531	12.14	...	G0	581*	10.03	.00	A0
482*	10.19	...	F2V	532	12.30	...	G0	582*	8.59	-.30	B8
483	11.77	...	G2	533	11.07	...	F0	583	12.02	+.25	A3
484	11.39	...	A0	534	11.73	...	G0:	584	11.99	...	G0
485	12.37	...	K0III	535	11.75	...	F5	585	11.98	+.10	A0

Table 1

Observational Data for Region LF2 (Cont'd)

Zone +30° (Cont'd)

No.	m_{pg}	R. I.	Sp.
586	12.65	...	K0
587	12.77	...	K0
588	12.23	...	A3
589	12.33	+.38	B9
590	12.15	...	G0
591*	8.83	-.31	B9
592	12.12	+.17	A2
593	12.80	...	G0
594	11.46	...	G0
595*	10.46	...	F8V
596	11.84	...	G0
597	12.30	...	A5
598	12.17	...	A0
599	11.42	+.31	A0
600	11.29	+.15	A0
601	12.65	...	K2
602	12.01	+.28	A5
603	10.13	...	F8V
604	11.79	...	F8
605*	11.45	+.38	B9
606	12.08	...	G2
607*	8.29	+.21	A0
608	12.32	...	G0
609	12.42	-.07	A0
610	11.21	...	G8III
611	12.04	+.31	B9
612	12.02	...	G0
613	12.39	+.35	A2
614*	9.76	+.08	A2
615	11.91	...	G0
616	12.32	...	K0III
617	11.07	...	F8

Zone +31°

1*	11.58	...	K0III
2*	9.62	-.22	A0
3	12.24	...	K0III
4*	11.56	...	G5V
5	10.55	+.17	A2
6	12.10	...	G0
7*	12.20	...	G8:
8*	11.17	...	K0III
9	12.56	+.14	A2
10	12.18	...	K0III
11*	10.60	-.08	A0
12	12.42	...	B8
13R	11.41	...	F5
14*R	9.08	...	M0III
15	12.46	...	K0:
16	11.67	...	F0
17	12.00	-.27	B9
18	11.97	...	G0
19*	9.90	-.15	A0
20	11.32	...	F5
21*	12.18	...	K3
22*	9.03	-.42	A0
23*	11.80	...	K2III
24	12.18	...	F5
25	12.05	...	F0
26*	11.04	...	K5III
27	12.36	...	G0
28	12.32	...	K5
29*	11.81	...	G8III
30	12.14	...	F8
31*	10.05	...	K0III
32*	9.27	...	K2III
33*	6.85	...	F5V
34	11.81	...	A3
35	12.27	...	B8
36*	11.32	+.08	A2
37	11.28	...	G5V
38	11.41	+.16	A3
39	11.04	-.15	A0
40	12.16	...	G8III
41*	9.66	-.23	B8
42*	10.95	...	K2V
43	11.77	-.05	A0
44	11.54	+.26	A5
45	12.12	+.09	A2
46*	11.04	...	G8III
47	11.61	-.34	B9
48	11.97	...	G0
49	11.07	+.01	A0
50*	10.12	-.78	A0
51*	11.52	...	G8III
52	12.41	+.23	A5
53	11.92	...	K0
54	11.97	...	K0
55*	9.03	-.06	A5
56	12.12	...	G8III
57	11.33	...	A0
58*	9.67	+.20	A2
59*	9.62	-.33	B8
60	11.63	...	K0III
61	12.07	...	G8III
62	11.98	...	G5V
63	11.32	+.12	A2
64R	11.51	...	F5
65	11.12	+.15	A5
66	11.75	...	F2
67	12.06	...	F5
68	12.05	...	F0
69	11.90	...	F0
70	12.01	+.02	A3
71	11.96	...	F5
72	11.21	...	F8
73	12.16	...	G8V
74*	10.58	-.16	B9
75*	11.07	...	F0
76*	9.79	...	K0IV
77	12.14	+.11	A3
78	11.86	...	G0
79	11.36	...	K2III
80	11.08	+.11	A3
81*	10.87	+.23	A3
82	12.20	+.12	A2
83	11.51	...	B8
84	12.06	...	G5III
85*	7.09	...	B0
86	12.08	...	F2
87	11.07	...	K0IV
88	11.82	...	F5
89*	10.43	...	F5III
90	10.81	...	B5
91	12.07	+.04	A0
92	11.46	...	G0
93*	11.56	+.28	A3
94	11.21	...	F5
95*	9.62	...	G5III
96*	9.62	-.27	A2
97*	9.44	-.41	B9
98	11.21	+.06	A5
99*	9.70	...	G8IV
100	11.08	...	F2
101*	9.47	-.34	A0
102*	10.64	...	F0
103	11.80	...	G0
104	11.51	+.27	A3
105*	9.10	...	K2III
106	12.05	...	K0III
107	11.20	...	G0
108	11.32	.00	A3
109	11.45	...	F2
110	11.41	...	F0
111*	11.41	...	F3
112	11.80	...	G5III
113	11.82	...	G0
114	11.29	+.31	A3
115*	10.54	...	F0V

Table 1

Observational Data for Region LF2 (Cont'd)

Zone +31° (Cont'd)

No.	m_{pg}	R. I.	Sp.	No.	m_{pg}	R. I.	Sp.	No.	m_{pg}	R. I.	Sp.
116	12.45	...	K0III	166	12.55	+.09	A2	216*	8.83	-.12	B9
117*	10.84	...	M0III	167	11.94	...	G5III	217	11.04	...	G5V
118*	7.90	-.03	A0	168	11.80	...	K0V	218*	9.97	...	F8V
119	10.70	-.36	A0	169*	8.50	...	G8III	219	12.35	...	F0
120*	8.66	-.43	B9	170	11.73	...	F5	220	11.37	+.09	A2
121	12.23	...	G5V	171*	9.03	-.36	A0	221	11.93	+.32	A3
122	12.54	...	K0III	172	12.42	...	A3	222	12.50	...	K3
123	12.67	...	G0	173*	10.27	...	G8IV	223*	8.40	-.60	B8
124	12.15	...	G0	174*	9.67	-.36	A0	224*	7.88	...	G8III
125*	9.22	-.21	A2	175	12.07	...	G0	225	12.04	...	G8III
126	12.19	...	A2	176*	7.53	-.15	A0	226	11.51	-.13	B8
127*	11.72	...	K0III	177	10.51	...	F2V	227	11.61	+.05	A0
128	12.36	...	G5V	178	10.55	...	G0IV	228	12.41	...	A3
129	12.02	...	M0V	179*	10.36	...	G0IV	229	12.17	...	G0:
130	11.93	...	G5III	180*	9.15	...	G0V	230	12.08	...	G8V
131	11.32	...	F0	181	11.08	...	F8	231	12.30	+.25	A5
132	12.39	...	G8	182	11.90	+.05	A0	232	11.93	...	G0
133	12.03	...	A3	183*	9.15	...	G5III	233	12.07	...	F0
134*	11.29	...	K0III	184	11.69	...	G0	234*	9.13	...	G5V
135*	8.55	...	K0III	185	11.64	...	F5	235	12.45	-.06	A2
136	12.56	...	G0	186*	8.83	-.14	A2	236	11.61	+.09	A3
137	11.85	...	G0	187	12.12	...	G0	237	12.00	...	F0
138	11.84	...	F2	188*	9.36	-.44	A0	238*	11.05	...	K0III
139	12.03	...	F2	189	11.71	...	K0III	239	11.96	...	G0:
140	11.50	...	G2V	190	11.03	-.05	A0	240	11.88	...	G0
141	12.10	...	G8III	191*	11.32	...	K0V	241	11.60	-.13	A2
142	12.37	...	A0	192*	11.32	+.25	A2	242	11.57	+.13	A3
143	11.41	...	F2	193*	9.33	...	G8III	243	11.20	...	G0
144*	9.33	...	M0III	194	12.25	...	A3:	244	12.39	...	F0:
145	11.58	...	F8	195	11.87	...	G0	245	11.97	...	F0
146	11.80	...	K2V	196	11.70	...	F0	246	10.37	-.53	B8
147*	9.74	...	G8IV	197*	11.94	...	K0III	247	11.93	...	G5
148	12.35	+.31	B9	198*	9.62	...	F8III	248	12.48	...	G2
149	12.28	-.14	A0	199*	9.97	...	G8III	249	12.27	...	G5
150	11.97	+.16	A5	200	11.56	...	G5III	250	12.08	...	K0
151	11.63	...	F0	201*	9.83	...	F8III	251*	11.21	...	F8
152	12.03	...	F0:	202	11.96	...	F0	252*	11.06	...	F0:
153*	10.19	...	G5IV	203	9.90	-.25	A0	253*	11.37	...	G8III
154	11.70	...	G0	204	11.97	...	F0	254	11.81	...	F8
155	11.08	-.15	A0	205	12.19	...	F2	255	12.21	...	K0
156	12.10	+.02	A3	206	12.24	-.29	A3	256	11.61	...	F5
157	11.82	...	F2	207	12.26	+.13	A3	257	12.45	...	G0
158*	9.12	...	K2III	208	12.23	...	G5V	258	12.46	...	A0
159	12.00	...	M2III	209*	11.32	...	K0V	259R	11.82	...	F0
160	11.61	...	F8	210	11.64	...	G5V	260	12.16	...	G0
161	12.03	...	G8	211	12.13	...	A3	261	12.41	...	G0
162	12.22	...	F2	212	12.38	...	F8	262*R	8.28	...	F0V
163	12.28	...	G8III	213*	9.72	-.05	A3-F2	263	11.86	...	G5V
164	11.36	-.29	A0	214	12.18	...	A2	264	11.91	...	B9
165	12.50	...	K5	215	12.03	...	G0	265	12.21	+.13	A0

Table 1

Observational Data for Region LF2 (Cont'd)

Zone +31° (Cont'd)

No.	m_{pg}	R. I.	Sp.	No.	m_{pg}	R. I.	Sp.	No.	m_{pg}	R. I.	Sp.
266	10.91	...	A0	291	12.08	...	G0	316	12.12	...	G0
267*	8.53	...	F8V	292	12.00	...	G5III	317*	12.10	...	K5III
268	12.73	...	K0	293*	9.76	-.13	A0	318	12.23	...	G0
269*	9.31	...	G5V	294	11.50	-.28	A0	319	11.87	-.03	A2
270	11.51	...	G0	295	12.51	...	G0	320	11.90	...	A5
271	11.47	...	F0	296	12.30	...	F8	321	12.03	...	G0
272*	10.82	+.34	A0	297	12.36	...	K5	322*	10.32	...	F5III
273	11.66	...	G8V	298	12.67	...	K2	323	12.36	...	G2
274	11.07	...	G8IV	299	11.80	+.15	A2	324	12.02	...	F8
275	12.06	...	G8	300	11.81	-.01	A2	325	11.40	...	F5
276*	10.42	...	F0V	301	12.52	...	G5IV	326	11.97	...	K0III
277*	9.53	...	F0III	302	12.41	...	K3	327	11.82	+.41	A5
278	11.98	+.08	A0	303	12.08	...	G5V	328	12.75	...	A0
279	12.08	-.05	A0	304	12.52	...	G8III	329*	11.36	...	K0III
280*	10.06	-.58	A0	305	12.39	...	A0	330	11.47	...	G0
281	12.10	...	F2	306	12.65	...	G0:	331	12.67	...	K5
282*	8.83	...	G8V	307	10.29	...	A0	332*	10.64	-.06	A2
283	11.28	+.18	A0	308	12.54	...	A0	333*	11.61	...	K3III
284	12.27	...	A0	309*	9.88	...	G8III	334*	11.17	+.15	A0
285	12.12	-.01	A2	310	11.16	+.09	B9	335	12.33	...	K2III
286	12.08	...	K0V	311*	11.07	...	G8III	336	11.84	+.23	B9
287	11.10	...	F5	312*	10.04	-.21	A2	337	11.94	...	B8
288	11.85	...	G5V	313	11.58	...	G0	338	11.83	...	G0
289	12.28	+.02	B9	314	12.42	...	A0	339*	11.57	...	M5III
290*	11.08	...	G8IV	315	12.19	...	F8				

TABLE 2

Remarks Concerning the Spectra of Table 1

No.	
	Zone +28°
46	*Hγ* strong; *Hδ* weak; K line strong
121	Hydrogen lines very sharp
182	G band visible; continuum to red of *Hγ* very strong for class F5; more like G8
248	*Hδ* very diffuse; G band present; hydrogen strong in ultraviolet
261	Metallic-line A star; G band present faintly
265	*Hδ* emission suspected; BG Cygni 10.4–12.1 period 292.4 days
281	Hydrogen lines sharp
284	*Hδ* very diffuse
312	Metallic-line A star; G band present
365	*Hδ* unusually strong
420	Metallic-line A star
445	Hydrogen lines very sharp
	Zone +29°
5	Hydrogen lines sharp
58	K line weak for class F0
79	Hydrogen lines broad and diffuse
105	G band present; K line weak for class F; ultraviolet hydrogen lines strong
166	HD photographic magnitude given
196	*Hδ* very strong
218	Probably metallic-line A star; G band trace; K weak for class
230	Broad emission at *Hγ* and *Hβ*; resembles P Cygni
247	Hydrogen lines have broad wings, sharp cores
313	*Hδ* very strong
327	Suspected double star
339	K line weak for class F0; G band present; hydrogen lines strong
393	K line weak for class F0; G band present; hydrogen lines strong
424	Principal characteristics of class A3, but G band present
440	*Hδ* very diffuse
457	Same characteristics as No. 440
594	SU Cygni 7.2–8.2 period 3.84 days
619	Trace of G band; K line somewhat weak for class A3
620	Hydrogen lines sharp
633	K line very diffuse
655	Hydrogen lines sharp
711	*Hδ* very strong
	Zone +30°
24	*Hδ* very strong for class F0
26	HD 183930 class K0; *HDC* appears to be in error here
28	K line weak for class F2; G band present; metallic lines present
158	HD 184738 Ocp; Beals classification BW0+P
250	*Hδ* very strong
259	Very close double
306	HD magnitude given
381	F5 characteristics except weak K line and strong hydrogen in ultraviolet
397	HD 186178 class K2; *HDC* appears to be in error here
425	F2 characteristics except weak K line and strong hydrogen in ultraviolet
454	HD magnitude given
509	*Hβ*, *Hγ*, *Hδ*, very sharp
556	K line weak for class F2; G band present; hydrogen lines sharp
560	Hydrogen lines sharp
	Zone +31°
13	Abnormally strong K line
14	HD 184149 gives class K
64	*Hδ* very strong
259	*Hδ* very diffuse
262	HD 186258 class A2; *HDC* appears to be in error here

TABLE 2—*Continued*

BD Numbers for a Few Stars in LF2

Zone +27°	Our No. 3 = +27°3440; No. 19 = +27°3455
Zone +28°	No. 12 = +28°3373; No. 50 = +28°3378; No. 101 = +28°3394; No. 152 = +28°3406; No. 220 = +28°3417; No. 279 = +27°3454; No. 307 = +28°3431; No. 363 = +27°3474
Zone +29°	No. 27 = +29°3618; No. 110 = +28°3380; No. 192 = +29°3655; No. 276 = +29°3672; No. 348 = +29°3686; No. 420 = +28°3434; No. 550 = +29°3714; No. 667 = +29°3734
Zone +30°	No. 34 = +30°3605; No. 111 = +30°3625; No. 236 = +30°3658; No. 306 = +29°3684; No. 397 = +30°3697; No. 459 = +29°3710; No. 549 = +30°3725; No. 607 = +30°3736
Zone +31°	No. 33 = +30°3622; No. 120 = +30°3656; No. 176 = +30°3673; No. 262 = +31°3722

The fourth column contains the spectral type and, for the stars later than F0, the luminosity class. The spectral classification agrees very closely with the system of the *Henry Draper Catalogue*. As has been shown in several recent publications[2,4] from this observatory, our classification of the late B stars has a tendency to be about 0.1 or 0.2 spectral subdivisions earlier than the HD class. Otherwise the agreement is very good. Both authors of this paper have classified the spectra in LF2 independently, and there appear to be no systematic differences in the assigned types.

The luminosity classes are on the system defined by the work of Morgan, Keenan, and Kellman.[5] For stars F8 and later and brighter than $m_{pg} = 11.0$, it was generally possible to distinguish four luminosity classes, viz., I (supergiant), III (giant), IV (intermediate), V (dwarf). For the early F stars and for the faint stars of all later types, only classes III and V were used. In many cases poorly exposed or overlapping spectra precluded the assignment of a luminosity class.

Remarks concerning individual spectra are given in Table 2, together with the BD equivalents already mentioned.

[4] J. J. Nassau and C. K. Seyfert, *Ap. J.*, **103**, 117, 1946; J. J. Nassau and D. A. MacRae, *Ap. J.*, **110**, 42, 1949.

[5] *An Atlas of Stellar Spectra* (Chicago: University of Chicago Press, 1943).

OH EMISSION BANDS IN THE SPECTRUM OF THE NIGHT SKY. II

A. B. MEINEL
Lick and Yerkes Observatories
Received May 1, 1950

ABSTRACT

A detailed analysis has been made of the vibrational constants for the ground state of *OH*, combining the observations of the night-sky rotation-vibration bands with laboratory data for the ultraviolet electronic *OH* bands. Systematic deviations were observed from the band positions predicted by ω_e and $\omega_e x_e$ from the ultraviolet bands. The deviations show, however, that the assignment of terms in $\omega_e y_e$, $\omega_e z_e$, . . . , would not have any physical significance. The relative intensities have been determined for the night-sky bands from 9000 to 5500 A. The resultant values show systematic changes of band intensity within each Δv sequence. A brief investigation of the band intensities under conditions of radiative equilibrium for cases of resonance and thermal excitation shows that the *OH* bands are probably produced by a chemical resonance mechanism and, further, that collisional de-excitation effects may be present. The temperature in the *OH* stratum was found to be 260° ± 5° K from the distribution of energy in the resolved *P* branches and from the ratio of intensity between the *P*, *Q*, and *R* branches.

(7, 2) 6870 A *OH* BAND

A spectrum obtained subsequent to the publication of the author's tables of wave lengths[1] has recorded the (7, 2) transition near 6870 A with sufficient intensity for measurement. Inasmuch as the *P* branch of this band is obscured by the O_2 telluric absorption band at 6900 A, the wave lengths for the *P* branches are uncertain. The relatively sharp *R* and *Q* branches, however, could be measured with good accuracy. The wave lengths and intensities for the (7, 2) *OH* band are shown in Table 1.

TABLE 1

SUPPLEMENTARY WAVE-LENGTH VALUES FOR THE (7, 2) *OH* BAND

$\lambda_{(air)}$ (A)	$\nu_{(vac)}$ (Cm^{-1})	*I*	Branch	$\lambda_{(air)}$ (A)	$\nu_{(vac)}$ (Cm^{-1})	*I*	Branch
6838.2	14619.7	6	*R*	6921	14(445)	1	P_1
6867.6	557.1	5	*Q*	6951	(382)	2	P_2
6893	(503)	1	P_1	6982	(318)	1	P_4

VIBRATIONAL CONSTANTS FOR *OH*

The vibrational constants for the $^2\Pi$ ground state of *OH* have been redetermined with more significance than was possible in the previous report[1] by the simultaneous use of high-dispersion data for the $v = 0$, 1, and 2 levels as obtained from the ultraviolet electronic *OH* bands. A further refinement was made by locating the origins of the infrared *OH* bands, using the rotational lines of the *P* branch wherever possible. For bands in which the doublet structure of the *P* branch was resolved, the mean position of the lines of equal *J* number was used. For the (7, 3) and (8, 3) bands, the strong component, $^2\Pi_{3/2}$, of the *J*-splitting was used. To avoid ambiguity, the origin of the *P* branch was taken as defined by the equation

$$\nu_0 = P_J(\nu) + (B_{v'} + B_{v''})J - (B_{v'} - B_{v''})J^2 . \quad (1)$$

It should be noted that this definition does not include a small constant term, $\Lambda(B_{v'} - B_{v''})$, which occurs in other definitions. Table 2 shows the wave-number positions of the

[1] A. B. Meinel, *Ap. J.*, **111**, 555, 1950.

origins for the *OH* bands. The (4, 0) band origin was estimated from the *P* line, and the *Q* branch, using the interval (origin − *Q*), was determined from the (6, 2) and (5, 1) bands. This procedure was necessary because most of the *P* branch of the (4, 0) band is obscured by the strong A-band absorption at 7600 A. The origin of the weak (7, 2) band was similarly estimated from the observed *Q* and *R* branches.

TABLE 2

EXTRAPOLATED *OH*-BAND ORIGINS

J	(7, 3) (Cm^{-1})	(6, 2) (Cm^{-1})	(5, 1) (Cm^{-1})	(9, 4) (Cm^{-1})	(4, 0) (Cm^{-1})	(8, 3) (Cm^{-1})	(7, 2) (Cm^{-1})
⅝	11325.9	11983.9	12633.6	12901.4	.....	13733.6	.....
							(*Q*−*R*)
½	26.2	83.6	33.4	898.2	13284.9	33.7	14564.9
					(*O*−*Q*)		(*O*−*Q*)
⅞	26.2	83.9	33.2	.....	13285.8	35.4	64.4
1½	.....	83.8	34.4	.....	.....	35.2	.....
Av.	11326.4	11983.8	12633.6	12899.8	13285.4	13734.5	14564.6
Comp.	11297.2	11957.7	12622.2	12879.4	13284.7	13707.5	14535.6
O−C	29.2	24.1	11.4	20.4	0.7	27.0	29.0

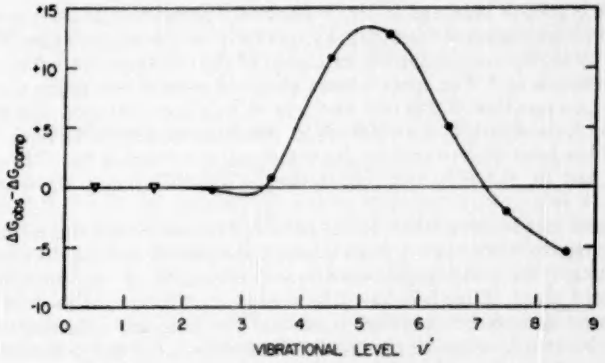

FIG. 1.—This graph shows the difference between $\Delta G_{v+1/2}$ observed for the higher levels and the $\Delta G_{v+1/2}$ terms predicted by the constants of *OH* determined from the electronic bands.

Systematic differences are observed when the measured band positions are compared to the band positions predicted by the values of ω_e and $\omega_e x_e$ that are well defined for the lowest vibrational levels by the electronic bands. The differences must arise from neglecting higher-order terms, such as $\omega_e y_e$, $\omega_e z_e$, etc. Figure 1 shows the difference in wave numbers between $\Delta G_{v+1/2}$ observed for the higher vibrational levels and the $\Delta G_{v+1/2}$ terms predicted by the known constants for the lower levels. From the shape of this curve, it is obvious that many higher-order terms would be required to adequately represent the vibrational levels up to $v = 9$. The nature of the potential function for the $^2\Pi$ state above $v = 4$ is therefore such that specifying an $\omega_e y_e$, . . . , would not have any physical significance. It is therefore felt that the constants for the $^2\Pi$ state of *OH* given

by Herzberg[2] cannot be modified to fit the observations of the rotation-vibration *OH* bands. These constants are as follows:

$$\omega_e = 3735.21 , \qquad \omega_e x_e = 82.81 .$$

It should be noted that the relative wave numbers determined by the author have a probable error of $< \pm 0.5$ cm^{-1}, while the absolute wave numbers may have a probable error as large as ± 2 cm^{-1}. An absolute error, however, does not affect the shape of the curve except near the ends, since it is determined from the wave numbers of overlapping transitions.

RELATIVE *OH*-BAND INTENSITIES

The spectra obtained by the author were microphotometered and reduced to correct relative intensities as described in the previous paper.[1] These intensities have provided a basis for comparing the relative *OH*-band intensities. The intensity for the weak (7, 2) band was determined from a recent spectrogram covering the 7000 A region in more detail. The *Q* branch of the *OH* bands was selected for intercomparison, since the *Q* branch is quite narrow, resembling more nearly a monochromatic line. The intensities of the *Q* branches are tabulated relative to the intensity of the 6300 A [*O* I] line. Since the 6300 A emission is very variable, with respect to both diurnal and auroral effects, the intensity was defined by the plates obtained on two quiet nights. The diurnal effect was averaged by exposures extending from approximately 1.5 hours after sunset to 1.5 hours before sunrise. As a consequence, most of the twilight enhancement was avoided. The effective intensity of the 6300 A [*O* I] line is therefore not much greater than it would be during the middle of the night.

The author is greatly indebted to Dr. J. Dufay for permission to refer to unpublished spectra of the visible region of the night-sky spectrum for the study of the *OH* intensities. Publications by Dufay concerning the extension of the *OH*-band system into the visible region are forthcoming.[3] The spectra were obtained with a two-prism Cojan spectrograph, having an aperture of 246 mm and a focal length of 160 mm. The resulting dispersion varied from 300 A/mm at 6000 A to 700 A/mm at 8000 A. With this spectrograph Dufay has been able to resolve the rotational structure of the *P* branches of the (8, 2), (9, 3), and (6, 1) *OH* bands, confirming the identification of these transitions by the author.[4]

The *OH*-band intensities relative to the 6300 A [*O* I] line have been estimated for the bands in the region 5000–6500 A from a microphotometer tracing of one of Dufay's spectra. Although the wave-length sensitivity calibration of the emulsion (Eastman 103*a*-E) was not given, it has been possible to estimate the band intensities by referring to the standard characteristics of this emulsion. The resulting values can therefore be used only to give rough values for the relative intensities. They are, however, of sufficient accuracy to enable an extension of the *OH* intensity scale.

The values of the *Q*-branch intensities of *OH* relative to the 6300 A [*O* I] line for all observed *OH* bands are given in Table 3. The intensities determined from bands observed by the author are given to three significant figures, except for the weak (7, 2) band at 6870 A. The intensities estimated from Dufay's spectra are given to two figures, although the second place is uncertain. The last column in Table 3 gives the relative numbers of transitions per second for each band, according to the equation

$$\frac{I_{em}}{p^4} = (\text{Const.})\, N_{v'} f_{v',v''} . \qquad (2)$$

[2] G. Herzberg, *Molecular Spectra*, Vol. 1 (New York: D. Van Nostrand Co., 1950).

[3] J. Cabannes, J. Dufay, M. Dufay, *C.R.*, **230**, 1233, 1950.

[4] A. B. Meinel, *Ap. J.*, **111**, 433, 1950.

The intensities of the bands in each Δv sequence show a strong increase with larger v'' values. A discontinuity, however, exists between $v'' = 9$ and $v'' = 10$. The transitions originating from $v'' = 9$ give rise to the strongest bands in the $\Delta v = 5$ and $\Delta v = 6$ sequences. This situation also appears to apply to the $\Delta v = 4$ sequence, since the (9, 5) band is in the 1μ region, where strong night-sky radiations have been detected.[1] On the other hand, no bands have been observed that originate from the level $v'' = 10$. This fact establishes an upper limit at

$$I(10, v'') < \tfrac{1}{20} I(9, v''). \tag{3}$$

TABLE 3

OH RELATIVE INTENSITY AND TRANSITION RATIOS

Transition (v', v'')	Intensity Ratio	Wave Number (Cm^{-1})	$[N_2'(OH)Q]/[N_2'(O\,{}^1S)]$
(7, 3)	25.00	11323	96.4
(6, 2)	9.25	11977	28.5
(5, 1)	5.25	12625	13.1
(4, 0)	1.00	13278	2.0
(9, 4)	2.88	12890	6.61
(8, 3)	1.50	13724	2.68
(7, 2)	0.63	14560	0.91
(6, 1)	0.30	15380	0.34
(5, 0)	<0.10	16200	<0.10
(9, 3)	0.50	15970	0.50
(8, 2)	0.30	16980	0.23

OH-BAND INTENSITIES IN RADIATIVE EQUILIBRIUM

RESONANCE EXCITATION

For the case in which the primary excitation mechanism populates a single excited level, the equilibrium equations for all lower vibrational levels may be readily obtained. In the following discussion we shall assume that the primary mechanism gives rise to a population in level $v = 9$. The population N_9 will then be distributed among the lower levels, according to the transition probabilities $9 \rightarrow 8$, $9 \rightarrow 7$, . . . , . In turn, the population that has appeared in level 8 will be redistributed among the still lower levels. The array of equations representing the resulting secular equilibrium conditions are as follows:

$$\begin{aligned}
1 &= N_9 f_{98} + N_9 f_{97} + N_9 f_{96} + N_9 f_{95} + \ldots + N_9 f_{90} \\
N_9 f_{98} &= N_8 f_{87} + N_8 f_{86} + N_8 f_{85} + \ldots + N_8 f_{80} \\
N_9 f_{97} + N_8 f_{87} &= N_7 f_{76} + N_7 f_{75} + \ldots + N_7 f_{70} \\
&\cdots\cdots\cdots\cdots\cdots\cdots\cdots \\
N_9 f_{91} + N_8 f_{81} + N_7 f_{71} + N_6 f_{61} + \ldots &= N_1 f_{10} \\
N_9 f_{90} + N_8 f_{80} + N_7 f_{70} + N_6 f_{60} + \ldots + N_1 f_{10} &= 1 .
\end{aligned} \tag{4}$$

In order to evaluate the equilibrium expressions for each vibrational level, we must investigate the transition probabilities. In the case of rotation-vibration bands, the

transition probabilities have a strong dependence on $\Delta v = v' - v''$. If the vibration of the molecule were strictly harmonic, the only permitted transitions would be transitions with $\Delta v = 1$. On the other hand, for anharmonic vibration, transitions with $\Delta v = 2, 3, \ldots$, become possible; however, the transition probability decreases rapidly with increasing Δv. The observed vibrational levels show that the *OH* molecule has a very anharmonic potential function for the ground $^2\Pi$ state. Preliminary computations show, however, that the transition probability decreases by an order of more than 10 with a change from $\Delta v = n$ to $\Delta v = n + 1$. If we assume that the transition probabilities are related by an equation of the form

$$f_{v',\,v''-1} = \eta\,(v')\,f_{v',\,v''} \qquad (\eta < \tfrac{1}{10}), \tag{5}$$

we can write

$$\begin{aligned} N_8 f_{87} &= N_9 f_{98}\left\{\frac{N_9 f_{98}}{N_9 f_{98} + \ldots + N_9 f_{91}}\right\}, \\ N_8 f_{86} &= N_9 f_{98}\left\{\frac{N_9 f_{97}}{N_9 f_{98} + \ldots + N_9 f_{91}}\right\}. \\ &\vdots \qquad\quad \vdots \end{aligned} \tag{6}$$

Then the equilibrium of level 7 is given by

$$N_9 f_{97} + N_8 f_{87} = N_9 f_{97} + N_9 f_{98}\left[\frac{N_9 f_{98}}{1 - N_9 f_{90}}\right]. \tag{7}$$

If we now use the above assumption for η, the total number of transitions per second into level 7 is given by

$$N_9 f_{97} + N_8 f_{87} = N_9 f_{98}\,[\eta + N_9 f_{98}]. \tag{8}$$

Again using the definition of η and $N_9 f_{98} = 1 - \eta + \eta^2 - \ldots$, we can write

$$N_9 f_{97} + N_8 f_{87} = N_9 f_{98}\,[1 + \eta^2 - \ldots], \tag{9}$$

from which we see that the total number of transitions per second into level 7 is equal to the total number of transitions into level 8, with an error of the order of η^2. This procedure can be extended to show that the total number of transitions per second into all levels subsidiary to 9 are very nearly equal to the number between 9 and 8. As a consequence of the above equilibrium conditions, we also can show that

$$\frac{N_v f_{\Delta v = n}}{N_{v-1} f_{\Delta v = n}} = \left[\frac{\eta\,(v)}{\eta\,(v-1)}\right]^{n-1}. \tag{10}$$

Since the observed band intensity is related to Nf by equation (2), we can evaluate the ratios of Nf for the observed bands. These ratios are shown in Table 4. The mean ratio, weighted according to the reliability of the band intensities, is approximately 2.8. The fact that this ratio is the same for the $\Delta v = 4$, 5, and 6 sequences indicates that η must be small. There are two possible explanations for the observed ratio of 2.8 for the bands. First, the ratio could be explained by an exponential increase in the transition probabilities, with v'' of the form

$$f_{\Delta v = n} = (2.8)^{v''}\,\eta^{n-1} f_{\Delta v = 1}. \tag{11}$$

A second explanation is that collisional de-excitation may be affecting the populations in each level.

The effective radiative transition probability when collisional de-excitation is present is

$$f^{(1)}_{v',v''} = \frac{1}{1 + \dfrac{c}{\sum_i f_{v',i}}} f_{v',v''}; \tag{12}$$

hence the collisional term must be comparable to the sum of the transition probabilities in order to be of importance. If we look at the expression for the transition probability of a vibrational transition,

$$P_{nm} = \frac{1}{a} \int_{-\infty}^{\infty} R_n R_m (p - p_0 u)\, du, \tag{13}$$

TABLE 4

OBSERVED *OH*-BAND *Nf* RATIOS

$\Delta v = 4$		$\Delta v = 5$		$\Delta v = 6$	
Transition	*Nf* Ratio	Transition	*Nf* Ratio	Transition	*Nf* Ratio
.....	.....	$\frac{(9,4)}{(8,3)}$	2.47	.....	.....
$\frac{(7,3)}{(6,2)}$	3.4	$\frac{(8,3)}{(7,2)}$	2.68	$\frac{(9,3)}{(8,2)}$	2.2
$\frac{(6,2)}{(5,1)}$	2.18	$\frac{(7,2)}{(6,1)}$	2.9	.....	.....
$\frac{(5,1)}{(4,0)}$	5.25	$\frac{(6,1)}{(5,0)}$	>3.4	.....	.....

we see that the transition probability is directly proportional to the coefficient of the change of the dipole moment with u, since $\int R_n R_m p\, du = 0$ from the orthogonality properties of the wave functions. Therefore, since the *OH* bands are entirely permitted, Σf cannot be small unless the $p_0 u$ term is small. The possibility of an experimental determination of the dipole moment of *OH* is being considered by Herzberg. On the other hand, if *OH* can combine readily with another constituent of the upper atmosphere, the reaction may produce a large collisional cross-section. Since $f_{\Delta v=1}$ is likely to be of the same order of magnitude for the higher vibrational levels, the collisional effect would be the same for each level, thereby producing the observed ratios. The question as to the origin of the observed ratio cannot be resolved, however, until accurate relative transition probabilities can be computed. This problem becomes very difficult for large values of v' and v''.

It is interesting to note that the *OH* bands arising from transitions to $v'' = 0$ are considerably weaker than anticipated from the ratio of 2.8. This effect may be due to reabsorption of the emissions by *OH* molecules in the lowest vibrational level.

THERMAL EXCITATION

If the mechanism producing the initial populations is due to "thermal excitation," not considering for the moment the observed break at $v = 9$, the ratio of the band

strengths will be different from the preceding case. The term "thermal excitation" does not imply thermodynamic equilibrium but indicates that the excitations are due to collisions with particles having a Maxwellian velocity distribution $f(E)$, characterized by a definite temperature. Since the relative concentration of OH must be small compared to the other constituents of the upper atmosphere, we can neglect the effect of the discrete energy states of OH on the velocity distribution of the particles. The rapid escape of energy in the form of radiation, however, will prevent the establishment of thermodynamic equilibrium populations in the excited states. Even when collisions are of sufficient frequency to produce noticeable collisional de-excitations, the nonconformance to thermodynamic equilibrium populations will hold because of the downward radiative cascade characteristic of rotation-vibration bands.

If we neglect collisional de-excitations on level v, then the total of all radiative transitions into v, plus the collisional excitations from the ground state into v, must equal the number of radiative transitions out of level v. The secular equations are then of the form

$$\sum_{i \geqslant v+1} N_i f_{i,\,v} + \int_{E_v}^{\infty} f(E)\, dE = \sum_{i \leqslant v} N_v f_{v,\,i}. \tag{14}$$

With the assumption that η is smaller than 0.1 we can extend the development of the preceding section to show that

$$N_v f_n = [\eta(v)]^{n-1} \sum_{i \geqslant v+1} \int_{E_i}^{\infty} f(E)\, dE, \tag{15}$$

where $\Delta v = n$. Then

$$\frac{N_v f_n}{N_{v-1} f_n} = \left[\frac{\eta(v)}{\eta(v-1)}\right]^{n-1} \sum_{i \geqslant v+1} \frac{\int_{E_i}^{\infty} f(E)\, dE}{\int_{E_{i-1}}^{\infty} f(E)\, dE} \tag{16}$$

or

$$\frac{N_v f_n}{N_{v-1} f_n} = \left[\frac{\eta(v)}{\eta(v-1)}\right]^{n-1} \left[1 + \frac{\int_{E_{v-1}}^{E_v} f(E)\, dE}{\sum_{i \geqslant v+1} \int_{E_i}^{\infty} f(E)\, dE}\right]^{-1} \leqslant \left[\frac{\eta(v)}{\eta(v-1)}\right]^{n-1}. \tag{17}$$

As a consequence, the total number of transitions and the intensity should increase for each successively lower vibrational level at the same rate, as new primary excitations are added. Such an excitation mechanism as thermal excitation would therefore favor the lower vibrational levels. The observed intensities, however, show a strong decrement in the opposite sense. This fact would mean that the effect of collisional de-excitation or the variation of the transition probability with v' would have to be increased over that required under the assumption that the primary excitation is predominantly to a single level. Moreover, thermal excitation would require a discontinuity in the transition probabilities between $v = 9$ and $v = 10$. It is therefore very likely that the observed OH bands are due to an energy resonance selectively populating the level $v = 9$.

TEMPERATURE OF THE OH STRATUM

The fact that the structure of the OH bands can be observed in detail offers an excellent opportunity to determine the temperature of the OH stratum. Three methods appear to be feasible. The first and most direct method is to use the rotational-line intensities of the $^2\Pi_{3/2}$ component of the resolved P branches. A second method is to utilize the

relative total intensities of the P, Q, and R branches. The third method is provided by the observation that the $^2\Pi_{1/2}$ component, which lies 138 cm^{-1} above the ground component $^2\Pi_{3/2}$, is considerably weaker. We shall examine each of these methods in detail.

P-BRANCH ROTATIONAL TEMPERATURE

The intensity of a rotational line is given by the expression

$$I_{em} = (\text{Const.})\, i(J')\, e^{-F(J')/kT}, \tag{18}$$

where $i(J')$ is the intensity factor and $F(J')$ is the rotational energy of the upper rotational level J'. For a $^2\Pi$ state in which there is no coupling between rotational and electronic motion (Hund's case a), the intensity factors $i(J)$ are given by

$$P(J') = \frac{(J'+1+\Omega)(J'+1-\Omega)}{J'+1},$$

$$Q(J') = \frac{(2J'+1)\,\Omega^2}{J'(J'+1)}, \qquad (\Omega = \tfrac{1}{2},\ \tfrac{3}{2}) \tag{19}$$

$$R(J') = \frac{(J'+\Omega)(J'-\Omega)}{J'}.$$

Since the coupling parameter A/B_v equals 7.3 for *OH*, the assumption of Hund's case a coupling is good only for very low J values. With the low temperature encountered in the upper atmosphere, however, the intensity drops off so rapidly that the lines of low J are the only lines of appreciable intensity.

The evaluation of $F(J') = B_{v'}J'(J'+1)$ depends upon both the mode of excitation and the density. If the excitation is from the ground level by electronic excitation and if the density is very low, then no redistribution of energy will occur among the rotational levels. In this case $F(J')$ should be evaluated with the rotational constant for the ground state. This effect has been noted in laboratory studies of H_2 emission bands at very low pressures.[2] On the other hand, if the *OH* molecule is formed in the excited state or if there is a collisional redistribution among the rotational levels, then the rotational constant for the upper state $B_{v'}$ should be used. Since a is large for the $^2\Pi$ state of *OH*, the value of $B_{v'}$, where

$$B_v = B_e - a\,(v+\tfrac{1}{2}) \qquad (B_e = 18.86),\ (a = 0.69), \tag{20}$$

will change considerably with v. The effect will be to change the computed temperature by the factor

$$\frac{B_{v'}}{B_e - \tfrac{1}{2}a}. \tag{21}$$

In all the following computations the value of the rotational constant for the *upper state* is assumed, since a preliminary determination by Roach and Elvey[5] places the *OH* stratum at about 80 km, where the atmospheric density is still high. This assumption is shown to be correct when we consider the temperature indicated by the relative total intensities of the P, Q, and R branches for different transitions.

The curves obtained for the rotational-line intensities of the P branch of the (6, 2) transition for temperatures of 100°, 200°, and 300° K are shown in Figure 2. The observed line intensities are given in Table 5. When two entries are shown under a single date, the

[5] Private communication.

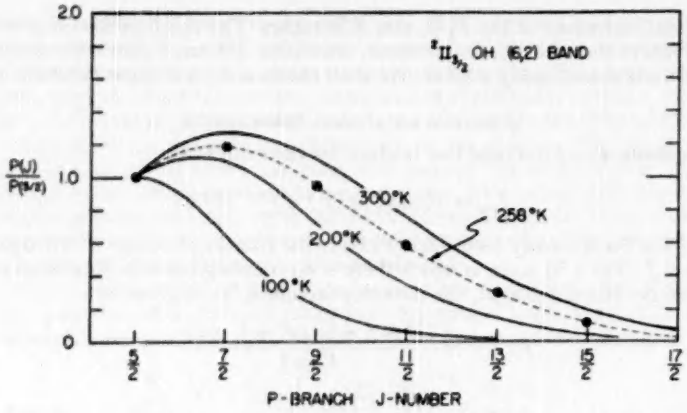

FIG. 2.—Rotational-line intensities for the resolved $^2\Pi$ P branch of the (6, 2) 8347 A band of *OH* as a function of the temperature.

TABLE 5

OBSERVED P-BRANCH ROTATIONAL-LINE INTENSITIES

(6, 2) 8347 A *OH* BAND

$P(J)$	Dec. 29	Dec. 29	Jan. 4	Jan. 6	Jan. 7	Jan. 7
3/2	1.00	1.00	1.00	1.00	1.00	1.00
5/2	1.29	1.26	1.07	1.18	1.15	1.18
7/2	0.98	1.00	0.91	1.01	0.98	0.92
9/2	0.62	0.64	0.62	0.60	0.58	0.59
11/2	0.35	0.34	.....	0.27	.....	0.28
13/2	.....	.....	.....	0.16	.....	.....

(6, 2) 8347 A *OH* BAND (*Continued*)

$P(J)$	Jan. 10	Jan. 19	Jan. 26	Jan. 27	Av.	258° K
3/2	1.00	1.00	1.00	1.00	1.00	1.00
5/2	1.32	1.09	1.14	1.24	1.19	1.19
7/2	0.89	0.81	0.95	0.97	0.94	0.95
9/2	0.49	0.54	0.61	0.62	0.59	0.59
11/2	0.16	0.32	0.30	0.35	0.30	0.30
13/2	0.11	0.19	0.12	.....	0.14	0.12

(5, 1) 7918 A *OH* BAND

$P(J)$	Jan. 6	Jan. 10	Jan. 19	Jan. 26	Av.	265° K
3/2	1.00	1.00	1.00	1.00	1.00	1.00
5/2	1.13	1.20	1.28	1.14	1.19	1.19
7/2	1.01	1.00	0.86	0.96	0.96	0.93
9/2	0.74	0.35	0.71	0.63	0.60	0.57
11/2	0.44	0.15	.....	.....	0.30	0.28

measurements are for different regions of the sky but are recorded on the same plate. The spectra obtained on January 19, 26, and 27, 1950, also showed auroral emissions at 8446 and 7774 A; however, no effect is apparent with respect to either the intensities or the rotational temperature of the *OH* bands. The average values observed for the (6, 2) band, plotted in Figure 2, correspond to a temperature of 258° ± 3° K, while for the (5, 1) band the temperature is 265° ± 5° K. The best mean value can be taken as 260° K.

RELATIVE BRANCH INTENSITY TEMPERATURE

We may obtain a second estimate of the rotational temperature by comparing the total intensities of the P, Q, and R branches. This method, however, is more sensitive than the P-branch method to changes in the molecular coupling. The theoretical values of the ratio P/Q and R/Q are plotted in Figure 3 for pure case a coupling and as a func-

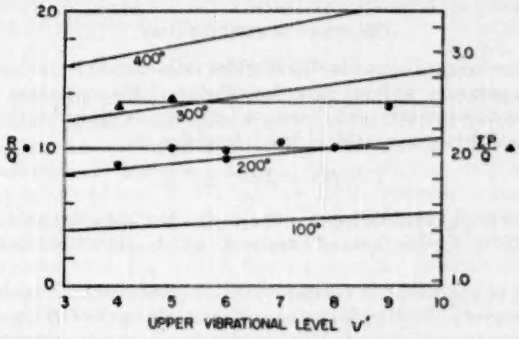

FIG. 3.— Branch intensity ratios for the *OH* bands as a function of the temperature

tion of the upper vibrational level of the transition. The circles represent observed ratios of R/Q, which can be readily determined, since both branches have the same general appearance. The triangles represent observed ratios of P/Q. The points for R/Q appear to fall systematically lower than those for P/Q. This effect can be attributed to the fact that the coupling is not strictly case a. The mean value of the temperature agrees well, however, with the value of 260° K determined from the rotational-line intensities within the P branch.

The assumption that the rotational constant should be taken as the B_v value for the upper state instead of $B_0 = B_e - \frac{1}{2}\alpha$ is shown to be correct in Figure 3. Instead of being constant, the points for the ratio R/Q for transitions having different upper vibrational levels have the same slope as the theoretical curve.

DOUBLET RATIO TEMPERATURE

The fact that the $^2\Pi_{1/2}$ state, which lies 138 cm^{-1} higher than the ground state $^2\Pi_{3/2}$, is considerably weaker would indicate a vibrational temperature. The observed ratio of the $^2\Pi$ components of the (6, 2) and (5, 1) transitions is

$$\frac{^2\Pi_{1/2}}{^2\Pi_{3/2}} = 0.317 = e^{A\hbar c/kT} = e^{A/0.695T}, \tag{22}$$

where $A = 138$ cm^{-1} for the doublet splitting. This ratio corresponds to a temperature of 172° ± 10° K.

The assumption that this value is a valid temperature presupposes that the excita-

tion mechanism does not redistribute the excitation energy between the $^2\Pi_{3/2}$ and $^2\Pi_{1/2}$ states. This supposition would be strictly correct if the excitation were radiative; however, the exciting emission would be at 3820 A. No strong emissions are present in this well-observed region. The possibility that the doublet ratio does indicate a temperature is not definitely excluded. The more likely explanation, however, is that the primary excitation energy is sufficient to populate the lower $^2\Pi_{3/2}$ component of the ninth vibrational level but is insufficient to populate strongly the higher $^2\Pi_{1/2}$ component. If, on the other hand, the energy spectrum of the excitation were due to a temperature and if the mean excitation energy exactly coincided with the $^2\Pi_{3/2}$ component of the level $v = 9$, then the ratio would indicate a correct temperature. Conversely, if this mechanism holds, we can reverse the reasoning to locate the mean energy of the primary excitation. If we assume a Boltzmann distribution of energies corresponding to a temperature of 260° K, the maximum of the excitation energy would be at 3.242 e.v.

OH STRATUM TEMPERATURE

In view of the preceding discussion, the doublet ratio cannot be seriously considered in establishing a temperature without exact knowledge of the excitation mechanism. The temperature of the *OH* stratum will therefore be taken as given by the relative branch intensities and the *P*-branch rotational-line intensities as

$$T(OH) = 260° \pm 5° \text{K}.$$

This value is rather high, considering that the author has obtained a temperature considerably less than 200° K for the O_2 band at 8640 A, which also arises from a stratum below 100 km.[6]

It is interesting to speculate on temperature determinations in the upper atmosphere in view of the discovery of hydride emission bands. Since the *OH* bands are extremely intense and since the transition probability is very small for the observed transitions, the number of *OH* molecules may be sufficient to contribute significantly to the composition of the upper atmosphere. Regardless of the origin of the *OH*, the dissociation equilibrium will favor atomic hydrogen in the extreme upper atmosphere. This hydrogen, however, would be very difficult to detect spectrographically, since the excited states are very high. As a consequence, no efficient excitation mechanism would be available from the low-energy sources present in the upper atmosphere. The presence of hydrogen, even in relatively small proportions, will very effectively lower the mean molecular weight of the upper atmosphere. It is well known that temperature determinations based on physical phenomena that require a knowledge of the molecular weight invariably give temperatures higher than are observed by spectroscopic methods. A solution to this long-standing discrepancy is therefore suggested by the presence of very intense hydride emission bands. In order to obtain quantitative data, however, information is needed with respect to the excitation mechanism and the absolute transition probabilities of the *OH* bands.

This investigation was sponsored by the Office of Naval Research.

[6] J. Kaplan, *Phys. Rev.*, **78**, 82, 1950.

ON THE IDENTIFICATION OF THE 3670 A BAND OF THE C_2 MOLECULE

JOHN G. PHILLIPS
Yerkes Observatory
Received March 28, 1950

ABSTRACT

By means of a rotational analysis of the 3670 A band, it is shown that the lower state is the $v''=6$ vibrational level of the $^1\Pi_u$ state of C_2. The identification of the upper state is uncertain, but it is most probably the $v' = 7$ vibrational level of the $^1\Pi_g$ state. It is found that the $^1\Pi_g$ state undergoes a strong vibrational perturbation. The presence of such a perturbation will affect the dissociation energy of the $^1\Pi_g$ state derived by a Birge-Sponer extrapolation.

A. INTRODUCTION

Whenever the spectrum of the C_2 molecule is produced in the laboratory, a few bands appear for which the electronic transitions have not yet been determined. The most intense of these additional bands appears at 3670 A, between the (5–4) and the (6–5) tail bands of the Deslandres-D'Azambuja system ($^1\Pi_g - {}^1\Pi_u$) at 3617 A and 3689A, respectively. The structure of the 3670 A band on high dispersion is exactly the same as the structures of these neighboring tail bands. It degrades to the red and consists of a single R and a single P branch. The Q branch is too faint to be observed. The similarity in appearance suggests that the 3670 A band is another member of the Deslandres-D'Azambuja system. Since the band appears in good intensity on plates of the C_2 molecule taken in this laboratory for other purposes,[1] an analysis of the band was undertaken to test the suggestion.

B. ROTATIONAL ANALYSIS

The rotational lines of the 3670 A band could be readily arranged into two series forming the R and P branches, and a parabola was derived which represented the two branches simultaneously. From this parabola relative quantum numbers could be assigned to the rotational lines, but, in view of the fact that the lines in the neighborhood of the band origin were too faint to be observed, it was impossible to find the absolute rotational numbering from the band itself. This was done in an indirect way, as follows.

Herzberg and Sutton in their work on the tail bands of the Deslandres-D'Azambuja system[2] had increased the known vibrational levels to $v' = 6$ of the $^1\Pi_g$ state and to $v'' = 5$ of the $^1\Pi_u$ state. It is easy to show that the 3670 A band, if it is a member of this system, cannot be a transition involving any of these known levels. Herzberg and Sutton found that the B_v''-versus-v''-curve of the lower, $^1\Pi_u$, state is strictly linear to $v'' = 5$. Therefore, no great error could be made if the constants B'' and D'' were computed for v'' equal to 6 and 7 by a short extrapolation from their data. The resulting constants were: $B_6'' = 1.5052\ \text{cm}^{-1}$, $D_6'' = 7.13 \times 10^{-6}\ \text{cm}^{-1}$, $B_7'' = 1.4880\ \text{cm}^{-1}$, and $D_7'' = 7.26 \times 10^{-6}\ \text{cm}^{-1}$. The usual equations were used to compute combination differences for these two additional vibrational levels of the lower state. Arbitrary sets of rotational numbers J were then assigned to the lines of the 3670 A band, and the corresponding observed combination differences, $\Delta_2F''(J) = R(J-1) - P(J+1)$, were compared with the computed sets for $v'' = 6$ and 7. It was found that one of the numberings provided combination differences which agreed exactly within the error of measurement with those

[1] John G. Phillips, *Ap. J.*, **110**, 73, 1949.

[2] G. Herzberg and R. B. Sutton, *Canadian J. Res.*, *A*, **18**, 74, 1940.

computed for the level $v'' = 6$. This numbering is the one given in Table 1, which lists the component lines of the two branches. The comparison of combination differences is shown in Table 2. The possibility of such an agreement's being fortuitous is so remote that it may be said definitely that the lower level of the 3670 A band is the $v'' = 6$ level of the $^1\Pi_u$ state of C_2 and that the correct rotational numbering of the band has been found. The adopted numbering was later confirmed by the discovery of a rotational perturbation setting in at $R(22)$ and $P(24)$, indicating that the rotational levels of the upper state with $J' = 23$ and higher were perturbed.

TABLE 1

WAVE NUMBERS OF LINES OF THE 3670 A BAND
($\nu_0 = 27220.16$ Cm^{-1})

J	$R(J)$ (Cm^{-1})	$P(J)$ (Cm^{-1})	J	$R(J)$ (Cm^{-1})	$P(J)$ (Cm^{-1})
1	27,224.76		19	27,188.47	27,088.80
2	226.57	27,213.66	20	182.00	077.25
3	227.85	209.86	21	174.77	065.49
4	228.77	205.55	22	166.91	053.07
5	229.17	200.84	23	161.85	040.07
6	229.17	195.68	24	151.81	026.11
7	228.77	190.11	25	143.77	014.96
8	227.85	184.09	26	133.55	26,999.18
9	226.57	177.64	27	124.44	985.22
10	224.76	170.73	28	113.14	969.03
11	222.66	163.46	29	103.08	954.19
12	219.87	155.64	30	090.82	
13	216.88	147.50	31	079.58	
14	213.20	138.76	32	066.28	
15	209.32	129.77	33	053.89	
16	204.68	120.11	34	039.41	
17	199.87	110.23	35	026.11	
18	194.39	099.79	36	010.27	

TABLE 2

COMPARISON OF OBSERVED COMBINATION DIFFERENCES OF 3670 A BAND WITH THOSE COMPUTED FOR $v'' = 6$ OF $^1\Pi_u$ STATE OF C_2

J	$\Delta_2F''(J)_{obs}$ (Cm^{-1})	$\Delta_2F''(J)_{comp}$ (Cm^{-1})	J	$\Delta_2F''(J)_{obs}$ (Cm^{-1})	$\Delta_2F''(J)_{comp}$ (Cm^{-1})
2	14.90	15.05	16	99.09	99.09
3	21.02	21.07	17	104.89	105.06
4	27.01	27.09	18	111.07	111.02
5	33.09	33.10	19	117.14	116.98
6	39.06	39.12	20	122.98	122.94
7	45.08	45.13	21	128.93	128.88
8	51.13	51.14	22	134.70	134.82
9	57.12	57.15	23	140.80	140.75
10	63.11	63.15	24	146.89	146.67
11	69.12	69.15	25	152.63	152.58
12	75.16	75.15	26	158.55	158.49
13	81.11	81.14	27	164.52	164.39
14	87.11	87.13	28	170.25	170.27
15	93.09	93.11			

With the rotational numbering known, it was immediately possible to find the rotational constants of the upper state. These are: $B'_v = 1.2910$ cm^{-1} and $D'_v = 16.8 \times 10^{-4}$ cm^{-1}. The band origin, ν_0, is at 27220.16 cm^{-1}. The rotational constants are presented in Table 3, which also includes, for comparison purposes, the constants of the $^1\Pi_g$ state as determined by Herzberg and Sutton. As will be shown below, the vibrational number of the upper state of the 3670 A band is uncertain, so that the symbol x has been used in Table 3 for the vibrational number.

C. DETERMINATION OF THE UPPER STATE

By introducing the origin of the 3670 A band into the energy-level diagram derived by Herzberg and Sutton, we find that the upper vibrational level is 1601.42 cm^{-1} above the $v' = 6$ level of the $^1\Pi_g$ state, as shown in Figure 1. This new level is indicated in the figure as having $v = x$. It is not possible to determine definitely the correct vibrational numbering of this level by extrapolation from the lower levels, since it lies above the extrapolated dissociation limit found by Herzberg and Sutton, shown in Figure 1 by the dashed line. Also no other bands are found in the spectrum arising from this new level.

TABLE 3

ROTATIONAL CONSTANTS OF THE $^1\Pi_g$ STATE

v	B_v (Cm^{-1})	$D_v \cdot 10^6$ (Cm^{-1})	v	B_v (Cm^{-1})	$D_v \cdot 10^6$ (Cm^{-1})
0	1.7734	7.1	4	1.6175	17
1	1.7490	8.0	5	1.5227	25
2	1.7186	9.1	6	1.4096	23
3	1.6784	12	x	1.2910	16.8

However, if the new level is associated with the $^1\Pi_g$ state, it may be shown that it is most probably the $v' = 7$ level, as follows: If it is assumed, for example, that the new level is the $v' = 8$ level, then the $v' = 7$ level must be present in the interval between the new level and the one with $v' = 6$. Bands arising from the $v' = 7$ level were looked for in the spectrum, but none were found in any of the regions corresponding to any likely location of the $v' = 7$ level. The nonexistence of these additional bands, while suggestive, cannot be taken as positive proof of the nonexistence of an intermediate level, since the overlap of wave functions might be such that the intensity of the (8–6) band is high.

The difficulty experienced in obtaining the correct identification of the upper level may be illustrated in another way. If the 3670 A band is identified as the (7–6) or possibly the (8–6) band, then it can be shown that a vibrational perturbation has displaced the upper level from its expected position. This is obvious, if $v' = 7$, because then $\Delta G_{6\,1/2}$ is twice as large as would be expected on the basis of an extrapolation from lower levels. The case of $v' = 8$ is illustrated in Figure 1. The potential curve to $v' = 6$ was derived from the known vibrational and rotational constants by the method of Klein.[3] Assuming that the new level has $v' = 8$, Oldenberg's equation,

$$\int \sqrt{2\mu\,[V(r) - E_v]}\,dr = h\,(v + \tfrac{1}{2}),$$

can be used to find the course of the potential curve between levels $v' = 6$ and $v' = 8$. In this equation μ is the reduced mass, $V(r)$ the potential energy at the internuclear distance r, and E_v the vibrational energy at level v. The resulting potential curve is shown in Figure 1 by the dotted line. It is difficult to imagine a set of circumstances which

[3] O. Klein, *Zs. f. Phys.*, **76**, 226, 1932.

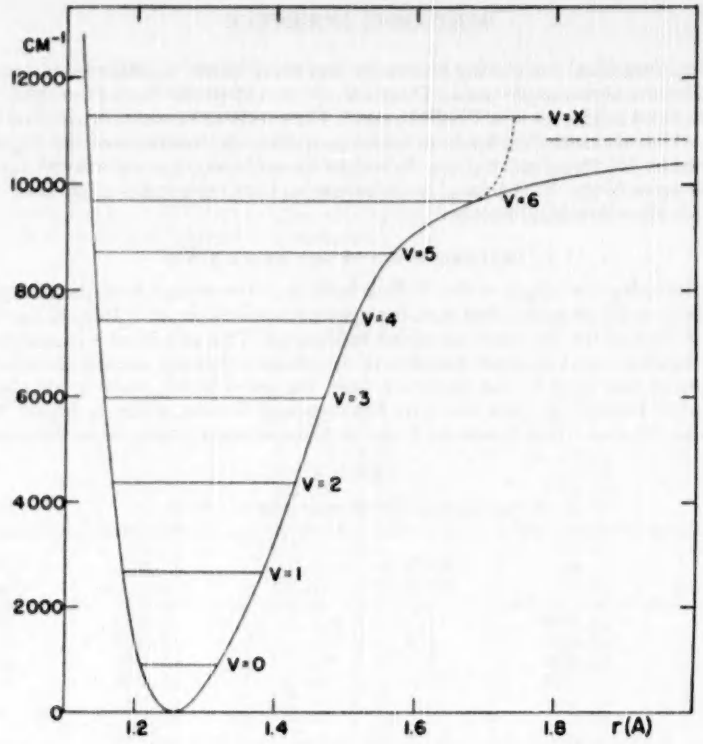

FIG. 1.—The potential curve and energy levels of the $^1\Pi_g$ state of the C_2 molecule

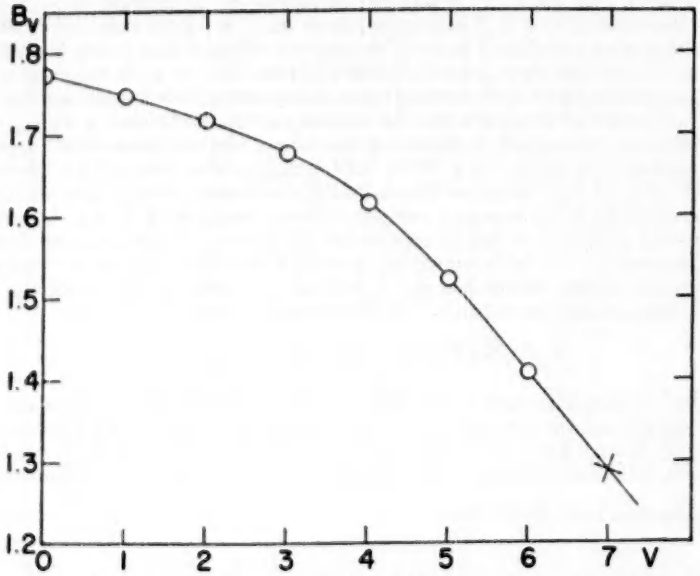

FIG. 2.—The rotational constants, B_v, of the $^1\Pi_g$ state of the C_2 molecule

would produce an unperturbed potential curve with such an inflection point. Thus the only possible explanation of the location of the upper vibrational level of the 3670 A band is that a vibrational perturbation is taking place. The perturbing state must be another $^1\Pi_g$ state, and bands would be expected to appear in the spectrum as the result of transitions between this new $^1\Pi_g$ state and the $^1\Pi_u$ state. The possibility exists that the 3670 A band is associated with this new transition. Thus it is not even possible to identify definitely the upper electronic state associated with the 3670 A band.

Such a vibrational perturbation would be expected to have little effect on the rotational constants of the perturbed vibrational states, since all rotational levels of a given vibrational state would be perturbed by approximately the same amount. In Figure 2 the rotational constants B_v of the $^1\Pi_g$ state are plotted against v. If the resulting curve is extrapolated to $v = 7$, a B_7 may be predicted which is close to that found for the upper level of the 3670 A band, indicated in the figure by x. This fact tends to support the suggestion that the upper level of the 3670 A band has $v' = 7$. However, it cannot be taken as a conclusive proof of the identification, since the agreement may be fortuitous if the 3670 A band is associated with a new transition from the perturbing $^1\Pi_g$ state.

To summarize the results of this section, it is most probable that the upper state of the 3670 A band is the $v' = 7$ vibrational level of the $^1\Pi_g$ state, which is therefore perturbed by another $^1\Pi_g$ state. The perturbation has the effect of reducing the vibrational quanta for levels with $v' \lesssim 6$ and of increasing the quantum for the level with $v' = 7$.

It is interesting in this connection to note that, in 1942, Gerö and Schmid[4] suggested that the rapid convergence of the lower vibrational levels of the $^1\Pi_g$ state of the Deslandres–D'Azambuja system, as observed by Herzberg and Sutton, was caused by a vibrational perturbation, so that the determination of the dissociation limit of this state by an extrapolation from the lower levels is not valid. The present discussion of the 3670 A band tends to support their argument. At the present time no improved suggestion as to the dissociation limit can be made, since the course of the potential curve for still higher vibrational energies is unknown.

In conclusion, I wish to thank Dr. G. Herzberg and Dr. S. Chandrasekhar for many helpful discussions during the course of this investigation.

[4] L. Gerö and R. F. Schmid, *Phys. Rev.*, **62**, 82, 1942.

FINE STRUCTURE OF N_2O BANDS IN THE INFRARED SOLAR SPECTRUM*

MARCEL V. MIGEOTTE†
Mendenhall Laboratory of Physics, Ohio State University, Columbus
Received April 12, 1950

ABSTRACT

Absorption bands due to N_2O in the earth's atmosphere have been observed and resolved under high dispersion near 8.6 μ, 4.5 μ, and 3.9 μ. The first of these is the band $2\nu_2$ observed by Plyler and Barker, while the second is the fundamental ν_3. This band is readily resolved in the atmosphere but is difficult to resolve in the laboratory. The N_2O band at 3.9 μ was observed and resolved in an exploration but was not measured again owing to technical difficulties.

The presence of N_2O in the earth's atmosphere was first suggested by A. Adel[1, 2] to explain a band appearing in the 7.6 μ region of the prismatic solar spectrum. The evidence for N_2O was further increased by finding an additional weak absorption band at 8.6 μ, which could also be attributed to N_2O.[2] In 1941 the same author[3] claimed to have identified the individual rotational lines of N_2O in the atmospheric spectrum around 7.7 μ. However, in 1943, G. B. B. M. Sutherland and G. S. Callendar[4] pointed out that the evidence for N_2O, while strong, was not entirely conclusive. In particular, it was noted that the high-resolution solar spectrograms published by A. Adel[5] in 1941 did not show the fine structure of the 8.6 μ band of N_2O.

In June, 1948, at the Pasadena meeting of the A.A.S., the present author[6] stated that the presence of N_2O in the earth's atmosphere was confirmed, as the fine structures of the N_2O bands at 8.6, 4.5, and 3.9 μ appeared clearly on new solar spectrograms taken at Columbus, Ohio. Independently, J. H. Shaw, G. B. B. M. Sutherland, and T. W. Wormell[7] found bands of N_2O at 4.5, 4.06, and 3.9 μ during the last week of July, 1948, on solar spectrograms taken at Cambridge, England, with a lithium fluoride prism. In 1949, R. McMath[8] and O. Mohler and A. K. Pierce[9] mentioned the presence of fine structures due to N_2O, between 2 and 3.6 μ, on solar spectrograms taken at the McMath-Hulbert Observatory, Pontiac, Michigan.

The purpose of this paper is to give the results of our observations made in the 8.6 and 4.5 μ regions of the solar spectrum. They were obtained at Columbus, Ohio, by using a prism-grating spectrograph built by Dr. R. Noble, under the direction of Professor H. H.

* Supported by the Air Materiel Command, Wright Patterson Air Force Base, and the Ohio State University Research Foundation.

† Now at the Institut d'Astrophysique, University of Liége, Belgium.

[1] *Ap. J.*, **88**, 186, 1938.

[2] *Ibid.*, **90**, 627, 1939.

[3] A. Adel, *ibid.*, **93**, 509, 1941.

[4] *Rep. Prog. Phys.*, **9**, 18, 1943.

[5] *Ap. J.*, **94**, 451, 1941.

[6] M. Migeotte, *A.J.*, **54**, 45, 1948. The confirmation of the atmospheric N_2O was first stated by the author at the Symposium on Molecular Structure and Spectroscopy, held at the Ohio State University, from June 14 to June 19, 1948.

[7] *Phys. Rev.*, **74**, 978, 1948.

[8] *A.J.*, **54**, 214, 1949.

[9] *Pub. A.S.P.*, **61**, 221, 1949.

Nielsen. It is an instrument of the Pfund type,[10] the parabolic mirrors having a focal length of 100 cm. A grating with 3600 lines per inch (dimensions: $5\frac{1}{2}'' \times 3\frac{1}{2}''$) was used for the 8.6$\mu$ region, and a grating with 7200 lines per inch (dimensions: $5\frac{1}{2}'' \times 4''$) for the 4.5 μ region. Both gratings were replicas made by R. W. Wood. The receiver was a Perkin-Elmer amplifier, the beam being chopped five times per second.

Figure 1 shows the fine structure obtained in the solar spectrum, between 8.56 and 8.84 μ on July 6, 1948. The record was taken at 9:30 and 10:00 A.M. (Eastern Daylight Saving time), the mean solar height being 51°. The intense absorption lines reproduced in Figure 1 can easily be found on the spectrograms published by A. Adel,[5] but the weak lines are new. Most of them correspond to the fine structure of the N_2O band $2\nu_2$ at 8.6 μ, published by E. K. Plyler and E. F. Barker.[11]

In Table 1 the measurements on the solar spectrum are given in the first and second columns. For the sharp lines, the accuracy on the wave numbers is estimated to about ± 0.05 cm^{-1}, which corresponds to ± 4 A, in the 8.6 μ region.

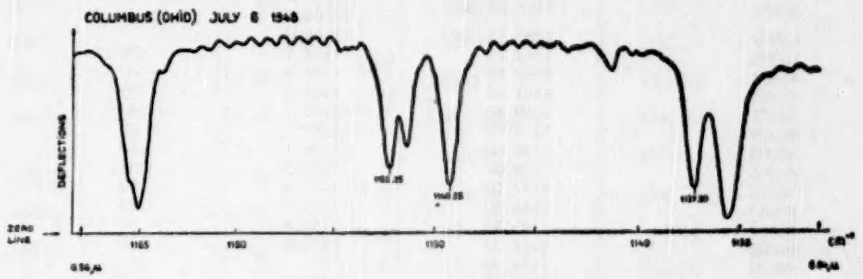

FIG. 1.—The solar spectrum between 8.56 μ and 8.84 μ

The abbreviations "*int.*" indicate the most intense lines, also observed by A. Adel. When a line appears only as an inflexion, the corresponding wave number is marked by "inf." In the third column the measurements of Plyler and Barker on N_2O are given. The wave numbers in parentheses indicate the N_2O lines which are masked by intense lines appearing in the solar spectrum. The last column gives the difference, sun−lab., when there is a correspondence between the lines appearing on the solar and the laboratory records. It shows a systematic difference of about 0.3 cm^{-1}. The measurements on the solar spectrum are based on a mean "spectrograph constant,"[12] which has been determined by using lines measured by A. Adel[5] at 1152.26, 1149.27, and 1137.19 cm^{-1}.

The laboratory data extend from 1203.0 to 1139.2 cm^{-1}, but, in the solar spectrum, most of the N_2O lines from the 8.6 μ band are masked by stronger absorption lines, outside the region given in Figure 1.

The solar spectrum between 4.46 and 4.59 μ is reproduced in Figure 2. It was recorded on June 16, 1948, from 12:00 to 12:30 (Eastern Daylight Saving time), the mean solar height being 71°. The measurements are listed in the first and second columns of Table 2, spacings in the third. For the sharp lines, the accuracy on the wave numbers is estimated to about ± 0.05 cm^{-1}, which corresponds to ± 1 A in the 4.5 μ region.

[10] For the description of an instrument using the same kind of optics for the grating spectrograph see *Phys. Rev.*, **38**, 2162, 1931.

[11] *Phys. Rev.*, **38**, 1827, 1931.

[12] For a definition of the spectrograph constant see C. F. Meyer, *The Diffraction of Light, X-rays, and Material Particles* (2d rev. ed.; Chicago: University of Chicago Press, 1949), p. 144.

The constant of the spectrograph[12] was computed by using four lines of *CO* located at 2158.98, 2155.28, 2128.36, and 2132.31 cm^{-1} in the solar spectrum.[13] These wave numbers have been computed by K. N. Rao,[14] who revised the values published by R. T. Lageman, A. H. Nielsen, and F. P. Dickey.[15]

TABLE 1

LINES OF N_2O BETWEEN 8.56 AND 8.84 μ IN THE SOLAR SPECTRUM

Solar Spectrum		N_2O Lines Measured by Plyler and Barker*	Diff Sun−Lab.
Wave Length (A)	Wave Number (Cm^{-1}) (Air)	Wave Number (Cm^{-1}) (Air)	(Cm^{-1})
85726	1166.50 (inf.)	(1167.8)	
85800	1165.50 (inf.)	(1166.4)	
85833	1165.05 (*int.*)	(1165.5) (1164.6)	
85929	1163.75 (inf.)	(1164.0)	
86003	1162.75	1163.1	−.35
86051	1162.10	1162.3	−.20
86103	1161.40	1161.6	−.20
86177	1160.40	1160.7	−.30
86229	1159.70	1159.9	−.20
86296	1158.80	1159.1	−.30
86356	1158.00	1158.3	−.30
86423	1157.10	1157.4	−.30
86483	1156.30	1156.6	−.30
86543	1155.50	1155.8	−.30
86602	1154.70	1155.0	−.30
86625	1154.40		
86659	1153.95	1154.2	−.25
86723	1153.10 (inf.)	1153.3	−.20
86787	1152.25 (*int.*)	(1152.6)	
86851	1151.39 (*int.*)	(1151.8)	
		(1151.0)	
		(1150.2)	
87013	1149.25 (*int.*)	(1149.5)	
87089	1148.25 (inf.)	1148.7	−.45
87138	1147.60	1148.0	−.40
87207	1146.70	1147.1	−.40
87268	1145.90	1146.3	−.40
87329	1145.10	1145.4	−.30
87386	1144.35	1144.7	−.35
87439	1143.65	1144.0	−.35
87458	1143.40		
87508	1142.75	1143.10	−.35
		(1142.20)	
87623	1141.25 (*int.*)	(1141.50)	
87696	1140.30	1140.70	−.40
87731	1139.85	(1140.0)	
87935	1137.20 (*int.*)	(1139.2)	
88059	1135.60 (*int.*)		
88222	1133.50		
88292	1132.60		

* *Phys. Rev.*, **38**, 1827, 1931.

[12] The presence of the *CO* lines in the solar spectrum has been reported by M. Migeotte, *Phys. Rev.*, **75**, 1108, 1949.

[14] K. N. Rao, private communication. A correction of 0.57 cm^{-1} was added to the values given by Rao, to obtain the wave numbers in air.

[15] *Phys. Rev.*, **72**, 284, 1947.

TABLE 2

THE SOLAR SPECTRUM BETWEEN 4.46 AND 4.59 μ

Wave Length (A)	Wave Number (Cm^{-1}) (Air)	Spacings	Wave Length (A)	Wave Number (Cm^{-1}) (Air)	Spacings
44838	2230.25	0.85	45284	2208.30	1.
44855	2229.40	0.65	45304	2207.30	1.
44868	2228.75	0.75	45325	2206.30	0.95
44883	2228.00	0.85	45344	2205.35	0.95
44900	2227.15	0.85	45364	2204.40	0.90
44917	2226.30	0.50	45382	2203.50	1.15
44928	2225.80 (inf.)	0.60	45406	2202.35	1.
44940	2225.20	0.55	45427	2201.35	0.85
44950	2224.65		45444	2200.50	1.15
			45468	2199.35	1.10
44972	2223.60	0.80	45491	2198.25	1.
44988	2222.80	0.80	45511	2197.25	1.15
45004	2222.00	0.95	45535	2196.10	1.05
45024	2221.05	0.90	45557	2195.05	1.
45042	2220.15	0.85	45578	2194.05	0.95
45059	2219.30	0.80	45597	2193.10	1.10
45075	2218.50	0.95	45620	2192.00	1.
45095	2217.55	0.90	45641	2191.00	1.
45113	2216.65	0.90	45662	2190.00	
45131	2215.75	0.95	45693	2188.50	
45151	2214.80	0.90	45712	2187.60	
45169	2213.90	0.90	45732	2186.65 (inf.)	
45187	2213.00	0.90	45755	2185.55	
45206	2212.10	0.95	45782	2184.25	1.10
45225	2211.15	0.85	45805	2183.15	1.05
45243	2210.30	1.	45827	2182.10	1.10
45263	2209.30	1.	45850	2181.00	
			45858	2180.60 (inf.)	
			45871	2180.00 (inf.)	
			45895	2178.85	
			45919	2177.75	
			45938	2176.85	

In Figure 2 a peak of less absorption has been marked at 2224.25 cm^{-1}. In this region the solar spectrum corresponds in general appearance with the ν_3 absorption band of N_2O, located at 2224.1 cm^{-1} by Plyler and Barker.[11] However, these authors do not give the measurements of the individual lines, and the following statement concerning the fine structure of this band may be quoted from their paper:

> Although many trials were made to determine the optimum conditions for resolution, no clear cut rotation series could be obtained. From certain sections of the band it is evident that the line spacing is the same as in the other fundamentals, but the envelope shows a scalloped appearance for all gas pressures, indicating superposed bands of appreciable intensity. As before, these are probably due to absorption by molecules already vibrating in the lowest frequency modes. The interaction between ν_2 and ν_3 is apparently large, so that the maximum of the positive branch for the first upper stage band falls very near the center of the primary band, which is so obscured that an accurate determination of its position is impossible. The fact that the 7.8 μ band is not so distorted indicates relatively less interaction between ν_1 and ν_2. The frequency indicated as the center, 2224.1 cm^{-1} is that of the lowest point in this portion of the curve.

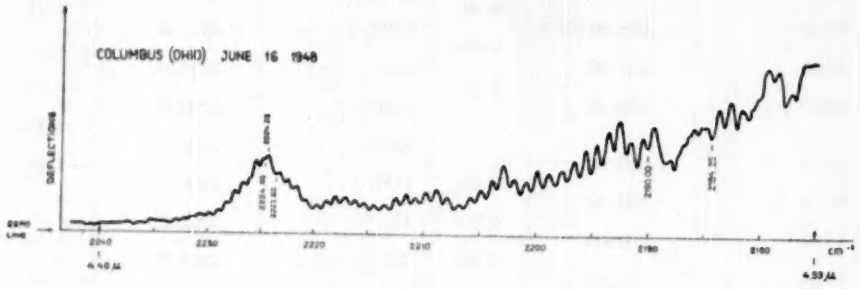

FIG. 2.—The solar spectrum between 4.46 μ and 4.59 μ

The position of this center agrees very well with the one observed in the solar spectrogram.

In the third column of Table 2 the listed differences agree with the spacings found in the N_2O bands located at 17.0, 8.57, and 7.77 μ. It is thus believed that the regularly spaced lines between 2230.25 and 2190.00 cm^{-1} are due to N_2O. The region between 2190.00 and 2184.25 cm^{-1} is perturbed, but the difference between these two lines is 5.75 cm^{-1}, corresponding to six intervals with a mean spacing of 0.95 cm^{-1}, so that the lines 2184.25, 2183.15, 2182.10, and 2181.00 cm^{-1} are also attributed to N_2O.

In the vicinity of 2224.25 cm^{-1} the solar spectrum reveals a regular fine structure, which, as appears from the statement quoted above, had been searched for in vain by Plyler and Barker. The appearance of this fine structure must be due to more favorable conditions, as far as pressure and temperature are concerned. Up to the present, it has not been possible for us to map again the 4.5 μ band of N_2O in the laboratory.

A regular fine structure was also found in the 3.9 μ region on solar spectrograms taken at Columbus, Ohio, but, owing to technical difficulties, new observations are needed before the measurements can be published.

It is a pleasure to thank Professor H. H. Nielsen for the facilities given to us during our stay at the Ohio State University. We have been stimulated by his great interest in our work.

PHOTOELECTRIC STUDIES. IV. COLOR-LUMINOSITY ARRAY FOR STARS IN THE REGION OF THE SUN*

OLIN J. EGGEN
Lick Observatory, University of California
Received March 20, 1950

ABSTRACTS

Introduction.—Magnitudes and colors of 180 stars have been determined with the photomultiplier photometer attached to the Lick Observatory 12-inch refractor; an additional 8 stars have been observed with the Crossley reflector.

Observations of the nearest stars.—The results of 245 observations of 78 stars within 14 parsecs of the sun are listed in Table 3. The color-luminosity array for these stars, derived from trigonometric parallaxes, is shown in Figure 1.

Subgiant extension of the bright-dwarf sequence.—The mean absolute photographic magnitude of 17 subgiants is $+3.60 \pm 0.13$(A.D.) and is apparently independent of the color C_p, which ranges from +0.32 to +0.97 mag. It appears that the secondary components of Algol-type eclipsing stars are subgiants.

Dwarf and subdwarf sequences.—The dwarf and subdwarf sequences intersect twice, once near $C_p = +0^m55$ and again near $C_p = +1^m30$.

Blue-dwarf and bright blue-dwarf sequences.—It appears that at least some of the fine structure in that portion of the color-luminosity array populated by the A-type stars probably is reflected in the spectra of these stars.

Rotational velocity.—The bright blue-dwarfs, which include the spectrum variables, appear to rotate more slowly, in the mean, than do the blue-dwarfs.

Concluding remarks.—The stars near the sun populate the same sequences in the color-luminosity array that are found in the four galactic clusters, Hyades, Pleiades, Coma Berenices, and Ursa Major.

I. INTRODUCTION

The preceding three papers[1] of this series have been concerned with the color-luminosity arrays for the stars in four galactic clusters. The present communication is the result of 605 observations of 180 near-by stars made in the last 18 months with the photomultiplier photometer on the Lick Observatory 12-inch refractor; 13 observations of 8 stars made with the Crossley 36-inch reflector are also included. The color system and magnitude convention used in the 12-inch work have been described in Paper I; colors and magnitudes observed with the reflector have been converted to the International System by means of the following formulae:

$$Pg_p = Pe_{cr} - 0^m19 - 0.15C_{cr},$$
$$C_p = +0^m76 + 0.86C_{cr}.$$

The effective wave lengths obtained with the photomultiplier and filters used in the Crossley installation will be discussed in more detail in a succeeding paper of this series, but the results obtained for the Harvard Standard Region C 12, given in Table 1, show the close agreement between refractor and reflector observations. As a further check on the Crossley results for the reddest stars, we may compare the observations of Barnard's star and 119 Tau.

STAR	12-INCH		CROSSLEY	
	Pg_p	C_p	Pg_p	C_p
Barnard's Star	11^m03	$+1^m52$	11^m02	$+1^m52$
119 Tau (CE Tau)	6.10	+1.79	6.09	+1.78

* *Contributions from the Lick Observatory*, Ser. II, No. 30.

[1] *Ap. J.*, **111**, 65, 81, 414, 1950. These will be referred to as "Papers I, II, and III."

If we take the observations of the Harvard Standard Region stars as typical for the magnitude range covered, the average deviation of a single determination from the mean magnitude and color, as a function of magnitude, is shown in the last two columns of Table 2, where the individual observations of these stars are listed. In order to extend the magnitude range to that represented by the observations made with the 12-inch, a few stars selected at random were added to those of the Standard Region in Table 2. Stars A and D in the Region C 12 are used for the determination of the extinction and its dependence upon color whenever this region is observable, so that some 50 observa-

TABLE 1

COLORS AND MAGNITUDES OF STARS IN HARVARD STANDARD REGION C 12

STAR	12-INCH REFRACTOR			CROSSLEY REFLECTOR			MEAN	
	P_{gp}	C_p	n	P_{gp}	C_p	n	P_{gp}	C_p
A	6m54	−0m04	.....	6m55	−0m05	.....	6m54	−0m045
C	7.34	+0.06	3	7.30	+0.07	1	7.33	+0.06
D	7.60	+1.12	.....	7.58	+1.12	.....	7.59	+1.12
E	7.88	+0.865	4	7.84	+0.86	1	7.87	+0.86
F	8.26	+0.24	4	8.30	+0.25	1	8.27	+0.24
G	8.33	+0.23	2	.....	.....	.....	8.33	+0.23
H	8.41	−0.01	4	8.44	0.00	1	8.42	−0.01
I	9.08	+1.16	3	9.10	+1.16	2	9.09	+1.16
L	9.38	+0.36	3	9.39	+0.35	1	9.38	+0.36
M	9.64	+1.20	3	9.66	+1.21	2	9.65	+1.20
N	9.93	+0.40	3	9.97	+0.38	2	9.95	+0.39
O	9.97	+0.955	3	.....	.....	.....	9.97	+0.955
P	10.10	+1.10	2	.....	.....	.....	10.10	+1.10

TABLE 2

INDIVIDUAL OBSERVATIONS OF STARS IN THE RANGE OF MAGNITUDE OBSERVED WITH THE 12-INCH REFRACTOR

STAR	(1)		(2)		(3)		(4)		(5)		MEAN		AVERAGE DEVIATION	
	P_{gp}	C_p	P_{gp}	C_p	P_{gp}	C_p	P_{gp}	C_p	P_{gp}	C_p	P_{gp}	C_p	P_{gp}	C_p
Sirius	− 1m54	−0m075	− 1m53	−0m08	−1m53	−0m07	−1m54	−0m07	−1m52	−0m07	− 1m53	−0m07	±0m01	±0m00
Vega	− 0 08	−0 075	− 0 07	−0 08	−0 09	−0 085	.....	.....	.....	.....	− 0 08	−0 08	± 01	± 00
Altair	+ 0 87	+0 165	+ 0 89	+0 165	.....	.....	.....	.....	.....	.....	+ 0 88	+0 165	± 01	± 00
Fomalhaut	+ 1 11	+0 02	+ 1 11	+0 005	.....	.....	.....	.....	.....	.....	+ 1 11	+0 015	± 00	± 01
ζ Her	+ 3 30	+0 53	+ 3 32	+0 53	.....	.....	.....	.....	.....	.....	+ 3 31	+0 53	± 01	± 00
γ Ser	+ 4 25	+0 41	+ 4 26	+0 40	.....	.....	.....	.....	.....	.....	+ 4 26	+0 405	± 01	± 01
61 UMa	+ 5 92	+0 63	+ 5 91	+0 63	+ 5 92	+0 63	+ 5 93	+0 63	.....	.....	+ 5 92	+0 63	± 01	± 00
C 12 A	+ 6 54	−0 04	+ 6 53	−0 04	+ 6 54	−0 05	+ 6 54	−0 04	−6 54	−0 04	+ 6 54	−0 04	± 00	± 00
C 12 C	+ 7 34	+0 06	+ 7 34	+0 06	+ 7 34	+0 06	+ 7 35	+0 06	−7 34	+0 06	+ 7 34	+0 06	± 00	± 00
C 12 D	+ 7 60	+1 12	+ 7 60	+1 12	+ 7 61	+1 125	+ 7 60	+1 12	−7 60	+1 12	+ 7 60	+1 12	± 00	± 00
C 12 E	+ 7 88	+0 86	+ 7 90	+0 86	+ 7 88	+0 85	+ 7 89	+0 87	.....	.....	+ 7 88	+0 86	± 01	± 00
C 12 F	+ 8 25	+0 235	+ 8 28	+0 24	+ 8 25	+0 235	+ 8 28	+0 24	.....	.....	+ 8 26	+0 24	± 02	± 00
C 12 G	+ 8 33	+0 235	+ 8 33	+0 22	.....	.....	.....	.....	.....	.....	+ 8 33	+0 23	± 00	± 01
C 12 H	+ 8 42	−0 02	+ 8 41	0 00	+ 8 41	−0 01	+ 8 39	0 00	.....	.....	+ 8 41	−0 01	± 01	± 01
C 12 I	+ 9 08	+1 16	+ 9 10	+1 16	+ 9 06	+1 14	.....	.....	.....	.....	+ 9 08	+1 16	± 01	± 01
C 12 L	+ 9 38	+0 36	+ 9 40	+0 38	+ 9 36	+0 34	.....	.....	.....	.....	+ 9 38	+0 36	± 01	± 01
C 12 M	+ 9 66	+1 20	+ 9 61	+1 22	+ 9 66	+1 19	.....	.....	.....	.....	+ 9 64	+1 20	± 02	± 01
C 12 N	+ 9 93	+0 42	+ 9 95	+0 40	+ 9 91	+0 395	.....	.....	.....	.....	+ 9 93	+0 40	± 01	± 01
C 12 O	+ 9 97	+0 96	+10 01	+0 955	+ 9 93	+0 95	.....	.....	.....	.....	+ 9 97	+0 955	± 03	± 00
C 12 P	+10 11	+1 11	+10 09	+1 09	.....	.....	.....	.....	.....	.....	+10 10	+1 10	± 01	± 01
+68°946	+10 36	+1 30	+10 34	+1 30	+10 36	+1 29	.....	.....	.....	.....	+10 36	+1 30	± 01	± 00
+4°3561	+11 03	+1 52	+11 07	+1 53	+10 99	+1 54	.....	.....	.....	.....	+11 03	+1 53	± 03	± 00
−4°4226	+11 25	+1 21	+11 23	+1 23	+11 33	+1 23	+11 23	+1 23	.....	.....	+11 27	+1 23	±0 04	±0 00

tions are available for these two stars; however, only 5 representative determinations are given in Table 2. A screen, absorbing 4.82 mag., was used for Sirius, Vega, and Altair. Although magnitudes and colors have been obtained for stars as faint as $Pg_p = 12^m5$ with the 12-inch refractor, the number of observations necessary to maintain the accuracy shown in Table 2 increases rapidly for stars fainter than $Pg_p = 11^m5$, and, except for special objects, observations are usually confined to stars brighter than $Pg_p = 11^m0$ with this instrument.

II. OBSERVATIONS OF THE NEAREST STARS

Table 3 lists the results for 245 observations of 78 stars within 14 parsecs of the sun. All but 8 of these stars have been observed with the 12-inch refractor, and each star was observed on at least two different nights. A few red dwarfs were observed as often as six to ten nights to test for variability in these stars. The various columns of Table 3 contain the following information: column 1, the current number; column 2, the *Henry Draper Catalogue* or *Durchmusterung* number, when available; column 3, other designations; columns 4 and 5, the 1900 positions; columns 6 and 7, the International photographic magnitude and color derived from the photoelectric observations; column 8, the number of nights each star was observed; column 9, the mean trigonometric parallax (these values are taken from Schlesinger's *Catalogue of Stellar Parallaxes*,[2] determinations made available since the completion of the catalogue have been incorporated into the means); column 10, the absolute photographic magnitude resulting from columns 6 and 9.

The color-luminosity array for the stars in Table 3 is shown in Figure 1. The filled circles represent stars within 10 parsecs of the sun, while the open circles represent the stars that are 10–14 parsecs distant. The continuous curves reproduced in Figure 1 have been taken directly from the previous papers of this series concerning the color-luminosity arrays for four galactic clusters: the zero point for all these arrays is determined by the Hyades cluster stars. The dashed lines in the color-luminosity array of Figure 1 represent the extensions added by the material in this paper. The few giant stars in the vicinity of the sun are not included in Table 3 or in Figure 1, but they will be discussed in a later paper of this series.

III. SUBGIANT EXTENSION OF THE BRIGHT-DWARF SEQUENCE

LUMINOSITY OF SUBGIANTS

The top section of Table 4 contains those stars in Table 3 which are classified with luminosity class IV in the system of the *Atlas*.[3] The middle section of Table 4 contains other parallax stars, more distant than 14 parsecs, for which available spectroscopic luminosity classifications indicate their subgiant nature. The bottom section of Table 4 contains five stars, for four of which no *Atlas* types are available. From the position of these stars in the color-luminosity array, however, we may assign the subgiant classification to them.

If we omit δ Gem, which falls on that portion of the bright-dwarf sequence defined by the cluster stars, we find that the straight mean of the luminosities of the subgiants in the first two sections of Table 4 is $\bar{M} = +3^m60 \pm 0^m13$ (A.D.). This result is the basis for the straight-line extension of the bright-dwarf sequence shown as a dashed line in Figure 1. If we assume that all subgiants redder than $C_p = +0^m32$ have $M = +3^m60$, we find the "photometric," (ptm), parallaxes given in the table. With but one exception, the photometric parallaxes all lie within the range of the individual trigonometric values;

[2] New Haven: Yale University Press, 1936.

[3] The Yerkes *Atlas of Stellar Spectra* (Chicago: University of Chicago Press, 1943), by Morgan, Keenan, and Kellman, will be referred to throughout this paper as the "*Atlas*." The *Atlas* luminosity classes will also be used: III = giants, IV = subgiants, and V = dwarfs.

TABLE 3

PHOTOELECTRIC OBSERVATIONS, LUMINOSITIES, AND TRIGONOMETRIC PARALLAXES FOR 78 STARS WITHIN 14 PARSECS OF THE SUN

No. (1)	HD (DM) (2)	Name (3)	α (1900) (4)	δ (1900) (5)	P_{Lp} (6)	C_p (7)	n (8)	π (Trig.) (9)	$M_{P_{Lp}}$ (10)
1*	+43°44 A	ADS 246 A	0h12m7	+43° 27′	+ 9m41†	+1m34	2	0″.284± 5	+11m67
2*	+43°44 B	ADS 246 B			+12 65†	+1 55	2	.284± 5	+14 91
3*	4614	η Cas	0 43 0	+57 17	+ 3 81	+0 46	3	.184± 5	+ 5 13
4*		Wolf 28	0 43 9	+ 4 55	+12 50†	+0 41	2	.243± 6	+14 43
5*	+61°195 A		0 56 3	+61 48	+10 81†	+1 29	1	.101± 7	+10 83
6*	+61°195 B	Wolf 47	0 57 0	+61 50	+14 90†	+1 29	1	.101± 7	+14 92
7	6582	μ Cas	1 01 6	+54 26	+ 5 69	+0 58	2	.133± 5	+ 6 31
8	10307	HR 483	1 35 7	+42 07	+ 5 36	+0 535	3	.087± 5	+ 5 06
9	10476	107 Psc	1 37 1	+19 47	+ 5 90	+0 71	3	.132± 6	+ 6 50
10	10700	τ Cet	1 39 4	−16 28	+ 4 05	+0 585	3	.298± 6	+ 6 42
11	10780	HR 511	1 40 4	+63 22	+ 6 22	+0 67	2	.111± 5	+ 6 43
12*	13974	δ Tri	2 10 8	+33 46	+ 5 28	+0 49	3	.098± 6	+ 5 24
13*	16160	HR 753 A	2 30 6	+ 6 25	+ 6 68	+0 89	2	.147± 4	+ 7 52
14*		HR 753 B			+12 94†	+1 32	1	.147± 4	+13 78
15	16895	θ Per	2 32 4	+48 48	+ 4 41	+0 395	3	.078± 5	+ 3 87
16	17925	HR 857	2 47 7	−13 11	+ 7 34	+0 96	1	.137± 6	+ 8 02
17	19373	ι Per	3 01 8	+49 14	+ 4 46	+0 50	3	.085± 4	+ 4 11
18	20630	κ Cet	3 14 1	+ 3 00	+ 5 33	+0 585	4	.106± 5	+ 5 46
19	22049	ε Eri	3 28 2	− 9 48	+ 4 87	+0 79	3	.303± 6	+ 6 87
20	26965	40 Eri A	4 10 7	− 7 49	+ 5 12	+0 725	2	.202± 3	+ 6 65
21	30652	π^2 Ori	4 44 4	+ 6 47	+ 4 02	+0 34	3	.128± 5	+ 4 02
22*	32147	HR 1614	4 55 9	− 5 52	+ 7 13	+0 96	3	.105± 4	+ 7 24
23	34411	λ Aur	5 12 1	+40 01	+ 5 12	+0 51	3	.068± 5	+ 4 28
24	36395	Cin 705	5 26 4	− 3 42	+ 9 12	+1 27	3	.166± 4	+10 22
25	37394	HR 1925	5 33 2	+53 26	+ 6 88	+0 75	3	.097± 5	+ 6 81
26*	38393	γ Lep A	5 40 3	−22 28	+ 3 88	+0 36	2	.122± 4	+ 4 31
27*	38392	γ Lep B			+ 6 98	+0 87	2	.122± 4	+ 7 41
28	39587	χ^1 Ori	5 48 5	+20 15	+ 4 86	+0 47	3	.104± 6	+ 4 98
29	48915	α CMa	6 40 7	−16 35	− 1 53	−0 07	5	.376± 3	+ 1 35
30	76943	10 UMa	8 54 2	+42 11	+ 4 28	+0 33	3	.073± 4	+ 3 60
31	82885	11 LMi	9 29 7	+36 16	+ 6 00	+0 66	3	.113± 6	+ 6 26
32	88230	Gmb 1618	10 05 3	+49 55	+ 7 96	+1 23	3	.220± 8	+ 9 67
33	+20°2465	Cin 1244	10 14 2	+20 22	+10 63	+1 32	3	.202± 6	+12 16
34*	90839	36 UMa A	10 24 2	+56 30	+ 5 19	+0 41	2	.082± 8	+ 4 76
35*	+56°1458	36 UMa B			+ 9 94	+1 21	4	.082± 8	+ 9 51
36*	+57°1266	36 UMa C			+ 8 99	+0 87	3	.082± 8	+ 8 56
37	95735	Lal 21185	10 57 9	+36 38	+ 8 78	+1 32	2	.392± 6	+11 75
38	+66°717	Cin 1383	11 14 8	+66 23	+10 52	+1 28	5	.120± 5	+10 92
39	101501	61 UMa	11 35 8	+34 46	+ 5 92	+0 63	4	.109± 9	+ 6 11
40	102870	β Vir	11 45 5	+ 2 20	+ 4 00	+0 49	3	.097± 6	+ 3 93
41	103095	HR 4550	11 47 2	+35 26	+ 7 05	+0 635	5	.108± 4	+ 7 22
42	109358	β CVn	12 29 0	+41 54	+ 4 72	+0 48	4	.108± 6	+ 4 93
43	111631	Cin 1633	12 45 6	− 0 13	+ 9 68	+1 26	3	.098± 7	+ 9 64
44	114710	β Com	13 07 2	+28 23	+ 4 63	+0 47	2	.121± 6	+ 5 05
45	115617	61 Vir	13 13 2	−17 45	+ 5 21	+0 60	3	.116± 6	+ 5 77
46	+11°2576	CC 782	13 24 9	+10 55	+10 37	+1 28	3	.123±10	+10 82
47	121370	η Boo	13 50 0	+18 54	+ 3 22	+0 52	3	.116±11	+ 3 54
48	141004	λ Ser	15 41 6	+ 7 40	+ 4 87	+0 52	2	.095± 5	+ 4 76
49	142860	γ Ser	15 51 9	+15 59	+ 4 26	+0 405	2	.078± 7	+ 3 72
50*	147379	Cin 2184 A	16 16 5	+67 29	+ 9 79	+1 23	4	.093± 4	+ 9 63
51	150680	ξ Her	16 37 5	+31 47	+ 3 31	+0 53	2	.113± 3	+ 3 57
52	151288	Cin 2238	16 41 4	+33 41	+ 9 34	+1 23	4	.113± 6	+ 9 60
53*	154363	CC 1017	16 59 8	− 4 54	+ 8 94	+1 07	4	.091± 4	+ 8 74
54*	−4°4226	CC 1018	17 00 0	− 4 55	+11 27	+1 23	4	.091± 4	+11 07
55	157214	72 Her	17 16 9	+32 36	+ 5 85	+0 49	2	.076± 6	+ 5 25
56	157881	Cin 2322	17 20 8	+ 2 14	+ 8 74	+1 21	9	.124± 5	+ 9 31
57*	160269	26 Dra	17 33 9	+61 58	+ 5 66	+0 48	5	.073± 4	+ 4 98
58	+68°946	Cin 2354	17 37 0	+68 26	+10 36	+1 30	3	0 213± 5	+11 94

TABLE 3—*Continued*

No. (1)	HD (DM) (2)	Name (3)	α (1900) (4)	δ (1900) (5)	P_{tp} (6)	C_p (7)	n (8)	π (Trig.) (9)	$M_{P_{0p}}$ (10)
59*	+4°3561	CC 1069	17h52m9	+ 4°25′	+11m03	+1m53	9	0″.543± 3	+14m71
60	166620	HR 6806	18 06.4	+38 28	+ 7.13	+0.79	3	.098± 7	+ 7.09
61*	170153	χ Dra	18 22.9	+72 41	+ 3.94	+0.395	3	.127± 7	+ 4.46
62	172167	α Lyr	18 33.6	+38 41	− 0.08	−0.095	3	.121± 4	+ 0.34
63	180617	CC 1143	19 12.1	+ 5 03	+10.36	+1.28	9	.170± 4	+11.51
64	185144	σ Dra	19 32.6	+69 29	+ 5.31	+0.715	3	.181± 4	+ 6.60
65	187642	α Aql	19 45.9	+ 8 36	+ 0.88	+0.165	2	.208± 5	+ 2.47
66	188512	β Aql	19 50.4	+ 6 09	+ 4.45	+0.77	10	.077± 5	+ 3.88
67	199305	Cin 2707	20 51.3	+61 49	+ 9.78	+1.27	4	.138± 5	+10.49
68*	201091	61 Cyg A	21 02.4	+38 15	+ 6.20†	+1.05	2	.296± 3	+ 8.56
69*	201092	61 Cyg B			+ 7.17†	+1.23	2		+ 9.53
70*	210027	ι Peg	22 02.4	+24 51	+ 4.05	+0.34	3	.077± 6	+ 3.48
71	−15°6290	CC 1387	22 47.9	−14 47	+11.43†	+1.35	1	.220± 11	+13.14
72	216899	CC 1392	22 51.8	+16 20	+ 9.89	+1.285	3	.161± 7	+10.92
73	216956	α Psc A	22 52.1	−30 09	+ 1.11	+0.015	2	.146± 7	+ 1.93
74	217014	51 Peg	22 52.6	+20 14	+ 5.92	+0.54	3	.072± 7	+ 5.21
75	219134	HR 8832	23 08.5	+56 37	+ 6.39	+0.875	4	.160± 6	+ 7.41
76		CC 1445	23 37.0	+43 39	+13.81†	+1.59	1	.316± 9	+16.31
77	+1°4774	Cin 3124	23 44.0	+ 1 52	+10.17	+1.24	3	.167± 6	+11.30
78*	224930	85 Peg	23 56.9	+26 33	+ 6.22	+0.55	5	0.086± 4	+ 5.89

* The notes for stars marked with an asterisk are as follows:

STAR

1, 2. $\rho \sim 40''$, $\theta \sim 60°$.

3. ADS 671, Δm $(Pg) > 4^m$, measured as one star.

4. Van Maanen 2.

5, 6. Common proper motion, $\rho \sim 300''$.

12. Spectroscopic binary.

13, 14. $\rho \sim 160''$, $\theta \sim 100°$.

22. The fact that this star lies 0.75 mag. above the dwarf sequence cannot be wholly the result of a poor parallax, for several modern determinations are in good agreement with one another. The radial velocity is variable in a long period, and the displacement from the dwarf sequence probably is due to a bright companion.

26, 27. ADS 4334, $\rho \sim 100''$, $\theta \sim 0°$.

34, 35, 36. Common proper motion and radial velocity.

50. ADS 10157, Δm $(Pg) > 3^m$, measured as one star.

53, 54. Common proper motion and radial velocity.

57. ADS 10660, Δm $(Pg) > 3^m$, measured as one star.

59. Barnard's proper-motion star.

61. Astrometric and spectroscopic binary.

68, 69. ADS 14636, $\rho \sim 30''$, $\theta \sim 140°$.

70. Spectroscopic binary.

78. ADS 17175, $\Delta m > 3^m$, measured as one star.

† Stars observed with the Crossley reflector.

the exception, 0″.080 for γ Cep, exceeds the mean trigonometric value, 0″.067 ± 5, by only two and a half times the probable error.

It is of interest to compare ε Cep and δ Gem with cluster stars of similar luminosity and color, as in the accompanying tabulation. The Mount Wilson spectral classifications

Star	M	C_p	Spectral Type	
			Mt. W.	*Atlas*
ε Cep	+2m45	+0m22	A6n	F0 V
Hyades 75	+2.55	+0.22	A2	A1, F5 IV=F0 II–III (metallic)
Hyades 47	+2.62	+0.225	A6n	A5(K), F2 (metallic)
δ Gem	+2.64	+0.225	A8n	F2 IV

for ε Cep and δ Gem are taken from *Mount Wilson Contributions*, No. 511;[4] the data for the metallic-line stars are from Paper I. The comparison indicates that the stars ε Cep

[4] *Ap. J.*, **81**, 189, 1934.

and δ Gem are quite similar to the two Hyades metallic-line stars; but perhaps the metallic-line tendencies, if present, are not so pronounced as in the Hyades stars.

Four stars in the last section of Table 4 do not have luminosity classifications available on the *Atlas* system, but spectroscopic absolute magnitudes are given in the Mount Wilson catalogue of spectroscopic parallaxes[4] (see accompanying table). Since the spectro-

Star	Sp.	M (Vis)	Star	Sp.	M (Vis)
74 Ori	F5	$+3^m4$	5 Ser	F6	$+3^m3$
40 Leo	F5	+3.3			
HR 5691	F6	+3.1	Mean	F5.5	+3.3

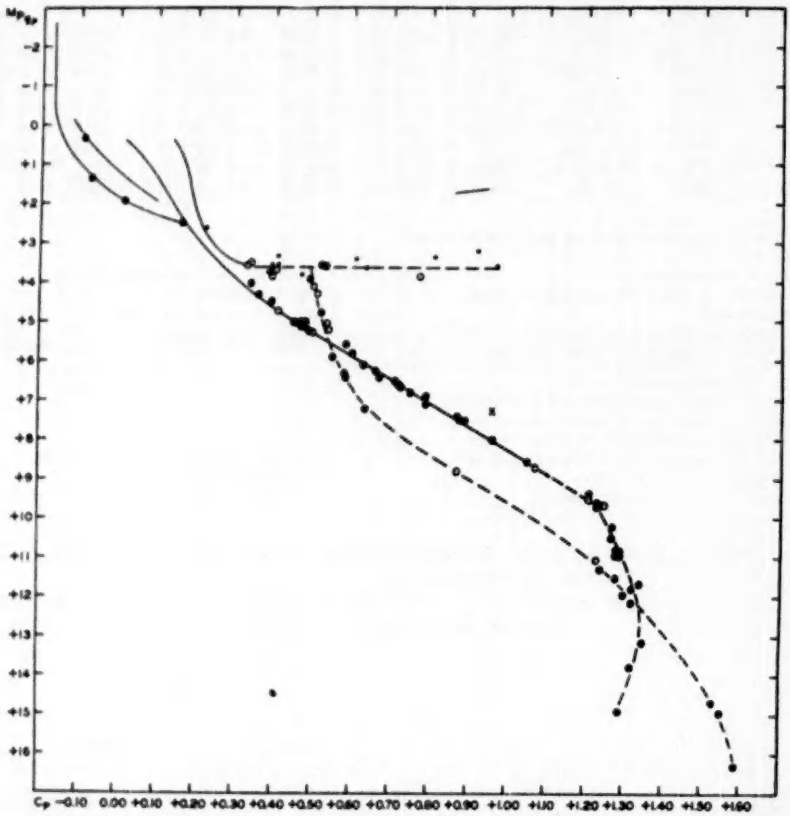

FIG. 1.—Color-luminosity array for stars within 14 parsecs of the sun. The filled circles represent stars within 10 parsecs; the open circles stars from 10 to 14 parsecs distant; and the small dots, along the subgiant extension of the bright-dwarf sequence, those more distant stars in Table 4 that were used to define this portion of the sequence. The continuous lines in the color-luminosity array are defined by cluster stars in Papers I, II, and III, while the dashed lines are added by the stars under the present discussion. The cross at $M = 7.24$, $C_p = 0.96$, represents HR 1614, which probably has an undiscovered bright companion.

TABLE 4

PHOTOMETRIC, SPECTROSCOPIC, AND TRIGONOMETRIC DATA FOR THE NEARER SUBGIANTS

Star	P_{fg}	C_p	n	π (Trig.)	π (Ptm)*	M (Trig.)	*Atlas*†	Remarks
10 UMa	4^{m}28	+0^{m}33	3	0".070 ± 9 (A) .071 ± 10 (M) 0.075 ± 6 (S)				Visual binary with $\Delta m = 1.8$ mag., so the observations probably are little affected
			Mean	0.073 ± 4	0".073	+3^{m}60	F4 IV	
γ Ser	4.26	+ .405	2	0.056 ± 10 (A) 0.101 ± 11 (M)				
			Mean	0.078 ± 7	.074	+3.72	F6 IV	
η Boo	3.22	+ .52	3	0.116 ± 11?	.119	+3.54	G0 IV	Trig. π quoted by Kuiper
ζ Her	3.31	+ .53	2	0.117 ± 9 (A) .110 ± 10 (M) .117 ± 10 (S) 0.104 ± 5 (y)				ADS 10157, $\Delta m = 2.8$ (visual)
			Mean	0.112 ± 3	.115	+3.57	G0 IV	
β Aql	4.45	+ .77	10	0.081 ± 9 (A) .065 ± 16 (S) .069 ± 11 (M) 0.082 ± 8 (Y)				
			Mean	0.072 ± 5	.068	+3.88	G8 IV	
δ Gem	3.75	+ .225	3	0.058 ± 9 (A) .063 ± 7 (M) 0.059 ± 8 (W)				See text
			Mean	0.060 ± 5	.063	(+2.64)	F2 IV	
τ Boo	4.82	+ .385	2	0.048 ± 10 (A) 0.075 ± 10 (M)				
			Mean	0.061 ± 7	.057	+3.75	F6 IV	
ι Psc	4.43	+ .395	3	0.071 ± 9 (M) 0.063 ± 9 (Y)				
			Mean	0.067 ± 6	.068	+3.56	F8 IV	
σ^2 UMa	5.08	+ .395	3	0.037 ± 10 (M) .040 ± 10 (y) 0.078 ± 10 (G)				
			Mean	0.053 ± 6	.051	+3.70	F6 IV	
θ Boo	4.41	+0.41	4	0.066 ± 10 (A) 0.071 ± 11 (M)				
			Mean	0.068 ± 7	0.069	+3.57	F6 IV	

* It should be noted that the differences between the π (Trig.) and π (ptm) are less than the probable errors of the trigonometric parallaxes in sixteen cases, equal in five cases, and greater in one case. A study of the probable errors given by Schlesinger on the basis of agreements between different determinations for each star shows that his probable errors should be reduced by an average factor of 0.7. With the recomputed values of the probable errors, it is found that π (Trig.) − π (ptm) is less in twelve cases and greater in ten. Since Schlesinger had, in general, increased the published probable errors in a manner described in the *General Catalogue of Stellar Parallaxes*, it appears that for these stars, at least, he was overpessimistic.

† The luminosity classes for ι Psc and χ Her are by Nassau and van Albada (*Ap. J.*, **107**, 16, 1948); those for 10 UMa, 10 Tau, and ν^2 CMa are unpublished values determined here by Mrs. Belserene (Emilia Pisani) in connection with Moore and Paddock's radial-velocity program of faint stars (*Ap. J.*, **112**, 48, 1950).

TABLE 4—*Continued*

Star	P_{fp}	C_p	n	π (Trig.)	π (Ptm)*	M (Trig.)	*Alias*†	Remarks
υ And	4^{m}43	+0^{m}41	3	0$''$064 ± 9 (A) 0.055 ± 12 (M)				
			Mean	0.061 ± 7	0$''$068	+3^{m}36	F8 IV	
χ Her	5.03	+ .47	2	0.064 ± 7 (A) 0.049 ± 9 (M)				
			Mean	0.057 ± 6	.052	+3.81	G0 IV	
10 Tau	4.66	+ .48	3	0.056 ± 8 (A) .047 ± 8 (M) 0.060 ± 10 (Y)				
			Mean	0.056 ± 5	.061	+3.40	F7 IV	
70 Vir	5.50	+ .635	3	0.037 ± 8 (A) 0.056 ± 10 (M)				
			Mean	0.042 ± 6	.042	+3.62	G5 IV–V	
η Cep	4.17	+ .81	5	0.069 ± 10 (A) .067 ± 13 (M) 0.069 ± 12 (y)				
			Mean	0.069 ± 7	.076	+3.36	K0 IV	
γ Cep	4.07	+ .92	2	0.066 ± 10 (A) .065 ± 8 (M) 0.070 ± 10 (G)				
			Mean	0.067 ± 5	.080	+3.20	K1 IV	
ν^2 CMa	4.88	+ .97	2	0.059 ± 9 (M) 0.051 ± 8 (Y)				
			Mean	0.055 ± 6	0.055	+3.58	K2 III–IV	
					Mean	+3.60 ± 0.13(A.D.)		
ϵ Cep	4.28	+ .22	3	0.030 ± 9 (A) .056 ± 10 (M) .063 ± 14 (y) 0.029 ± 13 (S)				Discussed in text
			Mean	0.043 ± 5	0.045	(+2.45)	F0 V	
74 Ori	5.30	+ .33	3	0.042 ± 7 (A)	.046	+3.42	.....	‡
40 Leo	5.07	+ .37	3	0.051 ± 11 (A)	.051	+3.60	.....	‡
HR 5691	5.51	+ .44	3	0.046 ± 6 (A) .045 ± 10 (M) 0.051 ± 9 (G)				
			Mean	0.047 ± 5	.042	+3.87	.....	
5 Ser	5.39	+0.47	3	0.033 ± 8 (A) .035 ± 12 (M) 0.048 ± 10 (Y)				
			Mean	0.038 ± 6	0.044	+3.29	.....	

‡ Further trigonometric parallaxes are necessary before 74 Ori and 40 Leo can be definitely assigned to the bright-dwarf or dwarf sequences. The fact that the luminosity difference between the two sequences near the color of these stars is very small will make the assignment difficult unless spectroscopic criteria are applicable.

scopic luminosity is in terms of visual magnitudes, we must add +0.4 mag., the color of F5.5 taken from Figure 2, to the mean, which yields $\bar{M} = +3^m.7$, in excellent agreement with the value of $\bar{M} = +3^m.60 \pm 0^m.13$ (A.D.) for the subgiants in Table 4.

The relationship between color and spectral types of the subgiants is given in Figure 2, from *Atlas* spectral types only. It is a curious fact that subgiants of type later than K2 must be quite rare, since none have been found in the following three independent surveys:

1. "*Atlas*."—No subgiants of type later than K2 are included in this monograph.
2. *Keenan*.[5]—In determining the spectroscopic luminosities and spectral types for stars brighter than the eighth visual magnitude and of *Henry Draper Catalogue* types G5–K5 in two fields—one in Cassiopeia and the other centered at the north galactic pole—Keenan found that "... among the stars later than K2, none was classified as a subgiant; this was true also of the calibration stars."
3. *McCuskey*.[6]—Observations of spectra of all stars to photographic magnitude 10.5 in a field in Aquila of 14.3 square degrees revealed no subgiants later than K0.

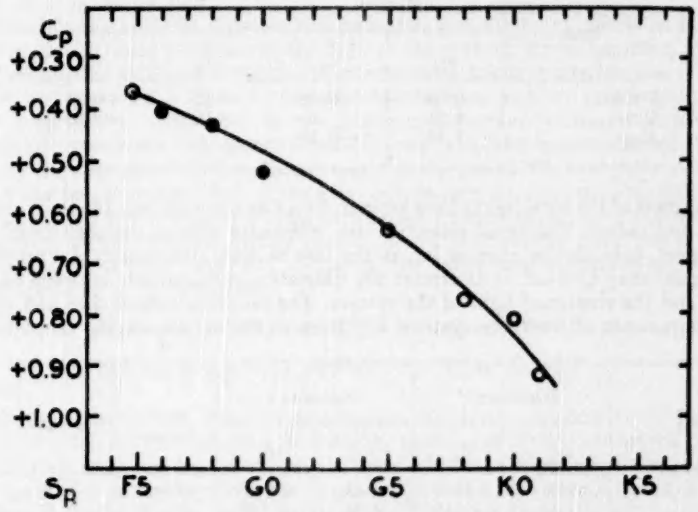

FIG. 2.—The color–spectral-type relationship for subgiants (luminosity class IV) in the *Atlas*. The open circles represent individual stars; the filled circles, means of two or more stars of the same spectral type.

Since the subgiants redder than $C_p = +0^m.32$ appear to be of constant photographic luminosity, surveys Nos. 2 and 3 above may indicate the luminosity function of subgiants in the regions covered. The lack of subgiants later than K2, however, might mean only that the spectroscopic-luminosity criteria are not valid for later types, since the brighter visual magnitude may place these stars, *spectroscopically*, in the category of normal giants.

Since the relationship between color and magnitude of the subgiants is dependent upon the region of the spectrum in which we observe these quantities, it is accidental that the photographic absolute magnitude is essentially constant for all subgiants redder than

[5] *Ap. J.*, 91, 506, 1940.

[6] *Ap. J.*, 109, 426, 1949.

$C_p = +0^m32$ (regardless of color).[7] It is, however, a fortunate accident, and it may have many astrophysical applications. A good example of such an application is to the study of those eclipsing systems possessing either one or two subgiant components. A program to observe these systems is now in progress at this observatory, and a few preliminary results, relevant to the subject under discussion, follow.

SUBGIANTS IN ECLIPSING BINARIES

Algols.—An Algol system usually contains a small, bright, late B- or early A-type component and a fainter, larger subgiant companion. Three classical examples of this type of system are U Cep, U Sge, and the prototype star itself. All three of these systems have been observed at maximum light, and U Cep and U Sge have also been observed during the total phase of the primary eclipse. The results are given in the accompanying tabulation. The depths of the total eclipses immediately give the luminosities of the brighter

Star	Maximum		Total Eclipse	
	P_{fp}	C_p	P_{fp}	C_p
U Cep	6^m63	-0^m06	9^m65	$+0^m75$
U Sge	6.31	− .10	9.92	+0.80
Algol	1.90	−0.10	.....	.....

stars, in terms of the total light of the system; hence we can compute the individual magnitudes and colors. The small reflection and ellipticity effects, deduced from existing light-curves, may also be allowed for. In the case of Algol, the results of a previous six-color study[8] may be used to determine the difference in magnitude between each component and the combined light of the system. The resulting magnitudes and colors for both components of the three systems are given in the accompanying tabulation. The

Star	Component 1		Component 2		M (2) (Assumed)	$M-m$	M (1)
	P_{fp}	C_p	P_{fp}	C_p			
U Cep	6^m65	-0^m14	9^m65	$+0^m75$	$+3^m60$	-6^m05	$+0^m60$
U Sge	6.32	− .15	9.92	+ .80	+3.60	−6.32	.00
Algol	1.96	−0.16	5.42	+0.59	+3.60	−1.82	+0.14

absolute magnitudes of the secondary components, M (2), are derived from the assumption that they are subgiants. The reason for this assumption is that the resulting moduli for the systems give luminosities for the primary components, M (1), that are consistent with the colors and spectral types. We see that these stars are very similar to some of the Pleiades stars that populate the blue-dwarf sequence discussed in Paper II; examples of such stars are Pleiades No. 67, with $M = +0^m20$ and $C_p = -0^m15$, and No. 28, with $M = +0^m53$, $C_p = -0^m13$.

These results, if the basic assumption of subgiant character for the secondary components is correct, show that negligible reddening or selective absorption, either circum-

[7] It might be pointed out that, even in terms of visual magnitude, the absolute magnitudes of the subgiants between $C_p = +0^m97$ and $C_p = +0^m32$ will vary only by 0.65 mag.

[8] *Ap. J.*, **108**, 1, 1948.

stellar or interstellar, affects the brighter stars of these three systems.[9] The eclipsing binaries U Cep and U Sge are too distant to have reliable trigonometric parallaxes, but the photometric parallax of Algol, 0".043, agrees well with two trigonometric values, 0".044 ± 4 (A) and 0".034 ± 5 (S),[10] both of which are based upon many plates.

AR Lacertae-type systems.—Another type of eclipsing system known to contain subgiant components is represented by the prototype, AR Lac. Photoelectric observations of this system by G. E. Kron[11] present the first photometric evidence for possible large-scale surface activity, such as dark and bright patches, on stars other than the sun. W. E. Harper[12] determined velocity-curves for both components of the system, and A. B. Wyse,[13] who classified the stars as G5 and K0, noted sharp emission features at H and K of *Ca* II. Observations of magnitude and color made at maximum light and at primary total eclipse give

$$\text{Maximum light: } Pg_p = 6^m.87\,, \qquad C_p = +0^m.66\,;$$

$$\text{Total eclipse: } Pg_p = 7^m.69\,, \qquad C_p = +0^m.83\,.$$

F. B. Wood[14] was unable to separate the reflection and ellipticity effects in the light-curve from the intrinsic variation of the light of the system. Kron, however, obtained light-curves during intervals when the source of the intrinsic variation was relatively quiescent; and from these curves we find that the depth of primary eclipse given above must be corrected by −0.07 mag., in the photographic region. Although the ellipticity and reflections effects are wave-length dependent, we have arbitrarily corrected the visual depth by the same amount, since the error introduced can hardly amount to more than 0.01 mag. We see, therefore, that at the total eclipse half the photographic light of the system is lost; this result we might have anticipated from our previous conclusion that, photographically, the subgiants redder than $C_p = +0^m.32$ have the same absolute magnitude, regardless of their color. We find, then, the colors and magnitudes of the individual components to be as follows:

$$\text{Blue component: } Pg = 7^m.65\,, \qquad C_p = +0^m.55\,;$$

$$\text{Red component: } Pg_p = 7^m.65\,, \qquad C_p = +0^m.82\,.$$

The modulus of the system, from the assumption that both components are subgiants with $M = +3^m.60$, is 4.05 mag., or a photometric parallax of 0".0155. From the colors of the components and from the color–spectral-type relation of Figure 2, we can estimate that the spectral type of the primary-eclipsed star, which is also known from the photometric data to be the smaller, is G2 and that the larger component is K0.

There are a few other stars mentioned in the literature that may be similar to AR Lac in that both components are subgiants. When approximate spectral classes are known for the components and both are later than, say, F5 but are separated by several subclasses and when the light-curve exhibits a total eclipse during which half the total photographic light is lost, the system is quite likely to be composed of two subgiants. If the

[9] Since the blue-dwarf sequence begins its nearly vertical rise at $C_p \sim -0^m.16$, the effects of selective absorption on the bright components would be conspicuous; this is one reason that the use of some B-type stars in detecting interstellar absorption is so successful.

[10] The following convention will be followed throughout in regard to the source of individual trigonometric parallaxes: (A) = Allegheny, (C) = Cape of Good Hope, (G) = Greenwich, (M) = McCormick, (S) = Sproul, (V) = Van Vleck, (W) = Mount Wilson, (Y) = Yale, and (y) = Yerkes. The probable errors are given in terms of 0".001.

[11] *Pub. A.S.P.*, **59**, 261, 1947.

[12] *Pub. R.A.S. Canada*, **27**, 146, 1933.

[13] *Lick Obs. Bull.*, **17**, No. 464, 37, 1934.

[14] *Princeton U. Obs. Contr.*, No. 21, 1946.

elements are known, we should expect the star of later spectral type to be the larger. A good example of such a system is RS Ari. Wyse[13] called the spectra F9 and G5, and stated: "The primary spectrum [F9] is intermediate between giant and dwarf." Many visual observations give the primary eclipse, which is total, a depth of 1.0 mag. From Figure 2 we find that a G5 star is 0.2 mag. redder than one of class F9, so that the photographic depth of the total eclipse, during which the F9 star is occulted, is 0.8 mag.; when allowance is made for reflection and ellipticity effects, we may conclude that, photographically, the stars are of about the same magnitude. The elements quoted by the Gaposchkins[15] indicate that the G5 star is the larger of the two.

A similar system is RW UMa, the components of which Wyse[13] has classified as F9 and G9. The primary eclipse is total, with a visual depth of 1.10 mag., or 0.75 mag. photographically if we correct for the difference in color between the two stars. Struve[16] determined the velocity-curve of the F9 star, which is the star occulted at the total eclipse. He also measured ". . . two fairly well-marked and narrow emission lines of *Ca* II K and H. These lines belong to the eclipsing star [G9] at primary eclipse and have about the same amplitude as the absorption lines of the [visually] brighter component [F9]."[17]

IV. DWARF AND SUBDWARF SEQUENCES

DWARFS

The dwarf sequence has been defined in Papers I, II, and III by the cluster stars that are gathered together in Table 5; they range in color from $C_p = +0^m02$ to $+1^m05$. The main sequence defined by these stars is given in Table 6, but the individual deviations from this main sequence are tabulated as O − S (observed *minus* sequence) in the last column of Table 5. The sequence between $C_p = +0^m06$ and $+0^m16$ is not well defined, owing to a real lack of cluster stars in this interval, and the main sequence is represented by only one point in this range. Table 7 contains the dwarf stars from Table 3, with the individual modern determinations of the trigonometric parallaxes and their means. The photometric parallaxes given in the penultimate column of Table 7 are derived from the colors of the stars and from the dwarf sequence of Table 6. In nearly every instance the photometric parallax falls within the range of the trigonometric determinations. There is some selection of the stars in Table 7, in that, generally, only stars with several modern determinations of parallax were included on the observing program. The values of O − S in Table 7 are in the sense of mean trigonometric parallax minus the photometric parallax. When we recall that the zero point of the dwarf sequence given in Table 6 is defined by the Hyades stars, the mean systematic difference in O − S of $-0''.001$ indicates the sameness of cluster and noncluster dwarfs.

A few dwarfs, more distant than 14 parsecs, are included in Table 8; the arrangement of the material is the same as in the previous table. Although it is true that for these stars the trigonometric parallaxes are, on the whole, rather discordant, the photometric parallax usually falls within the range of the individual determinations. Only those dwarfs redder than $C_p = +0^m20$ are discussed here; the bluer stars, that is to say, those earlier than about F0, are discussed in connection with the blue-dwarf and bright blue-dwarf sequences in Section V.

[13] *Variable Stars* ("Harvard College Observatory Monographs," No. 5 [Cambridge, 1938]).

[16] *Ap. J.*, **102**, 74, 1945.

[17] It is strange that, although the primary eclipse of RW UMa indicates that the components are of nearly equal photographic brightness, only the emission lines of the redder component are observed, while in WW Dra, for example, where the total eclipse exceeds 1.0 mag. photographically, Joy observed both absorption and emission lines of the fainter star. The emission lines in WW Dra, like those in RW UMa, give a velocity-curve which is a mirror image of that of the primary star, but the amplitudes of the absorption-line velocity-curves are quite unequal (*Ap. J.*, **94**, 407, 1941; *Mt. W. Contr.*, No. 654).

TABLE 5

LUMINOSITIES AND COLORS OF CLUSTER DWARFS

Name*	M_{Pg_p}	C_p	O−S	Name	M_{Pg_p}	C_p	O−S
C 130	+0m42	+0m03	−0m08	C 86	+4m32	+0m35	+0m02
C 107	+0.58	+ .03	+ .08	C 162	+4.32	+0.36	− .06
H 60	+0.96	+ .08	− .06	C 114	+4.37	+0.36	− .01
H 117	+1.28	+ .09	+ .04	HR 4867	+4.41	+0.36	+ .03
H 139	+1.27	+ .095	− .03	P 23	+4.43	+0.38	− .08
H 119	+1.30	+ .10	− .03	P 49	+4.55	+0.395	− .05
H 84	+2.10	+ .15	− .04	C 53	+4.55	+0.395	− .05
H 34	+2.20	+ .15	+ .04	H 19	+4.52	+0.40	− .11
H 141	+2.37	+ .16	+ .07	P 9	+4.57	+0.40	− .06
H 96	+2.50	+ .17	+ .05	C 58	+4.64	+0.40	+ .01
P 58	+2.60	+ .18	± .00	P 55	+4.72	+0.41	+ .03
H 39	+2.82	+ .20	± .00	H 10	+4.87	+0.43	+ .06
P 15	+2.86	+ .20	+ .04	P 53	+4.87	+0.45	− .08
P 20	+2.96	+ .21	+ .04	C 76	+4.98	+0.45	+ .02
H 8	+3.08	+ .22	+ .06	C 97	+5.02	+0.45	+ .06
H 102	+3.14	+ .23	± .00	C 85	+5.22	+0.475	+ .11
H 14	+3.25	+ .24	− .02	P 57	+5.13	+0.48	− .01
P 71	+3.26	+ .24	− .01	H 20	+5.15	+0.48	+ .01
H 4	+3.28	+ .24	+ .01	H 57	+5.15	+0.485	− .02
C 49	+3.52	+ .26	+ .02	P 32	+5.18	+0.49	− .02
37 UMa	+3.58	+ .27	− .02	H 15	+5.38	+0.50	+ .11
H 21	+3.61	+ .28	− .09	P 38	+5.28	+0.51	− .06
P 72	+3.66	+ .28	− .04	H 18	+5.44	+0.53	− .01
H 13	+3.76	+ .29	− .03	HD 115043	+5.63	+0.54	+ .11
C 19	+3.82	+ .29	+ .03	H 24	+5.79	+0.56	+ .13
C 36	+3.82	+ .29	+ .03	C 132	+5.86	+0.60	− .01
H 38	+3.88	+ .29	+ .09	CH 14	+6.10	+0.64	− .01
P 24	+3.97	+ .30	+ .08	CH 21	+6.53	+0.70	+ .06
C 118	+4.10	+ .33	− .05	H 89	+6.65	+0.72	+ .06
C 101	+4.14	+ .33	− .01	H 91	+6.72	+0.75	− .05
H 6	+4.15	+ .33	± .00	H 106	+7.02	+0.80	+ .05
P 42	+4.15	+ .33	± .00	H 53	+7.49	+0.87	± .00
H 138	+4.23	+ .34	± .00	H 90	+8.37	+1.03	− .08
C 90	+4.34	+0.345	+0.07	H 72	+8.54	+1.05	−0.03

* C = Coma Berenices; P = Pleiades; H = Hyades.

TABLE 6

THE DWARF SEQUENCE DEFINED BY CLUSTER STARS IN THE RANGE C_p = +0m02 TO +1m22

C_p	M_{Pg_p}	C_p	M_{Pg_p}	C_p	M_{Pg_p}	C_p	M_{Pg_p}
+0m02	+0m40	+0m38	+4m51	+0m66	+6m23	+0m94	+7m91
+ .04	+0.60	+ .40	+4.63	+ .68	+6.35	+0.96	+8.03
+ .06	+0.80	+ .42	+4.75	+ .70	+6.47	+0.98	+8.15
+ .10	+1.33	+ .44	+4.90	+ .72	+6.59	+1.00	+8.27
+ .16	+2.30	+ .46*	+5.01	+ .74	+6.71	+1.02	+8.39
+ .18	+2.60	+ .48	+5.14	+ .76	+6.83	+1.04	+8.51
+ .20	+2.82	+ .50	+5.27	+ .78	+6.95	+1.06	+8.63
+ .22	+3.02	+ .52	+5.39	+ .80	+7.07		
+ .24	+3.27	+ .54	+5.51	+ .82	+7.19	+1.08†	+8.75
+ .26	+3.50	+ .56	+5.63	+ .84	+7.31	+1.10	+8.87
+ .28	+3.70	+ .58	+5.75	+ .86	+7.43	+1.12	+8.99
+ .30	+3.89	+ .60	+5.87	+ .88	+7.55	+1.14	+9.11
+ .32	+4.07	+ .62	+5.99	+ .90	+7.67	+1.16	+9.23
+ .34	+4.23	+0.64	+6.11	+0.92	+7.79	+1.18	+9.35
+0.36	+4.38					+1.20	+9.47
						+1.22	+9.59

* For C_p = +0m46 to +1m22 the values of M may be computed from the relation $M = +2^m27 + 6.0\,C_p$.
† From C_p = +1m06 to +1m22 the main sequence is derived from the stars in Table 3.

SUBDWARFS

In 1922 Adams and Joy[18] discovered ". . . three stars of large proper motion, which, in absolute magnitude, seem to form a group midway between the faint 'white dwarfs' . . . and the stars of early type belonging to the main sequence"; they called these stars "intermediate white dwarfs." In 1938 Kuiper[19] pointed out that these stars existed all along the main sequence, and he stated that ". . . since these stars . . . are much more similar

TABLE 7

COMPARISON OF THE TRIGONOMETRIC AND PHOTOMETRIC PARALLAXES OF THE DWARFS IN TABLE 3

Star	Trigonometric Parallaxes						Ptm. π	O−S
	A	M	S	Y	Others	Mean		
η Cas A	0".179 ± 9	0".182 ± 8	0".194 ± 8			0".184 ± 5	0".175	+0".009
107 Psc	128 ± 7	146 ± 11				132 ± 6	.134	− .002
HR 511		111 ± 9			0".116 ± 10 (W)	111 ± 5	.105	+ .006
δ Tri	065 ± 9	135 ± 9	087 ± 11			098 ± 6	.096	+ .002
HR 753	149 ± 9	141 ± 7		0".153 ± 8		147 ± 4	.153	− .006
HR 857		139 ± 9			134 ± 10 (C)	137 ± 6	.137	.000
κ Cet	115 ± 7	092 ± 10		104 ± 10		106 ± 5	.125	− .019
ϵ Eri		303 ± 9		298 ± 10	301 ± 6 (C)	303 ± 6	.320	− .017
40 Eri A	201 ± 6	210 ± 9		200 ± 11	190 ± 9 (C)	202 ± 3	.200	+ .002
π^3 Ori	128 ± 8	156 ± 11		110 ± 9		128 ± 5	.110	+ .018
HR 1925 A	086 ± 8	105 ± 10				097 ± 5	.095	+ .002
γ Lep A	147 ± 9	104 ± 6			136 ± 8 (C)	122 ± 4	.125	− .003
γ Lep B	147 ± 9	104 ± 6			136 ± 8 (C)	122 ± 4	.125	− .003
χ^1 Ori	098 ± 8	110 ± 8				104 ± 6	.110	− .006
11 LMi A	127 ± 8	110 ± 11	113 ± 19		(.065) ± 8 (W)	113 ± 6	.112	+ .001
36 UMa A	074 ± 9	085 ± 9	102 ± 14			082 ± 8	.080	+ .002
61 UMa	109 ± 9					109 ± 9	.107	+ .002
β CVn	114 ± 9	107 ± 10	093 ± 18			108 ± 6	.110	− .002
β Com		124 ± 10	133 ± 18			121 ± 6	.122	− .001
61 Vir		131 ± 11		127 ± 9		129 ± 7	.128	+ .001
72 Her	071 ± 11	074 ± 11	062 ± 13			076 ± 6	.074	+ .005
26 Dra		073 ± 10	078 ± 16	0".078 ± 6		073 ± 4	.078	− .002
HR 6806	098 ± 9	109 ± 13				098 ± 7	.095	+ .003
χ Dra		124 ± 10	120 ± 9		136 ± 10 (G)	127 ± 7	.135	− .008
σ Dra	180 ± 7	184 ± 9			168 ± 12 (G)	181 ± 4	.178	+ .003
61 Cyg A	288 ± 6	310 ± 6	271 ± 14		0".320 ± 10 (W)	296 ± 3	.296	.000
51 Peg	072 ± 9	076 ± 10				072 ± 7	.083	− .011
HR 8832	0".140 ± 8	0".161 ± 10	0".179 ± 13			0".160 ± 6	0".168	−0".008
						Av. dev.		−0".001 ±0".005

to main-sequence stars than to white dwarfs, the name 'subdwarfs' is suggested for this class of stars, in analogy with 'subgiant.' " This group of objects contains "stars not over 2 or 3 mag. below the main sequence." In 1947 he further stated that ". . . subdwarfs are all or nearly all, high velocity stars."[20] Joy [21] has summarized the spectroscopic features that distinguish subdwarfs from ordinary dwarfs. We shall apply the term "subdwarf" to the stars populating that sequence which, in Figure 1, runs below and parallel

[18] *Ap. J.*, **56**, 262, 1922; *Mt. W. Contr.*, No. 244.

[19] *Ap. J.*, **89**, 548, 1938.

[20] *A.J.*, **53**, 149, 1948.

[21] *Ap. J.*, **105**, 96, 1947; *Mt. W. Contr.*, No. 726.

TABLE 8

PHOTOMETRIC AND TRIGONOMETRIC DATA FOR DWARFS MORE DISTANT THAN 14 PARSECS

Star	Ps_p	C_p	n	π (Trig.)	π (Ptm)
6 Cet	5m16	−0m36	3	0".062 ± 10 (Y)	0".070
−4°3049	8.02	+ .62	2	0.047 ± 12 (M) .065 ± 11 (Y) 0.043 ± 11 (C)	
			Mean	0.049 ± 7	.040
HR 4867	6.13	+ .36	5	0.038 ± 10 (A) 0.041 ± 11 (W)	
			Mean	0.039 ± 7	.045
HR 5455	6.46	+ .35	3	0.035 ± 6 (A) .051 ± 10 (M) 0.034 ± 8 (Y)	
			Mean	0.036 ± 4	.037
45 Boo	5.20	+ .34	2	0.058 ± 10 (A) 0.071 ± 12 (M)	
			Mean	0.063 ± 8	.064
+39°2950	9.27	+ .84	3	0.054 ± 7 (A) 0.062 ± 6 (y)	
			Mean	0.052 ± 6	.041
+0°3593	7.26	+ .68	3	0.082 ± 10 (A) .033 ± 12 (M) .073 ± 8 (Y) 0.047 ± 8 (W)	
			Mean	0.061 ± 5	.066
+1°3421	7.32	+ .43	3	0.040 ± 10 (A) 0.032 ± 8 (Y)	
			Mean	0.036 ± 6	.032
+4°3599	7.19	+ .475	6	0.051 ± 8 (A) .041 ± 9 (M) 0.033 ± 8 (Y)	
			Mean	0.041 ± 5	.038
θ Cyg	4.70	+0.30	2	0.060 ± 9 (A) 0.083 ± 11 (M)	
			Mean	0.067 ± 7	0.069

to the dwarf sequence from $C_p = +0^m60$ to $+1^m23$ and crosses the dwarf sequence at $C_p = +0^m55$ and $+1^m35$. Although this nomenclature presents a situation in which subdwarfs may be brighter than dwarfs, it is analogous to the fact that some "main-sequence dwarfs" are brighter than giants. As stated in Paper II, all these designations are unsatisfactory, and they should be replaced by less misleading ones as soon as the color-luminosity array is more completely mapped.

The stars populating the subdwarf sequence in Figure 1 are listed in Table 9, which also includes three probable subdwarfs found in the Hyades cluster. Two stars—Cin 1244, with $M = +12^m16$ and $C_p = +1^m32$, and Lal 21185, with $M = +11^m75$ and $C_p = +1^m32$—occur near the junction of the two sequences, so that it is difficult to say to which group they belong; both stars are omitted from Table 9.

TABLE 9

LUMINOSITIES AND COLORS OF SUBDWARFS

Star	$M_{P_{G_p}}$	C_p	Star	$M_{P_{G_p}}$	C_p	Star	$M_{P_{G_p}}$	C_p
β Vir*	3^m93	$+0^m49$	85 Peg A	5^m89	$+0^m55$	CC 1018	11^m07	$+1^m23$
ι Per	4.11	+ .50	Hyades 17‡	6.01	+ .565	Cin 3124	11.30	+1.24
λ Aur	4.28	+ .51	μ Cas	6.31	+ .58	CC 1143	11.51	+1.28
λ Ser	4.76	+ .52	Hyades 7‡	6.39	+ .58	Cin 2354	11.94	+1.30
HR 483	5.06	+ .535	τ Cet	6.42	+ .585	CC 1069	14.71	+1.53
51 Peg†	5.21	+ .54	HR 4550	7.22	+ .635	ADS 246 B	14.96	+1.55
Hyades 40‡	5.80	+0.55	36 UMa	8.56	+0.87	CC 1445	16.31	+1.59

* Three consistent determinations of the trigonometric parallax—0".100 ± 10 (A), 0".102 ± 9 (Y), and 0".093 ± 9 (M)—indicate that this star falls below the bright-dwarf sequence; however, the possibility that the star is a subgiant, with photometric parallax of 0".083, cannot be entirely eliminated.

† Two determinations of the trigonometric parallax, 0".072 ± 9 (A) and 0".076 ± 10 (M), place this star on the subdwarf sequence; but, since a parallax of 0".083 would place it on the dwarf sequence, the point is of low weight.

‡ The data for these stars are taken from Paper I.

Table 10 contains some of the stars in Table 3 that populate the dwarf sequence from $C_p = +0^m30$ to $+1^m30$, together with the spectral classes assigned these stars by Kuiper,[22] the Mount Wilson observers,[4] and the *Atlas*. The *Atlas* spectral types have been extended to stars later than K5 by Morgan.[23] The resulting color–spectral-type relationships for these stars are plotted in Figure 3, where the open circles represent individual stars and the filled circles are the means of two or more stars of the same spectral class. The crosses in all three cases represent the two components of 61 Cygni. It appears that, to $C_p \sim +0^m70$, the three systems of classification are quite similar, in that they give a linear relationship between color and spectral type; but, whereas the Yerkes systems show a sudden discontinuity at $C_p = +0^m70$ to $+0^m75$, spectral type K0–K1, the Mount Wilson system preserves the linear relationship to $C_p \sim +0^m90$, spectral type K5, where it then shows a somewhat less abrupt discontinuity. Since the color-luminosity array is linear to $C_p \sim +1^m23$, Figure 3 indicates that the Yerkes spectral types corresponding to $C_p = +0^m75$ to $+1^m23$ are compressed between K0 and K5, while the Mount Wilson system, for the same color range, contains types K0–M0. The second discontinuity, apparent at $C_p = +1^m23$ in all three parts of Figure 3, results from the sharp break in the color-luminosity array at this point.

The mean color–spectral-type relationships for the Mount Wilson and Yerkes systems are reproduced as the lines in Figure 4, while the points plotted in this figure represent the colors and spectral types of the subdwarfs given in Table 11 on these same sys-

[22] *Ap. J.*, **95**, 201, 1942.

[23] *Ap. J.*, **87**, 589, 1938.

tems. There appears to be a systematic difference in the relationship for the two kinds of stars, which amounts to three subclasses at F8 and disappears at G5. It is interesting that the two relationships merge at $C_p = +0^m.55$ to $+0^m.60$, which is near the point of intersection of the dwarf and subdwarf sequences in the color-luminosity array of Figure 1.

The systematic difference noted above may be due to certain spectroscopic peculiarities in subdwarfs. For example, a recent spectrophotometric study of bright stars in the range F8–M0 by T. Setterberg[24] indicates that the *CN* and *CH* molecular absorptions, as well as the atomic absorptions in the region λλ 4190–4340 A are weaker in the subdwarfs ι Per, λ Aur, and μ Cas than they are in dwarfs of the same color; this result is in agreement with Joy's[21] remark that "the spectroscopic features which distinguish subdwarfs from ordinary dwarfs are: for types A–M, a general weakening of the absorption spectrum. . . ."

TABLE 10

SPECTRAL TYPES FOR DWARFS IN THE COLOR RANGE FROM $C_p = +0^m.34$ TO $+1^m.30$

STAR	C_p	SPECTRAL TYPE			STAR	C_p	SPECTRAL TYPE		
		Kuiper	Mt. W.	*Atlas*			Kuiper	Mt. W.	*Atlas*
π^3 Ori	+0.34	F6	F5	F6 V	HR 6806	+0.79	K2	K2	.....
γ Lep A	+ .36	F6	F6	.....	γ Lep B	+0 .87	K3	K6	.....
χ Dra	+ .395	F8	F5	F6 V	HR 8832	+0 .875	K3	K5	K3 V
η Cas	+ .46	G0	F9	G0 V	HR 753 A	+0 .89	K3	K4	K3
χ^1 Ori	+ .47	G0	F9	G0 V	61 Cyg A	+1 .05	K3	K6	K5 V
β Com	+ .47	G0	G0	G0 V	Cin 2322	+1 .21	K7	M0	K6
β CVn	+ .48	G0	G0	G0 V	Cin 2238	+1 .23	K6	M0	K6
κ Cet	+ .585	G4	G5	G5 V	61 Cyg B	+1 .23	K5	M0	K6
61 Vir	+ .60	G5	G6	.....	Gmb 1618	+1 .23	K8	M0	K6
61 UMa	+ .63	G4	G6	G8 V	Cin 1633	+1 .24	K8	M0	.....
11 LMi	+ .66	G8	K0	.....	Cin 705	+1 .27	M1	M3	.....
HR 511	+ .67	K1	K0	.....	Cin 2707	+1 .27	M0+	M2	.....
107 Psc	+ .71	K0	G9	K0 V	Cin 1383	+1 .28	M1	M1	M1
σ Dra	+ .715	G9	K0	.....	CC 782	+1 .28	M1	M1	.....
40 Eri A	+ .725	K1	K0	.....	CC 1392	+1 .285	M2	M2 .5	.....
HR 1925	+ .75	K2	K1	.....	+61°195	+1 .29	M1+	.....	.....
ε Eri	+0 .79	K2	K2	.....					

The most obvious characteristic of the dwarf sequence is the abrupt break at $C_p \sim +1^m.23$.[25] From Figure 3 we see that this color corresponds to K6 on the Yerkes systems, or to M0 on the Mount Wilson system; in both cases, this is the point at which the *TiO* bands begin to show strongly in the spectra. A simple explanation of the break, then, would be that the *TiO* absorption band heads at λλ 4762, 4954, 5168, and 5445 A are affecting the observed colors, since the color defines only a small part of the shorter-wave-length side of the spectral energy-curve. There is some evidence, however, that the explanation is not so simple. For example, it is difficult to explain the fact that, although

[24] *Stockholm Obs. Ann.*, Vol. 15, No. 1, 1947.

[25] The existence of such a discontinuity was first pointed out by E. Hertzsprung in 1915, when he found a similar effect in his measurements of the effective wave lengths of absolutely faint stars. He concluded: "It is an obvious suggestion for the explanation of the fact noted above that the absolute magnitude +3 (sun = −0.33), corresponding to the temperature 3400° Abs. of a black body the size of the sun, represents the stage of a cooling star at which the formation of relatively dark solid matter on its surface begins, the remaining fluid giving practically all the radiation." Perhaps it is near this point in the color-luminosity array that the dwarfs reach a minimum effective temperature and become fainter as a result of decreasing size alone.

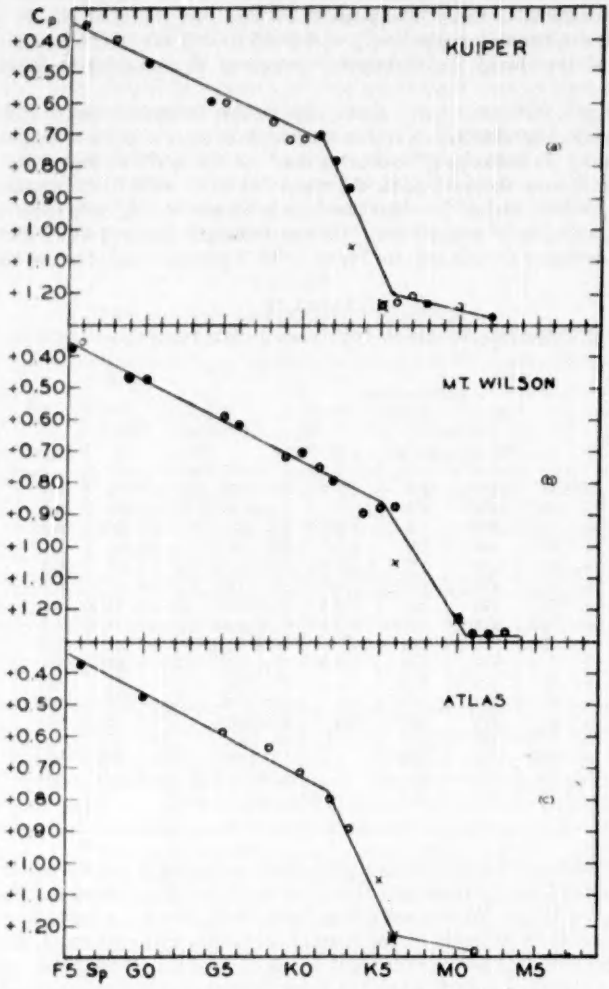

FIG. 3.—The color–spectral-type relationship for dwarfs classified by (*a*) Kuiper, (*b*) Mount Wilson, and (*c*) the authors of the *Atlas*. The open circles represent individual stars and the filled circles the means of two or more stars of the same spectral type; the crosses in all three sections of the figure represent the two components of 61 Cyg.

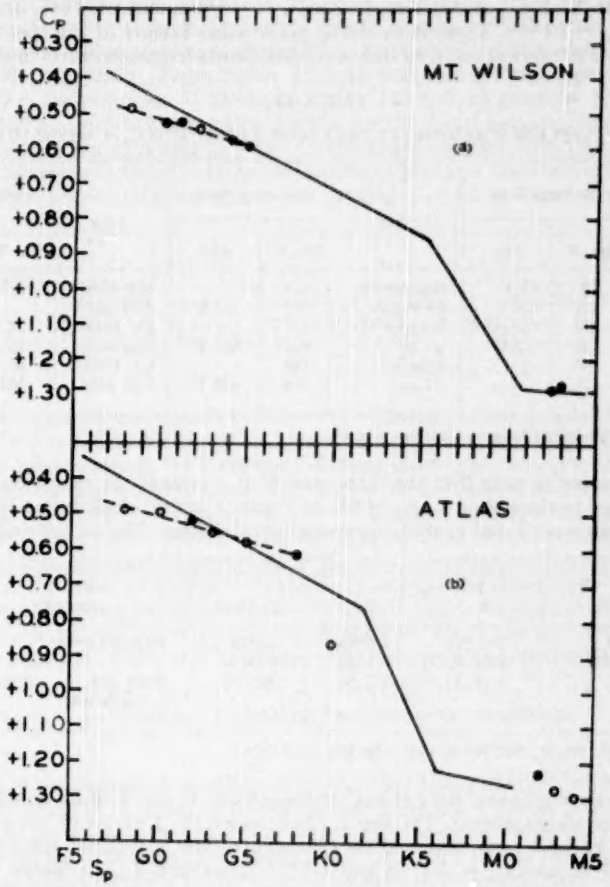

FIG. 4.—The color–spectral-type relationship for subdwarfs. The straight lines are reproduced from Fig. 3.

in the Mount Wilson system "the types of the M-dwarfs are based strictly upon the strength of the titanium oxide bands in the blue region of the spectrum,"[21] there exists a large color difference between dwarfs and subdwarfs of the same spectral subclass, as is the case with Wolf 47, an M6 dwarf with $C_p = +1^m.31$, and CC 1445, an M5.5 subdwarf with $C_p = +1^m.59$. There is evidently some other feature of the spectral energy-curve, besides *TiO* absorption, that differentiates dwarfs from subdwarfs in the M stars.

TABLE 11

SPECTRAL TYPES FOR SUBDWARFS IN THE COLOR RANGE FROM $C_p = +0^m.49$ TO $+1^m.30$

Star	Spectral Type		Star	Spectral Type		Star	Spectral Type	
	Mt. W.	*Atlas*		Mt. W.	*Atlas*		Mt. W.	*Atlas*
β Vir	F8	F8 V	Hyades 40	G3	.....	HR 4550	G5	G8 V
ϵ Per	G1	G0 V	85 Peg A	G1	G3 V	36 UMa C	.....	K0*
λ Aur	G0	G2 IV–V	Hyades 17	G5	.....	CC 1018	M3	M2
λ Ser	G0	G2 V	μ Cas	G4	G5 V	Cin 3124	M2	M2
HR 483	G0	.....	Hyades 7	G4	.....	CC 1143	M3	M3
51 Peg	G0	.....	τ Cet	G4	G8 V	Cin 2354	M3	M4

* 36 UMa C: Classified by Popper on the *Atlas* system.

It is interesting to note that the three stars that represent the extension of the subdwarf sequence to the red of $C_p = +1^m.32$ in Figure 1 are all classified as subdwarfs by Joy.[21] These stars are listed in the accompanying tabulation. The second and third stars

Star	M	C_p	Sp. (Joy)	Remarks
CC 1069	$+14^m.71$	$+1^m.53$	sdM4.5	Barnard's star
ADS 246 B	+14.91	+1.55	sdM4e	
CC 1445	+16.31	+1.59	M5.5e	Ross 248 ". . . probably a subdwarf"*

* *Ap. J.*, **105**, 96, 1947; *Mt. W. Contr.*, No. 726.

in this group show emission lines of both hydrogen and H and K of *Ca* II, while the first, Barnard's star, shows neither. The star L 726-8, which W. J. Luyten[26] has announced as an irregular variable, was observed on two nights. The individual results are $Pg_p = 13^m.92$ and $13^m.94$, and $C_p = +1^m.55$ and $+1^m.55$. The star is a close double, and Luyten gives 0.50 mag. as both the photographic and the photovisual magnitude difference between the components; he also gives the value 13.69 mag. as the total photographic magnitude of the system. If we adopt the value 0.50 mag. for the photographic Δm, we obtain from the photoelectric observations, Pg_p (A) $= 14^m.45$ and Pg_p (B) $= 14^m.95$; Joy and Humason[27] have classified this star as dM5.5e. Since the color of the system is similar to that of ADS 246 B, the stars probably are subdwarfs, although we cannot eliminate the possibility that one star is a dwarf and the other a subdwarf, of different colors, with a combined color of $+1^m.55$. If a value for $C_p = +1^m.55$ approximately represents the color of both components, then, by comparison with ADS 246 B and CC 1445, the parallax probably lies between $0''.1$ and $0''.2$; a more accurate value is not possible in view of the uncertainty introduced by the presence of a companion and the steepness of

[26] *Ap. J.*, **109**, 532, 1949.

[27] *Pub. A.S.P.*, **61**, 134, 1949.

the subdwarf sequence in this color region; Luyten estimates the parallax to be $0''.56 \pm 0''.07$.

It should, perhaps, be noted, although not stressed, that there is some suggestion in Figure 1 that the turning-back of the dwarf sequence, evident in the last observed point, Wolf 47, continues on through such stars as van Maanen No. 2 to the white dwarfs. Some support for this suggestion is offered by such stars as Wolf 489, which Kuiper[28] classifies as of the type K5±. From Figure 3 we see that this spectral type corresponds to $C_p = +1^m1 \pm$ and, since $m_v = 14^m3$ and $\pi = 0''.130 \pm 9$, as given by Kuiper, we find $M(Pg) = 16^m0 \pm$, which would place this star on the dwarf sequence between Wolf 47 and van Maanen No. 2. A search of the literature for parallax stars that populate this portion of the color-luminosity array yielded those given in the accompanying tabulation. These are stars contained in a recent catalogue of white dwarfs by Luyten[29] for

Star	Pg	I.C.	π (Trig.)	M(pg)	Star	Pg	I.C.	π (Trig.)	M(pg)
Vr 7	14^m0	-0^m3	Hyades	$+11^m0$	van Maanen 2	12^m6	$+0^m4$	$0''.243 \pm 6$	$+14^m5$
Vr 16	13.7	− .3	Hyades	+10.7	Wolf 457	16.0	+0.5	.078 ± 8	+15.5
Wolf 219	15.2	+0.3	$0''.067 \pm 8$	+14.3	Wolf 489	15.4	+1.1	0.130 ± 9	+16.0

which available parallaxes indicate a distance of 14 parsecs or less; in addition, two white dwarfs in the Hyades cluster are included, and the mean cluster parallax given in Paper I, $0''.0245$, is used to obtain the luminosity of these stars. The photographic magnitudes and colors are those given by Luyten. The magnitude and color obtained by Luyten for van Maanen No. 2, $Pg = 12^m6$ and I.C. $= +0^m4$, agrees well with the values in Table 3, $Pg_p = 12^m50$ and $C_p = +0^m41$. Also, the color of Wolf 489 is the same as that obtained above from the spectral type given by Kuiper. The colors and luminosities of these stars have been plotted in Figure 5. Taking into account the uncertainty in the photographic colors and the smaller parallaxes, Figure 5 is highly suggestive of a connection between the red and the white dwarfs. All the stars for which Luyten's magnitudes and colors have been used above will be observed on the present photoelectric program.

V. BLUE-DWARF AND BRIGHT BLUE-DWARF SEQUENCES

CLUSTER STARS

The stars in the Pleiades, Coma Berenices, and Ursa Major clusters, which were found in Papers II and III to populate the blue-dwarf sequence, are gathered together in Table 12. The mean sequence defined by these stars is given in Table 13. The individual deviations from this mean are tabulated as ΔM(O − S) in Table 12 for stars redder than $C_p = -0^m12$; the sequence is poorly defined between $C_p = -0^m12$ and -0^m17; and at $C_p = -0^m17$, $M = -0^m50$, the sequence seems to rise vertically to $M = -3$ mag. with no further change in color. The blue-dwarf sequence joins the dwarf sequence at $C_p = +0^m18$.

The stars in Papers I, II, and III which were found to populate the bright blue-dwarf sequence are listed in Table 14. The mean sequence is in Table 15.

"ATLAS" STARS

In Paper II it was pointed out that, in the Pleiades, the spectra of the bright blue-dwarfs indicate a smaller amount of $H\gamma$ and $H\delta$ absorption than do the spectra of blue-dwarfs of corresponding color. This effect probably is due to less pronounced wings of

[28] *Ap. J.*, **87**, 595, 1938. [29] *Ap. J.*, **109**, 528, 1949.

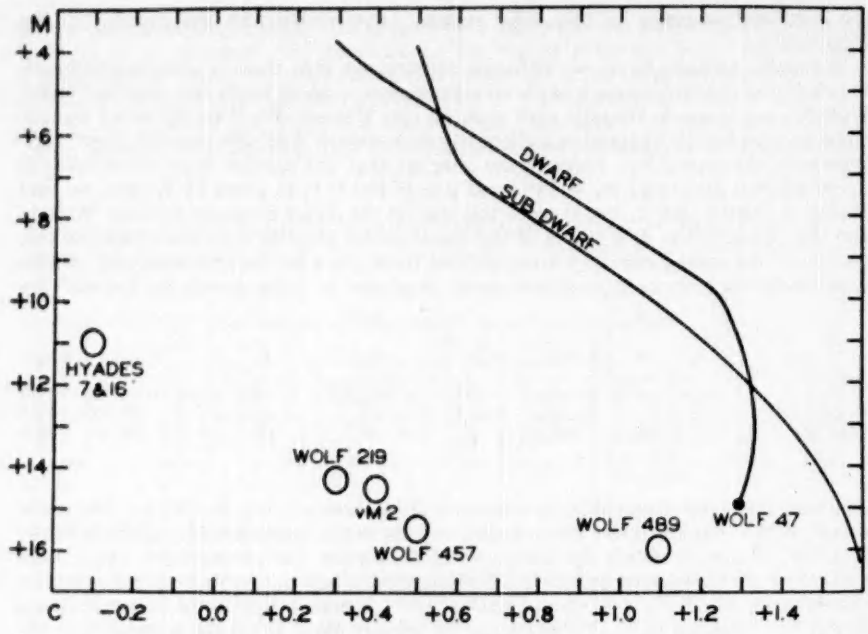

FIG. 5.—The position of the "white dwarfs" in the color-luminosity array. The large open circles represent stars within 14 parsecs for which photographic magnitudes and colors (Luyten) are available. The continuous curves are taken from Fig. 1.

TABLE 12

LUMINOSITIES AND COLORS OF BLUE-DWARF STARS IN GALACTIC CLUSTERS

Star	M_{Pg_p}	C_p	Δm(O−S)	Star	M_{Pg_p}	C_p	Δm(O−S)
P 17	−1^{m}70	−0^{m}18		P 69	+1^{m}70	−0^{m}01	−0^{m}07
P 48	−3.10	− .175		C 183	+1.78	.00	− .05
P 59	−2.33	− .17		P 46	+2.04	+ .05	− .04
P 54	−0.55	− .17		P 44	+2.11	+ .07	− .05
P 16	−0.35	− .17		P 64	+2.27	+ .08	+ .07
P 25	−2.09	− .16		C 139	+2.22	+ .09	± .00
P 67	+0.20	− .15		C 168	+2.28	+ .105	− .01
P 27	−0.16	− .145		C 145	+2.22	+ .11	− .09
P 28	+0.53	− .12	−0^{m}02	P 5	+2.38	+ .12	+ .03
P 63	+0.75	− .115	+ .12	P 66	+2.44	+ .125	+ .07
P 40	+0.94	− .09	− .03	C 104	+2.36	+ .13	− .03
P 43	+1.10	− .08	± .00	P 73	+2.41	+ .13	+ .02
P 70	+1.11	− .07	− .11	P 61	+2.44	+ .13	+ .05
P 45	+1.35	− .06	± .00	80 UMa	+2.45	+ .13	+ .06
P 33	+1.57	− .03	− .05	P 41	+2.65	+ .165	+ .12
P 68	+1.75	− .02	+ .05	P 3	+2.61	+0.17	+0.07
P 62	+1.79	−0.02	+0.09				

the hydrogen lines in the bright blue-dwarfs—an indication, according to the *Atlas*, of higher luminosity. In an attempt to separate the brighter A stars into the sequences discussed above, as well as to find additional spectroscopic evidence of differences in the spectra of stars populating the various sequences, the stars classified with luminosity classes IV and V and those of *Atlas* spectral types A0–A7 are discussed in the following paragraphs. The stars C Hya, λ UMa, 38 Lyn, and ζ Vir, are omitted for lack of reliable trigonometric parallaxes.

TABLE 13

THE BLUE-DWARF SEQUENCE DEFINED BY CLUSTER STARS

C_p	M_{Pg_p}	C_p	M_{Pg_p}	C_p	M_{Pg_p}	C_p	M_{Pg_p}
−0m12	+0m55	−0m04	+1m55	+0m04	+2m05	+0m12	+2m35
− .10	+0.85	− .02	+1.70	+ .06	+2.12	+ .14	+2.43
− .08	+1.10	± .00	+1.83	+ .08	+2.20	+ .16	+2.50
−0.06	+1.35	+0.02	+1.95	+0.10	+2.27	+0.18	+2.58

TABLE 14

LUNINOSITIES AND COLORS OF BRIGHT BLUE-DWARFS IN CLUSTERS

Star	M_{Pg_p}	C_p	ΔM(O−S)	Star	M_{Pg_p}	C_p	ΔM(O−S)
ε UMa	+0m01	−0m11	+0m03	P 22	+1m43	+0m03	−0m02
C 146*	+0.55	− .08	+ .15	C 10	+1.50	+ .05	− .10
γ UMa	+0.59	− .06	− .01	δ UMa	+1.70	+ .05	+ .10
β UMa	+0.66	− .05	− .04	P 77	+1.82	+ .08	± .00
C 160*	+0.88	− .03	− .02	C 62	+1.82	+ .09	− .06
P 47	+1.01	− .03	+ .11	P 75	+1.93	+ .09	+ .05
H 61	+1.18	± .00	− .01	H 50	+1.84	+ .095	− .08
P 56	+1.19	±0.00	±0.00	C 60	+1.98	+0.10	+0.03

* Slightly and erratically variable in magnitude (± 0m05, A.D.), and in color (± 0m02, A.D.).

TABLE 15

THE BRIGHT BLUE-DWARF SEQUENCE DEFINED BY CLUSTER STARS

C_p	M_{Pg_p}	C_p	M_{Pg_p}	C_p	M_{Pg_p}	C_p	M_{Pg_p}
−0m12	−0m15	−0m06	+0m60	±0m00	+1m19	+0m06	+1m68
− .10	+ .12	− .04	+0.80	+ .02	+1.37	+ .08	+1.82
−0.08	+0.40	−0.02	+1.00	+0.04	+1.53	+0.10	+1.95

SPECTRUM A0

γ *UMa*.—We have already shown, in Paper III, that this member of the Ursa Major cluster is a bright blue-dwarf.

α *Lyr* (*Vega*).—If we assume that Vega is a bright blue-dwarf, then from Table 15 we find $M = +0^m45$, or a photometric parallax of 0".127, which falls well within the range of the trigonometric values given in Table 16. Since a parallax of 0".173 would be required to make Vega a blue-dwarf, the assumption that it is a bright blue-dwarf seems to be correct.

TABLE 16

STANDARD A-TYPE STARS IN THE *Atlas*

Star	P_{ep}	C_p	n	*Atlas*	π (Trig.)	π (Ptm)	Sequence
γ UMa	2^{m}31	−0^{m}06	3	A0 V	0".046*	0".046	Bright blue-dwarf
α Lyr (Vega)	−0.08	− .075	3	A0 V	0.120 ± 6 (A) .134 ± 8 (M) 0.117 ± 13 (Y)		Bright blue-dwarf
				Mean	0.121 ± 4	.127	
α CrB	+2.12	− .05	3	A0 V	0.049 ± 9 (A) 0.053 ± 10 (M)		Bright blue-dwarf
				Mean	0.051 ± 7	.049	
α CMa (Sirius)	−1.53	− .07	5	A1 V	0.370 ± 5 (A) .360 ± 8 (M) .387 ± 9 (Y) 0.370 ± 11 (y)		Blue-dwarf
				Mean	0.373 ± 3	.367	
γ Gem	+1.88	− .065	2	A1 V	0.031 ± 8 (M) 0.047 ± 11 (y)		Bright blue-dwarf
				Mean	0.040 ± 6	.056	
β UMa	+2.23	− .05	5	A1 V	0.049*	.049	Bright blue-dwarf
β Aur	+1.84	+ .01	5	A2 IV	0.039 ± 4 (A) 0.029 ± 12 (M)		Dwarf
				Mean	0.034 ± 4	.035	
α PsA (Fomalhaut)	+1.11	+ .015	2	A3 V	0.134 ± 9 (Y) 0.157 ± 8 (C)		Blue-dwarf
				Mean	0.146 ± 6	.142	
δ UMa	+3.28	+ .05	3	A3 V	0.049*	.048	Bright blue-dwarf
β Leo	+2.11	+ .08	2	A3 V	0.066 ± 6 (A) .075 ± 11 (M) .103 ± 15 (y) 0.121 ± 15 (S)		Bright blue-dwarf
				Mean	0.083 ± 7	.089	
δ Her	+3.08	+ .04	3	A3 IV	0.032 ± 8 (A) 0.019 ± 10 (M)		Dwarf
				Mean	0.027 ± 6	.032	
β Ari	+2.65	+0.09	3	A5 V	0.075 ± 10 (A) .094 ± 13 (M) .040 ± 13 (y) 0.035 ± 12 (S)		Bright blue-dwarf
				Mean	0.063 ± 6	0.067	

* Cluster parallax from Paper III.

TABLE 16—*Continued*

Star	P_{ep}	C_p	n	Atlas	π (Trig.)	π (Ptm)	Sequence
δ Cas	+2m64	+0m10	3	A5 V	0".062 ± 10 (M) .025 ± 9 (y) 0.009 ± 9 (W)		Dwarf (?)
				Mean	0.033 ± 7	0".055	
80 UMa	+4.05	+ .13	4	A5 V	0.048*	.047	Blue-dwarf
α Aql (Altair)	+0.88	+ .165	2	A7 V	0.213 ± 8 (M) .217 ± 10 (Y) 0.187 ± 10 (y)		Blue-dwarf
				Mean	0.208 ± 5	.213	
α Cep	+2.42	+0.165	4	A7 V	0.069 ± 10 (A) .062 ± 7 (y) 0.064 ± 10 (G)		Bright-dwarf
				Mean	0.068 ± 4	0.068	

* Cluster parallax from Paper III.

α *CrB.*—The photometric parallax derived for this star on the assumption that it is a bright blue-dwarf, 0".049, is in excellent agreement with the trigonometric values in Table 16; a parallax of 0".070 would be required to place the star on the blue-dwarf sequence. It is noteworthy that if we assume membership in the Ursa Major cluster for α Coronae and compute the cluster parallax with the constants derived in Paper III, we find $\pi_c = 0".047$.

SPECTRUM A1

α *CMa* (*Sirius*).—The photometric parallax in Table 16 is derived from data in Table 12, with the assumption that Sirius is a blue-dwarf; the agreement with the trigonometric values is good.

α *Gem* (*Castor*).—The visual components of Castor are too close to be resolved with the 12-inch photometer, and so they are not included in Table 16; but, for the present purpose, we shall adopt the Harvard revised visual magnitudes[29a] of *m* (A) = 1m99 and *m* (B) = 2m85. If we assume that component A is a blue-dwarf and, as is indicated by the spectral type, similar to Sirius in color, we find a photometric parallax of 0".071, compared with the mean trigonometric value of 0".073 ± 3. The agreement is satisfactory, and we may assume that component A is a blue-dwarf. If we now apply the same parallax to component B, we find *M* (B) = +2m2, or +2m5 if we allow for the binary nature of this star. If the B component fell on the dwarf sequence, it would then be similar to such stars as Hyades Nos. 96 and 141 (Paper I), which have a mean *M* = +2m45 and C_p = +0m16. Both Hyades stars are metallic-line objects like α Gem B, a fact which supports our assumptions concerning component A.

γ *Gem.*—The trigonometric parallax of this star is small and uncertain, but the assumption that it is a bright blue-dwarf gives a photometric parallax that falls within the range of the trigonometric determinations; since the star is a long-period spectroscopic binary, the companion may have some influence on the magnitude and color.

β *UMa.*—We have already shown, in Paper III, that this member of the Ursa Major cluster is a bright blue-dwarf. The cluster parallax is given in place of the trigonometric values in Table 16.

[29a] *Harvard Mimeograms*, Ser. II, No. 2, 1938.

On the basis of the foregoing discussions, the *Atlas* standards at A1 V appear to consist of two blue-dwarfs, Sirius and α Gem A, and of two bright blue-dwarfs, γ UMa and probably γ Gem. In the *Atlas*, the authors state: "It is possible that the [hydrogen] wings are slightly less pronounced in the spectrum of γ Gem than in the other [A1 V] stars listed." We might expect a similar effect in β UMa as compared with Sirius.

SPECTRUM A2

β Aur.—The observed color and magnitude are $Pg_p = 1^m.84$ and $C_p = +0^m.01$, and, although the star is a spectroscopic and eclipsing binary,[30] the two stars are equally bright and probably of the same color, so that, correcting for the duplicity, we have $Pg_p = 2^m.59$ and $C_p = +0^m.01$ for each component. The dwarf sequence of Table 6 stops at $C_p = +0^m.02$; but, if we extrapolate to $C_p = +0^m.01$, we find $M = +0^m.30$, or a photometric parallax of 0".035 if the components are dwarfs; the mean trigonometric parallax in Table 16 is 0".034 ± 4. This star, like α CrB discussed above, is often assigned membership in the extended Ursa Major group. If we compute the cluster parallax with the constants derived for the cluster in Paper III, we find 0".034 in good agreement with the photometric value. The components of β Aur, therefore, probably are dwarfs similar to the brightest dwarfs thus far found in galactic clusters.

β Ser.—This star will be discussed in the following section concerning binary stars.

SPECTRUM A3

α PsA (Fomalhaut).—If Fomalhaut is a blue-dwarf, then, from Table 13, $M = +1^m.89$, and the photometric parallax is 0".142, very near the mean of the two trigonometric values in Table 16. The authors of the *Atlas* state: "α Pisces Australis gives spectroscopic evidence of having the lowest luminosity of any star in the table [of A3 stars]." Fomalhaut probably is the only A3 blue-dwarf in the *Atlas*.

δ UMa.—We have already shown in Paper III that this member of the Ursa Major cluster is a dwarf. The cluster parallax is given in place of the trigonometric values in Table 16.

β Leo.—The assumption that this star is a bright blue-dwarf leads to a photometric parallax of 0".089, which is in excellent agreement with the mean of the rather scattered trigonometric values. The authors of the *Atlas* state: "The hydrogen lines are weaker in the spectrum of β Leonis than in the other [A3] dwarfs. . . ."

δ Her.—The trigonometric parallax of this star is small and relatively uncertain, but the mean value gives $M = +0^m.24$, compared to $M = +0^m.60$ obtained from Table 6 under the assumption that the star is a dwarf; a parallax of 0".049 would be required to place it on the bright blue-dwarf sequence.

SPECTRUM A5

β Ari.—Although the individual values of the trigonometric parallax are rather discordant, this spectroscopic binary, with a period of 107 days, probably is a bright blue-dwarf, since the photometric parallax in Table 16, derived from this assumption, is in good agreement with the mean trigonometric value.

δ Cas.—This star is rather similar to β Ari in both magnitude and color, but the trigonometric determinations of the parallax are even more discordant than those for β Ari. From data in Tables 6, 15, and 13 we find $M = +1^m.33$, $+1^m.95$, or $+2^m.27$ for the assumptions that the star is a dwarf, bright blue-dwarf, or blue-dwarf, respectively. The corresponding photometric parallaxes are 0".055, 0".072, or 0".084, of which 0".055, from the assumption that the star is a dwarf, is the only value that falls within the rather large range of the trigonometric values.

80 UMa.—We have already shown in Paper III that this member of the Ursa Major

[30] The eclipses are only about 0.1 mag. deep, and the observed magnitude refers to maximum light.

cluster is a blue-dwarf. The cluster parallax is given in place of the trigonometric values in Table 16.

SPECTRUM A7

α Aql (*Altair*).—This star is situated near the junction of the blue-dwarf and dwarf sequences, so that it is difficult to decide to which it belongs; but the large rotational velocity, discussed later in this paper, supports its membership in the blue-dwarf sequence. It is interesting to note here that in Papers I and III it was found that several of the stars lying near the intersection of the blue-dwarf and dwarf sequences were metallic-line stars, and we might therefore expect the spectrum of Altair to show "metallic-line" tendencies.

α Cep.—From Tables 6 and 13 we find $M = +2^m45$ and 2^m54, respectively, from the assumptions that this star is a dwarf or a blue-dwarf. Either of these values for M would require a photometric parallax in excess of 0".1, as compared with the three accordant trigonometric values given in Table 16, 0".069 ± 10 (A), 0".062 ± 7 (y), and 0".064 ±

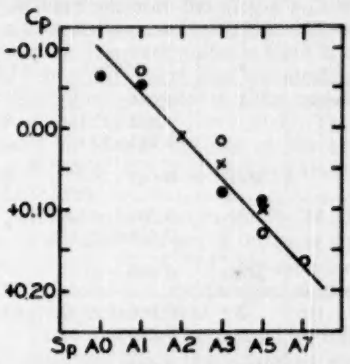

FIG. 6.—The color–spectral-type relationship for the A-type stars in the *Atlas*. The crosses indicate dwarfs; the open circles, blue-dwarfs; and the filled circles, bright blue-dwarfs.

10 (G), and with one discordant value, 0".094 ± 9 (M). The mean trigonometric parallax yields $M = +1^m58$, which makes the star similar to *υ* and 71 Tau, Nos. 66 and 70 in Paper I, which have mean $M = +1^m45$ and $C_p = +0^m18$. Both these Hyades stars fall on a portion of the bright-dwarf sequence that was shown in Paper I to contain rapidly rotating A5–A7 stars of luminosity class III; the mean rotational velocity of the two Hyades stars was noted in Paper I as 200 km/sec, which is the same as that observed for α Cep by Miss Westgate.[31] The fact that luminosity class V, instead of IV or III, is assigned to this star in the *Atlas* may be caused by the haziness of the spectral lines resulting from the large rotational velocity.

From the foregoing examples, it is apparent that at least some of the fine structure in that portion of the color-luminosity array populated by the A-type stars probably is reflected in the spectra of these stars. Close scrutiny of high-dispersion spectra of the brighter stars populating the dwarf, blue-dwarf, and bright blue-dwarf sequences may reveal further criteria for differentiating these stars purely from their spectra. If such a separation can be made, the spectroscopic method of deriving individual parallaxes would become precise and powerful. Figure 6 shows the rather ill-defined color–spectral-type relationship for the *Atlas* stars, discussed above.

[31] *Ap. J.*, **78**, 46, 1933.

PARALLAX STARS NOT IN THE "ATLAS"

A few additional parallax stars not included in the *Atlas* but with $C_p \leqq +0^m17$ have been observed; data for these stars are given in Table 17 and are discussed below.

λ *Gem.*—The photometric parallax derived from Table 15 on the assumption that the star is a bright blue-dwarf is in excellent agreement with the mean trigonometric value given in Table 17; but, since a slightly larger parallax of 0".049 would place the star on the blue-dwarf sequence, we cannot confidently eliminate the possibility that it falls on the latter sequence.

δ *Leo.*—The individual determinations of the trigonometric parallax of this star are quite discordant. The assumption that the star is a dwarf leads to a photometric parallax of 0".057, which is close to the mean of the trigonometric values; but, if the star is a bright blue-dwarf, the photometric parallax is 0".074, which is still within the range of

TABLE 17

STARS WITH $C_p \leqq +0^m17$ BUT NOT INCLUDED IN THE *Atlas*

Star	P_{Cp}	C_p	n	π (Trig.)	π (Ptm)	Sequence
λ Gem	3^m59	$+0^m04$	4	0".045 ± 7 (A) .034 ± 11 (M) 0.041 ± 12 (S)		Bright blue-dwarf
			Mean	0.041 ± 6	0".039	
δ Leo	2.55	+ .10	3	0.040 ± 6 (A) 0.078 ± 10 (M)		Dwarf (?)
			Mean	0.050 ± 5	.057	
ι UMa	3.30	+ .165	3	0.066 ± 7 (A) 0.066 ± 14 (M)		Blue-dwarf (?)
			Mean	0.066 ± 8	.069	
72 Oph	3.72	+0.08	4	0.035 ± 9 (A) .033 ± 11 (M) 0.047 ± 8 (Y)		Bright blue-dwarf
			Mean	0.040 ± 5	0.042	

the parallax determinations. We may conclude, with some uncertainty, that the star probably is not a blue-dwarf.

ι *UMa.*—This star is quite similar to Altair, in that it has the same color and a large rotational velocity. Also, like Altair, it occurs near the junction of the dwarf and blue-dwarf sequences, a fact that prohibits a definite assignment to either sequence. From Tables 6 and 13 we find, for $C_p = +0^m165$, $M = +2^m38$ and $+2^m52$, respectively, or photometric parallaxes of 0".069, dwarf, or 0".073, blue-dwarf. Either value for the photometric parallax is consistent with the trigonometric determinations given in Table 16.

72 Oph.—The trigonometric parallaxes are quite consistent with the assumption that this star is a bright blue-dwarf.

VI. VISUAL BINARIES

Although the trigonometric parallaxes of stars more distant than those listed in Table 3 are not trustworthy enough to use in the construction of accurate color-lumi-

nosity arrays, we are able to test the slopes of the various sequences and the relative position of one sequence to another, by the use of visual binaries and widely separated stars known to possess common proper motion and radial velocity. These systems may be regarded as small clusters;[32] and, when one component is properly fitted to a sequence of the color-luminosity array, the other component should fall into place on another, or the same, sequence. The systems observed in the present program are discussed below and are listed in Table 18. The six wide pairs included in Table 3 are not entered in Table 18. For purposes of comparison with visual binaries, the dwarf sequence defined by the cluster stars and given in Table 6 is extrapolated from $C_p = +1^m06$ to $+1^m22$; the extrapolated portion is given as the second section of Table 6.

111 Tau.—If the brighter star is a dwarf, we find, from Table 6, $M = +4^m82$, or a photometric parallax of 0".078, which, when applied to the fainter component, gives $M = +8^m30$ as compared to $+8^m39$, given in Table 6 for $C_p = +1^m02$.

ρ Gem.—If both stars are dwarfs, Table 6 gives $M = +3^m15$ and $+7^m25$, or moduli of $m - M = +1^m26$ and $+1^m16$. The mean photometric parallax is then 0".057, which is identical with the mean trigonometric value.

α Leo (*Regulus*).—If the companion is a dwarf, then $M = +6^m89$ from Table 6, and hence $M = -0^m83$ for Regulus. The companion is itself a binary, but the magnitude difference is great enough, 5 mag., to insure that the observed magnitude and color is that of the brighter component alone. Regulus is, then, a blue-dwarf similar to Pleiades No. 54 (Paper II) with $M = -0^m55$ and $C_p = -0^m17$. The Pleiades star is classified B8 by Morgan, and it has a rotational velocity of 300 km/sec, compared to B8 V (*Atlas*) and 200 km/sec for Regulus. The photometric parallax of the system, 0".041, is the same as the mean trigonometric value.

γ Vir.—This double is too close to be separated with the 12-inch photometer, but the components differ by only 0.04 mag.[33] and are of the same spectral type. From the observed magnitude and color we find $Pg_p = 3^m75$ for each component. If the stars are dwarfs, Table 6 gives $M = +3^m38$, or a photometric parallax of 0".084, which agrees well with the mean trigonometric value, 0".089 ± 7.

+7°2690 and +7°2692.—These two stars, separated by 500″, have a common proper motion. The Mount Wilson observers assign to the brighter star a spectroscopic absolute magnitude of +3.8 and spectral type G2. If the fainter star is a dwarf, then, from Table 6, we find $M = +8^m75$, or $m - M = +2^m31$, and a photometric parallax of 0".034. If we apply this photometric parallax to the brighter component, we find $M = +4^m66$. The brighter component is then a subdwarf similar to such stars in Table 9 as λ Ser, with $M = +4^m78$ and $C_p = +0^m52$, and λ Aur, with $M = +4^m28$ and $C_p = +0^m51$. We can eliminate the possibility that the fainter component lies on the subdwarf sequence, as defined in Table 9, because, if such were the case, M would be near +10.0 mag., which would give a photometric parallax of 0".06—a value ruled out by the trigonometric determinations given in Table 18. Combining $M = +4^m66$ and $C_p = +0^m52$, we find the visual absolute magnitude of the brighter star to be +4.1 mag., which is in reasonably good agreement with the value +3.8 mag. found spectroscopically.

α Lib.—The two components of this system are separated by 230″. The brighter component is given in the *Atlas* as a metallic-line star, but the separation between the K-line

[32] It is an attractive hypothesis to regard visual binaries as the remains of galactic clusters. For example, stars Nos. 145 and 146 in the Coma Berenices cluster (Paper III) are close enough together to be linked in ADS 8568. One of these stars is a spectrum variable, the other a metallic-line star, and they form a pair very similar to π Boo, ADS 9338, one component of which also is a spectrum variable and the other a metallic-line star. When disintegration of the Coma cluster is completed, perhaps by galactic rotation or by some other disrupting force, it is possible that the two Coma stars may hold each other by mutual attraction and become another binary system like π Boo. The systems of ε Lyr, Castor, and many others are highly suggestive of such an origin.

[33] J. Stebbins, *U. Illinois Bull.*, Vol. 4, No. 25, 1907.

TABLE 18

PHOTOMETRIC AND TRIGONOMETRIC DATA FOR VISUAL BINARIES
(Wide Pairs in Table 3 Excluded)

Star	P_{g_p}	C_p	n	π (Trig.)	π (Ptm)	Sequence
111 Tau A	5m36	+0m43	2	0".065 ± 8 (A)		Dwarf
B	8.84	+1.02	2	0.059 ± 9 (M)		Dwarf
			Mean	0.062 ± 7	0".078	
ρ Gem A	4.39	+0.23	2	0.062 ± 10 (A)		Dwarf
B	8.41	+0.83	2	0.055 ± 8 (M)		Dwarf
			Mean	0.057 ± 6	.057	
α Leo A	1.09	−0.16	2	0.067 ± 10 (M)		Blue-dwarf
B	8.81	+0.77	3	0.026 ± 8 (V)		Dwarf
			Mean	0.041 ± 6	.041	
γ Vir AB	3.00	+0.25	2	0.101 ± 15 (M)		Dwarfs
				0.088 ± 8 (Y)		
			Mean	0.089 ± 7	.084	
+7°2690	6.97	+0.52	2	0.025 ± 14 (W)		Subdwarf
+7°2692	11.06	+1.08	7	.028 ± 6 (A)		Dwarf
				.040 ± 10 (M)		
				0.010 ± 9 (Y)		
			Mean	0.026 ± 4	.034	
α Lib A	2.72	+0.08	5	0.069 ± 13 (M)		Dwarf
B	5.33	0.29	4	.047 ± 7 (Y)		Dwarf
				0.041 ± 17 (y)		
			Mean	0.051 ± 5	.049	
−15°4041	9.67	+0.65	5	0.051 ± 10 (M)		Subdwarf
−15°4042	10.09	+0.74	6	.050 ± 9 (C)		Subdwarf
				.040 ± 14 (D)		
				.046 ± 12 (y)		
				0.029 ± 7 (Y)		
			Mean	0.040 ± 4	.035	
−0°2944 AB	7.18	+0.67	5	0.059 ± 6 (A)		Dwarfs (?)
				.049 ± 8 (y)		
				.046 ± 10 (M)		
				.060 ± 12 (Y)		
				0.094 ± 11 (W)		
			Mean	0.057 ± 4	.047	
β Ser A	3.61	+0.03	5	0.035 ± 10 (A)		Dwarf
BC	8.51	+0.56	3	0.033 ± 10 (M)		Dwarfs
			Mean	0.034 ± 7	.024	
36 Oph AB	5.01	+0.75	5	0.165 ± 8 (Y)		Dwarfs
C	7.39	+1.02	3	0.190 ± 9 (C)		Dwarf
			Mean	0.175 ± 5	0.160	

TABLE 18—*Continued*

Star	Pg_p	C_p	n	π (Trig.)	π (Ptm)	Sequence
+8°3689.....	8^{m}25	+0^{m}59	3	0".033 ± 8 (A)		Dwarf
+8°3692.....	8.85	+0.69	3	.038 ± 9 (M)		Dwarf
				0.036 ± 7 (Y)		
			Mean	0.035 ± 4	0".033	
17 Cyg AB	5.25	+0.38	4	0.045 ± 5 (A)		Bright-dwarf
ADS 12889 AB	8.45	+0.89	4	.046 ± 7 (M)		Dwarfs
				0.049 ± 7 (y)		
			Mean	0.047 ± 4	0.047	

and the metallic-line type is only between A3 and A7, and the star is not included in A. Slettebak's[34] catalogue of metallic-line stars brighter than fifth magnitude and north of declination −20°. If the fainter star is a dwarf, $M = +3^m80$, and the photometric parallax is 0".049, compared with the mean trigonometric value, 0".051 ± 5. If we apply the photometric parallax to the brighter component, we find $M = +1^m17$. The bright star is then also a dwarf, for Table 6 gives, at $C_p = +0^m08$, $M = +1^m07$. If this star is a metallic-line star, it is the brightest one yet discussed; from its position in the dwarf sequence we would expect the *Atlas* classification to be A3–A5 V.

−15°4041 and −15°4042.—These two stars, separated by 300″, have a common proper motion and radial velocity. The large radial velocities of both components, +306 ± 2 km/sec for −15°4041 and +300 ± 3 km/sec for −15°4042, obtained by D. M. Popper,[35] prove that the components are physically connected. Popper classifies −15°4041 as sdG6. If we assume the stars to be subdwarfs and interpolate for $C_p = +0^m65$ and $+0^m74$ in Figure 1 or Table 9, we find $M = +7^m40$ and $+7^m80$ for the brighter and fainter stars, respectively. The photometric parallaxes, then, are both 0".035, as compared with the mean trigonometric value, 0".040 ± 4. Since a parallax of 0".019 would be required to put these stars on the dwarf sequence, we may conclude that both are subdwarfs and, as such, they fill the gap, in Table 9, between HR 4550 and 36 UMa C.

−0°2944.—This star, ADS 9544, is a close double, with a separation of about 0".1, with an orbital period probably less than 5 years. R. G. Aitken,[36] the only observer from whom measures are available, gives the components equal magnitude, but this observation cannot be conclusive in so difficult a pair. If we correct the observed magnitude for the duplicity of the star and assume that the components are of equal magnitude, we find $Pg_p = 7^m93$ for each star. From Table 6 we find $M = +6^m30$ if the stars are dwarfs, or a photometric parallax of 0".047, as compared with the mean trigonometric value 0".057 ± 4, which is formed from several discordant values. The system has a fairly high radial velocity of −70 km/sec and a large proper motion of 1".38. Since a parallax of 0".078 would place the stars on the subdwarf sequence, we cannot altogether eliminate the possibility that the stars are subdwarfs. If, however, we disregard the discordant Mount Wilson value for the trigonometric parallax, given in Table 18, and allow for a small difference in magnitude between the components, we can conclude that the stars are probably dwarfs.

β Ser.—The companion to β Ser is +15°2906, which is 1600″ distant from the brighter star but shares its proper motion. The brighter star is classified A2 IV in the *Atlas*, which

[34] *Ap. J.*, **109**, 547, 1949.

[35] *Ap. J.*, **95**, 307, 1942.

[36] *New General Catalogue of Double Stars* (Washington: Carnegie Institution of Washington, 1932).

is the same classification given β Aur. If, like β Aur, β Ser is a dwarf, then, from Table 6, $M = +0^m50$, and the photometric parallax is $0''.024$.[37] If we apply this parallax to the faint star, we find $M = +5^m40$, compared to $M = +5^m63$ given in Table 6 for $C_p = +0^m56$. The faint star is itself a visual binary, ADS 9766, the components of which are separated by 6″ and were observed in this program as one star. Since we find that the combined light of the system falls 0.23 mag. above the dwarf sequence, we would expect the magnitudes of the components to differ by about 1.5 mag. photographically, or approximately 1.2 mag. visually, which may be compared with 1.0 mag. given as the rough, visual estimate by double-star observers. We conclude that β Ser and both components of the fainter star are dwarfs.

36 Oph.—The close pair, AB, of this triple system was measured as one star, while the C component was measured separately. The components of the close pair are of equal magnitude; hence $Pg_p = 5^m76$ for each component. If the bright stars are dwarfs, we find $M = +6^m78$ from Table 6 and a photometric parallax of $0''.160$, which falls just outside the range of the two discordant trigonometric values given in Table 18. If we apply the photometric parallax to component C, we find $M = +8^m41$, compared to $M = +8^m39$ from Table 6 for $C_p = +1^m02$. All three stars, therefore, are dwarfs.

+8°3689 and +8°3692.—These two stars, separated by 600″, have common proper motion and radial velocity. If +8°3689 is a dwarf, then from Table 6, $M = +5^m81$, and the photometric parallax is $0''.032$, which agrees with the accordant trigonometric values. If we apply the photometric parallax to +8°3692, we find $M = +6^m41$, which is the same value given in Table 6 for $C_p = +0^m69$. We conclude that both stars are dwarfs.

17 Cyg and ADS 12889.—The star 17 Cyg is a visual binary, ADS 12913, with components that differ more than 3 mag. in brightness and that are separated by 25″. The pair ADS 12889, 52ˢ preceding and 7′ south of 17 Cyg, has the same proper motion and radial velocity. The components of ADS 12889 are of equal magnitude and, because of their small separation, were measured as one star; the large magnitude difference between the components of 17 Cyg makes it certain that the observations of this pair are uncontaminated by the closer companion. If we correct the observations of ADS 12889 for equal luminosity of the components, we find $Pg_p = +9^m20$ for each star. From the assumption that 17 Cyg is a subgiant, as is indicated by the spectroscopic absolute magnitude, we have $M = +3^m60$ and a photometric parallax of $0''.047$, which is the same as the mean of the trigonometric values; the latter in each case are the mean of the observed values for 17 Cyg and ADS 12889. If we apply the photometric parallax to the components of ADS 12889, we find $M = +7^m55$, whereas Table 6 gives, for $C_p = +0^m89$, $M = +7^m61$. Both components of ADS 12889 are probably dwarfs, but the magnitudes may be slightly unequal.

VII. ROTATIONAL VELOCITY

An AND As STARS

We may recall from Paper I that the bright-dwarf sequence of the Hyades cluster appears to be populated by stars that, on the average, possess higher speeds of rotation than do stars populating the dwarf sequence. It was concluded that the separation between these two sequences was not an effect of rapid rotation on either the colors or the luminosities of the bright-dwarfs; the effect is just opposite to that noted by Adams and Joy,[18] who first pointed out that the rapidly rotating A-type stars, designated as An stars, are, in the mean, of lower luminosity than the sharp-lined, or As, stars. If we convert the colors into spectral classes, the separation between the dwarf and the bright-dwarf sequences occurs between the late A-type giants and the early A-type "main-

[37] β Ser is often included as a member of the extended Ursa Major cluster. If we adopt the constants derived in Paper III for this cluster, we find a cluster parallax of $0''.024$, which is identical with the photometric parallax.

sequence" stars. In Paper II the color-luminosity array for the Pleiades stars added the blue-dwarf and bright blue-dwarf sequences to the fine structure in the region populated by the A-type stars. A discussion of the rotational velocities of these stars revealed that, at least for the Pleiades, the broad-lined, rapidly rotating n stars populate the blue-dwarf sequence, whereas the five stars that fall on the bright blue-dwarf sequence are sharp-lined objects; the rapidly rotating A-type giants, which populate the upper end of the Hyades' bright-dwarf sequence, are absent from the Pleiades. Table 19 reproduces the results obtained in Paper II for the run of the mean rotational velocity with luminosity of the blue-dwarfs in the Pleiades. Only four blue-dwarfs with available estimates of rotational velocity, which are not spectroscopic binaries, are added by the present discussion. These stars are Sirius, Fomalhaut, 80 Ursae Majoris, Altair, and ι Ursae Majoris, with rotational velocities of 0, 85, 200, 200, and 125 km/sec,[38] respectively. For comparison, the rotational velocities for the bright blue-dwarfs and the dwarfs are listed in Table 20, from which it appears that, on the average, both these sequences are populated by more slowly rotating stars than is the blue-dwarf sequence. The relatively large number of sharp-lined stars on the bright blue-dwarf sequence, as compared to the blue-dwarf

TABLE 19

RUN OF MEAN OBSERVED ROTATIONAL VELOCITIES WITH LUMINOSITY OF THE BLUE-DWARFS IN THE PLEIADES

$\overline{V_r \sin i}$ (Km/Sec)	M	No. of Stars	$\overline{V_r \sin i}$ (Km/Sec)	M	No. of Stars
170.....	-3^m to -1^m	4	100.....	$+2^m$ to $+2^m5$	4
180.....	-1 to $+1$	5	60.....	$+2.5$ to $+3$	4
130.....	$+1$ to $+2$	5			

sequence, suggests that the luminosity difference between the n and s stars noted by Adams and Joy was caused by the presence of both blue-dwarfs, predominately n stars, and bright blue-dwarfs, predominately s stars, in their material. From a compilation of the A-type stars in the Mount Wilson catalogue of spectroscopic parallaxes,[4] J. A. Hynek[39] found that, in the mean, the s stars are brighter than the n stars by 0.8 mag. for spectral types A0–A4; stars classified later than A4 are not included here for fear of vitiating the mean luminosities by including A-type stars populating the dwarf sequence. In approximate agreement with this result, Tables 13 and 15 show a difference of about 0.75 mag. between blue-dwarfs and bright blue-dwarfs for $C_p = -0^m12$ to $+0^m02$. Struve has suggested that the luminosity differences between n and s stars may be caused by (1) ". . . systematic errors in the spectral classification used by Adams and Joy. . . ," (2) ". . . the more luminous stars actually rotate more slowly than the less luminous stars. . . ," or (3) ". . . the decrease in surface gravity due to rapid rotation simulates [an] absolute magnitude effect. . . ."[40] Struve suggests that the absolute-magnitude effect might arise from the fact that, if a star of a given spectral class could be given rapid rotation, the higher level of ionization resulting from the lowered surface gravity would lead to an earlier spectral class, while the color of the star would remain

[38] The sources of the rotational velocities quoted in this paper are Miss Westgate (*Ap. J.*, **78**, 48, 1933) and C. T. Elvey (*Ap. J.*, **71**, 228, 1930); the rotational velocities of the Hyades and Pleiades stars, the work of Struve and of Struve and Smith, are taken from Papers I and II. Estimates of the rotational velocities of the Coma Berenices cluster stars are, unfortunately, not available.

[39] *Ap. J.*, **83**, 476, 1936.

[40] *Observatory*, **54**, 84, 1931.

the same.[41] In any case, the presence of two sequences, the blue-dwarf and bright blue-dwarf, probably is not an effect of rotation on the observed colors; for, if that were true, we would not expect the sharp demarcation between the sequences, as is observed, but, instead, a rather ill-defined region in which the position of each star was determined by its rotational speed and by the orientation of its rotational axis.

TABLE 20

ESTIMATED ROTATIONAL VELOCITIES OF DWARFS AND BRIGHT BLUE-DWARFS

DWARFS			BRIGHT BLUE-DWARFS		
Star	M (Ptm)	$V_r \sin i$ (Km/Sec)	Star	M (Ptm)	$V_r \sin i$ (Km/Sec)
δ UMa	+0m70	175	ϵ UMa	±0m00	25
H 60	+1.07	150	α Lyr	+0.40	0
H 117	+1.20	0	γ UMa	+0.60	125
H 139	+1.25	100	β UMa	+0.70	0
H 119	+1.33	50	P 47	+0.90	0
H 84	+2.15	25	H 61	+1.19	0
H 34	+2.15	0	P 56	+1.19	50
H 141	+2.30	0	P 22	+1.45	0
H 96	+2.45	0	λ Gem	+1.53	150
P 58	+2.60	50	P 77	+1.82	75
H 39	+2.82	0	β Leo	+1.82	125
P 15	+2.82	75	72 Oph	+1.82	75
P 20	+2.92	50	P 75	+1.88	75
H 8	+3.02	100	H 50	+1.92	0
H 102	+3.14	75			
H 14	+3.27	0			
P 71	+3.27	75			
H 4	+3.27	25			
H 21	+3.70	25			
H 13	+3.79	0			
H 38	+3.79	0			
H 6	+4.15	25			

MAGNETIC VARIABLES

The foregoing conclusion, that the bright blue-dwarfs rotate more slowly, in the mean, than do the blue-dwarfs, may have some bearing on the presence of stellar magnetic fields recently measured by H. W. Babcock. All the stars for which Babcock has announced magnetic fields are "peculiar"[42] A-type stars, the majority of which are also known to be spectrum variables. He concludes that it is "not impossible that future observations will show that all spectrum variables of type A have variable fields and, indeed, that the spectrum variability results from the magnetic variations."[43] Furthermore, con-

[41] The role of H^- in the opacity of the A-type stars has been recognized since the discussions by Struve and by Hynek were published. Chandrasekhar and Münch (*Ap. J.*, **104**, 446, 1946) have shown that, for those stars in which the contribution of both H^- and H are important, for a fixed effective temperature the color temperature is sensitive to small changes in pressure. If g_{grav} is diminished by rotation, then the pressure will decrease in such a way as to make the star appear bluer. An accurate computation of the magnitude of this effect would be difficult, but qualitatively we can see that it would operate to make a rapidly rotating star bluer than a nonrotating star.

[42] The term "peculiar" is used here to indicate those A-type stars showing strong spectral features attributed to the elements manganese, europium, chromium, and strontium. Such stars are to be differentiated from the other peculiar A-type stars usually designated as "metallic-line" stars.

[43] *Ap. J.*, **108**, 200, 1948.

cerning the connection between the star's velocity of rotation and its magnetic field, he adds: "The spectra of some normal main-sequence stars of early type such as Sirius (A0) and γ Geminorum (A3), show little or no evidence of the Zeeman effect on plates taken with the analyzer. As there is a great range in equatorial velocity among the A-type stars, from practically zero up to 250 km/sec, it is possible that Sirius and γ Geminorum have a low rate of axial rotation; and as a working hypothesis we may retain the modified proposition that the most intense magnetic activity occurs in the stars that are rotating most rapidly."[44]

SPECTRUM VARIABLES

There are three recognized spectrum variables included with the bright blue-dwarfs in Table 14: C 146 = 17 Coma, C 160 = 21 Coma, and ε UMa. The star 17 Com is described in the *Atlas* as being very similar to 78 Vir, which was the first star shown by Babcock to possess a magnetic field.[44] Also, 17 Com is very nearly matched in color and luminosity by α CVn,[45] which Babcock has recently announced to possess a magnetic field.[46] Unfortunately, the three spectrum variables in Table 14, with the addition of 78 Vir and α CVn, represent only about 20 per cent of the total known (1947). A. J. Deutsch,[47] however, has shown, from a consideration of the trigonometric parallaxes for more than half the total number of known spectrum variables, that as a group they lie between 0.5 and 1.2 mag. above the main sequence. Since the main sequence in this case probably refers to the blue-dwarf sequence, it appears reasonable to assume that at least the majority of spectrum variables populate the bright blue-dwarf sequence; some support is given this assumption by Deutsch's observation that "the peculiar A-stars generally exhibit less strongly winged hydrogen lines than do the main sequence stars of the same spectral type."[21]

To summarize, we may state the following conclusions concerning rotational velocities:

1. The bright blue-dwarfs rotate more slowly, in the mean, than do the blue-dwarfs. The separation between the two sequences in this respect, however, is not complete; for, although the zero rotational velocity of, say, Sirius, a blue-dwarf, may result from the fact that we are viewing this star nearly "pole-on," there are stars, such as γ UMa or λ Gem, which populate the bright blue-dwarf sequence and have rapid velocities of rotation.

2. If we associate magnetic fields with rapid rotation, then it is necessary to assume that the spectra of stars such as ε UMa, 17 Com, 21 Com, 78 Vir, and α CVn show negligible rotational disturbances because their axes of rotation are directed toward the sun. Since, according to Babcock, all spectrum variables of type A may possess variable

[44] 78 Vir was not included in the discussion of the bright blue-dwarf sequence because of its relatively small and uncertain trigonometric parallax, 0".018 ± 5. The observations of magnitude and color give $Pg_p = 4^m83$, $C_p = -0^m01$. If we assume the star to be a bright blue-dwarf, then, from Table 15, $M = +1^m10$, and the photometric parallax is 0".018. The assumption is usually made that this star belongs to the Ursa Major cluster, and the constants derived for this cluster in Paper III lead to the cluster parallax of 0".017 for 78 Vir.

[45] α CVn was not observed on the present program because of its small and uncertain trigonometric parallax and also because it is not possible to separate the visual components of the wide double with the 12-inch photometer. The individual visual magnitudes are given in *Harvard Mimeograms*, Ser. III, No. 2, as 2.74 and 5.26 mag. A. Deutsch (*Ap. J.*, **105**, 283, 1947) has classified the fainter component as F5 IV, which, from Fig. 2, corresponds to $C_p = +0^m37$ or Pg (B) $= 5^m63$. The brighter component is contained in Hertzsprung's catalogue of effective wave lengths (*B.A.N.*, **9**, 101, 1940); so, by converting c_2/T to C_p, we find $C_p = -0^m07$ or Pg (A) $= 2^m67$. Since the B component is a subgiant, we take $M = +3^m60$, and the modulus of the system is +2.03 mag., which gives a photometric parallax of 0".039; the mean trigonometric parallax is 0".033 ± 5. Applying the distance modulus, +2.03 mag., to the brighter star, we find $M = +0^m71$ at $C_p = -0^m07$, compared with $M = +0^m50$ for $C_p = -0^m07$ in Table 15, with the assumption that the star is a bright blue-dwarf.

[46] *Pub. A.S.P.*, **61**, 226, 1949.

[47] *Ap. J.*, **105**, 283, 1947.

magnetic fields and since we have found that at least the majority of the spectrum variables populate the bright blue-dwarf sequence, then it appears that intense magnetic fields are a feature of bright blue-dwarfs, or, more precisely, of those bright blue-dwarfs which have their poles of rotation directed toward the sun. The requirement that the pole of rotation be directed toward the sun is probably only an observational one, since the Zeeman effect would be lost in rotationally broadened lines.

3. There appears to be no correlation between color and spectrum, or magnetic variability among the bright blue-dwarfs. For example, Vega, with $C_p = -0^m075$, is of nearly the same color as 17 Com, $C_p = -0^m08$, and yet Vega is not a recognized spectrum variable. The same situation exists for 78 Vir, with $C_p = -0^m01$, which is similar to Hyades No. 61 or to Pleiades No. 56, both with $C_p = 0^m00$ in Table 14, but the two cluster stars are not recognized spectrum variables. It may be that spectrum variability, like magnetic variability, also requires that the stellar poles of rotation be directed toward the sun and that Vega, β UMa, and the other bright blue-dwarfs in Table 19, which show no rotational line-broadening, fail to do so because of a real lack of rapid rotation. It is possible, also, that the spectrum variables possess shells that are rotating much more slowly than are the photospheres of the stars; the association of rapid rotation with the presence of magnetic fields could then be preserved without the necessity of assuming that all spectrum variables are viewed pole-on.

VIII. CONCLUDING REMARKS

There are several obvious questions which present themselves in the interpretation of the foregoing data. The answers to some will require more observations, which are now being obtained at the Lick Observatory.

An important question pertains to what extent the various sequences represent real differences in the stars. The bright-dwarf and subdwarf sequences have been discussed at some length. We have seen that the separation between the blue-dwarf, bright blue-dwarf, and dwarf sequences is reflected in the spectra of these stars; our knowledge of Sirius and Vega alone, two early A-type stars with the well-determined difference in luminosity amounting to 1 mag., is convincing evidence for the reality of this separation. There is strong evidence that the spectrum and magnetic variables of class A occur among the bright blue-dwarfs and that the brighter components of at least three Algol-type eclipsing stars—U Cep, U Sge, and Algol—populate the blue-dwarf sequence. Unfortunately, it is in just such eclipsing systems that Struve has found spectroscopic evidence that the velocity-curves are not a true representation of the motions of the stars, so that we are not able to make use of the spectroscopic data to estimate the size and masses of the components. Among the brighter stars on the bright blue-dwarf sequence, only three are known spectroscopic binaries, and one of these, α CrB, is also an eclipsing star. D. B. McLaughlin[48] has studied α CrB spectroscopically and has found that its rotational period is much shorter than the period of revolution. In this respect α CrB is similar to the brighter stars of the U Cep and U Sge systems, for which Struve has also found a lack of equality between rotational and orbital velocities. The similarity, however, ends with this feature, for the Algol systems have periods less than 5 days and the components are subgiants, of larger size than the brighter stars by at least a factor of 2, compared to the well-separated components of α CrB, the fainter of which has only 30 per cent of the radius of the brighter. We also suspect that YZ Cas is a bright blue-dwarf. This system was not observed on the present program because the wide visual pair is not resolvable with the 12-inch photometer. However, two-color photometry by Kron[49] provides enough information to derive the approximate International magnitudes and colors of the components. From Kron's data we find Pg (A) $= 5^m76$, $C = -0^m01$, and

[48] *Pub. Obs. U. Michigan*, **5**, 91, 1933.

[49] *Ap. J.*, **96**, 87, 1942; *Contr. Lick Obs.*, Ser. II, No. 5, and *Lick Obs. Bull.*, **19**, 59, 1939.

Pg (B) = 8^{m}71, C = +0^{m}33. If we assume that the fainter component is a dwarf, then, from Table 6, M (B) = +4^{m}14 and, therefore, M (A) = +1^{m}19. From Table 15 we find that a bright blue-dwarf with C = −0^{m}01 has M = +1^{m}10. From the color of the dwarf component, C = +0^{m}33, which corresponds to dF5, we estimate the mass to be 1.5 ⊙, which, when combined with the mass functions, gives 3 ⊙ for the mass of the brighter star. From unpublished work Kron estimates the fainter components of α CrB to be of approximately solar type; hence, if, by analogy with the YZ Cas system, we assume it to be a dwarf of solar mass, we derive, from the mass function, 3 ⊙ as the mass of the brighter star. The resulting radii are then 2.7 ⊙ and 2.8 ⊙ for the bright blue-dwarf components of YZ Cas and α CrB, respectively. The radii derived for the dwarf components, 1.4 ⊙ and 1.0 ⊙, respectively, are consistent with the assumed masses for these stars. Although the values quoted above are necessarily rough, they provide us with an estimate that the masses and radii of bright blue-dwarfs exceed the solar values by a factor of 2–3. The distribution of the A-type eclipsing systems in the various sequences is further marked by the presence of β Aur on the dwarf sequence. The system of β Aur contains two very nearly equal dwarfs with masses of ∼2.2 ⊙ and radii of ∼2.4 ⊙; these values are somewhat smaller than those of the bright blue-dwarfs. To summarize, then: the somewhat limited data appear to separate the A-type eclipsing stars into the three sequences populated by the A-type stars, as follows:

1. Blue-dwarfs: Algol systems with large subgiants as the secondary components
2. Bright blue-dwarfs:[50] α CrB systems with relatively smaller dwarfs as secondary components
3. Dwarfs:[51] β Aur systems with both components very nearly equal in mass, luminosity, and temperature

The occurrence of the components of eclipsing stars on the various sequences will be discussed in more detail in a succeeding paper of this series.

Another question that might be mentioned here pertains to the distribution of the so-called "high-" and "low-velocity" stars among the various sequences. The most striking sequence in this respect is the subdwarf sequence, where all but two stars have peculiar space motions exceeding 70 km/sec. The two exceptions are 36 UMa C and ADS 246 B; the space motion of 36 UMa C is less than 30 km/sec, while that of ADS 246 is about 60 km/sec. It may be significant that both these stars have dwarf companions, although ADS 246 may escape the net for high-velocity stars because of the arbitrary limit of 70 km/sec and the high dispersion for the velocities of such stars. In contrast to the fact that all the single stars populating the subdwarf sequence have peculiar space motions in excess of 70 km/sec, the stars on the dwarf sequence contain a mixture of both high- and low-velocity stars. For example, the motions of the dwarfs 72 Her, CC 1017, and both components of 61 Cyg exceed 100 km/sec. It is interesting that, in contrast to the low-velocity system of 36 UMa, which contains a subdwarf and two dwarfs, we have the system of CC 1017 and 1018, with a peculiar space motion of over 100 km/sec, which also contains members of both sequences. A large number of high-velocity stars is found among the subgiants; for about 20 per cent of the stars in Table 4 are of this type, the most notable examples being ζ Her, γ Ser, and η Cep, all with peculiar space motions exceeding 100 km/sec.

I am indebted to my colleagues, Messrs. Herbig, Kron, Mayall, and Weaver, for discussions on some of the questions raised here.

[50] As a result of the large differences in size and luminosity of the components of these systems, both eclipses are very shallow and have been discovered by photoelectric methods only.

[51] WW and AR Aur probably are similar systems.

SPECTROGRAPHIC OBSERVATIONS OF W URSAE MAJORIS*

OTTO STRUVE AND HENRY G. HORAK
Yerkes and McDonald Observatories
Received April 21, 1950

ABSTRACT

Observations made at the McDonald Observatory indicate that $\gamma = -50$ km/sec, $K_1 = 125$ km/sec, and $K_2 = 250$ km/sec. The emission lines of *Ca* II are in phase with the more massive component of the binary and give $K_{Ca} = 190$ km/sec. The heavier component is in front during the principal minimum. There is a possibility that the contours of the absorption lines of the red component observed at phases in the vicinity of $0.25P$ were more diffuse in 1949 than in 1950 and that this led to a difference in the measured radial velocities.

The spectrographic orbit of W Ursae Majoris was determined by A. H. Joy in 1919.[1] From the measurement of ten Mount Wilson spectrograms secured during the winter of 1917–1918, he derived a set of approximate elements: $\gamma = -5$ km/sec, $K_1 = 134$ km/sec, $K_2 = 188$ km/sec, and $e = 0.00$. Because of the observational interest of this short-period eclipsing variable, the star was placed on the program of the McDonald Observatory, and two series of spectrograms were obtained: the first on January 19, 1949, and the second between January 19 and January 21, 1950. All plates were obtained with the Cassegrain spectrograph attached to the 82-inch reflector. Two quartz prisms and a camera 500 mm in focal length yielded a linear dispersion of 40 A/mm at λ 3933. The slit width was 0.05 mm.

The character of the spectrum has already been described by Joy. The type is approximately F8, and the lines are greatly broadened by the rapid rotation of the two components. Nevertheless, the doubling of the lines at the two elongations is very striking, as may be seen in Figure 1. As a rule, the violet component is slightly stronger, irrespective of whether it is produced by the more massive or by the less massive star.

The spectrograms were first measured by Horak and the list of lines which he used is given in Table 1. The results of his measurements, using all lines, are shown in Figure 2.

TABLE 1

STAR LINES USED IN W URSAE MAJORIS

Ca II	3933.67	*Fe* I	4143.72
Fe I	4005.26	*Hγ*	4340.49
Fe I	4045.82	*Fe* I	4415.14
Fe I	4071.75		

From an examination of the original plates it was concluded that the line *Fe* I 4046 gives better results than do the rest of the lines, many of which are seriously blended. Hence, on the later spectrograms he measured only this *Fe* I line. Table 2 gives the results of Horak's measures. Table 3 shows, for comparison, a set of measures by Struve. The agreement is satisfactory, and there is no appreciable systematic difference between the two measurers. There is, however, a conspicuous difference between the velocity-curves obtained from the line *Fe* I 4046 and that obtained from all lines listed in Table 1. Figures 3 and 4 give the results for *Fe* I 4046. The means of Struve's and Horak's meas-

* *Contributions from the McDonald Observatory, University of Texas*, No. 191.

[1] *Ap. J.*, **49**, 189, 1919.

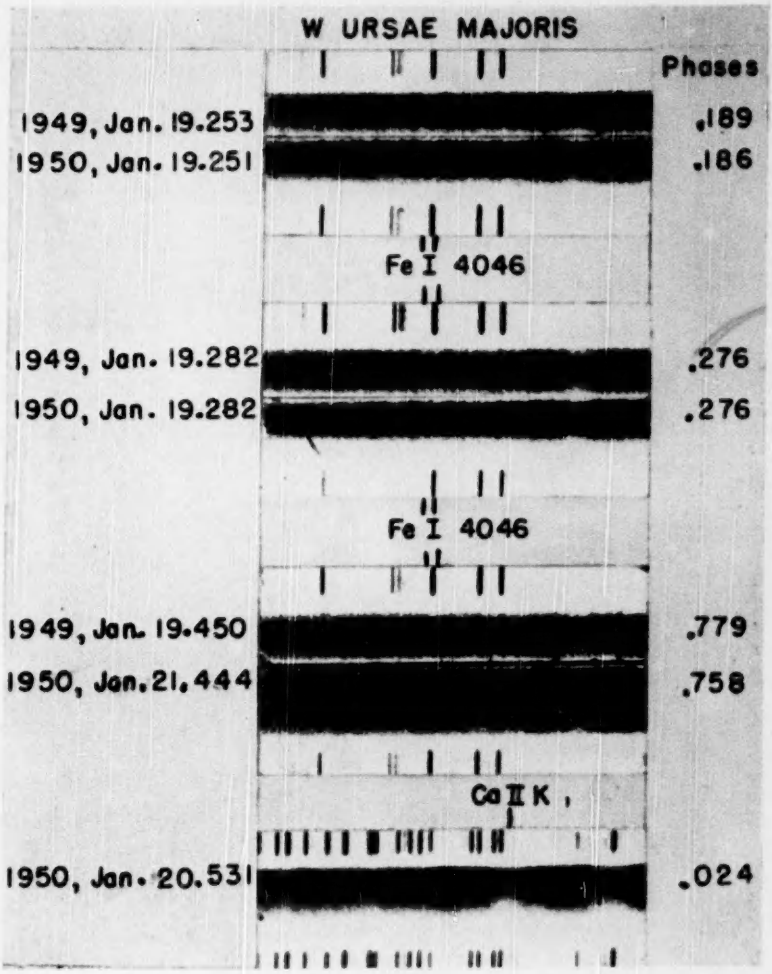
W URSAE MAJORIS
Phases
1949, Jan. 19.253
.189
1950, Jan. 19.251
.186
Fe I 4046
1949, Jan. 19.282
.276
1950, Jan. 19.282
.276
Fe I 4046
1949, Jan. 19.450
.779
1950, Jan. 21.444
.758
Ca II K
1950, Jan. 20.531
.024

FIG. 1

ures were plotted in Figure 3 for those plates that were measured by both observers. In Figure 4 Struve's measures are shown by crosses.

The difference between Figures 3 and 4, on the one hand, and Figure 2, on the other, is quite pronounced, and it is difficult to decide which pair of curves more nearly approaches the truth. It will be noticed that there is no great difference between Figures 3 and 4, and we conclude that there has been no change in the orbital elements between 1949 and 1950. A few of the measured points of the red component between phases 0.1*P*

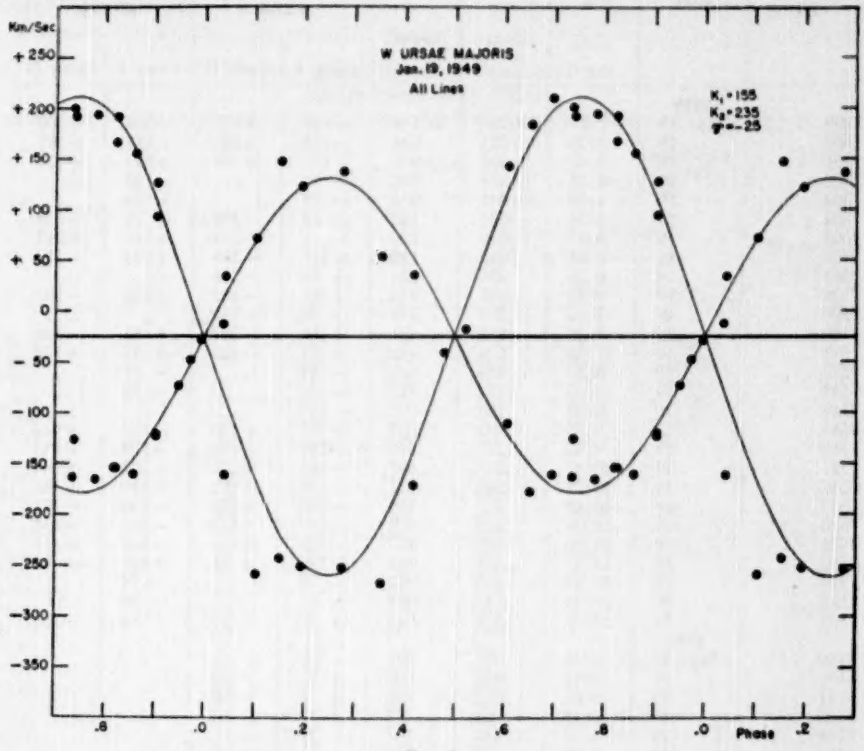

FIG. 2

and 0.3*P* lie systematically above the curve in 1949 (Fig. 3) and are on the curve or below it in 1950 (Fig. 4). This looks like a real effect, and we have carefully examined the corresponding plates in order to run down the cause of the discrepancy. Figure 1 shows three pairs of spectrograms. The two pairs at the top fall in the range of phases which we have just discussed. The pair at the bottom is in the other loop. It is perhaps significant that the red component of *Fe* I 4046 is more diffuse on the 1949 spectrograms than on those taken in 1950. Similarly, the red component of *Hδ* appears only as a diffuse shading on the red side of the stronger, violet component in 1949, while in 1950 the two components are distinctly resolved. It is probable, but by no means completely certain, that the contours of the red components at phases in the vicinity of 0.25*P* are slightly different and that this effect gives rise to the systematic behavior of the radial velocities. No such systematic effect can be detected at phases in the vicinity of 0.75*P*.

TABLE 2

RADIAL VELOCITIES OF W URSAE MAJORIS
(Measurements by H. Horak)

PLATE CQ	DATE	U.T.	PHASE		VELOCITIES (KM/SEC)			
					λ 4046		All Lines	
			Days	Period	Comp. I	Comp. II	Comp. I	Comp. II
	1949							
7499	Jan. 19	2:27	0.246	0.737	−188	+193	−164	+200
7500	19	3:08	.275	.824	−172	+186	−155	+191
7501	19	3:47	.302	.905	−152	+ 69	−123	+126
7502	19	4:21	.325	.974	− 74	.....	− 48	.....
7503	19	4:50	.011	.033	− 19	.....	− 13	.....
7504	19	5:23	.034	.102	+ 32	−295	+ 71	−259
7505	19	5:45	.050	.150	.....	−270	+147	−243
7506	19	6:05	.063	.189	+137	−289	+122	−252
7507	19	6:25	.077	.231	+ 52	−354	.....	.....
7508	19	6:46	.092	.276	+147	−282	+136	−253
7509	19	7:06	.106	.318	+ 20	−270	.....	.....
7510	19	7:24	.118	.354	+ 56	−289	+ 53	−268
7511	19	7:53	.138	.414	+ 23	−166	+ 35	−172
7512	19	8:22	.159	.477	− 55	.....	− 41	.....
7513	19	8:42	.173	.519	− 26	.....	− 18	.....
7514	19	9:04	.198	.593	−137	.....	.....	.....
7515	19	9:25	.202	.605	−107	+150	−112	+142
7516	19	9:46	.217	.650	−186	+153	−179	+183
7517	19	10:07	.232	.695	−163	+225	−162	+208
7518	19	10:28	.246	.737	−126	+192	−126	+192
7519	19	10:48	.260	.779	−156	+179	−166	+194
7520	19	11:07	.273	.818	−153	+137	−155	+166
7521	19	11:26	.286	.857	−192	+153	−161	+155
7522	19	11:47	.301	.902	−130	+ 91	−121	+ 93
7523	19	12:08	.316	.947	− 78	.....	− 74	.....
7524	19	12:31	.332	.995	− 61	.....	− 30	.....
7525	19	12:55	.014	.042	+ 22	−192	+ 34	−162
	1950							
8149	Jan. 19	4:42	.007	.021	− 46	.....	.....	.....
8150	19	5:22	.035	.105	+ 75	−263	.....	.....
8151	19	6:02	.062	.186	+ 39	−292	.....	.....
8152	19	6:45	.092	.276	+ 52	−302	.....	.....
8154	19	8:14	.154	.462	− 29	.....	.....	.....
8155	19	9:00	.186	.557	.....	+ 62	.....	.....
8156	19	9:47	.219	.656	−167	+147	.....	.....
8157	19	11:20	.283	.848	−132	+127	.....	.....
8158	19	12:00	.311	.932	− 84	+ 92	.....	.....
8159	19	12:42	.007	.021	− 40	.....	.....	.....
8170	20	8:14	.153	.459	− 35	.....	.....	.....
8171	20	9:16	.196	.587	−179	+ 39	.....	.....
8173	20	12:44	.008	.024	− 20	.....	.....	.....
8179	21	4:34	.000	.000	− 36	.....	.....	.....
8180	21	5:34	.041	.123	+ 32	−221	.....	.....
8181	21	6:35	.083	.249	+ 63	−286	.....	.....
8182	21	7:36	.126	.378	+ 66	−261	.....	.....
8183	21	8:37	.168	.504	− 41	.....	.....	.....
8184	21	9:38	.210	.629	−152	+111	.....	.....
8185	21	10:39	0.253	0.758	−172	+188	.....	.....

If we adopt the measurements of λ 4046 as the more reliable set, we conclude that the orbital elements are as follows:

$$\gamma = -50 \text{ km/sec}, \quad K_1 = 125 \text{ km/sec}, \quad K_2 = 250 \text{ km/sec}.$$

These elements differ appreciably from those obtained by Joy, especially in the case of the velocity of the center of mass of the system. Even if we adopt Figure 2 based upon the measurements of all lines, we find $\gamma = -25$ km/sec, which is still considerably lower than Joy's value of -5 km/sec.

TABLE 3

RADIAL VELOCITIES OF W URSAE MAJORIS
(Measurements by O. Struve)

Plate CQ	Date	U.T.	Phase		Velocities (Km/Sec)		
			Days	Period	λ 4046		Emission of Ca II
					Comp. I	Comp. II	
	1949						
7505	Jan. 19	5:45	0.050	0.150	+ 89.6	−288.4	.....
7506	19	6:05	.063	.189	+105.9	−307.6	.....
7507	19	6:25	.077	.231	+ 99.2	−346.9	.....
7508	19	6:46	.092	.276	+102.2	−278.7	.....
7509	19	7:06	.106	.318	+102.2	−284.7	.....
7510	19	7:24	.118	.354	+ 36.9	−311.3	.....
	1950						
8149	Jan. 19	4:42	.007	.021	.....	.....	− 26.7
8150	19	5:22	.035	.105	.....	.....	− 26.9
8151	19	6:02	.062	.186	+ 56.9	−311.4	+190.3
8152	19	6:45	.092	.276	+ 33.9	−333.7	+194.9
8153	19	7:30	.123	.369	+ 10.9	−203.3	.....
8154	19	8:14	.154	.462	.....	.....	+150.6
8155	19	9:00	.186	.557	.....	.....	−152.0
8156	19	9:47	.219	.656	.....	.....	−139.9
8157	19	11:20	.283	.848	.....	.....	−201.1
8158	19	12:00	.311	.932	.....	.....	−155.4
8159	19	12:42	.007	.021	.....	.....	− 50.9
8170	20	8:14	.153	.459	.....	.....	+ 79.9
8171	20	9:16	.196	.587	.....	.....	−137.3
8172	20	11:47	.301	.902	.....	.....	−243.6
8173	20	12:44	.008	.024	.....	.....	− 43.0
8179	21	4:34	.000	.000	.....	.....	− 50.4
8180	21	5:34	.041	.123	+ 42.7	−250.0	+174.3
8181	21	6:35	.083	.249	+ 78.3	−273.0	+146.8
8183	21	8:37	.168	.504	.....	.....	−165.1
8184	21	9:38	0.210	0.629	.....	.....	−189.6

The phases of the observations listed in Tables 2 and 3 were computed with the help of the elements:

$$\text{Principal minimum} = \text{JD } 2420980.8093 + 0.333636993E,$$

which were first derived by E. J. Woodward and adopted without change in the *General Catalogue of Variable Stars* by Kukarkin and Parenago for 1948.

The spectrograms obtained on January 19, 1949, gave some indication of diffuse emis-

sion lines of *Ca* II. However, the exposure times were not long enough to bring out these emission lines clearly. In 1950 the exposures were made long enough to reach the background intensity in the centers of the strong *Ca* II absorption lines. The existence of the emission lines immediately became apparent.[3] Table 3 lists the measured velocities from the bright line of *Ca* II 3933. There is only one component, and its variation in radial velocity is in phase with that of the more massive component of the binary. The ampli-

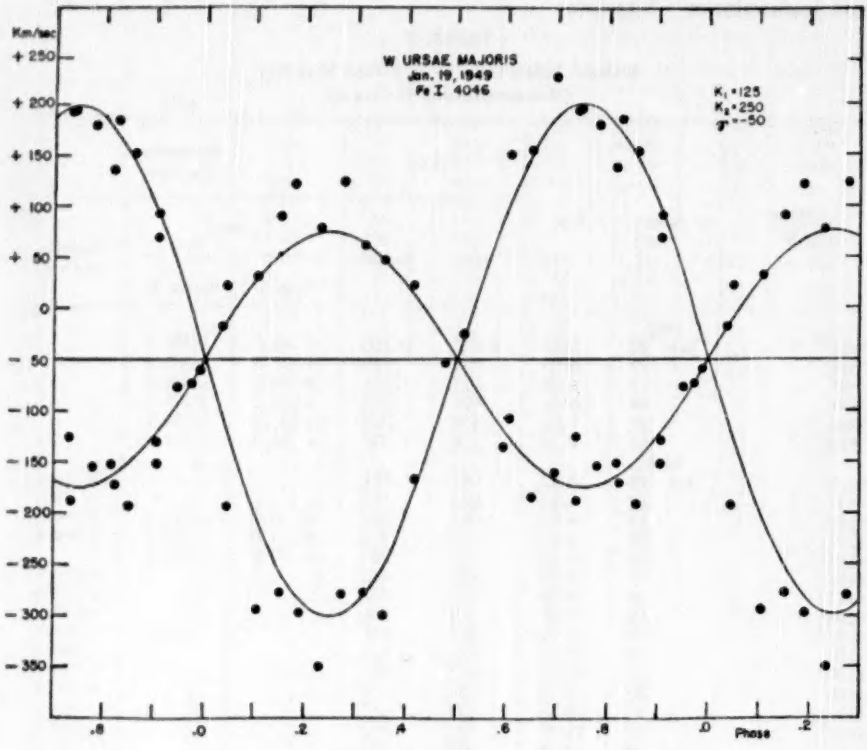

FIG. 3

tude of the variation of the emission line of *Ca* II is, however, much greater. This is shown in Figure 5. An enlargement of a plate showing the emission is reproduced at the bottom of Figure 1.

In conclusion, we may say that the observations of W Ursae Majoris are consistent with those previously published for other binaries of the same type. At principal minimum the less massive component is eclipsed by the more massive one: the mass ratio is $a = K_2/K_1 = 2.0$, which is not in agreement with the mass-luminosity relation; and the changes in the intensities of the two components are similar to those observed in many spectroscopic binaries of very short period.

[3] *Pub. A.S.P.*, **62**, 47, 1950.

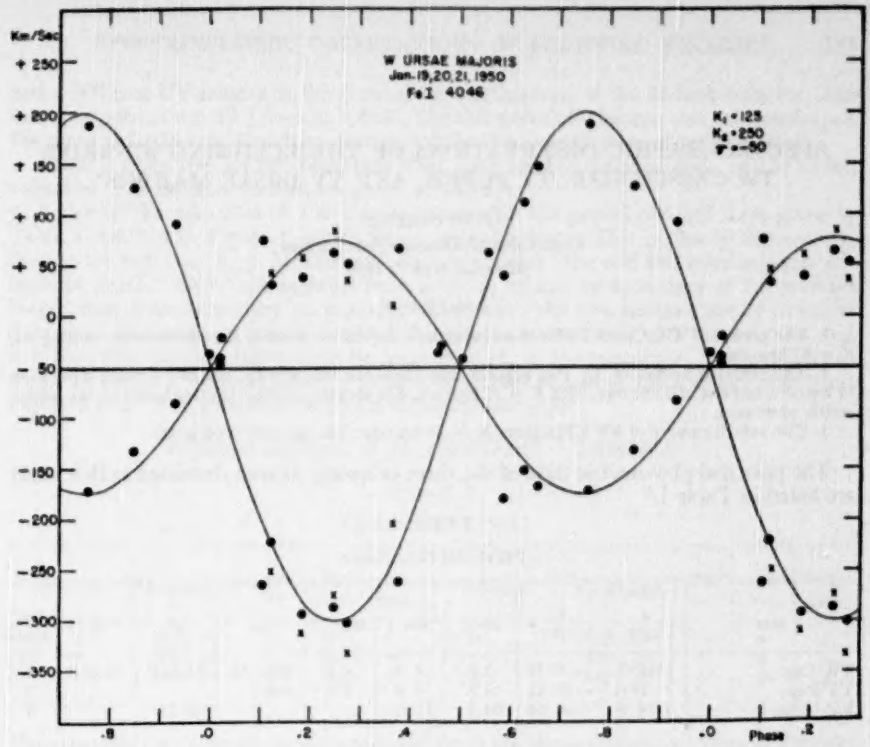
W URSAE MAJORIS
Jan. 19, 20, 21, 1950
Fe I 4046
K1 = 125
K2 = 250
γ = -50
Km/Sec
+250
+200
+150
+100
+50
0
-50
-100
-150
-200
-250
-300
-350
.8
.0
.2
.4
.6
.8
.0
Phase
.2

FIG. 4

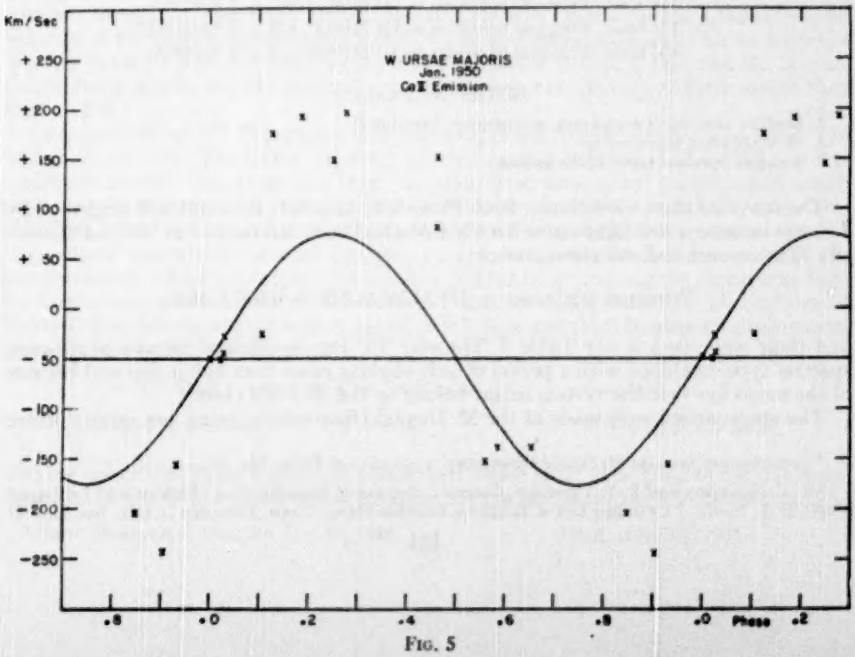
W URSAE MAJORIS
Jan. 1950
CaII Emission
Km/Sec
+250
+200
+150
+100
+50
0
-50
-100
-150
-200
-250
.8
.0
.2
.4
.6
.8
.0
Phase
.2

FIG. 5

SPECTROGRAPHIC OBSERVATIONS OF THE ECLIPSING BINARIES TW CASSIOPEIAE, TY PUPPIS, AND VV URSAE MAJORIS*

OTTO STRUVE
Yerkes and McDonald Observatories
Received May 1, 1950

ABSTRACT

1. The period of TW Cas is 1.428328 days, or half the value listed in the photometric catalogues; $K = 87$ km/sec.
2. The radial velocities of TY Pup suggest that there are two periods, one of 9.7 days, with $K = 74$ km/sec, and one of 0.581 day, with $K = 32$ km/sec. The shorter period is the one found by the photometric observers.
3. The velocity-curve of VV UMa gives $K = 59$ km/sec. The spectral type is A0.

The principal photometric data of the three eclipsing binaries discussed in this paper are listed in Table 1.[1]

TABLE 1

PHOTOMETRIC DATA

Star	α 1950	δ 1950	Max.	Min. I	Min. II	Sp.	D	d	Remarks
TW Cas	$2^h41^m.7$	$+65°31'$	8.3	8.9	8.9	B9+A0	$0.11P$	$0.01P$	1
TY Pup	7 30.6	−20 41	8.5	8.9	8.9	A9n	.....	.....	2
VV UMa	9 34.5	+56 14	10.1	11.0	.....	.....	0.21	.....	3

LIGHT-ELEMENTS

TW Cas: Principal minimum = JD 2419823.647 + 2.856656E,
TY Pup: Principal minimum = JD 2419455.618 + 0.58071564E,
VV UMa: Principal minimum = JD 2428925.135 + 0.687384E.

NOTES TO TABLE 1

1. Shallow annular? Two spectra, eccentricity, variable P.
2. W UMa type; two spectra?
3. Ranges? Spectral type? Little known.

The first two stars were chosen from Pierce's finding list, the third was suggested by J. Irwin because a new light-curve for VV UMa had been determined at Indiana University. The revised Indiana elements are:

$$\text{Principal minimum} = \text{JD } 2428925.135 + 0.6873748E,$$

and these were used in our Table 3. The star TY Pup is unusual because of its early spectral type combined with a period of only slightly more than half a day and because of the suspicion that the system might belong to the W UMa class.

The observations were made at the McDonald Observatory, using two quartz prisms

* *Contributions from the McDonald Observatory, University of Texas*, No. 192.

[1] B. V. Kukarkin and P. P. Parenago, *General Catalogue of Variable Stars* (Moscow and Leningrad, 1948); N. L. Pierce, "A Finding List of Eclipsing Variable Stars," *Contr. Princeton U. Obs.*, No. 22, 1947.

and a 500-mm UV camera in the Cassegrain spectrograph of the 82-inch reflector. The linear dispersion was 40 A/mm at λ 3933. The slit width of 0.05 mm was projected upon the plate as 0.025 mm. Emulsion Eastman 103*a*-O was used throughout this work.

Table 2 gives the list of absorption lines used for the determination of the radial velocities. The radial velocities are given in Table 3.

A plot of the velocities of TW Cas obtained with the period of 2.857 days given in Table 1 resulted in Figure 1, which shows a double wave. This is clearly not correct, despite the fact that R. J. McDiarmid[2] had found that "the odd and even minima differed in depth," that "the interval from primary eclipse to secondary is 7.8 minutes longer than from secondary to primary," and that "the two eclipses are of different duration." The evidence from the radial velocities is not consistent with these results, and it is desirable that the light-curve be redetermined. In the meantime, it seems best to adopt E. Zinner's[3] original period of 1^d10^h. Hence, the phases of TW Cas in Table 3 and Figure 2 have been computed with the following elements:

$$\text{Principal minimum} = \text{JD } 2419823.647 + 1.428328E .$$

TABLE 2

LIST OF STAR LINES

Element	Wave Length	TW Cas	TY Pup	VV UMa	Element	Wave Length	TW Cas	TY Pup	VV UMa
Ca II	3933.67	+	+	+	*Ca* I	4226.73	−	+	+
Fe I	4045.82	−	+	+	*Hγ*	4340.49	+	+	+
Hδ	4101.74	+	+	+	*Mg* II	4481.26	+	+	+

The spectrum, of class B9, is characterized by fairly sharp absorption lines of *Ca* II K and *Mg* II 4481. This and the absence of any rotational disturbance in the velocity-curve of Figure 2 indicate that the A star is small in size and has no excessive velocity of axial rotation, as we have found in U Cep, U Sge, and RZ Scu. On the contrary, the rotational velocity of the early-type component of TW Cas is unexpectedly small for an object of type A0 having a period of only 1.4 days. The periods of U Cep, U Sge, and RZ Scu are considerably longer, and the spectral types of the first two are only slightly earlier than that of TW Cas.

The spectrum of TY Pup shows only one component, which is broad and hazy. The type is about A9n. The radial velocities plotted against the period of 0.5807 day immediately showed that there is a large variation with some other period, upon which there may be superposed a variation with the half-day period of somewhat smaller amplitude in radial velocity. The spectrographic material is not sufficient to disentangle the two periods completely, and we can give only a very tentative interpretation of the measurements. The large-range variation was derived by estimating the departures from the mean curve for each date of observation. These values appear in the third column of Table 4. They are consistent with a period of 9.7 days and the following set of elements, derived graphically from Figure 3:

$P = 9.7$ days, $K = 74$ km/sec, $\omega = 100°$,

$\gamma = +4$ km/sec, $e = 0.45$, $T =$ Phase 7.1 days.

The last column of Table 4 gives the corrections which must be applied to the measured velocities of TY Pup in order to correct them for the motion in the 9.7-day period. The

[2] *Contr. Princeton U. Obs.*, No. 7, p. 16, 1924.

[3] *A.N.*, **190**, 337, 1911.

TABLE 3

RADIAL VELOCITIES OF TW CASSIOPEIAE

Plate No. CQ	Date	U.T.	Phase (Days)	Phase (Period)	Radial Velocities (Km/Sec)
	1950				
8023	Jan. 1	5:09	1.362	0.954	+ 24.9
8024	1	6:16	1.408	.986	− 18.0
8029	2	1:26	0.779	.545	+ 34.9
8030	2	2:55	0.841	.589	+ 20.4
8032	3	5:35	0.523	.366	− 86.6
8041	5	3:28	1.006	.704	+ 64.2
8042	5	4:30	1.049	.734	+ 63.0
8053	6	5:11	0.649	.454	− 24.5
8054	6	6:34	0.707	.495	− 48.5
8059	7	1:20	0.060	.042	− 41.1
8060	7	2:35	0.113	.079	− 65.7
8061	7	3:59	0.171	.120	− 88.9
8062	7	5:08	0.219	.153	− 86.6
8075	8	4:02	1.173	.821	+ 35.0
8076	9	1:50	0.653	.457	− 17.8
8077	9	3:20	0.716	.501	− 24.8
8078	9	4:49	0.778	.545	+ 9.4
8082	10	2:44	0.262	.183	− 91.1
8083	10	4:20	0.329	.230	−116.6
8089	11	2:04	1.234	.864	+ 42.9
8090	11	3:08	1.279	.895	+ 26.6
8091	11	4:09	1.321	.925	+ 20.3
8098	14	1:23	1.350	.945	+ 12.4
8099	14	2:29	1.395	.977	− 13.6
8100	14	3:36	0.013	.009	− 37.5
8111	15	1:26	0.923	.646	+ 48.2
8112	15	2:28	0.966	.676	+ 35.6
8113	15	3:30	1.009	.706	+ 49.8
8124	16	1:19	0.490	.343	− 93.5
8125	16	2:14	0.528	.370	− 60.9
8126	16	2:59	0.560	.392	− 66.6
8131	17	1:53	0.085	.060	− 69.1
8132	17	2:57	0.130	.091	− 64.1
8135	18	1:20	1.063	.744	+ 53.4
8136	18	2:11	1.098	.769	+ 69.9
8137	18	3:04	1.135	.795	+ 63.4
8141	19	1:24	0.636	.445	− 41.5
8142	19	2:08	0.667	.467	− 29.1
8143	19	2:56	0.700	.490	− 8.6
8160	20	1:27	0.210	.147	−100.2
8161	20	2:29	0.253	.177	−106.2
8174	21	1:30	1.212	.849	+ 65.6
8175	21	2:23	1.249	.874	+ 50.7
8176	21	3:09	1.281	.897	+ 43.5
8187	22	1:52	0.800	.560	+ 14.8
8188	22	2:55	0.844	.591	+ 36.8
8197	23	1:29	0.355	.249	−115.1
8198	23	2:28	0.396	0.277	−104.3

TABLE 3—*Continued*

RADIAL VELOCITIES OF TY PUPPIS

Plate No. CQ	Date	U.T.	JD	Phase		Radial Velocity (Km/Sec)	Corrected Radial Vel.
				Days	Period		
	1949						
7939	Dec. 25	9:18	2433275.887	0.398	0.685	− 6	+36
7940	25	10:20	275.931	.442	.761	+15	+57
7947	26	6:36	276.774	.124	.214	−44	−24
7948	26	7:39	276.819	.169	.291	− 8	+12
7949	26	8:42	276.862	.212	.365	−42	−22
7968	27	7:26	277.810	.579	.997	−18	−22
7969	27	8:09	277.840	.028	.048	+ 8	+ 4
7970	27	8:53	277.870	.058	.100	+27	+23
7971	27	9:48	277.908	.096	.165	+44	+40
7986	28	6:11	278.758	.366	.630	+58	+36
7987	28	6:58	278.790	.398	.685	+57	+35
7988	28	7:41	278.820	.428	.737	+85	+63
7989	28	8:27	278.852	.460	.792	+66	+44
	1950						
8025	Jan. 1	7:40	282.819	.362	.623	+24	+26
8026	1	8:57	282.873	.416	.716	+27	+29
8049	5	7:24	286.808	.286	.492	−12	0
8050	5	8:44	286.864	.342	.589	+26	+40
8067	7	7:31	288.813	.548	.944	+71	+43
8087	10	7:48	291.824	.075	.129	+29	−33
8088	10	8:54	291.870	.121	.208	+61	− 1
8095	11	6:02	292.751	.421	.725	+62	+84
8097	11	8:22	292.849	.519	.894	+46	+68
8104	14	5:38	295.735	.502	.864	−28	+ 2
8105	14	6:42	295.779	.546	.940	−10	+20
8106	14	7:43	295.822	.008	.014	− 4	+26
8107	14	8:46	295.865	.051	.088	+ 6	+36
8117	15	5:26	296.726	.331	.570	+43	+49
8118	15	6:32	296.772	.377	.649	+54	+60
8119	15	7:32	296.814	.419	.722	+45	+51
8120	15	8:38	296.860	.465	.801	+67	+73
8166	20	4:33	301.690	.069	.119	+58	+12
8167	20	5:30	301.729	.108	.186	+49	+ 3
8168	20	6:26	301.768	.147	.253	+34	−12
8169	20	7:14	301.801	0.180	0.310	+34	−12

TABLE 3—*Continued*

RADIAL VELOCITIES OF VV URSAE MAJORIS

Plate No. CQ	Date	U.T.	Phase (Days)	Phase (Period)	Radial Velocities (Km/Sec)
	1949				
7941	Dec. 25	11:56	0.467	0.679	+48.5
7972	27	11:10	.373	.543	+ 1.0
7973	27	12:25	.425	.618	+29.0
7990	28	9:37	.621	.903	+12.9
7991	28	11:00	.678	.986	− 5.8
7992	28	12:24	.050	.073	−60.4
8007	31	8:39	.144	.209	−71.4
8008	31	9:42	.188	.274	−75.5
8009	31	10:46	.233	.339	−72.1
8010	31	11:42	.272	.396	−38.7
8011	31	12:38	.310	.451	−18.3
	1950				
8027	Jan. 1	10:40	.540	.786	+50.7
8028	1	12:11	.604	.879	+ 5.3
8055	6	8:50	.653	.950	− 4.9
8056	6	9:50	.008	.012	−51.1
8057	6	11:00	.056	.081	−35.3
8058	6	12:20	.112	.163	−59.1
8068	7	8:43	.273	.397	−37.0
8069	7	9:45	.316	.460	+14.6
8070	7	10:48	.360	.524	−22.2
8071	7	11:55	.406	.591	+33.2
8108	14	10:00	.453	.659	+37.9
8109	14	11:02	.496	.722	+39.9
8110	14	12:07	.541	.787	+65.2
8121	15	9:54	.073	.106	−41.4
8122	15	10:57	.117	.170	−71.3
8123	15	12:03	.163	.237	−71.4
8195	22	10:58	.245	.356	−56.8
8196	22	11:58	0.287	0.418	−35.7

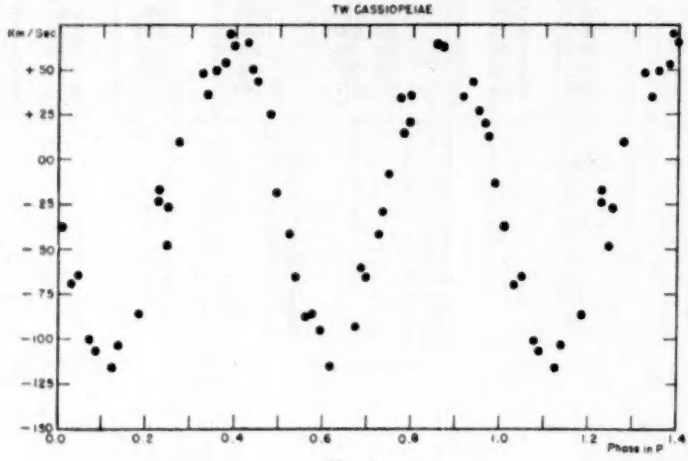

FIG. 1

corrected velocities are listed in the last column of Table 3 and are plotted in Figure 4. There is a general tendency in the points to conform to a sine-curve with $K = 32$ km/sec and $\gamma = +24$ km/sec, but the scatter is so large that a suspicion arises concerning the correctness of the longer period. The photometric observations by E. Hertzsprung[4] are

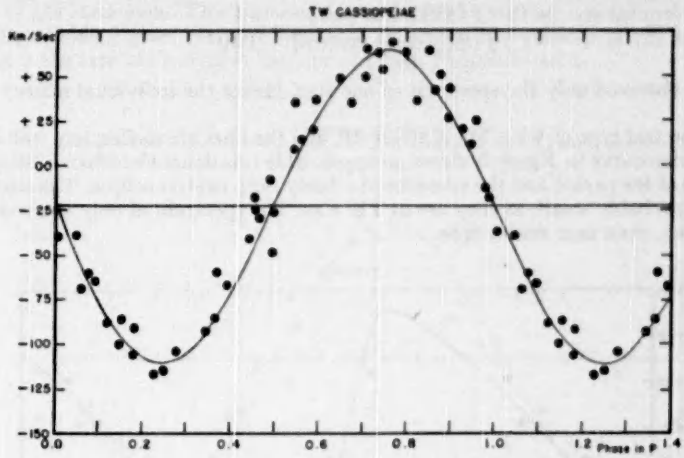

FIG. 2

TABLE 4

LONG-PERIOD OSCILLATION OF TY PUPPIS

Date	JD	Estimated Departures (Km/Sec)	Phase in Days ($P = 9.7$ Days)	Correction (Km/Sec)
1949				
Dec. 25.41	2433275.91	−42	0.00	+42
26.32	276.82	−26	0.91	+20
27.35	277.85	+ 3	1.94	− 4
28.31	278.81	+22	2.90	−22
1950				
Jan. 1.34	282.84	−19	6.93	+ 2
5.33	286.83	−17	1.22	+12
7.31	288.81	+41	3.21	−28
10.35	291.85	+44	6.24	−62
11.30	292.80	+ 6	7.19	+22
14.31	295.81	−26	0.50	+30
15.30	296.80	+ 6	1.49	+ 6
20.25	301.75	+50	6.44	−46

not compatible with any other period than the one given in Table 1. The existence of two periods in a spectroscopic binary, though not unique, is of considerable interest. But the present case is distinctly peculiar because the value of K in the long-period orbit is greater than in the short-period orbit. Even after correcting for the eccentricity of the long-period orbit, we still find that $K\sqrt{1 - e^2} = 67$ km/sec, which is twice the amplitude of the

[4] *B.A.N.*, **4**, 154, 1928; see also L. Campbell, *Harvard Bull.*, No. 858, p. 1, 1928.

short-period orbit. If this result is correct—and we again emphasize its preliminary nature—this would impose some severe restrictions upon the masses of the components which compose this triple system. The mass-functions of the close pair and the wide system are proportional to K^3P, respectively. This would result in

$$\frac{f(\mathfrak{M})\,[\text{close pair}]}{f(\mathfrak{M})\,[\text{wide system}]} \sim \frac{1}{100}.$$

We have observed only the spectrum of one star. Hence the individual masses are not known.

The spectral type of VV UMa is about A0, and the lines are moderately well defined. The velocity-curve in Figure 5 shows no appreciable rotational disturbance, despite the shortness of the period and the presence of a fairly deep central eclipse. The sizes of the stars are probably small, as they are in TW Cas. The spectrum of only one component can be seen, even near mid-eclipse.

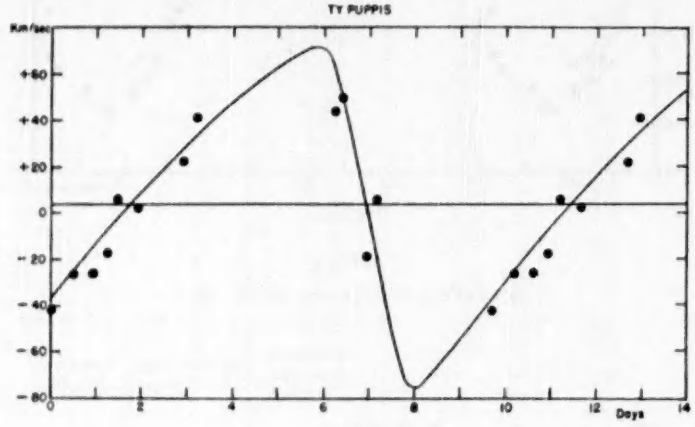

FIG. 3

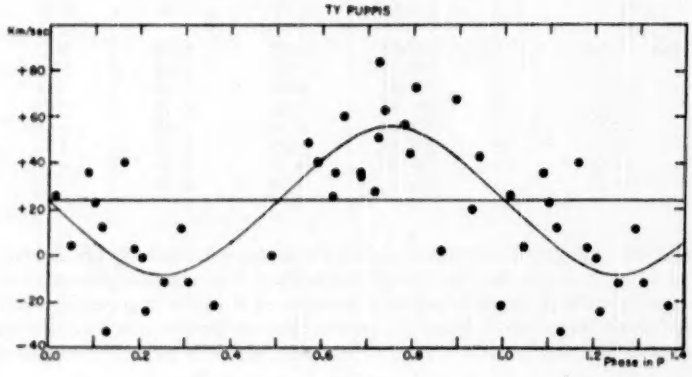

FIG. 4

Perhaps the most interesting result of this work consists in the small values found for the mass-functions of the short-period systems. This is an extension of the conclusion derived previously: the velocity-amplitudes of eclipsing systems of class A (for the brighter components) are systematically smaller than those of normal spectroscopic binaries of the same type. This phenomenon is especially striking among systems with $P < 1$ day. Table 5 gives the spectrographic elements. The velocity of the system of VV UMa is the sum of the two values derived from Figures 3 and 4.

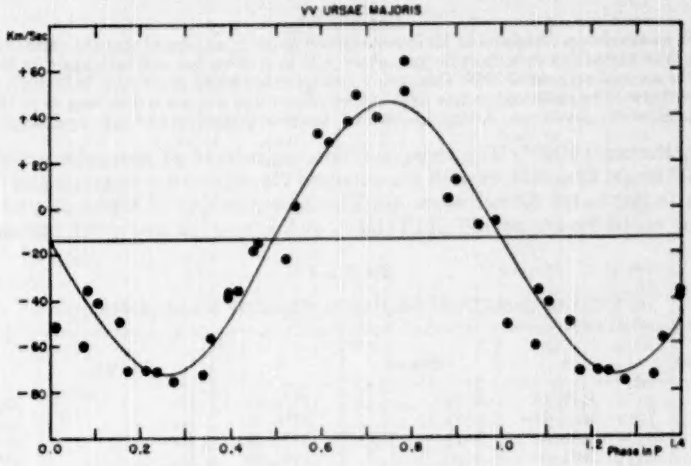

FIG. 5

TABLE 5

ORBITAL ELEMENTS

Star	P (Days)	γ (Km/Sec)	K (Km/Sec)	e	ω (Degrees)	T (Days)	$a \sin i$ (Km)	$f(\mathfrak{M})$ $\odot$
TW Cas....	1.43	−23	87	.....	.....	.....	1.7×10^6	0.098
TY Pup....	9.7	.....	74	0.45	100	ph 7.1	8.6×10^6	.266
TY Pup....	0.581	+28	32	.....	.....	.....	0.26×10^6	.002
VV UMa....	0.687	−13	59	.....	.....	.....	0.56×10^6	0.015

THE RADIAL VELOCITY OF GAMMA CASSIOPEIAE*

BURKE SMITH AND O. STRUVE
Yerkes and McDonald Observatories
Received May 1, 1950

ABSTRACT

From 59 spectrograms, obtained at McDonald Observatory, it was found that the radial velocity of absorption lines varied in a definite cycle from about +14 to −16 km/sec and back again, in 1940–1941, following the spectral outburst of 1939. This cycle is similar to one which occurred in 1935–1937, following the 1934 outburst. The emission borders were not so intense and did not last so long as in 1935–1937. There is no apparent correlation, during this interval, between brightness and velocity-changes.

During the years 1940–1947 a series of 59 spectrograms of γ Cassiopeiae was obtained at the McDonald Observatory with the standard Cassegrain spectrograph and 500-mm camera attached to the 82-inch telescope. The dispersion was 55 A/mm at $H\gamma$. Table 1 gives a list of the lines measured and Tables 2 and 3 show the absorption-line and emis-

TABLE 1

STELLAR LINES USED FOR RADIAL-VELOCITY MEASUREMENTS

Element	λ	Element	λ	Element	λ
H 21	3679.35	*H* 13	3734.37	*He*	3970.07
H 20	3682.81	*H* 12	3750.15	*He* I	4009.27
H 19	3686.83	*H* 11	3770.63	*He* I	4026.27
H 18	3691.56	*H* 10	3797.90	*Hδ*	4101.74
H 17	3697.15	*He* I	3819.68	*He* I	4120.90
H 16	3703.85	*H* 9	3835.39	*He* I	4143.76
He I	3705.14	*He* I	3888.65	*Hγ*	4340.47
H 15	3711.97	*Hζ*	3889.05	*He* I	4387.93
H 14	3721.94	*He* I	3964.73	*He* I	4471.58

sion-line velocities for each plate. These velocities, when averaged by days, are plotted in Figure 1, except for 1947. Although there is considerable scatter, the absorption velocities seem to have gone through a rather definite cycle between March, 1940, and January, 1942. If a smooth curve were drawn, the velocity during this period would vary from about +14 to −16 km/sec and back again. From January, 1942, on, there were fewer observations, and it is not possible to determine whether the velocity continued to follow the same pattern.

R. Baldwin[1] has published velocities for γ Cas from spectrograms taken at the University of Michigan during the period 1935–1937. The McDonald results follow rather closely the cycle obtained from his Ann Arbor plates, except that his velocities are, on the average, slightly lower and his cycle has a deeper minimum. In Figure 1 Baldwin's velocities for the *H* lines, with +8 km/sec added, have been superimposed on the McDonald results. The general trend and the length of the velocity-cycle is the same in both cases, and in each case the cycle occurred immediately following a spectral outburst.

* *Contributions from the McDonald Observatory, University of Texas*, No. 193.

[1] *Ap. J.*, **89**, 261, 1939.

TABLE 2

Absorption Velocities

Plate CQ	Date	U.T.	Vel (Km/Sec)	Plate CQ	Date	U.T.	Vel (Km/Sec)
	1940			829	May 20	11:18	−16.7
298	Jan. 31	5:15	− 1.4	901	July 30	3:24	− 2.9
299	31	5:43	− 0.3	902	30	3:40	−18.6
301	Feb. 1	1:06	− 9.8	903	30	3:50	−13.3
304	2	1:06	+ 2.3	904	30	3:53	−30.2
306	2	3:00	+11.5	1054	Nov. 9	1:00	−16.4
307	2	3:18	+11.0	1055	9	1:17	− 7.8
315	4	2:23	− 4.5		1942		
316	4	2:29	− 2.1	1188	Jan. 8	2:43	+ 7.0
317	4	2:39	− 4.9	1195	9	5:06	− 5.8
318	4	3:03	− 5.2	1505	July 3	11:00	−14.7
382	May 12	8:41	+ 7.3	1506	3	11:07	−23.5
383	12	9:20	+ 5.4		1943		
390	15	8:24	− 0.5	1883	Jan. 23	0:41	+ 6.5
391	15	8:47	− 1.1	1884	23	0:46	+ 4.5
438	July 1	10:58	+14.1	2177	June 24	11:04	−18.2
454	Aug. 15	11:20	+10.4	2178	24	11:11	−24.3
455	15	11:31	+ 5.1		1944		
514	30	11:30	− 8.5	3162	May 6	11:21	−18.8
534	Sept. 25	4:32	−12.2	3163	6	11:34	− 7.7
535	25	4:42	−13.3	3164	6	11:39	−15.7
541	Oct. 20	4:52	−22.8		1947		
542	20	5:04	− 6.3	5609	June 24	10:44	+ 5.8
543	20	5:10	− 3.2	5610	24	10:57	− 7.6
556	Nov. 12	7:12	−22.4	6134	Oct. 27	7:20	−20.8
557	12	7:26	+ 1.1	6135	27	7:36	−11.9
558	12	7:42	− 4.1	6158	28	7:15	−28.0
	1941						
581	Jan. 7	2:41	−18.2	6159	28	7:16	− 6.5
582	7	2:48	−10.7	6160	28	7:18	−31.7
583	7	2:57	− 3.8	6161	28	7:20	−36.3
620	18	1:06	− 7.3	6162	28	7:22	− 6.7
621	18	1:14	+ 5.9	6163	28	7:26	+ 0.3

TABLE 3

Emission Velocities

Plate	Date (1940)	λ 3835		λ 3889		λ 3970		$H\delta$		$H\gamma$		Mean Emission Velocity	
		V	*R*	*V*	*R*	*V*	*R*	*V*	*R*	*V*	*R*	*V*	*R*
298	Jan. 31	.....	.....	.....	.....	.....	+106	− 74	+129	− 96	+132	− 85	+122
299	31	−67	+ 98	−107	+109	− 63	+115	− 91	+119	− 91	+131	− 84	+114
304	Feb. 2	−55	+ 99	−103	+100	− 66	+124	− 88	+113	− 84	+133	− 79	+114
306	2	−54	+108	− 86	+120	− 57	+129	− 80	+137	−135	+135	− 82	+126
307	2	−46	+108	− 54	+135	− 51	+113	− 59	+129	− 79	+135	− 58	+124
315	4	.....	.....	.....	.....	.....	.....	− 96	.....	−110	+134	−103	+134
316	4	.....	.....	.....	.....	.....	.....	− 89	+129	−104	+140	− 96	+134
317	4	.....	.....	.....	.....	.....	.....	− 89	+103	−100	+131	− 95	+117
383	May 12	.....	.....	.....	.....	− 90	+ 67	− 91	+110	−121	+121	−101	+ 99
390	15	.....	.....	.....	.....	.....	.....	−151	.....	−136	.....	−144	.....
391	15	.....	.....	.....	.....	.....	.....	−151	.....	−219	.....	−185	.....
438	July 1	.....	.....	− 95	.....	.....	.....	− 96	.....	−105	.....	− 99	.....
455	Aug. 15	.....	.....	.....	.....	−103	.....	−111	.....	−136	.....	−117	.....
514	30	.....	.....	.....	.....	−116	.....	−118	.....	−133	.....	−122	.....
542	Oct. 20	.....	.....	− 87	+ 72	− 78	+ 84	− 75	+ 54	− 90	+ 87	− 83	+ 74
543	20	.....	.....	.....	.....	.....	.....	−111	.....	−111	.....	−111	.....

With regard to emission velocities, which were measured by setting on the point of maximum intensity, the results for 1940–1941 also follow the general pattern of those for 1935–1937, except that the emission was distinctly fainter in 1940. The emission borders had disappeared by about November, 1940, while, in the earlier cycle, emission continued to be strong well into the new spectral outburst, which occurred in 1937.

The spectrum of γ Cas early in 1940, as shown on McDonald plates (Fig. 2), has been described previously.[2] In February all lines were sharp, with a broad, faint, underlying absorption in many lines. The *H* lines, from *H* γ to *H* η were bordered with emission, and *H* β, which was visible on a few plates, also showed emission. There was no emission visible in the *He* I lines. The emission gradually weakened, and by November, 1940, it was no longer visible. At the same time the *H* lines were greatly broadened. By Septem-

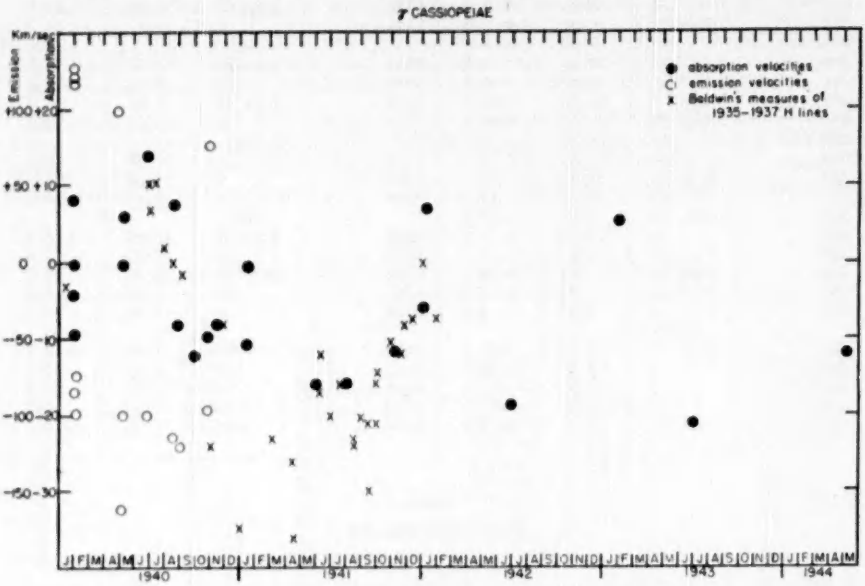
γ CASSIOPEIAE
Km/sec
Emission
Absorption
+100 +20
+50 +10
0 0
−50 −10
−100 −20
−150 −30
absorption velocities
emission velocities
Baldwin's measures of 1935–1937 H lines
J F M A M J J A S O N D J F M A M J J A S O N D J F M A M J J A S O N D J F M A M J J A S O N D J F M A M
1940
1941
1942
1943
1944

FIG. 1

ber 25, 1940, all lines were broad and rather fuzzy in appearance. A slight central core was still visible at λ 3889. In November, 1940, the *H* lines appeared to have a broad rectangular contour, with sharp edges, and λ 3889 still showed a central core. The line λ 3889 was measured as *He* I when the setting could be made on the core, otherwise it was measured as *H* ζ. By January 18, 1941, there was no central core visible in any of the lines, but on November 9, 1941, there was evidence of a slight emission border on the violet side of a few lines. From this date on until October 28, 1947, inclusive, there was not much change in the appearance of the spectrum. The emission was very faint.[3]

[2] Struve and Swings, *Harvard Ann. Card 545*, 1940; Struve and Greenstein, *Harvard Ann. Card 551*, 1940; Struve and Elvey, *Pub. A.S.P.*, **52**, 140, 1941; Swings and Struve, *Ap. J.*, **91**, 589, 1940; and Struve, *Physica*, **12**, 739, 1946.

[3] Through an unfortunate mistake in labeling the plates taken on January 18, 1941, a spectrogram of ζ Ophiuchi was inadvertently labeled Plate 621 of γ Cas. Since, at that time, the two stars had somewhat similar spectra, the error was not detected until after the publication of the paper by O. Struve in *Physica*, **12**, 744, 1946. The statement made in this article that on January 18 the absorption lines of γ Cas were abnormally broad must be withdrawn.

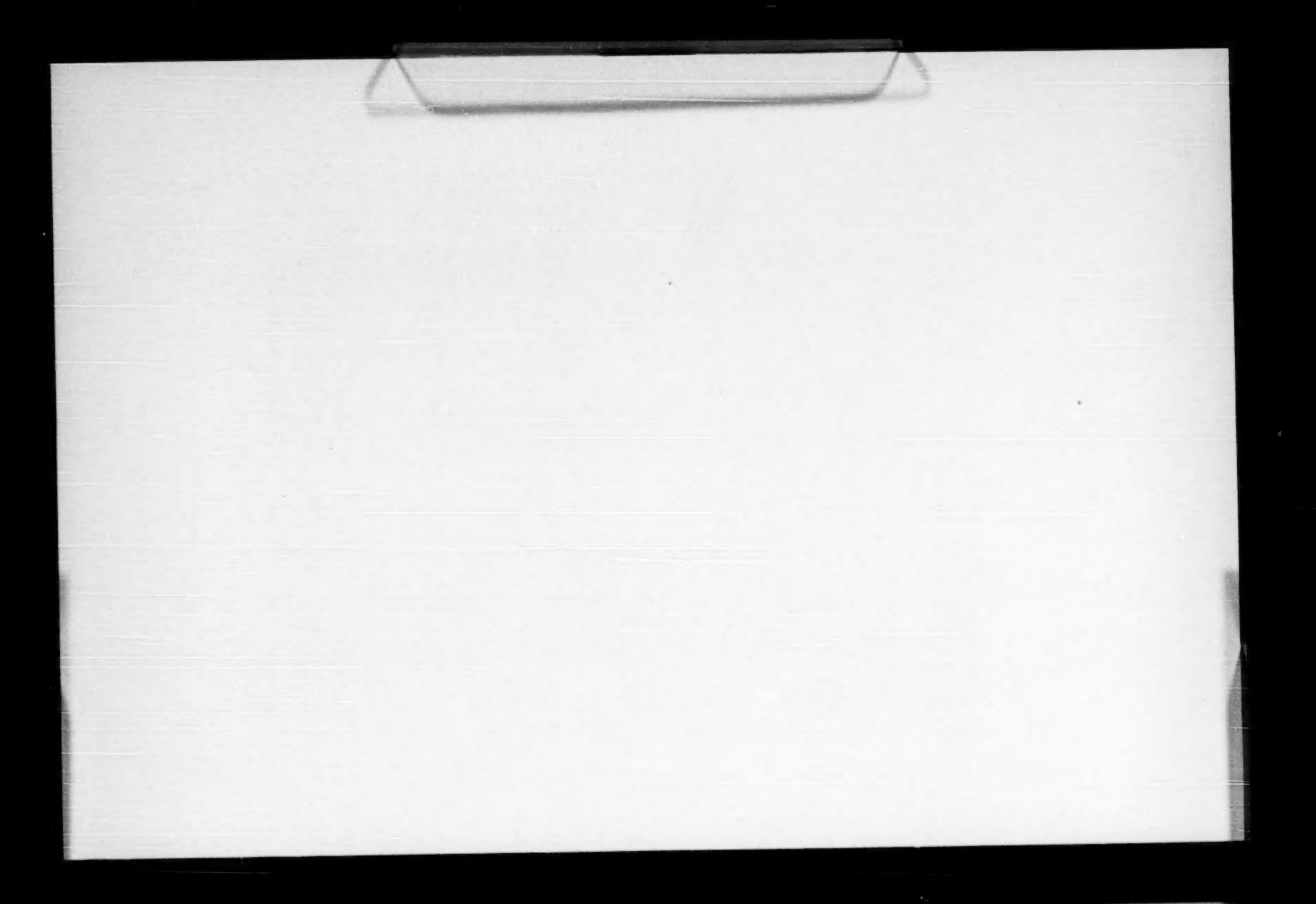

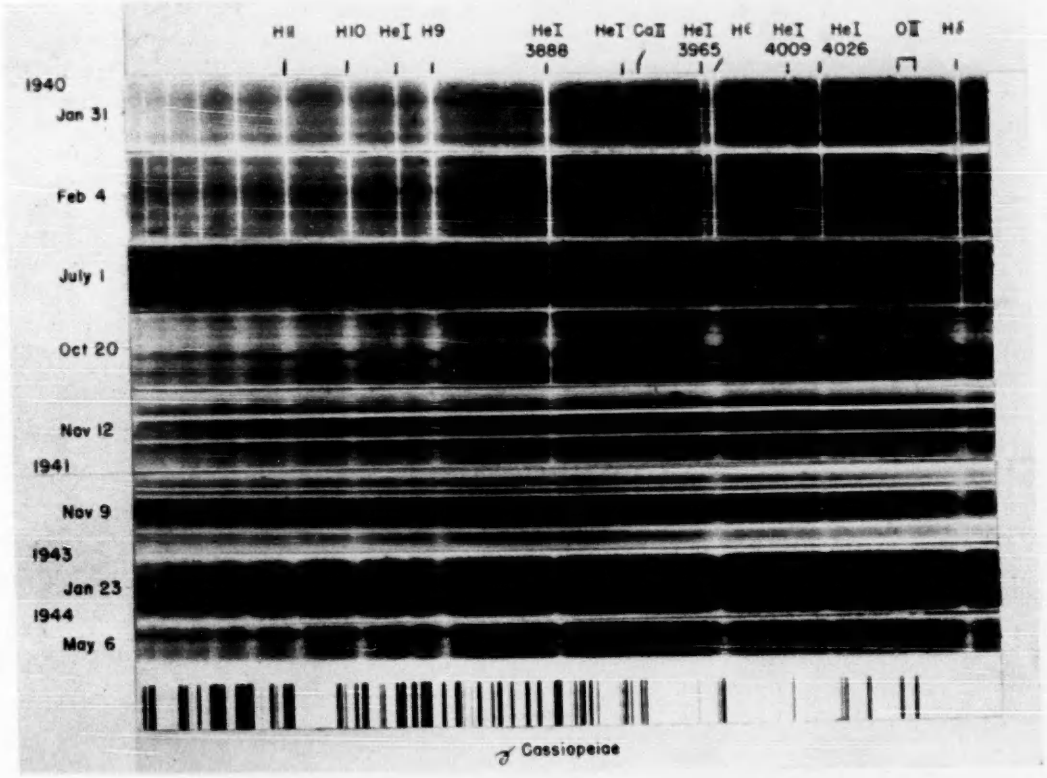
H11
H10
HeI
H9
HeI 3888
HeI
CaII
HeI 3965
H6
HeI 4009
HeI 4026
OII
H8
1940
Jan 31
Feb 4
July 1
Oct 20
Nov 12
1941
Nov 9
1943
Jan 23
1944
May 6
γ Cassiopeiae

FIG. 2

There has been some question as to whether the changes in brightness of γ Cas were correlated with the changes in spectrum or velocity. The magnitude was considered constant previous to 1936.[4] A spectral outburst occurred in 1934, and a velocity-cycle began in 1935. There was a marked increase in brightness from 2.2 mag. at the beginning of 1936 to about 1.6 mag. at the end of the cycle, in the early part of 1937. The magnitude then decreased during another spectral outburst to 2.4 at the end of 1937 and varied slightly between 2.2 and 2.4 in 1938. In 1939 the magnitude gradually decreased, while the star was again undergoing changes in spectrum. By the end of 1939 the magnitude had decreased to 3.0, and it remained around 2.8–3.0 during 1940. No published reports of brightness during 1941 are known. From reports of A.A.V.S.O. observers the star remained around 2.8–3.0 mag. during the years 1941–1949. There does not seem to be conclusive evidence of any close correlation between brightness and changes in spectrum or velocity.

The radial velocities recently published by V. F. Gase[5] agree fairly well with those given in this paper for the interval August–October, 1940; but our values obtained in 1941 are systematically smaller than those given in Miss Gase's Table IV. It is perhaps sufficient to conclude, from both series of measurements, that small, irregular fluctuations in the radial velocity were present in 1941 and probably also in the following years. But the most significant result is undoubtedly the absence of a negative displacement in the sharp lines produced by the shell, when compared to broad lines which were measured in the fall of 1940 and later.

[4] R. Prager, *Harvard Ann.*, **111**, 158, 1941; C. M. Huffer, *Ap. J.*, **89**, 139, 1938; L. Campbell, *Pop. Astr.*, **45**, 569, 1937; E. Cherrington, *Pop. Astr.*, **46**, 183, 1938; R. Rigollet, *L'Astronomie*, **52**, 129, 130, 1938; L. Campbell, *Pop. Astr.*, **48**, 385, 563, 1940; R. B. Baldwin and R. Torp-Smith, *Pop. Astr.*, **49**, 127, 1941; R. Rigollet, *L'Astronomie*, **55**, 87, 1941; and R. Rigollet and G. de Vaucouleurs, *L'Astronomie*, **60**, 91, 1946.

[5] *Izvestia Crimean Ap. Obs.*, **1**, Part I, 59, 1947.

ON THE CHANGE OF PERIOD OF ECLIPSING VARIABLE STARS

FRANK BRADSHAW WOOD
Steward Observatory, University of Arizona
Received January 31, 1950

ABSTRACT

Irregular period fluctuations of eclipsing systems are discussed. Part I points out that, when the elements of systems showing such fluctuations have been determined, the systems are, with one exception, at or near the limits of dynamical stability. Part II suggests a possible explanation of this correlation and of the period changes themselves.

I

One of the most surprising results of the study of eclipsing stars is that in many cases the period of light-variation is not constant. Frequently, the variation of period is itself periodic, and the plot against epoch of the differences in time between the observed minima and those computed from linear light-elements can be fitted by a sine-curve. If, in such a case, the plot of the time residuals of secondary minimum shows a curve of the same form but of opposite phase to that shown by the primary plot, we have evidence of a rotation of the line of apsides; a careful determination of the period of apsidal rotation and the elements of the system gives a means of determining the central condensation of at least one of the components. Apsidal motion may be expected whenever the secondary is not midway between the primaries.

In other cases the secondaries are located halfway between primaries, and a plot of their residuals gives a curve of the same form and phase as that of the primary. Here we have two possibilities, not necessarily mutually exclusive.

1. *Variation caused by changing light-time while the system moves in an orbit around a third body.*—This demands a strictly periodic change, usually corresponding to an elliptic orbit. (In some cases this assumption requires an extremely large orbit and an improbably great mass-function.) Horrocks[1] has shown that, in several cases where terms in the square of the epoch have been included in the light-elements, the variations are probably, in reality, of a long-period oscillatory nature.

2. *Disturbances in the mean longitude of the eclipsing pair.*—When all cases of periodic or regular variations are removed from consideration, many instances remain in which the period is by no means constant. In some cases the period seems to be changing almost continuously, but not in any regular manner; in others, a star which has shown a constant period for a considerable interval will shift, apparently suddenly, to a slightly different one. Such changes are of the general order of 10^{-5} or 10^{-6} of the period. It is extremely difficult to understand how a stable system can behave in such a manner; it is natural, therefore, to inquire into the stability of systems which have exhibited such behavior.

The stability of a close double-star system will depend not only on the size of the components relative to the size of the orbit and on the mass ratio but also on such factors as the shape of the orbit, the rotational speeds of the components, and the degree of central condensation of the stars. Fortunately, most eclipsing-star orbits are circular or nearly so, and the available evidence indicates, for most, a period of rotation equal to the period of revolution and, for all, a high degree of central condensation. Thus, for a first approximation, the Roche model, a circular orbit, and equality of rotation and revolu-

[1] *M.N.*, **101**, 237, 1941.

tion periods may be assumed. (If the second of these assumptions is invalid for a given system, the fact will be evidenced in the light- and velocity-curves. If the third assumption is invalid, evidence will be found in the velocity-curve unless the spectrum of the rapidly rotating component is invisible.) In such a case the limits of stability for a system of any given mass ratio can be computed. Perhaps the simplest method of doing this is to compute for the mass ratio in question the Jacobian limiting surface which contains the double point which appears when the ovals around the stellar centers touch one another.[2] This is a surface of zero relative velocity; if the system is to be stable, all parts of each star must lie within the Jacobian limiting surface surrounding that star. In bipolar co-ordinates the Jacobian limiting surface is given by

$$(1-\mu)\left(r_1^2+\frac{2}{r_1}\right)+\mu\left(r_2^2+\frac{2}{r_2}\right)=C'.$$

Here, μ and $1-\mu$ are the stellar masses, with $\mu \leqslant \frac{1}{2}$; the mass of the system and the distance between the centers are each unity. Moulton[3] has given a development and complete discussion of this formula. Numerical computation shows that the shortest equatorial radius of the less massive star, b_f, usually reaches the limiting surface first, as the mass ratio is increased. Hence, the above formula may be used to compute the values of r_2 at unit distance from the center of the more massive star. If the solution of the light-curve shows that b_f is near this limit, we may expect that the system at such points will be near the limits of stability. These limiting values of b_f for various mass ratios are given in the accompanying tabulation. In any system in which this criterion is violated, matter

m_1/m_2	1	1.5	2	2.5	3	4	5	6	7	8	10
$(b_f)_{\text{lim}}$	0.373	0.333	0.309	0.292	0.278	0.257	0.241	0.229	0.219	0.210	0.197

will flow out steadily from near the ends of the axis, b_f; for actual systems an apparent small margin of stability will by no means insure actual stability.

At first glance it appears that the application of this test for stability is simplicity itself. For stars which have exhibited sudden or irregular changes of period, take from the literature the computed values of b_f and the mass ratio and, by comparison with the above table, determine whether or not the star is near the limits of stability. In practice, however, this simple method is by no means adequate; various precautions must be observed. These fall into three general classes.

1. *The determination of the nature of the variation of period.*—Frequently, this presents no difficulties. While there are many cases of suspected variation of period which have not been confirmed, these suspected variations are nearly always of a periodic nature. The difficulty in many cases lies in determining whether an observed change really is a sudden one or whether we are observing part of a long-period oscillatory variation. This difficulty is often increased by the sparseness of recent determinations of the times of minimum. In this discussion, only stars whose variations of period are definitely irregular will be considered. Fortunately, enough stars are known so that a preliminary check may be made concerning the correlation between the approach to instability and the inconstancy of the period.

2. *The determination of the value of b_f.*—The determination of this factor requires care at several points. The light-curve must have been sufficiently well observed between eclipses to permit a reliable determination of the ellipticity. Both the nature of the eclipses and the accuracy of the observations must be such as to permit a reasonably de-

[2] *Contr. Princeton U. Obs.*, No. 21, p. 37, 1946.

[3] *Celestial Mechanics* (new ed.; New York: Macmillan Co., 1914), chap. viii.

terminate solution. Even when these criteria are satisfied, it is not permissible simply to take from the literature the computed values of b_f. These values are frequently found by multiplying a_f by the factor b/a determined from the observations between minima. But, for the consideration of stability, we are interested in the geometric ellipticity; the observations between minima yield the value of the photometric ellipticity. The two are not the same, and, especially in the older publications, the distinction is frequently not made. Further, the shapes of the two stars are rarely the same—and, if they are, the solution is likely to be indeterminate—and for the present purpose we wish to know the shape of the less massive star, not the average of both components. Thus the value of b_f cannot be taken from the literature without careful consideration of the factors involved in each case. Usually it will be advisable to compute it from the elements of the system (following Russell[4]) and then finally to make certain that this computed value does not require a light-curve of appreciably different shape from that actually observed.

3. *The determination of the mass ratio of the components.*—When this has been determined spectrographically, the value is usually reliable; when it is not reliable, the fact is almost inevitably indicated by peculiarities in the spectra or by wide discrepancies between the spectrographic and the photometric data. When the spectrum of the fainter component is not visible, the mass ratio may be computed from the relative luminosities. Here it is the intrinsic luminosity of the fainter component which is significant; that is, its luminosity after the reflection (or reradiation) effect has been eliminated. This again demands accurate observations outside eclipses. Further, as Struve[5] has recently emphasized, it must not be forgotten that the fainter components of many eclipsing systems are among the most notorious violators of the usual mass-luminosity relationship. In the cases in which this violation occurs, it seems to be rather consistently in one direction, that is, the star in each case is too bright for its mass. Thus the masses so determined will, in such cases, be too large, making the mass ratio consistently too small. The effect of this will be to make such systems appear more stable than they are in reality. This effect must be kept in mind in the discussion of the systems to which it may apply.

Even in view of the uncertainties introduced by these complications, enough stars have been sufficiently well observed to justify a preliminary investigation to attempt to determine whether stars showing irregular fluctuations of period are also near the limits of stability. For this purpose, the 546 stars in Pierce's *Finding List*[6] have been investigated. While this excludes the faintest stars as well as the far-southern ones, there are few systems sufficiently well observed to be of use in this survey which are not included; the labor of attempting such a survey without the use of the *Finding List* is prohibitive. The following are all those in the *Finding List* which show irregular variation of period and for which satisfactory elements are available.

1. *AO Cas.*—Few times of minimum of this star have been observed because of the shallow depths ($0^m.17$). Those that have been published have all been determined from photoelectric observations; they cannot be fitted satisfactorily by a constant period and indicate a rather sudden lengthening of the period. Unpublished observations, taken one and three years after those most recently published,[7] are satisfactorily fitted by the new period. (Spectrographic observations by Struve and Horak show further shortening.) The mass ratio, determined spectrographically by Pearce,[8] is nearly unity. In this case the brighter component appears to be at the limits of stability; its shortest equatorial radius is 0.377. The solution[7] is made by a combination of spectrographic and photometric data; it is sufficiently determinate to indicate clearly that the system is near instability.

[4] *Ap. J.*, **102**, 4, 1945.

[5] *Ann. d'ap.*, **11**, 117, 1948.

[6] *Contr. Princeton U. Obs.*, No. 22, 1947.

[7] *Ap. J.*, **108**, 28, 1948.

[8] *Pub. Dom. Ap. Obs., Victoria*, **3**, 275, 1926.

2. *U Cep.*—It is well known that the period of this star is not constant.[9] A complete discussion of the work to 1920 has been given by Dugan,[10] who gives for the shortest equatorial radius of the less massive star a value of 0.308. (In excellent agreement with this is the value of 0.310 found by Baker.[11]) Use of the geometric ellipticity of the fainter component, computed from Dugan's elements, in place of the photometric ellipticity, decreases this value to 0.304. This indicates that instability should set in at a mass ratio of about 2.1. The actual mass ratio is not easy to determine. The relative luminosities of the fainter sides of the two components, using the mass-luminosity relation in the form developed by Russell and Moore,[12] indicate a mass ratio of about 1.7; as pointed out previously, in such a system the actual mass ratio will probably be appreciably larger. The spectrographic evidence does not give a great deal of help on this point. Carpenter's[13] plates did not show the secondary spectrum; Kopal,[14] using Redman's spectra, derived a mass ratio of 3.2; Struve[15] found a ratio of nearly unity from his own measures and suggests about 1.4 as the best compromise that can at present be obtained from the spectrographic data. Struve points out the possibility that the velocity-curve may be distorted by absorption in gaseous streams. The eccentricity of the orbit is large, according to the spectrographic observations, and is negligible photometrically. The marked differences in the velocity-curves observed at different epochs give additional suggestions that the system is not a stable one. In view of the present evidence, it is reasonable to accept this system as one which is near the limits of dynamical stability.

3. *X Tri.*—The variation of period of this star was first noted by Gadomski.[16] More recently, Lange and Nekrassova[17] have discussed the period; their light-elements contain two sine terms. However, a plot of their residuals from linear elements shows that they can be well fitted by assuming a rather sudden change of period at about JD 2425000 with constant periods before and after that date. In either case the variation of period is irregular. Dugan[18] gives $a_f = 0.336$. With his value of b/a, $b_f = 0.312$. From the mass-luminosity-curve, Dugan found a mass ratio of 2.1. Using this and his elements to compute the geometric ellipticity, $b_f = 0.303$. For a mass ratio of 2.1, the limit of stability is 0.306. The system is thus extremely near instability.

4. *R CMa.*—The variation of period of this star was first announced by Dugan[19] and has been further investigated by Dugan and Wright[20] and by myself.[2] After remaining constant for more than thirty years, the period abruptly shortened and, when last observed, was decreasing still more. Visual observations of Wendell and Pickering, made with a polarizing photometer, showed a strange hump in the light-curve which was present on some nights and missing on others. My own observations of this star[2] indicate that it must be quite near the limits of stability; the only alternative to this is an almost incredibly small mass for both components.

5. *TW Dra.*—The variable period of this star has been discussed by Gadomski[21] and by Pearce.[22] The latter has also observed the secondary spectrum. From three observa-

[9] *Ap. J.*, **44**, 51, 1916.

[10] *Contr. Princeton U. Obs.*, No. 5, 1920.

[11] *Laws Bull.*, **2**, 247, 1921.

[12] *The Masses of the Stars* (Chicago: University of Chicago Press, 1940).

[13] *Ap. J.*, **72**, 205, 1930.

[14] *Harvard Bull.*, No. 914, 1940.

[15] *Ap. J.*, **99**, 230, 1944.

[16] *Warsaw Circ.*, No. 22; *Warsaw Repr.*, No. 15, 1932.

[17] *Astr. Circ.* (Kasan), No. 24, 1943.

[18] *Contr. Princeton U. Obs.*, No. 8, 1928.

[19] *Contr. Princeton U. Obs.*, No. 6, 1924.

[20] *Contr. Princeton U. Obs.*, No. 19, 1939.

[21] *Warsaw Pub.*, **8**, 51, 1933.

[22] *Pub. A.A.S.*, **9**, 131, 1938.

tions during totality he finds an approximate mass ratio of 3.6. Baker's[23] value of b_f is 0.314; with the geometric ellipticity of the fainter component computed from his elements and Pearce's mass ratio, $b_f = 0.289$, indicating instability at a mass ratio of 2.7. Even if the mass ratio is considerably less than the approximate value given by Pearce, the system will be at the stability limits. The orbit is slightly eccentric; this will increase somewhat the tendency of the system toward instability. Baker has called attention to the similarity of this system to U Cep.

6. *SZ Her.*—The variation of period has been discussed by various authors; perhaps the most extensive investigation is that of Dugan and Wright.[20] With the geometric ellipticity computed from Dugan's[19] elements, $b_f = 0.314$. This indicates that instability sets in at a mass ratio of about 1.9; from the luminosities of the components Dugan assumed a value of 2. Since the spectral types are not known, this value is only approximate; it does indicate that the system is probably near the limits of stability.

7. *β Lyr.*—The dynamics of this system have been extensively discussed by Kuiper.[24] He finds that the system is not a stable one; the change of period is well known.

8. *ST Per.*—In an earlier discussion of this star,[2] it was pointed out that the observations indicated a sudden period change; this is further confirmed by a later observation of Struve.[25] The elements indicate that the system is stable unless the mass ratio approaches 7; even allowance for uncertainties in the elements can reduce this value only to between 5 and 6. Ordinarily, this would not be seriously considered; however, the extremely small mass function of 0.008 found by Struve[25] indicates either a large mass ratio or an extremely small value for the mass of the fainter component. Even a mass ratio of 7 gives the G component a mass of only 0.51 ⊙. Struve also finds a strong indication of a rotational disturbance in the velocity-curve; this will increase the tendency toward instability. The system thus seems near the limits of stability; this is apparently another case in which the fainter component is much too bright for its mass.

9. *AR Lac.*—On the basis of present knowledge this star comprises the sole exception to the generalization that sudden period changes are found only in systems which are obviously near dynamical instability. The elements of the system[2] yield a value of b_f of 0.306, indicating instability at a mass ratio of 2. Harper's[26] spectrographic value is only slightly greater than unity. The solution, however, is complicated by the fact that one of the components is intrinsically variable. Wyse[27] found that one component showed emission in *Ca* II; recently, Joy and Wilson[28] have reported this occurring in both components. Kron[29] has suggested variable bright and dark patches on the surface of the G5 component. His evidence is based on an extensive series of photoelectric observations. If the fainter component is rotating in a period shorter than the period of orbital revolution, the tendency toward instability will be appreciably increased.

The other stars whose periods show sudden or irregular changes have not been sufficiently well observed to furnish elements as definitive as those in the systems just discussed. Ten such systems, however, do have solutions which are strong enough to indicate the general nature of the system, and these elements in every case indicate that the system is at or near the limits of stability. These ten systems are as follows.

10. *ZZ Cas.*—The irregular variation of period of this star has been well established by Dugan and Wright.[20] Struve[30] was unable to see the secondary spectrum; for the B component to have a normal mass, the mass ratio must be between 3 and 4. Gaposchkin[31] gives two approximate photometric solutions based on visual estimates by Zessewitsch.

[23] *Lowes Pub.*, **2**, 29, 1921.

[24] *Ap. J.*, **93**, 133, 1941.

[25] *Ap. J.*, **104**, 269, 1946.

[26] *J.R.A.S., Canada*, **27**, 146, 1933.

[27] *Lick Obs. Bull.*, **17**, No. 464, 37, 1934.

[28] *Ap. J.*, **109**, 231, 1949.

[29] *Pub. A.S.P.*, **59**, 261, 1947.

[30] *Ap. J.*, **106**, 92, 1947.

[31] *Veröff. Berlin-Babelsberg*, **9**, No. 5, 1932.

These indicate that b_f is in the neighborhood of 0.32 and that instability thus sets in at a mass ratio somewhat less than 2. As far as it goes, the evidence indicates that this system is at the stability limits.

11. *WZ And.*—Sudden change of period of this star has also been established by the work of Dugan and Wright,[20] who give a provisional solution from photographic estimates; Miss Slonim[32] has presented one based on Jordan's photographic measures. Both agree in finding large radii of the components relative to the size of the orbit. Instability sets in at a mass ratio of about 1.5; this is approximately what would be expected from the relative luminosities of the components.

12. *XZ And.*—This system has also had its irregular variation of period established by Dugan and Wright;[20] it is even more firmly established by later unpublished observations of Pierce and of Blitzstein. Dugan and Wright also presented a preliminary solution. From their elements, instability should be expected to occur at a mass ratio of about 1.6; a mass ratio of 2 was assumed by them from the relative brightness of the components.

13. *V Leo.*—The period of this star apparently remained constant from its discovery until 1943; estimates by Struve[33] in 1945 showed the minima occurring about half an hour before the predicted times. There are several photometric solutions, none of which is highly determinate. That of Fetlaar[34] from Nijland's visual estimates gives $r_1 = 0.30$. The assumption of a mass ratio of 3 (from the relative luminosities) yields a value of about 0.28 for b_f, which indicates that instability sets in at precisely this mass ratio.

14. *44 i Boo.*—This system has recently been discussed by Eggen.[35] The period shows fluctuations other than those produced by the long-period orbital motion. The solution is not highly definitive—as Eggen points out—but does indicate clearly that the components are near the limits of stability.

15. *U CrB.*—The irregular variation of period of this star has been the subject of several discussions; that of Dugan and Wright[20] is perhaps the most complete. Plaskett's[36] velocity-curve indicates a mass ratio of 2.6; his results are confirmed by Pearce.[37] Sahade and Struve[38] were unable to observe the secondary spectrum and suggest the presence of a gaseous stream. The complete absence of any observed secondary minimum in the light-curve indicates that the mass ratio should be high. The provisional solution of Dugan and Wright indicates that $a_f = 0.33$; on the assumption of $m_h/m_f = 2.6$, this indicates that $b_f = 0.30$, or instability at a mass ratio of about 2.3. Baker's[39] elements give a slightly lower value of b_f but still indicate that the system is near the limits of stability.

16. *RV Lyr.*—The irregular variation of period of this star has also been pointed out by Dugan and Wright.[20] The solution by Fetlaar[34] from Nijland's visual observations is not strong. It indicates instability for a mass ratio of 2; this is also the value suggested by the relative luminosities.

17. *U Peg.*—The variation of period of U Peg has been studied by Recillas and Woodward.[40] Shapley[41] made three solutions from Wendell's measures; they indicate for the fainter component a value of a_f of about 0.40. The solutions are somewhat indeterminate but leave little doubt that the system is not far from the stability limits.

18. *TV Peg.*—Dugan and Wright[20] pointed out the irregular variation of period of this star and made a provisional solution. From the elements so derived, instability should not set in until a mass ratio of between 3 and 4. Inasmuch as secondary minimum was too shallow to be observed, such a mass ratio does not appear improbable.

[32] *Bull. Tashkent Astr. Obs.*, No. 4, 1934.

[33] *Ap. J.*, **102**, 113, 1945.

[34] *B.A.N.*, **6**, 29, 1930.

[35] *Ap. J.*, **102**, 480, 1945.

[36] *Ap. J.*, **108**, 15, 1948.

[37] *Laws Bull.*, **2**, 233, 1921.

[38] *Pub. Dom. Ap. Obs., Victoria*, Vol. 1, No. 11, 1920.

[39] *A.J.*, **51**, 101, 1945.

[40] *Pub. A.A.S.*, **8**, 219, 1936.

[41] *Contr. Princeton U. Obs.*, No. 3, 1915.

19. *U Sge.*—In his study of U Sge, Joy[42] found a mass ratio of 3.3. This, combined with any of the various photometric solutions, indicates that the system is near instability. From the published observations it is impossible to determine whether the fluctuations observed in the period are irregular or oscillatory in nature. However, Dr. N. L. Pierce has recently sent me some unpublished times of minimum, including those of Struve and of Irwin; from these it appears highly probable that the variations are not simply periodic.

The preceding discussion thus indicates that an eclipsing system which shows irregular variation of period may be expected to be near the limits of dynamical stability. However, one further question must be asked before we can accept such a relationship with any degree of confidence. Are there systems near the limits of stability which have not exhibited such changes? If the answer is "Yes," such systems must be carefully considered before the preceding results can be regarded as anything more than a rather amazing coincidence. If the answer is "No," then we may with some confidence divide eclipsing systems into two general classes: one in which at least one component is near the stability limits and in which we may expect irregular variations of period to occur; the other in which both components appear stable and whose periods show no sudden fluctuations. (In reality, of course, there will be no sharp dividing line between the two classes; we may perhaps think of the irregular fluctuations as occurring more frequently, the nearer the star is to the stability limits.)

Again, and for the same reasons as before, the stars in Pierce's *Finding List* are considered. The criteria for establishing stability remain the same. The general results strongly confirm those previously reached; that is, the stars which have exhibited constant periods are those whose solutions indicate stability of the components. The following exceptions should be noted.

On the basis of the present solutions, the stars RT Scl, UU And, RV Per, SX Aur, and WZ Cyg appear to be near the limits of stability. The solutions available at present for these systems are unsatisfactory, however, either because the stars have not been adequately observed or because the solutions presented do not satisfactorily fit the observations. (The statement that a fit is not "satisfactory" rests in each case upon the opinion of the authority presenting the solution.) Even more important is the fact that the times of minimum of these stars have not been adequately observed throughout the years. It is to be expected that in most of these cases (the exceptions being those in which stronger solutions will show stable systems) close observation of these stars will show period fluctuations.[43] Another system which should be closely watched is ZZ Aur. Here a good solution by Pierce[44] is available. From mass-luminosity considerations, Pierce assumed a mass ratio of 4; this, combined with his elements, indicates instability of the system. Unfortunately, except for the years 1930–1937, this system has been very little observed. It must be borne in mind that, if this is one of the systems in which the fainter component departs appreciably from mass luminosity, the system may really be stable. For this to be true, the departure from mass luminosity must be in the opposite direction to that usually found in Algol systems. This system is not a "typical" Algol system, however, since the bright star is the larger; it is rather a typical main-sequence pair, so there is no reason to expect such a departure to be in the direction generally found in Algol systems. The system Z Dra is another which appears to be near the limits of stability. Further observation is needed to determine whether the observed fluctuations of period are irregular or oscillatory.

[42] *Ap. J.*, **71**, 336, 1930.

[43] Since writing the above, I have received the 1949 edition of *Astronomiczny*. In this, Szafraneic reports a minimum of RV Per falling 0.046 day earlier than the computed time. Whether this actually represents a sudden change in the period must be left to future observations.

[44] *A.J.*, **47**, 78, 1938.

To summarize the preceding, the observational evidence available at present indicates a rather striking connection between the dynamical stability of an eclipsing system and the irregular fluctuations of its period. The seven systems just listed offer an opportunity for further testing this connection. It is of interest to note that many of these nearly unstable systems also have asymmetrical light-curves. Taylor[45] has found that stars with asymmetry in their light-curves have relatively large components.

It may be appropriate here to emphasize further one consequence of the preceding ideas. The variation of period of the W UMa stars has been frequently commented upon. Both components of these systems are highly distorted; the effect of this distortion is strongly evident in the light-curve because the components are of comparable brightness. But in an Algol system the fainter component may be equally distorted with little effect on the light-curve, because of the small value of its luminosity compared to that of the primary. Thus the real criterion for variation of period is not the shape of the curve (although W UMa stars may well be expected to show variation of period, except perhaps in a few cases where the mass ratio is nearly unity) but the stability of the system itself. Thus the same basic mechanism may be considered responsible for irregular period changes in any type of eclipsing system.

II

In this section an attempt is made to suggest a possible physical mechanism to explain the relation developed in the preceding section and also to explain the period changes themselves. In this connection, attention should be called to the work of Kuiper[24] concerning the dynamics of the system β Lyr. Kuiper's work differs from this in that he considered only contact binaries, whereas this discussion treats separated stars in which one component is near the limits of stability. Actually, both cases may exist; although occasionally it may be uncertain to which one a given system belongs, it is certain that many systems exist which are not contact binaries and which do show such period changes; it is to them that this discussion pertains.

Assuming the Roche model and the law of gravitation, we may expect Kepler's third law, $m_1 + m_2 = a^3/P^2$, to hold in these systems. Hence, an observed change of period implies a change either in the combined mass of the components or in their separation or in both. The first inquiry must therefore be whether any phenomenon already observed is capable of causing such change.

The answer, based on our observation of the sun, is that a rather sudden change of mass seems indeed plausible. As is clearly and strikingly demonstrated by spectrohelio-kinematograms, eruptive prominences are continually occurring on the sun in which large amounts of solar material are expelled from the surface with explosive force. In some cases this material is ejected with speeds of the order of 200 km/sec and to distances of the order of the sun's diameter. In the case of the sun, of course, it seems probable that all the material so expelled eventually returns to the sun. But by no means would this necessarily be true in the case of a highly distorted star, located close to another star of equal or greater mass. Even if the eruptive forces which expelled the material were no greater than those observed on the sun, the more powerful eruptions would easily eject the matter beyond the Jacobian limiting surface, where it would be lost to the system. Indeed, in many cases recently described by Struve and his colleagues, spectrographic evidence alone shows that certain eclipsing systems are surrounded by streams of gas. It thus seems apparent that, from a qualitative viewpoint, forces possibly similar to those causing eruptive prominences on the sun, operating, probably greatly magnified, on those components of eclipsing systems which are already near the bounds of stability, could cause an actual loss of mass to the system and thus a change of period. It remains to be seen whether the amount of loss needed to cause a period change of the size observed is within the bounds of reason.

[45] *Ap. J.*, **94**, 46, 1941.

Kepler's law may be written as follows:

$$P^2 = \frac{a^3}{m_1 + m_2}. \tag{1}$$

P is, of course, expressed in years, a in astronomical units, and $(m_1 + m_2)$ in terms of the sun's mass as unity. Keeping a constant, for a first approximation, and considering the change of mass to occur in only one component, the change in period caused by a small change in m_2 is given by

$$dP = -a^3 \frac{dm_2}{2P(m_1 + m_2)^2} = -\frac{P dm_2}{2(m_1 + m_2)}. \tag{2}$$

For quantitative considerations, consider a system in which $(m_1 + m_2) = 2 \odot$ and $P = 2$ days; a will then be 0.039 A.U. If the change in period is 1 second—appreciably higher than many of those observed—then, from equation (2), $dm_2 = -2.32 \times 10^{-5} \odot$. Thus, in such a system, a loss of mass by one component of the order of 1/100,000 of the sun's mass will cause a change of period appreciably greater than those usually observed. Expressed as the loss of mass in relation to the mass of the system, $dm_2/(m_1 + m_2) = -1.16 \times 10^{-5}$.

There remain, however, two objections to consideration of this mechanism alone as responsible for the period changes; that is, it provides only for an increase in the period, whereas in many cases the period has been observed to decrease; also, by the third law of motion, the expulsion of a portion of a star's mass with explosive velocity may be expected to have some effect on the motion of the star. Computation of the Jacobian surfaces shows that the star is nearest instability at those portions of its surface near the ends of its shortest equatorial axis. If material is ejected from the end of this axis which is on the opposite side of the star from the direction of orbital motion, the effect will be to increase the star's velocity. This will increase the centrifugal force, and the star will move farther from the center of mass of the system until its increased energy has been expended as work against the gravitational field of the other component. The star will thus move to a greater distance from the center of mass, and the period of revolution will be lengthened. If the explosion occurs at the opposite end of the axis, the reverse will be true. It is necessary to determine how the effect on the period from this cause will compare with that from loss of mass; in actual practice, of course, both effects will be occurring simultaneously, sometimes reinforcing, sometimes tending to neutralize, one another, depending upon the position on the star's surface at which the ejection occurs.

It was found that, in the hypothetical system assumed previously, a loss of mass of $2.32 \times 10^{-5} \odot$ would suffice to cause a lengthening of the period of 1 second. Now, suppose this mass had been ejected with explosive velocity from an area near one of the ends of the shorter equatorial radius. What would be the effect on the period caused by the change in the star's motion thus developed? To determine this, information about the masses of the individual stars is needed; the assumption $m_1 = m_2 (= m \odot)$ will be made. In reality, m_2 is usually less than m_1, and the effect to be discussed will be magnified. A velocity of expulsion of 300 km/sec will be assumed. This is the velocity of the gaseous streams observed by Struve in β Lyrae and is little greater than that observed in some explosive prominences on the sun. Then, from the third law of motion, the change in the stars' velocity, dv, is

$$dv = 2.32 \times 10^{-5} \times 3 \times 10^7 \text{ cm/sec} = 696 \text{ cm/sec}. \tag{3}$$

The change in the star's kinetic energy for a small change of velocity is $dE = m_2 v dv$. This energy is expended in action against the gravitational field of the other star (as-

sumed constant for a first approximation) over the distance da, the change in distance from the center of the system. Thus:

$$m_2 v\, dv = \frac{G m_1 m_2}{a^2}\, da, \quad \text{or} \tag{4}$$

$$da = v a^2 \frac{dv}{G m_1}. \tag{5}$$

The orbital velocity of the star in this assumed case may easily be computed thus:

$$v = \frac{2\pi a}{P} = 2.12 \times 10^7 \text{ cm/sec}. \tag{6}$$

Hence, from equation (5), $da = 3.83 \times 10^7$ cm $= 2.55 \times 10^{-6}$ A.U. How will such a change affect the period? Again, from Kepler's third law, taking into account both the sudden decrease in mass and the impulsive change in momentum, we have

$$dP = \frac{-a^3 dm_2}{2P(m_1+m_2)^2} \pm \frac{3a^2 da}{2P(m_1+m_2)} = 3.12 \times 10^{-8} \pm 53.4 \times 10^{-8} \text{ years}. \tag{7}$$

The sign of the second term will depend upon the end of the axis at which the ejection occurs; the magnitude of this term is about 17 seconds. Thus, in the case considered, the primary cause of change of period is the change of motion of the star caused by the explosion. This can either shorten or lengthen the period, depending on the area of the star at which the explosion occurs, and, by observation, the periods of eclipsing systems are found to change in either direction. The loss of mass needed to cause a change of period of 1 second will be of the order of 10^{-6} $\odot$.

In summation, the preceding hypothesis suggests a possible explanation for the irregular changes of period which have long puzzled observers of eclipsing systems. In systems in which there is frequent ejection of material, the period changes may be almost continuous; in others, where only the largest of eruptive prominences escape, the system may remain constant for years. In such cases, when a change of period does occur, it may be a relatively large one. The value of about 10^{-6} of the mass of the star to be lost in such an explosion or series of explosions represents decidedly an upper limit. The changes of period actually observed are often considerably less than a second (although in some cases they are somewhat greater); the assumption $m_1 = m_2$ also tends to minimize the computed effect of a given ejection. In cases encountered in nature, a value of 10^{-7} or 10^{-8} may well prove more normal, although wide variations may be expected. If a change of period occurs on the average of once every 10 years, this will mean that in roughly 10^7 years the star will lose 0.1 of its total mass. This suggests that the condition of near-instability is a temporary one in the life of the system and that systems in such a condition are in a transition state.

The weakest part of the quantitative discussion of this hypothesis is the assumption of the Roche model. While this assumption is adequate for computations of stability as carried out in Part I, the changes considered in Part II are of the order of 10^{-6} P. If the Roche model is not assumed, then changes of matter within the stars themselves could, of course, conceivably cause period changes; the hypothesis just developed, however, requires only the operation of processes similar to those frequently observed on the sun. The changes in the physical elements involved in these period changes offer a test which is unfortunately many hundreds of times more delicate than can be attained by the best photometric and spectrographic observations.

Continued observations of the times of minimum of critical systems are badly needed,

as well as solutions based on accurate observations covering the entire curve. The need for spectrographic mass ratios in those systems in which both spectra are visible cannot be overemphasized. It should, finally, be emphasized that the correlation between stability and constancy of period as developed in Part I is independent of the correctness of the hypothesis suggested in Part II.

I am indebted to Drs. Newton Pierce, Otto Struve, John Irwin, and William Blitzstein for permission to use their unpublished times of minimum; I am especially indebted to Dr. Pierce for informing me of the existence of these observations. For a critical reading of the manuscript and helpful suggestions, I wish to thank Drs. Henry Norris Russell, Edwin F. Carpenter, and Newton L. Pierce.

NOTES

A NOTE ON ENERGY GENERATION

Energy-generation rates obtaining in stellar interiors were recomputed by using (*a*) new values of the nuclear cross-sections for the processes occurring in the carbon cycle and (*b*) the revised formula for the proton-proton reaction.

a) THE CARBON CYCLE

Cross-sections for the carbon cycle in the range of energy corresponding to stellar interiors, extrapolated from measurements near 100 kev, are as follows:[1]

C^{12}: $\sigma = \dfrac{0.0020}{E} \exp(-6E^{-1/2})$ barns,

C^{13}: $\sigma \geq \dfrac{0.01}{E} \exp(-6E^{-1/2})$ barns, (from single resonance at ~ 500 kev),

N^{14}: $\sigma = \dfrac{0.028}{E} \exp(-7E^{-1/2})$ barns,

N^{15}: $\sigma = \dfrac{110}{E} \exp(-7E^{-1/2})$ barns (1 barn $= 10^{-24}$ cm^2).

The following calculations on the carbon cycle were based on the $N^{14} + H^1$ reaction, N^{14} having the longest lifetime of the nuclei of the cycle, and its relative abundance, a_{14}, having the smallest relative change from its original to its equilibrium value. The energy generation per unit volume and per unit time is[2]

$$\epsilon_C \rho = \int_0^\infty \left[\frac{\rho a_{14}}{14 m_H}\right]\left[\frac{\rho X}{m_H}\frac{2}{\pi^{1/2}}\frac{1}{(kT)^{3/2}} e^{-E/kT} E^{1/2} dE\right]\left[\left(\frac{2E}{M}\right)^{1/2}\right]\left[\frac{C}{E} e^{-(E_0/E)^{1/2}}\right] \times [4 \times 10^{-5}]. \quad (1)$$

In this formula the terms in brackets are as follows: the first denotes the number of N^{14} nuclei per unit volume; the second the number of protons with energies in the range E to $E + dE$; the third the relative velocity with M (the reduced mass) expressed in mev/c^2; the fourth the effective cross-section for the $N^{14} + H^1$ reaction, with $E_0 = Z^2$ mev $= 49$ mev; and the last the energy production per capture.

For computational purposes, equation (1) was rewritten in the form:

$$\log \frac{\epsilon_C}{\rho X a_{14}} = \log A - \tfrac{5}{6} \log T + \log J(BT^{-1/3}), \quad (2)$$

with

$$A = \frac{2^{3/2} C k^{-5/6} 4 \cdot 10^{-5} E_0^{1/3}}{\pi^{1/2} M^{1/2} 14 (m_H)^2} \quad (3)$$

[1] R. N. Hall and W. A. Fowler, *Phys. Rev.*, **77**, 197, 1950. Values of the cross-sections were kindly communicated by Dr. Fowler to Dr. B. Strömgren in advance of publication.

[2] Cf. G. Gamow and E. Teller, *Phys. Rev.*, **53**, 608, 1938.

and

$$B = E_0^{1/3} k^{-1/3}, \tag{4}$$

while

$$J(BT^{-1/3}) = \int_0^\infty \exp\{-BT^{-1/3}(t + t^{-1/2})\}\, dt. \tag{5}$$

This transformation was effected by the following substitution:

$$t = \frac{E}{E_0^{1/3}(kT)^{2/3}}. \tag{6}$$

The integral (eq. [5]) was evaluated numerically for sixteen integral values of the temperature, and equation (2) was computed accordingly. The results are tabulated in Table 1, in which the temperature is given in millions of degrees, and the last column indicates the power of T upon which $\epsilon_C/\rho X a_{14}$ depends, and is computed simply as $(\Delta \log \{\epsilon_C/\rho X a_{14}\})/(\Delta \log T)$. An adequate representation of ϵ_C in regions of greatest contribution to the luminosity in the case of the sun ($T \sim 17$), may be given by

TABLE 1

T	log J	log $(\epsilon_C/\rho X a_{14})$	n
10	0.853−33	6.64−10	.....
11	.853−32	7.60−10	22.8
12	.728−31	8.44−10	22.1
13	.517−30	9.20−10	21.6
14	.230−29	9.89−10	21.0
15	.876−29	0.51	20.6
16	.472−28	1.08	20.1
17	.012−27	1.60	19.6
18	.520−27	2.09	19.2
19	.982−27	2.53	18.8
20	.417−26	2.95	18.7
21	.829−26	3.34	18.3
22	.211−25	3.71	18.0
23	.572−25	4.05	17.6
24	.907−25	4.37	17.4
25	0.232−24	4.68	.....

$$\epsilon_C = 1.0 \times 10^{-23} \rho X a_{14} T^{20}. \tag{7}$$

The lifetimes of the C^{12}, C^{13}, N^{14}, and N^{15} atoms, given by the reciprocal of the probability of collision with a proton, are[3]

$$\text{Lifetime} = \frac{1}{\rho X} \frac{4 \times 10^{-5}}{A m_H} \frac{(\rho X a)}{\epsilon}. \tag{8}$$

In equation (8), A is the atomic weight of the atom under consideration, and a is its relative abundance by weight. For $\rho X = 30$ and $T = 20$, and for $\rho X = 120$ and $T = 16$, the lifetimes are, numerically, as follows:

	$\rho X = 30,\ T = 20$	$\rho X = 120,\ T = 16$
C^{12}:	1.2×10^5 years,	1.3×10^6 years,
C^{13}:	2.8×10^4 years,	2.5×10^5 years,
N^{14}:	2.0×10^6 years,	3.7×10^7 years,
N^{15}:	520 years,	9.5×10^3 years.

[3] Cf. H. A. Bethe, *Phys. Rev.*, **55**, 440, 1939.

Alternatively, the relative abundances of the nuclei for $\rho X = 30$, $T = 20$, are

$$C^{12}:C^{13}:N^{14}:N^{15} = 1 : < \tfrac{1}{4} : 17 : \tfrac{1}{230},$$

while those for $\rho X = 120$, $T = 16$, are

$$C^{12}:C^{13}:N^{14}:N^{15} = 1 : < \tfrac{1}{5} : 28 : \tfrac{1}{135}.$$

b) COMPARISON WITH THE PROTON-PROTON REACTION

Calculations on the proton-proton reaction were carried out with the aid of the following formula:[4]

$$\epsilon_p = 1.91 \left(\frac{\rho}{100}\right)\left(\frac{X}{0.316}\right)^2\left(\frac{T}{15}\right)^4, \tag{9}$$

which depends on the applicability of the Gamow-Teller selection rules for this process. By definition, the luminosities L_p and L_c, due to the proton-proton reaction and carbon cycle, respectively, are

$$L_p = \int_0^R 4\pi r^2 \rho \epsilon_p dr = (3.78)(10)^{-6} \times 4\pi \left[\frac{(2.5)\,k}{4\pi G \mu H}\right]^{3/2} X^2 \rho_c^{1/2} T_c^{11/2} \int_0^{\xi_1} \xi^2 \theta^7 d\xi$$
$$= \frac{6.23 \times 10^{25}}{\mu^{3/2}} X^2 \rho_c^{1/2} T_c^{11/2}, \tag{10}$$

$$L_c = \int_0^R 4\pi r^2 \rho \epsilon_c dr = (1.0)(10)^{-23} \times 4\pi \left[\frac{(2.5)\,k}{4\pi G \mu H}\right]^{3/2} X a_{14} \rho_c^{1/2} T_c^{43/2} \int_0^{\xi_1} \xi^2 \theta^{23} d\xi$$
$$= \frac{2.84 \times 10^{7}}{\mu^{3/2}} X a_{14} \rho_c^{1/2} T_c^{43/2}. \tag{11}$$

In equations (10) and (11) the assumption has been made that, throughout regions in which both energy-producing mechanisms are operative, the temperature and density distributions are given by a polytrope of index 3/2. The two integrals occurring in equations (10) and (11) have been evaluated numerically and were found to equal 0.3396 and 0.0585, respectively. These values yield, for the relative contribution to the luminosity of the proton-proton reaction and the carbon cycle,

$$\frac{L_p}{L_c} = \left(\frac{X}{a_{14}}\right) \frac{(2.194)(10)^{18}}{T_c^{16}} \tag{12}$$

(T in millions of degrees).

Applying equations (10) and (11) to the sun, with $\rho_c = 157.5$,[5] $X = 0.74$, $a_{14} = 0.01$, $\mu = 0.60$, and $L = L_p + L_c$, one finds that T_c for the sun equals 15.7 million degrees. The values of T_c and μ are consistent with the mass-luminosity relation to the extent required in this preliminary calculation. Equation (12) indicates that, in the sun, energy production due to the proton-proton reaction outweighs the energy production due to the carbon cycle by a factor of 12.

Since the two sources of energy production discussed above are of comparable importance for stars similar to, or a little brighter than, the sun, a more nearly satisfactory procedure would be to reintegrate the equations of stellar structure, employing the con-

[4] L. Aller, *Ap. J.*, **111**, 176, 1950. The original calculations, due to H. A. Bethe and C. L. Critchfield (*Phys. Rev.*, **54**, 248, 1938), contain a numerical error of a factor of 2 in the Fermi (β-decay) constant and another factor of 2 in the cross-section for the proton-proton reaction. This was pointed out by G. Gamow and C. L. Critchfield and also by Edwin E. Salpeter in an informal communication to W. A. Fowler.

[5] M. H. Harrison, *Ap. J.*, **108**, 322, 1948.

tributions of both energy sources in computing the luminosity. It may then be possible to make further conclusions regarding secondary effects on the energy generation due to the change in model arising from the above computations. For stars 2 mag. or more brighter than the sun, the energy generation is evidently controlled almost exclusively by the carbon cycle.

The foregoing calculations were initiated at the suggestion of Professor Bengt Strömgren, to whom the writer owes many thanks for his co-operative interest in this investigation.

I. Epstein

Princeton University Observatory
May 26, 1950

ON THE TRANSITION PROBABILITIES OF C_2 SWAN BANDS

Robert B. King[1] has recently reported measurements of the intensities of Swan bands of carbon in furnace source and has compared the results of his experimental transition probabilities with the theoretical ones. For the latter he has used the calculated results of McKellar and Buscombe,[2] based upon the theory developed by Hutchisson.[3] In the comparative study, the experimental results of Johnson and Tawde[4] have also been subjected to discussion, and some peculiarities of intensity development in relation to theory have been shown.

In this connection it is interesting to draw attention to the investigations carried out in this laboratory and presented in a thesis by Patel,[5] wherein he obtained quantitative measures of Swan-band intensities in flames under about ten varied conditions. These results have been examined in the light of theory by computing the transition probabilities from Hutchisson's intensity integral. However, many of these computed values of Patel differ greatly from those of McKellar and Buscombe (as quoted in King's paper). In Table 1 are given the two sets of values of theoretical transition probabilities.

The disparity in the values in Table 1 derived from the same formula is not easily accountable, unless the constants used by the two authors differ markedly. As the original paper of McKellar and Buscombe is not within our reach, we cannot obtain satisfaction on this point. But it appears that the molecular constant to which the values are sensitive is Δr, the difference in internuclear distance in the two electronic states of C_2 (Swan). Patel's value of Δr is 0.046 A, which is not sensibly different from that of McKellar and Buscombe, viz., 0.047 A. It is also closer to the more recent estimate, 0.0457 A, of Phillips[6] from revised rotational analysis on Swan bands. Again in a recent work by Gopalkrishnan,[7] the calculations of Patel have been proved to be correct, and hence there seems little doubt about the values of theoretical transition probabilities given by him.

Now, coming to the question of the degree of agreement between theory and experiment, one has to remember that Hutchisson's intensity integral, from which the calculations have been made, is worked out on the assumption of the harmonic nature of nuclear oscillations, besides the symmetry of the molecule. But in the electronic band system as that of the present C_2 molecule, anharmonicity sets in after the first few vibrational levels, and this would bring in increasing departure in bands associated with higher and higher vibrational quanta. Hence higher sequences or higher members in sequences are expected to show more rapid departure between theory and experiment.

[1] *Ap. J.*, **108**, 429, 1948.
[2] *Pub. Dom. Ap. Obs., Victoria*, **7**, 361, 1948.
[3] *Phys. Rev.*, **36**, 410, 1930.
[4] *Proc. R. Soc. London, A*, **137**, 575, 1932.
[5] Ph.D. thesis, Bombay University, 1947.
[6] *Ap. J.*, **108**, 434, 1948.
[7] Ph.D. thesis, Bombay University, 1949 (in submission).

TABLE 1

Band	McKellar and Buscombe	Patel	Band	McKellar and Buscombe	Patel
0, 0	1.000	1.000	3, 1	0.149	0.137
0, 1	0.354	0.335	3, 2	.392	.394
0, 2	0.048	0.043	3, 3	.022	.....
			3, 4	.498	.502
1, 0	0.324	0.307	3, 5	.....	.259
1, 1	0.436	0.459			
1, 2	0.511	0.493	4, 2	.215	.202
1, 3	0.121	0.103	4, 3	.334	.330
			4, 5	.435	.405
2, 0	0.034	0.061	4, 6	.....	.459
2, 1	0.422	0.409			
2, 2	0.144	0.164	5, 4	0.246	.554
2, 3	0.544	0.533	5, 7	.....	0.493
2, 4	0.203	0.185			

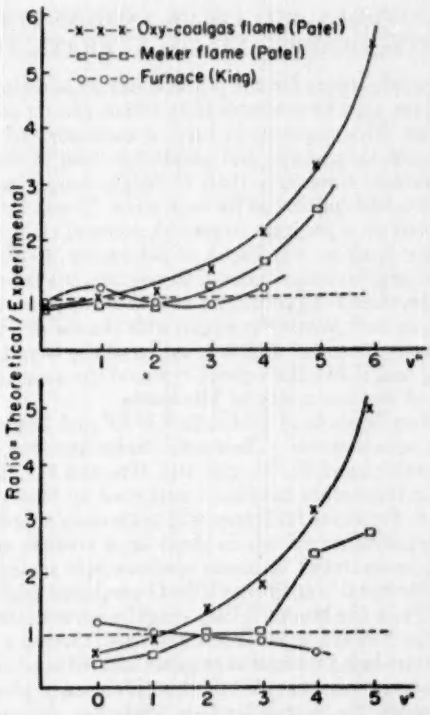

FIG. 1

That may be the reason why King has noticed a tendency of the experimental values of the higher members of sequences λ 5635 and λ 4737 in his furnace source to rise more rapidly than the theoretical ones. Such behavior has been found by Patankar[8] in another symmetric molecule N_2. Patel has noted a similar departure, but a systematic one, in his work on flame sources; but he finds that the experimental values, instead of gaining over the theoretical ones, fall short of them, a phenomenon which is contrary to that of the furnace findings of King. Figure 1 illustrates how, with increasing v' and v'' values, the disparity increases. The horizontal broken straight line indicates the ideal agreement of experimental results with theory, while the points below this line indicate the gain of experimental values over the theoretical ones, and those above it the opposite. The behavior due to the results of King and of Patel is shown side by side. Details of the investigation are being incorporated in a paper under preparation.

N. R. Tawde
J. M. Patel

Spectroscopic Laboratories
Royal Institute of Science
Bombay, India
October 20, 1949

APPARENT MAGNITUDES AND COLOR INDICES FOR SEVENTY-FOUR WHITE DWARFS AND DEGENERATE STARS

Before a really adequate theory for the physical nature of white dwarfs can be formulated, observational data must be available from which, among others, the linear dimensions can be calculated. This requires, in turn, a knowledge of the luminosities—and therefore of the apparent magnitudes and parallaxes—and of the surface brightnesses. Even though at the present time more than 120 white dwarfs are known, accurate apparent magnitudes have been published for only a few. It was for these reasons that the present writer embarked on a program to provide some of these missing data.

Originally, when the program was begun in September, 1944, it was planned to determine only the photographic magnitudes of these stars, but the ease and accuracy with which the program developed suggested its extension to photovisual magnitudes and hence to color indices as well. Work was begun with the aid of a grant from the Society of Sigma Xi; it was later extended with a grant from the Gould Fund of the National Academy of Sciences; and it has throughout received the generous financial support of the Graduate School of the University of Minnesota.

All known white dwarfs north of declination $-30°$ and brighter than the sixteenth magnitude have now been observed. Their magnitudes have been determined by direct comparison with Selected Areas 92, 96, 100, 104, 108, and 112. The photographic magnitudes for the stars in these areas have been published by Mount Wilson;[1] the writer is greatly indebted to Dr. Frederick H. Seares, who generously supplied photovisual magnitudes down to the sixteenth magnitude in these same areas in advance of publication. For the photographic magnitudes Eastman spectroscopic plates 103*a*-O without filter were used; for the photovisual magnitudes 103*a*-G emulsions and a No. 12 "minus-blue" filter were employed. Since the Mount Wilson magnitudes were determined with a silver-on-glass mirror and the Steward reflector is aluminized, there is a slight difference in the color systems—blue stars being somewhat brighter and red stars somewhat fainter in our system than in the International one. While this difference is advantageous in the sense that it appears to broaden the color-index base, there has, unfortunately, been no occa-

[8] *Proc. Phys. Soc. London*, **55**, 396, 1943.

[1] *Papers of the Mt. Wilson Observatory*. Vol. **4**, 1930.

TABLE 1

MAGNITUDES AND COLORS FOR 74 WHITE DWARFS AND DEGENERATE STARS

STAR	1950 R.A.	1950 Dec.	PROVISIONAL I.C.	m_{pg}	m_{pv}	ADOPTED I.C.
L 505-1	$0^h 00^m.1$	−34° 30′	+0.2	15.02	14.76	+0.26
LDS 1 A	08.7	−21 00	+0.2	12.29		
LDS 1 B	08.7	−21 00	+0.5	14.03		
W 1	11.1	+ 0 03	+0.1	15.40	14.94	+ .46
L 1011-71	33.1	+ 1 37	+0.3	15.26	15.02	+ .24
vMa 1	0 46.5	+ 5 11	+0.4	12.93	12.25	+ .69
L 796-10	53.3	−11 45	+0.3	15.09	15.06	+ .03
W 1516	1 15.4	+15 56	−0.2	13.55	13.78	− .23
R 548	33.7	−11 36	+0.2	13.92	14.22	− .30
L 870-2	35.5	− 5 16	+0.2	12.98	12.75	+ .23
Oxf +25:6725	2 05.9	+25 00	0.0	12.93	13.31	− .38
h Per 1166	14.0	+56 53	−0.3	13.16	13.75	− .59
*L 587-77 A	3 26.8	−27 34	−0.1	13.88	13.52	+ .36
W 219	41.6	+18 18	+0.3	15.13	14.40	+ .73
Z 3	50.7	+10 36	−0.2	12.52	12.88	− .36
Z 4	3 52.5	+ 9 37	0.0	14.23	14.08	+ .15
Z 10	4 07.3	+17 54	−0.2	14.00	13.99	+ .01
Z 2	10.0	+11 45	−0.4	13.20	13.83	− .63
o Eri BC	13.0	− 7 44		9.17		
VR 7	21.0	+16 14	−0.3	14.07	13.98	+ .09
VR 16	4 25.7	+16 52	−0.3	13.53	14.00	− .47
Z 9	29.4	+17 38	0.0	14.03	13.79	+ .24
Z 7	31.0	+12 35	−0.4	13.55	14.09	− .54
L 1244-26	6 12.4	+17 45	−0.4	12.65	13.37	− .72
SA 26-82	39.6	+44 43	0.0	16.07	16.09	− .02
He 3	6 44.3	+37 36	−0.3	11.24	12.04	− .80
L 384-24	7 32.0	−42 47	0.0	13.82		
*L 745-46 A	38.0	−17 17	−0.1	12.84	13.01	− .17
L 817-13	52.8	−14 38	0.0	13.32	13.53	− .21
L 532-81	8 39.7	−32 47	−0.2	11.71	11.65	+ .05
*LDS 235 B	8 45.3	−18 48	−0.1	14.63	15.08	− .45
LDS 275 A	9 35.0	−37 07	0.0	14.86	14.71	+ .15
LDS 275 B	35.0	−37 07	+0.1	15.16	15.01	+ .15
SA 29-130	43.5	+44 08	+0.1	12.90	13.47	− .57
L 898-25	10 55.1	− 7 15	+0.1	14.35	14.31	+ .04
L 971-14	11 15.8	− 2 58	0.0	14.87	15.00	− .13
R 627	21.7	+21 39	+0.3	13.77	14.31	− .54
*L 1405-40	47.7	+25 35	+0.1	15.39	15.66	− .27
L 1261-24	54.2	+18 39	+0.2	15.43	15.65	− .22
Z 28	12 30.0	+41 46	+0.3	15.37	15.50	− .13
W 457	12 57.7	+ 3 46	+0.5	15.98	15.83	+ .15
Z 43	13 14.0	+29 22	0.0	11.90	12.86	− .96
BD −7:3632	27.7	− 8 18	+0.1	12.12	12.52	− .40
W 489	34.3	+ 3 58	+1.1	15.53	14.76	+ .77
*LDS 455 A	34.3	−16 04	0.0	14.94	15.29	− .35
Grw +70:5824	13 37.8	+70 33	−0.1	12.26	12.88	− .62
*L 619-50	48.1	−27 18	+0.1	15.03	15.38	− .35
L 1126-68	14 48.4	+ 7 47	0.0	15.05	15.43	− .38
R 808	15 59.6	+36 58	0.0	14.13	14.11	+ .02
R 640	16 26.8	+36 51	+0.3	13.46	13.79	−0.33

TABLE 1—*Continued*

Star	1950 R.A.	1950 Dec.	Provisional I.C.	m_{pg}	m_{pv}	Adopted I.C.
L 1491-27	16h37m4	+33°32′	+0.2	14.22	14.34	−0.12
L 845-70	17 08.5	−14 45	+0.2	14.12	14.19	− .07
*W 672 A	16.2	+ 2 00	0.0	14.24	14.27	− .03
L 1208-132	18 18.2	+12 38	+0.3	15.90	15.69	+ .21
R 137	24.8	+ 4 02	−0.3	13.77	13.84	− .07
L 994-27	18 57.6	− 1 30	+0.4	16.83	.....	.....
Grw +70:8247	19 00.6	+70 34	−0.2	12.71	13.02	− .31
*LDS 678 A	17.7	− 7 46	−0.3	11.89	12.03	− .14
*LDS 683 B	32.9	−13 36	−0.1	15.04:	15.34	− .30
L 1573-31	40.4	+37 24	−0.4	14.11	14.30	− .19
L 1140-73	19 41.9	+ 8 47	0.0	14.16	13.72	+ .44
L 709-20	52.9	−20 37	0.0	14.61	14.93	− .32
L 997-21	54.0	− 1 09	0.0	13.62	13.62	.00
L 710-30	20 07.3	−21 55	+0.2	14.41	14.16	+ .25
W 1346	32.3	+24 55	−0.2	11.16	11.46	− .30
R 198	21 24.8	+54 59	−0.4	14.43	14.53	− .10
Grw +73:8031	26.6	+73 25	−0.3	12.56	12.90	− .34
*LDS 749 B	29.6	0 00	0.0	14.21	14.57	− .39
Grw +82:3818	36.7	+82 49	−0.1	12.51	13.06	− .55
L 930-80	45.0	− 7 58	0.0	14.23	14.73	− .50
*L 1512-34 A	23 41.4	+32 15	+0.1	13.04	12.84	+ .20
*LDS 826 A	51.5	−33 33	0.0	14.59	14.34	+ .25
L 505-42	51.7	−36 50	+0.3	14.80	14.78	+0.02
L 362-81	59.6	−43 25	+0.2	12.81	.....	.....

TABLE 2

DOUBLE STARS

Star	A	pg	pv	I.C.	B	pg	pv	I.C.
L 587-77	nf	13.88	13.52	+0.26	sp	15.61:	13.54	+2.07
L 745-46	fo	12.84	13.01	−0.17	pr	17.60	16.01	+1.59
LDS 235	nf	12.65	11.43	+1.22	sp	14.63	15.08	−0.45
L 1405-40	nf	15.39	15.66	−0.27	sp	16.38	15.45	+0.93
LDS 455	nf	14.94	15.29	−0.35	sp	15.18	14.00	+1.18
L 619-49/50	nf	13.92	12.32	+1.60	sp	15.03	15.38	−0.35
W 672	np	14.24	14.27	−0.03	sf	15.55	14.09	+1.46
LDS 678	sf	11.89	12.03	−0.14	np	13.72	11.91	+1.81
LDS 683	nf	14.8:	13.55	+1.3:	sp	15.04:	15.34	−0.30
LDS 749	sp	10.97	10.07	+0.90	nf	14.21	14.57	−0.36
L 1512-34/35	so	13.04	12.84	+0.20	no	13.31	11.42	+1.89
LDS 826	so	14.59	14.34	+0.25	no	15.04	13.44	+1.60

sion as yet to determine the relationship between the two systems by observing standard stars.

In general, as many different stars and as many different Selected Areas as feasible were used in each case; however, many of the photovisual magnitudes of the faintest white dwarfs depend upon comparison with one single star in a single Selected Area. The brightness of the stars was determined by eye estimates, using the Argelander step-method. The first photographic observations were made by the writer in September, 1944, and were continued by Dr. Jose during the years 1944–1946 and by the writer during short visits to Tucson in March, 1945, and March, 1946. The later photographic observations and all the photovisual observations were made by the writer alone during brief visits to Tucson in March, 1947, March and September, 1948, March, 1949, and March, 1950. In each case the writer's stay extended over only ten nights at maximum, and consequently, because of the pressure for time, observations had to be made under circumstances that were far from favorable. Plates simply *had* to be taken—often when the sky was photometrically doubtful, when the stars were in large hour-angles, or when large differential extinction corrections had to be applied; many plates showing slight trails or slightly out-of-focus images had to be used; and bad seeing was the rule, thus rendering observations on close double stars especially difficult. In fact, nearly all the cardinal sins of photometry had to be committed if the program was to be completed at all, even in five years' time.

Consequently, the accuracy of the results is considerably less than what could be obtained under ideal conditions: discussion of the internal disagreements among plates indicates an average mean error for a photographic or a photovisual magnitude as determined from a single plate of 0.12 mag. For stars of high declination and of the optimum magnitude range from 13 to 15, the accuracy is considerably better and the mean error probably only half this amount; for stars south of declination $-20°$ it must be considerably worse, while, in addition, for these far southern stars serious systematic errors may be present in the magnitudes, owing to uncertainties in the extinction correction. It is hoped, however, that these uncertainties do not affect the adopted color indices too seriously. If plates were taken under good conditions and showed images of good quality, three pairs of plates were considered sufficient, but in some cases as many as seven or eight pairs were taken. The average is 4.2 pairs of plates per star; hence it is believed that the mean error of the finally accepted photographic or photovisual magnitudes is around ± 0.06 mag. and that of the color indices around ± 0.085 mag.

The data are collected in Table 1, the several columns of which give, in order, the star's designation, the position for 1950, the provisional color index as determined at Tucson by the differential method, the photographic and photovisual magnitudes, and the adopted color index. For six stars it has not been possible to obtain yellow plates, and no photovisual magnitudes or color indices are accordingly shown. Twelve stars in this table, marked with an asterisk, are components of binaries of which the other component appears to be an ordinary red dwarf. Further data for both the components of these systems are given in Table 2.

The writer is greatly indebted to Dr. Paul D. Jose, acting director of the Steward Observatory, University of Arizona, from 1942 to 1946, not only for his permission to use the 36-inch reflector for this purpose but for his active participation in the program and the taking of numerous blue plates; and he is also indebted to Dr. Edwin F. Carpenter, who, after his return from active service to the directorship of the Steward Observatory, has continued to allow the telescope to be used for this program.

W. J. LUYTEN

UNIVERSITY OF MINNESOTA
April 5, 1950

THE SPECTRUM OF YY GEMINORUM (CASTOR C)

The orbit of Castor C was determined by A. H. Joy and R. F. Sanford in 1926.[1] The most remarkable feature of the spectrum of this double-lined red-dwarf system is the presence of strong emission lines of *Ca* II and *H* in both components. On the Mount Wilson plates the more massive star had stronger absorption lines than did the less massive

TABLE 1

RADIAL VELOCITIES OF YY GEMINORUM

Plate	Date	U.T.	Phase (Days)	Phase (Period)	Radial Velocities (Km/Sec)			
					Absorptions		Emissions	
					Comp. I	Comp. II	Comp. I	Comp. II
	1948							
CQ 7176	Nov. 17	8h34m	0.674	0.828	−100.6	+107.1	.....	.....
7177	17	9:34	.716	.879	− 66.2	+ 81.8	− 89.3	+ 95.1
f/2 G 11366	18	8:58	.063	.077	.....	− 54.9	+ 73.3	− 54.1
11382	19	10:40	.318	.391	.....	.....	+ 64.6	− 86.5
11400	23	10:33	.243	.298	+121.0	−110.3	+113.8	−120.2
11401	23	11:10	.268	.329	+129.3	−111.8	+110.6	−108.6
11402	23	12:00	.303	.372	+ 61.0	−114.5	+ 83.3	− 92.2
11408	24	10:08	.411	.505	+ 4.5	.....	− 1.0	.....
11409	24	10:38	.432	.531	− 5.1	.....	− 1.1	.....
11414	25	12:00	.674	.828	− 93.0	+122.1	−117.5	+126.4
11415	25	12:32	.696	.855	−115.0	+119.3	− 81.0	+119.2
11420	26	11:41	.033	.041	+ 10.4	.....	+ 18.1	.....
11421	26	12:29	.066	.081	− 5.5	.....	+ 67.3	− 65.1
11440	28	10:38	.360	.442	− 17.5	.....	+ 5.1	.....
11444	29	12:20	.617	.758	−106.8	+135.1	−132.9	+114.4
11449	30	12:35	.813	.998	− 6.8	.....	− 6.0	.....
11459	Dec. 1	12:30	.181	.222	+149.0	−102.6	+137.2	−130.2
11481	3	11:24	.506	.621	.....	.....	− 77.7	+ 98.3
11482	3	11:59	.530	.651	−100.6	.....	−106.0	+106.0
11483	3	12:28	.550	.675	−117.1	+ 84.4	−129.4	+127.3
CQ 7300	4	7:20	.523	.642	− 49.6	+116.2	− 92.8	+ 75.7
7366	10	11:51	.197	.242	.....	.....	+112.5	−126.8
CG 7412	16	12:03	.505	.620	−119.1	+ 58.9	− 76.8	+ 79.3
	1949							
CG 7558	Feb. 13	8:14	.718	.882	− 74.5	+ 70.5	− 85.1	+ 87.3
7561	14	5:22	.784	.963	− 51.7	+ 6.4	− 30.1	+ 33.5
7562	14	6:33	.019	.023	+ 2.6	.....	+ 12.8	− 29.1
7563	14	7:47	.070	.086	+ 52.8	− 58.5	+ 59.7	− 64.2
7566	17	6:20	.567	.696	−146.3	+ 83.8	−112.8	+113.9
7567	17	7:12	.603	.741	−120.8	+105.0	−130.5	+111.9
7568	17	8:03	.638	.784	−123.6	+135.9	−119.9	+115.3
7569	19	6:00	.110	.135	+ 90.9	− 97.8	+ 88.8	− 93.3
7570	19	6:52	0.146	0.179	+ 83.0	−110.5	+108.7	−112.0

star, and there was no indication of any variation in the intensities of these lines. However, the emission lines of the more massive component were twice as strong as those of the less massive component when the former was receding and the latter approaching. When the positions of the two components in the spectrum were reversed, the emission lines of the more massive star were estimated to be, on the average, about 20 per cent

[1] *Ap. J.*, **64**, 250, 1926.

weaker than the emission lines of the less massive star. This periodic variation in the relative intensities of the emission lines bears a certain resemblance to the well-known variation of the absorption lines in early-type spectroscopic binaries having very short periods and in W Ursae Majoris binaries; but in these latter two groups of objects the violet component is always the stronger, irrespective of whether it comes from the more massive or from the less massive star in each system. Joy and Sanford suggested that the variation of the emission lines in Castor C might be caused by "the effect of the rapid orbital motion in a resisting medium," which "might be such as to cause the higher atmosphere which produces the emission to be dragged behind." This might then explain the strengthening of the bright lines in the receding star.

Because of the interest attached to this phenomenon, Castor C was placed upon the spectrographic observing program of the McDonald Observatory, and thirty-two spectrograms were obtained with the Cassegrain spectrograph attached to the 82-inch reflector. Three different combinations of cameras and prisms were used. In Table 1 "CQ" designates the quartz prisms and 500-mm UV camera, giving a dispersion of 40 A/mm at λ 3933; "CG" designates the glass prisms and 500-mm camera, giving a dispersion of 26 A/mm at λ 3933; and "*f*/2 G" designates the glass prisms and 180-mm Schmidt camera, giving a dispersion of 50 A/mm at λ 3933.

Table 1 lists the spectrograms and the radial velocities obtained from the absorption lines and from the emission lines. Figure 1 shows the velocities plotted against the period of 0.8142822 day, which is the value found originally by Van Ghent in 1931. His photometric elements were adopted without change in the *1948 Catalogue of Variable Stars* by Kukarkin and Parenago. The elements of our velocity-curves are: $\gamma = 0$ km/sec; $K_1 = K_2 = 125$ km/sec. Although the scatter of the observations is large, we find equal masses for the two components; this is contrary to the Mount Wilson results. Since their velocity-curves are at least as reliable as those obtained at McDonald, we are inclined to believe that there has been a real change in the value of K_1, for which Joy and Sanford obtained 114 km/sec. The value of K_2 is substantially the same in both sets of observations, and the difference in γ of 4 km/sec is probably not significant.

It is of special interest that the McDonald spectrograms show no appreciable variation in the intensities of the emission lines. A careful study of our plate material gave only one observation in which the red component was distinctly stronger than the violet. This was on December 4, spectrogram CQ 7300, but even on this anomalous plate the red component was only a small fraction of its intensity stronger than the violet component. An inspection of spectrogram *d* in Plate IX, facing page 255 of the article by Joy and Sanford, shows conclusively that not a single spectrogram of our series comes anywhere near to showing the marked difference between the emission components which they had observed.

We have, as yet, no indication as to whether the phenomenon of variability in the emission lines is periodic. However, it looks as though the changes might be sporadic. Our plate CQ 7300 with a phase of 0.642*P* is almost exactly matched by two spectrograms taken the preceding night. At phase 0.675*P* the two components are equal in intensity, and on the preceding plate, at phase 0.651*P*, the violet component looks slightly stronger than the red.

It is impossible without much additional material to discuss this phenomenon further, but it is perhaps significant that Katherine C. Gordon and Gerald E. Kron have recently discovered appreciable changes in the light-curves of Castor C obtained in different seasons.

The great sharpness of the emission lines constitutes another interesting problem. According to Joy and Sanford, the distance between the centers of the two stars is 2,700,000 km. The Mount Wilson discussion of the photometric light-curve gave $r_1 = r_2 = 0.2\,(a_1 + a_2) = 500{,}000$ km $= 0.7\,\odot$. Allowing for the inevitable spreading of the photographic image by the changing radial velocity during the exposure (which for

the highest dispersion was approximately 1 hour), we find that the emission components are not much broader than the comparison lines obtained with a slit of 0.1 mm, which is projected upon the plate as a width of 0.05 mm. Thus, at the two elongations, the separation between the two emission components of the calcium lines is approximately four or five times the width of each emission line. In most spectroscopic binaries with calcium emission lines the source of the radiation is located at the tidal bulges of each component. In Castor C there is no clear evidence of a variation in the line width. Yet it is reasonable to suppose that the calcium gases are not subject to appreciable darkening

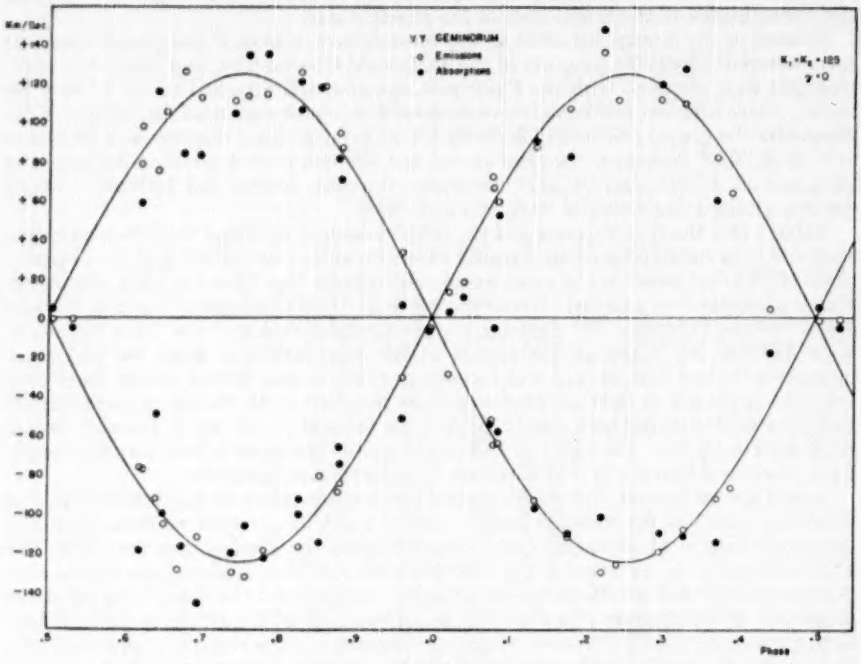

FIG. 1

at the limb. Consequently, the narrow widths of the lines must signify that the rotational velocities are small. This, in turn, means that the stars are small in size. Adopting the Mount Wilson value for $a_1 + a_2 = 2{,}700{,}000$ km, we estimate that the radius of each star is approximately 300,000 km, or about 0.5 $\odot$. Allowing for the uncertainty of the estimate, this is probably compatible with the photometric values of r_1 and r_2.

Spectroscopically, there is a vast difference between the rotational broadening of the lines of Castor C and any typical W Ursae Majoris binary. In the latter the absorption lines, as well as the *Ca* II emission lines, are greatly broadened by rotation, and this broadening is conspicuous even with the smaller dispersions used at the McDonald Observatory. This is due partly to the shorter periods of the W Ursae Majoris systems, accounting for a factor of about 2 in the rotational velocities, and partly to the greater size of the stars, accounting for another factor of 2.

The question has arisen as to whether, with the relatively high surface gravities of the late-type dwarfs, the emission lines of hydrogen would show a noticeable broadening

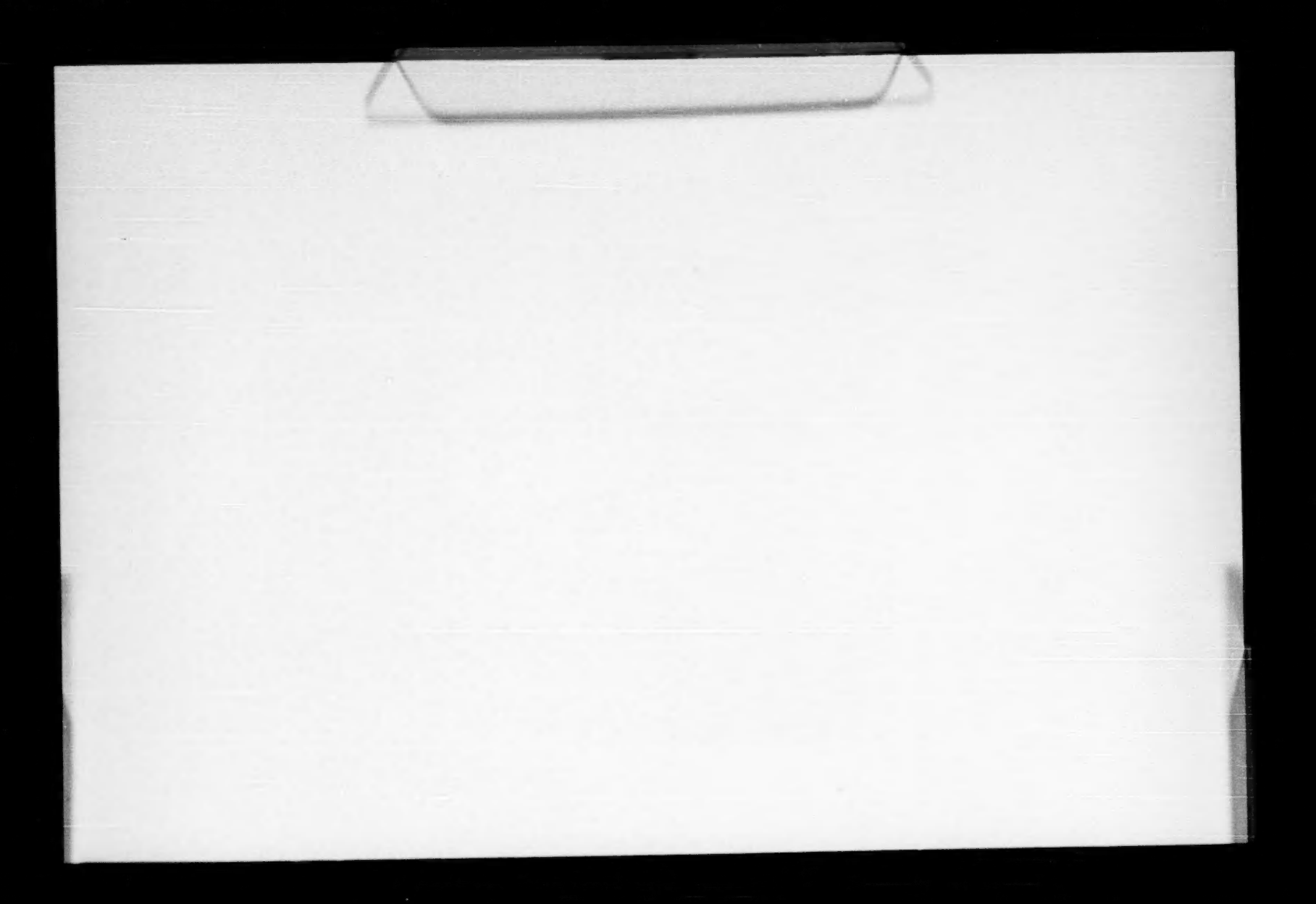

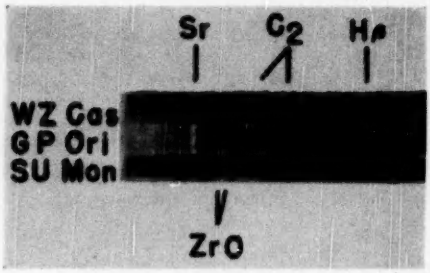

FIG. 1.—Part of the photographic region of the spectrum of three cool stars. The resonance line of *Sr*I is very strong in the spectrum of GP Orionis.

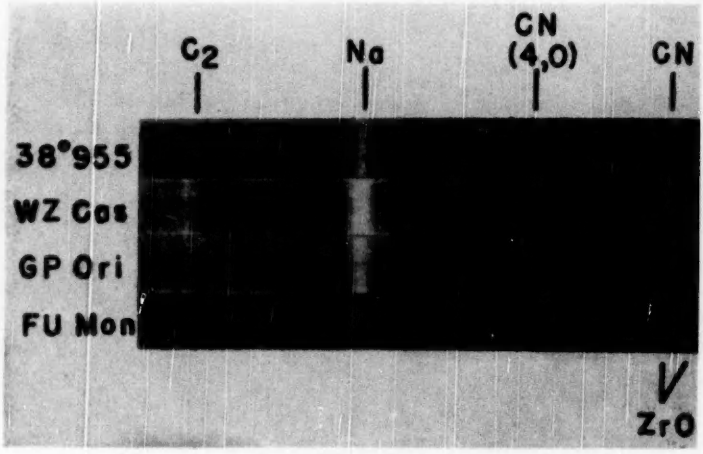

FIG. 2.—The visual region of the spectrum of four cool stars. The upper two objects are carbon stars, while the lower two are members of class S.

caused by Stark effect. With the higher dispersions employed at McDonald, *Hδ* and *He* do not look appreciably different in width than do *Ca* II H and *Ca* II K. Incidentally, *He* appears approximately with its normal intensity, and it is not noticeably reduced by any overlying *Ca* II vapor. The higher members of the Balmer series, which were not seen by Joy and Sanford, presumably because of the absorption of light in their spectrograph, can easily be traced with our quartz optics as far as *H* 15. It is significant that *H* 10, *H* 11, and *H* 15 appear as diffuse condensations in the continuous spectrum of the star, without revealing the duplicity shown by the lower members of the series. This is noticeable particularly on our spectrogram CQ 7177, taken at phase 0.879*P*. We have no other plate, long enough exposed, that would correspond to a phase of greater separation between the components. If this observation should be confirmed, it would serve as a clue for finding the location of the emitting *H* gas. Incidentally, *H* 12, *H* 13, and *H* 14 are not clearly visible on our spectrogram. This may be due to a photographic effect produced by the weakening of the (underexposed) continuous spectrum of the red dwarf by heavy absorption features in the region λλ 3720–3750. But it is perhaps significant that these same lines are also weak in long-period variables at phases preceding maximum light, presumably due to overlying absorption.[2]

O. Struve
G. Herbig
H. Horak

Yerkes and McDonald Observatories
April 6, 1950

THE SPECTRUM OF GP ORIONIS

The spectrum of the red star GP Orionis[1] was noted by Baldwin and Hamlin[2] to show exceptionally strong sodium D lines. Weak bands of *ZrO* and *TiO* were also present in the visual region of the spectrum, according to their observations. More recently, however, McKellar[3] and Sanford[4] have considered GP Orionis to be a carbon star. To investigate the nature of this object, a number of low-dispersion spectra have been obtained of it and of other cool stars at the McDonald Observatory. Several spectra are shown in Figures 1 and 2; the dates of observation are given in the accompanying tabulation.

Wave-Length Region	Star	Date	Wave-Length Region	Star	Date
Photographic	WZ Cas	Jan. 2, 1949*	Visual	WZ Cas	Dec. 21, 1949
	GP Ori	Apr. 16, 1948		GP Ori	Apr. 24, 1948
	SU Mon	Nov. 16, 1946		FU Mon	Dec. 22, 1949
Visual	+38°955	Dec. 22, 1949			

* The writer is indebted to Dr. G. H. Herbig for obtaining this spectrogram for him.

Figure 1 shows the photographic region of the spectrum of GP Orionis, along with that of the cool carbon star, WZ Cassiopeiae,[5] and SU Monocerotis, which has been

[2] See, e.g., P. W. Merrill, the upper spectrum of R Hydrae in Pl. I, *Ap. J.*, **103**, 6, 1946.

[1] BD+15°726: $\alpha = 4^h57^m1$, $\delta = +15°11'$ (1900). The photographic magnitude varies from 11.8 to 13.6, but details of the light-curve are not known.

[2] *Ann. Dearborn Obs.*, Vol. **4**, Part 15, 1940.

[3] *J.R.A.S. Canada*, **38**, 237, 1944.

[4] *Pub. A.S.P.*, **61**, 43, 1949.

[5] See P. C. Keenan and W. W. Morgan, *Ap. J.*, **94**, 501, 1941.

classified as type S2 by Dorothy Davis.[6] The outstanding feature of the spectrum of GP Orionis is the extraordinary strength of the resonance line of neutral strontium. The weakness of molecular features in the spectrum of GP Orionis is quite apparent: the C_2 bands are exceedingly weak, if not absent, but the *ZrO* bands near λ 4640 are probably present. It is of considerable interest that the hydrogen lines appear in emission in the spectrogram of WZ Cassiopeiae reproduced. Emission at $H\beta$ was noted by the early Yerkes observers[7] but apparently has not been seen since.

The region of the spectrum of GP Orionis surrounding the D lines is shown in Figure 2. For comparison are included the spectra of WZ Cassiopeiae and of two stars classified by Merrill, Sanford, and Burwell[8] as of types N and S, respectively—+38°955 and FU Monocerotis (HD 44544). A considerable similarity exists between the spectra of GP Orionis and FU Monocerotis. The C_2 band at λ 5635 does not appear to be present in either, although bands of the red system of *CN* are definitely present. The (0, 0) band of *ZrO*, starting at λ 6474, is probably present in both, although it is blended on the long-wave-length side by the strongest head of the (6, 2) band of the red system of *CN* at λ 6494. The great enhancement of transitions arising from the ground level in WZ Cassiopeiae which is apparent from the strength of the D lines and the resonance doublet of *Li* I at λ 6708[9] is shown also by the intensity of the (4, 0) red-system *CN* band.

From these spectra it appears that GP Orionis must be considered an S-type star. Yet, though undoubtedly a very cool star, its spectrum does not show strong bands of *TiO*—a phenomenon which is exhibited also by the cool carbon stars. In the latter stars it has long been concluded that carbon is abnormally abundant relative to oxygen and that much of the oxygen is taken up in the unobservable molecule *CO*. Might we not suspect that stars of the type of GP Orionis also have a somewhat abnormal abundance of carbon? It is apparent that an increase in the abundance of carbon relative to oxygen will reduce the formation of metallic oxides, but those molecules of the highest dissociation potentials (*ZrO*, *YO*, *LaO*) will be less affected than those of lower dissociation potentials.[10] A very low-opacity atmosphere would, however, be necessary to produce strong bands of any oxides under these circumstances. Qualitatively it appears that the occurrence of spectra such as those of GP Orionis, FU Monocerotis, and some other S-type stars could be due to an atmospheric carbon abundance intermediate between that in ordinary stars and that in the objects which are now recognized as carbon stars—an idea which is essentially due to Fujita.[11] The existence of considerable variation in the carbon content of the atmospheres of the carbon stars is strongly indicated by the work of Keenan and Morgan on the classification of these stars.[5] Further evidence is provided by the recent discovery that several K-type stars which had been previously noted to show strong resonance lines of *Ba* II also show the (0, 0) band of C_2 in unusual strength, in addition to abnormally strong bands of *CN* and *CH*. All these bands, however, are much weaker than in the presently recognized carbon stars. These objects, of which HR 774 is typical, seem to be clear cases of intermediate carbon abundance; they are being studied at present by Dr. Keenan and the writer.

WILLIAM P. BIDELMAN

YERKES AND MCDONALD OBSERVATORIES
June 7, 1950

[6] *Pub. A.S.P.*, **46**, 267, 1934.

[7] G. E. Hale, F. Ellerman, and J. A. Parkhurst, *Pub. Yerkes Obs.*, Vol. **2**, 1903.

[8] *Pub. A.S.P.*, **45**, 307, 1933.

[9] See A. McKellar, *Observatory*, **64**, 4, 1941.

[10] K. Wurm has discussed in *Ap. J.*, **91**, 103, 1940, the dependence of the *ZrO*/*TiO* ratio on the partial density of free oxygen atoms.

[11] *Japanese J. Astr. and Geophysics*, **17**, 17, 1939; **18**, 45, 1940; **18**, 177, 1941.

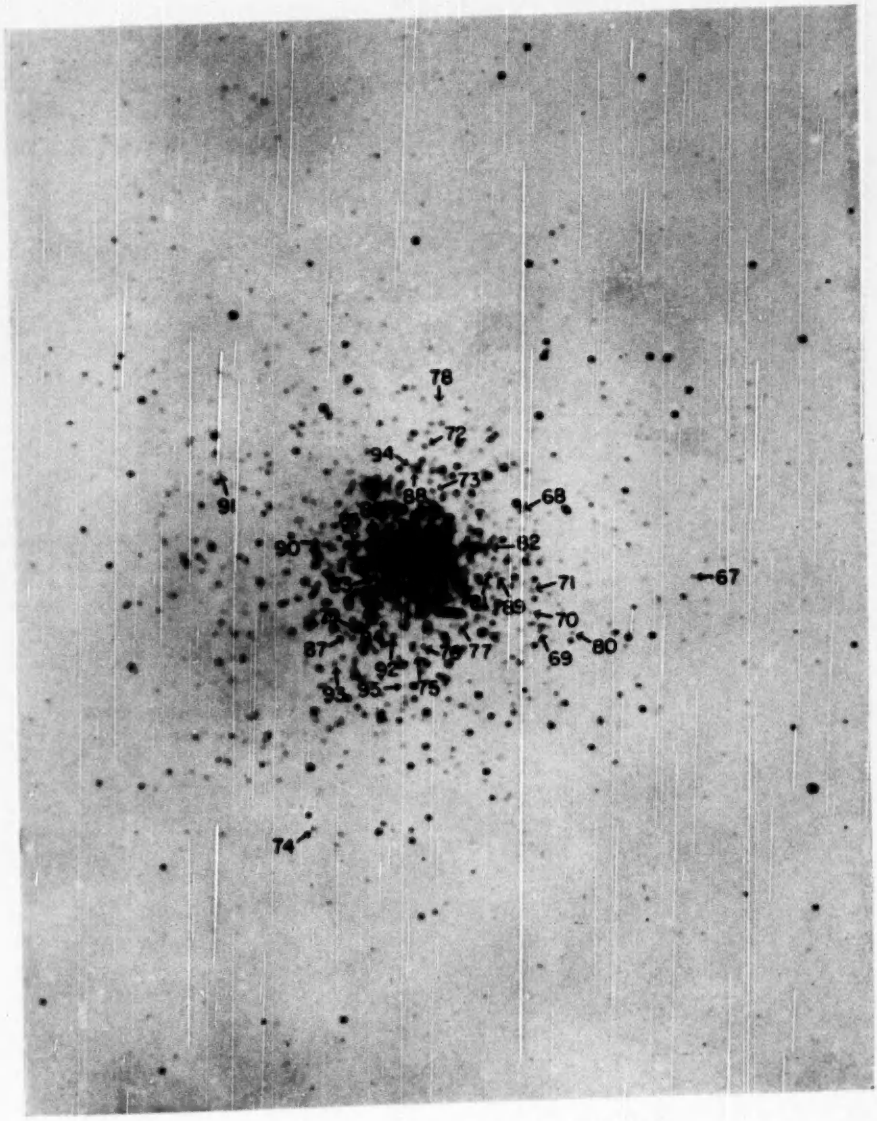

FIG. 1.—Identification of new variable stars in M 15

TWENTY-NINE NEW VARIABLE STARS IN THE GLOBULAR CLUSTER M 15

NGC 7078 = M 15, a condensed globular cluster of class IV, can be considered quite rich in variable stars. The *Catalogue of 1116 Variable Stars in Globular Star Clusters* of H. B. Sawyer gives the positions and magnitudes of 66 variables in this cluster, discovered by Bailey on Arequipa and Mount Wilson plates. Eight additional variables were found by Guthnick and Prager, according to a short communication (*Sitzungsberichte Preussischen Akademie der Wissenschaften*, **28**, 508, 1925), but the positions were not indicated. Of these 66 variables, only 3 are within a distance of 50″ from the center, probably because the central part was too congested on Bailey's plates to permit accurate search in this area.

TABLE 1

NEW VARIABLES IN M 15

No.	x	y	Küstner No.	No.	x	y	Küstner No.
67	−86″.6	−10″.4	227	82	−20″.7	+ 1″.5	.....
68	−31.8	+12.6	420	83	+16.3	− 7.4	.....
69	−37.0	−25.2	.....	84	+18.5	−16.3	.....
70	−34.0	−19.2	.....	85	+20.7	+ 2.2	.....
71	−34.8	−12.6	.....	86	+12.6	+ 4.4	.....
72	− 2.2	+34.8	556	87	+23.7	−23.7	.....
73	− 3.7	+20.0	.....	88	+ 2.2	+26.6	.....
74	+36.3	−85.8	754	89	−23.7	− 6.7	463
75	+ 2.2	−30.3	.....	90	+31.1	+ 4.4	.....
76	+ 0.7	−28.9	.....	91	+67.3	+28.9	847
77	−11.8	−22.9	.....	92	+ 9.6	−25.2	610
78	− 6.7	+47.4	533	93	+27.4	−33.3	705
79	+21.5	−23.7	.....	94	+ 3.7	+28.9	.....
80	−47.4	−26.6	345	95	+ 5.2	−40.0	599
81	−21.5	− 5.9	.....				

I have had the opportunity to examine two series of plates taken by Dr. A. Brown at the Cassegrain focus of the 82-inch reflector of the McDonald Observatory, in blue and yellow light. The scale is 1 mm = 7″.4, and, with exposure times ranging from 1 to 10 minutes, it is possible to observe single stars, without serious blending, to a distance of about 30″ from the center of the cluster. Twenty-nine new variables were found, mostly near the central part, and 55 of the 66 variables previously known were rediscovered. Of the 11 undiscovered, 3 (Nos. 26, 28, and 31) are too far from the center, in a zone which was not searched with particular attention, and 2 (Nos. 27 and 34) probably do not vary at all. The real percentage of the known variables found in this search is therefore 90 per cent. The new variables are marked in Figure 1.

Table 1 contains the positions of the 29 new variables. Successive columns give the number of the new variables, consecutively from the last known variable in this cluster; the x and y co-ordinates in seconds of arc; and the number in Küstner's *Catalogue*.

The material does not allow the derivation of accurate magnitudes and periods; it is, however, sufficient to conclude that 28 of the new variables are of the RR Lyrae type, with a mean magnitude of around 15.7. Variable No. 86 is probably a long-period cepheid with an amplitude of about 1.2 mag. and a mean magnitude of 14.0.

I wish to express my gratitude to Dr. A. Brown, who kindly placed his plates of M 15 at my disposal for measurements at the blink microscope.

L. ROSINO

YERKES OBSERVATORY
March 1950

ZEEMAN SHIFTS FOR STELLAR DIPOLES AND QUADRUPOLES WITH INCLINED AXES

Recent measurements of stellar magnetic fields by H. W. Babcock[1] have raised the question of how large the observed Zeeman shift would be for a magnetic star with an axis inclined to the line of sight. The necessary formulae to answer this question can be derived as follows:

For measurements made through an analyzer for circularly polarized light, F. H. Seares[2] and H. W. Babcock[3] have shown that the shift measured in the light of one surface element of the star is proportional to the component of the magnetic field in the line of sight. Hence the shift measured in the light of the star as a whole is determined by the effective field strength, H_e, which is the line-of-sight component of the magnetic field averaged over the visible hemisphere:

$$H_e = \frac{\int\int H_\zeta I \, d\xi \, d\eta}{\int\int I \, d\xi \, d\eta} . \tag{1}$$

Here H_ζ is the magnetic component in the line of sight, I the surface brightness, and $d\xi d\eta$ the surface element of the stellar disk. The co-ordinate system ξ, η, and ζ is chosen to be oriented so that ζ is parallel to the line of sight, and the unit of length is chosen to be equal to the radius of the star.

If one introduces a second co-ordinate system—x, y, and z—oriented so that z is parallel to the magnetic axis, one has, for the magnetic field on the surface of the star, with $x^2 + y^2 + z^2 = 1$,

Dipole: $$H_x = x\left(\tfrac{3}{2}z\right) H_p , \qquad H_y = y\left(\tfrac{3}{2}z\right) H_p , \qquad H_z = \left(\tfrac{3}{2}z^2 - \tfrac{1}{2}\right) H_p ; \tag{2}$$

Quadrupole: $$H_x = x\left(\tfrac{5}{2}z^2 - \tfrac{1}{2}\right) H_p , \quad H_y = y\left(\tfrac{5}{2}z^2 - \tfrac{1}{2}\right) H_p , \quad H_z = z\left(\tfrac{5}{2}z^2 - \tfrac{3}{2}\right) H_p . \tag{3}$$

Here H_p is the field strength at the pole. With the transformation

$$x = \zeta \sin i + \xi \cos i , \qquad y = \eta , \qquad z = \zeta \cos i - \xi \sin i , \tag{4}$$

where i is the inclination of the magnetic axis to the line of sight, one can obtain expressions for the magnetic component in the line of sight, H_ζ, in terms of ξ, η, ζ, and i.

Now, to compute the effective field H_e, one may introduce the expressions for H_ζ into equation (1) and, at the same time, substitute for I the usual expression for the surface brightness

$$I = 1 - u + u\zeta , \tag{5}$$

where u is the limb-darkening coefficient. The integrations over ξ and η occurring in equation (1) can be performed analytically, with the following results:

Dipole: $$H_e = \frac{15 + u}{15 - 5u} \cdot \frac{H_p}{4} \cdot \cos i , \tag{6}[4]$$

Quadrupole: $$H_e = \frac{u}{3 - u} \cdot \frac{H_p}{4} \cdot \frac{1 + 3\cos 2i}{4} . \tag{7}$$

[1] *Ap. J.*, **108**, 201, 1948.

[2] *Ap. J.*, **38**, 99, esp. eq. (21), 1913.

[3] *Ap. J.*, **105**, 105, esp. eq. (8), 1946.

[4] Equation (6) is in satisfactory agreement with H. W. Babcock's result for $i = 0$ and $u = 0.45$ (*Ap. J.*, **105**, 105, esp. eq. [10], 1946).

It is seen that the dependence of the effective field on the inclination i has a simple harmonic form in both cases. The dependence on the limb darkening u is moderate for the dipole and large for the quadrupole.

In the special case of a uniform disk ($u = 0$), according to equation (7), a quadrupole cannot be measured in the integrated light of a star, from any inclination. In general ($u \approx 0.5$), a quadrupole has to be of the order of ten times stronger than a dipole to give the same measured effect.

All the above results hold only if the surface brightness I and the equivalent widths of the lines measured are unaffected by the magnetic field and hence independent of the magnetic latitude.

MARTIN SCHWARZSCHILD

PRINCETON UNIVERSITY OBSERVATORY
May 31, 1950

REVIEWS

Einführung in die sphärische Astronomie. By ADALBERT PREY. Vienna: Springer Verlag, 1949. Pp. 316+123 figs. $5.50 (unbound).

This textbook on spherical astronomy was primarily written as an introduction to the field of astrometry. In his Introduction the author remarks that a book on this subject tends to appear outdated because basically new ideas have not been added to this field of astronomy in the last hundred to a hundred and fifty years. It is somewhat of an academic question to distinguish between basically new ideas and new methods, but a modern book on spherical astronomy should cover such important subjects as heliographic co-ordinates used in the study of sun spots and other solar phenomena associated with them; the methods of reduction of photographic plates for the determination of parallaxes, proper motions, mass ratios, etc.; as well as a discussion of double-star orbits. None of these subjects is covered in this book.

The chief divisions are: "The Spherical Astronomy" (165 pp.), "The Astronomical Instruments" (55 pp.), "The Determination of Geographic Co-ordinates" (60 pp.), and an appendix on "The Method of Least Squares" (29 pp.).

The division on spherical astronomy follows the conventional pattern of previous textbooks. It should be noted that the author quotes the formulas for the general precession for 1850 published by Oppolzer in 1881 rather than the values determined by Newcomb and adopted by international agreement. If the author wished to show the precessional quantities in a time series, he should have quoted the more recent paper by de Sitter (*B.A.N.*, Vol. **8**, No. 307, 1938). This important paper was apparently unknown to the author, since he later refers to an earlier paper by de Sitter on the same subject, which was published in 1915.

The author's values for the annual aberration and for the constant of refraction are also at variance with those now generally accepted.

It is regrettable to find that, in the part on astronomical instruments, eight pages out of fifty have been spent on the description of two instruments which have long been considered obsolete, namely, the ring micrometer and the heliometer.

In the part on the determination of geographic co-ordinates the usual methods for determining such co-ordinates are discussed. While this is important in understanding the basic problems, it is felt that some of the modern tables for obtaining quick solutions for navigational purposes should have received some mention.

The publishers should be commended for their high standards in quality of printing and paper.

K. AA. STRAND

Dearborn Observatory
Northwestern University

THE OBSERVATORY

FOUNDED 1877

* * *

A Magazine presenting current developments in Astronomy for the Amateur and Professional Astronomer. Articles, Correspondence, Notes on Observations, and Reviews of Books. The Journal is published by the Royal Astronomical Society and contains the Monthly Notices (Geophysical) of the Royal Astronomical Society and the Proceedings which follow are also fully reported.

* * *

Annual subscription for 6 issues post free 30/- should be sent to

The Editors, ROYAL OBSERVATORY
Greenwich, London S.E. 10

THE ATMOSPHERES OF THE EARTH AND PLANETS

Papers presented at the Fiftieth Anniversary Symposium of the Yerkes Observatory—September, 1947

Edited by GERARD P. KUIPER

CONTRIBUTORS: A. Adel, H. Brown, S. T. Chamberlin, [illegible], T. Dunham, E. Durand, J. Franck, J. L. Greenstein, G. [illegible], [illegible], Z. Kopal, G. P. Kuiper, M. V. Migeotte, C.-G. Rossby, L. Spitzer, F. Spurgo, H. C. van de Hulst, F. L. Whipple

366 pages 6¾×9¾ Illustrated $5.00

THE UNIVERSITY OF CHICAGO PRESS